

Institut für Physik und Astronomie
Astrophysik II

The H I Lyman α opacity at redshift $2.7 \leq z \leq 3.6$

Dissertation
zur Erlangung des akademischen Grades
"doctor rerum naturalium"
(Dr. rer. nat.)
in der Wissenschaftsdisziplin "Astrophysik"

eingereicht an der
Mathematisch-Naturwissenschaftlichen Fakultät
der Universität Potsdam

von
Dominik Hildebrandt

Potsdam, den 30.01.2015

This work is licensed under a Creative Commons License:
Attribution 4.0 International
To view a copy of this license visit
<http://creativecommons.org/licenses/by/4.0/>

Published online at the
Institutional Repository of the University of Potsdam:
URN urn:nbn:de:kobv:517-opus4-78355
<http://nbn-resolving.de/urn:nbn:de:kobv:517-opus4-78355>

Contents

Abstract	iii
Zusammenfassung	v
List of Figures	vii
List of Tables	xi
Abbreviations	xiii
1 The H I Lyα opacity	1
1.1 Introduction	1
1.2 The Intergalactic Medium and its Reionization	2
1.3 Investigating the redshift evolution of τ_{eff}	9
1.3.1 Instruments	9
1.3.2 Background sources	10
1.3.3 Quasar spectra	11
1.4 Historical remarks	12
1.5 Observed quantities	14
1.5.1 The effective optical depth	14
1.5.2 The Gunn-Peterson optical depth	19
1.6 Motivation for this work	24
2 Data selection and analysis	29
2.1 Sample selection	29
2.2 Discussion of quasar sightlines	31
2.2.1 J132029-052335	32
2.2.2 J162116-004250	32
2.2.3 J212912-153841	34
2.2.4 J004131-493611	35
2.2.5 J012403+004432	36
2.2.6 J111113-080401	36
2.2.7 J005758-264314	37
2.2.8 J123055-113909	38
2.2.9 J010604-254651	38
2.2.10 J014214+002324	39
2.2.11 J111350-153333	40

2.2.12	J115538+053050	41
2.2.13	J124957-015928	41
2.3	Fitting procedures	42
2.3.1	FITQSOSPLINE	43
2.3.2	CANDALF	44
2.3.3	Results of the line-fitting procedure with CANDALF	45
3	H I Lyα forest statistics	47
3.1	The column-density distribution	48
3.2	Doppler-parameter distribution	51
3.3	$b(N)$ distribution	53
3.4	Number-density evolution	58
4	The H I Lyα opacity at redshift $z \sim 3$	61
4.1	Methodology	61
4.2	Results	65
4.3	Systematics	69
4.3.1	Shifting the redshift bounds of the 3 proper Mpc segments	69
4.3.2	Correction for metal absorption lines	72
4.3.3	Simulations	73
5	Discussion and Conclusions	85
5.1	Discussion	85
5.1.1	High-resolution data	85
5.1.2	Low-resolution (SDSS) data	92
5.2	Conclusions	97
5.2.1	Conclusions from this work	98
5.2.2	Literature comparison	100
5.2.3	Future prospects	102
A	Equations	105
A.1	Derivation of Eq. (1.7)	105
A.2	Derivation of Eq. (1.11)	105
A.3	Derivation of Eq. (1.17)	107
B	Technical details of the line-fitting procedure with CANDALF	109
C	Segment flux histograms	115
D	Absorption spectra	123
E	Absorption line data	157
	Bibliography	283

Abstract

Most of the baryonic matter in the Universe resides in a diffuse gaseous phase in-between galaxies consisting mostly of hydrogen and helium. This intergalactic medium (IGM) is distributed in large-scale filaments as part of the overall cosmic web. The luminous extragalactic objects that we can observe today, such as galaxies and quasars, are surrounded by the IGM in the most dense regions within the cosmic web. The radiation of these objects contributes to the so-called ultraviolet background (UVB) which keeps the IGM highly ionized ever since the epoch of reionization.

Measuring the amount of absorption due to intergalactic neutral hydrogen ($\mathrm{H}\,\mathrm{I}$) against extragalactic background sources is a very useful tool to constrain the energy input of ionizing sources into the IGM. Observations suggest that the $\mathrm{H}\,\mathrm{I}$ Lyman α effective optical depth, τ_{eff} , decreases with decreasing redshift, which is primarily due to the expansion of the Universe. However, some studies find a smaller value of the effective optical depth than expected at the specific redshift $z \sim 3.2$, possibly related to the complete reionization of helium in the IGM and a hardening of the UVB. The detection and possible cause of a decrease in τ_{eff} at $z \sim 3.2$ is controversially debated in the literature and the observed features need further explanation.

To better understand the properties of the mean absorption at high redshift and to provide an answer for whether the detection of a τ_{eff} feature is real we study 13 high-resolution, high signal-to-noise ratio quasar spectra observed with the Ultraviolet and Visual Echelle Spectrograph (UVES) at the Very Large Telescope (VLT). The redshift evolution of the effective optical depth, $\tau_{\mathrm{eff}}(z)$, is measured in the redshift range $2.7 \leq z \leq 3.6$. The influence of metal absorption features is removed by performing a comprehensive absorption-line-fitting procedure.

In the first part of the thesis, a line-parameter analysis of the column density, N , and Doppler parameter, b , of ≈ 7500 *individually* fitted absorption lines is performed. The results are in good agreement with findings from previous surveys.

The second (main) part of this thesis deals with the analysis of the redshift evolution of the effective optical depth. The τ_{eff} measurements vary around the empirical power law $\tau_{\mathrm{eff}}(z) \propto (1+z)^{\gamma+1}$ with $\gamma = 2.09 \pm 0.52$. The same analysis as for the observed spectra is performed on synthetic absorption spectra. From a comparison between observed and synthetic spectral data it can be inferred that the uncertainties of the τ_{eff} values are likely underestimated and that the scatter is probably caused by high-column-density absorbers with column densities in the range $15 \leq \log N \leq 17$. In the real Universe, such absorbers are rarely observed, however. Hence, the difference in τ_{eff} from different observational data sets and absorption studies is most likely caused by cosmic variance. If, alternatively, the disagreement between such data is a result of an too optimistic estimate of

the (systematic) errors, it is also possible that all τ_{eff} measurements agree with a smooth evolution within the investigated redshift range. To explore in detail the different analysis techniques of previous studies an extensive literature comparison to the results of this work is presented in this thesis.

Although a final explanation for the occurrence of the τ_{eff} deviation in different studies at $z \sim 3.2$ cannot be given here, our study, which represents the most detailed line-fitting analysis of its kind performed at the investigated redshifts so far, represents another important benchmark for the characterization of the H I Ly α effective optical depth at high redshift and its indicated unusual behavior at $z \sim 3.2$.

Zusammenfassung

Der Großteil der baryonischen Materie des Universums, die im Wesentlichen aus Wasserstoff und Helium besteht, befindet sich in Form von diffusem Gas zwischen den Galaxien. Dieses intergalaktische Medium (IGM) bildet großräumige Strukturen aus, dessen Fäden als "kosmisches Netz" bezeichnet werden. Die leuchtkräftigen extragalaktischen Objekte, die man heutzutage beobachten kann (z.B. Galaxien und Quasare), sind von diesem IGM umgeben und befinden sich in den dichtesten Regionen innerhalb des kosmischen Netzes. Die von diesen Objekten ausgehende ultraviolette (UV) Strahlung ist Bestandteil des UV-Strahlungshintergrunds, der seit der Reionisationsphase den hochionisierten Zustand des IGM aufrecht hält.

Eine Auswertung des absorbierten Strahlungsanteils durch den noch im IGM vorhandenen neutralen Wasserstoff (HI) entlang der Sichtlinie zu einer beobachteten extragalaktischen Hintergrundquelle lässt auf den Energieeintrag der Strahlungsquellen ins IGM schließen. Aus geeigneten Messdaten lässt sich schlussfolgern, dass sich die effektive optische Tiefe von HI ($\text{Ly}\alpha$ Übergang) mit abnehmender Rotverschiebung verringert, was im Wesentlichen auf die Expansion des Universums zurückzuführen ist. Einige Arbeiten finden jedoch bei der ausgewiesenen Rotverschiebung $z \sim 3.2$ einen kleineren Wert für die effektive optische Tiefe als erwartet, ein Trend der möglicherweise mit der vollständigen Reionisation von Helium im IGM und einem Anstieg der Intensität des UV-Hintergrunds in Verbindung steht. Die Detektion und mögliche Ursache einer Abnahme der effektiven optischen Tiefe bei $z \sim 3.2$ ist in der Literatur kontrovers diskutiert und die beobachteten Besonderheiten machen eine weitere Untersuchung erforderlich.

Um die Eigenschaften der mittleren Absorption bei hoher Rotverschiebung besser zu verstehen und um einen Lösungsansatz für die Debatte zu liefern, untersuchen wir 13 hoch aufgelöste Quasarabsorptionsspektren mit einem hohen Signal-zu-Rauschen Verhältnis, die mit dem Instrument UVES des *Very Large Telescope* (VLT) aufgenommen wurden. Die Entwicklung der effektiven optischen Tiefe wird im Rotverschiebungsbereich $2.7 \leq z \leq 3.6$ gemessen. Die Messung wird um den Beitrag von Metallen durch die detaillierte Anpassung von Linienprofilen an die beobachtete Absorption korrigiert.

Im ersten Teil der Arbeit wird eine Auswertung der Parameter der ≈ 7500 *einzelnen* angepassten Absorptionslinien (Säulendichte N und Doppler-Parameter b) vorgenommen. Die entsprechenden Ergebnisse stimmen im Rahmen der Messunsicherheiten mit Literaturwerten überein.

Der Hauptteil der Arbeit beschäftigt sich mit der Berechnung der effektiven optischen Tiefe in Abhängigkeit von der Rotverschiebung $\tau_{\text{eff}}(z)$. Es stellt sich heraus, dass die τ_{eff} -Messwerte um ein empirisches Potengesetz der Form $\tau_{\text{eff}}(z) \propto (1+z)^{\gamma+1}$ mit $\gamma = 2.09 \pm 0.52$ streuen. Die gleiche Auswertung wie für die Beobachtungsdaten wird für synthetische

Spektren durchgeführt. Ein Vergleich dieser Daten legt nahe, dass die Größe der Unsicherheiten der τ_{eff} -Messwerte wahrscheinlich unterschätzt wird und dass die Streuung der Datenpunkte auf Absorber hoher Säulendichte ($15 \leq \log N \leq 17$) zurückzuführen ist. Solche Absorber sind im beobachtbaren Universum jedoch selten, sodass der Unterschied in den τ_{eff} -Messwerten bei verschiedenen Zusammenstellungen von Beobachtungsdaten und Studien zum Absorptionsverhalten höchstwahrscheinlich durch kosmische Varianz bedingt ist. Sollte jedoch die fehlende Übereinstimmung dieser Daten eine Folge zu optimistischer (systematischer) Fehlerabschätzungen sein, so ist es ebenfalls denkbar, dass die τ_{eff} -Messwerte mit einer gleichmäßigen Entwicklung über den untersuchten Rotverschiebungsbereich hinweg konsistent sind. Um die wesentlichen Unterschiede in den Untersuchungsmethoden vorheriger Studien zu untersuchen, wird in dieser Arbeit ein umfassender Vergleich der Ergebnisse dieser Arbeit mit entsprechender Literatur vorgenommen.

Eine endgültige Erklärung für das Auftreten einer Abweichung in $\tau_{\text{eff}}(z)$ vom empirischen Potenzgesetz, wie sie von einigen Studien bei $z \sim 3.2$ gefunden wurde, kann in dieser Arbeit zwar nicht gegeben werden, dennoch stellt sie die bislang umfassendste Parameterbestimmung von Absorptionslinien ihrer Art im untersuchten Rotverschiebungsbereich dar. Sie ist somit ein weiterer wichtiger Schritt in Richtung des ganzheitlichen Verständnisses der effektiven optischen Tiefe bei hohen Rotverschiebungen und deren möglicherweise ungewöhnlichem Verlauf bei $z \sim 3.2$.

List of Figures

1.1	Dark Matter density field at redshift $z = 0$	4
1.2	Redshift evolution of chemical abundances and gas temperature during inhomogeneous He II reionization	6
1.3	Absorption spectrum of the quasar Q0420-388	11
1.4	Redshift evolution of the number of absorption lines in quasar spectra	13
2.1	Redshift coverage of the observed quasar spectra used in this work	31
2.2	Absorption spectrum of the quasar J132029-052335	32
2.3	Absorption spectrum of the quasar J162116-004250	32
2.4	Absorption spectrum of the quasar J212912-153841	34
2.5	Absorption spectrum of the quasar J004131-493611	35
2.6	Absorption spectrum of the quasar J012403+004432	36
2.7	Absorption spectrum of the quasar J111113-080401	36
2.8	Absorption spectrum of the quasar J005758-264314	37
2.9	Absorption spectrum of the quasar J123055-113909	38
2.10	Absorption spectrum of the quasar J010604-254651	38
2.11	Absorption spectrum of the quasar J014214+002324	39
2.12	Absorption spectrum of the quasar J111350-153333	40
2.13	Absorption spectrum of the quasar J115538+053050	41
2.14	Absorption spectrum of the quasar J124957-015928	41
3.1	Doppler-parameter distribution of identified metal absorption lines	48
3.2	Column-density distributions of H I Ly α absorption lines	50
3.3	Doppler-parameter distributions of H I Ly α absorption lines	52
3.4	$b(N)$ distributions of H I Ly α absorption lines	54
3.5	Lower cutoff envelope in the $b(N)$ distributions of H I Ly α absorption lines	57
3.6	Number-density evolution of H I Ly α absorption lines	59
4.1	Proper distance	64
4.2	Histograms of the model mean flux	65
4.3	Redshift evolution of the effective optical depth	67
4.4	Comparison of the redshift evolution of the effective optical depth for various absorption line selections	68
4.5	Power-law analysis of $\tau_{\text{eff}}(z)$	70
4.6	Same as Fig. 4.2 using a different redshift grid	71
4.7	Redshift evolution of the effective optical depth for two different grids of 3 proper Mpc segments	72

4.8	Redshift coverage of the synthetic quasar spectra used in this work	74
4.9	Example of a synthetic quasar absorption spectrum	75
4.10	Redshift evolution of the effective optical depth from synthetic quasar spectra featuring H I Ly α absorption lines with lognormal Doppler-parameter distributions and different column-density distributions	77
4.11	Redshift evolution of the effective optical depth from synthetic quasar spectra featuring H I Ly α absorption lines with different column-density distributions and a fixed Doppler parameter	77
4.12	Redshift evolution of the effective optical depth from synthetic quasar spectra featuring H I Ly α absorption lines with lognormal Doppler-parameter distributions and a fixed column density	79
4.13	Redshift evolution of the effective optical depth from synthetic quasar spectra featuring H I Ly α absorption lines with fixed Doppler parameters and a fixed column density	80
4.14	Same as Fig. 4.10 a computed in half the redshift bin size	81
4.15	Same as Fig. 4.14 shown in a smaller redshift range and offset vertically by a constant amount to match the τ_{eff} evolution measured from the corrected model flux at redshift $z \sim 3.54$	82
5.1	Effective-optical-depth measurements from different works	86
5.2	Comparison of the effective-optical-depth measurements from this work to those found by Kim et al.	87
5.3	Redshift evolution of the effective optical depth from the segment flux average and pixel flux average for two different flux selections	88
5.4	Comparison of the effective-optical-depth measurements from this work to those found by Bernardi et al. and Faucher-Giguère et al.	89
5.5	Same as Fig. 4.2 with the observed (uncorrected) flux used after degrading the quasar spectra to SDSS resolution	93
5.6	Comparison of the redshift evolution of the effective optical depth measured in this work for different spectral resolutions	94
5.7	Comparison of the effective-optical-depth measurements from this work to measurements from SDSS (low-resolution) data	95
5.8	Comprehensive comparison of measurements of the effective optical depth available in the literature to the measurements presented in this work	97
B.1	Hydrogen absorption features of a selection of absorbers	112
C.1	Mean (observed and model) flux histograms	116
C.2	Mean flux histograms from synthetic spectra	117
C.3	Mean flux histograms from synthetic spectra exhibiting H I Ly α absorption lines with Doppler parameters drawn from a lognormal Doppler-parameter distribution and column densities in the range $12 \leq \log N_{\text{H}_1} \leq 17$ and $12 \leq \log N_{\text{H}_1} \leq 22$	119
C.4	Same as Fig. C.3, but the H I Ly α absorption lines have fixed Doppler parameters	119
C.5	Same as Fig. C.3, but the H I Ly α absorption features have fixed column densities	120

C.6 Same as Fig. C.3, but the H _I Ly α absorption lines have fixed Doppler parameters and fixed column densities	121
D.1 Normalized absorption spectrum of the quasar J004131-493611 and its fit .	124
D.2 Normalized absorption spectrum of the quasar J212912-153841 and its fit .	127
D.3 Normalized absorption spectrum of the quasar J111350-153333 and its fit .	130
D.4 Normalized absorption spectrum of the quasar J010604-254651 and its fit .	132
D.5 Normalized absorption spectrum of the quasar J014214+002324 and its fit .	135
D.6 Normalized absorption spectrum of the quasar J115538+053050 and its fit .	138
D.7 Normalized absorption spectrum of the quasar J123055-113909 and its fit .	140
D.8 Normalized absorption spectrum of the quasar J005758-264314 and its fit .	142
D.9 Normalized absorption spectrum of the quasar J124957-015928 and its fit .	144
D.10 Normalized absorption spectrum of the quasar J162116-004250 and its fit .	147
D.11 Normalized absorption spectrum of the quasar J132029-052335 and its fit .	149
D.12 Normalized absorption spectrum of the quasar J012403+004432 and its fit .	152
D.13 Normalized absorption spectrum of the quasar J111113-080401 and its fit .	155

List of Tables

1.1	Literature investigating the redshift evolution of the effective optical depth	26
2.1	Signal-to-noise ratio of quasar spectra	33
3.1	Fit parameters of the column-density distribution	51
3.2	Values of the Doppler-parameter distribution	53
3.3	Fit parameters of the $b(N)$ distribution	56
3.4	Fit parameters of the number-density evolution	58
4.1	Fit parameters of the redshift evolution of the effective optical depth . . .	66
4.2	Effective-optical-depth values	69
4.3	Fit parameters of the redshift evolution of the effective optical depth from synthetic spectra	76
5.1	Quasar spectra used in various studies	91
B.1	Specific fixed-parameter absorption lines	111
E.1	Freely iterated H I Ly α absorption lines	157

Abbreviations

AGN	Active Galactic Nucleus
AJ	Astronomical Journal
AMD	absolute mean deviation
ApJ	The Astrophysical Journal
ApJS	The Astrophysical Journal Supplement Series
ARA&A	Annual Review of Astronomy and Astrophysics
astro-ph	http://de.arxiv.org/archive/astro-ph (Astrophysics)
A&A	Astronomy and Astrophysics
a.u.	arbitrary units
BAL	broad absorption line
BBN	Big Bang nucleosynthesis
CCD	charge-coupled device
CDM	cold Dark Matter
CMB	Cosmic Microwave Background
DLA	damped Ly α absorber
dof	degrees of freedom
edn.	edition
eds.	editors
ESI	Echellette Spectrograph and Imager (Keck II)
ESO	European Southern Observatory
FIR	far infrared
FWHM	full width at half maximum
GRB	gamma-ray burst
H I	neutral hydrogen
He II	singly ionized helium
HIRES	High Resolution Echelle Spectrometer (Keck I)
HST	Hubble Space Telescope
IAU	International Astronomical Union
IGM	intergalactic medium
ISBN	International Standard Book Number
LLS	Lyman limit system
LUQAS	Large Sample of UVES Quasar Absorption Spectra
Ly α , Ly β , ...	Hydrogen spectral series of transitions involving the ground state
MIKE	The Magellan Inamori Kyocera Echelle spectrograph (Magellan II)
MNRAS	Monthly Notices of the Royal Astronomical Society
Mpc	megaparsec
nol	number of lines

PASA	Publications of the Astronomical Society of Australia
QSO	quasi-stellar object; synonym for quasar
SDSS	Sloan Digital Sky Survey
SDSS-DR	SDSS data release
SMBH	super-massive black hole
SQUAD	The Spectral Quasar Absorption Database
<i>S/N</i>	signal-to-noise ratio
UVB	ultraviolet background
UVES	Ultraviolet-Visual Echelle Spectrograph (VLT)
vol.	volume
VLT	Very Large Telescope
VPFIT	Voigt profile fitting program
WMAP	Wilkinson Microwave Anisotropy Probe

Chapter 1

The H I Ly α opacity

1.1 Introduction

The first quasar was observed half a decade ago in 1960 (see Burbidge 1967). Quasars are point sources similar to stars which gives them the denotation quasi-stellar object (QSO). The observed spectrum of a quasar shows a multitude of broad emission lines. The identification of these emission lines with their rest-frame counterparts and the found redshift led to the indication of the extragalactic origin of a quasar as a ‘nuclear region of a galaxy’ (Schmidt 1963). Since then many quasars have been observed and their redshift determined and ever since they were objects of study.

Gunn and Peterson (1965) derived theoretically that most of the hydrogen in the intergalactic medium (IGM) must be highly ionized, presuming that most of the matter exists in a gaseous phase between galaxies and consists to a large extent of hydrogen. Rees and Sciama (1967) claimed that heavy elements are less abundant in the intergalactic gas than in galaxies. Such elements could be seen in absorption in quasar spectra. Schmidt (1969) mentioned the uncertainty of the origin of the absorption lines seen in quasar spectra¹, as well as of the nature of the quasar redshifts². In the late 1960s, absorption lines in quasar spectra were identified by finding a multitude of absorption lines at the same redshift, possibly from different ions. Such redshifted systems could not account for all absorption lines found in a quasar spectrum. Lynds (1971) asserted that numerous unidentified strong absorption lines shortward of the H I Lyman-alpha emission line³ of a quasar can be accounted for by H I Ly α transitions (see also Oemler and Lynds 1975; Ellis 1978; Young et al. 1979). Sargent et al. (1980) presumed the H I Ly α absorption lines to be of intergalactic origin and assigned them to two distinct populations: H I Ly α clouds, pressure confined by a surrounding IGM, and metal line systems, associated with galactic halos. Weymann et al. (1981) called the numerous single absorption lines with a velocity separation larger than 3000 km s^{-1} from the H I Ly α emission line and shortward

¹Absorption features may be caused by ejecta from the host QSO or by intervening matter along the line of sight to the QSO.

²In order to explain the large observed redshifts of quasars three main hypotheses emerged: The cosmological, the Doppler (considering local explosions) and the gravitational hypothesis (considering QSOs as massive compact objects).

³Throughout this work the electron transitions of atoms or ions from an excited state to the ground state known as the Lyman series will be denoted as Ly α , Ly β , Ly γ , etc., respectively. H I refers to neutral hydrogen, while H II denotes ionized hydrogen. Abbreviations are also used for other chemical elements.

the H I ‘Ly α forest’.

Today the cosmological hypothesis to explain the large observed quasar redshifts is commonly accepted. Quasars reside within galaxies surrounded by the IGM, which mostly consists of hydrogen and helium (see §1.5.2). In the late Universe ($z < 6$) hydrogen is mostly ionized (e.g., Fan et al. 2006), allowing for a study of the small fraction of neutral hydrogen that is seen in absorption in the quasar spectra.

The enrichment of the IGM with metals is a large field of research. In this work, metal absorption is not studied in detail but considered as contamination in the quasar spectra. For the aim of this work it is important to remove the contribution of metals to the absorption features of the H I Ly α forest. The ‘decontaminated’ H I Ly α forest is analyzed to investigate the H I Ly α opacity.

The H I Ly α opacity is visualized through the effective optical depth⁴, τ_{eff} , which is a measure of the mean transmitted flux. The exact definition of this quantity will follow below. Estimates of the effective optical depth can give an insight on the energy input from ionizing sources into the IGM and the detailed contribution from ionizing sources such as quasars and star-forming galaxies. This could in principle lead to the understanding of the ionizing history and the evolution of galaxies and quasars.

In theory, the effective-optical-depth evolution, $\tau_{\text{eff}}(z)$, follows a pure power law. As will be seen later this is a direct outcome of the empirical power-law evolution of the number density of H I Ly α absorbers as inferred from the H I Ly α absorption features imprinted on the observed spectral energy distribution from quasars.

A power-law evolution of τ_{eff} is observed by some works analyzing low-resolution quasar spectra (Dall’Aglio et al. 2009; Becker et al. 2013). In high-resolution studies (Faucher-Giguère et al. 2008b; Dall’Aglio et al. 2008), a deviation from a pure power law is seen at $z \approx 3.2$. This downward feature is quite narrow ($\Delta z \sim 0.3$). The reality of the downward feature in the redshift evolution of the effective optical depth requires further research. In this work, I present the most detailed analysis of $\tau_{\text{eff}}(z \sim 3.2)$ inferred from high-resolution quasar spectra to date contributing to the discussion of the controversy regarding the observation of the τ_{eff} feature.

A possible explanation of the downward feature is based on the reionization of helium. If He II reionization is completed at redshift $z \sim 3.2$, the cosmic ultraviolet background (UVB) may harden for neutral hydrogen. This increases the observed flux at this redshift and, hence, relatively decreases the H I Ly α opacity. A more detailed discussion will follow in the next section.

1.2 The Intergalactic Medium and its Reionization

The matter, which constitutes the IGM that can be observed directly, consists of ions (baryonic nuclei) and atoms (baryon-electron recombinations). Only in very special environments molecules can form (e.g., Richter et al. 2013). Baryons are hadronic sets of quarks and the electron is a typical lepton. Another matter constituent of the Universe

⁴In principle, the effective optical depth can be measured for any atom or ion. Since other chemical elements are not investigated here, the term ‘effective optical depth’ in this work refers exclusively to measurements regarding neutral hydrogen and, in particular, its Ly α transition.

is Dark Matter, which can only be observed indirectly through its gravitational influence. In the literature the preferred cosmological model assumes a flat Universe containing cold Dark Matter (CDM) and Dark Energy (cosmological constant Λ). The flat Λ CDM cosmology (e.g., Hinshaw et al. 2013; and the Planck Collaboration 2013; see also Zhang et al. 1995; Miralda-Escudé et al. 1996; Bi and Davidsen 1997) affects structure formation and the expansion of the Universe. In the following, a qualitative picture of the ionization history of the Universe is given. For a more detailed view on this topic I refer to the literature cited.

The Big Bang model to explain the existence of the Universe is very complex especially at very early times. For simplicity, I skip to a stage in the history of the Universe shortly after the Big Bang, where the Universe has cooled significantly. According to Big Bang nucleosynthesis only light elements could form sufficiently shortly after the Big Bang (see §1.5.2). This mainly means hydrogen and helium. Hydrogen makes up roughly 75% of the total baryonic mass and helium approximately 25%. After decoupling of photons from baryonic matter at redshift $z \sim 1000$, recombination led to a largely neutral Universe (Peebles 1968). These photons can be observed at present as the Cosmic Microwave Background (CMB; e.g., the Planck Collaboration 2013). Assuming that the Big Bang led to a turbulent Early Universe, density fluctuations in the matter content grew with time due to the gravitational force. Since Dark Matter is five times more abundant than baryonic matter (see Hinshaw et al. 2013), it is the driving force in the formation of structure, with baryonic matter following on its trails. Gravitation drives matter into the denser regions and creates adjacent voids. The resulting structure is called the ‘cosmic web’ (Bond et al. 1996; Springel et al. 2005; see Fig. 1.1). Filamentary structures pervade space and the most dense regions are found in intersections of the filaments.

If a sufficient amount of cold gas is present on small scales, it collapses gravitationally and heats up in the center of mass to several 10^6 K allowing for thermonuclear fusion. The released radiation counters the infall of matter and culminates in hydrostatic equilibrium. The first stars are born from metal-free gas and make up a population on their own, Population III stars (e.g., Venkatesan et al. 2003). Radiation pressure drives ambient gas away from the star and high-energy photons ionize the stars’ environments to the extent of the Strömgren sphere (Strömgren 1939). Outside the Strömgren sphere the recombination rate within the gas outbalances the ionization rate due to photons and the energy output from the star is depleted, leaving the gas neutral. It is evident that the ionized volume depends on the density distribution of the gas in the proximity of the star, as well as on the spectral energy distribution and the lifetime of the star. The ionized volume will not be ideally spherical but be shaped by density inhomogeneities (compare Figs. 4 and 5 of McQuinn et al. 2009). The ionization fronts depend on the abundance of the respective chemical element and its ionization cross section, as well as on the luminosity of the ionizing source. The ionization front of He II is expected to be thicker than for hydrogen due to the lower helium abundance and the lower cross section of He II (Miralda-Escudé 1998).

Any source of radiation will ionize hydrogen and helium in its environment if the source produces photons above the ionization potential of hydrogen ($E_{\text{LL}}^{\text{H}\,\text{I}} \simeq 13.6$ eV, $\lambda_{\text{r},\text{LL}}^{\text{H}\,\text{I}} \simeq 912$ Å) and helium ($E_{\text{LL}}^{\text{He}\,\text{I}} \simeq 24.6$ eV, $\lambda_{\text{r},\text{LL}}^{\text{He}\,\text{I}} \simeq 504$ Å; $E_{\text{LL}}^{\text{He}\,\text{II}} \simeq 54.4$ eV, $\lambda_{\text{r},\text{LL}}^{\text{He}\,\text{II}} \simeq 228$ Å). The formation of such sources within hierarchical structure formation processes marks the advent of the reionization of the Universe (Arons and Wingert 1972; Madau et al.

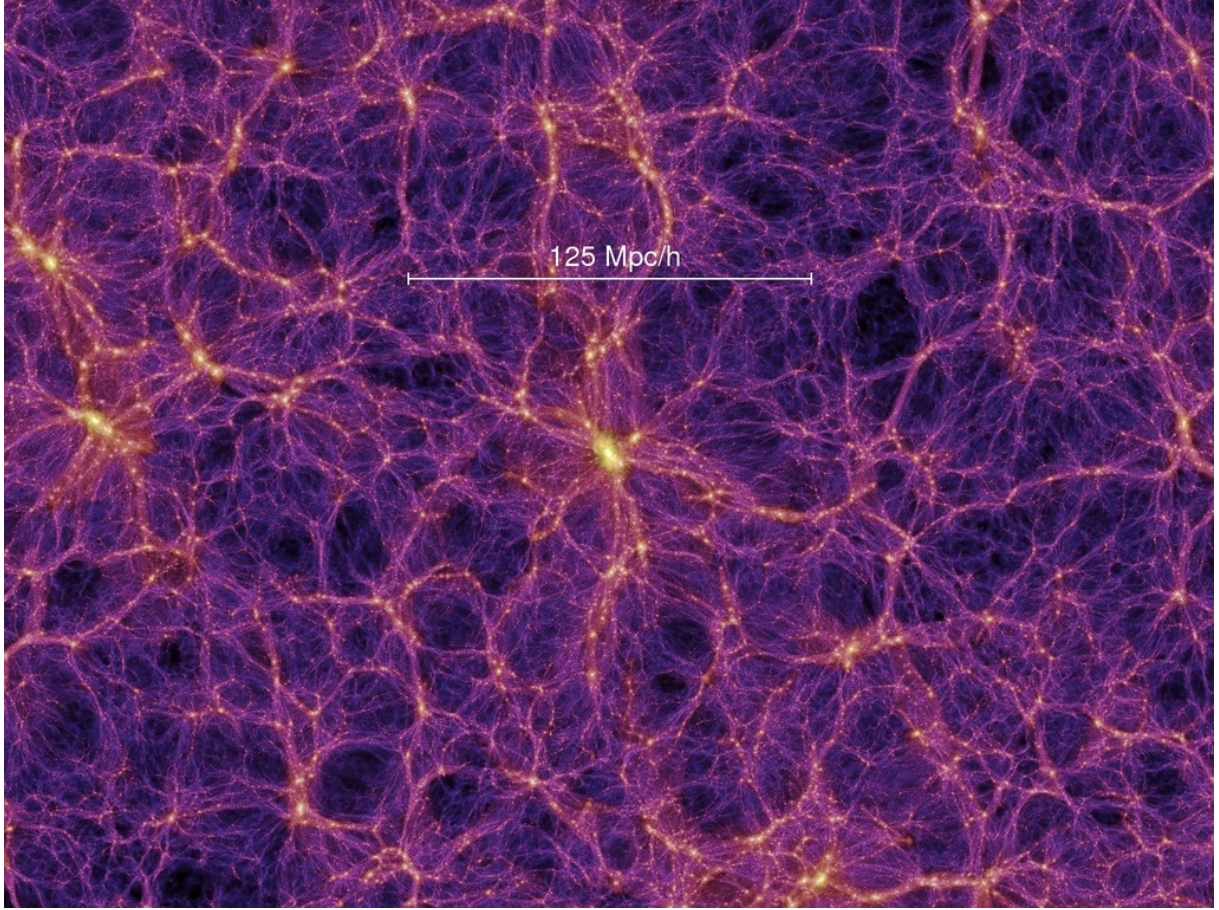


Figure 1.1. Dark Matter density field at redshift $z = 0$, colour-coded by density and local Dark Matter velocity dispersion (Millennium Simulation Project; Springel et al. 2005).

1999; Miralda-Escudé et al. 2000; Gnedin 2000; Hui and Haiman 2003; Furlanetto and Oh 2008a; McQuinn et al. 2009; Furlanetto 2009; Compostella et al. 2013). The higher ionization threshold of He II and the larger He II recombination coefficient compared to that of hydrogen (Miralda-Escudé and Rees 1994) favor a delay of full reionization of helium compared to that of hydrogen. The CMB may give insights on the initial epoch of hydrogen reionization since free electrons will interact with the CMB photons through Thomson scattering (Haiman and Knox 1999). Shaver et al. (1999b) suggest that H I reionization could leave sharp features in the cosmic background due to redshifted H I 21 cm line emission (radio) and hydrogen recombination radiation (optical/near-IR). According to Syunyaev (1968) the Universe was neutral at least until redshift $z \sim 300$.

In the neutral Universe numerous Population III stars will form. Though they can in principle be found throughout the entire space, the largest probability for a star to form is in filaments and especially in knots. Stellar formation and hierarchical structure formation will eventually provide a plethora of ionizing sources: stars, star clusters, protogalaxies (Gnedin 2000), minigalaxies (Haiman and Knox 1999), galaxies (Benson et al. 2002), protouniquasars, miniquasars (Madau et al. 2004), and quasars or other active galactic nuclei (AGNs; Barthel 1989). Due to stellar nucleosynthesis, which produces elements as heavy as iron, and supernova nucleosynthesis a (post-)stellar environment will be enriched with heavier elements than hydrogen and helium (e.g., Cen and Bryan 2001, see also Ricotti

et al. 2002), so that the new generation of stars will contain heavy elements at birth.

Stars produce far less ionizing photons compared to quasars, even if these stars are taken into account collectively as found in galaxies. If galaxies harbour a super-massive black hole (SMBH) in their center and if this SMBH is fed with infalling material (e.g., Salpeter 1964) it becomes an AGN. The lifetime of a quasar depends on the amount of material available. The radiation pressure from the quasar will counteract the accretion ('feedback'; Hopkins et al. 2006) and hence, limit the lifetime additionally. Since a sufficient amount of infalling material will be available in the most dense regions of the Universe, quasars are possibly more rare than their stellar hosts.

Assuming that the quasar ionizes its proximity to a larger spatial extent than its host galaxy is capable of, the outer regions will start to recombine after the shutdown of the quasar. Though, the outer regions may be reionized again, if the quasar is powered another time by anew infalling gas, e.g., through major merger events (Hopkins et al. 2006), or if the reionized region is consumed by the Strömgren spheres of external sources (Compostella et al. 2013). Hence, source lifetimes may play a role in the overall evolution of the reionization process (Sokasian et al. 2002). Merger events of galaxies will probably alter the ionization state of the surrounding gas. The stellar populations undergo turbulent motion which could spread out the stars spatially, leading to more diffuse ionizing radiation and allowing the surrounding gas to recombine more efficiently; or turbulent gas motion could trigger additional star formation, although this is more likely to occur once the merging is complete since the surrounding gas will fall back onto the deeper potential well.

Ionizing sources form in the densest regions of the Universe. Hence, the sources have to reionize their surrounding environment first, before the radiation can escape into regions of lower gas density (Sokasian et al. 2002). If the production of ionizing photons is not sufficient enough, the source will only surround itself with an ionized bubble of gas, but not be capable of contributing to full reionization (Ricotti et al. 2002). Such dense regions, including those which do not harbour ionizing sources at all, have to be reionized by external sources. On the importance of local sources of radiation in the intervening absorbing gas towards bright background sources see Miralda-Escudé (2005) and Schaye (2006).

Reionization will be complete if regions, occupied by the same ionized species, overlap and fill the entire space (Miralda-Escudé and Rees 1994). Hence, the Universe becomes transparent to the respective ionizing photons. The overlap depends on the number of ionizing sources, their spatial distribution and lifetimes, and the spatial extent of their ionized environment, which in turn depends on the emissivity of the source and the gas density distribution. The larger the Strömgren spheres, the less numerous the sources can be to still complete reionization. Figure 1.2 shows the redshift evolution of important species fractions and the IGM temperature during reionization.

Photons produced by a background source are scattered by intervening material along the line of sight. Hence, a spectrum of an extragalactic source will show absorption features due to intergalactic hydrogen and helium. If metals are present along the sightline, these will produce additional absorption features in a spectrum. The continuous suppression of flux in a spectrum is known as the Gunn-Peterson trough (Gunn and Peterson 1965).

Neutral hydrogen is seen in absorption in the spectra of quasars (e.g., Lynds 1971). Evi-

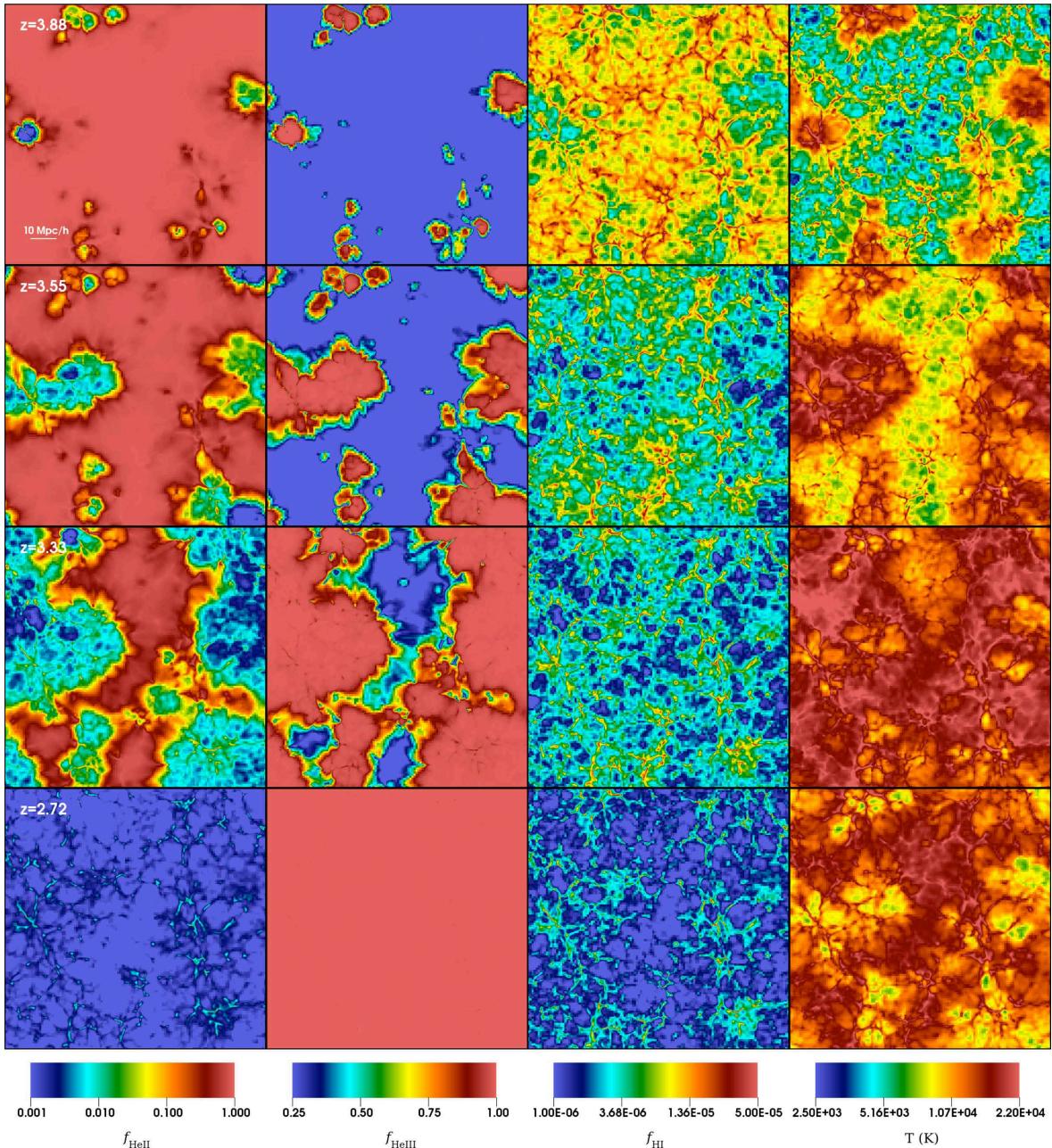


Figure 1.2. Redshift evolution of the fractional abundance, f , of He II, He III, and H I, and the IGM temperature, T , during inhomogeneous He II reionization (taken from Compostella et al. 2013).

dently, the hydrogen content of the Universe must be largely reionized by redshift $z \approx 6$ since the H I Gunn-Peterson trough of H I Ly α at rest-frame wavelength $\lambda_{r,\text{Ly}\alpha}^{\text{H}\,\text{I}} \simeq 1216 \text{ \AA}$ is absent in quasar spectra below this redshift value, but can be observed in spectra taken from quasars with higher emission redshift (e.g., Fan et al. 2006). Possibly, helium is singly ionized approximately at the same time as hydrogen since its ionization potential is not much higher. Though single He I absorption could be detected (Reimers et al. 1992), observations of the He I Gunn-Peterson trough ($\lambda_{r,\text{Ly}\alpha}^{\text{He}\,\text{I}} \simeq 584 \text{ \AA}$) were unsuccessful (Beaver et al. 1991; Reimers and Vogel 1993; Reimers et al. 1997). He II Ly α Gunn-Peterson absorption ($\lambda_{r,\text{Ly}\alpha}^{\text{He}\,\text{II}} \simeq 304 \text{ \AA}$) was first observed by Jakobsen et al. 1994 at $3.1 < z < 3.3$ in the quasar spectrum of Q0302-003 ($z_{\text{em}} \simeq 3.286$; Jakobsen et al. 1994; Hogan et al. 1997; Heap et al. 2000; Jakobsen et al. 2003; Syphers and Shull 2014).

Detection of He II in absorption is difficult due to H I absorption at lower redshifts, especially due to H I Lyman limit systems (LLSs) which suppress the flux completely below $\lambda_r \simeq 912 \text{ \AA}$, the eponymous Lyman limit or ionization threshold (also referred to as the Lyman edge, Jakobsen et al. 1994). The flux suppression is unavoidable at least locally due to neutral hydrogen in the interstellar medium of the Milky Way (Davidson et al. 1996), limiting detections of He II absorption to $z > 2$.

Few other sightlines have been discovered to feature He II absorption: HS1700+64 ($z_{\text{em}} \simeq 2.72$; Davidson et al. 1996; Fechner et al. 2006), HE2347-4342 ($z_{\text{em}} \simeq 2.885$; Reimers et al. 1997; Kriss et al. 2001; Smette et al. 2002; Shull et al. 2004; Zheng et al. 2004b; Shull et al. 2010), PKS1935-692 ($z_{\text{em}} \simeq 3.18$; Anderson et al. 1999), and Q1157+3143 ($z_{\text{em}} \simeq 3$; Reimers et al. 2005). Though, the comprehensive study of other objects started recently (e.g., Zheng et al. 2004a, 2008; Syphers et al. 2009a,b, 2011a, 2012; Worseck et al. 2011). Despite the successful observations of neutral hydrogen and helium in quasar spectra and more importantly the lack of it at certain redshifts, the question on the dominating ionizing sources responsible for reionization is difficult to answer (see e.g., Meiksin 2005). Possibly, the reionization of hydrogen was completed at $z = 6$ by galaxies (softer UVB, Faucher-Giguère et al. 2009), perhaps close to the peak in the cosmic star-formation rate (Hernquist and Springel 2003; Faucher-Giguère et al. 2008a). If star formation in the host galaxies and activity of the galactic nucleus are correlated (Franceschini et al. 1999), this may be difficult to reconcile since the quasar space density is observed to decline above $z \sim 2.5$ (Shaver et al. 1999a; Fan et al. 2001; Richards et al. 2006; Hopkins et al. 2007; Brusa et al. 2009). Though, in turn, the peak in the quasar space density between $2 < z < 3$ may be in concordance with the potential end of helium reionization at $z \lesssim 3$ due to a significant contribution to the UVB from quasars (e.g., Agafonova et al. 2005, 2007; Gleser et al. 2005; Bolton et al. 2006; Paschos et al. 2007; Faucher-Giguère et al. 2008a; Furlanetto and Oh 2008b; Bolton et al. 2012). As mentioned above, the ability to reionize the Universe depends on the spectral energy distribution of the ionizing sources, especially at 1 and 4 Ryd. Measurements of the metagalactic ionizing flux hint on the sources of reionization and its epoch. Besides the condensed sources of ionizing photons, reprocessing of ionizing radiation by the IGM (Haardt and Madau 1996) has to be taken into account.

A change in the ionizing spectrum at $z \approx 3$ was suggested by Songaila and Cowie (1996) and Songaila (1998) due to rapid evolution in the column-density ratio $N(\text{Si IV})/N(\text{C IV})$ at this redshift. The change in the metagalactic UVB at $z \simeq 3$ could be attributed to the end epoch of He II reionization. The column-density ratio of the ions mentioned above

may be a sensitive probe of the UVB since the ionization potentials ($E_{\text{LL}}^{\text{Si IV}} = 45.1 \text{ eV}$, $E_{\text{LL}}^{\text{C IV}} = 64.5 \text{ eV}$) are comparable to that of He II. Though, Kim et al. (2002b) challenge the significance of $N(\text{Si IV})/N(\text{C IV})$ as a probe of He II reionization and find no sharp change in $N(\text{Si IV})/N(\text{C IV})$ in the redshift range $1.6 < z < 3.6$. No evolution was found in this column-density ratio by Boksenberg et al. (1998, supplemented by Boksenberg et al. 2003) across $z \sim 2.2 - 3.8$ and in the median pixel-optical-depth ratio $\tau(\text{Si IV})/\tau(\text{C IV})$ studied by Aguirre et al. (2004) at $1.5 \lesssim z \lesssim 4.5$. A combination of column-density ratios (Boksenberg et al. 1998) or other metals (e.g., Vladilo et al. 2003) might be good tracers of the ionization evolution.

The reionization history impacts on the thermal history of the IGM (e.g., Miralda-Escudé and Rees 1994; Haehnelt and Steinmetz 1998; Tittley and Meiksin 2007; see also Theuns et al. 2002b; Meiksin et al. 2010). The temperature in the IGM increases following reionization. The increase in temperature is significantly affected by radiative transfer effects (Abel and Haehnelt 1999), which affect the UVB (Maselli and Ferrara 2005). Such an increase of the temperature was found by Schaye et al. (2000) at $z \sim 3$ (see also Ricotti et al. 2000; Lidz et al. 2010), but not by McDonald et al. (2001) and Zaldarriaga et al. (2001). Post-reionization, the temperature should decline due to cooling by expansion of the Universe (Theuns et al. 2002b; Hui and Haiman 2003), although slower than expected by pure adiabatic expansion due to continuing photoheating of the gas (Theuns et al. 2002c). The expansion of the Universe also effects the H I Ly α opacity, in that it decreases the effective optical depth (Theuns et al. 2002a). If He II reionization leads to a sudden jump in the temperature, this may lead to a sudden decrease in the effective optical depth (τ_{eff} , see §1.5) since this quantity depends on the hydrogen recombination coefficient, which is temperature dependent (see, e.g., Eqs. 1.53 and 1.35). A higher temperature reduces the number of recombinations and, hence, increases the observed flux. Performing hydrodynamical simulations, a sharp feature in $\tau_{\text{eff}}(z)$ was predicted by Theuns et al. (2002a) corresponding to a sudden temperature jump. Such a sharp feature in $\tau_{\text{eff}}(z)$ was found by Bernardi et al. (2003) studying Sloan Digital Sky Survey (SDSS) quasar spectra. Bolton et al. (2009b) challenge the findings of Theuns et al. (2002a) and show by performing hydrodynamical simulations that rapid reheating of the IGM during He II reionization is unlikely to lead to a confined feature in the effective-optical-depth evolution. Rather, a sudden drop in $\tau_{\text{eff}}(z)$ will be followed by a slow recovery of this quantity. Bolton et al. (2009a) even suggest ‘a more gradual, moderate temperature boost’ in the first place from their study of quasar photoheating of the IGM during He II reionization through analytical arguments and numerical radiative transfer models. Furlanetto and Oh (2008a) argue that the inferred temperature evolution from measurements depends on the used method. Recent temperature measurements show a rise in the temperature at the mean density (see, e.g., Hui and Gnedin 1997 for a mathematical framework) from redshift $z \simeq 4.4$ to $z \simeq 2.8$ (Becker et al. 2011), which implies an extended period of heat injection in the IGM. The rise in temperature is most likely due to photoheating during helium reionization. At lower redshifts (Boera et al. 2014), heating of the (low-density) IGM by extragalactic very-high-energy gamma rays as emitted by TeV blazars (AGNs) may become important (e.g., Chang et al. 2012; Puchwein et al. 2012).

Given the various studies on helium reionization, this phase transition of the Universe may be completed (though see Davies and Furlanetto 2014) somewhat between $z \approx 2.7$ (Dixon and Furlanetto 2009; Worseck et al. 2011) and $z \approx 3.4$ (Lidz et al. 2010), perhaps

beginning at $z \gtrsim 4.4$ (Becker et al. 2011). The redshift at which helium is completely reionized may be determined more precisely by other observational techniques, such as observations of the He II Ly β optical depth (e.g., Syphers et al. 2011b).

The detection of He II supports the standard Big Bang model (Hogan et al. 1997; Jakobsen et al. 2003) and allows for the observation of the foreground proximity effect (Heap et al. 2000; Jakobsen et al. 2003; Worseck and Wisotzki 2006; Worseck et al. 2007; Syphers and Shull 2014).

An investigation of the H I optical depth, such as presented in this thesis, provides important information on the physical conditions in the IGM during an important epoch in the Universe.

If a narrow feature in $\tau_{\text{eff}}(z)$ is present, it is likely produced by other means but the temperature evolution during extended He II reionization (McQuinn et al. 2009; see also Compostella et al. 2013), e.g., by a rapid change in the hydrogen photoionization rate (Bolton et al. 2009a) due to ionizing-radiation reprocessing in the IGM or opacity changes of H I LLSs (Bolton et al. 2009b).

1.3 Investigating the redshift evolution of τ_{eff}

1.3.1 Instruments

In the following, a rough outline on instrumental possibilities, which are used to investigate the effective optical depth, and their limitations is given. Photons are detected by telescopes. These instruments can be divided into two classes, namely space-based and earth-bound telescopes. Space-based telescopes do not have to deal with the difficulties arising from light passing through the Earth's atmosphere. Therefore, they are able to detect even ultraviolet photons which are otherwise absorbed by the atmosphere. Though, the installation in space may restrict the set-up of a telescope with respect to the transport (e.g., weight) and funding (e.g., repairs, external orbit adjustments due to a particle-driven decrease in altitude). Technically, observations with the Hubble Space Telescope (HST) often have a lower signal-to-noise ratio (S/N) and lower resolution compared to optical spectra taken from the ground. Earth-bound telescopes have to account for scintillation and the atmospheric absorption. Observation windows extent in rest-frame wavelength λ_r roughly across $3000 \text{ \AA} < \lambda_r < 30 \mu\text{m}$ (two orders of magnitude, covering near-ultraviolet, visible, and infrared light, though spectral gaps are present and far-infrared photons⁵ cannot be detected) and $1 \text{ cm} < \lambda_r < 15 \text{ m}$ (within the radio band).

The most common element in the Universe is hydrogen (see §1.5.2). Its intergalactic occurrence manifests itself by interaction with photons. The presence of neutral hydrogen is observable in absorption against extragalactic background sources (see §1.3.2). The lowest excitation energy is provided by H I Ly α photons with $\lambda_r \simeq 1215.67 \text{ \AA}$. Due to the expansion of the Universe, as studied by, e.g., Knut Lundmark, Georges Lemaître, and Edwin Hubble (Steer 2012), emitted photons with wavelength λ_r become redshifted and are detected at higher wavelengths

$$\lambda_{\text{obs}} = \lambda_r \cdot (1 + z), \quad (1.1)$$

⁵The far-infrared (FIR) spectrum is defined from $\lambda_r \simeq 30 \mu\text{m}$ up to $\lambda_r \simeq 1 \text{ mm}$ and followed by radio wavelengths (including microwaves over $1 \text{ mm} \lesssim \lambda_r \lesssim 1 \text{ m}$).

where z means the redshift. In this context, the proper distance⁶ between two objects in the Universe is found by integrating the inverse Hubble parameter, $H(z)$, over redshift (e.g., Davis and Lineweaver 2004),

$$L = \frac{1}{R_0} \cdot \frac{c}{1+z} \int_{z_{\text{em}}}^z \frac{dz'}{H(z')}.$$
 (1.2)

Herein, the proper distance, L , depends on the observed redshift, z , and on the redshift of emission, z_{em} , as well as the present-day scale factor, $R_0 = 1$; c is the speed of light in vacuum. The redshift, z , is related to the scale factor, $R(t)$, by

$$R(t) = (1+z)^{-1}$$
 (1.3)

(e.g., Sandage 1961), so that $R_0 = R(t=0)|_{z=0} = 1$. The larger the redshift separation between two objects, the larger their separation in proper distance and the larger the look-back time due to the finite speed of light. Equation (1.2) will be essential for the analysis in this work.

The visual regime of the electromagnetic spectrum is about $4000 \text{ \AA} < \lambda_{\text{obs}} < 7000 \text{ \AA}$. The redshift range for investigating extragalactic neutral hydrogen in Ly α ($\lambda_r \simeq 1215.67 \text{ \AA}$) with earth-bound telescopes from the visual regime using Eq. (1.1) is therefore $2.3 < z < 4.8$. As mentioned above, the observation window due to atmospheric absorption demands the use of space-based telescopes for low-redshift studies at $z < 1.5$ ($\lambda_{\text{obs}} < 3000 \text{ \AA}$). The upper redshift limit for studying extragalactic hydrogen is redshift $z \approx 6$ (e.g., Fan et al. 2006).

1.3.2 Background sources

To study the IGM in absorption spectra, background sources are required. Sufficiently bright sources are quasars (e.g., Burbidge 1967) which make up a class of active galactic nuclei (AGNs; see, e.g., Barthel 1989; Kazanas et al. 2012) and are observed as point sources featuring a broad spectral energy density distribution. Historically, quasars are the most common extragalactic objects used to study the IGM. The quasar emission redshifts range from $z \simeq 0.158$ (Schmidt 1963) to beyond redshift $z = 6$ (Fan et al. 2006). The quasar with the highest emission redshift known to date is ULAS J112001+064124 with $z_{\text{em}} > 7$ (e.g., Momjian et al. 2014).

Galaxies with a high star-formation rate host many young stars, which in principle emit hard photons to interact considerably with the IGM through radiative transfer. The spectrum of a galaxy is the superposition of the light emitted by any star residing in the galaxy. A galactic spectrum shows absorption lines from matter intrinsic to the galaxy. These are difficult to distinguish from absorption lines from intervening matter along the line of sight to the galaxy. The spectra of gamma-ray bursts (GRBs; e.g., Woosley and

⁶Conceptionally many different distance measures can be defined, though they are possibly convertible into each other (depending on the nature of the distances and the underlying space-time). An intuitive definition is the comoving distance, which implies a constant distance between two objects that are affected only by the expansion of the Universe. The proper distance, as measured by using a universal scale, is found by scaling the comoving distance with a time dependent quantity, the scale factor.

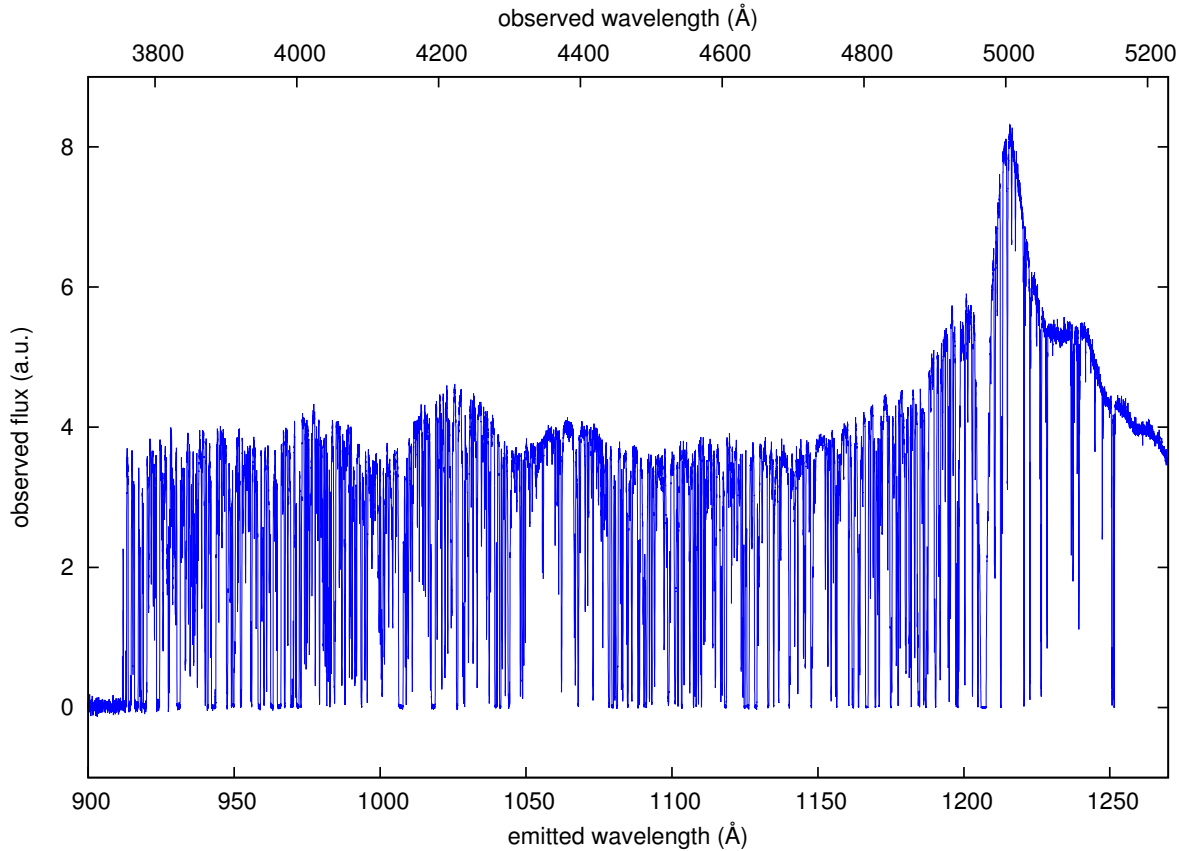


Figure 1.3. Absorption spectrum of the quasar Q0420-388 with an emission redshift of $z_{\text{em}} \simeq 3.118$.

Bloom 2006) can in principle also be used to study the intergalactic medium (Miralda-Escudé 1998).

This work is based on high-quality quasar spectra to study the absorption behaviour of intergalactic neutral hydrogen. Due to the expansion of the Universe quasars can be used as background sources to study intervening material along the observed sightline. The emitted photons from the quasar are redshifted and absorbed by the intergalactic gas at various redshifts. Therefore, the H I Ly α forest is observed in quasar spectra blueward of the H I Ly α emission line of the quasar.

1.3.3 Quasar spectra

Figure 1.3 shows an absorption spectrum of a quasar at redshift $z_{\text{em}} \simeq 3.118$ obtained with the Ultraviolet and Visual Echelle Spectrograph (UVES, Dekker et al. 2000) at the Very Large Telescope (VLT) at Cerro Paranal in northern Chile.

The emitted wavelength axis, or rest-frame wavelength, λ_r , is shown with regard to the emission features of the quasar spectrum. Prominent emission lines can be identified with H I Ly α at $\lambda_r \approx 1216$ Å, H I Ly β at $\lambda_r \approx 1026$ Å and the N V doublet at $\lambda_r \approx (1239, 1243)$ Å. Emission features may vary in strength and width from quasar to quasar. Another significant feature in this spectrum is the depletion of the spectral energy density at $\lambda_r \approx 912$ Å. Continuous absorption occurs due to the ionization of hydrogen. In the shown example, continuous absorption due to the damped Ly α absorber (DLA)

close to the quasar depletes the emitted flux already before the observation threshold ($\lambda_{\text{obs}} = 3000 \text{ \AA}$).

The detailed shape of a quasar's spectral energy density as a function of wavelength is unknown due to the numerous absorption features in the spectrum. As a first approximation the continuous radiation is assumed to display a smooth function of wavelength. The continuum is usually estimated from the transmission peaks seen in the quasar spectrum. This procedure is less successful if the quality of the spectrum is insufficient. Low resolution biases the continuum estimate towards lower values, and a low S/N adds uncertainties to the transmission peaks. The number of absorption features decreases with decreasing redshift due to structure formation and the expansion of the Universe, which drives matter apart that is not gravitationally bound. At redshift $z \gtrsim 4$ cumulative absorption becomes significant.

The knowledge of the continuum is crucial in order to remove features intrinsic to the quasar. This assures the statistical significance of an analysis of the absorption features and the inferred neutral hydrogen fraction of the IGM.

High-resolution, high S/N quasar spectra make it possible to estimate the continua locally. At high redshift continuum corrections may be considered to account for cumulative absorption. For low-quality spectra continua are usually extrapolated from an apparent power law redward of the H I Ly α emission line. In the process, overlying emission lines have to be accounted for. This region of the spectrum is almost free from absorption features, except for metal transitions at redshifts lower than the H I Ly α emission line, but with higher rest-frame wavelength. Typical candidates are C IV, Fe II, Mg II, and Si IV.

As mentioned above, the H I Ly α forest is built up of numerous H I Ly α absorption features, at shorter wavelengths superposed with higher order H I Lyman series absorption features. The absorption features at different redshifts vary in strength and line profiles. DLAs are believed to be associated with galaxies, though these are possibly not luminous enough to be observed as counterparts to the absorption features. Especially dense absorbers exhibit various metal absorption lines. These will remove additional flux in a quasar spectrum and have to be disentangled from the H I Ly α forest for an analysis of hydrogen absorption such as presented in this work. The effect of metals on the flux measurements will be discussed with respect to the effective optical depth in Chapter 4.

As mentioned above, the absorption-line density in the H I Ly α forest decreases with decreasing redshift due to the expansion of the Universe. This is illustrated in Fig. 1.4 by several quasar spectra with different emission redshifts. An increase in emission redshift leads to a spectrum dominated by more numerous and saturated absorption lines. The continuum becomes more difficult to estimate and especially at redshifts $z > 4$ the continuum fit becomes problematic (McDonald et al. 2000) due to the uncertainty of the amount of absorption.

1.4 Historical remarks

The study of absorption lines in spectra is about 200 years old and began with the observation of refracted light emitted by the Sun. The technological advances in photography in the 19th century led to further progress in astrophysics. It was possible to obtain images of celestial objects and also to record stellar spectra on photographic plates. In

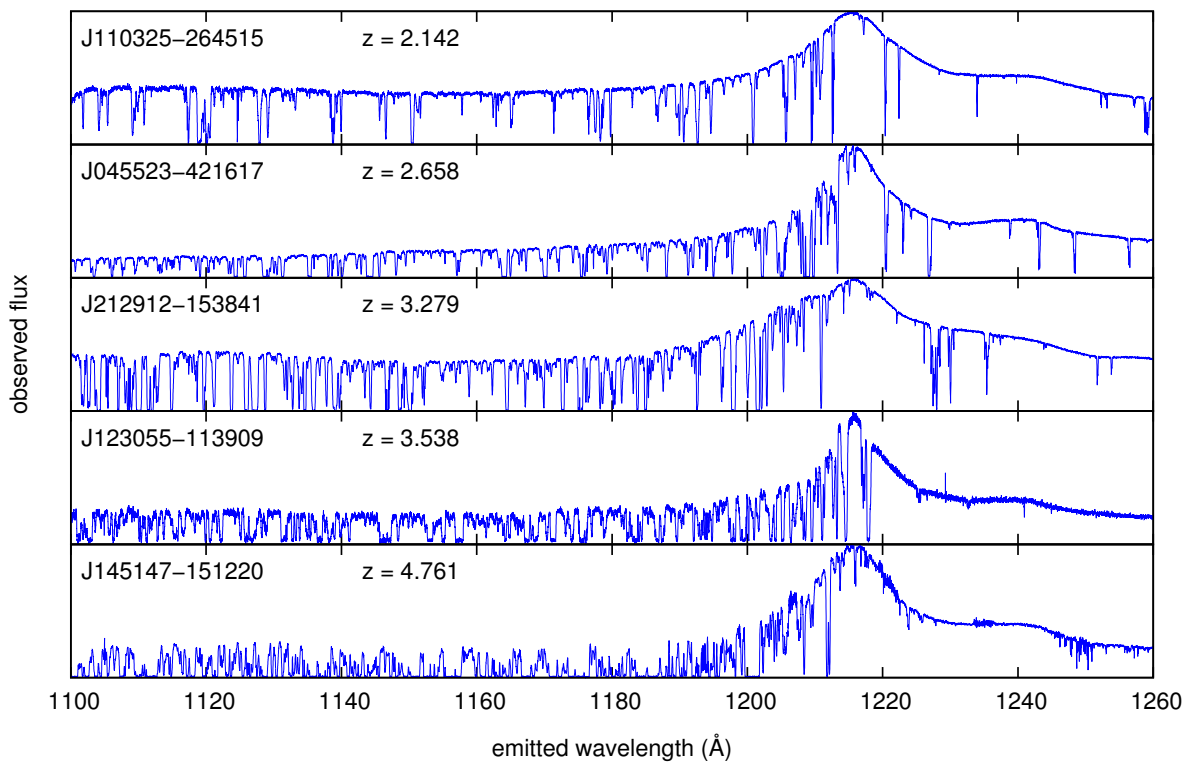


Figure 1.4. Quasar absorption spectra shown in the quasars' rest frame. The redshift, z , at which each quasar is observed is labelled in each panel and increases from top to bottom. The spectra are taken from the Spectral Quasar Absorption Database (see §2; names are given in the respective panels). The continuum emission becomes increasingly difficult to determine with higher emission redshift.

the late 19th and early 20th century stellar spectra were studied extensively, which led to the classification scheme of stars based on spectral characteristics.

For a recorded spectrum of a quasar on a photographic plate see Figs. 1 of Lynds (1971) and Oemler and Lynds (1975). The latter show also the intensity over wavelength display of the corresponding spectrogram.

The intensity-wavelength display became much easier with the advent of charge-coupled devices (CCDs) in the 1980s and made it convenient to apply a profile-function analysis to the absorption features seen in quasar spectra. Several supporting computer programs have been developed, such as AUTOVP (Davé et al. 1997), VPFIT⁷ (Carswell et al. 1987), and CANDALF⁸. Line identification, line blending, spectral noise, and the uncertainty of the continuum level are difficulties which are inevitable in this kind of analysis (Machacek et al. 2000; Oemler and Lynds 1975), especially at higher redshift.

The higher the resolution is, the more detailed the absorption features appear. Low resolution smoothes the absorption features. Hence, a line profile is only an approximation to a rather complex absorption structure from intergalactic gaseous clumps or density fluctuations. This natural complexity may give rise to the problems of line blending. Addition-

⁷<http://www.ast.cam.ac.uk/~rfc/vpf.fit.html>

⁸Written by Robert Baade.

ally, noise and the continuum uncertainty make it difficult to determine absorption-line equivalent widths (e.g., Oemler and Lynds 1975) and absorption-line profiles.

1.5 Observed quantities

Rather than consisting of clouds (Sargent et al. 1980), the canonical picture of the IGM today assumes that it is structured by density fluctuations of gas in cosmological structures (Bi and Davidsen 1997), which absorb photons. The fraction, f_ν , of the quasar continuum flux, $f_{\nu,\text{cont}}$, being observed in transmission, $f_{\nu,\text{obs}}$, depends on the optical depth, τ , of the intergalactic gas,

$$f_\nu(\tau) = \frac{f_{\nu,\text{obs}}}{f_{\nu,\text{cont}}} = e^{-\tau}. \quad (1.4)$$

Two methods can be applied in order to reveal the structure of the intergalactic gas and, thus, the structure of the Universe. The evolution of the H I Ly α opacity with redshift can be determined from quasar spectra directly. But direct flux statistics suffer from the contamination of the H I Ly α forest with metals. The second approach is the analysis of absorption lines. Research can concern the redshift evolution of the number density of absorption lines (e.g., Peterson 1978) or column densities. Column densities can be computed from equivalent widths using the curve of growth estimates (Young et al. 1979) or determined by fitting absorption-line profiles to absorption features. The latter is performed easier on high-resolution data. In addition, absorption-line profiles give an insight into the thermal conditions of an absorber, taking into account the process of thermal line broadening. Both methods depend on the adopted quasar continuum level.

The simplest quantity to study from quasar spectra is the flux, f_ν , or, equivalently from Eq. (1.4), the optical depth, τ . Statistics using the optical depth or the transmitted flux are the mean opacity (Press et al. 1993), the cumulative H I opacity (Cen 1997; Machacek et al. 2000; Bi and Davidsen 1997), the optical depth probability distribution function (Machacek et al. 2000; Kim et al. 2001), the flux probability distribution (Jenkins and Ostriker 1991; McDonald et al. 2000; Machacek et al. 2000; Kim et al. 2001; Calura et al. 2012), and the computation of high-redshift colors of galaxies and quasars (Songaila 2004). Zuo (1993) introduced the effective optical depth, τ_{eff} , according to

$$e^{-\tau_{\text{eff}}} \equiv \langle e^{-\tau} \rangle = \langle f_\nu \rangle, \quad (1.5)$$

the mean (transmitted) flux⁹.

Comparing observations of τ_{eff} to their numerical simulation, McDonald et al. (2000) find a ‘remarkable’ agreement of the predicted flux distribution in the simulation with the observed distribution, supporting the H I Ly α forest theory based on gravitational evolution of primordial fluctuations. This result shows the importance of simulations and the required agreement with any quantity studied through observations.

1.5.1 The effective optical depth

There are different methods to measure τ_{eff} , depending on the quality and quantity of available spectra.

⁹Throughout this work, a quantity enclosed in angled braces means the arithmetic mean of this quantity.

Oke and Korycansky (1982) define the parameter

$$D = \left\langle 1 - \frac{f_{\nu,\text{obs}}}{f_{\nu,\text{cont}}} \right\rangle, \quad (1.6)$$

called flux decrement, where $D = D_A$ is measured from data ‘between emission [H I] Ly α and [H I] Ly β + O VI’ and $D = D_B$ is measured ‘between emission [H I] Ly β and the emission [H I] Lyman limit’. With D_B being larger than D_A , they have confirmed that the majority of absorption lines shortward of the H I Ly α emission line can be attributed to H I Ly α absorption at different absorption redshifts, as it was first suggested by Lynds (1971) due to his study of the quasar 4C05.034. Peterson (1978) has proposed to confirm H I Ly α absorption if the corresponding H I Ly β is studied. These three studies use quasar spectra from objects at redshift $z \sim 3$ and the spectrum studied by Lynds (1971) is also included in the studies by Peterson (1978) and Oke and Korycansky (1982) as object 0805+046.

Other D_A measurements at high redshift are conducted by, e.g., Steidel and Sargent (1987) and Schneider et al. (1989a,b). The latter find an increase of D_A with redshift among all the data mentioned above, together with the low redshift study from Bechtold et al. (1984) within the redshift range $1 < z < 5$ (see Fig. 6 of Schneider et al. 1989b). An analysis with revised and extended data is presented in Schneider et al. (1991, their Fig. 9) with the same trend of $D_A(z)$ over the redshift range $0 < z < 5$ (see also O’Brien et al. 1988) and is in agreement with Giallongo and Cristiani (1990) at $z \sim 3.2$.

Since for an observable x

$$\forall C \in \mathbb{R} : C \pm \langle x_i \rangle = \langle C \pm x_i \rangle \quad (1.7)$$

(see Appendix A.1 for a derivation), the flux decrement, D , and the average flux, f_ν , as defined above or the effective optical depth can be connected by

$$D = \left\langle 1 - \frac{f_{\nu,\text{obs}}}{f_{\nu,\text{cont}}} \right\rangle = 1 - \langle f_\nu \rangle = 1 - e^{-\tau_{\text{eff}}} \approx \tau_{\text{eff}}. \quad (1.8)$$

The last step is only valid if $\tau_{\text{eff}} \ll 1$. Hence, the trend of the flux decrement with redshift implies an evolution of the mean transmitted flux. The mean transmitted flux decreases with redshift. This trend can also be seen from the composite spectra for different redshift bins from a total of over 1000 SDSS quasar spectra with $2.75 \lesssim z_{\text{em}} \lesssim 4.3$ from Bernardi et al. (2003, Figs. 3 and 14). Songaila and Cowie (2002, their Fig. 3) show that the decrease continues for redshifts $4 < z < 6$. At redshift $z \sim 6$ the mean transmitted flux is found to be less than $f_\nu < 0.1$ (Becker et al. 2001).

The advantage of D_A measurements becomes clear with the following argument. The average of N independent measurements Q_i is $\langle Q_i \rangle = N^{-1} \sum_{i=1}^N Q_i$. If the total data set is split into m bins, each containing the same number $n = N/m$ of measurements, the average of the Q_i in the k th bin is

$$\langle Q_i \rangle_k = \frac{1}{n} \sum_{i=1+(k-1)\cdot n}^{n+(k-1)\cdot n} Q_i = \frac{1}{n} \sum_{i=1-n+k\cdot n}^{k\cdot n} Q_i. \quad (1.9)$$

In Eq. (1.9), the index i has to cover the Q_i enclosed in the k th bin. This is accomplished by shifting the index by $(k - 1) \cdot n$, where the factor $(k - 1)$ allows an initial value $k = 1$ for the index k , equivalent to the first bin. Since $\langle Q_i \rangle_k$ is the average of the Q_i in the k th bin, the average of the $\langle Q_i \rangle_k$ for the m bins is

$$\begin{aligned} \langle \langle Q_i \rangle_k \rangle &= \frac{1}{m} \sum_{k=1}^m \langle Q_i \rangle_k = \frac{1}{m} \sum_{k=1}^m \frac{1}{n} \sum_{i=1-n+k \cdot n}^{k \cdot n} Q_i \\ &= \frac{1}{m \cdot n} \sum_{k=1}^m \sum_{i=1-\frac{\mathcal{N}}{m}+k \cdot \frac{\mathcal{N}}{m}}^{k \cdot \frac{\mathcal{N}}{m}} Q_i = \frac{1}{\mathcal{N}} \sum_{i=1}^{\mathcal{N}} Q_i \stackrel{!}{=} \langle Q_i \rangle. \end{aligned} \quad (1.10)$$

Since $\sum_{j=a}^b 1 = b + 1 - a$, it can be shown that the double sum in Eq. (1.10) contains \mathcal{N} independent indices. Let i_u and i_l be the upper and lower limit of the index i , respectively, then

$$\sum_{k=1}^m [i_u + 1 - i_l] = \sum_{k=1}^m \left[\left(k \cdot \frac{\mathcal{N}}{m} \right) + 1 - \left(1 - \frac{\mathcal{N}}{m} + k \cdot \frac{\mathcal{N}}{m} \right) \right] = \sum_{k=1}^m \frac{\mathcal{N}}{m} = \mathcal{N},$$

showing that the second to last step in Eq. (1.10) is valid. Hence, D_A measurements can be seen as independent of spectral resolution. High-resolution data can be degraded to mimic low-resolution spectra and from Eq. (1.10) follows that the flux decrement, or the mean transmitted flux, computed from either of the two cases, should be approximately the same.

Jenkins and Ostriker (1991, their page 3) mention that D_A is influenced by the number density of absorbers and also by the absorption-line-parameter distributions. For absorption-line studies, as performed in this work, it is interesting to see how the flux decrement is connected to absorption-line parameters. Giallongo and Cristiani (1990) use absorption-line statistics from the literature to compute synthetic spectra from which the average flux decrement at a given redshift is derived (see their Fig. 2). Jenkins and Ostriker (1991) link the absorption-line parameters mathematically to the mean transmitted flux (see their Eq. 2.3). Both works consider the number, \mathcal{N} , of absorbing clouds in the redshift interval $z \rightarrow z + dz$ with intrinsic equivalent widths between $W \rightarrow W + dW$. Kennefick et al. (1995) make use of absorption-line-parameter distributions of the column density, N , and the Doppler parameter, b , $d^3\mathcal{N}/dz db dN$, to generate model quasar spectra. They normalize $d\mathcal{N}/dz \propto (1+z)^{\gamma_{app}}$ to match the observed D_A .

Let $\eta(z, b, N)$ be the mean number of absorbers per unit redshift, Doppler parameter, and column density and $\tau_A(z, b, N)$ the optical depth of a single absorber. The effective optical depth is then found to be

$$\tau_{\text{eff}} = \int_0^\infty \int_0^\infty \int_{z_1}^{z_2} [1 - e^{-\tau_A(z, b, N)}] \eta(z, b, N) dz db dN \quad (1.11)$$

(see Appendix A.2 for a derivation). Since spectra are observed on wavelength scale λ_{obs} , the conversion to redshift follows from Eq. (1.1) with the rest-frame wavelength $\lambda_r = \lambda_\alpha \simeq 1216 \text{ \AA}$. Hence,

$$\frac{d\lambda_{\text{obs}}}{dz} = \lambda_\alpha$$

and

$$\frac{d\lambda_{\text{obs}}}{d\lambda_r} = 1 + z_A$$

(where z_A means the redshift of the absorber), so that

$$dz = \frac{1 + z_A}{\lambda_\alpha} d\lambda_r. \quad (1.12)$$

Converting Eq. (1.11) to rest-frame wavelength λ_r at z_A using Eq. (1.12), we have

$$\begin{aligned} \tau_{\text{eff}}(z_A) &= \int_0^\infty \int_0^\infty \int_{\lambda_1}^{\lambda_2} [1 - e^{-\tau_A(\lambda_r, b, N)}] \eta(z, b, N) \frac{1 + z_A}{\lambda_\alpha} d\lambda_r db dN \\ &\simeq \frac{1 + z_A}{\lambda_\alpha} \int_0^\infty \int_0^\infty \eta(z_A, b, N) \underbrace{\int_{\lambda_1=0}^{\lambda_2=\infty} [1 - e^{-\tau_A(\lambda_r, b, N)}] d\lambda_r db dN}_{W_\lambda(b, N)}. \end{aligned} \quad (1.13)$$

In Eq. (1.13) is made use of the fact that $\tau_A(z, b, N)$ sharply peaks at the redshift of the absorber if strongly saturated absorbers and DLAs are excluded, so that $\eta(z, b, N) \rightarrow \eta(z_A, b, N)$ and $1 - e^{-\tau_A(\lambda_r, b, N)} \rightarrow 0$ for $\lambda_r \ll \lambda_\alpha$ and $\lambda_r \gg \lambda_\alpha$. Thus, extending the limits $\lambda_1 \rightarrow 0$ and $\lambda_2 \rightarrow \infty$ is valid. $W_\lambda(b, N)$ is the rest-frame equivalent width.

Empirically, the absorption-line parameters are found to be uncorrelated (Rauch et al. 1992; Lu et al. 1996)¹⁰. The column-density distribution follows a power law of the form $dN/dN \propto N^{-\beta}$ (e.g., Tytler 1987; Hu et al. 1995; Kirkman and Tytler 1997; Janknecht et al. 2006), with a possible departure from a single power law at higher column densities (e.g., Petitjean et al. 1993; Lu et al. 1996; Kim et al. 1997, 2002a). The Doppler-parameter distribution, dN/db , is close to a truncated Gaussian (e.g., Hu et al. 1995; Lu et al. 1996) or a distribution with a sharp low- b cutoff found by Hui and Rutledge (1999). The redshift evolution of the number density is well approximated by a power law of the form $dN/dz \propto (1 + z)^{\gamma_{\text{app}}}$ (e.g., Murdoch et al. 1986; Rauch et al. 1992; Bechtold 1994; Kim et al. 2002a; Janknecht et al. 2006), though its evolution may be more complicated at redshifts $z < 2$ (see Fig. 18 of Janknecht et al. 2006). Therefore, the mean number of absorbers per unit redshift, Doppler parameter, and column density can be parameterized as

$$\frac{d^3N}{dz db dN} = \eta(z, b, N) = f(z)g(b)h(N). \quad (1.14)$$

Assuming $f(z) = dN/dz = N_0 \cdot (1 + z)^\gamma$, Eq. (1.13) becomes for $z_A = z$

$$\begin{aligned} \tau_{\text{eff}}(z) &= \frac{1 + z}{\lambda_\alpha} \int_0^\infty \int_0^\infty N_0 (1 + z)^\gamma g(b) h(N) W_\lambda(b, N) db dN \\ &= (1 + z)^{\gamma+1} \underbrace{\frac{N_0}{\lambda_\alpha} \int_0^\infty \int_0^\infty g(b) h(N) W_\lambda(b, N) db dN}_{\equiv \tau_0}. \end{aligned} \quad (1.15)$$

¹⁰Pettini et al. (1990) found a correlation between column density, N , and Doppler parameter, b , for low-column-density absorbers, though see Rauch et al. (1993).

It can be seen that Eq. (1.15) is independent of the exact form of $F(b, N) = g(b)h(N)$ and even allows for a correlation of b and N . For the interpretation of the empirical results concerning the number density $f(z) = dN/dz$, a theoretical approach is possible.

In the following, a spatially flat geometry of the Universe is assumed (e.g., the Planck Collaboration 2013; Hinshaw et al. 2013). Let $dN_{\text{total}}/dV = n$ be the number density of absorbers per unit proper volume, which is in turn $dV = A dL$ with the area of the cross sections, A , perpendicular to the length, L . We further assume that the invariant metric absorber cross section is $\sigma = \pi r_0^2$ (Lu et al. 1991), where r_0 is a characteristic radius (Peterson 1978), and that the absorbers have a constant characteristic density per unit comoving volume (Peterson 1978). Then, the number, N , of intervening absorbers along a line of sight is $dN = \sigma A^{-1} dN_{\text{total}} = \sigma n dL$, where $\sigma \cdot A^{-1}$ is the probability to intersect an absorber along the sightline. Given a constant number density per unit comoving volume, n_0 , it is $n = (1 + z)^3 n_0$. Hence, the number density becomes

$$\frac{dN}{dz} = \sigma n \frac{dL}{dz} = \pi r_0^2 (1 + z)^3 n_0 \frac{dL}{dz}. \quad (1.16)$$

In Appendix A.3 it is shown for proper length L that

$$\frac{dL}{dz} = \frac{c}{(1 + z)H(z)} \quad (1.17)$$

(e.g., Peterson 1978), where

$$H(z) = H_0 [\Omega_M (1 + z)^3 + \Omega_k (1 + z)^2 + \Omega_\Lambda]^{1/2} \quad (1.18)$$

is the Hubble parameter.

Solving the Einstein field equations presuming the Cosmological Principle, which implies the metrical form $ds^2 = c^2 dt^2 - R^2(t)d\chi^2$ (see Sandage 1961), leads to the Friedmann equations. According to Sandage (1961), $d\chi$ represents an auxiliary three-space of constant Riemannian curvature. $R(t)$ is the so called ‘scale factor’ in Eq. (1.3). One of the two Friedmann equations can be written in the form

$$H^2 \equiv \left(\frac{\dot{R}}{R} \right)^2 = \frac{8\pi G}{3} \rho_{\text{total}} - \frac{kc^2}{R^2} + \frac{\Lambda c^2}{3},$$

with gravitational constant G , matter and energy density ρ_{total} , spatial curvature k/R^2 , and cosmological constant Λ . For simplicity, the density parameters

$$\Omega_\Lambda = \frac{\Lambda c^2}{3H_0^2}, \quad \Omega_k = -\frac{kc^2}{(R_0 H_0)^2}, \quad \text{and} \quad \Omega_M = \frac{8\pi G}{3H_0^2} \rho_0$$

are defined, where $R_0 = 1$ is the scale factor today and $\rho_0 = \rho \cdot R^3/R_0^3$ is the matter density today (energy induced by radiation is neglected as observed today). The density parameters can be compared between different cosmological models. It is

$$\frac{H^2}{H_0^2} = \frac{\Omega_M}{R^3} + \frac{\Omega_k}{R^2} + \Omega_\Lambda,$$

which implies $1 = \Omega_M + \Omega_k + \Omega_\Lambda$.

In a flat Universe ($\Omega_k = 0$, e.g., Hinshaw et al. 2013) Eq. (1.16) becomes

$$\frac{d\mathcal{N}}{dz} = \frac{c\pi r_0^2 n_0}{H_0} \frac{(1+z)^2}{[\Omega_M(1+z)^3 + \Omega_\Lambda]^{\frac{1}{2}}} = \underbrace{\frac{c\pi r_0^2 n_0}{H_0 \cdot \Omega_M^{\frac{1}{2}}}}_{\mathcal{N}_0} \frac{(1+z)^2}{\left[(1+z)^3 + \frac{\Omega_\Lambda}{\Omega_M}\right]^{\frac{1}{2}}}. \quad (1.19)$$

It is $\Omega_\Lambda < 1$ since $\Omega_M > 0$. Hence, Ω_Λ/Ω_M can be neglected at high redshifts ($z > 2$) and we have

$$\frac{d\mathcal{N}}{dz} \simeq \mathcal{N}_0 \cdot (1+z)^{\frac{1}{2}}. \quad (1.20)$$

Hence, for a non-evolving population of absorbers with cosmic time it is $\gamma = \frac{1}{2}$ in Eq. (1.15). Peterson (1978) was the first who investigated the redshift evolution of the number density and finds the absorbers to be strongly evolving in the redshift range $1.8 < z < 3.6$, $\gamma > 1$. In contrast, Sargent et al. (1980) find no evolution in the number density at similar redshifts, though see Weymann et al. (1981, their section 5.1).

The exponent γ in Eq. (1.15) is the intrinsic evolutionary rate exponent (Zuo 1993). It differs from the observed evolutionary rate exponent γ_{app} since the observed redshift evolution of the number density $d\mathcal{N}/dz \approx \mathcal{N}_0 (1+z)^{\gamma_{app}}$ is subject to line blending and the influence of noise (Liu and Jones 1988, $\gamma > \gamma_{app}$). Hence, if the assumption about the intrinsic evolutionary rate exponent γ is correct, it can be determined by estimating the redshift evolution of the effective optical depth $\tau_{eff}(z)$ from Eq. (1.15). This method is superior to the determination of γ_{app} by line counts.

1.5.2 The Gunn-Peterson optical depth

The Gunn-Peterson optical depth, τ_{GP} , is observed as the continuous suppression of emitted flux in quasar spectra due to absorption by smoothly distributed gas of neutral hydrogen in the IGM. By comparing τ_{GP} from hydrodynamic simulations for an appropriate cosmological model with the observed effective optical depth, it is possible to draw conclusions about the baryon or the ionizing radiation content in the Universe. The latter may constrain contributions to the UVB from ionizing sources (e.g., quasars and star-forming galaxies) which is important in order to better understand the end of the hydrogen reionization epoch.

The optical depth of an absorber depends on the absorption coefficient, κ , and the considered path length, s ,

$$d\tau = \kappa ds. \quad (1.21)$$

The absorption coefficient in SI¹¹ units is

$$\kappa = \frac{1}{4} \frac{e^2}{\epsilon_0 m_e c} f n(s) \Phi(\Delta\nu) \quad (1.22)$$

(e.g., Gunn and Peterson 1965), where e is the elementary charge, ϵ_0 the electric constant, m_e the electron mass, c the speed of light in vacuum, f the oscillator strength of the

¹¹Refers to the International System of Units. The abbreviation follows from French: *Le Système international d'unités*.

considered electron transition, $n(s)$ the volume number density of the particles, and $\Phi(\Delta\nu)$ the profile function.

Hence, local integration of Eq. (1.21) gives

$$\tau = \frac{1}{4} \frac{e^2}{\epsilon_0 m_e c} f \underbrace{\Phi(\Delta\nu)}_{N} \int_0^s n(s') ds', \quad (1.23)$$

with column density N . Assuming a Gaussian profile with Doppler width $\Delta\nu_D$,

$$\Phi(\Delta\nu) = \frac{1}{\sqrt{\pi} \Delta\nu_D} \exp \left[- \left(\frac{\Delta\nu}{\Delta\nu_D} \right)^2 \right], \quad (1.24)$$

where $\Delta\nu_D = \nu_c \cdot b/c$ (with Doppler parameter b and central frequency ν_c) and $\Delta\nu = \nu_r - \nu_c$ (with rest-frame frequency ν_r), we get

$$\tau(\nu_r) = \frac{1}{4\sqrt{\pi}} \frac{e^2}{\epsilon_0 m_e} \frac{f N}{\nu_c b} \exp \left[- \left(\frac{c}{b} \cdot \frac{\nu_r - \nu_c}{\nu_c} \right)^2 \right]. \quad (1.25)$$

On cosmological scales the observed frequency, ν_{obs} , changes with distance since it relates to different rest-frame frequencies, ν_r , due to the redshift, z . Following Eq. (1.1) we have

$$\nu_r = \nu_{\text{obs}} \cdot (1 + z). \quad (1.26)$$

Therefore, the integration of Eq. (1.21) considering an observed, cosmological object in a flat Universe at emission redshift z_{em} becomes

$$\tau = \frac{1}{4} \frac{e^2}{\epsilon_0 m_e c} f \int_0^{z_{\text{em}}} n(z) \Phi[\nu_{\text{obs}}(1+z) - \nu_c] \frac{dL}{dz} dz, \quad (1.27)$$

where $s = L$ is the proper length. With Eq. (1.17) we have

$$\tau = \frac{1}{4} \frac{e^2}{\epsilon_0 m_e c} f \int_0^{z_{\text{em}}} \underbrace{\frac{c \cdot n(z)}{(1+z) H(z)}}_{\equiv q(z)} \Phi[\nu_{\text{obs}}(1+z) - \nu_c] dz. \quad (1.28)$$

Since the profile function peaks sharply at the redshift of the absorber z_A , so that $q(z) \rightarrow q(z_A)$, we are left with the integral

$$\tau(z_A) \simeq \frac{1}{4} \frac{e^2}{\epsilon_0 m_e c} f \frac{c \cdot n(z_A)}{(1+z_A) H(z_A)} \int_0^{z_{\text{em}}} \Phi[\nu_{\text{obs}}(1+z) - \nu_c] dz \quad (1.29)$$

that can be solved by substituting $\xi = \nu_{\text{obs}}(1+z) - \nu_c$, so that $d\xi/dz = \nu_{\text{obs}}$. Hence,

$$\int_0^{z_{\text{em}}} \Phi[\nu_{\text{obs}}(1+z) - \nu_c] dz \simeq \int_{-\infty}^{\infty} \Phi[\nu_{\text{obs}}(1+z) - \nu_c] dz = \int_{-\infty}^{\infty} \frac{\Phi(\xi)}{\nu_{\text{obs}}} d\xi = \frac{1}{\nu_{\text{obs}}}. \quad (1.30)$$

In Eq. (1.30) the limits can be extended artificially due to the shape of the profile function if the absorber has a sufficiently large redshift ($z_A > 0$) but is distant enough to the observed object ($z_A < z_{\text{em}}$). The profile function is defined to fulfill

$$\int_{-\infty}^{\infty} \Phi(\xi) d\xi = 1. \quad (1.31)$$

Hence, Eq. (1.29) leads to

$$\tau(z_A) \simeq \frac{1}{4} \frac{e^2}{\epsilon_0 m_e c} f \cdot \frac{n(z_A)}{(1+z_A) H(z_A)} \cdot \frac{c}{\nu_{\text{obs}}} \quad (1.32)$$

with $c/\nu_{\text{obs}} = \lambda_{\text{obs}}$. Applied to hydrogen ($f = f_\alpha \simeq 0.416$, $\lambda_{\text{obs}}/(1+z_A) = \lambda_\alpha \simeq 1215.67 \text{ \AA}$, $n = n_{\text{H}_1}$) and by dropping the index on the redshift, we arrive at

$$\tau_{\text{GP}}(z) \simeq \frac{1}{4} \frac{e^2}{\epsilon_0 m_e c} f_\alpha \lambda_\alpha \frac{n_{\text{H}_1}(z)}{H(z)}. \quad (1.33)$$

Equation (1.33) is called the Gunn-Peterson optical depth (e.g., Fan et al. 2006) since it was firstly derived by Gunn and Peterson (1965).

The ionization ratio of a species with number density n is determined by

$$\frac{n_{\text{ion}}}{n_{\text{atom}}} = \frac{\Gamma}{\Sigma}, \quad (1.34)$$

with ionization rate Γ and recombination rate Σ . Ionization is driven by radiation, collisions, or charge exchange with other species. Recombination is due to captured electrons and charge exchange. Neglecting charge exchange processes and collisional ionization for the typical conditions in the IGM while focussing on hydrogen (hence, dielectronic recombination is disregarded), we are left with

$$\frac{n_{\text{H}_{\text{II}}}}{n_{\text{H}_1}} = \frac{\Gamma_{\text{photo}}}{\alpha_{\text{rad}}(T) \cdot n_e} \quad \Leftrightarrow \quad n_{\text{H}_1} = \frac{\alpha_{\text{rad}}(T) n_e n_{\text{H}_{\text{II}}}}{\Gamma_{\text{photo}}}, \quad (1.35)$$

where $\alpha_{\text{rad}}(T)$ is the temperature-dependent radiative recombination coefficient, n_e is the electron number density, and Γ_{photo} is the photoionization rate. For our purposes, only the average intergalactic radiation field needs to be considered for Γ_{photo} , far away from local sources (i.e., galaxies and their nuclei).

In the following, a simplistic picture of the Universe and the origin of its content is described, in order to introduce the baryonic density parameter Ω_b (cf. Eq. 1.18): In the standard model of Big Bang theory the matter in our Universe emerged from the Big Bang and existed as a plasma until the expansion of the Universe cooled it sufficiently, causing recombination of electrons with existent atomic nuclei. Big Bang nucleosynthesis (BBN) allowed for the build-up of nuclei from protons and neutrons (baryons). Stable nuclei resulting from the BBN process are from the chemical elements hydrogen (${}^1\text{H}$, ${}^2\text{H}$), helium (${}^3\text{He}$, ${}^4\text{He}$), lithium (${}^6\text{Li}$, ${}^7\text{Li}$), and beryllium (${}^9\text{Be}$). ${}^4\text{He}$ is a considerable threshold for the BBN process since reactions of ${}^4\text{He}$ with protons or itself lead to unstable nuclei with 5 and 8 nucleons. Therefore, sufficient production of heavier elements is due to

other means than the BBN, such as the evolution and explosion of stars. Assuming that the total baryonic mass in the Universe, m_b , is composed of hydrogen and helium (as in primordial gas), $m_b = m_H + m_{He}$, we find with the mass fraction of helium,

$$Y \equiv \frac{m_{He}}{m_b} = \frac{m_{He}}{m_H + m_{He}} = \frac{1}{\frac{m_H}{m_{He}} + 1} \Leftrightarrow m_{He} = \frac{Y}{1 - Y} m_H, \quad (1.36)$$

the relation

$$m_b = m_H + m_{He} = m_H + \frac{Y}{1 - Y} m_H = \frac{1}{1 - Y} m_H. \quad (1.37)$$

Hence, with the mass density, $\rho = m/V$, we have

$$\rho_b = \frac{1}{1 - Y} \rho_H. \quad (1.38)$$

It is a reasonable¹² assumption that all hydrogen is found in the form of 1H and all helium as 4He . In this case, the mass of a hydrogen nucleus is the proton mass, m_p . Hence, the hydrogen mass density can be expressed as

$$\rho_H = m_p n_H, \quad (1.39)$$

with the hydrogen number density n_H . Combining Eqs. (1.38) and (1.39) we get

$$\rho_b = \frac{1}{1 - Y} m_p n_H \quad (1.40)$$

as well as the density parameter for the baryons, Ω_b , which is defined equivalently to the matter density parameter, Ω_M , from Eq. (1.18),

$$\Omega_b \equiv \rho_b \cdot \frac{8\pi G}{3H_0^2} = \frac{8\pi G}{3H_0^2} \cdot \frac{m_p}{1 - Y} n_H. \quad (1.41)$$

This leads us to

$$n_H = \frac{3H_0^2}{8\pi G} \cdot \frac{1 - Y}{m_p} \cdot \Omega_b. \quad (1.42)$$

In an expanding Universe n_H from Eq. (1.42) is the comoving hydrogen number density. By introducing the comoving volume $V_c = V/R^3(t) = V(1+z)^3$ for a flat Universe, where V is the proper volume and $R(t) = (1+z)^{-1}$ the relating scale factor (see Eq. 1.3), the proper hydrogen number density at all cosmic times is

$$n_H(z) = \frac{3H_0^2}{8\pi G} \cdot \frac{1 - Y}{m_p} \cdot \Omega_b (1+z)^3. \quad (1.43)$$

The total hydrogen number density, n_H , contains neutral hydrogen, n_{H_I} , and ionized hydrogen, $n_{H_{II}}$ (cf. Eq. 1.35). If the intergalactic hydrogen is highly ionized (Gunn and Peterson 1965), the total hydrogen number density is $n_H = n_{H_I} + n_{H_{II}} \simeq n_{H_{II}}$. Assuming that the baryonic matter in the Universe is composed of hydrogen and helium only (cf.

¹²The relative atomic mass A_r , which includes all isotopes, is approximately the mass (or nucleon) number. The mass number refers to the most abundant isotope which is by far 1H and 4He for hydrogen and helium, respectively.

Eq. 1.36), the free electrons stem from the ionized atoms in an assumed electrically neutral Universe,

$$n_e = n_{\text{H II}} + \underbrace{n_{\text{He II}} + 2 \cdot n_{\text{He III}}}_{\equiv \vartheta \cdot n_{\text{He}}} \simeq n_{\text{H}} + \vartheta \cdot n_{\text{He}}. \quad (1.44)$$

Herein, ϑ is ranging from zero (all helium is neutral) to 2 (helium is completely ionized), and the total helium number density is

$$n_{\text{He}} = \frac{m_{\text{He}}}{4 \cdot m_p}, \quad (1.45)$$

neglecting the mass excess and the difference in nucleon mass, $m_p \approx m_n$ (neutron mass). The total helium mass, m_{He} , is assumed to be made up from ${}^4\text{He}$, the most abundant isotope of helium. Hence, using Eq. (1.36), Eq. (1.44) becomes

$$n_e \simeq n_{\text{H}} + \frac{\vartheta}{4} \cdot \frac{m_{\text{He}}}{m_p} = n_{\text{H}} + \frac{\vartheta}{4} \cdot \frac{Y}{1-Y} \cdot \underbrace{\frac{m_{\text{H}}}{m_p}}_{n_{\text{H}}} = \left(1 + \frac{\vartheta}{4} \cdot \frac{Y}{1-Y}\right) n_{\text{H}} \equiv \psi \cdot n_{\text{H}} \quad (1.46)$$

with

$$\psi(\vartheta, Y) \equiv 1 + \frac{\vartheta \cdot Y}{4(1-Y)}. \quad (1.47)$$

If all helium in the Universe is neutral, $\vartheta = 0$, then $\psi = 1$. For fully ionized helium ($\vartheta = 2$) with a mass fraction of $Y = 0.2477$ (Peimbert et al. 2007), $\psi \approx 1.165$.

With all the assumptions made above, Eq. (1.35) can be expressed as

$$n_{\text{H I}}(z) = \frac{\alpha_{\text{rad}}(T) n_e(z) n_{\text{H II}}(z)}{\Gamma_{\text{photo}}} \simeq \frac{\alpha_{\text{rad}}(T)}{\Gamma_{\text{photo}}} \psi n_{\text{H}}^2(z). \quad (1.48)$$

Combining Eqs. (1.33), (1.48), and (1.43) we get

$$\begin{aligned} \tau_{\text{GP}}(z) &\simeq \frac{\psi}{4} \cdot \frac{e^2}{\epsilon_0 m_e c} \cdot f_\alpha \lambda_\alpha \cdot \frac{(1+z)^6}{H(z)} \cdot \frac{\alpha_{\text{rad}}(T)}{\Gamma_{\text{photo}}} \cdot \left(\frac{3H_0^2}{8\pi G} \cdot \frac{1-Y}{m_p} \cdot \Omega_b \right)^2 \\ &= \frac{\psi}{4} \cdot \frac{f_\alpha \lambda_\alpha}{\epsilon_0 m_e c} \cdot \left(\frac{1-Y}{m_p} \right)^2 \cdot \left(\frac{3e}{8\pi G} \right)^2 \cdot \frac{\alpha_{\text{rad}}(T)}{\Gamma_{\text{photo}}} \cdot \frac{H_0^4}{H(z)} \cdot \Omega_b^2 (1+z)^6. \end{aligned} \quad (1.49)$$

For visual clarity, we define with $\mathcal{C}(\psi(\vartheta, Y), Y) = \mathcal{C}(\vartheta, Y)$

$$\mathcal{C}(\vartheta, Y) = \mathcal{C}_{\text{He}} \equiv \frac{1}{4} \left(1 + \frac{\vartheta}{4} \cdot \frac{Y}{1-Y} \right) \cdot \frac{f_\alpha \lambda_\alpha}{\epsilon_0 m_e c} \cdot \left(\frac{1-Y}{m_p} \right)^2 \cdot \left(\frac{3e}{8\pi G} \right)^2, \quad (1.50)$$

which is a constant for a given ionization state and mass fraction of helium. Using the Hubble parameter (Eq. 1.18) for a Universe with zero curvature ($\Omega_k = 0$) and neglecting dark energy, which is approximately valid for high redshift, $H(z) \approx H_0 \Omega_M^{1/2} (1+z)^{3/2}$, we get

$$\tau_{\text{GP}}(z) \approx \mathcal{C}_{\text{He}} \cdot \frac{\alpha_{\text{rad}}(T)}{\Gamma_{\text{photo}}} \cdot \frac{H_0^3}{\Omega_M^{1/2}} \cdot \Omega_b^2 (1+z)^{4.5}. \quad (1.51)$$

Equation (1.51) is valid for a uniform medium at a given redshift, though it can be extended to include density fluctuations (Rauch et al. 1997; McDonald and Miralda-Escudé 2001) using the overdensity

$$\Delta \equiv \frac{\rho_{\text{H}}}{\bar{\rho}_{\text{H}}} = \frac{n_{\text{H}}}{\bar{n}_{\text{H}}}. \quad (1.52)$$

If Eqs. (1.33) and (1.34), and, therefore, Eq. (1.48), are considered locally, and since Eqs. (1.38) to (1.43) refer to the mean number density ($n_{\text{H}} \rightarrow \bar{n}_{\text{H}} = n_{\text{H}}/\Delta$) at a given redshift in a clumpy IGM, Eq. (1.51) can be expressed as

$$\tau_{\text{GP}}(z) \approx \mathcal{C}_{\text{He}} \cdot \frac{H_0^3 \Omega_b^2}{\Omega_M^{\frac{1}{2}} \Gamma_{\text{photo}}} \cdot \alpha_{\text{rad}}(T) \Delta^2 (1+z)^{4.5} \quad (1.53)$$

(still ignoring the effects of peculiar velocities and thermal broadening). Here, appropriate assumptions about the distribution and ionization state of helium have to be made in order for \mathcal{C}_{He} to be a constant.¹³ The density distribution and density-temperature relation $T(\Delta)$ (equation of state), that is contained implicitly in the radiative recombination coefficient, have to be estimated by hydrodynamic simulations for an appropriate cosmological model (McDonald and Miralda-Escudé 2001). Comparing the observed flux decrement from Eq. (1.8) to the flux decrement from simulations $D_{\text{sim}} = 1 - e^{-\tau_{\text{GP}}}$, the observed mean flux can be linked to the baryon density and ionizing background. Following the literature, the unitless parameter is defined as

$$\mu \equiv \frac{H_0 \Omega_b^2}{\Omega_M^{\frac{1}{2}} \Gamma_{\text{photo}}} \quad (1.54)$$

(cf. Miralda-Escudé et al. 1996; Rauch et al. 1997; McDonald et al. 2000). Assuming that a simple scaling of the optical depth with μ in the simulation does not change the density and temperature of the gas (Rauch et al. 1997), Ω_b and Γ_{photo} are determined by μ and the cosmological parameters (H_0 , Ω_M). Given an ionizing radiation field, it is possible to obtain an estimate for Ω_b (Rauch et al. 1997, see also Weinberg et al. 1997; Bi and Davidsen 1997) and vice versa (McDonald et al. 2000; McDonald and Miralda-Escudé 2001). The evolution of Γ_{photo} with redshift may constrain contributions to the UVB from different sources such as quasars and star-forming galaxies (Bajtlik et al. 1988; McDonald and Miralda-Escudé 2001) or the IGM itself (Haardt and Madau 1996). The end of the hydrogen reionization epoch (e.g., Miralda-Escudé et al. 2000; Becker et al. 2001; Songaila and Cowie 2002; Fan et al. 2006) may, thus, be better understood. The proximity effect (Bajtlik et al. 1988) gives the opportunity to infer the quasar contribution to the intensity of the UVB (e.g., Cooke et al. 1997; Dall'Aglio et al. 2008).

1.6 Motivation for this work

Empirically, the redshift evolution of the effective optical depth, $\tau_{\text{eff}}(z)$, follows a smooth power law. Several studies report on the detection of a narrow feature in the otherwise smooth redshift evolution of τ_{eff} (Bernardi et al. 2003; Faucher-Giguère et al. 2008b;

¹³In the simplest case helium is neglected.

Dall’Aglio et al. 2008). Bernardi et al. (2003) use low-resolution SDSS quasar spectra, while Faucher-Giguère et al. (2008b) and Dall’Aglio et al. (2008) use high-resolution quasar spectra. As will be seen later, the τ_{eff} features found by these studies are observed at similar redshift ($z \sim 3.2$) and are similar in size.

Pâris et al. (2011) and Becker et al. (2013) also use low-resolution SDSS quasar spectra to measure $\tau_{\text{eff}}(z)$ and do not find a narrow deviation from the empirical power law. Though, Pâris et al. (2011) find a break in the redshift evolution of the mean flux at $z \sim 3$. Although a definite explanation is not yet found, why a sharp feature should occur in a smooth power-law evolution of the effective optical depth, a detailed investigation of this puzzling aspect is desired.

In this work, I use the method from Faucher-Giguère et al. (2008b) to infer the redshift evolution of the effective optical depth. I will check the success of this method against synthetic spectra. Faucher-Giguère et al. (2008b) use a statistical approach to account for metal absorption in quasar spectra. In this work, the imprint of metal absorption in quasar spectra is removed in detail by the use of absorption-line fits to the normalized spectra. In order to account for metal absorption lines in the quasar spectra in the best possible way, I fitted the 7491 absorption lines found in the considered redshift ranges of the spectra *individually*. This is a very time-consuming procedure.

The method, used in this work, to remove the contribution of metals to the observed absorption in quasar spectra using absorption-line fits is similar to the approach of Kim et al. (2007). They use 18 high-resolution quasar spectra, of which 11 have emission redshifts $z_{\text{em}} < 2.7$ and only two spectra cover the redshift range around $z \sim 3.2$, making the research of the potential onset of a narrow τ_{eff} feature statistically uncertain. Compared to Kim et al. (2007), in this work the number of sightlines used to infer $\tau_{\text{eff}}(z)$ above $z = 2.7$ is almost tripled. *Thus, such a precision measurement of the effective optical depth across the redshift range $2.7 \lesssim z \lesssim 3.6$ is done for the first time in this work.*

This work is structured as follows. In Chapter 2 the data used in this work is presented and the line-fitting procedure is described. A statistical analysis of the line-fitting parameters is performed in Chapter 3. The method to infer $\tau_{\text{eff}}(z)$, the results regarding this measurement, and the discussion of systematics are presented in Chapter 4. I compare the $\tau_{\text{eff}}(z)$ measurement from this work to the literature in §5.1 (see also Table 1.1) and try to find a consistent picture that can explain the various measurements. I conclude in §5.2.

Table 1.1. Literature investigating the redshift evolution of the effective optical depth. This includes estimates of single values at a given redshift, average values for individual quasar sightlines, and the mean flux inferred from all quasar spectra intersected by a given redshift bin. The columns are (1) the reference; (2) specifications of the quasar sample (number of sightlines used, the quality of the spectra, and the observatory); (3) criteria of investigation which include sightline selections, continuum estimates, the analyzed H α forest range in rest-frame wavelength λ_r , and high-column-density-absorber as well as metal contribution; (4) the redshift range investigated; (5) the method to infer the mean flux and τ_{eff} ; (6) the results.

Reference	no.	QSO Sample	instrument	Criteria of Investigation	Redshift	Statistical Method	Results
Tytler et al. (2004)	77	FWHM $\sim 250 \text{ km s}^{-1}$ $S/N \sim 2 - (> 50)$	Kast/Lick	no BAL quasars; continuum fitted; $\lambda_r = (1070 - 1170) \text{ \AA}$	$z = 1.9$	mean flux decrement D_A from pixel flux decrement scaled to the expected value at $z = 1.9$	$D_A = 0.151 \pm 0.007$, reduces if corrected for metals and high-column-density absorbers, see their §§7.8, 11.2
Janknecht et al. (2006)	3	$R \gtrsim 38\,000$ $S/N \sim 3 - 25$	HIRESS/Keck, UVES/VLT	continuum fitted; metals eliminated by masking	$1.81 \leq z \leq 1.91$	mean normalized flux from the respective spectral parts	$\langle f_\nu \rangle = 0.895 \pm 0.02$, $\tau_{\text{eff}} = 0.111 \pm 0.02$
Songaila and Cowie (2002)	15	$R \sim 5300$	ESI/Keck	continuum extrapolated	$3.8 \leq z \leq 5.5$	mean fluxes per spectrum from four equidistant bins of $\Delta\lambda_r = 25 \text{ \AA}$ within $\lambda_r = (1075 - 1175) \text{ \AA}$; in their §4 they also introduce the average of the mean fluxes (including literature values) in a given redshift bin	$\langle f_\nu \rangle \propto (1 + z)^{-7.1}$, data points show a large scatter
Kim et al. (2002a)	8	$R \sim 45\,000$ $S/N \gtrsim 35$	UVES/VLT	continuum fitted; $\lambda_r \sim (1026 - 1216) \text{ \AA}$ presumably excluding the proximity region; DLAs excluded; metals subtracted from the spectra using VPFIT	$1.5 \leq z \leq 3.6$	mean flux per spectrum	trend of decreasing τ_{eff} with decreasing redshift
Schaye et al. (2003)	21	FWHM = 6.6 km s $^{-1}$ $S/N \gtrsim 40$	UVES/VLT, HIRESS/Keck	continuum fitted; $\lambda_r \sim (1026 - 1216) \text{ \AA}$ without quasar proximity zone ($\Delta v = \max[4000 \text{ km s}^{-1}, 8 \text{ Mpc} \cdot H(z)/h]$)	$1.65 \lesssim z \lesssim 4.45$	mean flux from H α forest of a spectrum split into two parts with (i) all pixels and (ii) after removal of pixels presumably contaminated by metals, atmospheric lines, or absorbers with high-column densities (log $N \geq 19$)	$\tau_{\text{eff}} = \tau_0 \cdot \left(\frac{1+z}{4}\right)^\alpha$ $\log \tau_0 = -0.40 \pm 0.02$, $\alpha = 3.40 \pm 0.23$
Songaila (2004)	50	$R \sim 5\,300 - 36\,000$	ESI/Keck, HIRESS/Keck	continuum fitted ($z_{\text{em}} < 4.5$) and extrapolated ($z_{\text{em}} > 4.5$)	$2.0 \leq z \leq 6.3$	the average from mean fluxes of $\Delta\lambda_r = 15 \text{ \AA}$ bins between $\lambda_r \sim (1080 - 1185) \text{ \AA}$ of a spectrum was computed in bins of six data points	$\log \tau_0 = -0.44 \pm 0.01$, $\alpha = 3.57 \pm 0.20$
Kim et al. (2007)	18	$R \sim 45\,000$ $S/N \gtrsim 25 - 30$	UVES/VLT	continuum fitted; $\lambda_r \sim (1026 - 1216) \text{ \AA}$ without quasar proximity zone ($\Delta v = 4000 \text{ km s}^{-1}$); LLSS included, sub-DLAs and DLAs excluded; metals subtracted from the spectra using VPFIT	$1.7 \leq z \leq 3.2$	mean flux for each line of sight	τ_{eff} increases with redshift
Dall'Aglio et al. (2008)	40	$R \sim 45\,000$ $S/N \sim 70$	UVES/VLT	continuum fitted; $\lambda_r \sim (1026 - 1216) \text{ \AA}$ without quasar proximity zone ($\Delta v = 5000 \text{ km s}^{-1}$); LLSS and DLAs excluded	$2.0 \lesssim z \lesssim 4.5$	H α forest split into two equidistant parts in redshift	a trend of decreasing τ_{eff} with decreasing z with scatter caused by cosmic variance,
Calura et al. (2012)	8	FWHM $\sim 6.7 \text{ km s}^{-1}$ $S/N = 25 - 150$	UVES/VLT	continuum fitted; $\lambda_r \sim (1026 - 1216) \text{ \AA}$ without quasar proximity zone ($\Delta v = 4000 \text{ km s}^{-1}$); LLSS, sub-DLAs, and DLAs excluded; metals masked	$2.8 \lesssim z \lesssim 3.6$	$\langle f_\nu \rangle$ computed for two bins per spectrum	trend of increasing τ_{eff} with redshift with scatter

Table 1.1. Continued

Reference	no.	QSO quality	Sample instrument	Criteria of Investigation	Redshift	Statistical Method	Results
Rauch et al. (1997)	7	FWHM = 6.6 km s ⁻¹	HRS/Keck	continuum fitted; $\lambda_r \sim (1026 - 1216)$ Å without quasar proximity zone ($r = 5h^{-1}$ Mpc); excluding DLAs, unidentified strong absorption lines with $b < 10$ km s ⁻¹ , and metal lines	1.5 ≤ $z \leq 4.5$	mean of the quantity $D = 1 - e^{-\tau}$ in $\Delta z = 1$	$\langle z \rangle = 2.29$; $\langle D \rangle = 0.186$ $\langle z \rangle = 3.02$; $\langle D \rangle = 0.321$ $\langle z \rangle = 3.98$; $\langle D \rangle = 0.539$
Bernardi et al. (2003)	1061	$\Delta v = 150$ km s ⁻¹ $S/N \sim 3$	SDSS	spectra with the most prominent BALs and DLAs removed; $\lambda_r = (1080 - 1160)$ Å	2.6 < $z < 4.1$	minimization approach to solve for the absorbed flux and continuum of composite spectra, allowing for Gaussian deviations from smooth power laws; a deviation in the redshift evolution of τ_{eff} and intrinsic quasar emission lines on the continuum in the H I Ly α forest	$\tau_{\text{eff}} = \tau_0 \cdot (1 + z)^{\gamma+1}$, $\tau_0 = 0.0028 \pm 0.0011$, $(\gamma + 1) = 3.69 \pm 0.22$, shows a deviation in a range of $\Delta z = 0.1$ at $z = 3.15$
Viel et al. (2004)	27	$R \gtrsim 40\,000$ $S/N > 50$	UVES/VLT (LUQAS)	continuum fitted; sub-DLAs and DLAs excluded	2 ≤ $z \leq 3$	mean flux in three given redshift ranges	$2.0 < z < 2.3$, $\langle z \rangle = 2.125$ ▲ $\langle f_{\nu} \rangle = 0.849 \pm 0.008$, ▲ $\tau_{\text{eff}} = 0.163 \pm 0.009$, ▲ $\langle f_{\nu} \rangle = 0.800 \pm 0.008$, ▲ $\tau_{\text{eff}} = 0.223 \pm 0.014$, ▲ $\langle f_{\nu} \rangle = 0.730 \pm 0.011$, ▲ $\tau_{\text{eff}} = 0.315 \pm 0.015$
Tytler et al. (2004)	77	FWHM ∼ 250 km s ⁻¹ $S/N \sim 2 - (> 50)$	Kast/Lick	no BAL quasars; continuum fitted; $\lambda_r = (1070 - 1170)$ Å	1.6 < $z < 2.4$	mean flux decrement D_A from pixel DA(z) = 0.147 · $\left(\frac{1+z}{1+1.9}\right)^{2.57}$ flux decrement of all quasars contributing in bins of $\Delta z = 0.08$	for redshifts $z < 5.5$ (including Songaila, 2004, data supplementing down to redshift $z = 3$): ▲ $\tau_{\text{eff}} = \tau_0 \cdot \left(\frac{1+z}{0.5}\right)^{\gamma+1}$, $\tau_0 = 0.85 \pm 0.06$, $(\gamma + 1) = 4.3 \pm 0.3$
Fan et al. (2006)	19	different	various (see their Table 1)	continuum extrapolated; $\lambda_r = (1040 - 1216)$ Å without quasar proximity zone	4.9 ≤ $z \leq 6.3$	mean flux in $\Delta z = 0.15$ redshift bins along each line of sight; see also their §3.3	mean flux decrement D_A from pixel DA(z) = 0.147 · $\left(\frac{1+z}{1+1.9}\right)^{2.57}$ flux decrement of all quasars contributing in bins of $\Delta z = 0.08$ for redshifts $z < 5.5$ (including Songaila, 2004, data supplementing down to redshift $z = 3$): ▲ $\tau_{\text{eff}} = \tau_0 \cdot \left(\frac{1+z}{0.5}\right)^{\gamma+1}$, $\tau_0 = 0.85 \pm 0.06$, $(\gamma + 1) = 4.3 \pm 0.3$
Kim et al. (2007)	18	$R \sim 45\,000$ $S/N \gtrsim 25 - 30$	UVES/VLT	continuum fitted; $\lambda_r \sim (1026 - 1216)$ Å without quasar proximity zone ($\Delta v = 4000$ km s ⁻¹); LLSS included, sub-DLAs and DLAs excluded; metals subtracted from the spectra using VPFFIT	1.7 ≤ $z \leq 3.2$	mean flux from pixels of all quasars contributing in a given $\Delta z = 0.2$ redshift bin	downward deviation from the smooth power law $\tau_{\text{eff}} = \tau_0 \cdot (1 + z)^{\gamma+1}$, $\tau_0 = 0.0054 \pm 0.0101$, $(\gamma + 1) = 2.96 \pm 0.83$
Faucher-Giguère et al. (2008b)	86	FWHM ≥ 6 km s ⁻¹ $S/N \gtrsim 10$ pixel ⁻¹	ESI/Keck, HIRES/Keck, MIKE/Magellan	continuum fitted; $\lambda_r \sim (1026 - 1216)$ Å without quasar proximity zone ($R_{\text{proper}} = 25$ Mpc); excluding systems with $\log N_{\text{H}_1} > 19$ (SLLSs, DLAs) and their associated metal lines	2.0 ≤ $z \leq 4.2$	average flux in $\Delta z = 0.1$ redshift bins from the mean flux in 3 proper Mpc intervals per quasar, corrected for systematic continuum bias using mock spectra	downward deviation from the smooth power law $\tau_{\text{eff}} = \tau_0 \cdot (1 + z)^{\gamma+1}$, $\log \tau_0 = -2.21 \pm 0.09$, $\gamma = 2.04 \pm 0.17$, 'tentative' feature within $3.2 \lesssim z \lesssim 3.4$
Dall'Aglio et al. (2008)	40	$R \sim 45\,000$ $S/N \sim 70$	UVES/VLT	no BAL quasars; continuum fitted; $\lambda_r = (1025 - 1180)$ Å	2.0 ≤ $z \lesssim 4.5$	mean flux from all quasars contributing to a respective redshift bin of size $\Delta z = 0.1$	$\tau_{\text{eff}} = \tau_0 \cdot (1 + z)^{\gamma+1}$, $\log \tau_0 = -2.28 \pm 0.03$, $\gamma = 2.13 \pm 0.04$
Dall'Aglio et al. (2009)	1733	$R \sim 2000$, $S/N \gtrsim 10$ at $\lambda_r \sim 1450$ Å	SDSS-DR5				

Table 1.1. *Continued*

Reference	no.	QSO quality	Sample instrument	Criteria of Investigation	Redshift	Statistical Method	Results
Pâris et al. (2011)	2576	$R \sim 1800$, $S/N > 8$ at $\lambda_r \sim 1280 \text{ \AA}$	SDSS-DR7	no BAL quasars and lines of sight containing DLAs; continuum from PCA without BAL quasars and objects where the peak of the [H] β Ly α emission line was greater than 10 times the continuum level near a rest wavelength of 1280 \AA ; used 26 composite spectra in redshift bins of $\Delta z_{\text{em}} = 0.1$ in the range $2.2 \leq z \leq 4.4$ and $\Delta z_{\text{em}} = 0.2$ at higher redshift from individual quasar spectra with absolute magnitudes $M_i > -29.0$ and ‘corrected for telluric emission line residuals in the red’; $\lambda_r \sim (1041 - 1175) \text{ \AA}$	$2.3 < z < 4.0$	mean flux between $\lambda_r = (1080 - 1160) \text{ \AA}$ in redshift bins of $\Delta z = 0.1$	decrease of mean flux with redshift steepens at $z \sim 3$
Becker et al. (2013)	6065	$\Delta v \sim 69 \text{ km s}^{-1}$	SDSS-DR7	$2 < z < 5$	mean flux as a fraction of its value at $z = 2.15$ from flux ratios of separate composites at the same rest wavelength, scaled to values at $z \leq 2.5$ from Faucher-Giguère et al. (2008b)	smooth decline of the mean transmitted flux with redshift	
this work	13	$R \geq 40\,000$ $S/N \gtrsim 15$	UVES/VLT	$2.7 \leq z \leq 3.6$	average flux in $\Delta z = 0.1$ redshift bins from the mean fitted/model flux in ~ 3 proper Mpc intervals per quasar	τ_{eff} increases with redshift	

Chapter 2

Data selection and analysis

2.1 Sample selection

The aim of this work is to investigate the redshift evolution of the effective optical depth (§1.5). In particular, I want to check the existence of a narrow feature in $\tau_{\text{eff}}(z)$ at redshift $z \sim 3.2$, which is found quite controversial in the literature. In order to measure the effective optical depth from quasar spectra, the H I Ly α ($\lambda_{\text{r,Ly}\alpha}^{\text{H}_1} \simeq 1216 \text{ \AA}$) forest without higher order of the Lyman series is analyzed. In principle, it would be possible to account for absorption features in the H I Ly α forest from H I Ly β ($\lambda_{\text{r,Ly}\beta}^{\text{H}_1} \simeq 1026 \text{ \AA}$), H I Ly γ ($\lambda_{\text{r,Ly}\gamma}^{\text{H}_1} \simeq 973 \text{ \AA}$), and even higher orders, to use the complete H I Ly α forest of a single spectrum. This approach demands a complex fitting procedure of line profiles to the absorption features detected in a spectrum (§2.3.2). Absorption features of different neutral hydrogen Lyman transitions found at the same redshift have to be fitted simultaneously. Subsequently, the H I Ly α information has to be extracted by removing higher order Lyman series contamination. There is no simple way to perform such a procedure. It is already complicated for metal absorption features (see §2.3) and these are much rarer than the absorption features due to neutral hydrogen.

The rest-frame wavelength $\lambda_{\text{r,Ly}}^{\text{H}_1}$ of each Lyman transition can be computed by inserting integer values $n \geq 2$ into Rydberg's formula for the Lyman series

$$\lambda_{\text{r,Ly}}^{\text{H}_1} \simeq 912 \text{ \AA} \left(1 - \frac{1}{n^2}\right)^{-1}. \quad (2.1)$$

It can be seen from Eq. (2.1) that the relative difference of adjacent Lyman rest-frame wavelengths becomes smaller with larger n . This means that absorption-line blends due to higher order Lyman transitions mask H I Ly α absorption severely if the Lyman limit ($n \rightarrow \infty$) is approached. The small amount of additional spectral information blueward of the H I Ly β emission line regarding H I Ly α absorption does not justify the huge effort to account for higher order Lyman transitions in this spectral region. Hence, I used the H I Ly α forest from the H I Ly α emission line of a spectrum down to the corresponding H I Ly β emission line. This spectral region provides a fair amount of spectral coverage in order to investigate H I Ly α absorption features.

The Spectral Quasar Absorption Database (SQUAD) provided by Michael T. Murphy consists of 389 quasar spectra at various predetermined emission redshifts ($0 < z_{\text{em}} \lesssim 5$)

observed with the Ultraviolet and Visual Echelle Spectrograph (UVES, Dekker et al. 2000) at the Very Large Telescope (VLT) at the ESO Paranal Observatory. The data reduction procedure is summarized by Richter et al. (2011). The typical spectral resolution is $R \sim 45\,000$ while the signal-to-noise ratio (S/N) can vary significantly (see below).

Since in the literature a narrow downward deviation in the otherwise smooth redshift evolution of the effective optical depth is centered at $z \sim 3.2$, I chose this redshift as a lower limit of the emission redshifts for a subsample of SQUAD spectra. Since the precision measurement of $\tau_{\text{eff}}(z)$ in this work relies on profile fits to absorption features in quasar spectra which depend on estimates of the corresponding quasar continuum, the upper limit is set to $z_{\text{em}} = 4$. Above this redshift absorption-line blending becomes too severe to estimate the continuum reliably. The SQUAD provides 29 quasar spectra with the H_I Ly α emission line at redshifts $3.2 \lesssim z_{\text{em}} < 4$. Hence, the H_I Ly α forest covers the redshift range $2.55 \lesssim z < 4.00$. The lower redshift limit is due to the H_I Ly β absorption (see above). This redshift range is sufficiently large to see a narrow ($\Delta z \sim 0.3$) feature in the redshift evolution of the effective optical depth at $z \simeq 3.2$.

Partially, the quasar spectra exhibit spectral gaps, are of insufficient quality, do not exhibit H_I Ly α emission lines (from which I intended to redetermine the emission redshift), or contain DLAs. DLAs are usually accompanied by a large amount of metal absorption features at the same redshift and, hence, provide a great opportunity to identify metal transitions within the H_I Ly α forest. This is crucial in order to derive the effective optical depth from the observed flux. On the other hand, the line-fitting procedure used in this work (§2.3.2) does not work for the profile shape of DLAs, specifically the damping wings. Therefore, DLA-contaminated regions have to be excluded from the quasar spectra.

The final SQUAD subsample used in this thesis consists of 13 quasar spectra, which have appropriate spectral coverage for an analysis of the H_I Ly α forest, as well as exhibit the H_I Ly α emission line. This emission line is also used as a point of reference in the continuum fitting (§2.3.1).

Along a line of sight the UVB hardens if the background quasar is approached. Close to the background quasar the ionized fraction of neutral hydrogen is increased relative to the general IGM (the ‘proximity effect’, Bajtlik et al. 1988). This has to be accounted for in order to measure an unbiased $\tau_{\text{eff}}(z)$.

Two absorption lines at redshifts z_1 and z_2 , respectively, are separated in velocity (v) space by

$$\frac{\Delta v}{c} = \frac{z_2 - z_1}{\frac{z_2 + z_1}{2} + 1} \quad (2.2)$$

(Sargent et al. 1980), where c is the speed of light in vacuum. Identifying $z_2 = z_{\text{em}}$ and $z_1 = z$ close to the emission redshift, it follows

$$\frac{\Delta v}{c} \simeq \frac{z_{\text{em}} - z}{z_{\text{em}} + 1}. \quad (2.3)$$

The proximity region of a quasar can be defined in various ways (see Table 1.1). I chose $\Delta v = 5000 \text{ km s}^{-1}$ (Dall’Aglio et al. 2008) in Eq. (2.3) to identify $z = z_{\text{prox}}$ as the approximate boundary above which the quasar affects the IGM. Figure 2.1 illustrates the redshift coverage of the 13 quasar spectra used in this work.

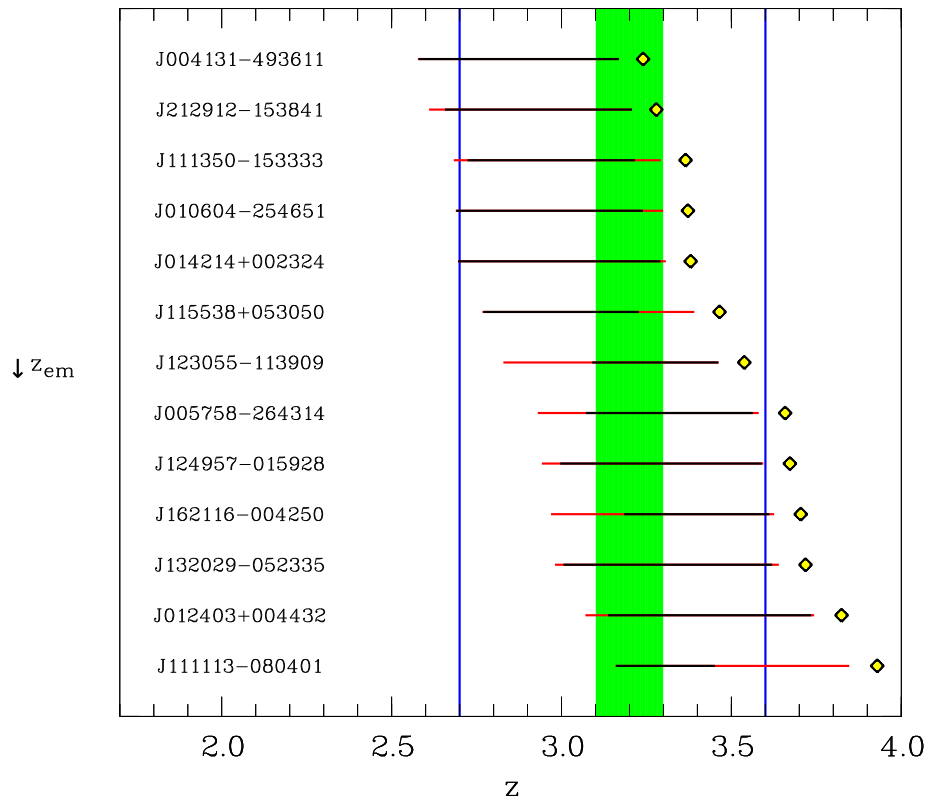


Figure 2.1. The 13 quasar spectra used in this work (J2000 names on the left) in increasing emission redshift from top to bottom (as indicated with the lozenge on the right-hand side). The green vertical band indicates the selection criterion for the quasar spectra in order to look for a deviation from a smooth power law of the redshift evolution of the effective optical depth. The horizontal lines mark the spectral range from the H I Ly β emission line to the proximity zone of the quasar in redshift space, with the black line denoting the spectral range used to analyze the H I Ly α forest (see Chapters 3 and 4). The blue vertical lines mark the bounds of the redshift range used in this work ($2.7 \leq z \leq 3.6$).

2.2 Discussion of quasar sightlines

In the following, the individual quasars and notable features of their spectra are discussed. In this context, the redshifts given for absorption systems are inconsistent across the spectra, sometimes denoting the strongest absorption component and sometimes the center of the absorption system. They may have to be redetermined if the systems are analyzed in more detail. For the purposes of this work the approximate absorption redshift is sufficient.

Metal absorption lines can best be identified by the occurrence of multiplets of the same ion and similar absorption features of different ions of the same species at the same redshift. Strong, saturated H I Ly α absorbers likely feature metal absorption and redward of the H I Ly α emission line of the quasar any absorption feature is due to metals. Line blending, especially with the H I Ly α forest, is a problem for the identification of metal absorption features.

The following overview may not be a complete summary of the features along each line of sight. The corresponding figures show the H I Ly α forest region (not the spectral fit) of

the respective quasar spectrum. The observed flux is displayed in arbitrary units (a.u.). The continuum estimate from cubic spline interpolation (see §2.3.1) is shown as a red solid line. The part of the H I Ly α forest that is used for the analysis in this work is shown in blue. In Table 2.1 S/N estimates for the quasar spectra at various observed wavelengths are listed.

2.2.1 J132029-052335

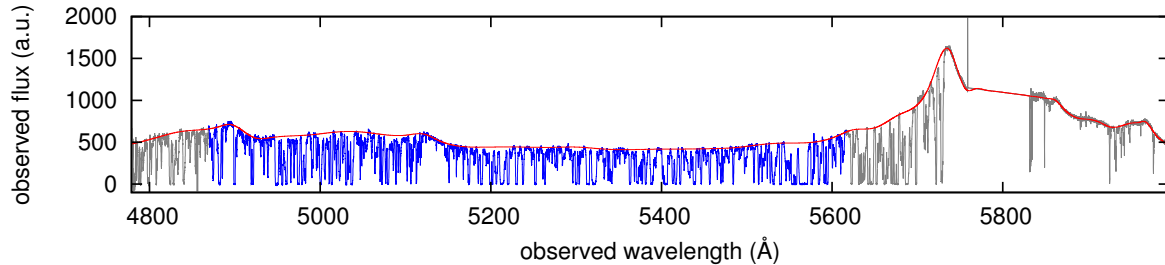


Figure 2.2. Absorption spectrum of the quasar J132029-052335. The analyzed H I Ly α forest is shown in blue. The red solid line represents the fitted continuum onto the spectrum.

The central wavelength of the H I Ly α and H I Ly β emission line is at $\lambda_{\text{obs}} \simeq 5735 \text{ \AA}$ and $\lambda_{\text{obs}} \simeq 4838.9 \text{ \AA}$, respectively. Hence, the emission redshift is at $z_{\text{em}} \approx 3.718$. The proximity effect is diminished at $z_{\text{prox}} \simeq 3.639$ ($\lambda_{\text{obs}} \simeq 5639.35 \text{ \AA}$). The spectrum shows spectral gaps in the observed wavelength ranges 4518 \AA to 4777 \AA and 5759 \AA to 5831 \AA . The first spectral gap limits the use of H I Ly β absorption components for comparison with the respective H I Ly α absorption features.

At low redshift strong Fe II and Mg II absorption features ($z \simeq 1.404$) are identified, as well as strong Fe II and weak Mn II absorption features at $z \approx 1.528$.

Various C IV and Si IV doublets are seen in the spectrum at redshifts $2.8 < z < 3.4$.

2.2.2 J162116-004250

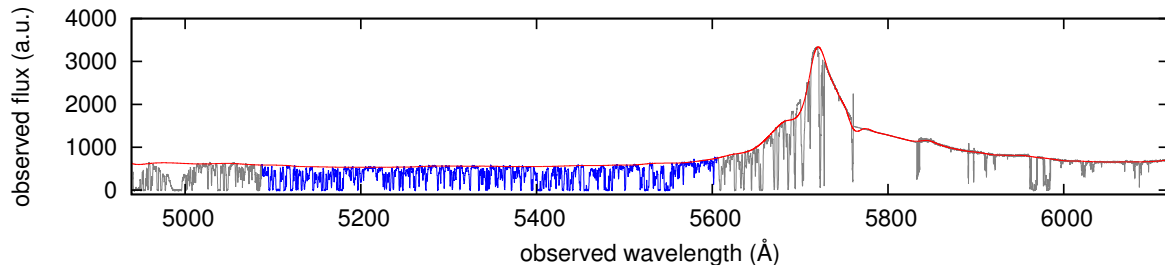


Figure 2.3. Absorption spectrum of the quasar J162116-004250. The analyzed H I Ly α forest is shown in blue. The red solid line represents the fitted continuum onto the spectrum.

The quasar emission redshift is $z_{\text{em}} \simeq 3.704$. The observed wavelengths for the respective transitions in H I Ly α and H I Ly β are $\lambda_{\text{obs}} \simeq 5718.5 \text{ \AA}$ and $\lambda_{\text{obs}} \simeq 4825 \text{ \AA}$. The proximity effect affects the spectrum down to $z_{\text{prox}} \approx 3.626$ ($\lambda_{\text{obs}} \simeq 5623.1 \text{ \AA}$). In this spectrum

Table 2.1. Signal-to-noise ratio per pixel for each quasar at different observed wavelengths in the spectrum.

QSO	z_{em}	λ (Å)	S/N
J004131-493611	3.240	4606	53
		4620	54
		4868	59
		5445*	31
J005758-264314	3.658	5010	44
		5955*	43
J010604-254651	3.372	4888	24
		4995	22
		5485*	25
J012403+004432	3.824	5366	25
		5500	27
		6145*	33
J014214+002324	3.380	5075	25
		5107	27
		5560*	28
J111113-080401	3.929	5257	22
		6195*	32
J111350-153333	3.365	5070	28
		5495*	37
J115538+053050	3.465	4878	20
		4883	21
		5569*	23
J123055-113909	3.538	5098	15
		5621*	25
J124957-015928	3.672	4874†	46
		5055†	48
		5740*	79
J132029-052335	3.718	5398	44
		5990*	47
J162116-004250	3.704	5283†	57
		6115*	67
J212912-153841	3.279	4490	84
		4977	124
		5414*	132

† Uncertain continuum level.

* Redward of the H I Ly α emission line.

spectral gaps are present at 4519 \AA to 4776 \AA and 5760.5 \AA to 5832.5 \AA . The first gap limits the use of the H I Ly β absorption features for comparison with the imprints on the spectrum of the respective H I Ly α transitions. The latter one is a spectral gap redward of the H I Ly α emission line.

The H I Ly α forest of this spectrum is cut blueward of $\lambda_{\text{obs}} \simeq 5086.9\text{ \AA}$ for the analysis due to the presence of a DLA at $z \simeq 3.106$ and strong Fe II absorption features ($z \approx 1.134$). The DLA exhibits C II, presumably blended C III, C IV, O I (two transitions can be seen, the probable third one would be completely blended), Si II, saturated Si III, and Si IV, which is partially cut off due to a spectral gap. The O I absorption features have not been recognized as such before the absorption-line fitting, so that one absorption feature that falls in the range of the H I Ly α forest has been interpreted as being due to H I Ly α . The components were fitted with Doppler parameters $b < 8\text{ km s}^{-1}$ and are therefore not taken into account for the analysis (see Chapters 3 and 4).

More imprints on this spectrum are due to absorption by Na I and Ca II at redshift $z = 0$, C IV in the range $2.8 < z < 3.4$ and two low-redshift absorbers. One of the two low-redshift absorbers is found at $z \approx 1.175$; Mg II absorption is evident and a thin Fe II absorption line is present at the same redshift. Other iron transitions are not seen within possible blends with the H I Ly α forest. The second low-redshift absorber ($z \approx 1.134$) shows very strong Mg II absorption, similarly complex Fe II absorption, and in comparison structurally very different Mg I absorption.

2.2.3 J212912-153841

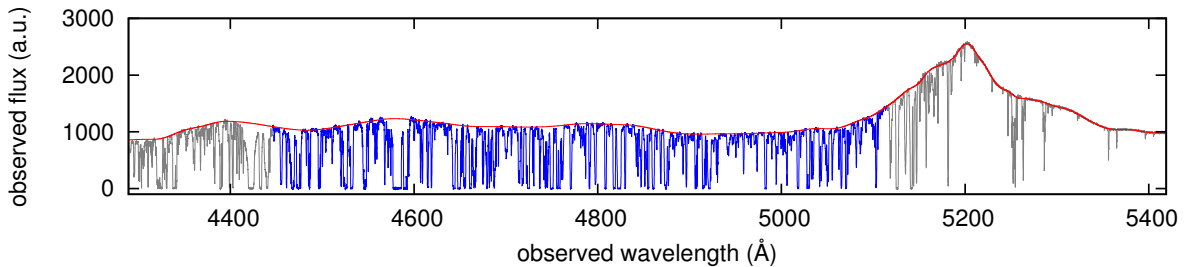


Figure 2.4. Absorption spectrum of the quasar J212912-153841. The analyzed H I Ly α forest is shown in blue. The red solid line represents the fitted continuum onto the spectrum.

The H I Ly α (H I Ly β) emission line is observed at approximately 5202 \AA (4389.2 \AA ; $z_{\text{em}} \simeq 3.279$). Blueward of $z_{\text{prox}} \approx 3.208$ ($\lambda_{\text{obs}} \simeq 5115.24\text{ \AA}$) the proximity effect of the quasar becomes negligible. The spectrum contains spectral gaps at $5604\text{ \AA} \lesssim \lambda_{\text{obs}} \lesssim 5672\text{ \AA}$ and $6658\text{ \AA} \lesssim \lambda_{\text{obs}} \lesssim 6692\text{ \AA}$. This sightline exhibits a lot of metal absorption features.

A strong absorber at $z \approx 2.769$ shows metal absorption of C II, probably saturated C III, C IV, an ambiguous N II absorption feature (though the structure is similar to those of other species at the same redshift and N II is the only ion found to explain the detected feature, a second transition may have left an imprint in the noisy part of the spectrum), O I (two transitions evident and one would be blended in the H I Ly α forest), O VI, Al II, Al III, Si II, Si III, Si IV, Fe II, and Ni II (two transitions are weak and one is marginal).

A DLA at $z \simeq 2.638$, which limits the redshift range of the analyzed H I Ly α forest, exhibits presumably C II (structure is saturated) with possible C IV in a spectral gap, Mg I,

Mg II, Al II, Al III, Si II, Si III, Si IV, Fe II, Ni II (all three transitions evident), and possibly O VI, though blended with absorption features of the H I Lyman series.

The detection of another absorber ($z \approx 2.023$) suffers from the spectral gaps in this spectrum. Though C II, C IV, Mg II, Si II with Si III presumably blended within a saturated spectral region, Si IV, and Fe II absorption features are seen, possible Mg I and Al III absorption features fall into the range of the spectral gaps. The respective Al II components have not been recognized during the absorption-line fitting, so that these absorption features were fitted as H I Ly α lines. However, the resulting Doppler parameters are $b < 10 \text{ km s}^{-1}$ and, thus, these absorption lines are disregarded for the analysis (see Chapters 3 and 4).

Additional absorption is due to Ca II and Na I at $z = 0$, as well as Si IV and C IV at redshifts $1.7 < z < 3.3$.

2.2.4 J004131-493611

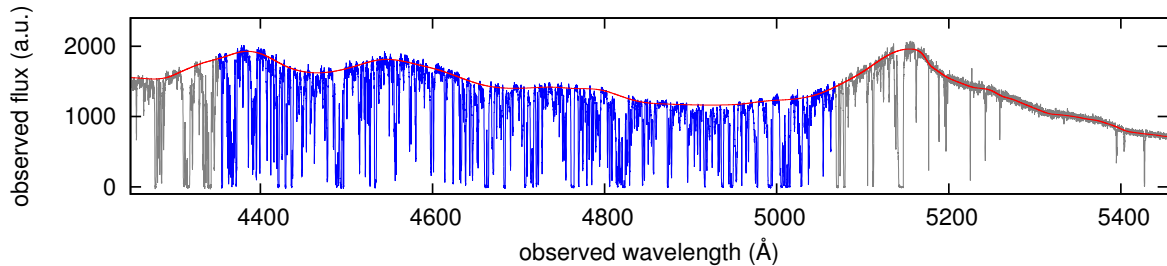


Figure 2.5. Absorption spectrum of the quasar J004131-493611. The analyzed H I Ly α forest is shown in blue. The red solid line represents the fitted continuum onto the spectrum.

This quasar emits at a redshift of $z_{\text{em}} \approx 3.24$ ($\lambda_{\text{obs, em}}^{\text{H I Ly}\alpha} \simeq 5155 \text{ Å}$, $\lambda_{\text{obs, em}}^{\text{H I Ly}\beta} \simeq 4349.5 \text{ Å}$). The upper limit of the observed wavelength range, within which the H I Ly α forest is not affected by the proximity effect of the quasar, is $\lambda_{\text{obs}} \simeq 5069 \text{ Å}$ ($z_{\text{prox}} \simeq 3.17$). The spectrum is incomplete in the range $5601 \text{ Å} < \lambda_{\text{obs}} < 5676 \text{ Å}$.

Several C IV doublets can be identified at redshifts $1.4 < z < 3.3$. Furthermore, three strong absorbers are detected, which exhibit various metal absorption features:

- ▶ $z \simeq 3.232$: C III, C IV, Si III, Si IV, N III, N V, O VI;
- ▶ $z \simeq 2.11$: blended C IV, Mg II, marginal Mg I, Al II, Al III, Si II, possibly blended Si III, Si IV, and Fe II;
- ▶ $z \simeq 1.497$: blended or saturated C IV, Mg I, Mg II, Al II, Al III, probably Si II (just one transition within the spectral range) and presumably Si IV (noisy region of the spectrum), Fe II, Mn II (three transitions), and it is also possible that all three Ni II transitions are seen in absorption, though their component structure is ambiguous.

At a redshift of $z \simeq 2.248$ a DLA exhibits C IV, Mg II, Al II, Al III, Si II (though most transitions contribute to blends), blended Si III, Si IV, Fe II, Cr II (three transitions), Mn II (two transitions are seen, although it is difficult to unambiguously detect the third one, which is either not present or lost in a data anomaly), marginal Ni II, possibly Zn II, probably C II, and possibly Mg I.

2.2.5 J012403+004432

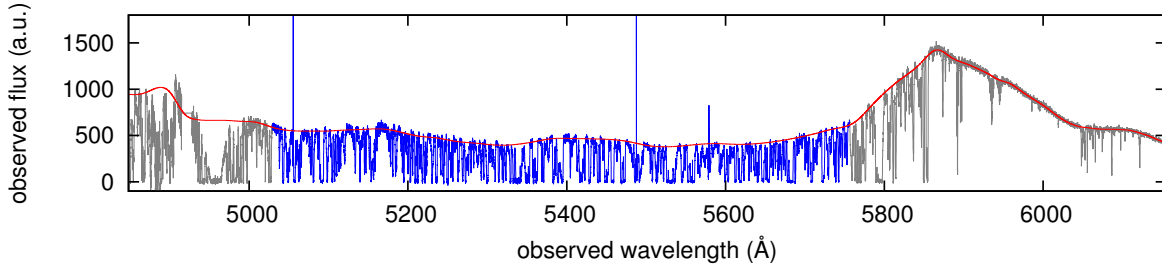


Figure 2.6. Absorption spectrum of the quasar J012403+004432. The analyzed H_I Ly α forest is shown in blue. The red solid line represents the fitted continuum onto the spectrum.

This spectrum exhibits the emission lines of H_I Ly α and H_I Ly β at $\lambda_{\text{obs}} \simeq 5865 \text{ \AA}$ and $\lambda_{\text{obs}} \simeq 4948.6 \text{ \AA}$, respectively, corresponding to a redshift of $z_{\text{em}} \approx 3.824$. The proximity to the quasar influences absorption features of the H_I Ly α forest down to $z_{\text{prox}} \simeq 3.744$ ($\lambda_{\text{obs}} \simeq 5767.2 \text{ \AA}$). Furthermore, the spectrum exhibits flux oscillations in the observed wavelength ranges $4799 \text{ \AA} < \lambda_{\text{obs}} < 4809.5 \text{ \AA}$, $4837.5 \text{ \AA} < \lambda_{\text{obs}} < 4850 \text{ \AA}$, and $4914.5 \text{ \AA} < \lambda_{\text{obs}} < 4928 \text{ \AA}$, though they are of minor importance.

The observed flux in this spectrum is diminished due to various C IV and Si IV absorption features at redshifts $2.8 < z < 3.7$, as well as partially suppressed due to the cut of the sightline through a DLA at redshift $z \simeq 3.078$ (close to the H_I Ly β emission line). Exhibited metal transitions by the DLA are rare: C IV, Si II, one transition of Fe II (other transitions are not within the covered spectral range), and probably C II.

2.2.6 J111113-080401

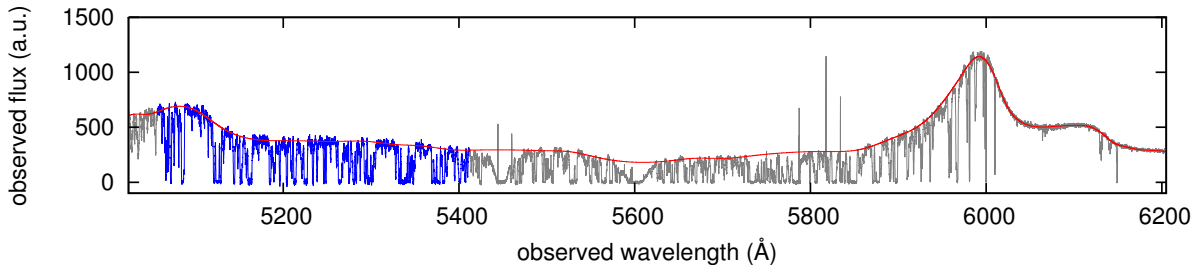


Figure 2.7. Absorption spectrum of the quasar J111113-080401. The analyzed H_I Ly α forest is shown in blue. The red solid line represents the fitted continuum onto the spectrum.

This spectrum exhibits hydrogen emission lines at redshift $z_{\text{em}} \simeq 3.929$ (e.g., H_I Ly α at $\lambda_{\text{obs}} \simeq 5992 \text{ \AA}$, H_I Ly β at $\lambda_{\text{obs}} \simeq 5055.8 \text{ \AA}$). The ultraviolet radiation from the quasar compared to the extragalactic background is negligible blueward of $\lambda_{\text{obs}} \simeq 5892.1 \text{ \AA}$ ($z_{\text{prox}} \simeq 3.847$).

The line of sight to the quasar J111113-080401 intersects two extragalactic structures, which appear as DLAs in the quasar's spectrum. Therefore, the spectrum is cut above $\lambda_{\text{obs}} = 5412 \text{ \AA}$ for the analysis. In the following the respective metal transitions exhibited by the DLAs are noted:

- ▶ $z \simeq 3.482$: C II, C IV, Al II, Si II, Si III, Si IV;
- ▶ $z \approx 3.608$: C II and by 100 km s^{-1} offset C IV (C III may be blended in a saturated part of the spectrum), N II (one transition seen, another one would reside in the noisy part of the spectrum), maybe O I (one transition blended with Si II at a different redshift and one transition presumably blended within the H I Ly α forest), Al II, Si II, Si III, Si IV (offset by 100 km s^{-1}), Fe II (one transition in the spectral range).

Another absorber at $z \approx 3.761$ features C II, C III, C IV, Al II, Si II, Si IV, and possibly blended Si III.

More absorption features due to C IV and Si IV are found at redshifts $2.9 < z < 3.9$.

2.2.7 J005758-264314

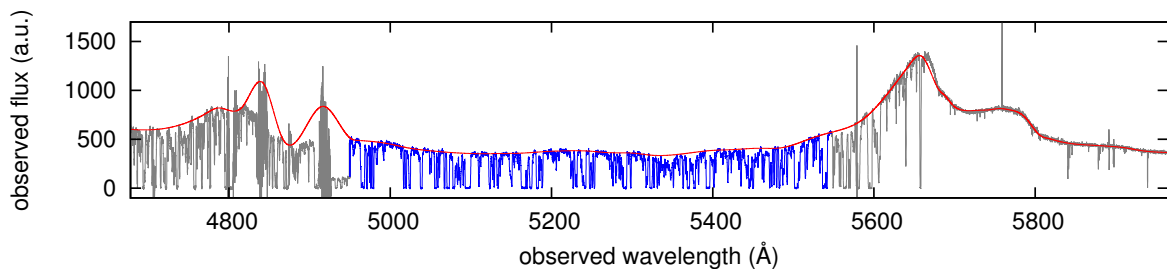


Figure 2.8. Absorption spectrum of the quasar J005758-264314. The analyzed H I Ly α forest is shown in blue. The red solid line represents the fitted continuum onto the spectrum.

Important emission features of the quasar are the H I Ly β line at $\lambda_{\text{obs}} \simeq 4778.2 \text{ Å}$, the onset of the proximity zone at $\lambda_{\text{obs}} \simeq 5568.6 \text{ Å}$ ($z_{\text{prox}} \approx 3.581$) and the H I Ly α line at $\lambda_{\text{obs}} \simeq 5663 \text{ Å}$ ($z_{\text{em}} \simeq 3.658$). Parts of the spectrum exhibit flux oscillations of a typical width of $\Delta\lambda_{\text{obs}} \approx 10 \text{ Å}$ ($4797 \text{ Å} - 4810 \text{ Å}$, $4836 \text{ Å} - 4847 \text{ Å}$, $4912.5 \text{ Å} - 4924 \text{ Å}$). Therefore, the spectrum is cut below $\lambda_{\text{obs}} = 4950 \text{ Å}$ for the analysis.

Low-redshift absorbers and their metal transitions are listed here:

- ▶ $z \approx 0.566$: Mg I, Mg II, Fe II;
- ▶ $z \approx 1.268$: C IV, Si II (only one transition in the spectral range), Si IV (doublet in a very noisy part of the spectrum), Mg I, Mg II, Fe II, Al III, and presumably blended Al II;
- ▶ $z \simeq 1.319$: C IV, marginal Mg I, Mg II, Al II, marginal Al III (one transition probably blended), Fe II;
- ▶ $z \approx 1.534$: Mg I, Mg II, a single clear Si II transition, Fe II and Mn II (three transitions).

Strong C IV absorption can be seen at $z \simeq 3.192$, accompanied by strong hydrogen absorption and Si IV. The corresponding Si III is presumably blended.

More C IV absorption features are detected at $2.6 < z < 3.7$.

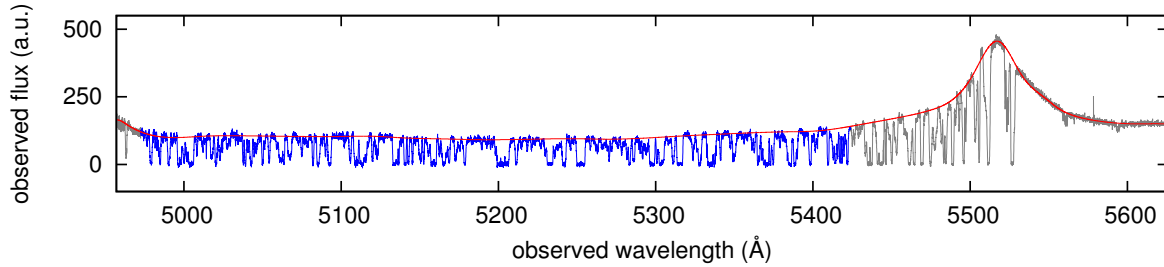


Figure 2.9. Absorption spectrum of the quasar J123055-113909. The analyzed H I Ly α forest is shown in blue. The red solid line represents the fitted continuum onto the spectrum.

2.2.8 J123055-113909

The important range of this spectrum for the analysis of the H I Ly α forest is $\lambda_{\text{obs}} \simeq 4655 \text{ \AA}$ (H I Ly β emission line) to $\lambda_{\text{obs}} \simeq 5425 \text{ \AA}$ (onset of the proximity effect, $z_{\text{prox}} \simeq 3.463$). The emission redshift is $z_{\text{em}} \simeq 3.538$, estimated from the H I Ly α emission line ($\lambda_{\text{obs}} \simeq 5517 \text{ \AA}$). Spectral gaps are present at $\lambda_{\text{obs}} \simeq 4523.5 \text{ \AA}$ to $\lambda_{\text{obs}} \simeq 4778.5 \text{ \AA}$ (making the comparison of H I Ly β to H I Ly α absorption in this spectral range impossible) and at $\lambda_{\text{obs}} \simeq 5760 \text{ \AA}$ to $\lambda_{\text{obs}} \simeq 5834 \text{ \AA}$. The spectrum also exhibits flux oscillations in the ranges $\lambda_{\text{obs}} \simeq 4837 \text{ \AA}$ to $\lambda_{\text{obs}} \simeq 4848 \text{ \AA}$ and $\lambda_{\text{obs}} \simeq 4914 \text{ \AA}$ to $\lambda_{\text{obs}} \simeq 4928 \text{ \AA}$. Due to these spectral flaws the spectrum is cut below $\lambda_{\text{obs}} \simeq 4972.6 \text{ \AA}$ for the analysis.

This line of sight does not intersect absorbers with identified metals, except for a few, which exhibit C IV absorption features redward of the H I Ly α emission line of the quasar at redshifts $3.2 < z < 3.4$.

2.2.9 J010604-254651

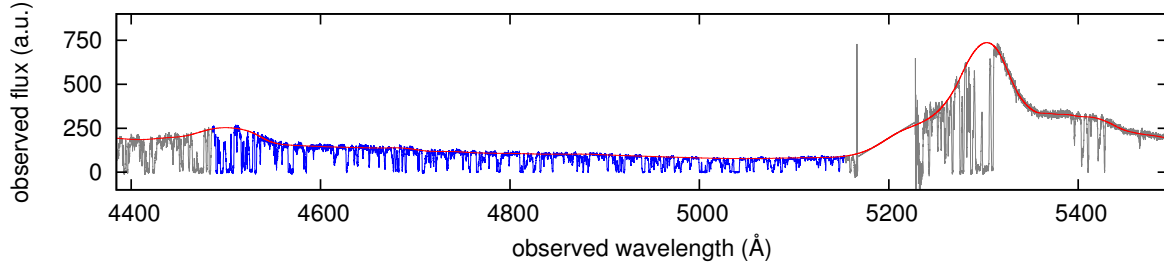


Figure 2.10. Absorption spectrum of the quasar J010604-254651. The analyzed H I Ly α forest is shown in blue. The red solid line represents the fitted continuum onto the spectrum.

Blueward of the H I Ly α emission line ($\lambda_{\text{obs}} \simeq 5315 \text{ \AA}$, $z_{\text{em}} \simeq 3.372$) the proximity effect becomes negligible at $z_{\text{prox}} \simeq 3.299$ ($\lambda_{\text{obs}} \simeq 5226.3 \text{ \AA}$). This means a separation in redshift of $\Delta z \simeq 0.61$ to the H I Ly β emission line ($\lambda_{\text{obs}} \simeq 4484.5 \text{ \AA}$). A spectral gap in this spectrum is present in the range $5167 \text{ \AA} \lesssim \lambda_{\text{obs}} \lesssim 5228 \text{ \AA}$, which limits the redshift range of the H I Ly α forest for the analysis in this work.

A low-redshift absorber at $z \approx 0.974$ features Mg I, Mg II, and Fe II absorption. Unfortunately, this absorber was not considered during the line fitting. One of its Fe II absorption features is blended with one transition of Si IV at a different redshift ($\lambda_{\text{obs}} \approx 4703 \text{ \AA}$)

and was fitted as such. This influenced the line fit of the single H I Ly α absorber at $\lambda_{\text{obs}} \simeq 4734.3 \text{ \AA}$, blended with the second Si IV transition of the doublet. The uncorrected fit parameters for the H I Ly α absorber are $\log N = 13.818$ and $b = 39.918 \text{ km s}^{-1}$; they are too low. Since this is only one single absorption line, the erroneous values are statistically insignificant. The Fe II absorption features from other transitions are detected in the H I Ly α forest and have been misinterpreted as being due to H I Ly α . The corresponding Doppler parameters are all lower than $b = 9 \text{ km s}^{-1}$ and, therefore, these absorption lines are anyhow accounted for for the analysis (see Chapters 3 and 4).

This spectrum also contains a single component C IV doublet at $z \approx 2.124$, which was identified after the line fitting was concluded. Hence, the doublet has been fitted as H I Ly α by mistake, but the Doppler parameters are smaller than $b = 5 \text{ km s}^{-1}$ and, hence, disregarded for the analysis. The C IV doublet is probably accompanied by Si IV absorption, though the Si IV doublet structure is ambiguous. Nevertheless, this Si IV absorption resides blueward of the H I Ly β emission line and is, therefore, not relevant for the analysis.

Two high-redshift absorbers at $z \simeq 3.356$ and $z \simeq 3.362$, respectively, exhibit N V and marginal N III (N IV does not lie within the covered spectral range), as well as Si III and Si IV detections.

Another absorber at redshift $z \simeq 2.245$ exhibits C II, Si IV, and Al III. Also, absorption features due to Si II (limited spectral range) and Al II (blended) are probably detected. If C IV is present in this absorber it was not accounted for during the line fitting. However, some of the possible components are nevertheless discarded for the analysis due to the small b values.

2.2.10 J014214+002324

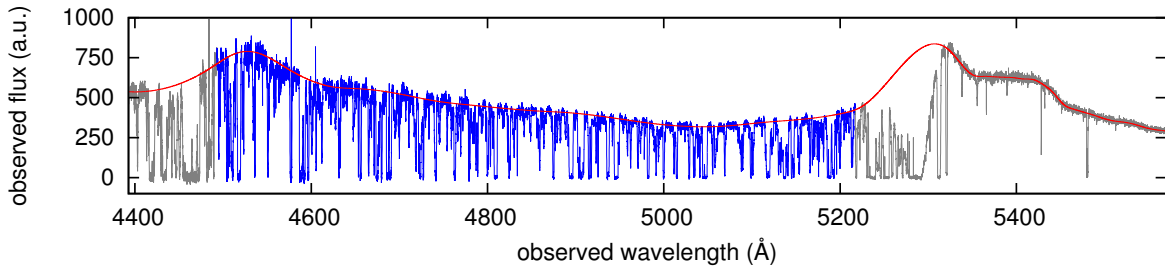


Figure 2.11. Absorption spectrum of the quasar J014214+002324. The analyzed H I Ly α forest is shown in blue. The red solid line represents the fitted continuum onto the spectrum.

The emission redshift of the quasar is $z_{\text{em}} \simeq 3.38$, corresponding to an observed wavelength of $\lambda_{\text{obs}} \simeq 5325 \text{ \AA}$ ($\lambda_{\text{obs}} \simeq 4493 \text{ \AA}$) for the H I Ly α (Ly β) emission line and a proximity effect limit of $z_{\text{prox}} \simeq 3.307$ ($\lambda_{\text{obs}} \simeq 5236.2 \text{ \AA}$). The spectrum exhibits a spectral gap in the range $\lambda_{\text{obs}} \simeq 5760 \text{ \AA}$ to $\lambda_{\text{obs}} \simeq 5835 \text{ \AA}$.

An absorber at $z \simeq 3.377$, close to the H I Ly α emission line of the quasar, is evident within the covered spectral range in neutral hydrogen (Ly α , Ly β , and Ly γ), but not in any metal transitions.

An absorber at $z \approx 2.675$ exhibits C IV, Al II, Si II, and, if at all, blended Si III and blended

Si IV within the $\text{H I Ly}\alpha$ forest.

Two blended absorption features exhibit a similar metal content. The absorber at $z \approx 3.306$ exhibits presumably C II and C III , C IV , presumably N II and N III , Si II , Si III , and Si IV . The absorber at $z \approx 3.31$ exhibits maybe C II and C III , definitely C IV , presumably N II and N III , N V , Si II , Si III , and Si IV .

At $z \approx 3.347$, a DLA exhibits C II , possibly blended C III , C IV , presumably O I (though two of three transitions are blended), Al II , Si II , probably saturated Si III , and Si IV .

Various absorption features of Si II , Si IV , and C IV can be found redward of the $\text{H I Ly}\alpha$ emission line at redshifts $2.6 < z < 3.4$.

2.2.11 J111350-153333

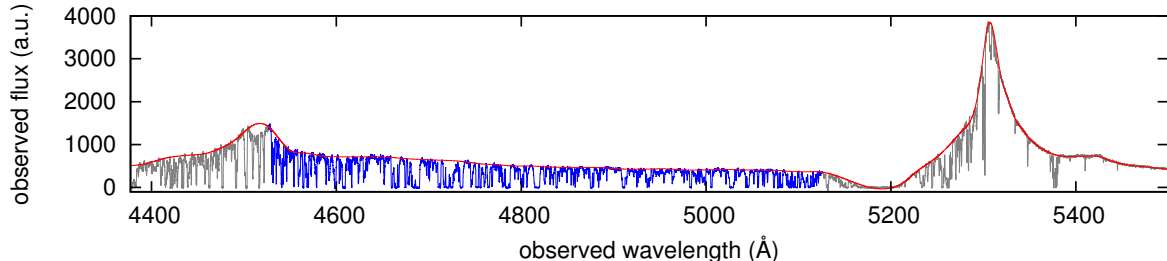


Figure 2.12. Absorption spectrum of the quasar J111350-153333. The analyzed $\text{H I Ly}\alpha$ forest is shown in blue. The red solid line represents the fitted continuum onto the spectrum.

The $\text{H I Ly}\alpha$ ($\text{Ly}\beta$) emission line is redshifted to $\lambda_{\text{obs}} \approx 5307 \text{ Å}$ ($\lambda_{\text{obs}} \approx 4477.8 \text{ Å}$; $z_{\text{em}} \approx 3.365$). The proximity effect must be considered redward of $\lambda_{\text{obs}} \approx 5218.5 \text{ Å}$ ($z \approx 3.293$). A spectral gap is apparent in the range $5600 \text{ Å} \lesssim \lambda_{\text{obs}} \lesssim 5674 \text{ Å}$.

Two low-redshift absorbers at $z \approx 0.817$ and $z \approx 1.039$, respectively, exhibit absorption features of Mg II and Fe II . The latter system contains also Mg I . If Mg I absorption of the first low-redshift absorber would be present, it is blended with a DLA at a different redshift. This DLA at $z \approx 3.267$, which limits the analyzed spectral range of the $\text{H I Ly}\alpha$ forest to blueward of $\lambda_{\text{obs}} \approx 5125.4 \text{ Å}$, exhibits (within the spectral range) C II , ambiguous C III , C IV , O I (two transitions are seen, a third falls into the $\text{H I Ly}\beta$ range of the DLA), Al II , ambiguous Si I , Si II , ambiguous Si III , Si IV , and a single Fe II transition.

A complex absorber at redshift $z \approx 2.963$ features C II , C IV , Si II , Si III , and Si IV . Similar species are detected for an absorber at $z \approx 3.136$, except for singly ionized carbon and silicon.

The spectral gap denies the check on Si IV transitions at redshift $z \approx 3.039$. At this redshift C III and C IV are evident, but the detection of Si III is tentative since other silicon transitions are absent.

Plenty of absorption features redward of the $\text{H I Ly}\alpha$ emission line of the quasar can be ascribed to C IV and Si IV absorbers at redshifts $2.7 < z < 3.3$.

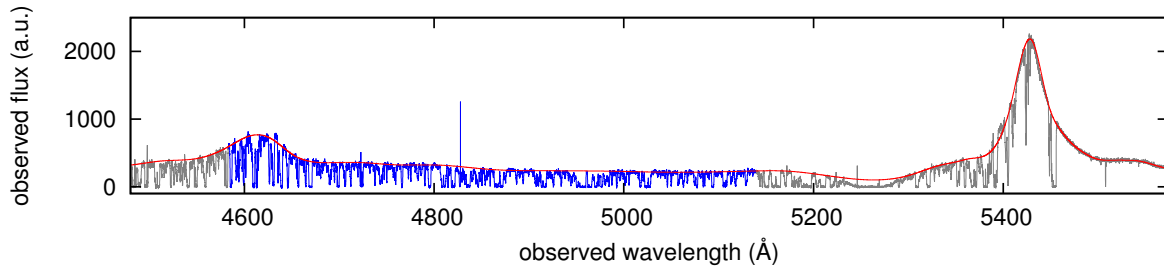


Figure 2.13. Absorption spectrum of the quasar J115538+053050. The analyzed H I Ly α forest is shown in blue. The red solid line represents the fitted continuum onto the spectrum.

2.2.12 J115538+053050

The hydrogen emission lines of the quasar are redshifted ($z_{\text{em}} \approx 3.465$) to $\lambda_{\text{obs}} \simeq 5427.4$ Å (H I Ly α) and $\lambda_{\text{obs}} \simeq 4579.4$ Å (H I Ly β). The proximity effect is expected to be important down to $z_{\text{prox}} \simeq 3.39$ ($\lambda_{\text{obs}} \simeq 5336.9$ Å). In the wavelength range $\lambda_{\text{obs}} \simeq 5600$ Å to $\lambda_{\text{obs}} \simeq 5675$ Å the spectrum exhibits a spectral gap.

Numerous C IV and Si IV absorption features can be identified redward of the H I Ly α emission line at redshifts $2.8 < z < 3.5$.

A DLA is detected at $z \approx 3.327$ and exhibits saturated C II, possibly C III (if present, it is blended or strongly saturated), C IV, strong Al II, Al III, saturated Si II, Si III, less prominent Si IV, and Fe II (though only one transition lies within the covered spectral range). Ni II may also be detected but the observed wavelength of two of three available transitions falls into the spectral gap. The spectrum is cut above $\lambda_{\text{obs}} \simeq 5138.7$ Å for the analysis due to the influence of the DLA at higher observed wavelength.

A C IV doublet at $z \approx 2.034$ was identified after the line fitting was concluded and has been regarded by mistake as H I Ly α absorption lines during the line fitting. Due to the small Doppler parameters, these lines are anyway not considered for the analysis in this work. Neither other ions nor atoms are seen in absorption at this redshift.

2.2.13 J124957-015928

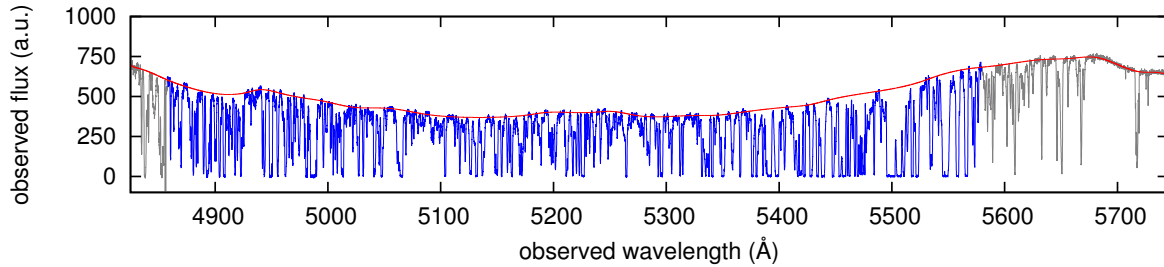


Figure 2.14. Absorption spectrum of the quasar J124957-015928. The analyzed H I Ly α forest is shown in blue. The red solid line represents the fitted continuum onto the spectrum.

This spectrum exhibits the H I Ly α emission line at $\lambda_{\text{obs}} \simeq 5680$ Å corresponding to an emission redshift of $z_{\text{em}} \simeq 3.672$. This places the H I Ly β emission line at $\lambda_{\text{obs}} \simeq 4792.5$ Å. The proximity effect of the quasar is taken into account redward of $z_{\text{prox}} \approx 3.594$ ($\lambda_{\text{obs}} \simeq$

5584.3 \AA). The spectral gap in the range $\lambda_{\text{obs}} \simeq 4518.5\text{ \AA}$ to $\lambda_{\text{obs}} \simeq 4776.5\text{ \AA}$ limits the use of H I Ly β absorption and hinders metal identifications.

Besides Na I at redshift $z = 0$ and a few Si IV absorption features at redshifts $3.4 < z < 3.5$, an extragalactic absorber at $z \simeq 3.102$ is detected, which exhibits C II, C IV, Si II, presumably saturated Si III, Si IV, and Fe II.

2.3 Fitting procedures

The main goal of this work is to measure the effective optical depth of hydrogen from quasar spectra. A quasar spectrum exhibits absorption features caused by various chemical elements (neutral species and ions). Gaining information about the amount of absorption ascribed to hydrogen only is a challenging task. The metal contribution to the absorption in the H I Ly α forest can be estimated (Tytler et al. 2004) or determined directly (Kim et al. 2007). Both methods have their disadvantages. An estimate depends on the underlying assumptions and may not be accurate; and the direct metal-absorption-line identification is imperfect since metal absorption features may be missed due to absorption-line blending or insufficient spectral coverage of a quasar spectrum. In this work, metal absorption features are removed with a direct approach. This means all the metal absorption features within the spectrum at various redshifts have to be identified and sorted out.

In general, saturated H I Ly α absorption features are likely accompanied by metal absorption (Songaila and Cowie 1996). High-column-density hydrogen absorbers such as LLSs and DLAs most certainly exhibit metal absorption. Since the rest-frame wavelength of metal transitions is often larger than that of H I Ly α , metal absorption lines can be observed in quasar spectra, although hydrogen absorption at the same redshift does not fall into the observed spectral range. Hence, it is important to identify metals directly, which is easiest redward of the H I Ly α emission line where only metal absorption is seen.

The removal of metal absorption is quite complicated due to line blending. Masking metal absorption features is a common method (Janknecht et al. 2006; Kim et al. 2007; Faucher-Giguère et al. 2008b). The masking has a crucial disadvantage. It is difficult to apply to metal absorption features which are blended with H I Ly α absorption lines. Removing the masked spectral region will then remove information about the hydrogen flux decrement.

In this work, instead of masking identified absorption lines, their influence on the H I Ly α opacity is removed by spectral fitting (Kim et al. 2007). Spectral fitting mimics the quasar flux using a superposition of profile functions. Each profile function is assumed to represent a single absorption component. This assumption is not ideal since it suggests that absorbers are distinct entities rather than density fluctuations in the IGM. However, the advantage of this procedure is the possibility to remove single profiles from the model, leaving a spectrum only with the desired species. A critical point may be the loss of noise information after the line-fitting procedure has been applied. Its significance can be estimated by comparing the effective optical depth measured from the model flux with the measurement using the observed spectrum.

In order to fit absorption lines in a spectrum, the continuum flux emitted by the quasar must be known. The continuum estimation and the line fitting can be performed simul-

taneously with the program CANDALF (§2.3.2). However, this process is rather difficult to perform consistently across a whole spectrum since a spectrum usually exhibits too many absorption features to be handled by CANDALF within a sole run. Therefore, the spectrum has to be split into several sections. Determining the sections conveniently is a time-consuming process. They have to be chosen in advance and, subsequent to the fitting procedure, the continuity of the continuum from adjacent sections has to be evaluated. Possibly, the sections have to be refined and refitted for a reasonable continuum estimate.

A spectrum normalized in advance can be treated more easily and precisely with CANDALF. Hence, a program to estimate the continuum of a spectrum independently of the spectral fit is used. I will refer to this program as FITQSOSPLINE. In §2.3.1 the specifications of FITQSOSPLINE as given in the program's preamble are outlined. In §2.3.2 the spectral fit with CANDALF will be described in detail. The line-fitting results are presented in §2.3.3.

2.3.1 FITQSOSPLINE

The program FITQSOSPLINE has been provided by G. Worseck and A. Dall'Aglio. It is used to compute the quasar continuum by cubic spline interpolation of continuum regions without absorption. The used algorithm is based on Young et al. (1979) and Carswell et al. (1982).

The flux decrement of a background quasar's continuum emission due to intervening absorbers is larger blueward of the H I Ly α emission line than redward. The use of FITQSOSPLINE offers the possibility to treat the spectrum as two distinct parts with the emission redshift of the quasar as necessary point of reference.

In general, a quasar continuum can be described as a power law and additional emission line features. The trend of the continuum is different for each quasar. With FITQSOSPLINE a spectrum is split into equidistant sections. In each section a cubic spline is fitted to represent the continuum flux and separate splines are connected smoothly via shared knots between next neighbours.

The cubic spline interpolation is, amongst other parameters, dependent on the initial number of pixels per section. The input of FITQSOSPLINE comprises an initial number of pixels for both the spectral part blueward of the H I Ly α emission line of the quasar and redward. In each section pixels assigned to potential absorption features are neglected. This is an iterative process. The pixel farthest from the mean flux is removed with each iteration until either the average noise in the section exceeds the flux standard deviation or the remaining pixel number drops below a predetermined value. The latter is necessary in the presence of strong absorption. In the H I Ly α forest only pixels below the mean flux are affected, accounting for frequent absorption. Since redward of the H I Ly α emission line absorption features are rare, in this part of the spectrum pixels are removed below and above the mean.

Subsequently, the size of sections within the H I Ly α forest is halved if the slope between corresponding spline knots exceeds a given value. This foremost affects the continuum fit to emission line wings. Afterwards the spline knots are determined again. Also, pixels associated with spikes in the spectrum (upward flux excesses) are removed from the respective section if they deviate from the remaining pixels by more than 2σ .

The smoothing of the continuum is applied by comparing flux values from three adjacent sections at a time. If the flux of the central section is lower than a predefined amount of each of the adjacent sections, the central section is neglected. In the case of comparable flux of the adjacent sections (within 5 %), their mean flux is used instead.

On the remaining data the cubic spline interpolation is performed. In order to determine the continuum for a quasar spectrum, I adjusted the initial number of pixels per section and the selection threshold for the remaining pixels. Figures showing all quasar spectra used in this work and their continua can be found in §2.2. No other parameters are varied for the continuum estimation besides the emission redshift and the aforementioned numbers of pixels.

2.3.2 CANDALF

The profile-fitting routine CANDALF has been written by Robert Baade. It uses the Levenberg-Marquardt algorithm in order to fit a spectrum by applying non-linear least squares. The required profile functions to fit the absorption features are of Doppler shape (Eq. 1.24). The computed spectrum is convolved with a Gaussian, $P(\lambda)$, of width $\text{FWHM} = \lambda/R$, where λ denotes the wavelength and R the resolution of the spectrum. Therefore, the spectral resolution R of the data has to be known. The convolution takes into account the broadening of absorption lines due to the instrument, this means the line spread function.

In order to fit a spectrum, an initial guess of the parameters of the individual absorption lines (redshift z , Doppler parameter b , and column density N) and of the continuum is required (see below). The continuum is estimated locally as a Legendre polynomial up to fourth order.

An advantage of CANDALF with respect to other line-fitting programs is that the continuum and the line parameters are estimated simultaneously. However, the simultaneous fitting is a time-consuming process if a total H I Ly α forest, with $\sim 10^3$ absorption features at high redshift, is fitted. Therefore, I used FITQSOSPLINE to determine the quasar continua (see §2.3.1). In order to reduce the computation time, the program runs with CANDALF were done with a constant continuum of value 1 using the normalized spectra. This allows for choosing spectral sections for the fitting with regard to absorption features only and considerably shortens the time necessary to set up the fitting procedure.

One disadvantage of CANDALF is that only Doppler profiles are fitted. In general, an absorption line is best modeled by a Voigt profile, i.e., the convolution of a Lorentz profile, which represents the natural line broadening and broadening due to particle collisions, and a Doppler profile, which takes into account the particle motions. The Doppler profile outlines the core of an absorption line, while the Lorentz profile accounts for the damped absorption line wings. Apparently, DLA profiles are dominated by the damping wings. Though, for the majority of absorption features in the H I Ly α forest the Lorentz profile can be neglected. As mentioned above, using CANDALF relies on this approximation, i.e., the shape of DLAs cannot be fitted appropriately with this program. Therefore, I skipped DLA-contaminated regions of the quasar spectra for the analysis.

The optical depth of an absorption line (Eq. 1.21) is proportional to the integral of its profile function times the volume number density of the particles within the absorber along

the line of sight through the absorber. Equation (1.25) follows from local integration and can be expressed in terms of wavelength, $\lambda = c/\nu$,

$$\tau(\lambda_r) = \frac{1}{4\sqrt{\pi}} \frac{e^2}{\epsilon_0 m_e} \frac{\lambda_c f N}{cb} \exp \left[- \left(\frac{c}{b} \cdot \frac{\lambda_r - \lambda_c}{\lambda_c} \right)^2 \right], \quad (2.4)$$

where the quantities are the same as defined in §1.5.2. In an expanding Universe the exponential function of Eq. (2.4) changes to account for the redshift, z , of the absorption line of a species with rest-frame wavelength λ_0 ,

$$\tau(\lambda_{\text{obs}}) = \frac{1}{4\sqrt{\pi}} \frac{e^2}{\epsilon_0 m_e c} \frac{\lambda_0 f N}{b} \exp \left[- \left(\frac{c}{b} \cdot \frac{\lambda_{\text{obs}} - \lambda_{c,\text{obs}}}{\lambda_{c,\text{obs}}} \right)^2 \right], \quad (2.5)$$

where $\lambda_{c,\text{obs}}/\lambda_0 = 1 + z = \lambda_{\text{obs}}/\lambda_r$. Using Eq. (1.4) and considering the line broadening due to the instrument (see above), the observed flux $f(\lambda_{\text{obs}})$ is

$$f(\lambda_{\text{obs}}) = f_{\text{cont}}(\lambda_{\text{obs}}) \cdot e^{-\tau(\lambda_{\text{obs}})} \otimes P(\lambda_{\text{obs}}), \quad (2.6)$$

where $f_{\text{cont}}(\lambda_{\text{obs}})$ is the continuum flux.

Hence, for a given species (rest-frame wavelength λ_0 , oscillator strength f) and initial guesses on the observed central wavelength, $\lambda_{c,\text{obs}}$, column density, N , and Doppler parameter, b , the output of CANDALF comprises the best-fit parameters for an absorption line. Besides an absorption-line list with the adjusted parameters, including also the corresponding redshift, z , and the equivalent width, and their respective errors, the fit of the spectral section is put out. It is convenient to put in the resulting parameters again to check for convergence. Although addressing single absorption lines as input for CANDALF is more time consuming than the use of automatic line-fitting programs, its advantage is the precise knowledge of the absorption-line parameters of any species identified in the H I Ly α forest.

With CANDALF it is also possible to fit absorption lines interdependently, i.e., with the same redshift, column density, and Doppler parameter. This is useful for doublets such as C IV, Si IV, Al III, and others. Line blending makes the determination of absorption-line parameters difficult, but coupling transitions of an ion leads to a more accurate estimate of the parameters and may even reveal blended absorption features of another species (e.g., decomposing hydrogen absorption features from spectral imprints of metals). Interdependent absorption-line fitting could in principle also be used to determine the line parameters of H I Ly α absorption features more precisely by taking into account the corresponding H I Ly β transition, and higher orders of the Lyman series.

For technical details of the line-fitting procedure with CANDALF see Appendix B.

2.3.3 Results of the line-fitting procedure with CANDALF

In this section an overview of the fitting results is given with regard to the absorption-line parameters using the program CANDALF. A visual representation of the fitted quasar spectra can be found in Appendix D.

The line-fitting procedure with CANDALF of 13 high-resolution quasar spectra resulted

in 7491 absorption lines. To reach convergence, it is occasionally (for a few percent of all fitted absorption lines) necessary to fix one or more parameters of an absorption line. For all intents and purposes this is not desirable since anything can be fitted this way without implying reasonable properties of an absorber. Once the fit converges with fixed parameters, it may be possible to release these parameters again for further iterations. The line-fitting procedure performed in this work led to parameters kept fixed for 4 % of all fitted absorption lines (see also Appendix B). Any absorption line that has fixed parameters has at least a fixed Doppler parameter. Out of the total 298 fixed-parameter absorption lines, 285 (96 %) have Doppler parameters of $b \leq 2 \text{ km s}^{-1}$. In the case of H I Ly α absorption lines these are likely due to noise, missed metals, and saturation effects. It is not likely that the fixed-parameter absorption lines affect the statistical analysis considering the overall amount of absorption lines. Another 505 absorption lines are due to identified metals. Their Doppler parameter distribution is shown in Fig. 3.1.

Altogether, the line-fitting procedure with CANDALF resulted in 6688 fitted absorption lines due to H I Ly α without any fixed parameters. The absorption lines with $b > 10 \text{ km s}^{-1}$ are listed in Appendix E. An analysis of the line parameters is presented in the next chapter.

Chapter 3

H I Ly α forest statistics

The main result of this thesis, concerning the H I Ly α opacity, is presented in Chapter 4. In this chapter, the distributions of absorption-line parameters are analyzed. This analysis comprises the column-density distribution (§3.1), the Doppler-parameter distribution (§3.2), the $b(N)$ distribution (§3.3), and the number-density evolution (§3.4).

The most time-consuming part of this thesis has been the absorption-line fitting procedure. I have fitted in total 7491 individual absorption lines using the line-fitting program CANDALF (see §2.3). In some regions of the fitted quasar spectra absorption lines have been fitted with fixed line parameters in order to reach convergence with CANDALF. These lines are of insignificant number and most of them have small Doppler parameters ($b \leq 2 \text{ km s}^{-1}$; see §2.3.3). Their impact on the line parameters of the other fitted absorption features should be negligible. Excluding the fixed-parameter absorption lines from the total line sample leaves 7193 lines for absorption-line statistics. Throughout this chapter, further references to fitted absorption lines will only be made to the sample comprising these 7193 absorption lines with freely iterated parameters (505 identified metal absorption lines and 6688 lines due to H I Ly α).

Narrow H I Ly α absorption lines, $b < 15 \text{ km s}^{-1}$, can usually be attributed to metal transitions, noise, or line blending (Lu et al. 1996; Rauch et al. 1997). Figure 3.1 shows the Doppler-parameter distribution of the metal absorption lines identified in the 13 quasar spectra used in this work¹. The b distribution peaks at $\sim 5 \text{ km s}^{-1}$ and declines rather steeply down to 16 km s^{-1} with a flat tail at larger Doppler parameters. From Fig. 3.1 it seems reasonable to assume that the majority of metal absorption lines has Doppler parameters $b \lesssim 15 \text{ km s}^{-1}$.

The Doppler parameter, b , has a thermal contribution, b_{th} , a turbulent contribution, b_{nt} , including all non-thermal processes (e.g., particle collisions), and a contribution from the Hubble expansion, b_{Hubble} , if the absorber is large enough to be affected by the cosmolog-

¹Not shown are four metal absorption lines with larger Doppler parameters. Each two transitions belong to O VI and Fe II, respectively, show the same absorption pattern, and were fitted interdependently. O VI is observed in the quasar spectrum J004131-493611 at $\lambda_{\text{obs}} \simeq 4366.7 \text{ \AA}$ ($\lambda_r \simeq 1031.9 \text{ \AA}$) and $\lambda_{\text{obs}} \simeq 4390.8 \text{ \AA}$ ($\lambda_r \simeq 1037.6 \text{ \AA}$). Fe II is observed in the quasar spectrum J162116-004250 at $\lambda_{\text{obs}} \simeq 5514.1 \text{ \AA}$ ($\lambda_r \simeq 2586.7 \text{ \AA}$) and $\lambda_{\text{obs}} \simeq 5542.9 \text{ \AA}$ ($\lambda_r \simeq 2600.2 \text{ \AA}$). O VI leaves a severely blended spectral imprint and the respective Doppler parameters are possibly overestimated. The Fe II absorption lines also arise in blends.

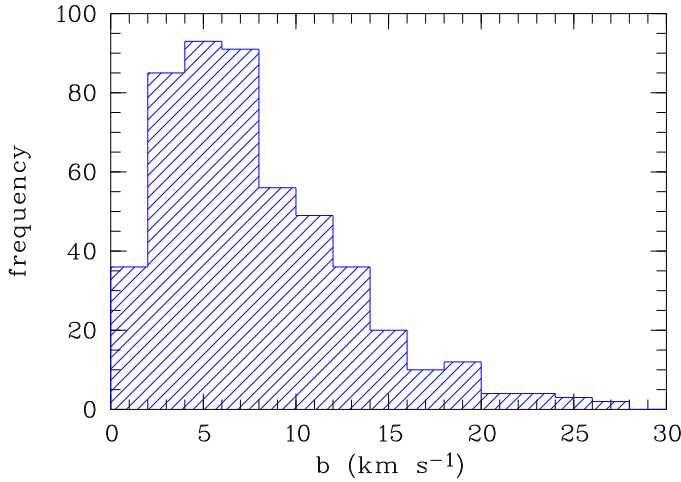


Figure 3.1. Distribution of the Doppler parameter, b , of identified metal absorption lines in bins of size $\Delta b = 2 \text{ km s}^{-1}$.

ical expansion. It is customary and convenient to add these contributions in quadrature,

$$b^2 = b_{\text{th}}^2 + b_{\text{nt}}^2 + b_{\text{Hubble}}^2. \quad (3.1)$$

Note that this is only true if the line profile is a Gaussian, and if the turbulent motion of the gas follows a Gaussian distribution (which is not necessarily true in general). The thermal contribution is given by

$$b_{\text{th}} = \sqrt{\frac{2kT}{m}}, \quad (3.2)$$

corresponding to the most probable thermal speed of the absorbing particles (e.g., atoms, molecules) which obey a Maxwell-Boltzmann distribution. Herein, $k = 1.380\,649 \times 10^{-23} \text{ J K}^{-1}$ is the Boltzmann constant, T is the temperature of the gas, and m is the particle mass. For pure hydrogen, $m = 1.673\,533 \times 10^{-27} \text{ kg}$, we have $b_{\text{th}} \approx 0.1285 \text{ km s}^{-1} \sqrt{T/\text{K}}$. Therefore, a Doppler parameter of $b \simeq 15 \text{ km s}^{-1}$ would correspond to a temperature of $T \approx 13\,500 \text{ K}$ in the purely thermal case. In reality, this temperature is likely to be an upper limit and it is already well below the mean temperature of the IGM at the considered redshift ($\sim 20\,000 \text{ K}$), justifying the selection criterion regarding narrow absorption lines. Hence, for the H I Ly α statistics investigated in this chapter only H I Ly α lines with $b \geq 15 \text{ km s}^{-1}$ are used. This sample consists of 4742 lines.

3.1 The column-density distribution

The (differential) column-density distribution function (CDDF) describes the number of absorbers, \mathcal{N} , in a given column-density interval, ΔN , per absorption distance, X ,

$$f_{\text{CDD}} = \frac{d\mathcal{N}}{dN \cdot X}, \quad (3.3)$$

where

$$X = \sum_{i=1}^n X_i \quad (3.4)$$

is the sum over all n contributing quasars, and

$$X_i(z) = \int_{z_1}^{z_2} \frac{(1+z)^2 H_0}{H(z)} dz \quad (3.5)$$

(Bahcall and Peebles 1969). Here, z_1 and z_2 denote the limits of the considered redshift range. The Hubble constant, H_0 , and the Hubble parameter, $H(z)$, are the same as in Eq. (1.18). The function

$$X_i(z) = \int_{z_1}^{z_2} f(z) dz, \quad (3.6)$$

where $f(z) \equiv (1+z)^2 [H_0/H(z)]$, can be approximated by Simpson's rule (e.g., Stoer 1989),

$$\int_{z_1}^{z_2} f(z) dz \approx \frac{z_2 - z_1}{6} \cdot \left[f(z_1) + 4f\left(\frac{z_1 + z_2}{2}\right) + f(z_2) \right]. \quad (3.7)$$

Hence, for a given redshift interval (z_1, z_2) , the absorption distance, X , can be computed by considering all contributing quasar sightlines. The total number of absorption lines in the respective redshift bin is counted within column-density bins in order to measure f_{CDD} . The error of the CDDF is simply the scaled Poisson error,

$$\sigma_f^2 = \sigma_N^2 \left(\frac{\partial f}{\partial N} \right)^2 \Rightarrow \sigma_f = \frac{\sqrt{N}}{\Delta N \cdot X}, \quad (3.8)$$

where $\sigma_N = \sqrt{N}$ is the Poisson error.

In this work, the CDDF is measured in three redshift bins, $(z_1, z_2) = (2.7, 3.0)$, $(3.0, 3.3)$, and $(3.3, 3.6)$. The resulting column-density distributions are shown in Fig. 3.2. Empirically, the CDDF is found to follow a power law of the form $f_{\text{CDD}}(N) = A \cdot N^{-\beta}$ (e.g., Tytler 1987), with a possible departure from a single power law at higher column densities (e.g., Petitjean et al. 1993). Following Kim et al. (2002a), the power-law fit in this work is performed in the column-density range $13.0 \leq \log N \leq 17.0$. The respective fit parameters are given in Table 3.1. The fit parameters found by Kim et al. (2002a) at redshift $\langle z \rangle = 3.3$, $\log A = 9.18 \pm 1.31$ and $\beta = 1.55 \pm 0.03$, are in good agreement with the values derived in this work at $\langle z \rangle = 3.15$, $\log A = 8.98 \pm 0.32$ and $\beta = 1.55 \pm 0.02$. At lower redshifts, $0.5 < z < 2.0$, Janknecht et al. (2006) find $\log A = 9.9 \pm 0.3$ and $\beta = 1.63 \pm 0.02$ for lines in the comparable column-density range $13.0 \leq \log N \leq 16.5$. These values are larger than those derived in this work. This may indicate that the slope, β , increases with decreasing redshift for the considered column-density range, as suggested by Kim et al. (2002a). However, the β values obtained in this work show a different evolution, although, judging by the estimated errors, it is a marginal one. The slope increases from $\beta = 1.47$ at $\langle z \rangle = 3.45$ to $\beta = 1.55$ at $\langle z \rangle = 3.15$ and drops again to $\beta = 1.51$ at $\langle z \rangle = 2.85$. Based on Fig. 3.2 it appears that the larger β value measured in the central redshift bin is caused by a lower number of high-column-density absorbers ($\log N > 14.5$) compared to the adjacent redshift bins. This could be due to cosmic variance in the quasar spectra since such high-column-density absorbers are rare.

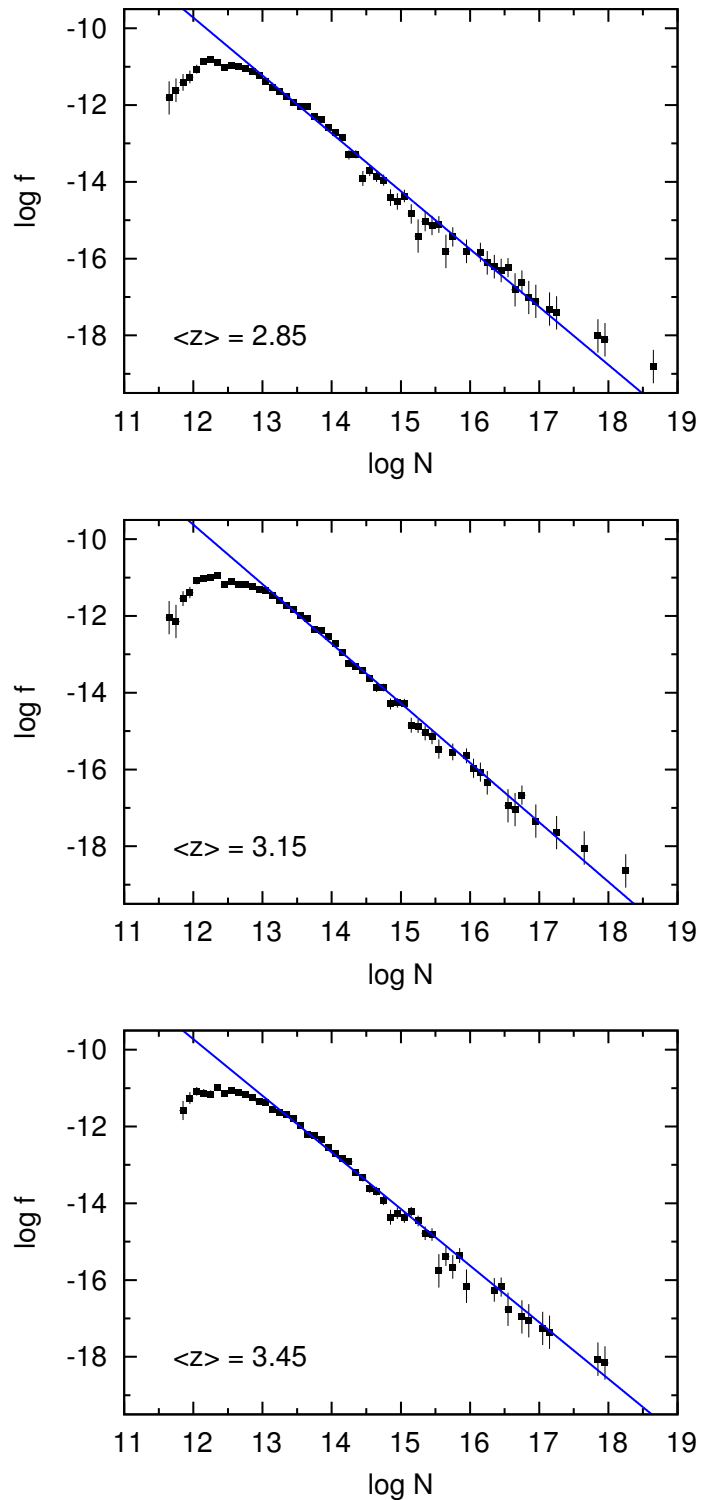


Figure 3.2. Column-density distributions of all H I Ly α absorption lines with Doppler parameters $b \geq 15 \text{ km s}^{-1}$ for three different redshift bins. The parameters of the power-law fit (blue solid line) are given in Table 3.1.

Table 3.1. Parameters of the power-law fit to the column-density distribution in the column-density range $13 \leq \log N \leq 17$ using the empirical form $f_{\text{CDD}}(N) = A \cdot N^{-\beta}$.

$\langle z \rangle$	$\log A$	β
2.85	8.36 ± 0.40	1.51 ± 0.03
3.15	8.98 ± 0.32	1.55 ± 0.02
3.45	7.97 ± 0.37	1.47 ± 0.03

From Fig. 3.2 can be seen that the column-density distribution is well described by a single power law over the column-density range considered for the fit, $13 \leq \log N \leq 17$. At $\log N \lesssim 13.0$ a departure from the empirical power law becomes apparent, which is the result of incomplete absorption-line counts due to line blending. This indicates that the completeness limit of the sample is $\log N \approx 13.0$.

3.2 Doppler-parameter distribution

Figure 3.3 shows the Doppler-parameter distributions of the H I Ly α absorption lines from this work in the redshift range $2.7 \leq z \leq 3.6$ in three equidistant redshift bins ($\Delta z = 0.3$; same as in §3.1). Only absorption lines with column densities above the completeness limit (see §3.1), $13.0 \leq \log N \leq 17.0$, are considered. The upper column-density limit, $\log N = 17$, is chosen to exclude LLSs. Not shown in Fig. 3.3 are lines with Doppler parameters $b > 100 \text{ km s}^{-1}$; 4 lines at $\langle z \rangle = 2.85$, 1 at $\langle z \rangle = 3.15$, and another 4 at $\langle z \rangle = 3.45$.

The Doppler-parameter distribution from this study is similar to b distributions found at comparable redshifts from other surveys (Hu et al. 1995; Lu et al. 1996), i.e., the bulk of the absorption lines has Doppler parameters in the range $15 - 40 \text{ km s}^{-1}$ with a peak at $b \sim 25 \text{ km s}^{-1}$, and the distribution flattens to even larger b values. The cutoff at $b = 15 \text{ km s}^{-1}$ seen in the distributions from this work is due to the selection criterion regarding narrow absorption lines (see above).

The mean Doppler parameter is $b_{\text{mean}} = (31 \pm 14) \text{ km s}^{-1}$, $(30 \pm 12) \text{ km s}^{-1}$, and $(31 \pm 15) \text{ km s}^{-1}$ at redshifts $\langle z \rangle = 2.85$, 3.15, and 3.45, respectively, and the median values are $b_{\text{median}} = 27.1 \text{ km s}^{-1}$, 27.1 km s^{-1} , 24.3 km s^{-1} at the respective redshifts (see also Table 3.2). There is no strong indication of evolution with redshift of any of the two quantities. Kim et al. (2002a) find $b_{\text{mean}} = 31.6 \text{ km s}^{-1}$ and $b_{\text{median}} = 28.1 \text{ km s}^{-1}$ at $\langle z \rangle = 3.3$ for the column-density range $13.0 \leq \log N \leq 17.0$ also used here. These values are in good agreement with those from this work, though the median b value of 24.3 km s^{-1} at $\langle z \rangle = 3.45$ is slightly lower compared to the other median Doppler parameters from both, this work and Kim et al. (2002a).

For the typical temperature ($T \sim 20\,000 \text{ K}$) of the IGM at redshift $z \sim 3$, the purely thermal contribution to the Doppler parameter is $b_{\text{th}} \simeq 18 \text{ km s}^{-1}$ (Eq. 3.2). This indicates that non-thermal mechanisms and the cosmological expansion contribute significantly to the broadening of absorption lines (Eq. 3.1) in order to reproduce the mean and median Doppler parameters measured in this work. Since the temperature is a key property of absorbers, a method that constrains the temperature of the low-density IGM is described

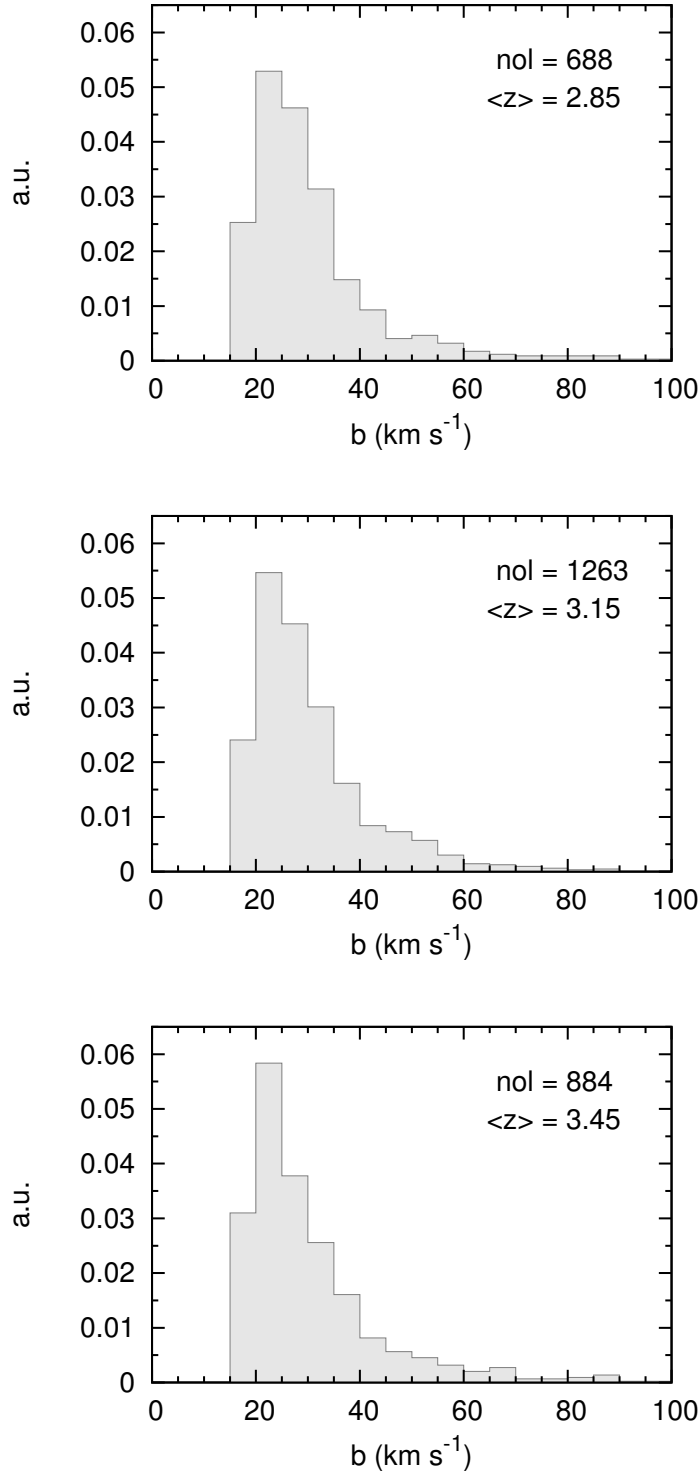


Figure 3.3. Normalized Doppler-parameter distributions of H I Ly α absorption lines. Each panel shows the Doppler parameters of the total number of lines (n_{ol} ; $13.0 \leq \log N \leq 17.0$), in the redshift bin of width $\Delta z = 0.3$ at the mean redshift $\langle z \rangle$, in bins of width $\Delta b = 5 \text{ km s}^{-1}$. The low- b cut in the distribution is due to the exclusion of narrow ($b < 15 \text{ km s}^{-1}$) lines from the sample (see text).

Table 3.2. Values of the Doppler-parameter distributions for three redshift bins with mean redshift $\langle z \rangle$. Listed are the number of lines (nol) in a given redshift bin, the mean Doppler parameter, and the median of the respective distribution.

$\langle z \rangle$	nol	b_{mean} (km s^{-1})	b_{median} (km s^{-1})
2.85	688	31 ± 14	27.1
3.15	1263	30 ± 12	27.1
3.45	884	31 ± 15	24.3

in the next section. It is more difficult to infer the temperature of high-density absorbers, but the H I Ly α forest absorption is caused mostly by the low-density gas. Note, however, that the overdensity of the gas (Eq. 1.52) associated with a given column density increases with decreasing redshift (Davé et al. 1999) due to the expansion of the Universe (Schaye et al. 2000).

3.3 $b(N)$ distribution

After discussing the distribution of the column densities, N , and Doppler parameters, b , individually in the previous sections, the $b(N)$ distribution will be considered. The $b(N)$ distributions for all absorption lines fitted as H I Ly α in the redshift bins used in §§3.1 and 3.2 are shown in Fig. 3.4.

Regarding the $b(N)$ distribution, the possibility to observe an absorption line depends on the optical depth of the line at the line center, as well as the signal-to-noise ratio, S/N , and the resolution, R , of the studied spectrum. At the line center, Eq. (2.5) gives

$$\tau(\lambda_{\text{obs}} = \lambda_{c,\text{obs}}) = \frac{1}{4\sqrt{\pi}} \frac{e^2}{\epsilon_0 m_e c} \frac{\lambda_0 f N}{b}. \quad (3.9)$$

Hence, the optical depth of an absorption line at the line center becomes minimal if the ratio N/b is minimal. The apparent detection limit in the quasar spectra used in this work, inferred from the H I Ly α absorption line with the lowest optical depth at the line center, is shown as the blue dashed line in each panel of Fig. 3.4. The selection criterion for narrow H I Ly α absorption lines is shown as the red horizontal dash-dotted line. This criterion was applied in §§3.1 and 3.2 since H I Ly α absorption lines with $b < 15 \text{ km s}^{-1}$ are most likely due to metal absorption, noise, or line blending. These narrow lines are left in the $b(N)$ distribution for comparison. It is apparent from Fig 3.4 that the column density and the Doppler parameter of absorption lines are generally uncorrelated (see also Rauch et al. 1993; Lu et al. 1996).

Kirkman and Tytler (1997) find a correlation between the lowest Doppler parameters at a given column density and the corresponding column densities of H I Ly α absorption lines with $\log N > 12.5$ towards the quasar HS1946+7658 ($z_{\text{em}} = 3.05$). Using simulations, Schaye et al. (1999) connect the $b(N)$ cutoff with a power-law equation of state (temperature-density relation) for the low-density gas. By using hydrodynamic simulations, Schaye et al. (2000) calibrate the relations between the parameters of the $b(N)$ cutoff from observations and the equation of state of the low-density IGM in order to infer the evolution of the temperature of the IGM (see §1.2). Hence, following Schaye

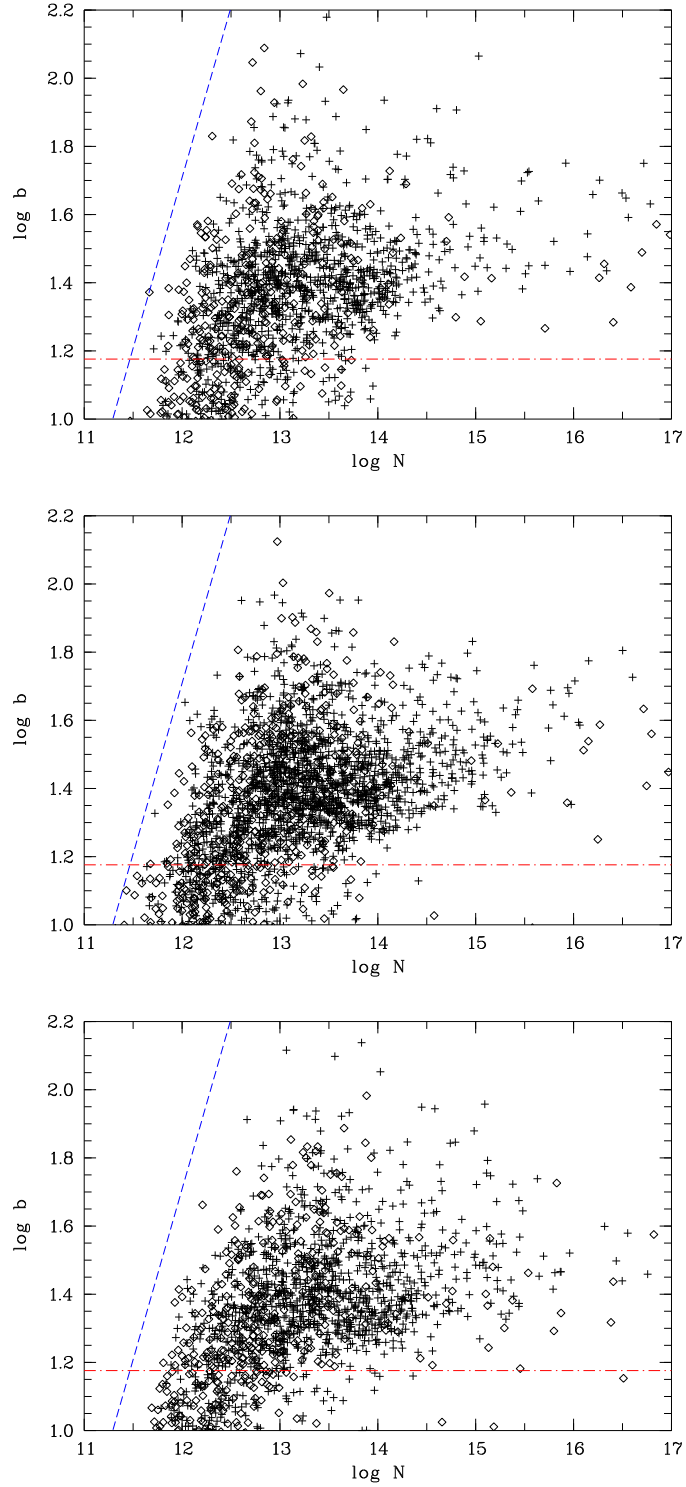


Figure 3.4. $b(N)$ distribution of HI Ly α absorption lines for three different redshift intervals; top: $2.7 < z < 3.0$, middle: $3.0 < z < 3.3$, bottom: $3.3 < z < 3.6$. Absorption lines with a relative error of $\leq 40\%$ in column density *and* Doppler parameter are shown as crosses. The remaining lines with larger errors are shown as open lozenges. Also plotted are the apparent optical-depth detection limit (blue dashed line) and the narrow-line criterion ($b = 15 \text{ km s}^{-1}$, red dash-dotted line).

et al. (2000), it is in principle possible to put constraints on the reionization history of the Universe by measuring the thermal evolution in the redshift range $2.7 < z < 3.6$ using the data of this work, which may give an insight on the occurrence of He II reionization in particular. But, since the application of the required simulations is beyond the scope of this work, such a detailed measurement is not performed here. Nevertheless, it is possible to obtain a rough upper limit of the temperature of the low-density IGM by measuring the lower cutoff envelope of the $b(N)$ distribution.

Assuming that the lowest b values in the $b(N)$ distribution at a given column density are due to purely thermal broadening, an upper limit of the IGM temperature can be inferred by measuring the lower cutoff envelope of the $b(N)$ distribution at a given redshift. I used the iterative method from Schaye et al. (1999) to measure the low- b cutoff. The procedure is described in the following.

A function of the form

$$\log b_{\text{co}}(\log N) = \log b_0 + (\Gamma - 1) \cdot \log N \quad (3.10)$$

is fitted to the entire sample of H I Ly α absorption lines in the $b(N)$ distribution. Then, the absolute mean deviation (AMD) of the b values from the resulting regression line is computed considering all absorption lines. Those lines with b parameters above a chosen threshold are removed from the sample for the next step, i.e., lines with Doppler parameters

$$\log b > \log b_{\text{co}} + (f_{\text{AMD}} \cdot \text{AMD}). \quad (3.11)$$

The factor f_{AMD} can be adjusted in an arbitrary way in order to match the regression line to the $b(N)$ distribution. A smaller f_{AMD} results in a smaller χ^2 value. For example, Schaye et al. (2000) use $f_{\text{AMD}} = 1$ and Kim et al. (2002b) use $f_{\text{AMD}} = 0.5$. In this work, the selection-threshold factor is $f_{\text{AMD}} = 0.2$.

The remaining lines are used for the next iteration, i.e., the regression is performed using the subsample and again the AMD is computed considering the *entire* sample used for the iterative method. These steps are repeated until convergence is achieved. In order to avoid unphysically narrow absorption lines, which are due to profile fitting of line blends, from the subsample, for which convergence was achieved, absorption lines with Doppler parameters

$$\log b < \log b_{\text{co}} - (f_{\text{AMD}} \cdot \text{AMD}) \quad (3.12)$$

are also removed. With the remaining absorption lines in the $b(N)$ distribution the regression is performed again. The resulting regression line is the lower Doppler-parameter cutoff in the $b(N)$ distribution.

In this work, the sample used for the iterative method comprises absorption lines with Doppler parameters $b \geq 15 \text{ km s}^{-1}$ (narrow-line criterion introduced at the beginning of this chapter) in the column-density range $13.0 \leq \log N \leq 14.5$. The lower column-density limit corresponds to the incompleteness threshold estimated in §3.1 and the upper limit is roughly the column density at which the density of the number of data points for a given column density in the scatter plot (Fig. 3.4) decreases. Hence, a sharp low- b cutoff in the $b(N)$ distribution is difficult to determine at larger column densities. Furthermore, the temperature-density relation is only valid in the low-density regime. Therefore $\log N = 14.5$ is a conservative upper limit. Additionally, only lines with a relative error

Table 3.3. Parameters of the lower cutoff envelope in the $b(N)$ distribution at a given redshift $\langle z \rangle$. Listed are the number of lines (nol) used for the iterative method (see text), and the intercept and slope of the regression line (Eq. 3.10), as well as the cutoff b value, b_{co} , at a given column density, $\log N = 13.6$.

$\langle z \rangle$	nol	$\log b_0$	$(\Gamma - 1)$	$b_{\text{co}}(13.6)$ (km s^{-1})
2.85	467	-0.477 ± 0.099	0.128 ± 0.007	18.5 ± 5.9
3.15	865	0.448 ± 0.072	0.061 ± 0.005	18.7 ± 4.4
3.45	592	0.538 ± 0.074	0.054 ± 0.005	18.7 ± 4.5

$\leq 25\%$ in Doppler parameter *and* column density (Kim et al. 2002b) are used for the iterative method in order to sharpen the cutoff (Schaye et al. 1999).

The lower cutoff envelope in the $b(N)$ distribution at a given redshift (Fig. 3.4) is shown in Fig. 3.5. The fit parameters are given in Table 3.3. These values can be compared to the measurement of Kim et al. (2002b) at $\langle z \rangle = 3.3$ since these authors use the same column-density range at this redshift, $13.0 \leq \log N \leq 14.5$, as used in this work. They find $\log b_0 = -0.413 \pm 0.116$ and $(\Gamma - 1) = 0.122 \pm 0.008$ at $\langle z \rangle = 3.3$, which agree better with the fit parameters found in this work at redshift $\langle z \rangle = 2.85$, $\log b_0 = -0.477 \pm 0.099$ and $(\Gamma - 1) = 0.128 \pm 0.007$, than those estimated at higher redshifts, where the slope $(\Gamma - 1)$ is roughly half the value of the slope at $\langle z \rangle = 2.85$. Accordingly, the axis intercept, $\log b_0$, is larger at higher redshifts. At a fixed column density, $\log N = 13.6$, Kim et al. (2002b) find the lower cutoff b value $b_{\text{co}}(13.6) = (17.2 \pm 1.0) \text{ km s}^{-1}$. This value is found within the estimated error of the $b_{\text{co}}(13.6)$ measurements in this work at the three given redshifts, $(18.5 \pm 5.9) \text{ km s}^{-1}$ at redshift $\langle z \rangle = 2.85$, $(18.7 \pm 4.4) \text{ km s}^{-1}$ at redshift $\langle z \rangle = 3.15$, and $(18.7 \pm 4.5) \text{ km s}^{-1}$ at redshift $\langle z \rangle = 3.45$ (see also column 5 of Table 3.3). In this work, the error of $b_{\text{co}}(13.6)$ is found by error propagation of the errors on the fit parameters $(\Gamma - 1)$ and $\log b_0$. The similarity of the measured $b_{\text{co}}(13.6)$ values from this work indicate that the lower cutoff envelopes pivot at b values at the column density of $\log N \sim 13.6$ for the three redshift ranges considered in this work (see also Kim et al. 2002b).

The inferred low- b cutoff with the iterative method can be shifted towards larger b values by choosing a larger f_{AMD} since less lines are excluded in each iteration. The lower $b_{\text{co}}(13.6)$ value measured by Kim et al. (2002b) is likely due to the smaller number of absorption lines used by these authors compared to the line number used here for a given redshift interval. Kim et al. (2002b) use 275 lines for their lower-cutoff-envelope measurement at $\langle z \rangle = 3.3$, which is roughly half the number of lines used in the lower redshift bin considered in this work. At higher redshifts the line number used for the linear regression in this work is even larger.

The $b_{\text{co}}(13.6)$ values measured in this work translate to the upper limits of the temperatures of $T_{\text{ul}} \simeq 20\,700 \text{ K}$ at redshift $\langle z \rangle = 2.85$ and $T_{\text{ul}} \simeq 21\,200 \text{ K}$ at higher redshifts (Eq. 3.2). These temperatures are only slightly above the mean temperature of the IGM at redshift $z \sim 3$ ($T \sim 20\,000 \text{ K}$). Note, that an evolutionary behaviour of the temperature can not be inferred from the $b_{\text{co}}(13.6)$ values measured at different redshifts since the overdensity of the gas at a given column density increases with decreasing redshift.

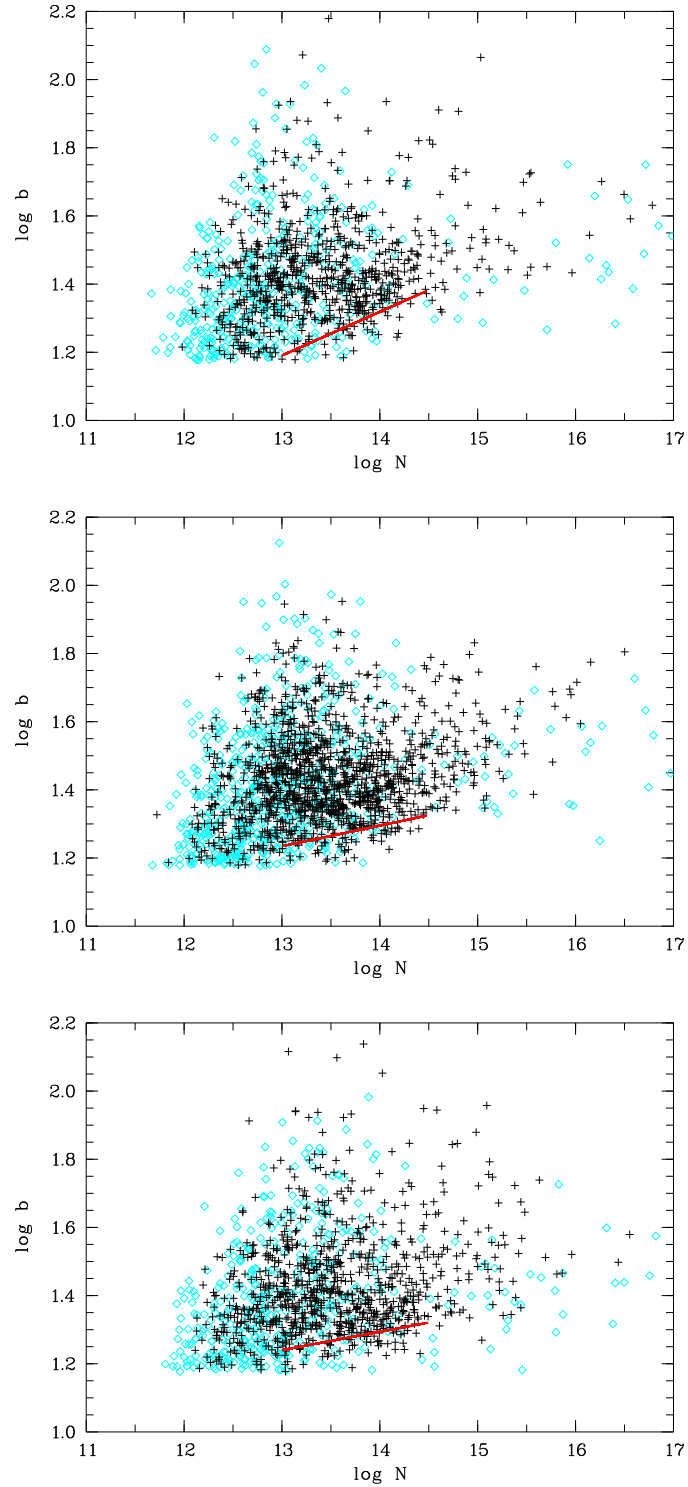


Figure 3.5. Same as Fig. 3.4. Absorption lines with $b < 15 \text{ km s}^{-1}$ are removed from the sample. Lines with a relative error of $> 25\%$ in Doppler parameter or column density are shown as open lozenges (cyan). Of the remaining data points (black crosses) only lines in the column-density range $13.0 \leq \log N \leq 14.5$ are used to determine the lower cutoff envelope of the $b(N)$ distribution (red solid line). Fit parameters of the regression line are given in Table 3.3.

Table 3.4. Fit parameters from the power-law fit of the form $dn/dz = n_0(1 + z)^{\gamma_{\text{app}}}$ to the redshift evolution of the number density, dn/dz , for two column-density ranges, $\log N$.

$\log N$	n_0	γ_{app}
13.0 – 17.0	44.9 ± 21.2	1.62 ± 0.33
13.644 – 17.000	12.0 ± 8.0	2.01 ± 0.47

3.4 Number-density evolution

The number-density evolution is the redshift-dependent mean number of absorbers per unit redshift. Figure 3.6 shows the number of H I Ly α absorbers that have Doppler parameters $b \geq 15 \text{ km s}^{-1}$ for two column-density ranges, $13 \leq \log N \leq 17$ (upper panel) and $13.64 < \log N \leq 17.00$ (lower panel), in redshift bins of size $\Delta z = 0.1$ in the redshift range $2.7 < z < 3.6$. As expected, the number density decreases with decreasing redshift. This can be explained as follows (see also, e.g., Meiksin 2009). As the Universe expands, the physical gas density of absorbers in the low-density IGM decreases. This also leads to fewer recombinations per unit time. Both processes result in a decreasing neutral hydrogen fraction in the absorber with decreasing redshift. Since the number of absorbers decreases with increasing gas density (and, hence, column density) at a given redshift due to hierarchical structure formation, the cosmological expansion leads to fewer observed absorbers with decreasing redshift for a fixed column-density range. This means, an increasing number of absorbers drops below the column-density threshold with decreasing redshift. However, towards lower redshifts ($z < 2$) the UVB intensity decreases due to the decline of the number of observed quasars (e.g., Hopkins et al. 2007), which leads to a larger recombination rate compared to higher redshifts. Hence, the number-density evolution flattens at $z < 2$ (e.g., Janknecht et al. 2006).

Empirically, the number-density evolution, dn/dz , can be described by a power law of the form

$$\frac{dn}{dz} = n_0(1 + z)^{\gamma_{\text{app}}} \quad (3.13)$$

(e.g., Murdoch et al. 1986; Janknecht et al. 2006). The parameters of the power-law fits to the number-density evolution from this work using different column-density ranges ($\log N_{\min} \leq \log N \leq 17.0$ with $\log N_{\min} = 13.0$ and $\log N_{\min} = 13.644$, respectively) are given in Table 3.4. The slopes of the number-density evolution for the two considered column-density ranges are consistent within the error bars. Since $\gamma_{\text{app}} > 1$ for both column-density ranges, the population of these high-column-density absorbers in the redshift range $2.7 < z < 3.6$ strongly evolves with cosmic time (see §1.5.1 and Eq. (1.20) in particular).

In Fig. 3.6 the respective power-law fit to the data shown in each panel is represented by the red solid line. Kim et al. (2002a) performed a maximum-likelihood fit to their data combined with literature values in the redshift range $1.5 < z < 4.0$ that is shown in the lower panel of Fig. 3.6 by the blue dashed line. The column-density range $13.64 < \log N \leq 17.00$ has been chosen for the data of this work to be comparable to the data of Kim et al. (2002a). These authors find a slope of $\gamma_{\text{app}} = 2.47 \pm 0.18$ that is in good agreement with the slope estimated here, $\gamma_{\text{app}} = 2.01 \pm 0.47$. Kim et al. (2002a) also find a trend

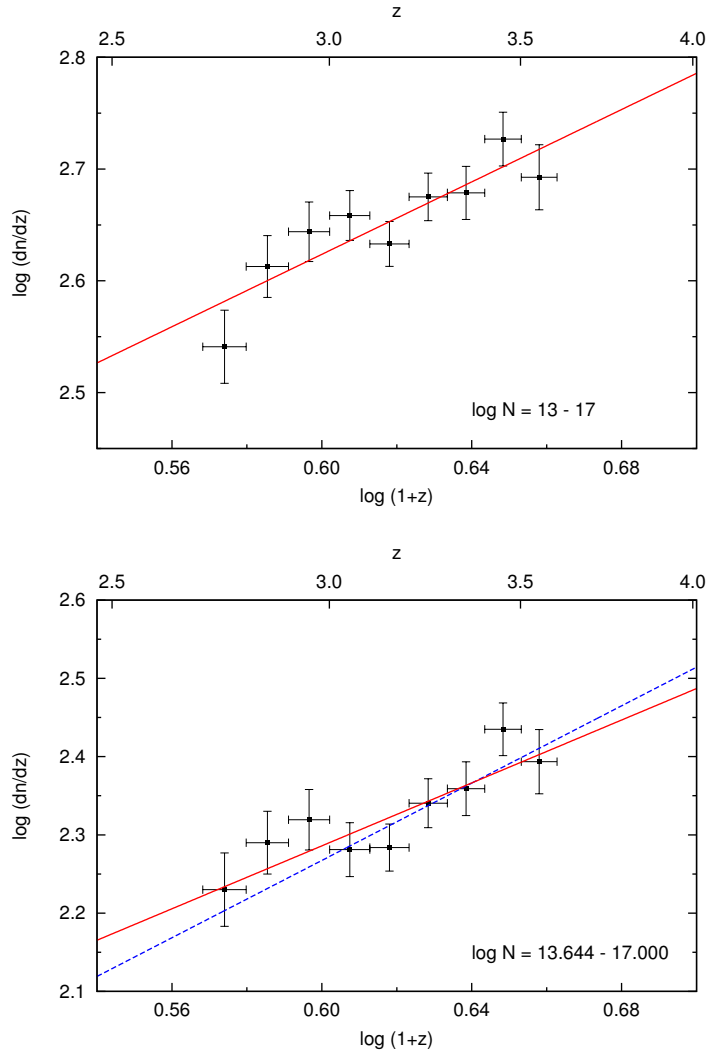


Figure 3.6. Number-density evolution of H I Ly α absorption lines with Doppler parameters $b \geq 15 \text{ km s}^{-1}$ and column densities in the range $13 \leq \log N \leq 17$ (upper panel) and $13.64 < \log N \leq 17.00$ (lower panel). The red solid line in each panel is the best-fit power law of the form $dn/dz = n_0(1+z)^{\gamma_{\text{app}}}$ to the respective data (parameters given in Table 3.4). The dashed blue line in the lower panel is the maximum-likelihood fit from Kim et al. (2002a) to their data combined with literature values in the redshift range $1.5 < z < 4.0$, $(n_0, \gamma_{\text{app}}) = (6.1, 2.47 \pm 0.18)$.

of increasing γ_{app} with higher column-density threshold while the upper column-density limit is kept fix (their Fig. 10). The measurements of this work confirm this trend. Kim et al. (2002a) discuss two possible explanations for this behaviour of γ_{app} . The γ_{app} trend could be due to more severe blending of absorption lines with lower column densities at higher redshift, or be caused by an intrinsic evolution of the H I Ly α forest.

As pointed out by Liu and Jones (1988), the apparent evolutionary rate exponent γ_{app} is smaller than the intrinsic exponent due to line blending effects. The intrinsic evolutionary rate exponent γ_{int} can be determined from the redshift evolution of the effective optical depth (Zuo 1993). This measurement is part of the analysis presented in the next chapter. The τ_{eff} measurements are not restricted to a certain column-density range, which makes a direct comparison of γ_{int} to γ_{app} measured from the number-density evolution difficult. Hence, I compare the measured slope γ_{int} of the redshift evolution of the effective optical depth to γ_{app} measured for the larger column density range used to infer dn/dz in this work, $13.0 < \log N \leq 17.0$. I find $\gamma_{\text{int}} = 2.09 \pm 0.52$, which is indeed larger than the value $\gamma_{\text{app}} = 1.62 \pm 0.33$.

Note, however, that the main characteristics of the number-density evolution shown in Fig. 3.6 resemble the evolution of the effective optical depth (see, e.g., Fig. 4.3 d). This is expected since both quantities trace the amount of neutral hydrogen at a given redshift. In particular, there might be a ‘dip’ at $z \sim 3.1$ or ‘bump’ at $z \sim 2.9$ in the number-density evolution. However, the presence and/or significance of any deviation from a smooth power law will be discussed in detail with respect to the effective optical depth in the next chapter.

Chapter 4

The H I Ly α opacity at redshift $z \sim 3$

As mentioned in §1.3, the redshift evolution of the effective optical depth can best be measured in the redshift range $1.5 < z < 4.0$ from quasar spectra observed with earth-bound telescopes. The lower and higher redshift limit is due to atmospheric absorption and uncertain continuum estimates, respectively. Some studies (Bernardi et al. 2003; Faucher-Giguère et al. 2008b; Dall’Aglio et al. 2008) find a downward deviation from the expected smooth evolution of τ_{eff} . This feature is of comparable size ($\Delta z \sim 0.3$) and found at similar redshift ($z \sim 3.2$) in all of the aforementioned studies. Assuming that the $\tau_{\text{eff}}(z)$ feature is real, it could be caused by an increase in the temperature of the IGM or the hydrogen photoionization rate due to He II reionization (see §1.2). However, other works (Dall’Aglio et al. 2009; Pâris et al. 2011; Becker et al. 2013) do not find such a feature in $\tau_{\text{eff}}(z)$, suggesting that it may not be real but rather the product of systematic errors in the analysis. Possible error sources are differences in the removal of metal absorption from the quasar spectra, uncertainties in the continuum estimation of quasar spectra, and the method to infer the effective optical depth. The $\tau_{\text{eff}}(z)$ measurement from this work is addressed in this chapter. In §4.1 the method used in this work to measure the redshift evolution of the effective optical depth, $\tau_{\text{eff}}(z)$, using 13 observed quasar spectra (see §2.1) is presented in detail. The results are presented in §4.2 and the effect of systematics on the measurement is discussed in §4.3. For a comparison with τ_{eff} estimates found in the literature see §5.1.

4.1 Methodology

The pixel mean flux, $\langle f_\nu \rangle$ (Eq. 1.5), can be measured in redshift bins of different sizes, ranging from a few pixels in the H I Ly α forest to all pixels in the redshift range between the H I Ly β and the H I Ly α emission lines. In addition, the pixels of a single spectrum that fall into a given redshift range or the pixels of all spectra, which are intersected by a given redshift bin, can be used to infer τ_{eff} . For a summary of the statistical methods used to measure the effective optical depth found in the literature see Table 1.1. The comparison of measurements from individual lines of sight produces a large scatter in the $\tau_{\text{eff}}-z$ plane. A more precise measurement of the effective optical depth can be obtained by averaging the absorption from all quasar spectra using only those pixels which contribute to a given redshift bin. For example, the Sloan Digital Sky Survey data releases (SDSS-DR) feature thousands of low-resolution ($R \simeq 2000$) quasar spectra. It is common to construct

composite spectra from hundreds of quasar spectra with similar emission redshifts in order to study details of the emission properties of quasars (see, e.g., Vanden Berk et al. 2001; Brotherton et al. 2001). Composite spectra can also be used to analyze the redshift evolution of the mean flux (e.g., Bernardi et al. 2003; Becker et al. 2013). Unfortunately, it is not possible to account for metal absorption in low-resolution quasar spectra by direct identification. Even though it is possible to apply statistical methods to correct for metal contamination in quasar spectra with low resolution, they lack the precision required to measure τ_{eff} at high accuracy.

In order to infer the redshift evolution of the effective optical depth at $z \sim 3$ more precisely by removing the contribution of metals a detailed analysis of high-resolution data is needed. The SQUAD database provides 13 quasar spectra suited for such an analysis (see §2.1). Note, however, that constructing composite spectra is not possible in this case since more sightlines would be necessary.

In this work two different approaches are considered to compute the effective optical depth. In the first approach, the observed flux from the quasar spectra is used directly. In the second approach, the model flux obtained from absorption-line fits (see §§2.3.2 and 2.3.3) is used instead.

The use of the model flux allows for different selections of the fitted absorption lines for the analysis. For example, by using all fitted absorption lines, the model flux can be compared directly to the observed flux. If the model and the observed fluxes are equal within the measurement errors, the evolution of the effective optical depth inferred from both approaches should agree. Note that the agreement between the observed and the model fluxes is one of the constraints imposed on the fitting procedure, and it is, thus, guaranteed by any objectively satisfactory fit. This is important because it is the basis of the methodology used in this work to compute τ_{eff} more precisely. The reason behind this is that the use of the model flux to remove contaminating absorption features – such as metal absorption lines – from the H I Ly α forest is easier than using the observed flux. Removing absorption features imprinted on the continuum flux requires masking (see §2.3). This is difficult to apply to blended absorption features. But removing absorption features from the model flux is possible since the parameters of individual absorption lines are known from the fitting procedure (see below).

For the analysis in this work the observed flux and the model flux, derived from all fitted absorption lines, is used. In addition, the model flux derived from a selection of fitted absorption lines is used:

- 1) H I Ly α absorption lines with freely iterated fitting parameters (which means that from all fitted absorption lines identified metal lines and fitted lines with fixed¹ parameters are excluded);
- 2) same as above, additionally narrow absorption lines with Doppler parameters of $b < 15 \text{ km s}^{-1}$ following Rauch et al. (1997) are rejected (see also Chapter 3).

As described in §2.3.2, the absorption features in each spectrum were fitted with CANDALF. The underlying assumption is that the absorption features in a quasar spectrum

¹Occasionally, during the absorption-line fitting procedure with the program CANDALF, absorption-line parameters had to be fixed rather than freely iterated in order to reach convergence. The corresponding lines unlikely influence the results in this work. For further details see §§2.3.2, 2.3.3, and Appendix B.

can be decomposed into individual absorption lines each with a smooth profile (e.g., Gaussian). CANDALF yields the parameters (z , b , N) for each absorption line. Hence, from the model flux individual absorption features – such as identified metal transitions – can be removed. If metal absorption lines are removed from the model flux, the remainder of the model flux should be similar to the observed flux unaffected by metal absorption. The second selection criterium given above is the most conservative to determine $\tau_{\text{eff}}(z)$. Narrow H I Ly α absorption lines, which could be in reality missed metal absorption lines or noise features, are removed to avoid misidentification of hydrogen absorption lines.

In summary, the data are analyzed using four different flux selections:

- a) the observed flux;
- b) the model flux including all fitted absorption lines;
- c) the model flux excluding identified metal absorption lines and fitted absorption lines with a fixed fitting parameter;
- d) same as c), excluding additionally narrow absorption lines ($b < 15 \text{ km s}^{-1}$).

The analysis of each flux selection sample is performed in the same way. In the following, the method used in this work, which is based on the method used by Faucher-Giguère et al. (2008b), is outlined. The steps are as follows:

- ▶ Create a linear redshift grid with 2×10^4 points using steps of $\text{d}z = 10^{-4}$, from $z_{\text{mean}} = 2.00005$ to redshift $z_{\text{mean}} = 3.99995$.
- ▶ Compute the proper length, $\text{d}L$ (Eq. 1.17), in proper Mpc,

$$\begin{aligned} \text{d}L &= \frac{c}{1+z} \cdot \frac{\text{d}z}{H_0 \sqrt{\Omega_M \cdot (1+z)^3 + \Omega_\Lambda}} \\ \Leftrightarrow \frac{\text{d}L}{\text{d}z} &= c H_0^{-1} [\Omega_M \cdot (1+z)^5 + \Omega_\Lambda \cdot (1+z)^2]^{-\frac{1}{2}} \equiv \mathfrak{L}(z), \end{aligned} \quad (4.1)$$

where $c \equiv 299\,792.458 \text{ km s}^{-1}$, $H_0 = 72 \text{ km s}^{-1} \text{ Mpc}^{-1}$, $\Omega_M = 0.27$, and $\Omega_\Lambda = 0.73$ (Spergel et al. 2003, Wilkinson Microwave Anisotropy Probe [WMAP] data only), which corresponds to a matter-dominated (neglecting energy induced by radiation as observed today), flat ($\Omega_k = 0$) Universe. The function $\mathfrak{L}(z)$ (Fig. 4.1) is continuous and the area beneath the curve gives the proper distance between any two chosen redshifts. Therefore, the proper distance can be approximated with rectangles $\mathfrak{L}(z_{\text{mean}}) \text{d}z$ with z_{mean} as introduced above. This gives roughly the proper distance, L , as by integrating Eq. (4.1) from $z_{\text{mean}} - \frac{\text{d}z}{2}$ to $z_{\text{mean}} + \frac{\text{d}z}{2}$.

- ▶ Combine adjacent redshift bins until the sum of partial proper distances is equal to 3 proper Mpc (Faucher-Giguère et al. 2008b). Due to the redshift grid, the proper Mpc segments are in the range between $\mathfrak{L}_{\text{min}}^{\text{seg}} = 3.00008 \text{ Mpc}$ and $\mathfrak{L}_{\text{max}}^{\text{seg}} = 3.04212 \text{ Mpc}$ with an average of $\mathfrak{L}_{\text{mean}}^{\text{seg}} = 3.01529 \text{ Mpc}$ and a median of $\mathfrak{L}_{\text{median}}^{\text{seg}} = 3.01383 \text{ Mpc}$. This procedure results in 177 segments along the grid in the redshift range $2.000 \leq z \leq 3.987$.

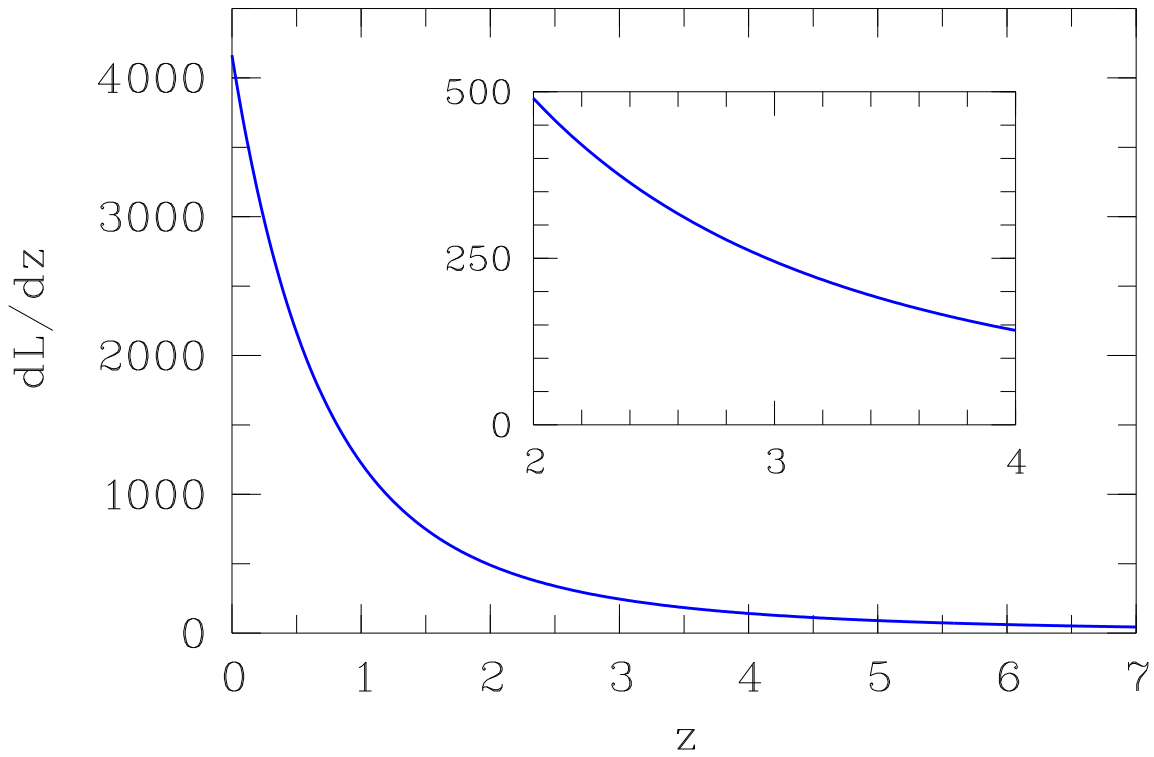


Figure 4.1. Proper distance per unit redshift as a function of z in a matter-dominated, flat Universe. The embedded panel shows a close-up to the redshift range $2 \leq z \leq 4$.

- ▶ Calculate the arithmetic mean flux per 3 proper Mpc segment from the pixels of a quasar spectrum contained within the respective segment. Pixels were accounted for only once in adjacent segments. This method was introduced by Faucher-Giguère et al. (2008b) and makes use of the central limit theorem. If the flux-probability distribution is the same within any 3 proper Mpc segment with the segments being independent of each other, the arithmetic mean flux from all segments is normally distributed.

Due to the redshift coverage of the quasar spectra used in this work (see Fig. 2.1) and for statistical significance, I decided to concentrate on the redshift range $2.7 \leq z \leq 3.6$. Within this redshift range there are 67 segments along the grid. The redshift range was split into 9 redshift bins of size $\Delta z \simeq 0.1$. The limits of these redshift bins depend on the exact size of the enclosed segments. If the analyzed H I Ly α forest of each of the 13 quasar spectra would span the redshift range $2.7 \lesssim z \lesssim 3.6$ then each spectrum would contribute 67 mean-flux measurements to the analysis. In reality the spectra span a shorter redshift range (black horizontal lines in Fig. 2.1). In each redshift bin the 3 proper Mpc segments from any contributing quasar spectrum are stacked. If the mean flux of the i -th segment is $\langle F \rangle_i$, the average flux computed from the segments in a given redshift bin is $\langle f_\nu \rangle = \langle \langle F \rangle_i \rangle$ with standard deviation $\sigma_{\langle F \rangle_i}$. The effective optical depth can then be computed by $\tau_{\text{eff}} = -\ln \langle f_\nu \rangle$ (see Eq. 1.5), its error being the standard deviation, $\sigma_{\langle F \rangle_i}$, divided by the square root of the number of segments, N , since the mean-flux measurements of the segments are

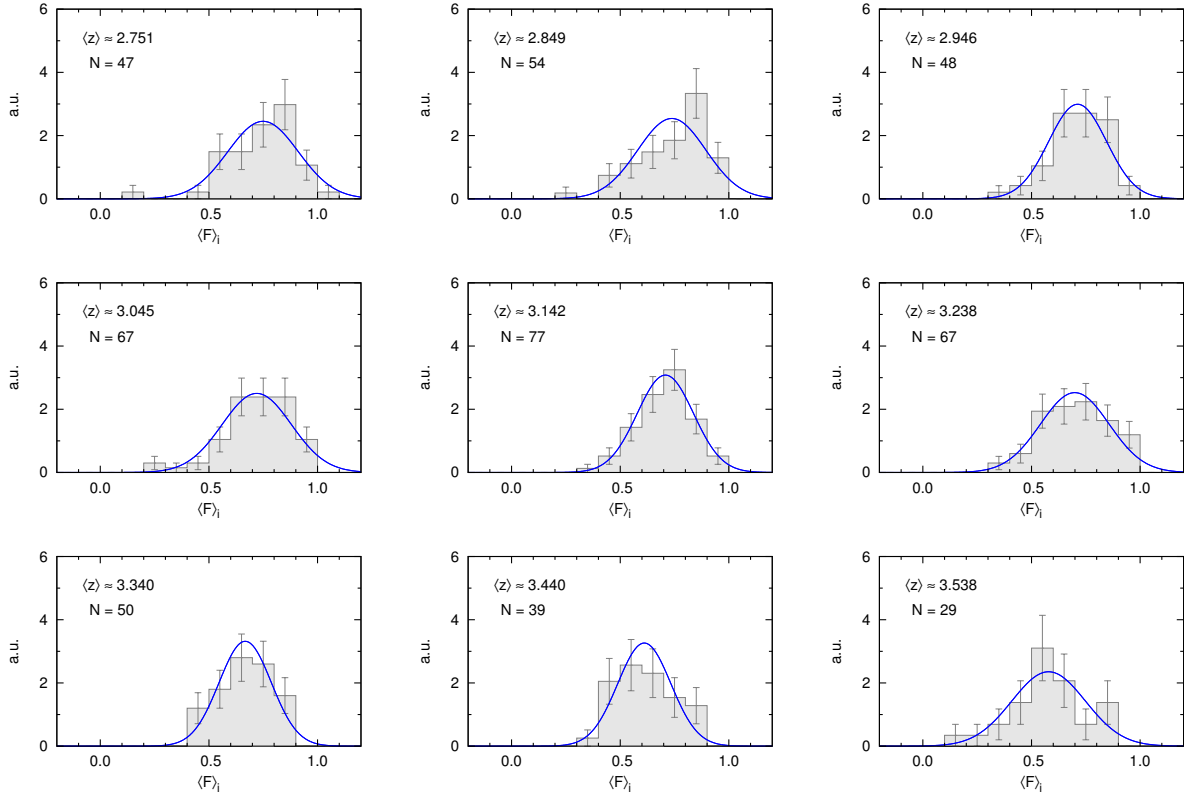


Figure 4.2. Histograms of the model mean flux $\langle F \rangle_i$ of the $\sum_{i=1}^N 1 = N$ contained segments from the 13 quasar spectra used in this work (if contributing, see Fig. 2.1) in redshift bins of size $\Delta z \simeq 0.1$ with a mean redshift $\langle z \rangle$. This measurement excludes metal absorption lines, absorption lines with fixed fitting parameters, and lines with Doppler parameters smaller than $b = 15 \text{ km s}^{-1}$ (see text). The Gaussian (blue curve) has the same mean flux and standard deviation as the respective histogram (see text), and is plotted for display purposes only. The histograms are normalized and displayed in arbitrary units (a.u.).

independent of each other, and divided by the average flux, $\langle f_\nu \rangle$, so that

$$\sigma_{\tau_{\text{eff}}} = \frac{\sigma_{\langle F \rangle_i}}{\sqrt{N} \cdot \langle f_\nu \rangle}. \quad (4.2)$$

Figure 4.2 shows the mean-flux distribution of the segments contained in each of the 9 redshift bins for the corrected² model flux (see also Appendix C). Since the segments are expected to be normally distributed, a Gaussian with the same mean $\langle f_\nu \rangle$ and standard deviation $\sigma_{\langle F \rangle_i}$ as the respective histogram is plotted for comparison (blue curve).

4.2 Results

As mentioned above, in this work four different flux selections for the computation of $\tau_{\text{eff}}(z)$ are considered. The redshift evolution of the effective optical depth obtained in

²Throughout this work, the corrected model flux means the model flux corrected for metal, fixed-parameter, and narrow absorption lines, i.e., model flux selection 2 (see text).

Table 4.1. Best-fit parameters from the power-law fit of the form $\tau_{\text{eff}} = \tau_0 \cdot (1 + z)^{1+\gamma}$ to the $\tau_{\text{eff}}(z)$ measurements from different flux selections (see §4.1).

flux selection	τ_0	γ	reference
a) observed flux	0.0086 ± 0.0072	1.71 ± 0.58	Fig. 4.3 a
b) model flux	0.0090 ± 0.0074	1.68 ± 0.58	Fig. 4.3 b
c) model flux selection 1)	0.0058 ± 0.0043	1.96 ± 0.51	Fig. 4.3 c
d) model flux selection 2)	0.0045 ± 0.0034	2.09 ± 0.52	Fig. 4.3 d

each case is shown in Fig. 4.3. Apparently, the relative position of the data points depends only weakly on the selection method. In general, the effective optical depth increases with redshift, as expected since the H I density increases with redshift due to the contraction of the Universe. Theoretically, the redshift evolution of τ_{eff} may be expected to follow a power law since the observed redshift evolution of the number density of hydrogen absorbers can empirically be described as a power law (see §1.5.1, in particular Eq. 1.15, and §3.4). As can be seen from Figs. 4.3 a–4.3 d, a single power law does not fit the data very well, which partially may be due to the restricted redshift range considered ($\Delta z \approx 0.9$). In this respect, a few outliers could have a significant impact on the general evolution. For the best-fit parameters using a single power law see Table 4.1. Assuming that a power law is a fair description of the redshift evolution of the effective optical depth shown in Fig. 4.3, we arrive at the following possibilities:

- i) If one fits a power law only through the first three redshift bins and the last two, a drop of the effective optical depth in the redshift range $3.0 < z < 3.4$ becomes apparent, which may correspond to a downward feature seen in other works (Bernardi et al. 2003; Faucher-Giguère et al. 2008b; Dall’Aglio et al. 2008).
- ii) If two power laws are considered with a break at $z \approx 3.2 - 3.4$ following Pâris et al. (2011), the slope would be smaller at lower redshift indicating a flatter evolution in the effective optical depth than at higher redshifts.

Figure 4.4 shows a comparison of the results shown in Figs. 4.3 a–4.3 d. The respective values of the effective optical depth are listed in columns 2 – 5 of Table 4.2. The τ_{eff} measurements using the observed flux and the model flux including all absorption lines fitted with CANDALF agree very well with each other. This is not surprising since the model flux using all absorption lines follows the observed flux closely (see Appendix D). Also, the distributions of 3 proper Mpc segments at a given redshift using both fluxes are highly similar (compare Figs. C.1 a and C.1 b). The excellent agreement between the τ_{eff} measurements using the observed flux and the model flux, respectively, justifies the use of the model flux in order to remove individual absorption features from the model flux for a corrected measurement of the redshift evolution of the effective optical depth. From Fig. 4.4 it can be seen that excluding absorption lines does not alter the shape of the redshift evolution of τ_{eff} , but only its amplitude. This suggests that the overall evolution of τ_{eff} is rather insensitive to contamination by metal lines and/or the presence of narrow ($b < 15 \text{ km s}^{-1}$) absorption lines (fixed-parameter lines likely contribute little to τ_{eff} , see §2.3.3 and Appendix B). This may be due to the presence of metal and narrow absorption lines at all redshifts. Despite the apparent lack of a trend in the metal pollution, only few

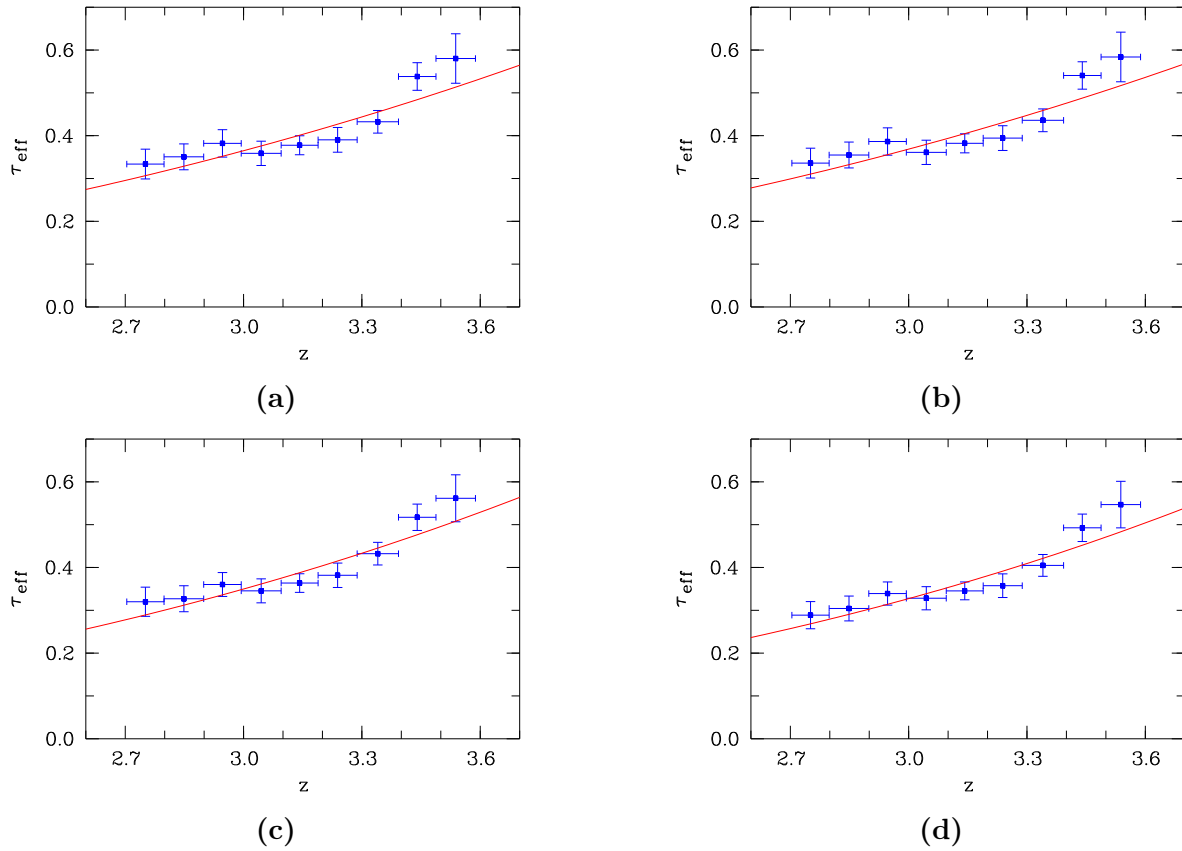


Figure 4.3. Redshift evolution of the effective optical depth. The red, solid line represents the best fit to the data with the empirical power law $\tau_{\text{eff}} = \tau_0 \cdot (1 + z)^{1+\gamma}$. The values of the fit parameters for each case are listed in Table 4.1. The flux used is (a) the observed flux, (b) the model flux, (c) the model flux excluding metal absorption lines and absorption lines with fixed fitting parameters, and (d) the model flux excluding metal absorption lines, absorption lines with fixed fitting parameters, and lines with Doppler parameters smaller than $b = 15 \text{ km s}^{-1}$.

identified metals seem to be present in the redshift bin at $z = 3.34$. The probability of finding metal absorption lines in blends within the H I Ly α forest increases with redshift because the amount of H I Ly α absorption features increases due to the larger amount of neutral hydrogen following the reionization history of the Universe (see §1.2). However, the number of metal absorption features also increases with redshift and metal absorption is seen at $z > 3.34$. There is no apparent reason for the lack of metals at $z \simeq 3.34$.

The ideal measurement of the redshift evolution of the effective optical depth comes from flux which is due to H I Ly α only. In this work such a measurement is $\tau_{\text{eff}}(z)$ computed from the model flux corrected for metal absorption lines, fixed-parameter lines, and narrow absorption lines, which is shown in Fig. 4.3 d. It can be seen that a single power law does not fit the data properly. Figure 4.5 a shows the same data points plotted in a logarithmic scaling in the ordinate. In order to investigate if a broken power law fits the data well I divided the data points into two samples: a low-redshift sample and a high-redshift sample. The high-redshift sample comprises those data points which were not considered in the low-redshift sample. An exception is the break point. The break point separates the redshift samples and is considered in both samples. At least two data points are necessary for a power-law fit in logarithmic space. This means that either the low-redshift or the

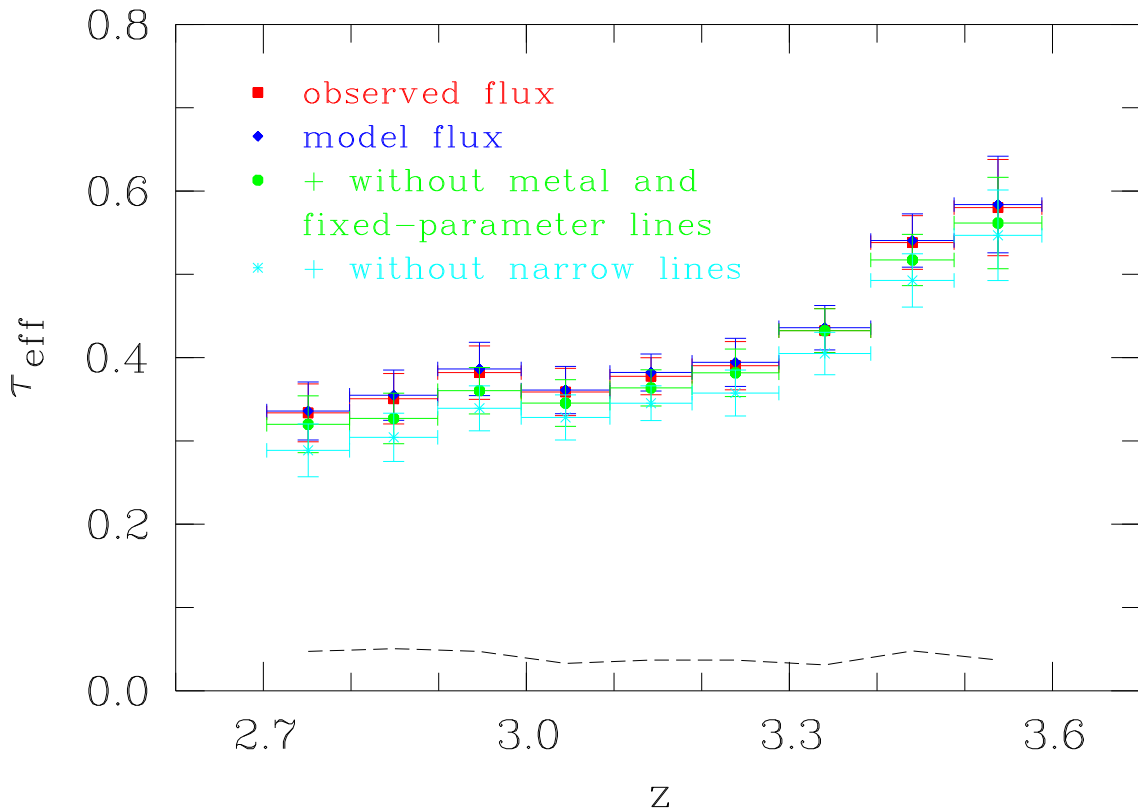


Figure 4.4. Comparison of the results for each flux selection to show the effect of removed absorption lines on the redshift evolution of the effective optical depth. Note that the data points in each case are identical to the corresponding data points shown in Fig. 4.3. The dashed line shows the interpolated contribution to τ_{eff} from contaminating absorption features, i.e., the difference between the model flux (blue lozenges) and the model flux corrected for metal, fixed-parameter and narrow lines (cyan asterisks, see column 6 of Table 4.2).

high-redshift sample contain a minimum of two data points while the other contain the maximum of eight data points. This leaves 7 possibilities to fit a broken power law to the data. The combinations of the low-redshift and high-redshift data points are 2 and 8, 3 and 7, 4 and 6, etc. Figure 4.5 b depicts the dependence of the final sum of squares of residuals³ on the break point at different redshifts. The final sum of squares of residuals reaches a minimum with a break point at $z \approx 3.238$. The corresponding power-law fits are shown in Fig. 4.5 c (grey solid lines). The existence of a power-law break could only be confirmed if data points lower than $z = 2.7$ and higher than $z = 3.6$ were included. The constrained analyzed redshift range may hinder determining the actual trend in the redshift evolution of the effective optical depth. This could be overcome by considering additional sightlines that cover lower and higher redshifts beyond the redshift range discussed here or by comparison to other works, though it is difficult to compare different methods to infer the effective optical depth reliably.

There is some uncertainty inherent to the method used in this work to determine the

³The residual means the difference between a data point and the estimated value from the power-law fit to the data. The sum of the squared residuals gives the overall difference. Since the power law is fitted iteratively the final sum of squares of residuals corresponds to the best fit.

Table 4.2. Values of the effective optical depth for the four flux selections. Listed are the average redshift, the τ_{eff} values for the observed flux, the model flux, the model flux excluding metal and fixed-parameter absorption lines, and the model flux corrected for metal, fixed-parameter, and narrow lines. The values in column 6 are $\tau_{\text{eff,metals}} = \tau_{\text{eff}}^{\text{mod}} - \tau_{\text{eff}}^{\text{cor}}$.

$\langle z \rangle$	$\tau_{\text{eff}}^{\text{obs}}$	$\tau_{\text{eff}}^{\text{mod}}$	$\tau_{\text{eff}}^{\text{nom}}$	$\tau_{\text{eff}}^{\text{cor}}$	$\tau_{\text{eff,metals}}$
2.751	0.334 ± 0.035	0.336 ± 0.035	0.320 ± 0.034	0.289 ± 0.032	0.047
2.849	0.351 ± 0.030	0.355 ± 0.030	0.327 ± 0.030	0.304 ± 0.029	0.051
2.946	0.382 ± 0.032	0.386 ± 0.032	0.360 ± 0.028	0.339 ± 0.027	0.047
3.045	0.359 ± 0.028	0.361 ± 0.028	0.345 ± 0.028	0.328 ± 0.027	0.033
3.142	0.378 ± 0.022	0.382 ± 0.022	0.364 ± 0.022	0.345 ± 0.021	0.037
3.238	0.390 ± 0.029	0.394 ± 0.029	0.382 ± 0.029	0.358 ± 0.028	0.037
3.340	0.432 ± 0.026	0.436 ± 0.027	0.432 ± 0.026	0.405 ± 0.025	0.031
3.440	0.538 ± 0.032	0.541 ± 0.032	0.517 ± 0.031	0.493 ± 0.032	0.048
3.538	0.580 ± 0.058	0.584 ± 0.058	0.562 ± 0.055	0.547 ± 0.054	0.037

effective optical depth but it has no impact on the conclusions drawn above. The mean flux computed from the 3 proper Mpc segments shall obey the central limit theorem, i.e., it should be approximately normally distributed. The observed, normalized flux values range from 1, if the observed flux is almost unabsorbed as at low redshift, to 0, if the observed flux is mostly suppressed as at high redshift ($z > 5$). The constrained range of the normalized flux values may cut off any Gaussian distribution if the extreme cases are approached. Nevertheless, the arithmetic mean can be computed and although the error estimate may be more uncertain, the conclusions drawn from the mean flux may still be the same. In this work, these extreme cases are not approached using the observed or model flux.

4.3 Systematics

In this chapter, an analysis of the potential systematic errors on the measurement of the H I Ly α opacity is presented. The effect of the choice of redshift bin size on the measurement is investigated in §4.3.1. In §4.3.2, an alternative method to correct for the presence of metal absorption lines following Faucher-Giguère et al. (2008b) is presented, which could be applied to τ_{eff} measurements in studies where a direct estimate of the contribution of metal absorption lines to the effective optical depth is not possible. The reliability of the method used in this work to compute the redshift evolution of the effective optical depth is assessed by the use of simulations in §4.3.3.

4.3.1 Shifting the redshift bounds of the 3 proper Mpc segments

The method to compute the redshift evolution of the effective optical depth used in this work is based on the set-up of the 3 proper Mpc segments (see §4.1). From a computational point of view it is possible to measure the 3 proper Mpc segments starting at $z = 0$. For simplicity, I started the measurement at $z = 2.0$. Depending on the starting point, the 3 proper Mpc redshift bounds change. In the following it will be discussed whether the

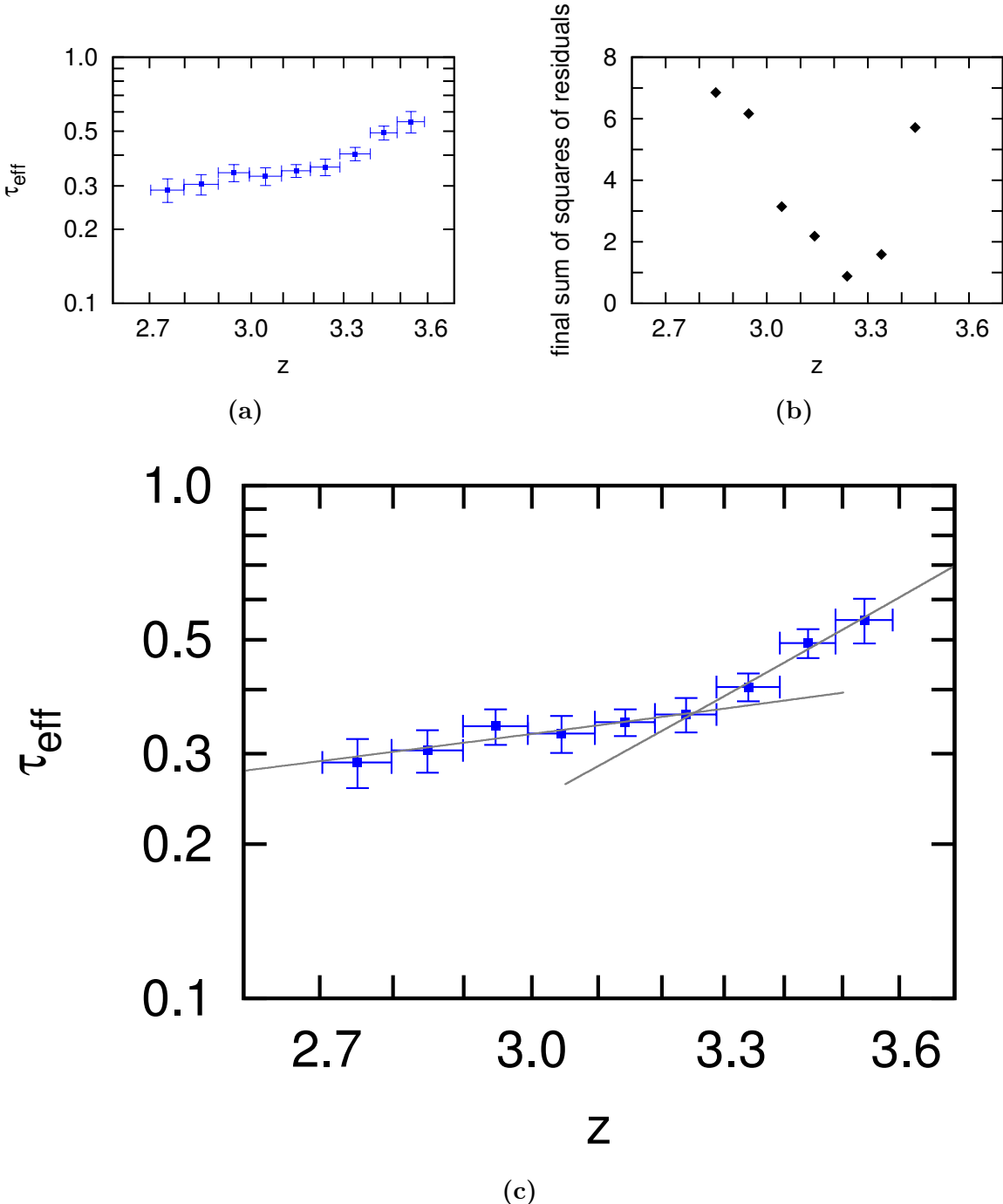


Figure 4.5. Fit in the form of a broken power law to the redshift evolution of the effective optical depth. (a) Same as Fig. 4.3 d in logarithmic scale in $\tau_{\text{eff}}(z)$. (b) Final sum of squares of residuals depending on the assumed break of a fitted power law to the data points of Fig. 4.5 a (see text). (c) Best broken-power-law fit to the data of Fig. 4.5 a as judged by Fig. 4.5 b. Redshift $z \approx 3.24$ marks the power-law break. The slope is $1 + \gamma$ with $\gamma = 0.57 \pm 0.32$ and $\gamma = 5.59 \pm 0.63$ for the low-redshift and high-redshift data points, respectively.

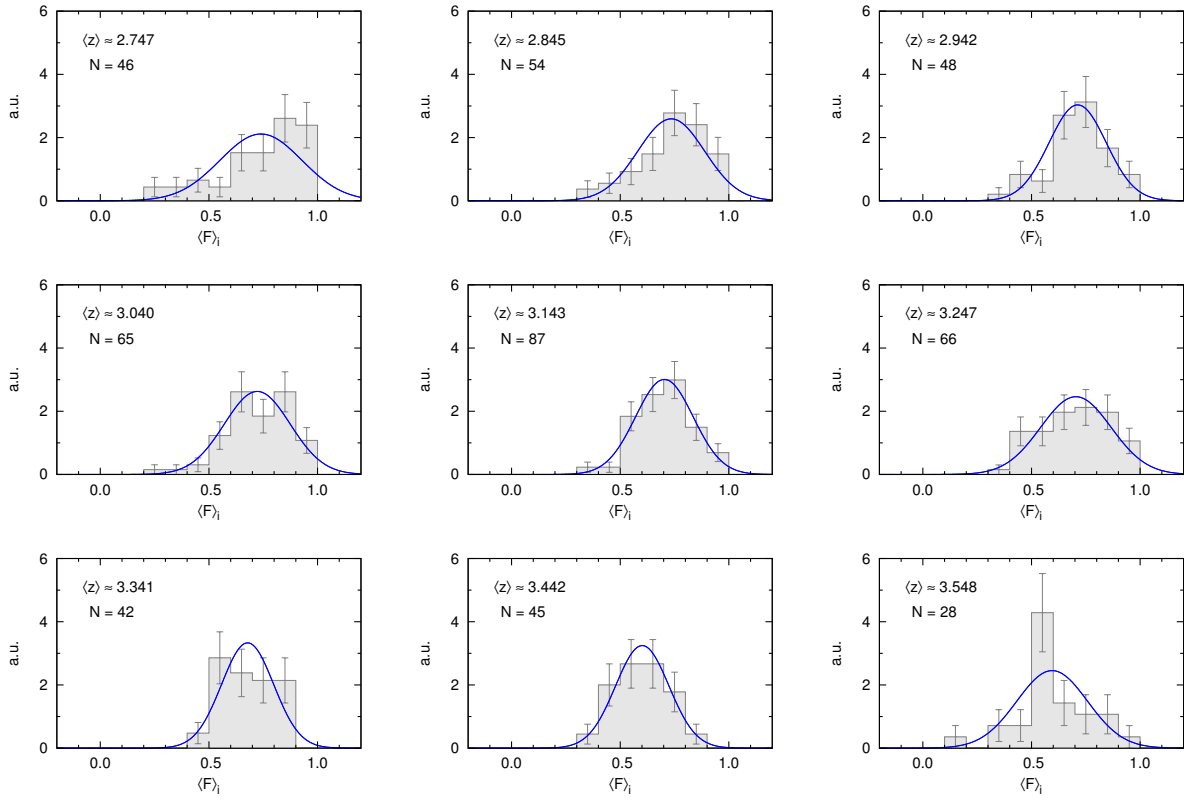


Figure 4.6. Same as Fig. 4.2 with the 3 proper Mpc segments calculated beginning at $z = 2.7$ instead of $z = 2.0$.

choice of the starting point affects the results significantly.

According to Eq. (1.10) the redshift bounds of the segments do not matter for computing τ_{eff} if each segment contains the same number of pixels and if all pixels are accounted for. As can be seen from Eq. (4.1) and Fig. 4.1, with increasing redshift the same proper distance covers larger redshift ranges. This is only partly compensated by the increasing separation of adjacent pixels with redshift. Hence, 3 proper Mpc segments contain more pixels at higher redshift. If the bounds of the 3 proper Mpc segments are shifted, some of the pixels are lost for or moved into adjacent redshift bins. According to the Cosmological Principle, a sufficiently large number of sightlines, and therefore segments, yields a $\langle F \rangle_i$ distribution in a given redshift bin that approaches the true distribution in that bin. Hence, a shift in the starting point for the computation of the 3 proper Mpc segments should be unimportant if there are enough data.

To test this, I measured the 3 proper Mpc segments additionally from $z = 2.7$ for the model flux corrected for metal, fixed-parameter, and narrow absorption lines. Thereby, the shift in the segment boundaries corresponds to roughly 40 % of a given segment in redshift, although the shift increases slightly with redshift from about 37 % in the first segment to about 42 % in the last one. The resulting mean-flux distribution for redshift bins of size $\Delta z \simeq 0.1$ is shown in Fig. 4.6 and can be compared to Fig. 4.2. The individual distributions are quite similar and the Gaussian shape of the histograms is at least tentative in both of the figures at any redshift. The comparison of the evolution of the effective optical depth derived from the two 3 proper Mpc set-ups using the corrected

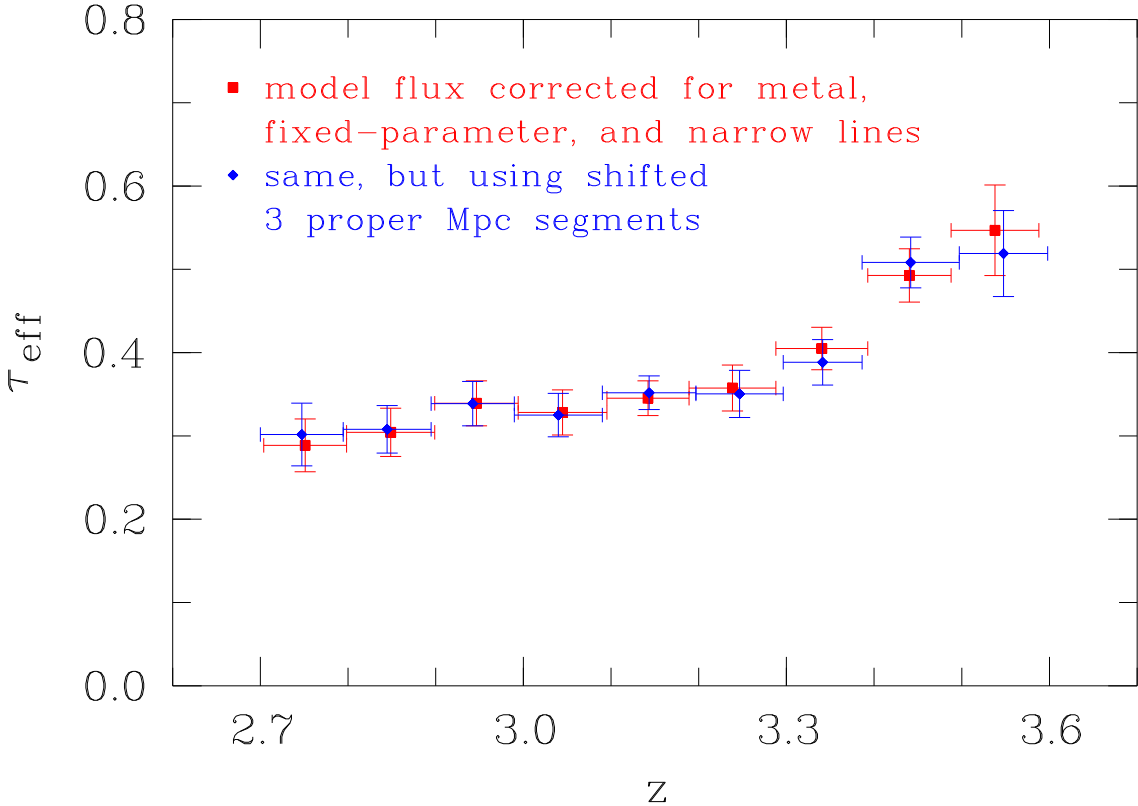


Figure 4.7. Redshift evolution of the effective optical depth for two different grids of 3 proper Mpc segments. Data points for segments starting at $z = 2.0$ (red; same as Fig. 4.3 d) are compared to those starting at $z = 2.7$ (blue).

model flux is shown in Fig. 4.7. Even though there is some difference in the measured values in each case, the data points agree within the error bars. Apparently, the quasar spectra sample used in this work consists of a sufficient amount of data. The last redshift bin used for the computation of τ_{eff} has the most uncertain flux distribution due to the small number of segments contained in that bin. Therefore, it may be more sensitive to a shift of the redshift bounds of the 3 proper Mpc segments.

4.3.2 Correction for metal absorption lines

The contribution of metal absorption lines to the effective optical depth can be quantified as follows, using the values listed in Table 4.2. At a given observed wavelength, λ_{obs} , the optical depth τ_{total} is the sum over the optical depth τ_i of the \mathcal{N} transitions contributing at λ_{obs} ,

$$\tau_{\text{total}} = \sum_{i=1}^{\mathcal{N}} \tau_i, \quad (4.3)$$

such that

$$f_{\nu} = e^{-\tau_{\text{total}}} = e^{-\sum_{i=1}^{\mathcal{N}} \tau_i} = \prod_{i=1}^{\mathcal{N}} e^{-\tau_i}. \quad (4.4)$$

Each of these transitions features a different rest-frame wavelength so that they can be accounted for independently (Faucher-Giguère et al. 2008b), hence,

$$\langle f_\nu \rangle = \prod_{i=1}^N \langle e^{-\tau_i} \rangle \equiv \prod_{i=1}^N e^{-\tau_{\text{eff},i}}. \quad (4.5)$$

Considering the transitions of H I Ly α and metals, and using Eq. (1.5), we get

$$e^{-\tau_{\text{eff}}} \equiv \langle f_\nu \rangle = e^{-\tau_{\text{eff},\alpha}} \cdot e^{-\tau_{\text{eff,metals}}}, \quad (4.6)$$

so that

$$\underbrace{\tau_{\text{eff}}}_{\equiv \tau_{\text{eff}}^{\text{mod}}} = \underbrace{\tau_{\text{eff},\alpha}}_{\equiv \tau_{\text{eff}}^{\text{cor}}} + \tau_{\text{eff,metals}}. \quad (4.7)$$

The value of $\tau_{\text{eff,metals}} = \tau_{\text{eff}}^{\text{mod}} - \tau_{\text{eff}}^{\text{cor}}$ is given in column 6 of Table 4.2 and can be used for metal correction in an otherwise metal contaminated measurement of the effective optical depth. The dashed line in Fig. 4.4 interpolates the redshift evolution of $\tau_{\text{eff,metals}}$. This quantity is rather constant within the considered redshift range.

4.3.3 Simulations

In addition to observational data I used synthetic quasar absorption spectra to investigate various aspects of the flux statistics. The main purpose of this exercise is to perform a quality assessment of the method to compute the redshift evolution of the effective optical depth used in this work. The synthetic spectra have a better resolution than the observed quasar spectra but were sampled onto pixels of the same size as the observed spectra. The synthetic spectra are noise-free and include absorption by H I Ly α only.

The synthetic spectra were created using a Monte-Carlo simulation following Tepper-García and Fritze (2008) in the following way. For a given redshift, a random number of H I Ly α absorption lines is drawn from a distribution constrained by observations of the mean number density of H I Ly α absorbers $d^3N \propto f(z)g(b)h(N)dz db dN$ (see §1.5.1 and Chapter 3), assuming the number of lines along the sightline follows a Poisson distribution. Here, $f(z) \propto (1+z)^\gamma$, $g(b)$, and $h(N) \propto N^{-\beta}$ are the distribution of redshifts, Doppler parameters, and column densities, respectively. The parameters (z, b, N) of each line are then randomly drawn from their corresponding distribution. The absorption of each line is calculated assuming a Voigt profile, and the normalized absorption spectrum including the absorption of all lines is then overlayed onto an unabsorbed quasar spectrum template. We use the quasar template given by Brotherton et al. (2001). The chosen distribution parameters for the simulations are $\gamma = 1.5$, $\beta = 1.5$ (the column density distribution function is assumed to follow a single power law), and a lognormal distribution $g(b)$ (rather than a cut-off Gaussian). The latter implies that the logarithm of b is normally distributed,

$$g(b; \mu, \sigma) = \frac{1}{\sqrt{2\pi}\sigma b} \exp \left[-\frac{1}{2} \left(\frac{\ln b - \mu}{\sigma} \right)^2 \right]. \quad (4.8)$$

In this case, the mean μ and the standard deviation σ of $\ln b$ are related to the expected value μ' and standard deviation σ' of the Doppler parameter b via

$$\mu' = \exp \left[\mu + \frac{1}{2}\sigma^2 \right] \quad (4.9)$$

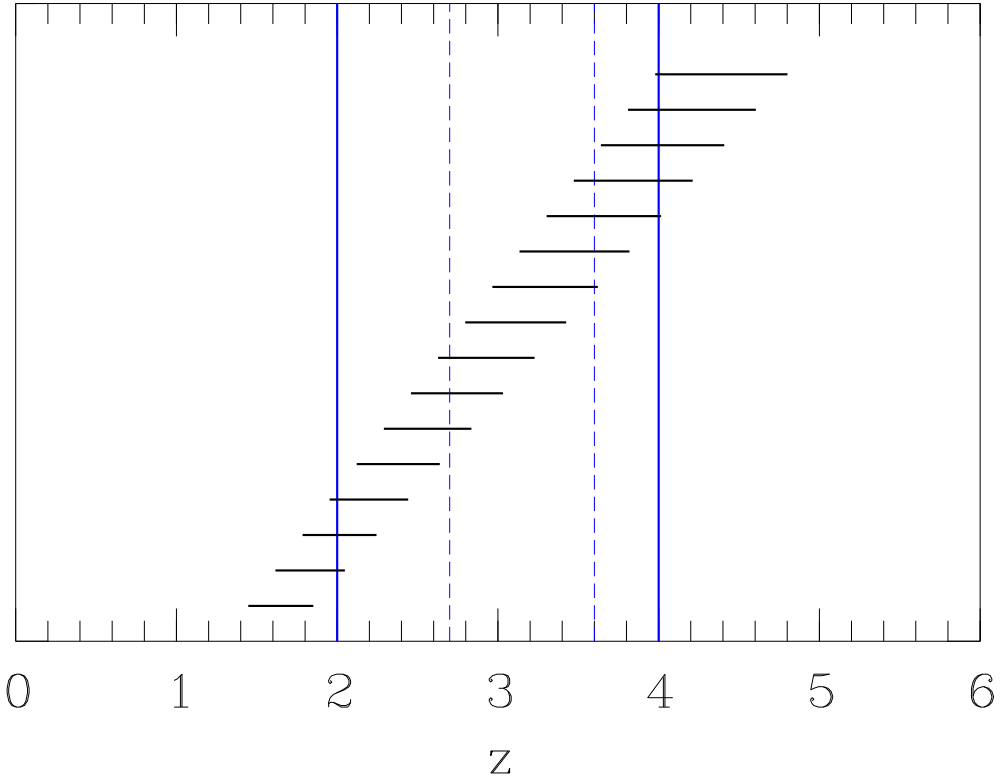


Figure 4.8. Redshift coverage of the 16 synthetic spectra (horizontal lines) between the H I Ly β emission line and the assumed proximity zone of the quasar. The blue vertical lines mark the limits of the analyzed redshift range for $\tau_{\text{eff}}(z)$ using the synthetic spectra (solid lines) and the 13 observed quasar spectra (dashed lines).

and

$$\sigma' = (\exp [\sigma^2] - 1)^{\frac{1}{2}} \mu' \quad (4.10)$$

(see, e.g., Tepper-García and Fritze 2008). In this work, $\mu' = 25 \text{ km s}^{-1}$ and $\sigma' = 15 \text{ km s}^{-1}$.

A set of synthetic spectra consists of 16 sightlines with emission redshifts in the range $1.9 \leq z_{\text{em}} \leq 4.9$ separated in redshift space by $\Delta z_{\text{em}} = 0.2$ (see Fig. 4.8). The analysis of the synthetic spectra was done in the same way as for the 13 observed quasar spectra. This includes the used redshift range between the H I Ly β emission line and the proximity zone of the quasar, and the computation of $\tau_{\text{eff}}(z)$. An example of a synthetic quasar absorption spectrum is shown in Fig. 4.9.

Twelve different sets of synthetic spectra were used in order to study the effect of parameter distributions on $\tau_{\text{eff}}(z)$. This may give insight into whether a deviation from an otherwise smooth evolution of the effective optical depth may not be of physical origin but rather caused by the analysis method, and to whether it is linked to the line-number-density evolution. Note that, by construction, a downward feature is not expected to be present in $\tau_{\text{eff}}(z)$ inferred from the synthetic spectra. We systematically investigate the effect of each parameter (b, N) on the evolution of τ_{eff} by varying either both parameters, by varying only one of them while keeping the other one fixed, or by keeping both of

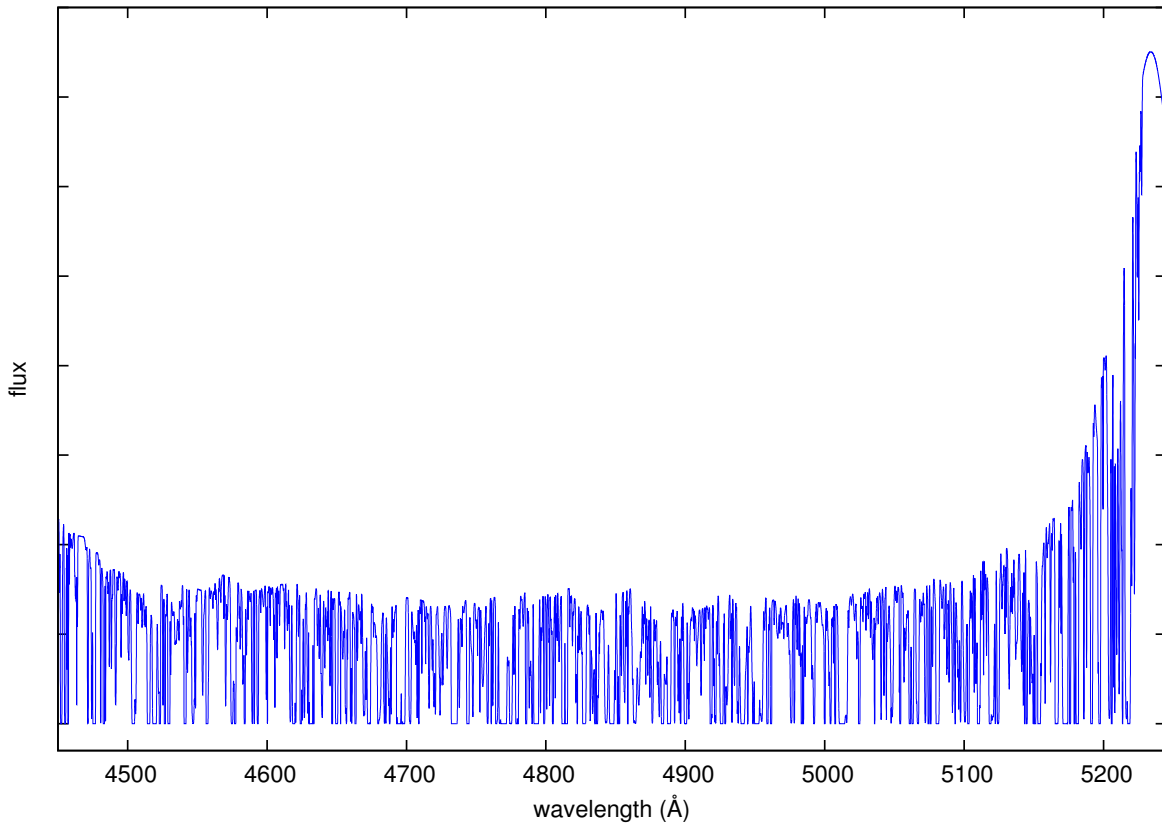


Figure 4.9. Example of a synthetic quasar absorption spectrum of a source at redshift $z_{\text{em}} = 3.3$. See text for details.

them fixed at different values. Although this approach leads to unrealistic line distributions and, hence, to an unrealistic evolution of τ_{eff} in each case, it is extremely convenient in order to isolate the effect of each parameter on the measured τ_{eff} . The number density is the same for any of the sets of synthetic spectra, $dN/dz \propto (1+z)^{\gamma \equiv 1.5}$. For each set the redshift evolution of the effective optical depth was computed and a power law of the form $\tau_{\text{eff}}(z) \propto (1+z)^{\gamma_{\text{free}}+1}$ was fitted to the result.

Table 4.3 summarizes the results of the power-law fits to the evolution of τ_{eff} inferred from the synthetic spectra. In columns 2 and 3 the different parameter distributions used to create the synthetic spectra are listed. The slope of the power-law fit to the redshift evolution of the effective optical depth is listed in column 4. The reduced χ^2 value is computed by dividing the χ^2 value by the number of degrees of freedom (dof). The number of degrees of freedom is the difference between the number of data points and the number of free parameters. The reduced χ^2 value is given in column 5. Since the expected power-law slope is $\gamma_{\text{free}} = \gamma \equiv 1.5$, a power law with this slope is also fitted to the evolution of the effective optical depth. The reduced χ^2 value for $\gamma = 1.5$ is given in column 6. Figures of the evolution of the effective optical depth are listed in column 7.

The evolution of τ_{eff} is insensitive to the redshift bin size (see rows 1 and 2 of Table 4.3). This is at least true for redshift bins of size $\Delta z \simeq 0.1$ and 0.2. Hence, computing $\tau_{\text{eff}}(z)$ from the observed quasar spectra in redshift bins of $\Delta z \simeq 0.1$ is appropriate (Figs. 4.3 and 4.4). In principle, smaller redshift bins should allow for a more precise study in terms

Table 4.3. Power-law-fit results for the redshift evolution of the effective optical depth computed from sets of synthetic spectra for two different redshift bin sizes (Δz). The sets differ in the parameter distributions of absorption lines used to create the synthetic spectra. The column-density range of the absorbers is given in column 2 and the Doppler-parameter distribution in column 3. The fitted power-law slope and the reduced χ^2 value from the power-law fits are given in columns 4 and 5, respectively. Column 6 contains the reduced χ^2 value from fixed-slope power-law fits with $\gamma = 1.5$. Figure references can be found in column 7.

#	$\log N$	b	γ_{free}	$\chi^2_{\gamma_{\text{free}}}/\text{dof}$	$\chi^2_{\gamma=1.5}/\text{dof}$	reference
$\Delta z \simeq 0.1$						
1	12 – 17	lognormal [‡]	1.29 ± 0.12	1.024	1.127	Fig. 4.14
$\Delta z \simeq 0.2$						
2	12 – 17	lognormal [‡]	1.28 ± 0.13	1.004	1.224	Fig. 4.10 a
3	12 – 22	lognormal [‡]	1.55 ± 0.14	1.412	1.273	Fig. 4.10 b
4	12 – 17	25 km s^{-1}	1.53 ± 0.15	1.792	1.600	Fig. 4.11 a
5	12 – 22	25 km s^{-1}	1.82 ± 0.13	1.530	2.417	Fig. 4.11 b
6	13	lognormal [‡]	1.48 ± 0.07	1.712	1.537	Fig. 4.12 a
7	14	lognormal [‡]	1.45 ± 0.05	0.417	0.417	Fig. 4.12 b
8	15	lognormal [‡]	1.44 ± 0.14	1.355	1.235	Fig. 4.12 c
9	17	lognormal [‡]	1.60 ± 0.23	2.039	1.858	Fig. 4.12 d
10	13	25 km s^{-1}	1.45 ± 0.08	2.152	2.000	Fig. 4.13 a
11	14	25 km s^{-1}	1.56 ± 0.07	0.710	0.692	Fig. 4.13 b
12	15	25 km s^{-1}	1.58 ± 0.14	1.337	1.238	Fig. 4.13 c
13	17	25 km s^{-1}	2.11 ± 0.37	4.907	5.741	Fig. 4.13 d

[‡] The expected value and the standard deviation of the lognormal distribution is $b = 25 \text{ km s}^{-1}$ and $b = 15 \text{ km s}^{-1}$, respectively.

of redshift evolution although more data would be required to avoid increasing the uncertainty (since smaller bins result in less 3 proper Mpc segments in each bin for a given data set).

Comparing Figures 4.10 a and 4.10 b, it can be seen that including high-column-density absorbers with $\log N = 17 – 22$ contributes little to the effective optical depth if the respective power-law fits with slope $\gamma = 1.5$ (dashed black line) are considered. Even though high-column densities imply a high opacity, such systems are rare. The normalization of the power law increases about 5 % if high-column density absorbers are included, though within the error this increase could be far less. Comparing the slope-fitted power laws (solid red lines) shows a larger difference in the evolution since the slopes already differ (γ_{free} in row 2 and 3 of Table 4.3). The decrease in the normalization is insignificant compared to the steepening in the slope. $\tau_{\text{eff}}(z \lesssim 2.3)$ is comparable for both column-density ranges, but $\tau_{\text{eff}}(z = 4)$ increases by more than 10 % if high-column-density absorbers are included. The same conclusions can be drawn comparing Figs. 4.11 a and 4.11 b, and the parameters of the respective power-law fits.

Using the same column-density distribution but different Doppler-parameter distributions to create synthetic spectra may give an insight on the impact of the Doppler parameter on

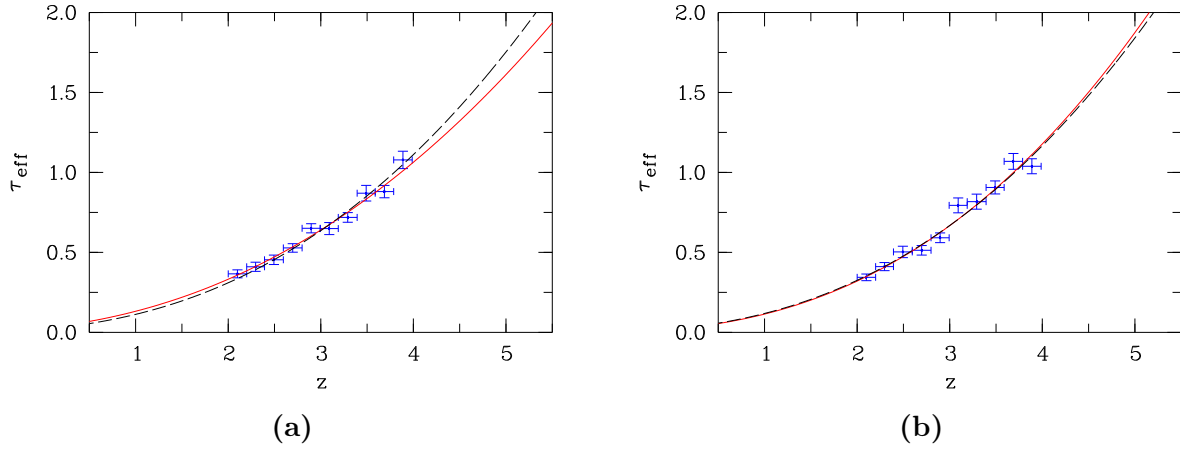


Figure 4.10. Redshift evolution of the effective optical depth from synthetic quasar spectra featuring H I Ly α absorption lines with lognormal Doppler-parameter distributions and different column-density distributions (rows 2 and 3 in Table 4.3). Column densities are within the range from $\log N_{\text{H}\text{I}} = 12$ to $\log N_{\text{H}\text{I}} = 17$ (a) and $\log N_{\text{H}\text{I}} = 22$ (b). The lines are power-law fits of the form $\tau_{\text{eff}}(z) = \tau_0 \cdot (1 + z)^{\gamma+1}$ to the respective data points. The dashed black line in each panel has $\gamma \equiv 1.5$ (input value) and the red solid line has $\gamma = 1.28 \pm 0.13$ (a) and $\gamma = 1.55 \pm 0.14$ (b).

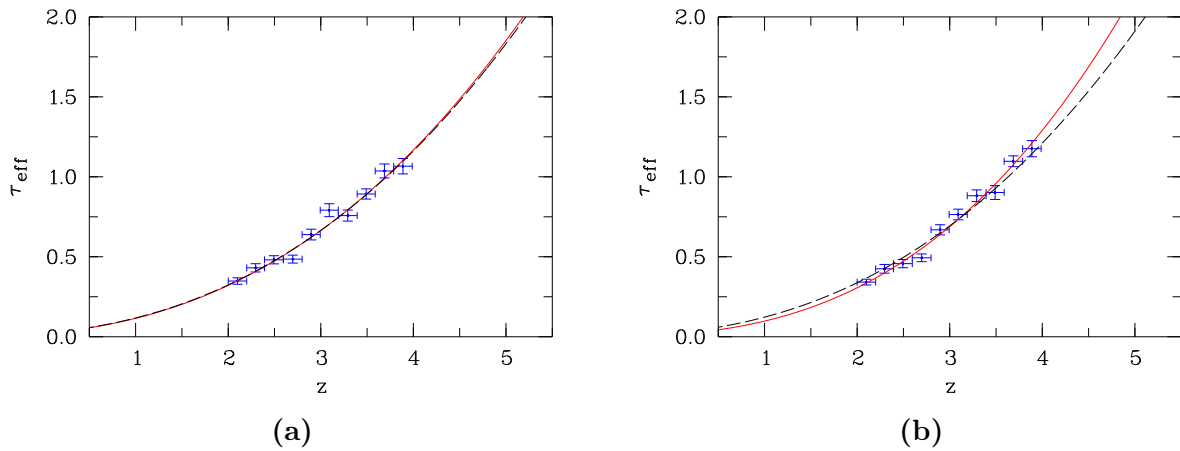


Figure 4.11. Redshift evolution of the effective optical depth from synthetic quasar spectra featuring H I Ly α absorption lines with different column-density distributions and a fixed Doppler parameter, $b = 25 \text{ km s}^{-1}$ (rows 4 and 5 in Table 4.3). Column densities are within the range from $\log N_{\text{H}\text{I}} = 12$ to $\log N_{\text{H}\text{I}} = 17$ (a) and $\log N_{\text{H}\text{I}} = 22$ (b). The lines are power-law fits of the form $\tau_{\text{eff}}(z) = \tau_0 \cdot (1 + z)^{\gamma+1}$ to the respective data points. The dashed black line in each panel has $\gamma \equiv 1.5$ (input value) and the red solid line has $\gamma = 1.53 \pm 0.15$ (a) and $\gamma = 1.82 \pm 0.13$ (b).

$\tau_{\text{eff}}(z)$ inferred from these spectra. Since the lognormal distribution already peaks quite sharply, testing Doppler parameters on their impact on $\tau_{\text{eff}}(z)$ is difficult. Hence, other than the lognormal distribution, the only different approach considered in this work is to create synthetic spectra with a fixed b value of 25 km s^{-1} .

Consulting Table 4.3 and comparing Figs. 4.10 a and 4.11 a, or Figs. 4.10 b and 4.11 b, gives an insight on a relative change in the redshift evolution of the effective optical depth. Considering the power-law fits with $\gamma = 1.5$ the normalization is marginally larger for a fixed Doppler parameter. This means, that the effective optical depth is systematically larger for a fixed Doppler parameter at all redshifts. This can be explained as follows. The most probable Doppler parameter of the lognormal distribution lies somewhat below 20 km s^{-1} , though the average Doppler parameter should be higher due to the high- b tail. Judging from the similar τ_{eff} evolution, 25 km s^{-1} should be close to the mean value, which is expected by the construction of the synthetic spectra. Although drawn from the same distribution, the Doppler-parameter distributions of different synthetic spectra will be slightly different due to statistical fluctuations. A shift to a Doppler parameter close to the mean for absorbers which have lognormally distributed b values smaller than the average, increases the effective optical depth. This effect is not fully compensated by those absorbers whose Doppler parameters from the high- b tail are reduced to $b = 25 \text{ km s}^{-1}$. The overall absorption increases for a fixed value of $b = 25 \text{ km s}^{-1}$ by about 4%. These conclusions depend somewhat on the error estimate of the normalization which allows for no difference in $\tau_{\text{eff}}(z)$ at all using the two Doppler-parameter approaches.

Fitting a power law to the data with the slope as a free parameter (red solid line in the figures) results in a larger slope and a smaller normalization for fixed Doppler parameters compared to the case of a lognormal distribution. The difference in the normalization is insignificant compared to the change in slope. The relative change of the effective optical depth is even smaller when high-column-density absorbers are included. The slope is steeper for each Doppler-parameter distribution if the high-column-density absorbers are included (see Table 4.3 rows 2 and 3, as well as 4 and 5).

The influence of the Doppler parameter on $\tau_{\text{eff}}(z)$ may be constrained better if lognormal distributions are considered which peak at different values due to shifting or broadening of the distribution. This is left for future work.

Comparing the $\gamma = 1.5$ power laws of the respective panels in Figs. 4.12 and 4.13 shows that using the fixed Doppler parameter rather than the lognormal distribution increases the normalization about 4% on average, ranging between 1% (top left panel) and 8% (top right panel). Hence, the effective optical depth increases at all redshifts. This is the same trend as mentioned above. Increasing the fixed column density of absorbers intersecting a given line of sight (Figs. 4.12 and 4.13) increases the effective optical depth as well, as expected.

Figure 4.14 shows the redshift evolution of the effective optical depth inferred from the same set of synthetic spectra as the evolution shown in Fig. 4.10 a, but computed in about half the redshift bin size (see Table 4.3, row 1). The data points show some scatter around an ideal power law. The scatter could most likely be reduced if more sightlines are used. Figure 4.14 indicates that the error of the synthetic data points may be underestimated since a power law is expected to be recovered. It is likely that the uncertainties on the τ_{eff} measurements found in the literature are too optimistic as well. This could mean that in

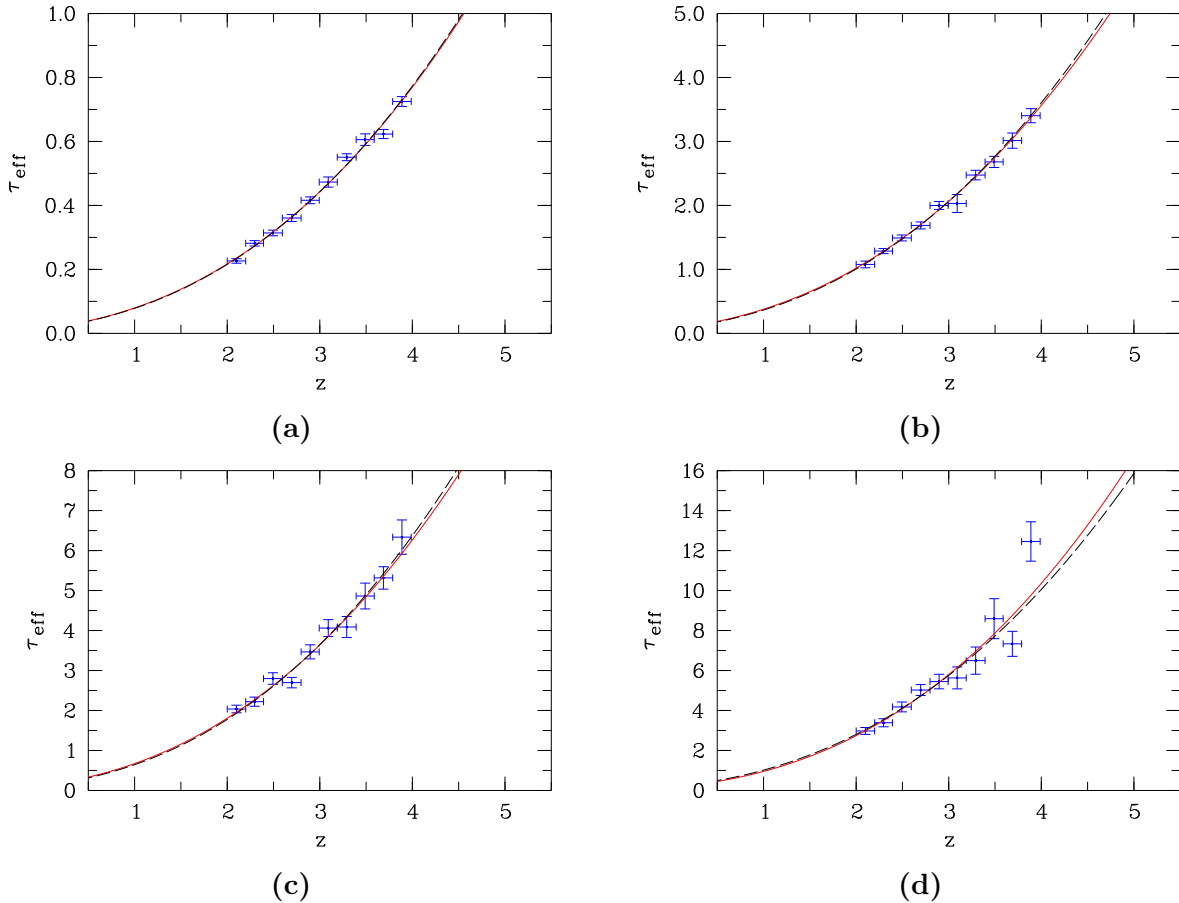


Figure 4.12. Redshift evolution of the effective optical depth from synthetic quasar spectra featuring H I Ly α absorption lines with lognormal Doppler-parameter distributions and a fixed column density: (a) $\log N_{\text{H}\,1} = 13$; (b) $\log N_{\text{H}\,1} = 14$; (c) $\log N_{\text{H}\,1} = 15$; (d) $\log N_{\text{H}\,1} = 17$ (rows 6 – 9 in Table 4.3). The lines are power-law fits of the form $\tau_{\text{eff}}(z) = \tau_0 \cdot (1 + z)^{\gamma+1}$ to the respective data points. The dashed black line in each panel has $\gamma \equiv 1.5$ (input value) and the red solid line has $\gamma = 1.48 \pm 0.07$ (a), $\gamma = 1.45 \pm 0.05$ (b), $\gamma = 1.44 \pm 0.14$ (c), and $\gamma = 1.60 \pm 0.23$ (d).

reality all measurements agree with a smooth evolution of the effective optical depth. Due to the known input slope ($\gamma \equiv 1.5$) the inferred power-law slope $\gamma = 1.29 \pm 0.12$ (red solid line in Fig. 4.14) may imply that the error of the power-law slope may be underestimated, too. The deviation of the recovered power-law slope from the input value may be a result of the restricted redshift range used. It may also be a result of statistical fluctuations in the number density and in the parameter distributions. Statistical fluctuations should be smoothed out by using more quasar spectra. On a test sample of 29 synthetic spectra in the redshift range $2 \leq z \leq 4$ with $\Delta z_{\text{em}} = 0.1$, the same exercise has been performed, which indeed resulted in reduced scatter of the data points around a smooth power law; also the input slope was recovered within the uncertainty.

From the comparison of the reduced χ^2 values from Table 4.3, there are no obvious differences between a power law with a free parameter γ_{free} and a fixed slope $\gamma = 1.5$ visible. $\Delta\chi^2 \lesssim 0.22$ is found in all cases, which supports a recovery of the input slope with the applied method. Exceptions are the sets of synthetic spectra with a fixed column density ($\log N = 17$, row 13), and a column-density distribution that extends to high-

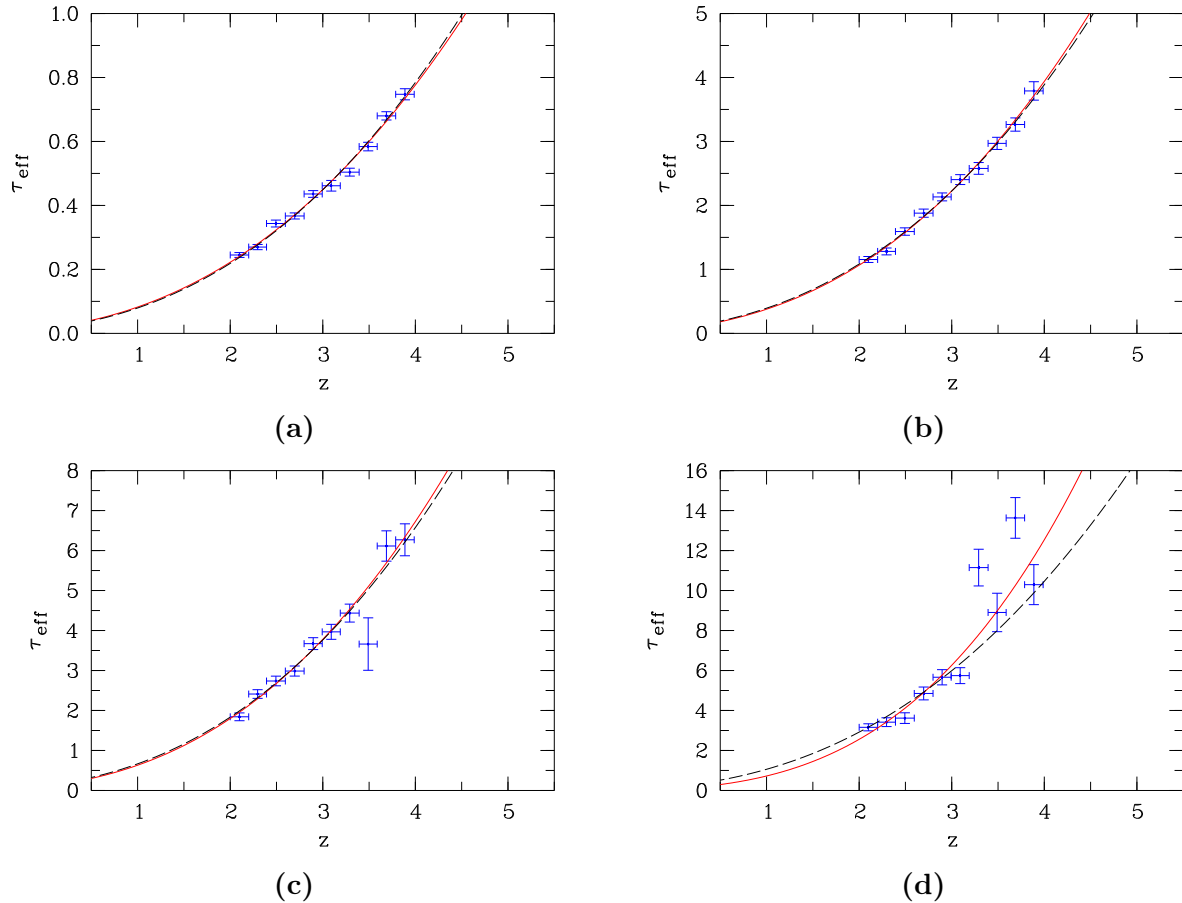


Figure 4.13. Redshift evolution of the effective optical depth from synthetic quasar spectra featuring H I Ly α absorption lines with fixed Doppler parameters ($b = 25 \text{ km s}^{-1}$) and a fixed column density: (a) $\log N_{\text{H}\text{I}} = 13$; (b) $\log N_{\text{H}\text{I}} = 14$; (c) $\log N_{\text{H}\text{I}} = 15$; (d) $\log N_{\text{H}\text{I}} = 17$ (rows 10 – 13 in Table 4.3). The lines are power-law fits of the form $\tau_{\text{eff}}(z) = \tau_0 \cdot (1 + z)^{\gamma+1}$ to the respective data points. The dashed black line in each panel has $\gamma \equiv 1.5$ (input value) and the red solid line has $\gamma = 1.45 \pm 0.08$ (a), $\gamma = 1.56 \pm 0.07$ (b), $\gamma = 1.58 \pm 0.14$ (c), and $\gamma = 2.11 \pm 0.37$ (d).

column-density absorbers ($\log N > 17$, row 5), both featuring a fixed Doppler parameter ($b = 25 \text{ km s}^{-1}$). Note that these cases are, however, of no relevance given their idealised nature, and are only useful to assess the impact of each parameter (b, N) on the inferred value of γ . In general, the $\chi^2_{\gamma=1.5}/\text{dof}$ is often lower than the χ^2/dof due to the extra free parameter.

Regarding the slopes, larger differences are found in the rows 1, 2, 5, and 13. In these cases, the fitted value of γ only marginally recovers the input value. The larger differences may hint at an underestimate of the error on the power-law slope. This is the same conclusion as drawn from the comparison of the power-law fits to the data points in Fig. 4.14 (see above). This may be true for the literature values as well.

As can be seen in the figures listed in column 7 of Table 4.3, the power laws for both slopes are barely distinguishable in the redshift range used for the power-law fitting ($2 \leq z \leq 4$). They differ significantly only at larger redshifts. An exception to this shows the set of synthetic spectra with fixed column densities ($\log N = 17$) and fixed Doppler parameters ($b = 25 \text{ km s}^{-1}$; Fig. 4.13 d). With such high column densities the synthetic spectra

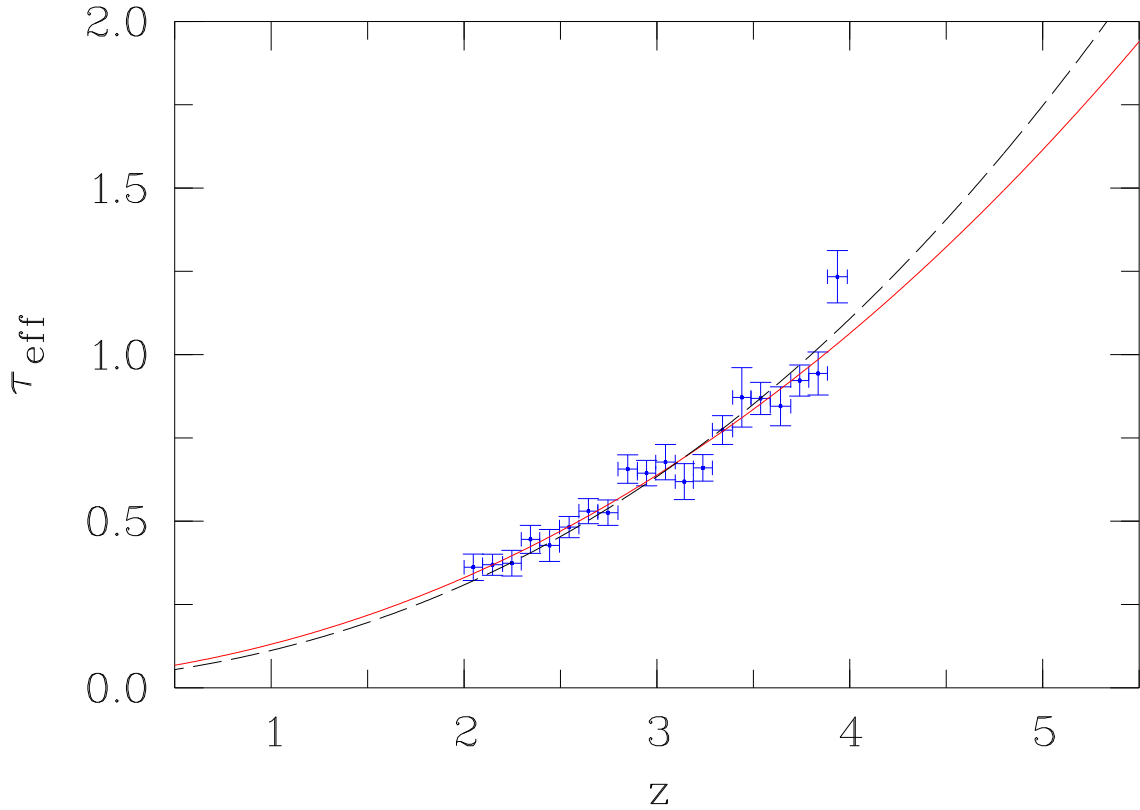


Figure 4.14. Redshift evolution of the effective optical depth from synthetic quasar spectra featuring H I Ly α absorption lines with parameters drawn from column-density and Doppler-parameter distributions constrained by observations (row 1 in Table 4.3). Column densities are in the range from $\log N_{\text{H}\,\text{I}} = 12$ to $\log N_{\text{H}\,\text{I}} = 17$; Doppler parameters are distributed lognormally with a mean $b = 25 \text{ km s}^{-1}$ and a width $b = 15 \text{ km s}^{-1}$. The lines are power-law fits to the data points of the form $\tau_{\text{eff}}(z) = \tau_0 \cdot (1 + z)^{\gamma+1}$. The dashed black line has $\gamma \equiv 1.5$ (input value), which corresponds to the input value, and the red solid line has $\gamma = 1.29 \pm 0.12$, which corresponds to the value recovered from the same analysis used on observed quasar spectra.

feature very little flux at redshifts $z > 3.1$. This statistically has an impact on $\tau_{\text{eff}}(z)$, as can be seen from the two outliers in Fig. 4.13 d and the increased scatter in Figures 4.12 d and 4.13 d, respectively. In order to reduce statistical scatter introduced by the procedure to draw absorption-line parameters from the number-density evolution, more synthetic spectra are needed for the analysis. A larger analyzed redshift range may better constrain the slope of $\log \tau_{\text{eff}}(z)$.

Figure 4.15 shows a comparison of the results obtained from the analysis of synthetic spectra (red lozenges) with the results obtained from the analysis of observed spectra (blue squares). $\tau_{\text{eff}}(z)$ computed from the synthetic spectra (see row 1 in Table 4.3) was shifted arbitrarily by a constant offset to match the corrected model flux at $z \sim 3.54$. This scaling accounts for the potential differences in the UVB adopted by the studies that yield the line-parameter distributions and those that provide measurements of the evolution of the effective optical depth. It is interesting to note that, although the synthetic data have been generated from a smooth line-number-density distribution, the evolution of the effective optical depth obtained from these data feature a significant deviation from a smooth evolution, akin to that observed in real data. Figures 4.12 and 4.13 show that

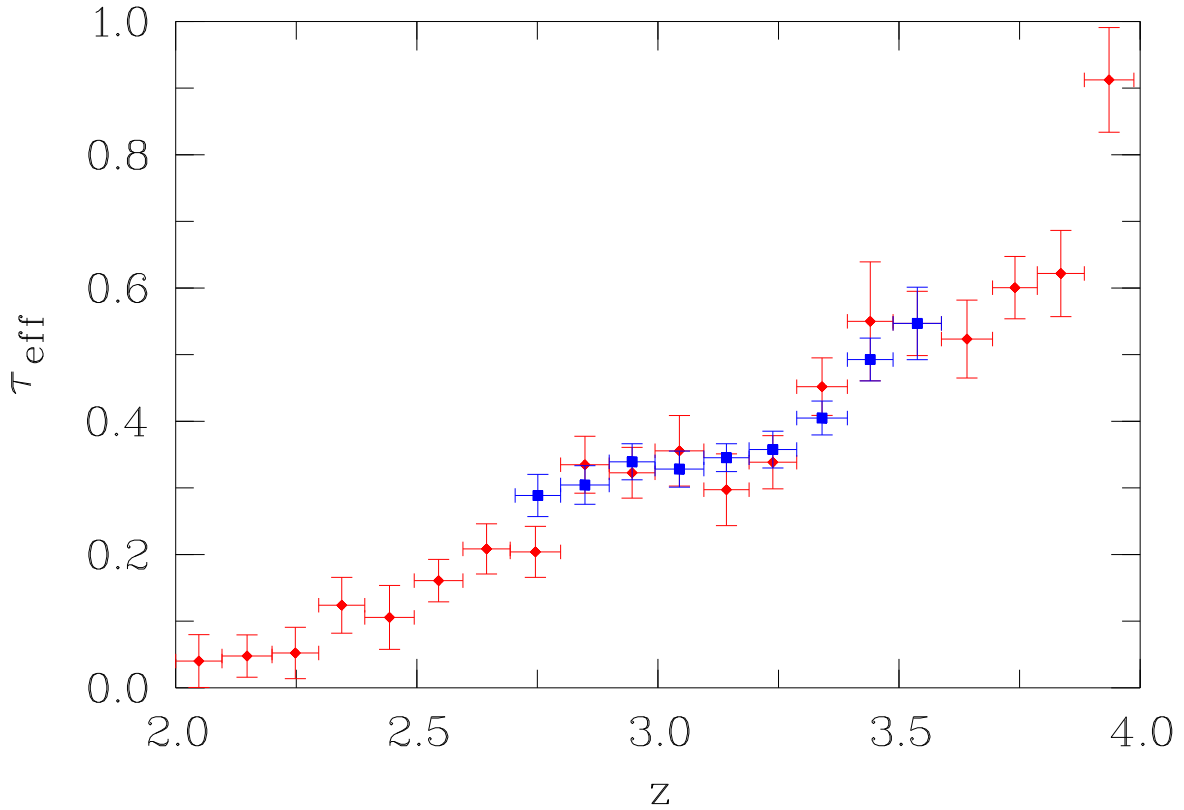


Figure 4.15. Same as Fig. 4.14 (red lozenges) shown in a smaller redshift range and offset vertically by a constant amount to match the τ_{eff} evolution measured from the corrected model flux (blue squares) at $z \sim 3.54$.

high-column-density ($\log N > 15$) absorbers produce a large scatter in τ_{eff} at any given redshift. In the real Universe, such absorbers are rare. Hence, the difference in τ_{eff} from different data sets is most likely caused by cosmic variance, and the disagreement between data sets is probably caused by a too optimistic estimate of the errors. We discuss these issues in more detail in the next chapter.

A question that arises is, whether a deviation from a smooth evolution of τ_{eff} could be recovered with the analysis method adopted here applied to synthetic data in which such a feature has been *introduced* by hand. The number-density evolution, column-density distribution, and Doppler-parameter distribution may contribute to the presence of a feature, perhaps entangled. To test their method, Pâris et al. (2011) introduce a downward feature in the number-density evolution and draw their synthetic spectra from absorption-line-parameter distributions similar to the ones used in this work. Pâris et al. (2011) find that the mean-flux evolution measured from these spectra agrees excellently with the theoretical input. A better test to discover an artificially introduced feature uses the normalized flux directly, imposing the flux evolution on individual synthetic spectra (Becker et al. 2013). Such a test is beyond the scope of this study and is left for future work.

In order to study the impact of the parameter distributions on the behaviour of $\tau_{\text{eff}}(z)$ analyzing several sets of synthetic spectra with a smaller number of spectra rather than fewer sets with more sightlines seemed more promising. The use of synthetic spectra created from specific absorption-line-parameter distributions was done in this way for the

first time. Building on this analysis it is possible to perform a more detailed investigation using a larger number of synthetic spectra created with particularly chosen absorption-line-parameter distributions. Nevertheless, the method used in this work to compute $\tau_{\text{eff}}(z)$ recovers the input slope in the considered redshift range. Hence, the computation of $\tau_{\text{eff}}(z)$ from observed spectra with this method and a sufficient amount of data should give reliable results and may answer the question on the existence of a downward feature in the smooth power-law evolution of the effective optical depth. The analysis of synthetic quasar absorption spectra hints at a smooth evolution of the effective optical depth with any deviation being an artifact of underestimated errors on the τ_{eff} measurements. We have shown in §4.2 that the redshift range investigated in this work ($2.7 \lesssim z \lesssim 3.6$) is too small to determine the redshift evolution of the effective optical depth reliably. The analysis of a set of synthetic spectra suggests that the redshift range $2 \leq z \leq 4$ may be appropriate. Furthermore, the use of more sightlines for the analysis likely reduces the scatter in the τ_{eff} measurement.

Chapter 5

Discussion and Conclusions

5.1 Discussion

In this section the results of this work regarding the redshift evolution of the effective optical depth, $\tau_{\text{eff}}(z)$, are compared to the literature. In principle, two types of data are found in the literature which are used to measure $\tau_{\text{eff}}(z)$. The Sloan Digital Sky Survey (SDSS) data releases are advantageous due to the large number (several 10^3) of quasar spectra available. Unfortunately, these quasar spectra are of low resolution. High-resolution quasar spectra are obtained, e.g., with UVES/VLT or HIRES/Keck and allow for precision measurements of $\tau_{\text{eff}}(z)$. Usually, several 10 such quasar spectra are analyzed in a single investigation. In the following I will consider both approaches for a comparison to the τ_{eff} measurement from high-resolution quasar spectra of this work.

5.1.1 High-resolution data

The comparison of τ_{eff} measurements from different works that use high-resolution quasar spectra is shown in Fig. 5.1. The data listed in Table 1.1 are used which are comparable to this work in terms of the computation of the effective optical depth (flux averages from all sightlines used intersecting a given redshift slice) and the (tentative) claim of a downward feature in its redshift evolution. This includes Faucher-Giguère et al. (2008b, red lozenges) and Dall'Aglio et al. (2008, black stars and dashed line). Although their method differs and they use low-resolution quasar spectra, the result of Bernardi et al. (2003) is also included (solid line) for completeness. Thereto, the data of Kim et al. (2007) are shown (green circles) since their second to last data point falls below their general trend, though they do not put emphasize on it. For comparison, the $\tau_{\text{eff}}(z)$ measurement inferred from the observed flux from this work is shown (blue rectangles). The τ_{eff} measurement from this work and the raw measurement of Faucher-Giguère et al. (2008b) are not corrected, neither for continuum bias, nor metal contamination. Faucher-Giguère et al. (2008b) apply these corrections to their data. These corrections do not change the evolution of their τ_{eff} measurement in shape, but lead to an offset of the data points to lower fluxes, i.e., to larger effective-optical-depth values. This offset is gradually increasing with redshift, especially above $z = 3.5$, where the data of this work are scarce. Therefore, I conclude that the redshift evolution of τ_{eff} can qualitatively be determined without the need of too careful corrections of the continuum or metal contamination (see also Fig. 4.4 and the

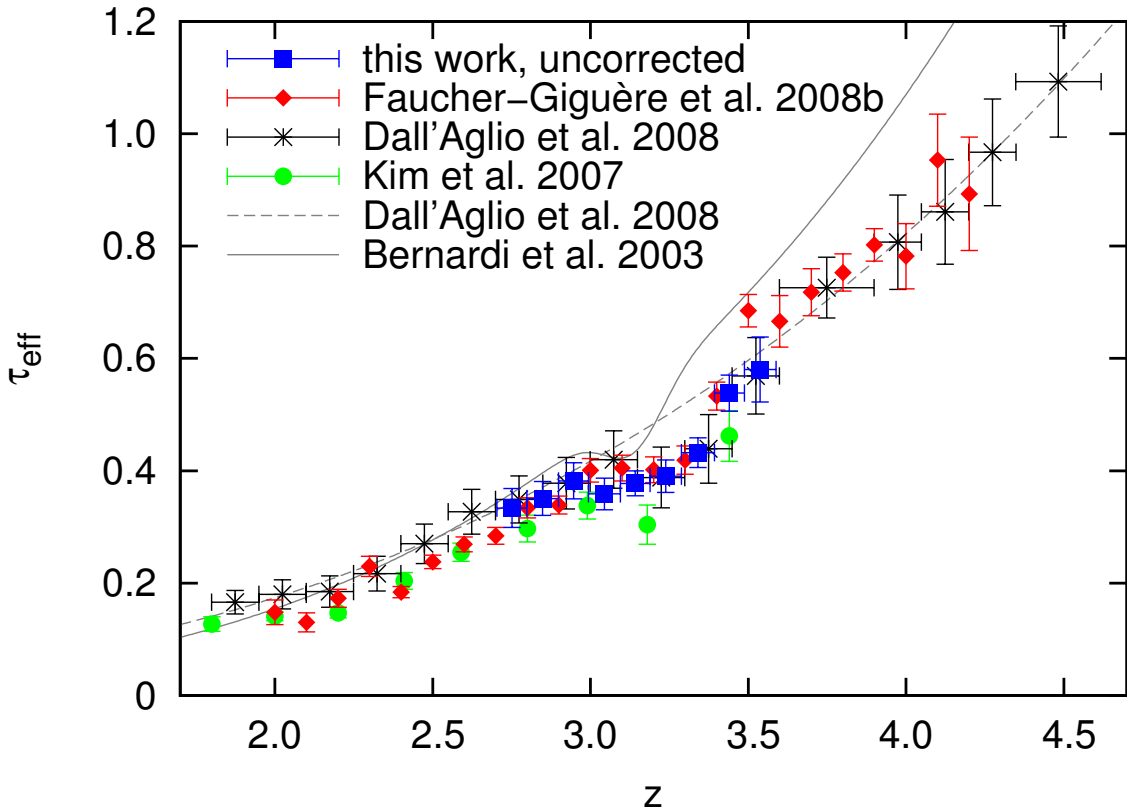


Figure 5.1. Effective-optical-depth measurements from different works. The solid line shows the evolution of the effective optical depth found by Bernardi et al. (2003) for their $S/N > 4$ quasar spectra. The black-asterisk symbols are taken from Dall'Aglio et al. (2008), as well as their power-law least-squares fit to the data (dashed line). The filled symbols are data from Kim et al. (2007, green circles), Faucher-Giguère et al. (2008b, red lozenges, their raw measurements), and this work (blue rectangles, observed flux from Fig. 4.3 a).

respective text references). Faucher-Giguère et al. (2008b) mask absorption lines with $\log N \geq 19$ and accompanying metal lines. Though, they show that their measurement is insensitive to masking metal lines associated with DLAs. DLAs were excluded from the analyzed redshift range in the quasar spectra analyzed in this work, so that the data are comparable, assuming that the continuum for a given observed spectrum would be found to be very similar. The respective measurements agree extraordinary well except for $\tau_{\text{eff}}(z \approx 3.5)$. This is the redshift bin in which there are the least number of segments in this work (Fig. 4.2).

Dall'Aglio et al. (2008) exclude pixels contaminated by LLSSs and DLAs. They apply a continuum correction using sets of synthetic spectra. Though, the correction is insignificant for redshifts up to $z \approx 3.5$ (see their Fig. 2, top panel). The τ_{eff} measurement of Dall'Aglio et al. (2008) agrees very well with the measurement from this work. Their data differs slightly from that of Faucher-Giguère et al. (2008b) at lower redshift, which may be partly due to the different redshift-bin size.

Kim et al. (2007) exclude absorption systems with $\log N \geq 19$. Their data points lie systematically below the ones of this work. Kim et al. (2007) remove metal contamination by use of their absorption-line fits. Since in Fig. 5.1 the data of this work obtained from

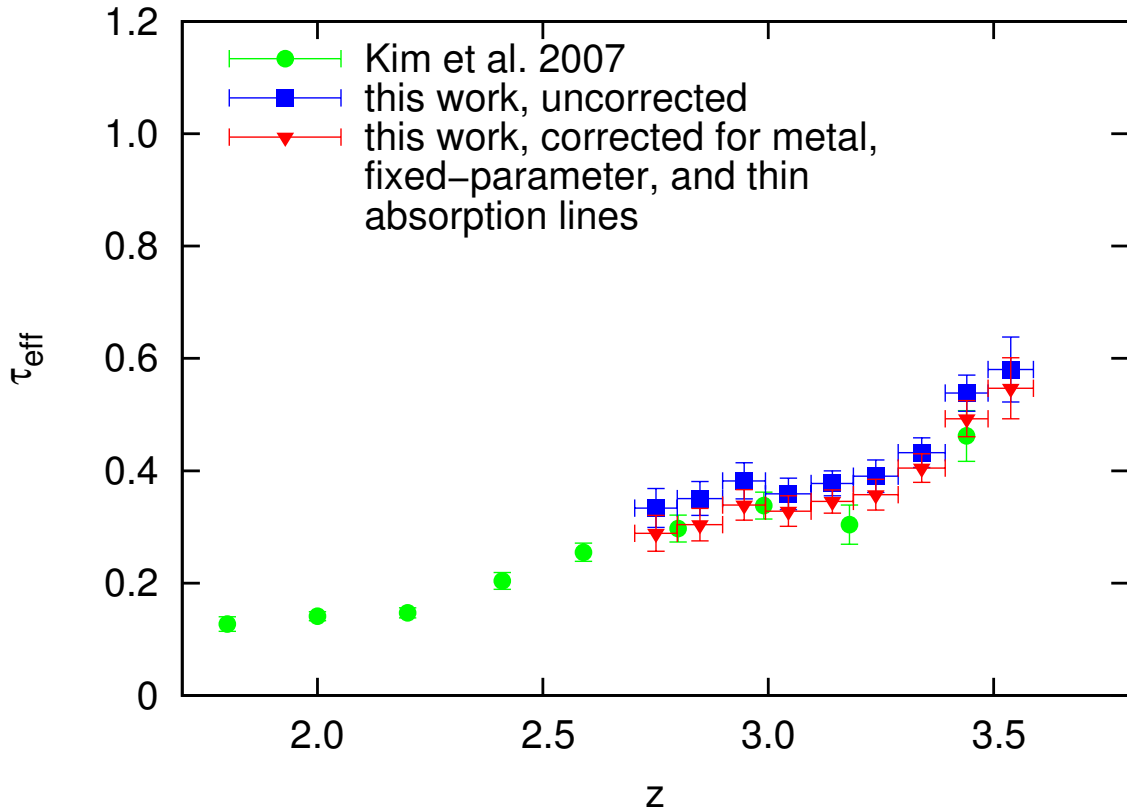


Figure 5.2. Effective-optical-depth measurements. The data shown represent a subset of the data shown in Fig. 5.1. Note that the redshift axis is shorter than in Fig. 5.1 for presentational purposes. The filled symbols represent data from Kim et al. (2007, green circles) and this work (blue rectangles, observed flux). In addition to the measurement using the observed flux of the quasar spectra (see Fig. 4.3 a), the measurement of the effective optical depth after the removal of absorption lines, which are presumably not H I Ly α , is shown (red triangles – shown as cyan stars in Fig. 4.4; see also Fig. 4.3 d).

the observed flux are plotted, the discrepancy may stem from the removal of the influence of metals by Kim et al. (2007). To check for this, in Fig. 5.2 is plotted the effective optical depth computed from the 13 quasar spectra used in this work based on the observed flux (blue rectangles) and the model flux corrected for metal, fixed-parameter, and narrow absorption lines (red triangles). The measurement by Kim et al. (2007) agrees very well with the measurement from the corrected model flux. The data from Kim et al. (2007) lie also systematically below the measurement from Dall'Aglio et al. (2008) in Fig. 5.1. Kim et al. (2007) use a sample of 18 quasar spectra that is included in the 40 sightlines analyzed by Dall'Aglio et al. (2008) except for J2233-606 and Q1101-264. Hence, it may not be surprising that the trend of τ_{eff} is similar. The discrepancy can again be ascribed to the metal contamination since Dall'Aglio et al. (2008) do not account for it.

The good agreement of the τ_{eff} measurements of Kim et al. (2007) with those of this work (corrected model flux) may support the existence of a downward feature in the redshift evolution of the effective optical depth at $z \sim 3.2$. On the other hand, combining these measurements also allows for a smooth redshift evolution of the effective optical depth around which the data points may scatter. At redshifts $z > 3$ the τ_{eff} measurements of this work should be more accurate than those found by Kim et al. (2007) since these

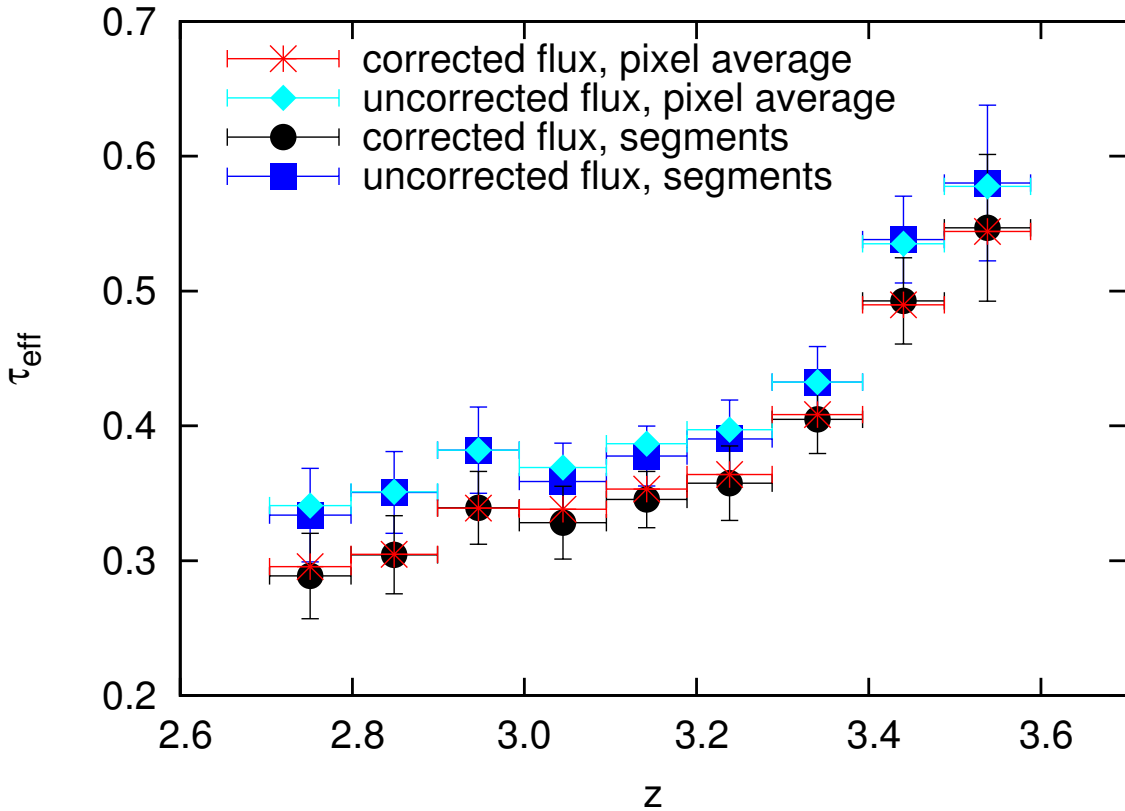


Figure 5.3. Redshift evolution of the effective optical depth from the segment flux average and pixel flux average for two different flux selections: observed flux and model flux corrected for metal, fixed-parameter, and narrow line absorption. Error bars on the pixel flux average are not shown. See text for details.

authors use a smaller number of sightlines at these redshifts (see below).

Kim et al. (2007) use those pixels from a quasar spectrum which fall in the respective redshift bin to compute the average pixel flux over all sightlines intercepted by the redshift bin. In Fig. 5.3 $\tau_{\text{eff}}(z)$ inferred from the method of Kim et al. (2007) and from the method used in this work are compared. The measurements indicated by ‘segments’ are taken from this work and are the same as in Figs. 4.3 a (uncorrected flux) and 4.3 d (corrected flux), respectively, and the same as the respective measurements indicated by ‘this work’ in Fig. 5.2. The measurements indicated by ‘pixel average’ are computed following Kim et al. (2007). These measurements agree well with the respective measurements using the method from this work to compute $\tau_{\text{eff}}(z)$. The error on the pixel-flux average is about an order of magnitude larger than computed from the segments since the scatter is larger. Kim et al. (2007) compute the error on their measurement by bootstrap resampling. Since the τ_{eff} measurement from both methods (average segment flux and average pixel flux) agree very well, the main difference seems to be only the error computation. Hence, I skipped the computation of the error on the pixel flux average since the bootstrap resampling apparently gives similar errors to the ones inferred in this work for the segment flux average (see Fig. 5.2). Since the correction of the observed flux for metal absorption does not alter the shape of the measured $\tau_{\text{eff}}(z)$ (see Fig. 4.4), I conclude that the Kim et al. (2007) measurement would be comparable to the data of Faucher-Giguère et al.

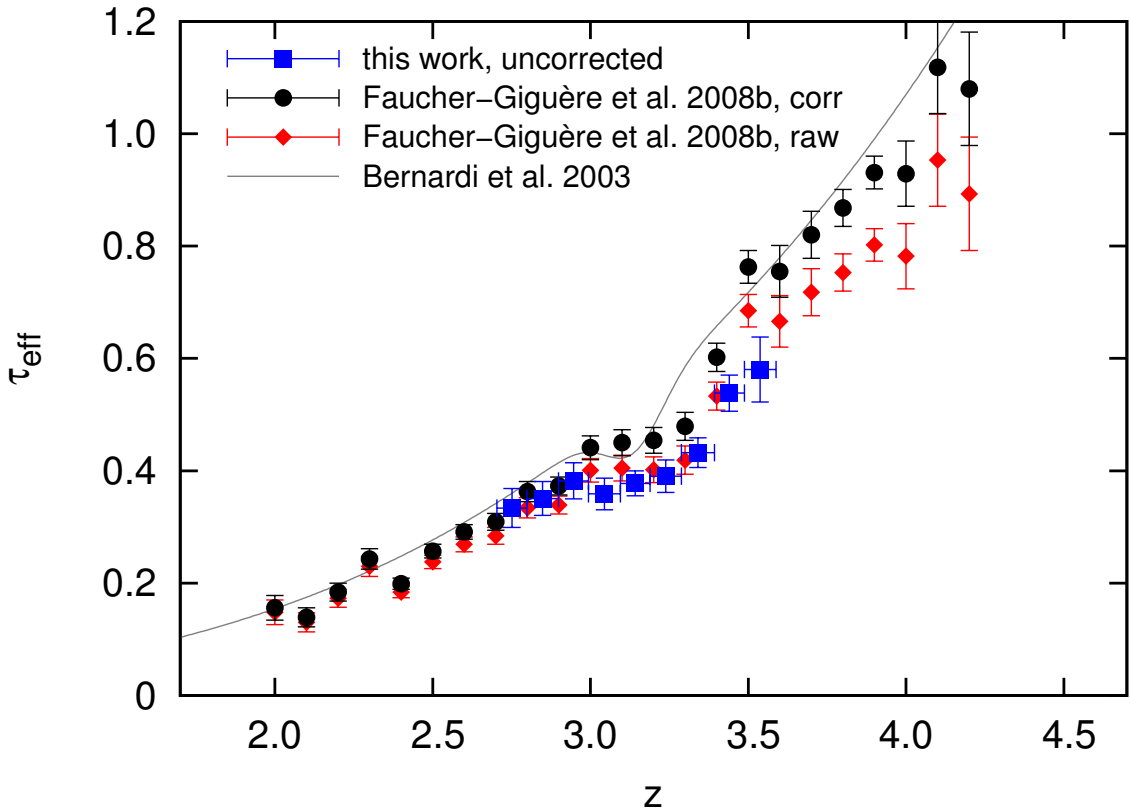


Figure 5.4. Effective-optical-depth measurements from different works. The solid line is the result taken from Bernardi et al. (2003) from their minimization approach. The blue rectangles are data from this work (observed flux), which can be compared to the data taken from Faucher-Giguère et al. (2008b, red lozenges). Shown as black circles are the data from Faucher-Giguère et al. (2008b) corrected for continuum bias, which agree better with the Bernardi et al. (2003) measurement than the raw measurement of Faucher-Giguère et al. (2008b).

(2008b), Dall’Aglio et al. (2008), and this work (observed flux) if metals would not have been accounted for in the quasar spectra used by Kim et al. (2007).

Except for Bernardi et al. (2003), all groups account for the proximity zone of the quasar in the absorption spectra (see Table 1.1) and use high-resolution, high-signal-to-noise quasar spectra. The result that these groups see a similar trend in $\tau_{\text{eff}}(z)$ using comparable data sets lends support for the existence of a real downward feature in the otherwise smooth redshift evolution of the effective optical depth. The observed feature has a width of $\Delta z = 0.3 - 0.5$ based on Fig. 5.1.

Bernardi et al. (2003) use about 1000 SDSS quasar spectra (sightlines with strong DLAs are removed). These authors introduce a method which estimates the quasar continuum as a function of rest-frame wavelength simultaneously with the redshift evolution of the mean transmission in the H I Ly α forest. Faucher-Giguère et al. (2008b) show that their effective-optical-depth measurement corrected for continuum bias agrees very well with the data of Bernardi et al. (2003) if binned and offset vertically with a constant value in logarithmic space, accounting for normalization uncertainties in the τ_{eff} measurement of Bernardi et al. (2003) (see §5.2.3 and Fig. 13 of Faucher-Giguère et al., 2008b, as well as §3.2 of Bernardi et al., 2003). In Fig. 5.4 the same data points are shown as in Fig. 5.1

without the measurement of Kim et al. (2007) and Dall’Aglio et al. (2008). Also included in the Figure is the measurement of Faucher-Giguère et al. (2008b) corrected for continuum bias. Note that their quoted errors may be underestimated at least in the case of the corrected measurement. More precise error estimates can be found in Table 4 of Faucher-Giguère et al. (2008b). As can already be seen from Fig. 5.4, the difference of the measurement from Bernardi et al. (2003, solid line) to those from high-resolution data may stem from the different methods used to estimate the continuum. The minimization approach applied by Bernardi et al. (2003) may underestimate the continuum or high-resolution data may need to be corrected for continuum bias, as done by Faucher-Giguère et al. (2008b, black circles). In this case the measurement of Bernardi et al. (2003) and the high-resolution data (Fig. 5.1) imply the existence of a downward feature in the otherwise smooth redshift evolution of the effective optical depth.

The downward deviation from a smooth power-law evolution of the effective optical depth inferred in this work can in principle be seen from the data alone but becomes more conclusive if compared to other high-resolution data (Kim et al. 2007; Dall’Aglio et al. 2008; Faucher-Giguère et al. 2008b) due to the narrow redshift range analyzed in this work. The feature seen in these works is similar in width and depth (Fig. 5.1). Although a statistical origin of the feature is possible, it is curious that the feature is seen at similar redshifts in all of these works. Assuming that some quasar spectra are shared among different works and that these spectra show an increase in the observed flux at $z \sim 3.2$, these spectra may influence the evolution of τ_{eff} inferred from all quasar spectra used in the respective analyses such that a downward feature is seen in the evolution of the effective optical depth measured by those works at similar redshifts. Table 5.1 lists the quasar spectra with emission redshifts $z_{\text{em}} > 3$ that are used by the works mentioned above and are shared at least between two different works. From Table 5.1 it can be seen that only one sightline was used in three of the works (J212912–153841), but no sightline was used in all of the works. This agreement is insufficient to account for a feature seen by all the works unless all those sightlines show an increase in the observed flux around $z = 3.2$. This could be checked if $\tau_{\text{eff}}(z)$ is measured from individual sightlines. I leave an analysis of single lines of sight for future work.

Kim et al. (2007) use effectively only two sightlines from which they can measure $\tau_{\text{eff}}(z)$ above $z = 3$, PKS2126-158 ($z_{\text{em}} = 3.279$) and Q0055-269 ($z_{\text{em}} = 3.655$). The latter being the only sightline which contributes to their highest redshift measurement.

Dall’Aglio et al. (2008) use a homogeneous sample of quasar spectra with regard to their emission redshift (several sightlines within emission redshift bins of size $\Delta z_{\text{em}} = 0.1$) in the ranges $2.1 < z_{\text{em}} < 3.3$ and $3.65 < z_{\text{em}} < 3.79$. Their sample misses quasar spectra with emission redshifts in the range $3.3 < z_{\text{em}} < 3.65$ and features only two quasar spectra with emission redshifts larger than $z_{\text{em}} = 3.79$ ($z_{\text{em}} = 4.697$ and $z_{\text{em}} = 4.766$). It is not clear how this influences the evolution of τ_{eff} , though a more homogeneous sample at high redshift would be statistically preferable. It has to be noted, however, that the H I Ly α forest covers a larger redshift range at higher redshifts. In total, Dall’Aglio et al. (2008) use 9 quasar spectra with emission redshifts of $z_{\text{em}} = 3.2 - 3.8$.

Faucher-Giguère et al. (2008b) measure $\tau_{\text{eff}}(z)$ separately using quasar spectra which have been observed via the Magellan and the Keck observatory, respectively. Though both measurements give consistent results, Fig. 14 of Faucher-Giguère et al. (2008b) shows a downward feature only in the Keck data points, which show in general larger scatter. The

Table 5.1. Quasar spectra used by the different works with emission redshifts $z_{\text{em}} > 3$ ordered by emission redshift. Each checkmark states contribution of the respective sightline to the $\tau_{\text{eff}}(z)$ measurement by these authors.

QSO	z_{em}	this work	Faucher-Giguère et al. (2008b)	Dall'Aglio et al. (2008)	Dall'Aglio et al. (2008b)	Kim et al. (2007)
HE0940-1050 [†]	3.089 [‡]	—	—	✓	✓	✓
Q0420-388 [†]	3.120 [‡]	—	—	✓	✓	—
CTQ0460 [†]	3.141 [‡]	—	✓	✓	✓	—
J212912-153841*	3.279*	✓	—	✓	—	—
J014214+002324*	3.380*	✓	✓	—	—	—
J115538+053050*	3.465*	✓	✓	✓	✓	✓
Q0055-2659 [†]	3.665 [‡]	—	—	—	—	—
J162116-004250*	3.704*	✓	✓	—	✓	—
J132029-052335*	3.718*	✓	—	✓	—	—
PKS2000-330 [†]	3.786 [‡]	—	✓	✓	—	—

* J2000 name.

[†]Quasar names taken from Dall'Aglio et al. (2008).

^{*}Redshift estimated from H I Ly α emission.

[‡]Redshift taken from Dall'Aglio et al. (2008).

Keck quasar spectra make up the majority of the sightlines analyzed by Faucher-Giguère et al. (2008b). As seen from their Fig. 2, these authors use 27 sightlines in the redshift range $3.1 \leq z_{\text{em}} \leq 3.7$.

The multitude of quasar spectra that are used by both, Kim et al. (2007) and Dall’Aglio et al. (2008), have emission redshifts below $z_{\text{em}} = 3$ and are therefore not important for the downward feature at $z \sim 3.2$. Though, they indirectly influence a detection of a feature since they are responsible for the lower redshift end of the inferred τ_{eff} redshift evolution. Only two quasar spectra with $z_{\text{em}} < 3$ were used by both, Dall’Aglio et al. (2008) and Faucher-Giguère et al. (2008b). These are Q2206–1958 and HE1347–2457. Each quasar spectrum was observed by a different instrument for different samples. Bernardi et al. (2003) use hundreds of quasar spectra. An agreement of sightlines to the other works mentioned above using high-resolution data is likely but seems insignificant due to the amount of sightlines used by Bernardi et al. (2003).

In principle, the possibility of a statistical origin of the τ_{eff} feature is not ruled out given that the distribution of sightlines in emission redshift space is not ideal for the Dall’Aglio et al. (2008) sample (Kim et al., 2007, use basically a subset of that sample and effectively only two sightlines for computing τ_{eff} above $z = 3$) and given that the τ_{eff} feature found by Faucher-Giguère et al. (2008b) stems basically from the Keck data, which produce a large scatter in the τ_{eff} measurements inferred from them. It only seems coincidental that a deviation from a smooth power law evolution of the effective optical depth is due to different statistical origins but occurs at similar redshifts with similar width. But, a similar deviation is found by analyzing a set of synthetic spectra in this work (see Fig. 4.15) that should not be present (by design of the synthetic spectra).

The quasar spectra used by Bernardi et al. (2003) have lower resolution than those used in this work and those used by Kim et al. (2007), Faucher-Giguère et al. (2008b), and Dall’Aglio et al. (2008). In the following it is shown that the resolution is unimportant for the computation of $\tau_{\text{eff}}(z)$ if the same quasar continuum is considered.

The 13 quasar spectra used in this work are degraded to SDSS resolution ($R \simeq 2000$) by convolution after being normalized. All absorption features are left in. The effective optical depth is computed from the degraded spectra in the same way as described in §4.1. The distribution of the 3 proper Mpc segments is shown in Fig. 5.5 and can be compared to Fig. C.1 a (observed flux). The redshift evolution of the effective optical depth measured from the high-resolution data is compared to the degraded-resolution counterpart in Fig. 5.6.

The agreement of the τ_{eff} measurements from the different resolutions is reassuring. Apparently, the inferred evolution of the effective optical depth is insensitive to the spectral resolution if the continuum of a spectrum is the same regardless of resolution. Hence, the discrepancy between the Bernardi et al. (2003) measurement and the high-resolution data must come from an effect other than the difference in spectral resolution between the data sets. But the resolution may still be important indirectly for a τ_{eff} measurement through the continuum estimation and the removal of metal absorption features.

5.1.2 Low-resolution (SDSS) data

Besides by Bernardi et al. (2003), SDSS quasar spectra are used by Dall’Aglio et al. (2009), Pâris et al. (2011), and Becker et al. (2013). These studies differ in the method to

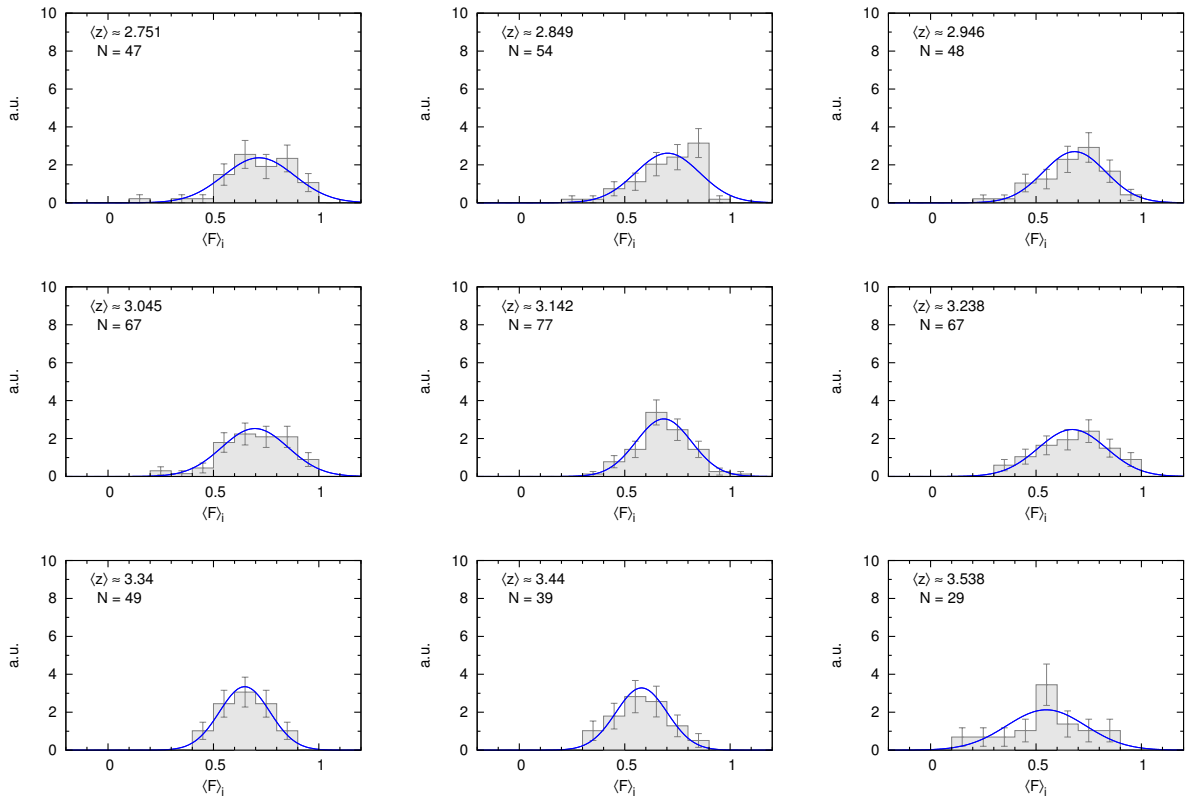


Figure 5.5. Same as Fig. 4.2 with the observed (uncorrected) flux used after degrading the quasar spectra to SDSS resolution, $R \simeq 2000$.

estimate quasar continua or to compute the average flux. Their findings regarding $\tau_{\text{eff}}(z)$ are compared to the τ_{eff} measurement from this work in Fig. 5.7. The high-resolution measurement from this work shown in Fig. 5.7 is made from the observed flux since it is compared to low-resolution measurements, which most likely include metal absorption. Though, Becker et al. (2013) state that their approach on the τ_{eff} measurement accounts for metals. This is due to their way to construct composite spectra and the scaling of their relative τ_{eff} measurement from these composites to the metal-corrected measurement of Faucher-Giguère et al. (2008b) at redshift $z \sim 2$ (see Becker et al., 2013, §2.2.1). The low-resolution data shown in Fig. 5.7 are in good agreement with each other. Though, the evolution found by Dall'Aglio et al. (2009) seems to be tilted compared to the other two measurements. This may be explained by the continuum correction Dall'Aglio et al. (2009) apply (see their Fig. 6). Possibly, the continuum is overestimated at $z < 2.7$ and underestimated at $z > 3.8$. Notably, Dall'Aglio et al. (2009) have no explanation for the apparent underestimation of their τ_{eff} measurements at $z \gtrsim 3.5$ compared to the measurements from Faucher-Giguère et al. (2008b). As mentioned by Becker et al. (2013), the continuum corrections of Dall'Aglio et al. (2009) may be biased since they are estimated from Monte Carlo simulated spectra using observed parameter distributions which may have inaccuracies and are found by studying high-resolution quasar spectra whose continuum estimates may be uncertain. Becker et al. (2013) ask for caution if their own data is compared to the Pâris et al. (2011) measurement since Pâris et al. do not account for metal absorption. They also mention that some systematic effects regarding the con-

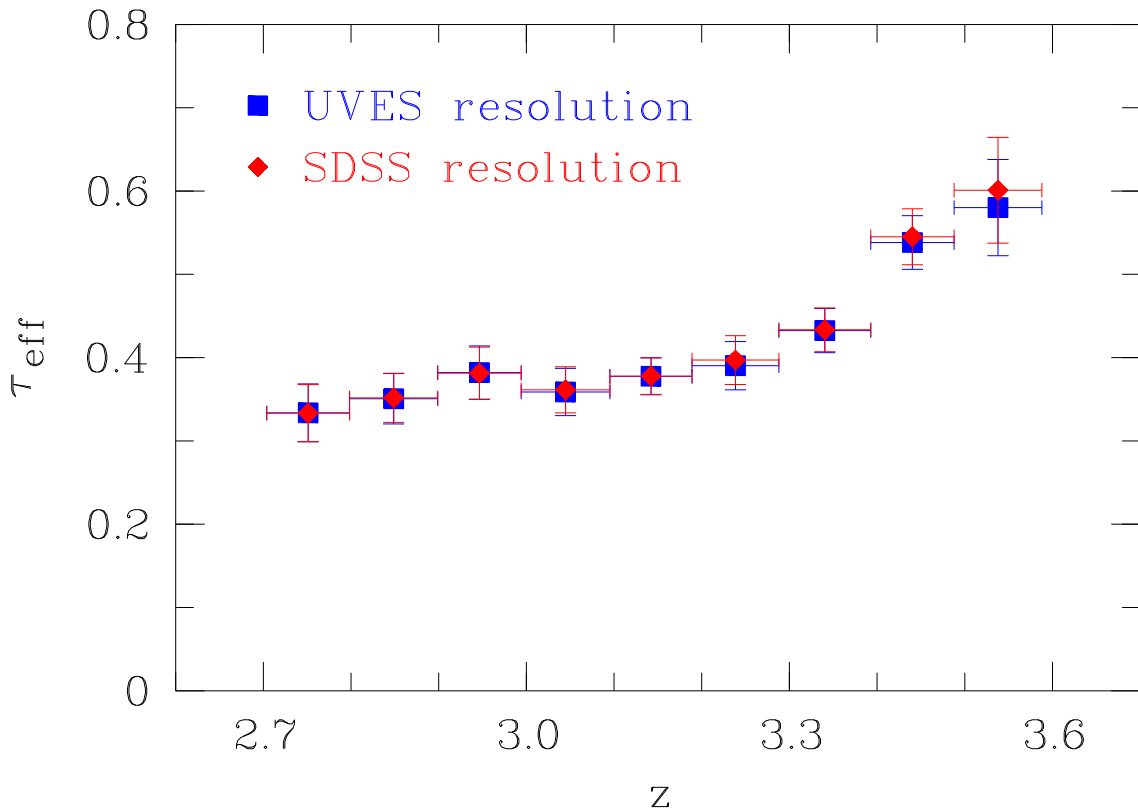


Figure 5.6. Redshift evolution of the effective optical depth computed from the observed flux of the 13 quasar spectra used in this work (blue squares) and from the same normalized spectra degraded to SDSS resolution (red lozenges).

tinuum estimate of Pâris et al. may compensate for the different amplitude of τ_{eff} .

All SDSS measurements shown in Fig. 5.7 differ at $3.0 < z < 3.4$ from the measurement of this work. This could be due to the binning in redshift space, although it is intriguing that the SDSS data seem to trace a single power law in the redshift evolution of the effective optical depth whereas the high-resolution data points exhibit a downward feature (compare to Fig. 5.1). Nevertheless, this could be coincidental and a relic of scaling differences due to the continuum placement. Also, Bernardi et al. (2003) find a feature in their τ_{eff} measurement using SDSS data. The discrepancy from the τ_{eff} measurement inferred in this work to the Dall’Aglio et al. (2009) and Pâris et al. (2011) measurements may be explained by a bias in their continuum estimate or continuum correction. In the case of the Becker et al. (2013) data this may be due to their normalization to the Faucher-Giguère et al. (2008b) data at $z \leq 2.5$ which were corrected for metal absorption using measurements from Schaye et al. (2003). Becker et al. (2013) consider this as a potential source of systematic error on their final τ_{eff} values, albeit a small one. Hence, it is possible that some systematic offset places the low-resolution measurements too high and that the τ_{eff} measurement from this work shows only scatter around the smooth τ_{eff} evolution estimated from low-resolution quasar spectra. This would be in accordance with the results of §§4.2 and 4.3.3 and could be tested, if a large number of high-resolution quasar spectra is analyzed.

Dall’Aglio et al. (2009) do not see a feature in their $\tau_{\text{eff}}(z)$ estimate even before their con-

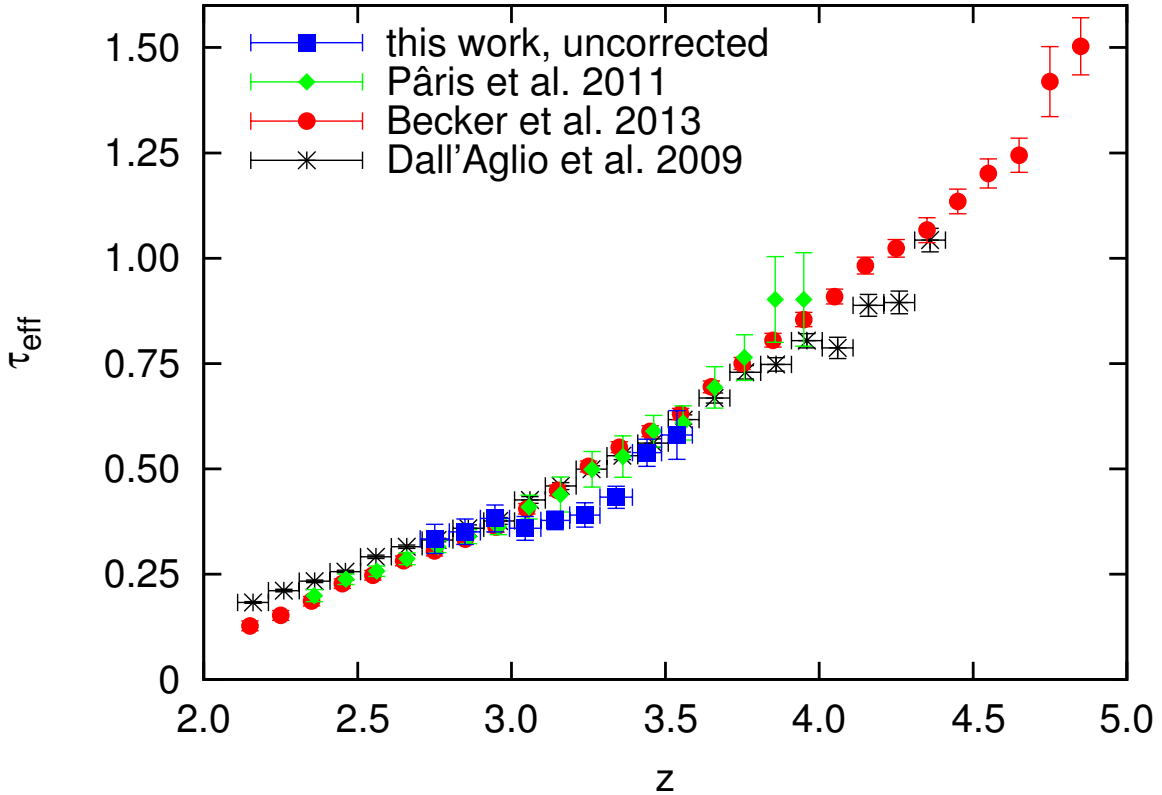


Figure 5.7. Effective-optical-depth measurements from different works. The data are taken from Dall’Aglio et al. (2009, black stars), Pâris et al. (2011, green lozenges), Becker et al. (2013, red circles), and this work (blue rectangles, observed flux).

tinuum correction that accounts for resolution effects and line blending. Their continuum estimate is based on a cubic-spline interpolation, a local continuum fit. As shown above, the resolution of quasar spectra has no significant effect on the redshift evolution of the effective optical depth. Dall’Aglio et al. (2009) apply the same method to infer the τ_{eff} measurement as Kim et al. (2007), but they do not correct the observed flux for metal contamination. Hence, the data are comparable to the τ_{eff} measurement from this work using the observed flux as shown in Fig. 5.7. The difference in the effective optical depth measurements from Dall’Aglio et al. (2009) and this work may imply that a large set of quasar spectra is necessary to infer $\tau_{\text{eff}}(z)$ precisely. This statement is supported by the conclusions from simulations (see §4.3.3 and particularly Fig. 4.15) and makes a possible feature in $\tau_{\text{eff}}(z)$ seen in the data of this work spurious.

Dall’Aglio et al. (2009) use 1733 low-resolution SDSS quasar spectra in their analysis and Dall’Aglio et al. (2008) study 40 high-resolution quasar spectra. Dall’Aglio et al. (2008) remove LLS and DLAs from the quasar spectra used in their analysis and Dall’Aglio et al. (2009) do not account for such high-column-density absorbers. As seen in §4.3.3, high-column-density absorbers ($\log N \geq 17$) have a negligible effect on the redshift evolution of the effective optical depth and the $\tau_{\text{eff}}(z)$ measurement is insensitive to the resolution of the data. Hence, these differences should have no affect on the evolution of τ_{eff} inferred in both studies. Yet, Dall’Aglio et al. (2009) find a pure power-law evolution and Dall’Aglio et al. (2008) find a downward feature in $\tau_{\text{eff}}(z)$ at $z \sim 3.3$, albeit tentatively. The only

apparent difference in both studies is the number of sightlines that have been analyzed, which hints on a spurious feature.

The quasar spectra of this work are selected in order to cover the redshift range $3.1 < z < 3.3$. Hence, this is the statistically dominant redshift range. Assuming that this means that $\tau_{\text{eff}}(z)$ has the correct amplitude in the redshift bins $\langle z \rangle \simeq 3.15, 3.25$, it could also mean that the τ_{eff} measurements in the outer redshift bins may be outliers. For instance, from Fig. C.1 can be seen that the first three redshift bins ($z < 3$) and the last three redshift bins ($z > 3.3$) contain ~ 50 segments, while the inner three redshift bins contain ~ 70 segments. For the redshift bin at $\langle z \rangle \simeq 3.05$ the larger number of segments can be explained by the contribution of the sightlines J124957-015928 and J132029-052335 (see Fig. 2.1). Though it seems to be quite a coincidence that the difference in the segment numbers manifests itself in the τ_{eff} values estimated from the mean flux in those segments placed systematically too high, except for the redshift bin at $\langle z \rangle \simeq 3.35$. It is rather likely that the τ_{eff} values estimated in this work scatter around a power law as seen in Fig. 4.3. Clearly, a larger number of high-resolution quasar spectra should be analyzed in order to check the conclusions above. Ideally, some 10^4 quasar spectra would be required in order to improve upon the sample of 6065 SDSS quasar spectra used by Becker et al. (2013).

Pâris et al. (2011) claim to see a departure from a smooth power law in the mean-flux redshift evolution at $z \sim 3.2$ (see their §4.1 and Fig. 15, left panel) using a similar set of SDSS quasar spectra to that of Bernardi et al. (2003). Analyzing a newly defined set of quasar spectra from SDSS-DR7, Pâris et al. (2011) claim to find a definite break in the evolution of the mean flux at $z \sim 3$. By comparison to Fig. 5.7, this is equal to a steeper slope of $\tau_{\text{eff}}(z)$ at higher redshift. Pâris et al. (2011) caution, that their procedures may slightly smooth out a more prominent feature at this redshift.

It may be possible that a few sightlines (of the order of 100 as for high-resolution data) may lead to a downward departure on the otherwise smooth evolution of τ_{eff} that gets smoothed out to a break for a larger number of quasar spectra (~ 1000) and vanishes completely for some thousand spectra (as used by Becker et al. 2013). This may be explained by selection biases in the early SDSS data releases or by statistical fluctuations in the evaluation of the mean flux from these quasar spectra. The amplitude of the τ_{eff} measurements is subject to the continuum placement and the absorption features left in (e.g., DLAs, metals).

Dall'Aglio et al. (2009) may not see a feature since they use a sufficient amount of quasar spectra (1733) that is almost twice as much as the Bernardi et al. (2003) sample. The discovery of the feature by Bernardi et al. (2003) may partly be due to sightlines containing DLAs which they did not remove (Pâris et al., 2011, had 837 quasar spectra by avoiding broad absorption lines (BALs) and DLAs while Bernardi et al., 2003, had 1061). However, we have shown in §4.3.3 that the presence of high-column-density systems (LLS, DLAs) does not affect appreciably the evolution of τ_{eff} .

The continuum estimate is perhaps the largest source of uncertainty. The continuum estimate from a principle component analysis (PCA) and from an extrapolation of a power law fitted to the red side of the H I Ly α emission line (as done by Pâris et al. 2011) may miss the bumps found in the mean continuum (e.g., Bernardi et al. 2003) and, hence, suppress the discovery of the downward feature in $\tau_{\text{eff}}(z)$. Bernardi et al. (2003) use a minimization approach to circumvent a direct continuum estimate. This marks a possibly

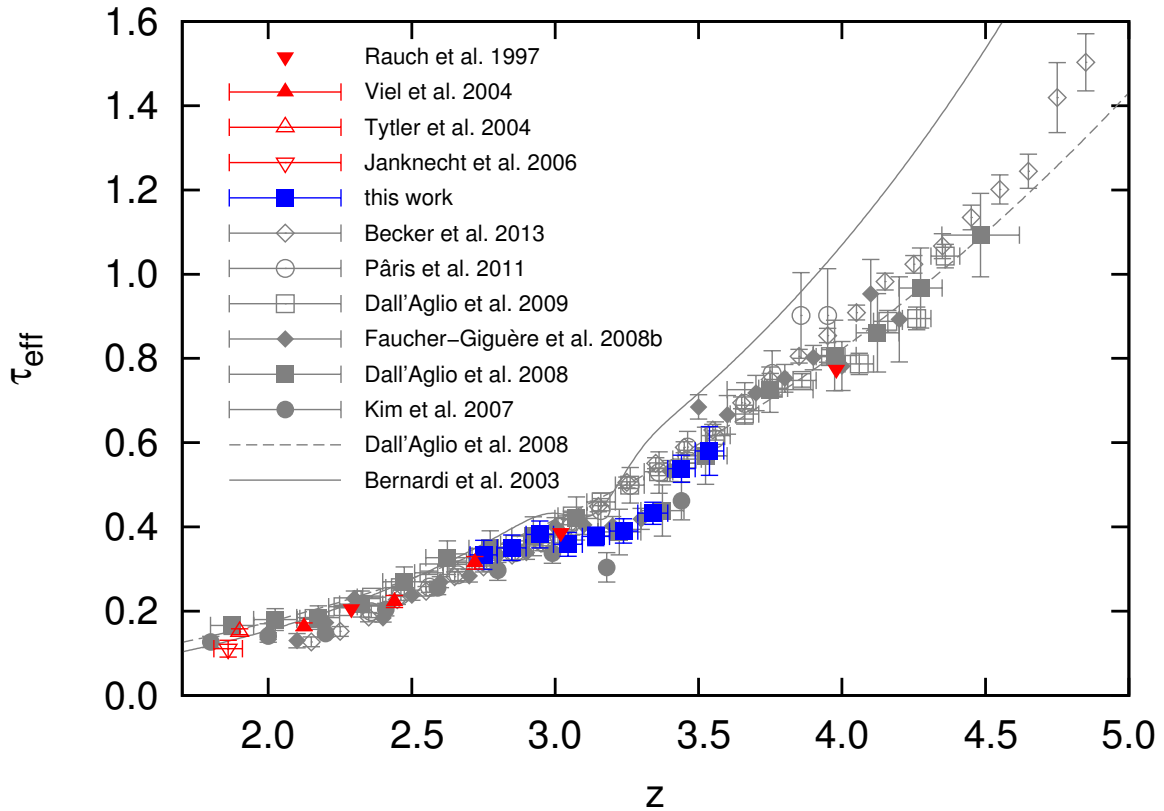


Figure 5.8. Comparison of measurements of $\tau_{\text{eff}}(z)$ available in the literature to the measurements presented in this work (see text).

crucial difference in the analysis of the data compared to other works using SDSS spectra. However, Bernardi et al. (2003) show that a feature in their evolution of the effective optical depth is retained if instead of a bumpy continuum on their composite spectra to account for emission lines in the H I Ly α forest a featureless power law is used (see their Fig. 12). Though, the amplitude of $\tau_{\text{eff}}(z)$ differs since a featureless power law underestimates the continuum flux in the H I Ly α forest where the emission lines are present. Nevertheless, their iterative method using composites is still different compared to other SDSS quasar spectra studies. In tests by Becker et al. (2013) using the iterative method, no prominent feature in the evolution of τ_{eff} is found.

Figure 5.8 summarizes the various τ_{eff} measurements available in the literature (see Table 1.1). Grey symbols and lines correspond to data previously shown and discussed. Red symbols correspond to measurements shown in this work for the first time. These values do not allow for investigating a detailed evolution of the effective optical depth on their own but are plotted for completeness. The estimates of τ_{eff} agree generally very well with one another. Due to the expected large scatter sightline averages are not shown.

5.2 Conclusions

The conclusions from this work are presented in three sections. The first part is a summary of the results from this work. In the second part the findings from the comparison of τ_{eff}

measurements from the literature to the measurement of this work are summarized. The last part comprises future prospects.

5.2.1 Conclusions from this work

The aim of this study has been the measurement of the effective optical depth, with regard to intergalactic hydrogen, which is a measure of the mean transmitted flux of the observed background sources. Hydrogen is the most abundant element in the Universe. Therefore, the H I Ly α effective optical depth is a very useful tool to constrain the energy input of ionizing sources, such as (star-forming) galaxies and active galactic nuclei, into the intergalactic medium (IGM). The advent of sources of radiation reionized the IGM that consists mostly of hydrogen and helium. The reionization of hydrogen is complete at redshift $z \sim 6$ (e.g., Fan et al. 2006), whilst the full reionization of helium is delayed due to the higher ionization potential of singly ionized helium. Observations suggest that the reionization of helium may be complete at redshift $z \sim 2.7$ (e.g., Worseck et al. 2011). In this case, the harder radiation should have an impact on the neutral hydrogen fraction at this redshift that might be visible in the redshift evolution of the effective optical depth measured from neutral hydrogen. Empirically the effective optical depth should follow a smooth power law. At redshifts $z \sim 3.2$ some studies find a deviation from a smooth power law of the H I effective optical depth which may be attributed to He II reionization. Though, this deviation is found controversial in the literature and simulations suggest that such a deviation is not required even in the case of He II reionization.

In this study I have used 13 high-resolution ($R \sim 45\,000$), high signal-to-noise ratio ($S/N \sim 40$) quasar spectra included in SQUAD, which were observed with UVES/VLT, with emission redshifts in the range $3.2 < z_{\text{em}} < 4.0$ in order to measure the effective optical depth for an important epoch in the evolution of the Universe, $2.7 \leq z \leq 3.6$. The measurement has been performed for redshift bins of size $\Delta z \simeq 0.1$. In order to see the impact of absorption features on $\tau_{\text{eff}}(z)$, several selections of absorption lines have been used to compute the effective optical depth. The selections comprise

- a) the observed flux,
- b) the model flux using all fitted absorption lines,
- c) the model flux corrected for metal absorption and fixed-parameter absorption lines (which are due to convergence issues and make up only $\approx 4\%$ of all fitted lines; see §2.3.3),
- d) and the model flux corrected for metal, fixed-parameter, and narrow ($b < 15 \text{ km s}^{-1}$) H I Ly α absorption lines.

The effective optical depth was computed based on the method used by Faucher-Giguère et al. (2008b).

I have fitted 7491 absorption lines individually that are found in the spectral range of each spectrum in between the H I Ly β emission line and the approximate onset of the proximity influence of the quasar on the IGM. The absorption-line fits have been used to remove the imprint of metals on each quasar spectrum. To remove metals in this way makes the measurement of the effective optical depth in this study the most significant at

redshifts $z > 2.7$ to date. Spectral regions contaminated by DLAs have been excluded.

An analysis of the absorption-line parameters was also performed in the redshift range $2.7 \leq z \leq 3.6$. The amount of data used in this work is the largest for such an analysis at these redshifts to date. Removing identified metal absorption lines, fixed-parameter lines, and narrow ($b < 15 \text{ km s}^{-1}$) absorption lines from the 7491 fitted absorption lines leaves 4742 lines (due to H I Ly α only) to estimate key parameters of the H I Ly α forest statistics in the redshift range $2.7 \leq z \leq 3.6$ concerning the column density, N , and the Doppler parameter, b . The fixed-parameter and narrow absorption lines are likely due to missed metals, noise features, and line blending.

In the following the results of this work are summarized.

H I Ly α forest statistics:

- ▶ The column-density distribution function is well described by a single power law of the form $f_{\text{CDD}}(N) = A \cdot N^{-\beta}$. The estimated parameters, $\log A$ and β , for three adjacent redshift bins of size $\Delta z = 0.3$ show marginal evolution over the redshift range $2.7 \leq z \leq 3.6$ based on the estimated errors. The parameter values are slightly larger at $\langle z \rangle = 3.15$ than at lower and higher redshift. The estimated slope is $\beta = 1.51 \pm 0.03$ at $\langle z \rangle = 2.85$, $\beta = 1.55 \pm 0.02$ at $\langle z \rangle = 3.15$, and $\beta = 1.47 \pm 0.03$ at $\langle z \rangle = 3.45$.
- ▶ The Doppler-parameter distribution shows the bulk of values in the range $b = (15 - 40) \text{ km s}^{-1}$. The mean value of the distribution is $b_{\text{mean}} \approx 30 \text{ km s}^{-1}$ and the median value is $b_{\text{median}} \approx 27 \text{ km s}^{-1}$. These values do not evolve with redshift.
- ▶ Assuming that the lowest b value at a given column density in the $b(N)$ distribution represents the temperature, a power-law fit to the lower cutoff envelope of the distribution has been performed in order to obtain an upper limit of the temperature of the low-density gas. The cutoff b values are found to follow $\log b_{\text{co}}(\log N) = (0.448 \pm 0.072) + (0.061 \pm 0.005) \cdot \log N$ at $z \sim 3.15$. The b_{co} value at $\log N = 13.6$ is $b_{\text{co}}(13.6) = 18.7 \text{ km s}^{-1}$ that corresponds to a temperature of the IGM of $T \approx 21\,000 \text{ K}$ at the corresponding density. The parameter $b_{\text{co}}(13.6)$ does not evolve with redshift.
- ▶ The number-density evolution can approximately be described by a power law of the form $dn/dz \propto (1 + z)^{1.62 \pm 0.33}$ for absorbers with column densities in the range $13 \leq \log N \leq 17$, which means that these absorbers significantly evolve with cosmic time. Similar to the effective optical depth the data points scatter around a smooth power law. This scatter is likely due to cosmic variance (see below).

Measurement of $\tau_{\text{eff}}(z)$:

- ▶ The τ_{eff} measurements using the observed flux and the model flux from all fitted absorption lines agree very well, justifying the absorption-line selection using the model flux to account for metal contamination in the quasar spectra.
- ▶ The qualitative redshift evolution of τ_{eff} is largely independent of the spectral contamination due to metals and narrow absorption lines.

- ▶ The effective optical depth increases with increasing redshift. A single power law does not fit the data well. This could be due to a downward feature at $z \sim 3.14$ or a break in the power-law evolution at $z \sim 3.24$. In order to determine the power-law deviation more precisely, the analysis presented in this work has to be extended in redshift space by the use of additional quasar spectra. Possibly, the deviation can be explained by scatter around a pure power law and is only apparent due to a too confined analyzed redshift range. This could be in agreement with the redshift evolution of the effective optical depth from the respective measurements of this work (corrected flux) combined with the measurements of Kim et al. (2007) at lower redshifts (see Fig. 5.2).
- ▶ The τ_{eff} measurements from this work could be used to account for metal absorption in studies in which the direct removal of contaminating metal-line absorption in the quasar spectra is not possible. For such a correction, the contribution of metals to τ_{eff} at a given redshift (Table 4.2, column 6) is subtracted from the uncorrected measurements (see §4.3.2).
- ▶ From simulations can be inferred that the error estimates of the τ_{eff} values computed in this work are too small, so that the τ_{eff} values may indeed underlie statistical scatter around a pure power law (Fig. 4.3) that is likely reduced if more sightlines (~ 30 , twice as many as used in this work) are used. As suggested by the simulations, the scatter may be caused by high-column-density absorbers ($15 \leq \log N \leq 17$).

It remains unclear which absorption-line parameter (distribution) could introduce a downward feature in the otherwise smooth evolution of τ_{eff} and how this would be related to the physical conditions in the IGM. From the results of this work can be implied that the redshift evolution of the effective optical depth is largely driven by the number-density evolution and that high-column-density absorbers could be responsible for scatter in the observational data. A decrease only in the number of high-column-density ($\log N > 15$) absorbers at $z \sim 3.15$, compared to lower and higher redshifts, would result in a steeper slope of the column-density-distribution function as found here (see above) and could, in principle, reduce the amount of observed absorption, i.e., result in the smaller τ_{eff} values estimated at this redshift (Fig. 4.3). It seems worthwhile to investigate the number-density evolution in more detail with regard to the redshift evolution of the effective optical depth, although line blending make an analysis problematic. The influence of absorbers with a given column density on $\tau_{\text{eff}}(z)$ could be investigated further by using a larger number of synthetic spectra created with particularly chosen absorption-line-parameter distributions. For example, the number of absorbers with a given column density could be increased or decreased at a given redshift in order to see the impact on $\tau_{\text{eff}}(z)$.

5.2.2 Literature comparison

- a) The most curious notice of the detection of a downward feature in the otherwise smooth evolution of the effective optical depth is the pure occurrence of the feature in $\tau_{\text{eff}}(z)$ inferred from different works at similar redshifts (Fig. 5.1). Though, as discussed above, this does not rule out the possibility that the feature has a statistical origin.

- b) Assuming that the effective optical depth follows a smooth evolution (e.g., Dall’Aglio et al. 2009; Becker et al. 2013) and that a detection of a downward feature in $\tau_{\text{eff}}(z)$ would be due to statistical biases, there should be found a bump in $\tau_{\text{eff}}(z)$, inferred from other quasar spectra than the ones used in the high-resolution works or by Bernardi et al. (2003) where the downward feature is seen, at the same redshift as the downward feature. To my knowledge, such a bump has not yet been reported. Note, that the downward feature in the effective optical depth evolution is equivalent to a ‘bump’ in the *mean flux* evolution (see below).
- c) Any method that infers the mean flux from observed quasar spectra should be able to recover the flux input that is introduced in mock spectra. The input recovery by Becker et al. (2013, see their §4) shows that their work leads arguably to the most precise measurement of the effective optical depth evolution to date. Though, there may still be concerns about the absolute scaling of their measurements with respect to the amount of absorption contributed by metals as mentioned earlier. Nevertheless, this does not effect the overall trend, which they find to follow closely to a pure power law. This makes the deviation as seen in high-resolution data spurious and may be explained by the two orders of magnitudes larger set of quasar spectra. The astonishing similarities of the constructed composite spectra by Becker et al. (2013) at any redshift may visualize the precision of their measurement (see their Fig. 2).
- d) As Becker et al. (2013) state, it may be possible that the SDSS data have converged up to now. The downward feature is found by Bernardi et al. (2003) and is claimed to be present in the analysis by Pâris et al. (2011) for which these authors use a specific subset of quasar spectra from the SDSS-DR7. This subset comprises spectra which have been observed up to the end of 2001, in order to mimic the Bernardi et al. (2003) sample. Pâris et al. (2011) also analyze general subsets of quasar spectra from the SDSS-DR7, similar to the Bernardi et al. (2003) sample. These subsets show a ‘bump’ or a break in the mean flux evolution. A single power law seems to be sufficient to describe the $\tau_{\text{eff}}(z)$ measurement by Dall’Aglio et al. (2009), who use SDSS-DR5 spectra. Pâris et al. (2011) declare a broken power law to be more likely to describe their data from SDSS-DR7. Becker et al. (2013) also use SDSS-DR7 quasar spectra and consider a single power law. The convergence of the SDSS data may be due to an increase in the amount of SDSS quasar spectra used for the analyses.
- e) The continuum estimation most likely does not play a crucial role in determining $\tau_{\text{eff}}(z)$ with regard to a downward feature, as long as the quasar spectra in a studied sample are treated consistently. As Becker et al. (2013) have impressively shown, composite spectra created from quasar spectra in redshift bins of $\Delta z_{\text{em}} = 0.1$ are alike even at different redshifts if the individual spectra have been normalized at a given rest-frame wavelength (Becker et al., 2013; they used $\lambda_r \sim 1285 \text{ \AA}$). They also showed their estimate of a mean continuum for the quasar spectra at any redshift, though not with the correct amplitude since for absolute scaling Becker et al. (2013) would need to have access to a composite spectrum at redshift $z = 0$. There are differences in the continuum estimates from different approaches, such as the

principle component analysis (PCA), the power-law extrapolation from redward of the H I Ly α emission line, and local fitting. These differences are expected to be of global significance in terms of the amplitude of $\tau_{\text{eff}}(z)$ since any local overestimate or underestimate will be canceled out by a sample of quasar spectra that are distributed evenly in emission-redshift space and of which several spectra contribute to the measurement at a given redshift. Hence, different approaches to estimate the continuum should lead to constant offsets between data or noticeable tilts of the τ_{eff} measurements. A local deviation in $\tau_{\text{eff}}(z)$ from a pure power law, as seen in the high-resolution data at $z \sim 3.2$, is unlikely to have an effect on the continuum estimation.

- f) Considering the solid angle, it seems more appropriate to ask, how many spectra are needed to see on average a homogeneous gas distribution in the IGM. Some 10^3 sightlines seem more promising than some 10^2 or only some 10. Since Becker et al. (2013) have shown that their method recovers a downward feature if it is introduced in individual mock spectra by design, it is tough to argue against their findings with respect to the observed redshift evolution of the effective optical depth. I tend to agree to their statement that the discoveries of a downward feature in $\tau_{\text{eff}}(z)$ appear to have been spurious (see below). Though, the occurrence of the $\tau_{\text{eff}}(z)$ feature is not yet fully understood.

The redshift evolution of the effective optical depth computed in this work agrees very well with the measurement of Faucher-Giguère et al. (2008b). The method used in this work is based on the method by Faucher-Giguère et al. (2008b) and the data used by both works are similar. Though, Faucher-Giguère et al. (2008b) use almost 3 times more high-resolution quasar spectra in the emission redshift range $3.2 < z_{\text{em}} < 4$. This emission redshift range covers all 13 quasar spectra used in this work. In both studies a downward feature in an otherwise smooth evolution of the effective optical depth could be present. The study by Dall'Aglio et al. (2009) is comparable to this work with regard to the τ_{eff} measurement. Dall'Aglio et al. (2009) use 1733 low-resolution quasar spectra and find no downward deviation from a smooth power law in $\tau_{\text{eff}}(z)$. There is no clear explanation for this.

5.2.3 Future prospects

To finally answer the question whether a downward feature in the otherwise smooth evolution of the effective optical depth is present, it is necessary to analyze a carefully selected sample of high-resolution quasar spectra. The quasar spectra must be distributed evenly in emission redshift space. The sample should preferably be homogeneous in terms of resolution, signal-to-noise ratio, and observational instrument. The number of quasar spectra should be of the order of 10^4 to improve at least the study of Becker et al. (2013) who analyzed 6065 low-resolution quasar spectra. The analysis of such a large quasar spectra sample is time consuming and could comprise the following methods:

- i) From the results mentioned above it is clear that a rough first estimate of $\tau_{\text{eff}}(z)$ is possible by estimating the continua of the quasar spectra automatically and computing the mean normalized flux as a pixel average over all pixels from contributing

quasar spectra in a given redshift bin. In principle, this should lead to the qualitative redshift evolution of the effective optical depth.

- ii) Composite spectra can be created from such a large sample. Depending on the redshift distribution of the individual quasar spectra, the redshift bins Δz_{em} for the construction of the composite should be chosen with care. The redshift evolution of the flux in the composite spectra can be studied, as well as the evolution of the composite continua.
- iii) For comparison, the continuum of the individual spectra can be estimated locally. This will be most time consuming and may suffer from inconsistencies. If many people contribute, there may be a subjective component to the analysis, although this may be constrained by creating subsamples of the individual quasar spectra which are homogeneously distributed over the whole emission redshift range covered by the full sample. In the case that a single person is working on this analysis, performance variability has to be considered since fitting continua on $\sim 10^4$ quasar spectra is rather exhausting work. This is also true if the continua can be estimated automatically and only have to be evaluated by eye. Corrections to the continua could be applied if necessary. Since metal absorption seems to be present at any redshift in the same amount, metal-absorption-line removal may be skipped but considered to offset the τ_{eff} measurement. The mean normalized flux can then be analyzed.

I consider this methodology the most promising in order to get a definitive answer on the redshift evolution of the H I Ly α opacity.

Appendix A

Equations

In the following, equations used in the main text are derived.

A.1 Derivation of Eq. (1.7)

This equation states, that if a constant real value C is added to (or subtracted from) the mean value of an observable x , it equals the mean value of the same constant real value added to (or subtracted from) the individual measurements x_i .

$$\begin{aligned} \forall C \in \mathbb{R} : C \pm \langle x_i \rangle &= C \pm \frac{1}{n} \sum_{i=1}^n x_i \\ &= \frac{1}{n} \left(nC \pm \sum_{i=1}^n x_i \right) \\ &= \frac{1}{n} \left(\sum_{i=1}^n C \pm \sum_{i=1}^n x_i \right) \\ &= \frac{1}{n} \sum_{i=1}^n (C \pm x_i) \\ &= \langle C \pm x_i \rangle \end{aligned} \tag{A.1}$$

A.2 Derivation of Eq. (1.11)

This equation relates the effective optical depth to the distribution functions of the intergalactic absorbers. The derivation is based on the derivations of Liske et al. (1998) and Zuo and Phinney (1993). Let $\eta(z, b, N)$ be the mean number of absorbers per unit redshift, Doppler parameter and column density:

$$\eta(z, b, N) = \frac{d^3 \mathcal{N}}{dz db dN}.$$

The mean total number of absorbers in the redshift range $z_1 \leq z \leq z_2$ is

$$m = \int_0^\infty \int_0^\infty \int_{z_1}^{z_2} \eta(z, b, N) dz db dN. \tag{A.2}$$

The average transmitted flux through a single absorber with optical depth $\tau_A(z, b, N)$ is

$$\langle e^{-\tau_A} \rangle = \int_0^\infty \int_0^\infty \int_{z_1}^{z_2} e^{-\tau_A(z, b, N)} \frac{\eta(z, b, N)}{m} dz db dN. \quad (\text{A.3})$$

The pixel optical depth $\tau_p(z)$ in a quasar spectrum results from the contribution of all absorbers at a given redshift z . Assuming N absorbers contribute independently to τ_p ,

$$\tau_p = \sum_{i=1}^N \tau_{A,i} \equiv \tau_{p,N},$$

then

$$e^{-\tau_{p,N}} = \exp \left[- \sum_{i=1}^N \tau_{A,i} \right] = \prod_{i=1}^N e^{-\tau_{A,i}}. \quad (\text{A.4})$$

Equation (A.4) gives, on average,

$$\langle e^{-\tau_{p,N}} \rangle = \left\langle \prod_{i=1}^N e^{-\tau_{A,i}} \right\rangle \equiv \left\langle \prod_{i=1}^N \langle e^{-\tau_A} \rangle \right\rangle = \prod_{i=1}^N \langle e^{-\tau_A} \rangle = \langle e^{-\tau_A} \rangle^N. \quad (\text{A.5})$$

Assuming a Poisson distribution of the absorbers along a line of sight, the probability mass function is

$$p(N; m) = \frac{m^N e^{-m}}{N!}. \quad (\text{A.6})$$

Hence, the effective optical depth can be expressed as

$$\begin{aligned} e^{-\tau_{\text{eff}}} &= \sum_{N=0}^{\infty} p(N; m) \langle e^{-\tau_{p,N}} \rangle = \sum_{N=0}^{\infty} p(N; m) \langle e^{-\tau_A} \rangle^N = \sum_{N=0}^{\infty} \frac{m^N e^{-m}}{N!} \langle e^{-\tau_A} \rangle^N \\ &= e^{-m} \underbrace{\sum_{N=0}^{\infty} \frac{(m \langle e^{-\tau_A} \rangle)^N}{N!}}_{\equiv \exp[m \langle e^{-\tau_A} \rangle]} = \exp[-m] \cdot \exp[m \langle e^{-\tau_A} \rangle] = \exp[-m(1 - \langle e^{-\tau_A} \rangle)]. \end{aligned} \quad (\text{A.7})$$

In Eq. (A.7) I made use of the definition of the exponential function,

$$e^x = \sum_{n=0}^{\infty} \frac{x^n}{n!}. \quad (\text{A.8})$$

Using Equations (A.3) and (A.2) the effective optical depth can now be expressed as

$$\begin{aligned}
\tau_{\text{eff}} &= m[1 - \langle e^{-\tau_A} \rangle] = m \left[1 - \int_0^\infty \int_0^\infty \int_{z_1}^{z_2} e^{-\tau_A(z,b,N)} \frac{\eta(z,b,N)}{m} dz db dN \right] \\
&= m - \int_0^\infty \int_0^\infty \int_{z_1}^{z_2} e^{-\tau_A(z,b,N)} \eta(z,b,N) dz db dN \\
&= \int_0^\infty \int_0^\infty \int_{z_1}^{z_2} \eta(z,b,N) dz db dN - \int_0^\infty \int_0^\infty \int_{z_1}^{z_2} e^{-\tau_A(z,b,N)} \eta(z,b,N) dz db dN \\
&= \int_0^\infty \int_0^\infty \int_{z_1}^{z_2} [1 - e^{-\tau_A(z,b,N)}] \eta(z,b,N) dz db dN. \tag{A.9}
\end{aligned}$$

A.3 Derivation of Eq. (1.17)

This equation relates the proper length to redshift. I start with the Friedmann-Lemaître-Robertson-Walker metric

$$ds^2 = c^2 dt^2 - R^2(t) d\chi^2, \tag{A.10}$$

where the line element $ds = 0$ (null-geodesic) at all times t for photons (Sandage 1961) as considered subsequently. The quantity c is the speed of light in vacuum. For zero curvature, $\Omega_k(k=0) = 0$, $d\chi$ is the comoving length and, hence, $R(t)d\chi = dL$ the proper length, so that

$$c^2 dt^2 = dL^2,$$

as well as

$$dL = c|dt|. \tag{A.11}$$

From $R(t) = (1+z)^{-1}$ (Eq. 1.3) follows

$$\dot{R}(t) = \frac{dR(t)}{dt} = -\frac{1}{(1+z)^2} \frac{dz}{dt} = -\frac{R(t)}{1+z} \frac{dz}{dt} \tag{A.12}$$

and

$$H(t) \equiv \frac{\dot{R}(t)}{R(t)} = -\frac{1}{1+z} \frac{dz}{dt} = H(z), \tag{A.13}$$

so that

$$dt = -\frac{1}{(1+z)H(z)} dz \tag{A.14}$$

and with Eq. (A.11)

$$dL = \frac{c}{(1+z)H(z)} dz. \tag{A.15}$$

Appendix B

Technical details of the line-fitting procedure with CANDALF

The program CANDALF (see §2.3.2) is used to fit absorption features in quasar spectra by profile functions. These profile functions are of Doppler shape. The necessary input parameters build up an absorption-line-parameter list. For each absorption line these parameters are the central observed wavelength $\lambda_{c,\text{obs}}$, the rest-frame wavelength λ_0 and oscillator strength f of the considered species, the column density N , and the Doppler parameter b . This list works as a reference from which the best spectral fit is determined by adjusting the given parameters considering non-linear least squares. The output comprises the adjusted parameters as a list.

In order to create a preliminary input absorption-line list for a spectral section, I determined the central observed wavelength for the most prominent absorption features. A sufficient first guess regarding an absorber's column density and Doppler parameter usually is $\log N = 13.5$ or $\log N = 14$ and $b = 25 \text{ km s}^{-1}$, respectively. However, these values are not appropriate for particularly weak or strong absorption lines. Leaving all parameters fixed during the preliminary runs with CANDALF, it was decided by comparing the raw fit with the original spectrum whether additional absorption lines are necessary and the set of absorption lines was extended accordingly. This concerns rather separate absorption features than blends. Possibly, it was necessary to modify the initial guesses for some of the parameters to reach convergence with CANDALF once the program was assigned to adjust these.

Since the input file with the absorption-line parameters and the output file with the adjusted parameters differ in format, I used a script written in PYTHON to generate a text file of input-file format containing the adjusted absorption-line parameters. The subsequent iteration with CANDALF was performed using the adjusted parameters. This usually improved the fit. Besides rearranging the output parameters per absorption line, PYTHON was used to compare the input parameters with the corresponding output parameters. When the input parameters differed from the corresponding output parameters by $\Delta \leq 0.05$ and, furthermore, the fit was accurate, the input absorption-line list was considered to be final. I assumed that robust line parameters would represent the best fit achievable. The arbitrary, though reasonable, deviation per respective unit, Δ , applies for each parameter – $\lambda_{c,\text{obs}}$ (in Å), $\log N$ (N in cm^{-2}), and b (in km s^{-1}). Agreement within Δ of all compared parameters is barely achievable due to the numerous absorption lines

per spectral section and the influence of blends and noise. By experience, the most likely source of discrepancy is the Doppler parameter. Some absorption lines became steadily broader with continuous iterations due to ambiguous absorption features, others became narrower because adjacent absorption lines made them unnecessary. Whenever required, the number of absorption lines was adjusted between program runs.

In the simplest way, the different formats of input file and output file are due to the listing of the respective parameter errors in the output file. Since PYTHON works with space character detection in text files, the presentational format of the error of the Doppler parameter, σ_b , results in an invalid comparison by using PYTHON with respect to the parameters $\log N$ and b , if exceeding $\sigma_b = 99.999 \text{ km s}^{-1}$. This problem cannot be overcome in a different manner than adjusting the corresponding input parameters, adding or removing absorption lines. Therefore, conditioned by the use of PYTHON, the final Doppler parameters of absorption lines have errors below the threshold of $\sigma_b = 100 \text{ km s}^{-1}$. For larger Doppler parameters the probability of a large error σ_b is higher and a few marginal absorption features with absorption lines of low column densities and large Doppler parameters could not be fit due to the issue outlined above.

The Doppler parameters of some absorption lines became very narrow ($b < 15 \text{ km s}^{-1}$). Though this is acceptable for metal absorption lines, because of their higher atomic weight, it seems unphysical for H I Ly α absorption lines with regard to the temperature of the IGM ($T \gtrsim 10^4 \text{ K}$). Such narrow H I Ly α absorption lines may be ascribed to unidentified metals. After all, the thermal contribution (Eq. 3.2) to the Doppler parameter (Eq. 3.1) is proportional to the square root of the ratio of the temperature T of the gas to the relative atomic mass A_r of the considered ion,

$$b_{\text{th}}^2 \propto \frac{T}{A_r}. \quad (\text{B.1})$$

Empirically, absorption lines with $b \lesssim 2 \text{ km s}^{-1}$ are unphysical compared to the resolution of the quasar spectra. In a technical view, they often have large error bars σ_b . Despite their questionable nature, I allowed certain H I Ly α absorption lines to stay in the absorption-line list, with a somewhat arbitrarily chosen fixed Doppler parameter $b_{\text{ll}} \equiv 2 \text{ km s}^{-1}$, in order to improve the fit or to facilitate convergence. Conditioned by their nature, I adopted b_{ll} also for critical, narrow metal absorption lines.¹ Figure 3.1 suggests that most of the hydrogen absorption lines with b_{ll} are noise since the most probable Doppler parameter of the identified metals lies in the range $2 < b/(\text{km s}^{-1}) < 8$. Indeed, 94 % of the H I Ly α absorption lines with $b = b_{\text{ll}}$ have low column densities, $\log N < 13$. However, Fig. 3.1 may not be representative of the Doppler-parameter distribution of metals if a sufficient amount of metal absorption lines was missed in the identification process. The 6 % of the H I Ly α absorption lines with b_{ll} and larger column densities are probably a relic of missed metal absorption features, as mentioned above, or due to saturation (see below).

¹The exception are two interdependent Fe II transitions. Their Doppler parameters of $b = 1.5 \text{ km s}^{-1}$ seemed to be the best fit, though adjacent H I Ly α absorption lines did not agree within Δ until these Doppler parameters were held fix. The respective metal component is also apparent in two additional unblended Fe II transitions. For the corresponding spectral section convergence was difficult to achieve in general.

Table B.1. Absorption lines with a fixed Doppler parameter, $b > 2 \text{ km s}^{-1}$.

QSO	z_{em}	$\lambda_0 (\text{\AA})$	$\lambda_{c,\text{obs}} (\text{\AA})$	$\log N$	$b (\text{km s}^{-1})$	reason to fix
J014214+002324	3.380	1215.670	4928.827	11.909	5.135	
J012403+004432	3.824	1215.670	5343.667	12.836	14.999	convergence
J111350-153333	3.365	2382.765	4858.333	16.831	3.500	
J212912-153841	3.279	1334.532	5029.316	18.016*	10.000	
J012403+004432	3.824	1215.670	5340.440	20.495*	12.000	saturation
J012403+004432	3.824	1215.670	5358.191	20.344*	6.870	
J212912-153841	3.279	1215.670	4660.682	14.413	18.000	
J212912-153841	3.279	1215.670	4736.752	15.270	8.000	
J212912-153841	3.279	1215.670	4744.009	14.081	6.800	
J132029-052335	3.718	1215.670	5112.660	14.442	5.000	no H I Ly β
J012403+004432	3.824	1215.670	5349.918	14.728	76.839	
J012403+004432	3.824	1215.670	5487.452	14.418	5.000†	
J012403+004432	3.824	1215.670	5488.143	19.125*	5.000†	

† Adjacent components separated by a flux-density spike.

* Would result in Voigt profiles.

The line-fitting procedure with CANDALF resulted in a total of 298 absorption lines with fixed parameters. Each of these lines had at least a fixed Doppler parameter. In particular, 285 (96 %) had Doppler parameters of $b \leq b_{\text{II}}$. Specifics of the remaining thirteen fixed-parameter absorption lines are given in Table B.1. The Doppler parameters of six listed absorption lines were held fix due to convergence issues with CANDALF. Due to saturation, the absorption-line flanks of four absorption lines among these appear too steep, so that their Doppler parameters became continuously smaller and their column densities increased simultaneously. A fixed b value made a robust fit possible. The Doppler parameters of seven more absorption lines were held fix due to absent H I Ly β absorption features, but H I Ly α is saturated. These absorption features could also be caused by complex metal absorbers.

With respect to the determination of the line parameters, saturated absorption features are a source of uncertainty. First, they could be complex strong metal absorption features which are regarded as H I Ly α . Insufficient spectral data or ambiguous higher-order Lyman series transitions could conceal such misidentifications. Second, the number of components of saturated absorption features is uncertain. With regard to metals, interdependent absorption-line fitting could solve this problem if one absorption feature is unsaturated. Regarding H I Ly α , higher-order Lyman series transitions could provide additional information. Though, higher-order Lyman series transitions arise in spectral regions with significant blending and the continuum estimation of their spectral regions is probably less accurate than redward of the H I Ly β emission line. Third, if saturated absorption lines are blended, the column density can become unreasonably high due to steep absorption-line flanks.

An absorber, seen as a single saturated component in H I Ly α , may actually show multiple

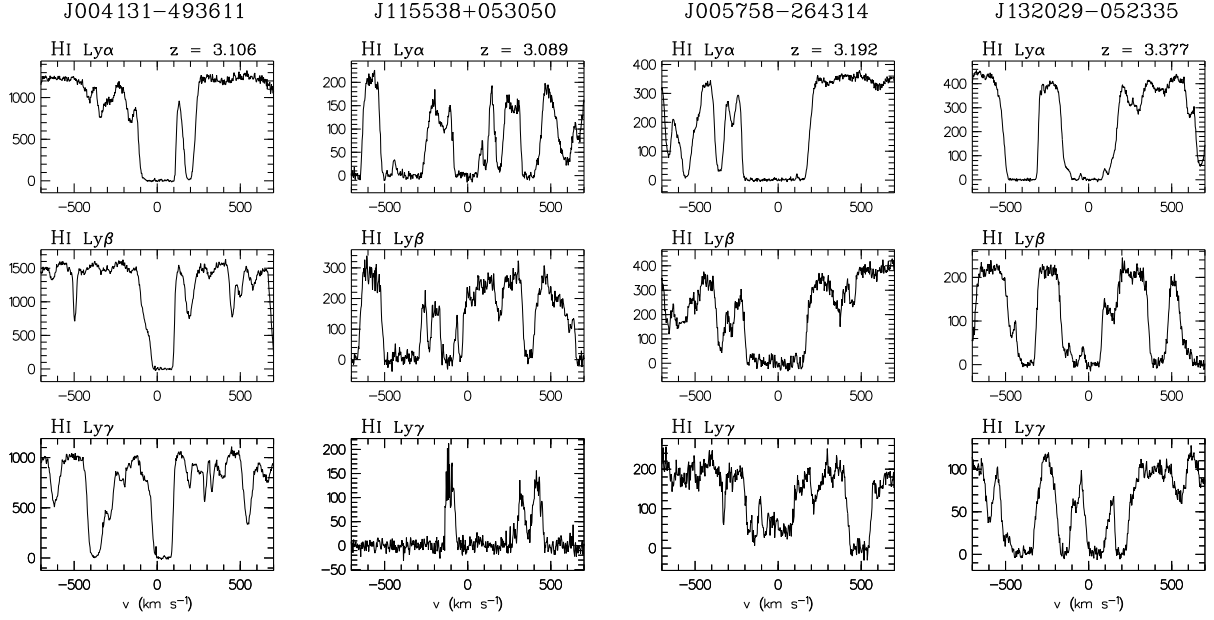


Figure B.1. Absorption features of the first three Lyman series transitions of absorbers intersecting different lines of sight. The ordinate has arbitrary flux-density units.

components in higher-order Lyman series transitions, which can only be accounted for if these are fitted simultaneously with their H I Ly α counterpart. In the case of missing or weak H I Ly β absorption features, the saturated H I Ly α absorption feature is presumably due to unidentified metals. If the Doppler parameter of a saturated H I Ly α absorption feature seems too narrow for an H I transition, the same conclusion may be drawn. It may occur that identified metal transitions are blended entirely with H I Ly α absorption features. Some absorption features are difficult to interpret. Figure B.1 shows some example hydrogen absorbers in the first three Lyman series transitions. For the spectral fit of the H I Ly α absorption features see the respective quasar spectra in Appendix D.

In order to verify the fit results from CANDALF regarding hydrogen absorbers, the parameters of the H I Ly α absorption lines were translated into H I Ly β absorption lines and compared with the respective absorption features in the H I Ly β region of the spectrum. This depends on the availability of spectral data. In order to have a consistent model, several conditions have to be fulfilled:

- ▶ The number of H I Ly α components must be the same as the estimated number of H I Ly β components.
- ▶ The absorbed flux from the H I Ly β absorption lines must not exceed the flux decrement in the H I Ly β region.
- ▶ The continuum estimate has to be considered with care since the continuum estimation is more uncertain in the spectral region in which higher-order Lyman series absorption is present.

In case of significant disagreement, I tried to fit H I Ly α and H I Ly β transitions simultaneously to improve the absorption-line parameters, using convenient spectral ranges. If required, H I Ly α absorption lines are added in the H I Ly β range to account for blends.

The improved H I Ly α parameters then were used for the actual spectral fit without interdependence with H I Ly β . When the revised absorption-line list led to an adequate fit, the H I Lyman series transition comparison was performed again. Though the comparison is not free of uncertainties, the final H I Ly α fits seem reasonable in general. Spectral data for matching the H I Lyman series transitions are insufficient for three of the 13 quasar spectra used in this work.

Appendix C

Segment flux histograms

The method used in this work to infer the redshift evolution of the effective optical depth is based on computing the average flux from all 3 proper Mpc segments of any quasar spectrum intersected by a given redshift bin (see Chapter 4). For each segment the mean flux from the pixels contained in the respective segment was computed. In this section, the mean-flux distribution of the segments in a given redshift bin is presented. This includes segment distributions from the 13 observed quasar spectra used in this work (Fig. C.1) and the synthetic spectra (Figs. C.2–C.6).

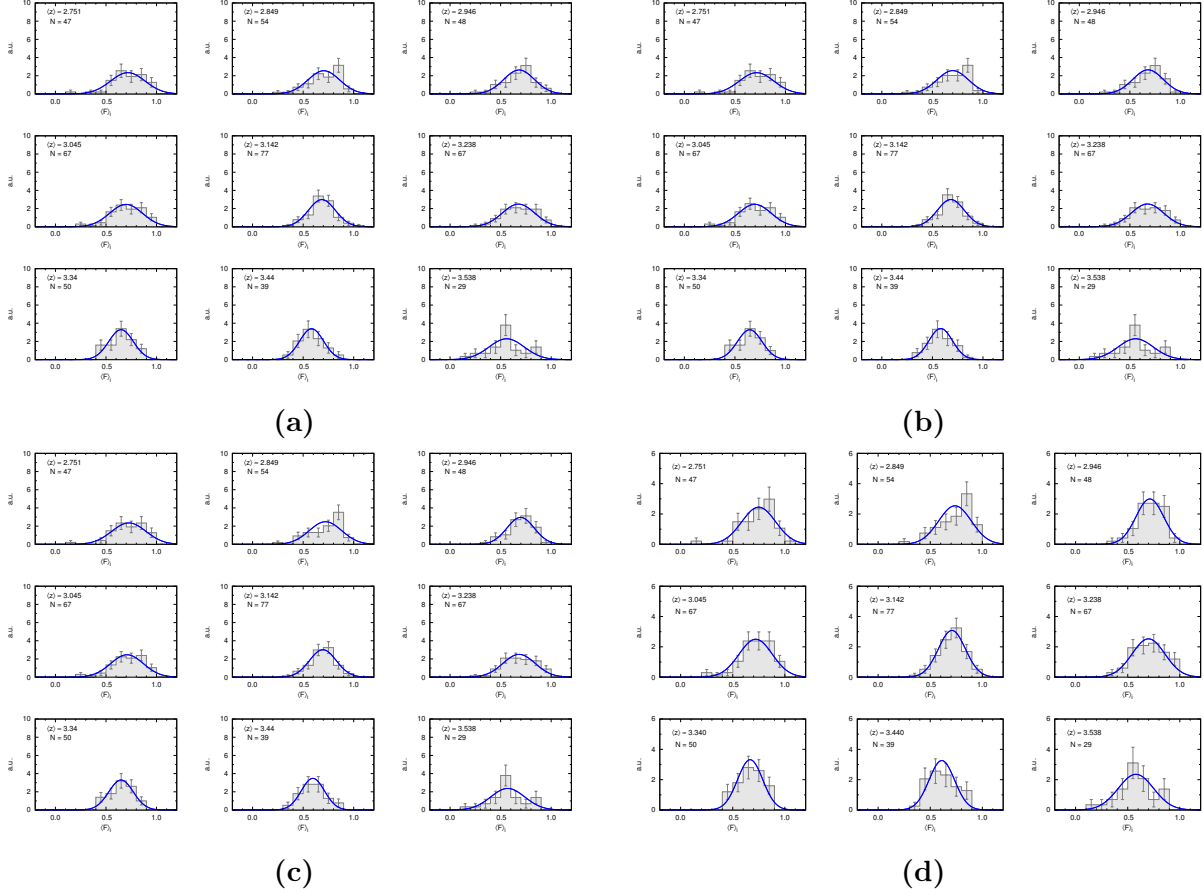


Figure C.1. Histograms of the mean flux $\langle F_i \rangle$ of the $\sum_{i=1}^N 1 = N$ contained segments from the 13 quasar spectra used in this work (if contributing) in redshift bins of size $\Delta z \simeq 0.1$ with a mean redshift $\langle z \rangle$. The Gaussian (blue curve) has the same mean flux and standard deviation as the respective histogram and is plotted for presentational purposes only. The flux used is (a) observed flux, (b) model flux, (c) model flux excluding metal absorption lines and absorption lines with fixed fitting parameters, (d) model flux excluding metal absorption lines, absorption lines with fixed fitting parameters, and lines with Doppler parameters smaller than $b = 15 \text{ km s}^{-1}$ (same as Fig. 4.2).

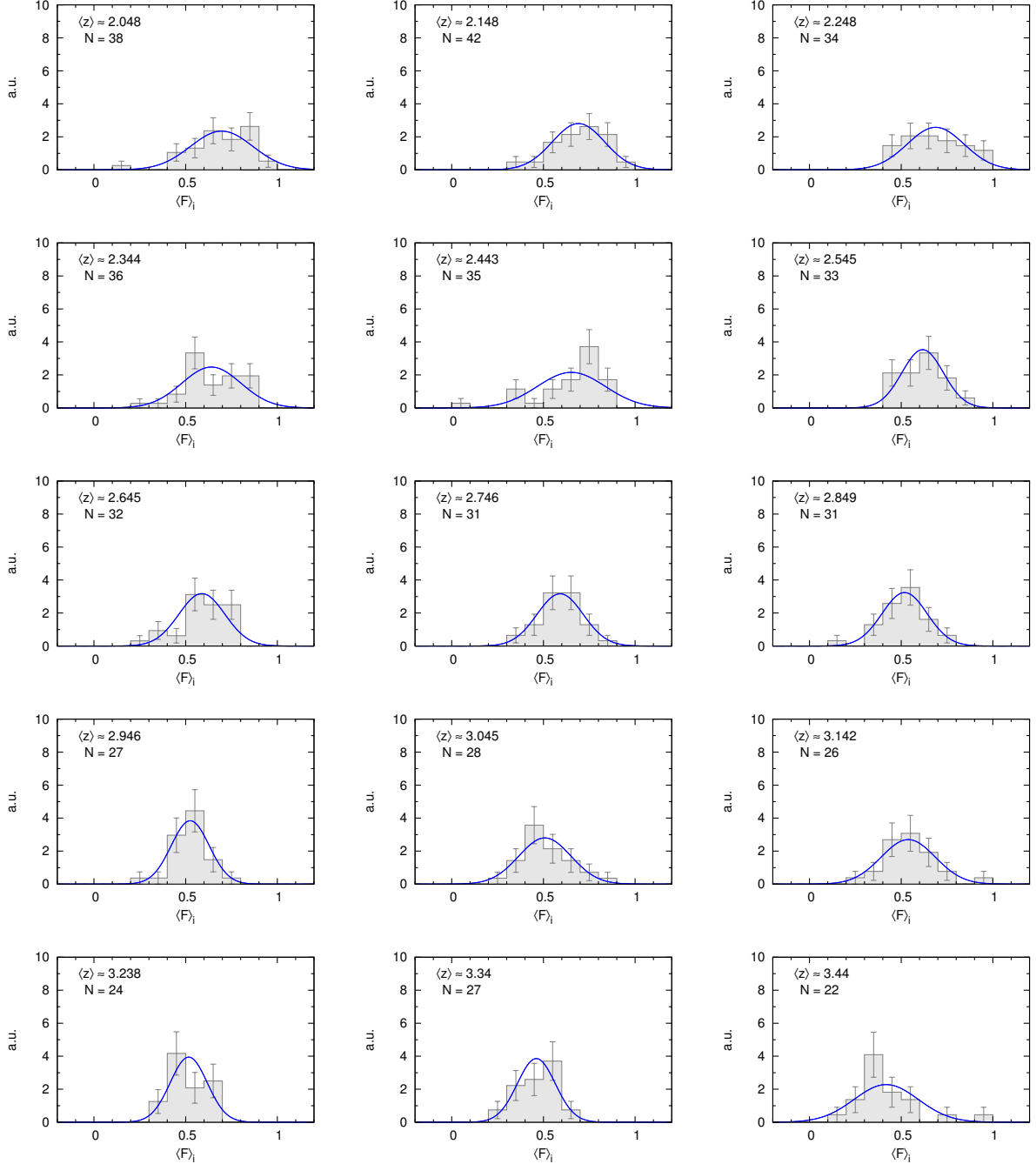


Figure C.2. Histograms of the mean flux $\langle F \rangle_i$ of the $\sum_{i=1}^N 1 = N$ contained segments from synthetic spectra used in this work (if contributing) in redshift bins of size $\Delta z \simeq 0.1$ with a mean redshift $\langle z \rangle$. The Gaussian (blue curve) has the same mean flux and standard deviation as the respective histogram and is plotted for presentational purposes only. The synthetic spectra exhibit H I Ly α absorption features only, with Doppler parameters drawn from a lognormal Doppler-parameter distribution and column densities in the range from $\log N_{\text{H}_1} = 12$ to $\log N_{\text{H}_1} = 17$ (see also row 1 in Table 4.3).

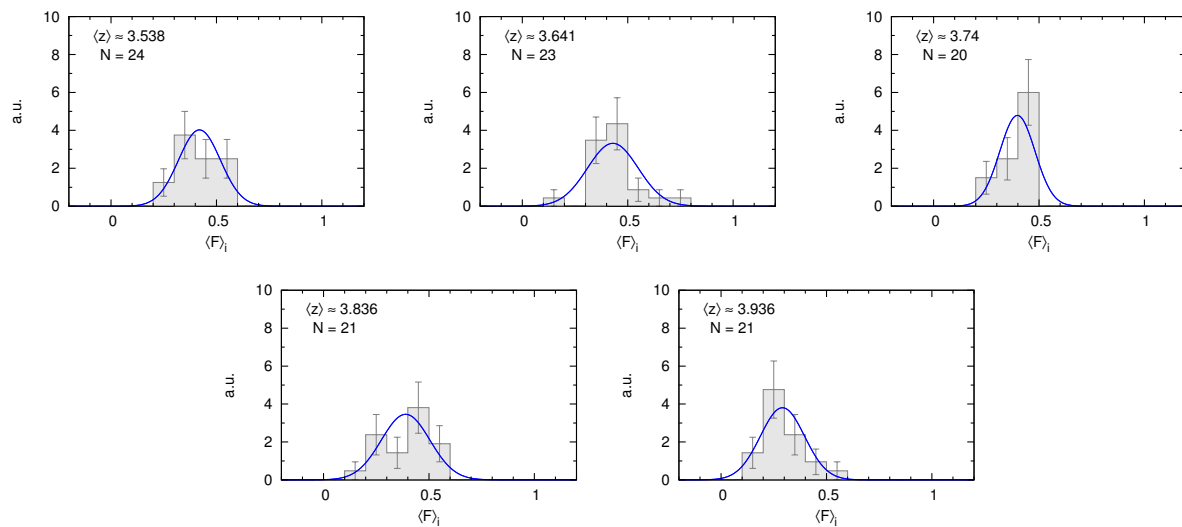


Figure C.2. *Continued*

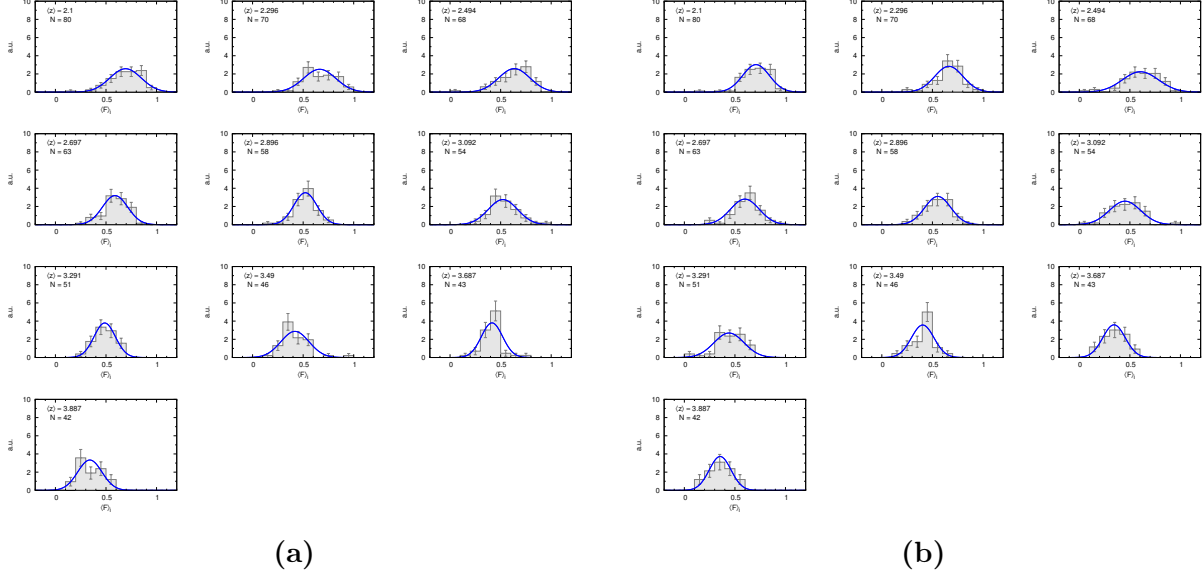


Figure C.3. Histograms of the mean flux $\langle F \rangle_i$ of the $\sum_{i=1}^N 1 = N$ contained segments from synthetic spectra used in this work (if contributing) in redshift bins of size $\Delta z \simeq 0.2$ with a mean redshift $\langle z \rangle$. The Gaussian (blue curve) has the same mean flux and standard deviation as the respective histogram and is plotted for presentational purposes only. The synthetic spectra exhibit H I Ly α absorption features only, with Doppler parameters drawn from a lognormal Doppler-parameter distribution and column densities in the range from $\log N_{\text{H}\,1} = 12$ to (a) $\log N_{\text{H}\,1} = 17$ and (b) $\log N_{\text{H}\,1} = 22$ (see also rows 2 and 3 in Table 4.3).

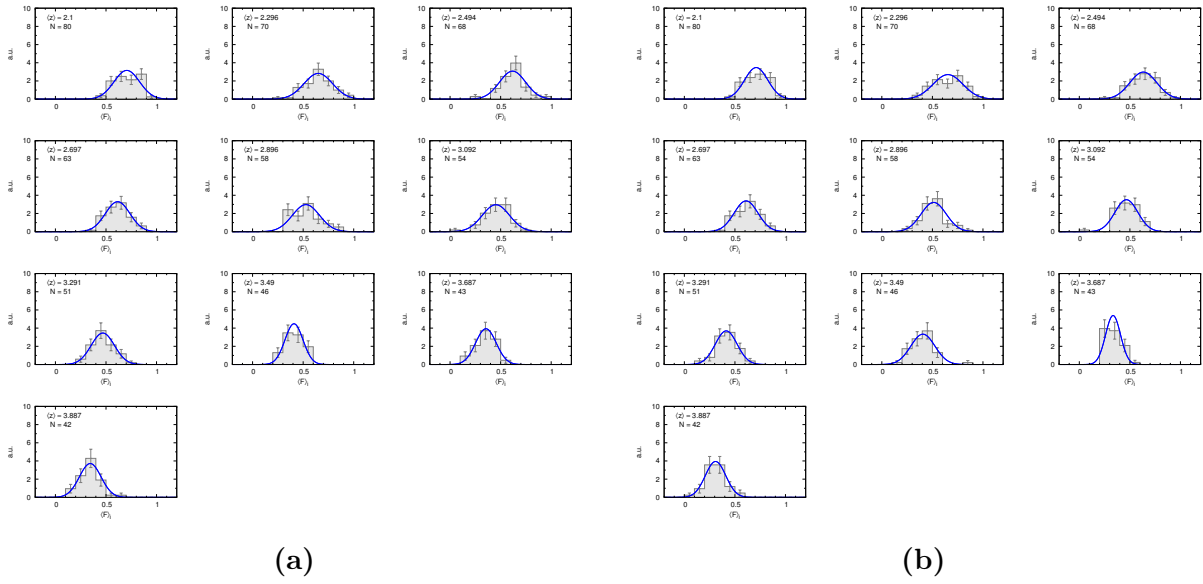


Figure C.4. Same as Fig. C.3. The synthetic spectra exhibit H I Ly α absorption features only, with fixed Doppler parameters ($b = 25 \text{ km s}^{-1}$) and column densities in the range from $\log N_{\text{H}\,1} = 12$ to (a) $\log N_{\text{H}\,1} = 17$ and (b) $\log N_{\text{H}\,1} = 22$ (see also rows 4 and 5 in Table 4.3).

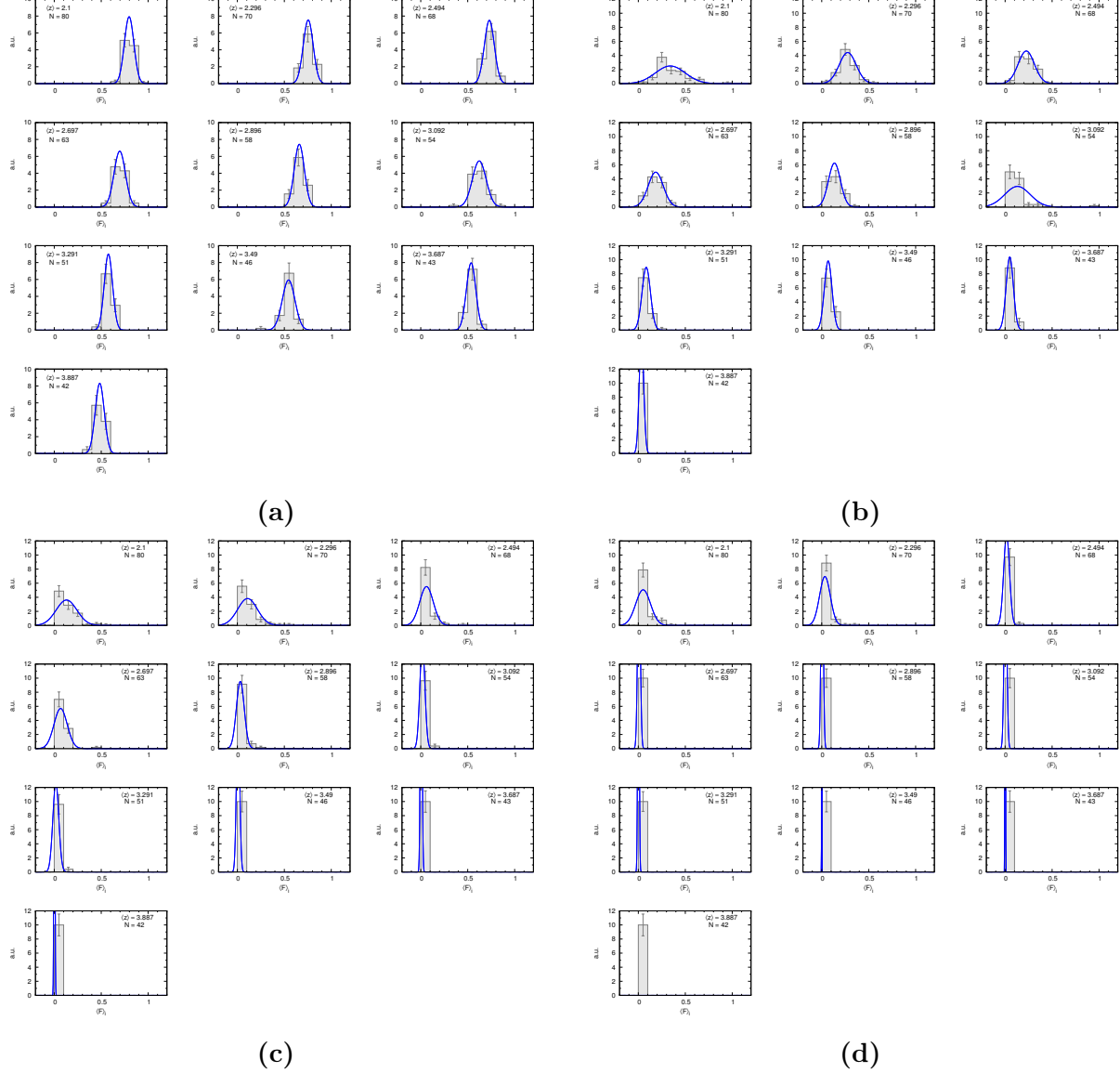


Figure C.5. Same as Fig. C.3. The synthetic spectra exhibit H I Ly α absorption features only, with Doppler parameters drawn from a lognormal Doppler-parameter distribution and with fixed column densities: (a) $\log N_{\text{H}\,1} = 13$; (b) $\log N_{\text{H}\,1} = 14$; (c) $\log N_{\text{H}\,1} = 15$; (d) $\log N_{\text{H}\,1} = 17$ (see also rows 6 – 9 in Table 4.3).

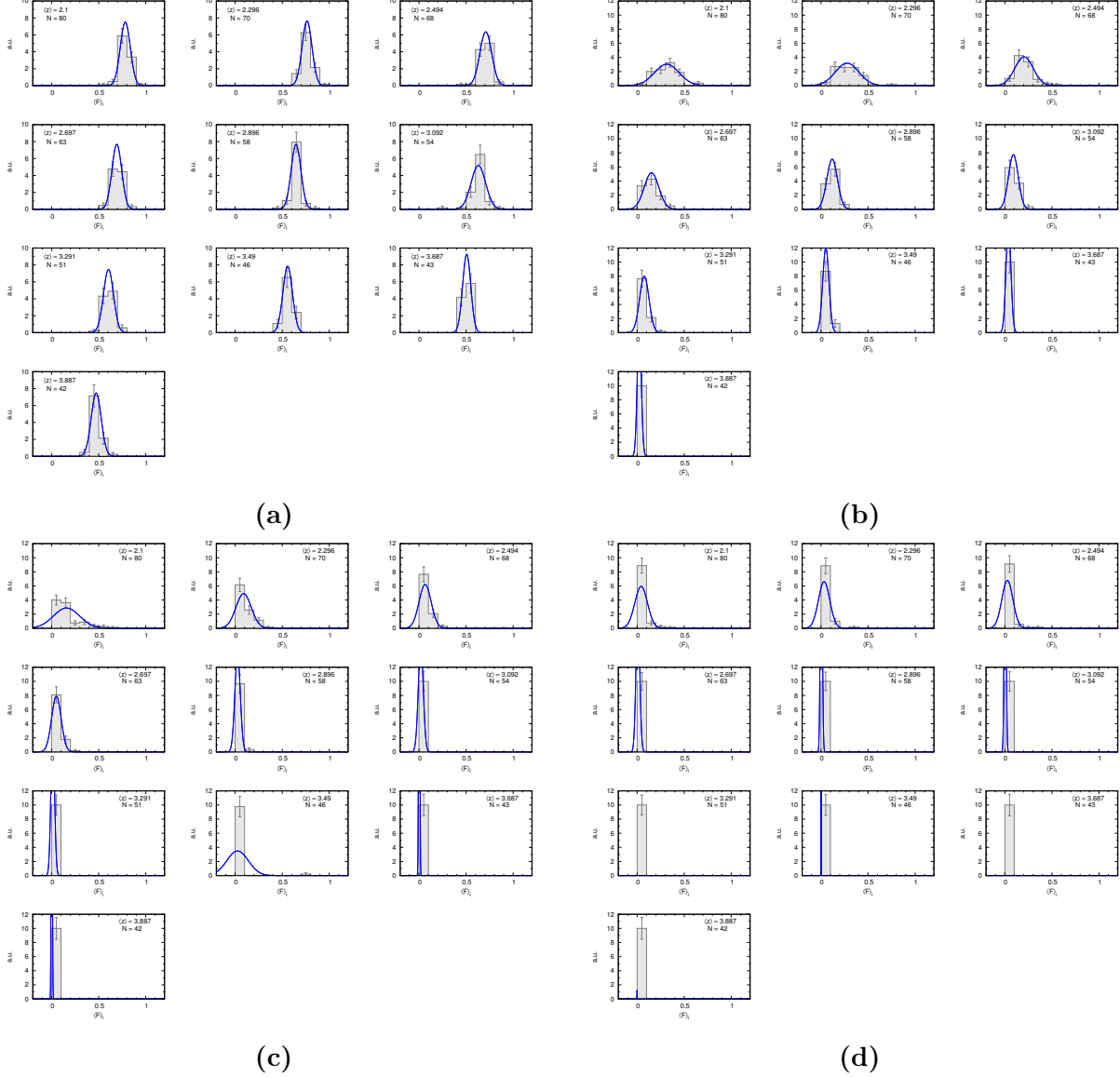


Figure C.6. Same as Fig. C.3. The synthetic spectra exhibit H_I Ly α absorption features only, with fixed Doppler parameters ($b = 25 \text{ km s}^{-1}$) and fixed column densities: (a) $\log N_{\text{H}\,I} = 13$; (b) $\log N_{\text{H}\,I} = 14$; (c) $\log N_{\text{H}\,I} = 15$; (d) $\log N_{\text{H}\,I} = 17$ (see also rows 10 – 13 in Table 4.3).

Appendix D

Absorption spectra

The following figures show the analyzed H I Ly α forest of the 13 quasar spectra used in this work in detail. Individual absorption lines are indicated by solid vertical lines above the spectral regions (see §2.3.2 for details on the line-fitting procedure). The quasar spectra were normalized by the respective continua denoted in the figures of §2.2. The quasar continua were computed with the method described in §2.3.1.

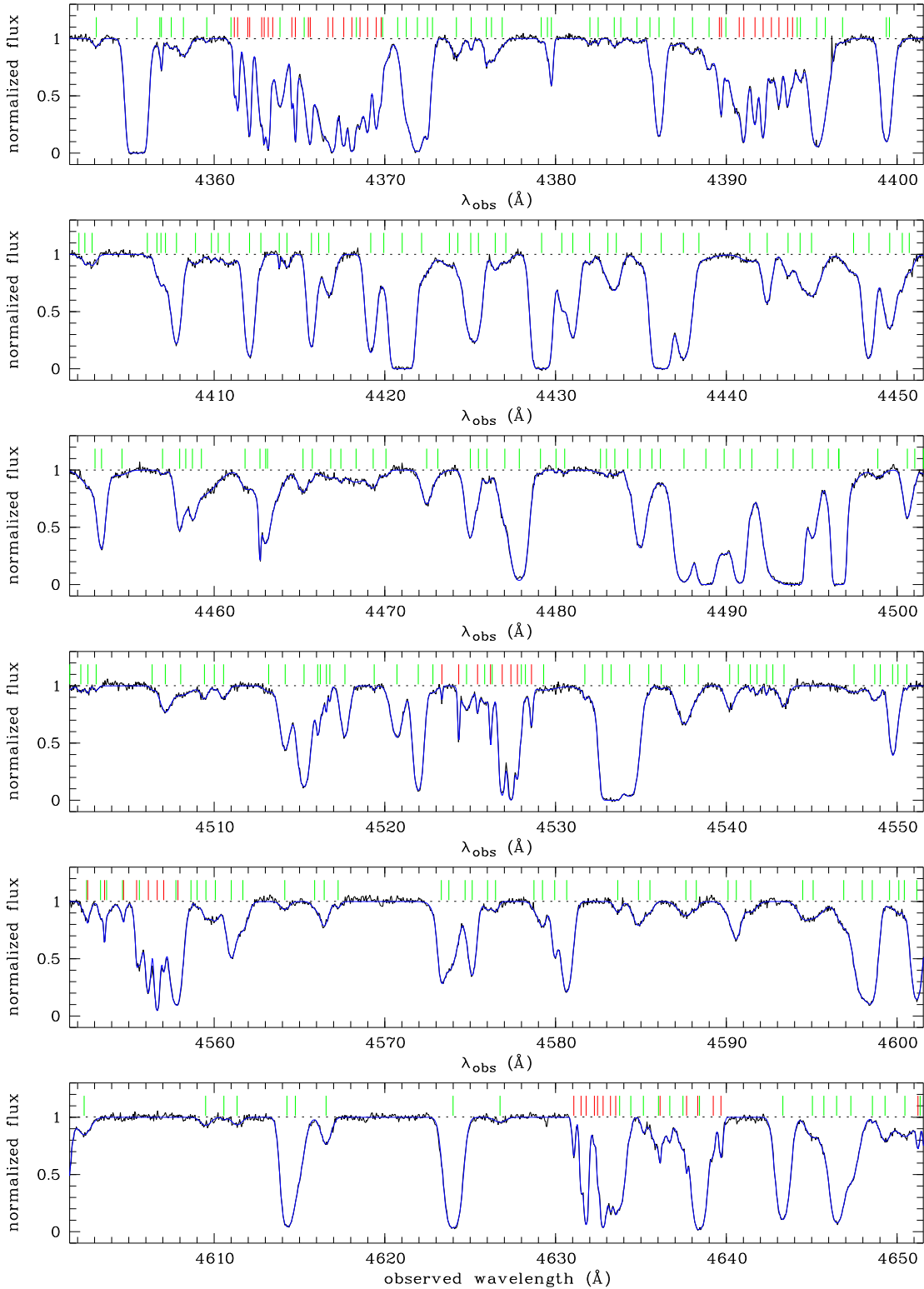


Figure D.1. The normalized absorption spectrum of the quasar J004131-493611 (black solid line) and its fit with CANDALF (blue solid line). Absorption-line components are indicated by vertical lines; assumed H I Ly α transitions (green) and identified metals (red).

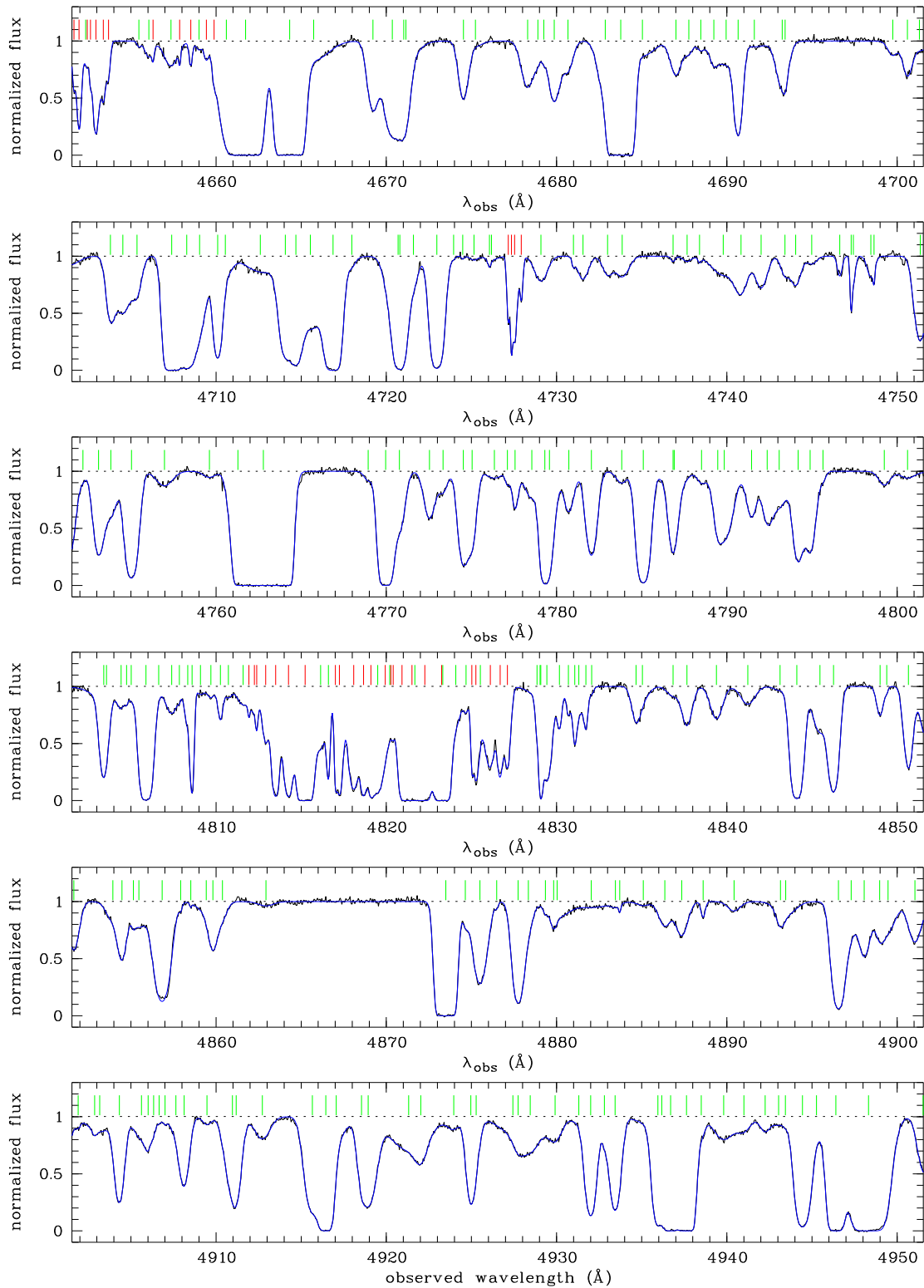


Figure D.1. *Continued*

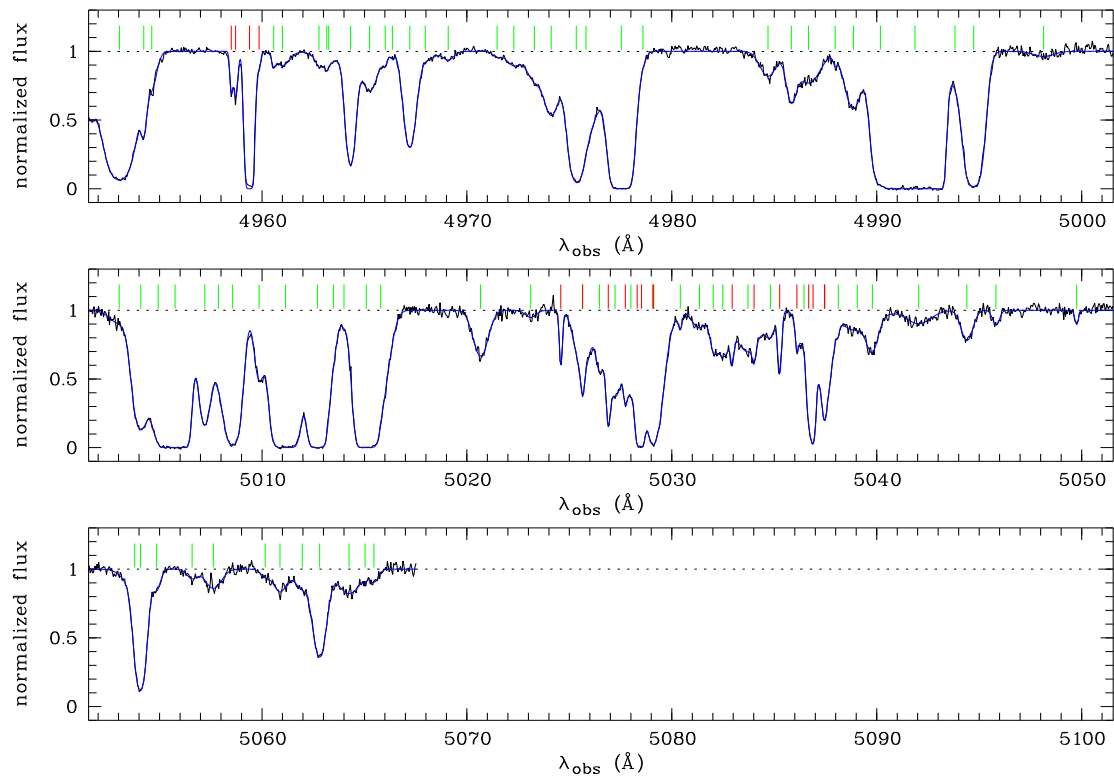


Figure D.1. *Continued*

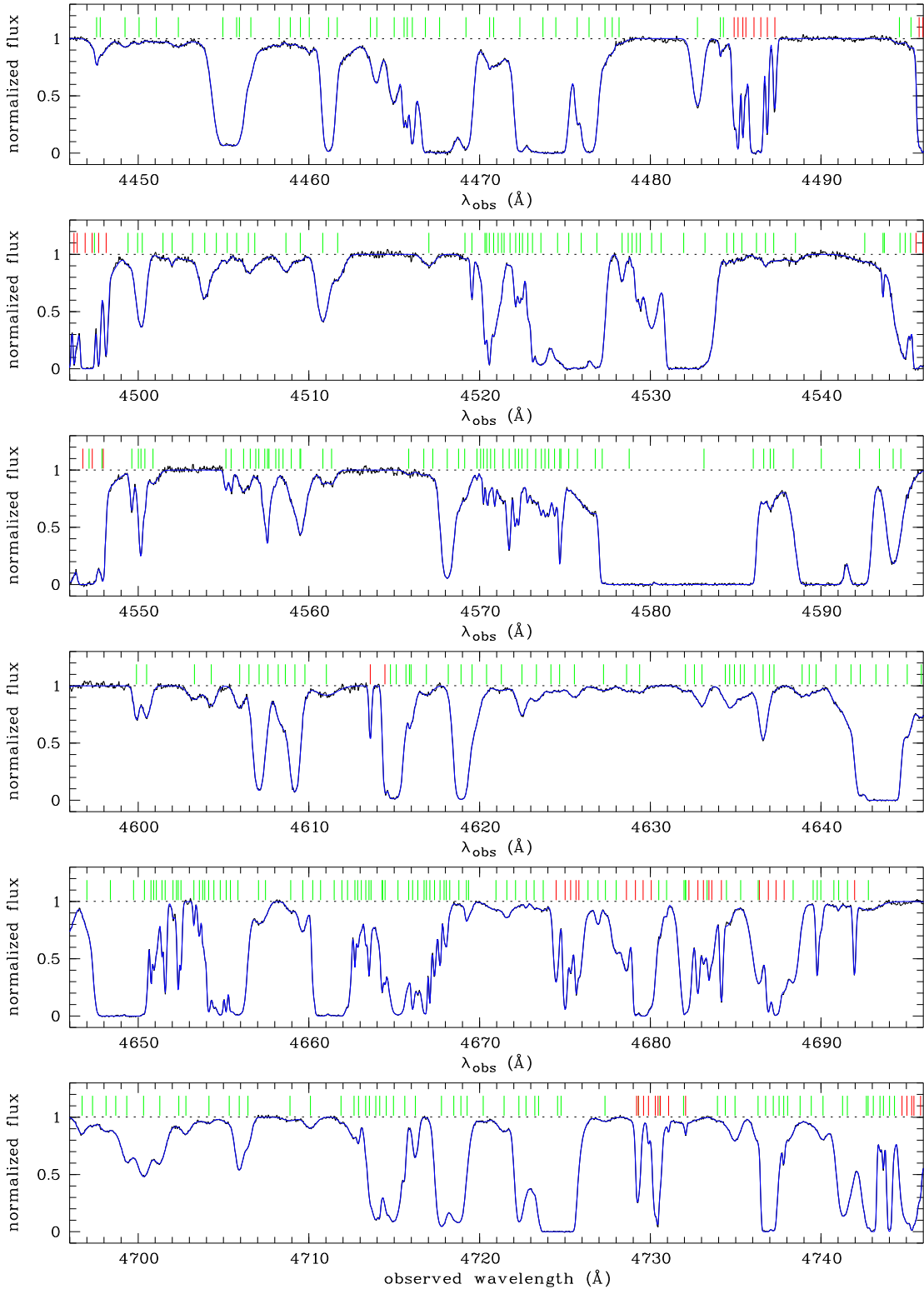
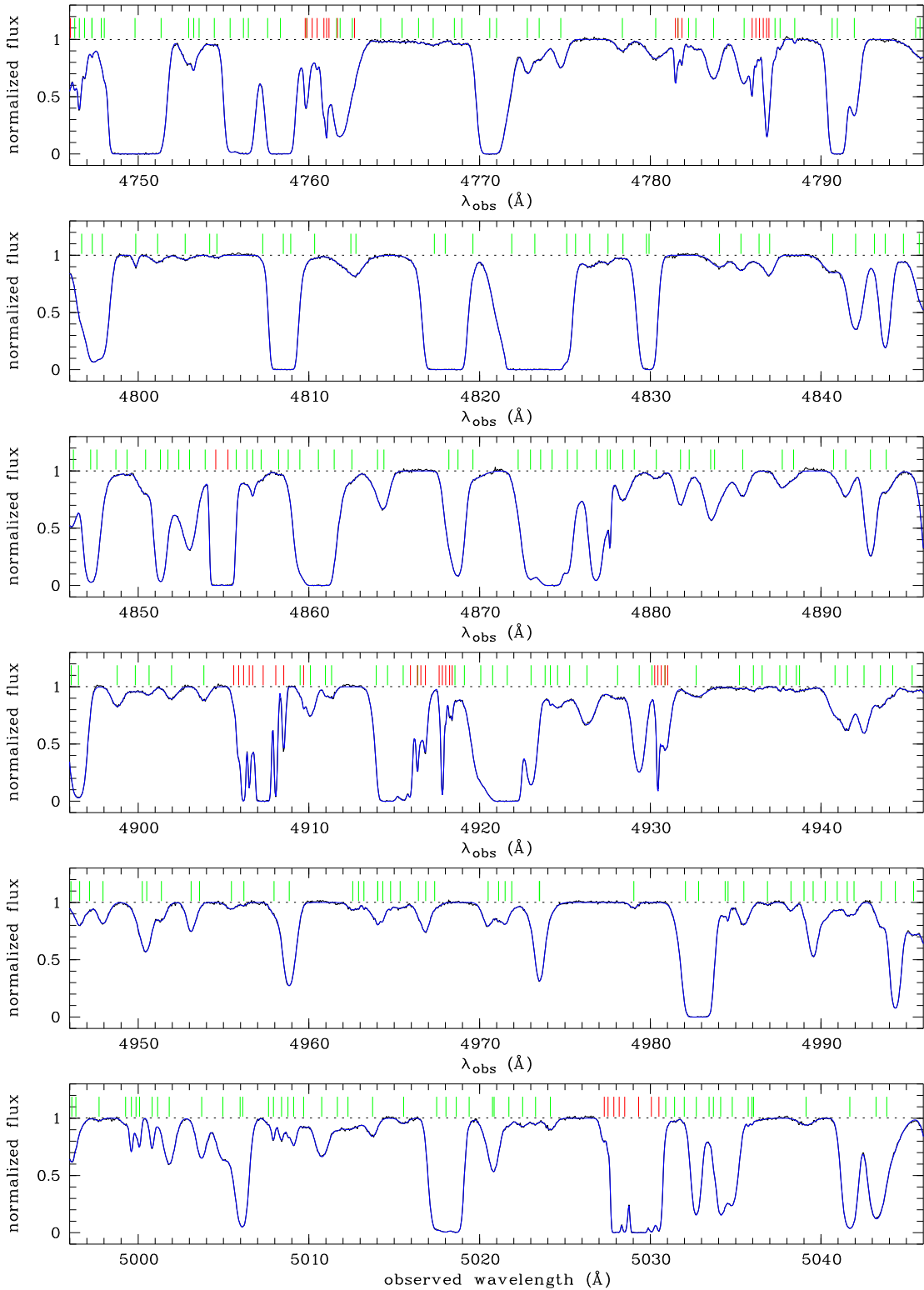


Figure D.2. The normalized absorption spectrum of the quasar J212912-153841 (black solid line) and its fit with CANDALF (blue solid line). Absorption-line components are indicated by vertical lines; assumed H I Ly α transitions (green) and identified metals (red).

Figure D.2. *Continued*

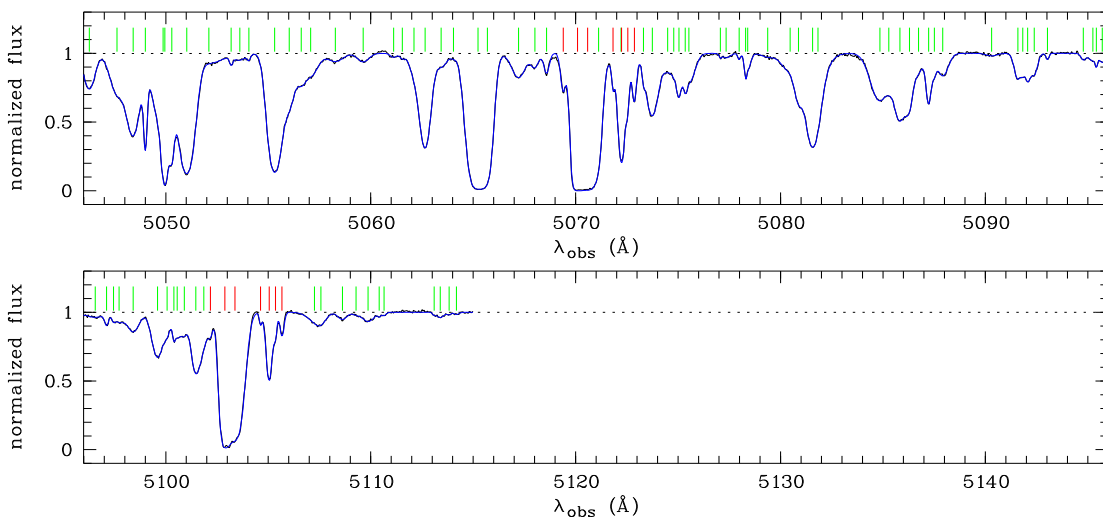


Figure D.2. *Continued*

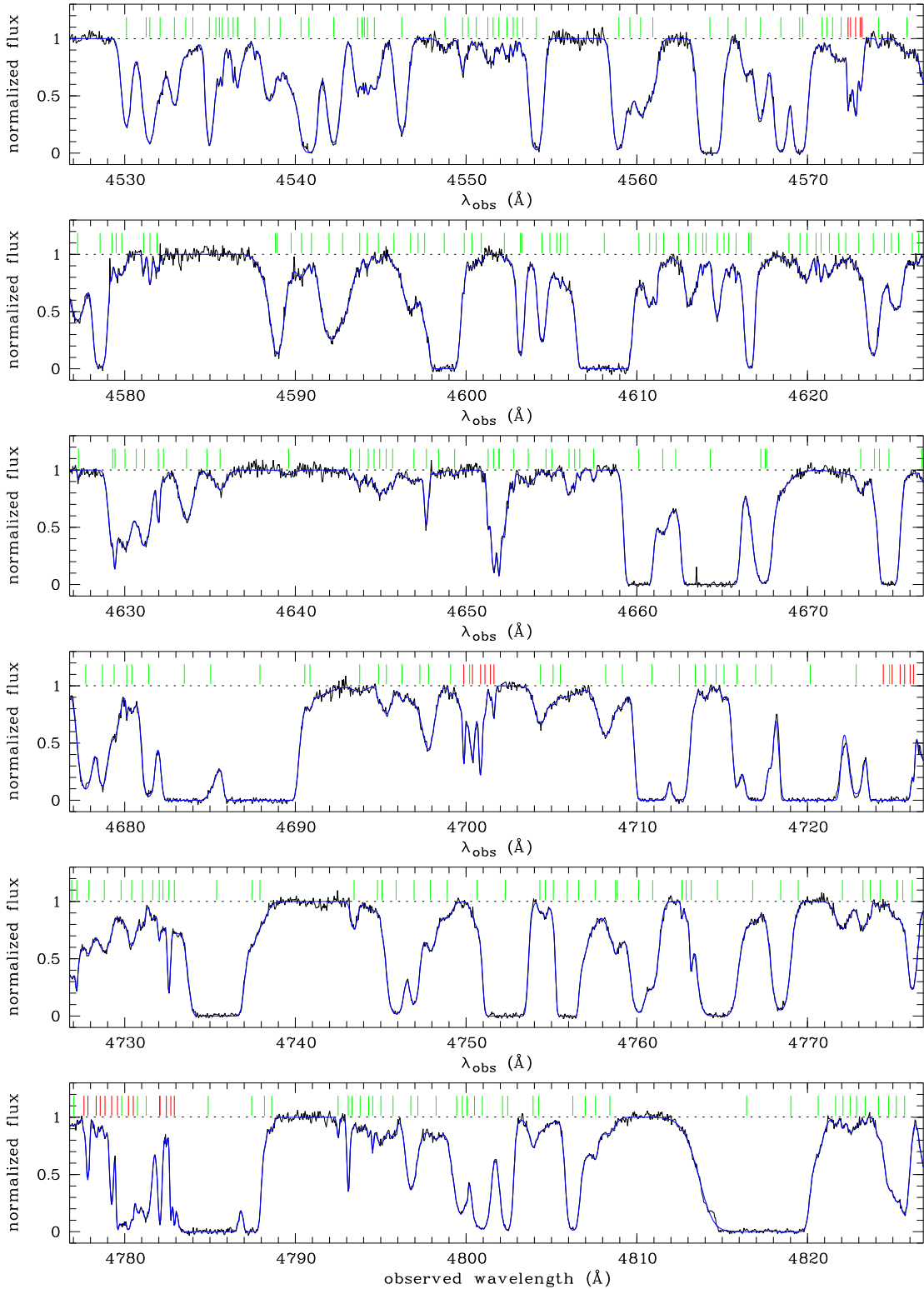


Figure D.3. The normalized absorption spectrum of the quasar J111350-153333 (black solid line) and its fit with CANDALF (blue solid line). Absorption-line components are indicated by vertical lines; assumed H I Ly α transitions (green) and identified metals (red).

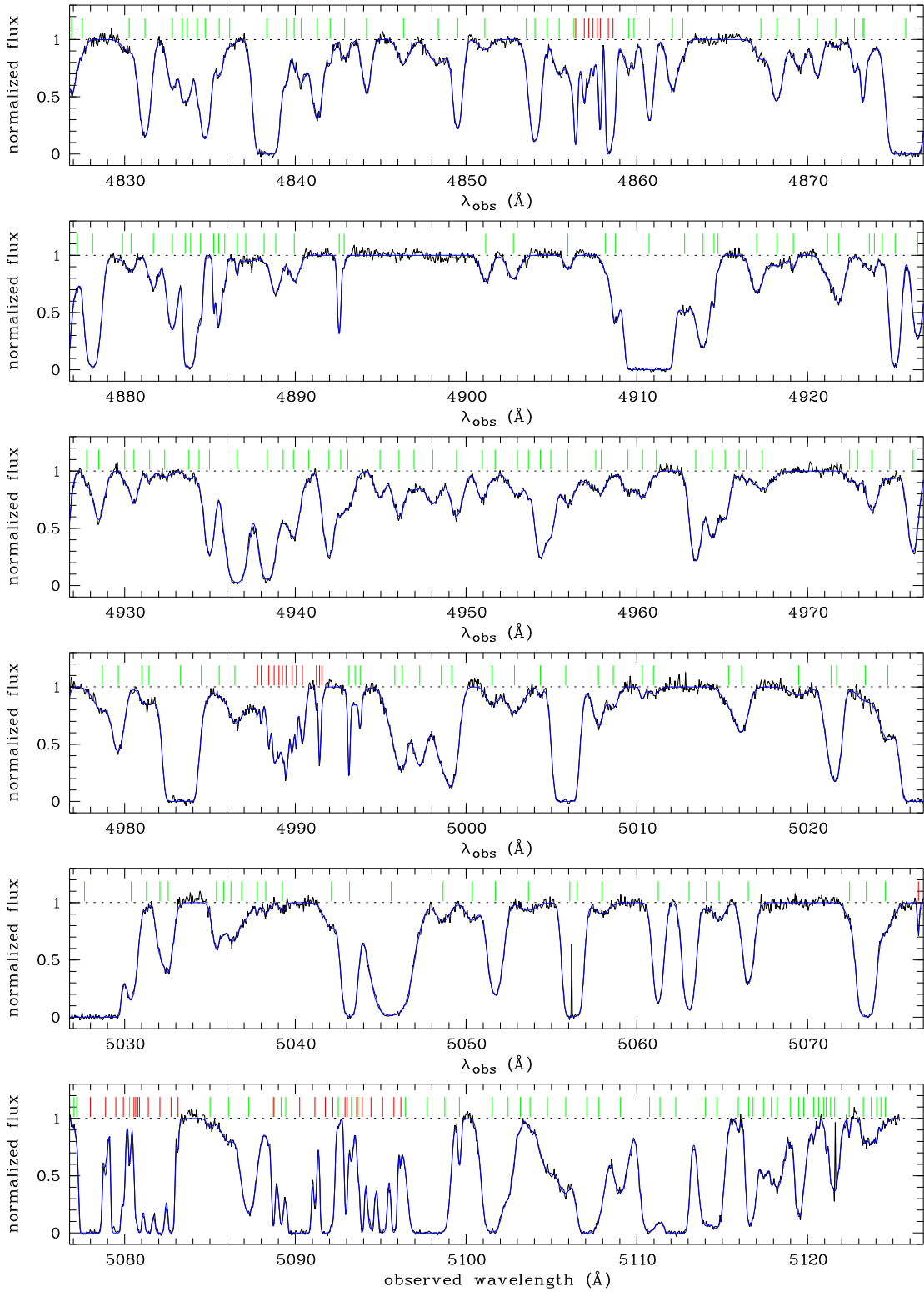


Figure D.3. *Continued*

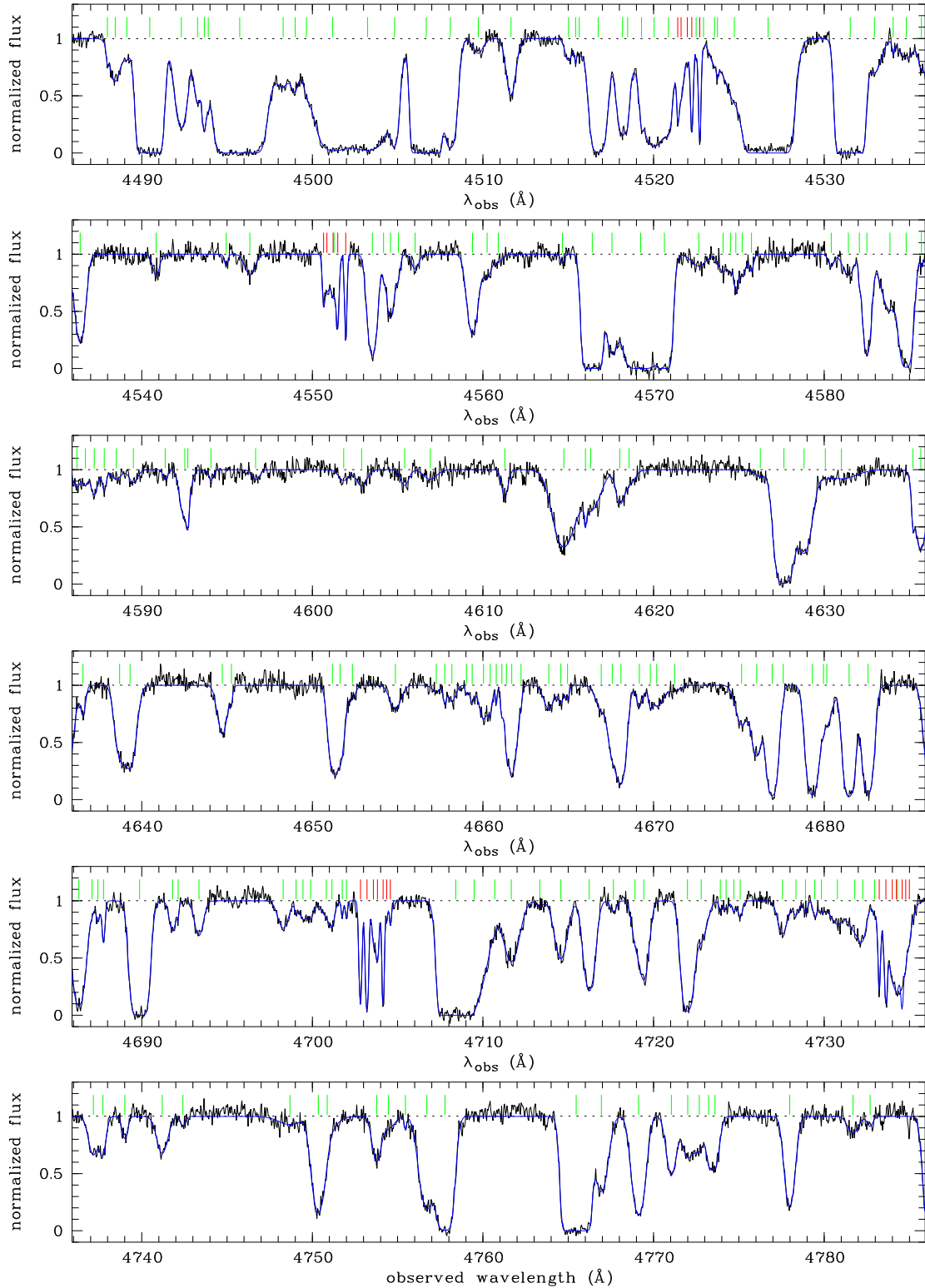


Figure D.4. The normalized absorption spectrum of the quasar J010604-254651 (black solid line) and its fit with CANDALF (blue solid line). Absorption-line components are indicated by vertical lines; assumed H I Ly α transitions (green) and identified metals (red).

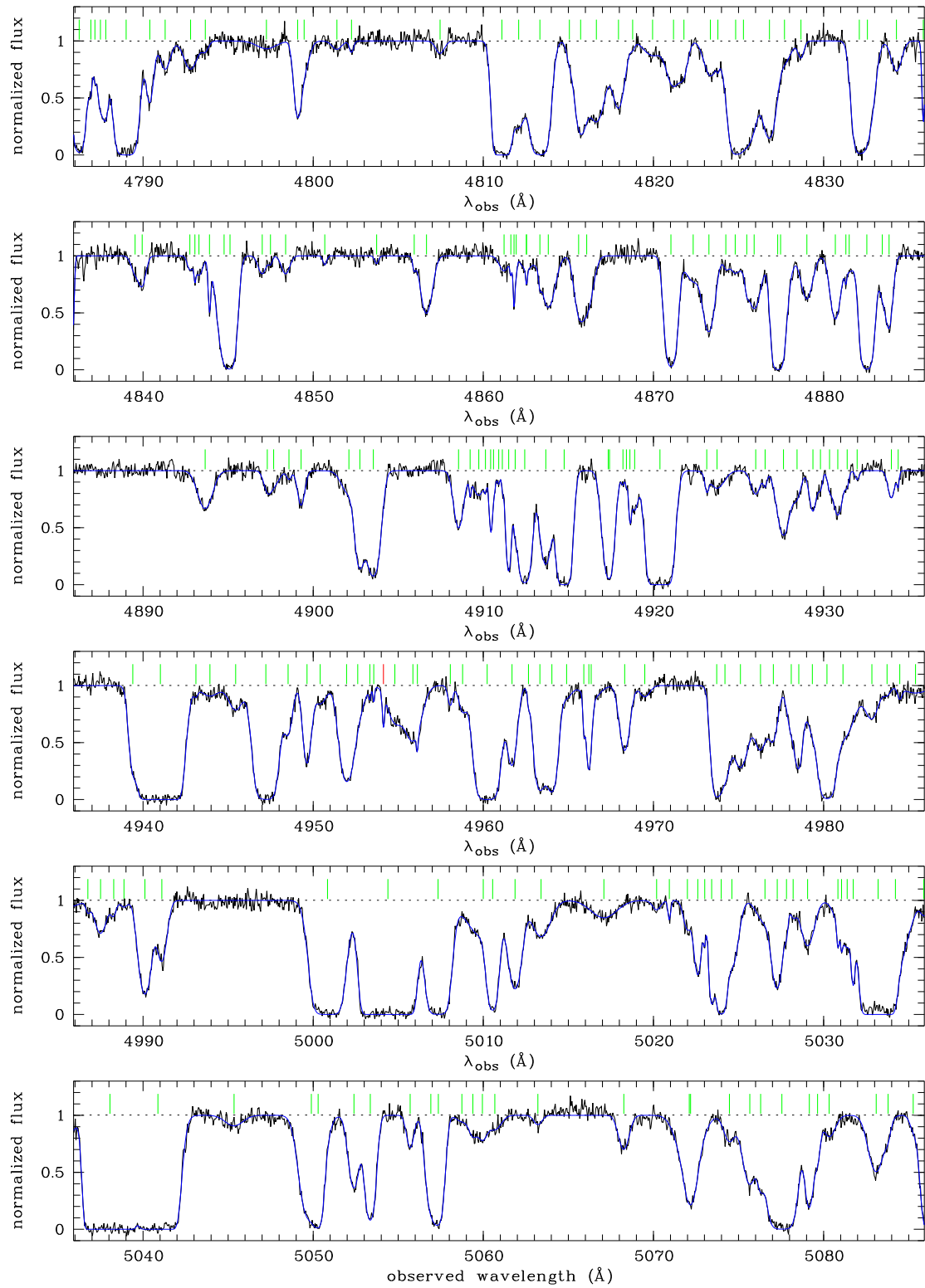


Figure D.4. *Continued*

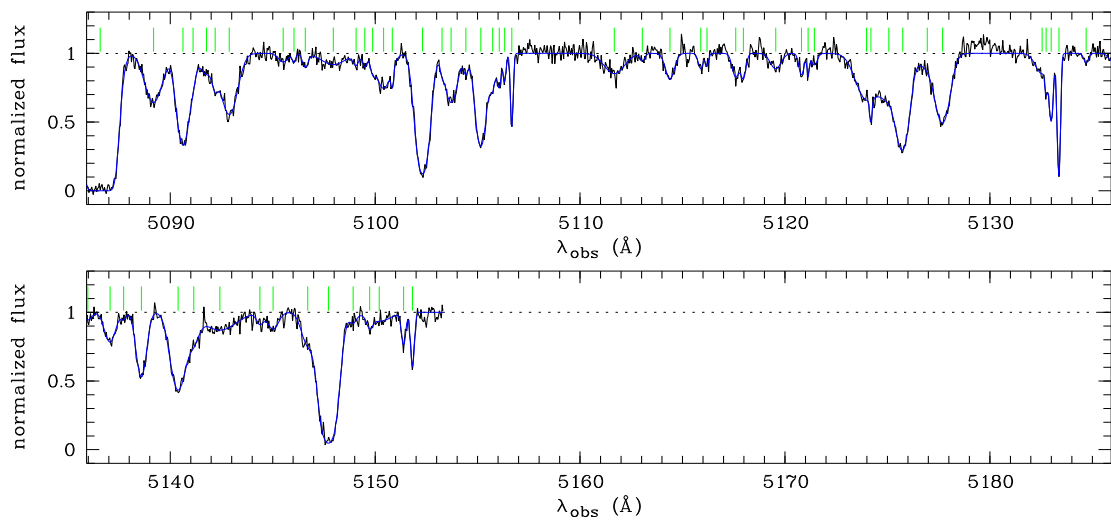


Figure D.4. *Continued*

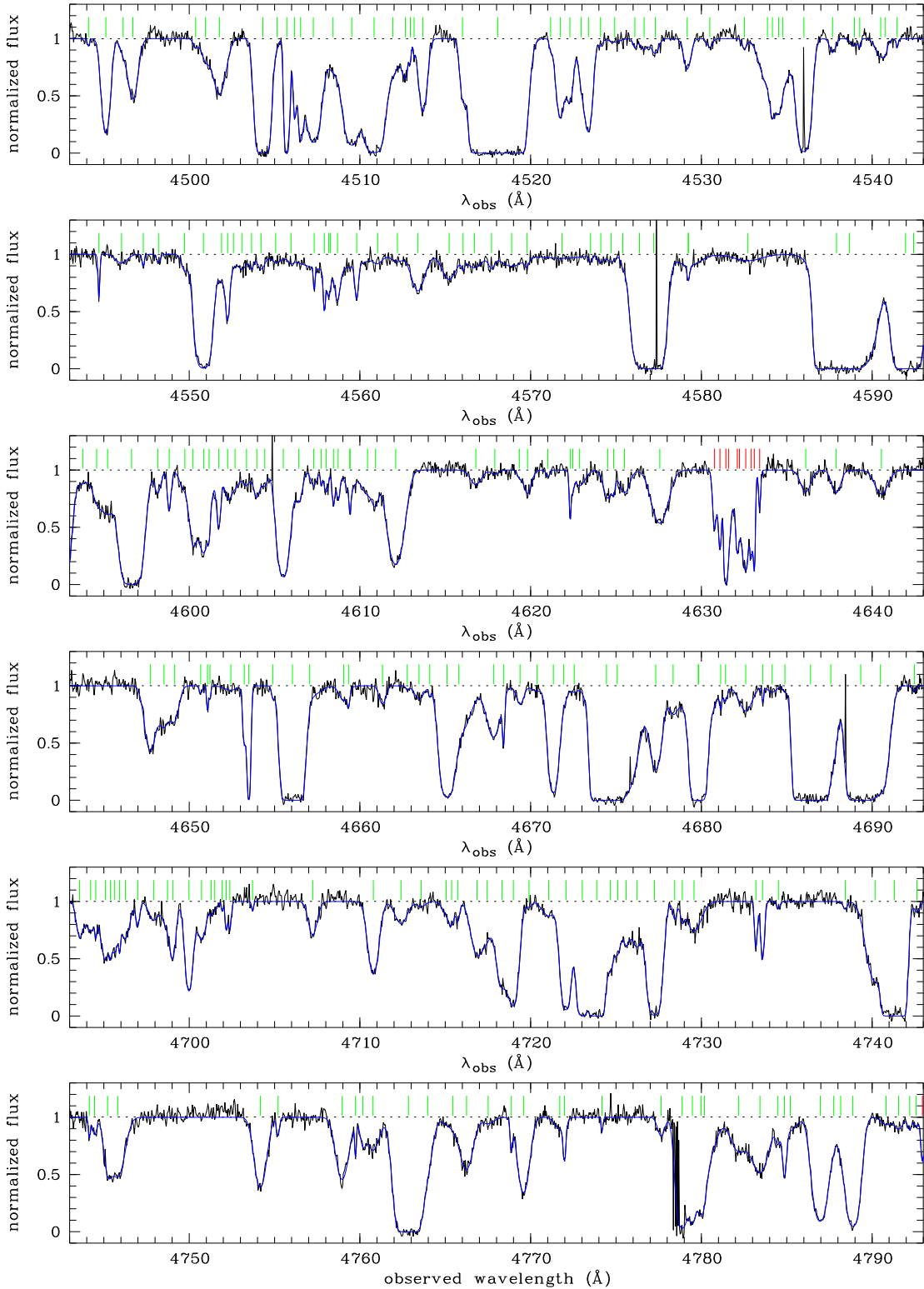


Figure D.5. The normalized absorption spectrum of the quasar J014214+002324 (black solid line) and its fit with CANDALF (blue solid line). Absorption-line components are indicated by vertical lines; assumed H α Ly α transitions (green) and identified metals (red).

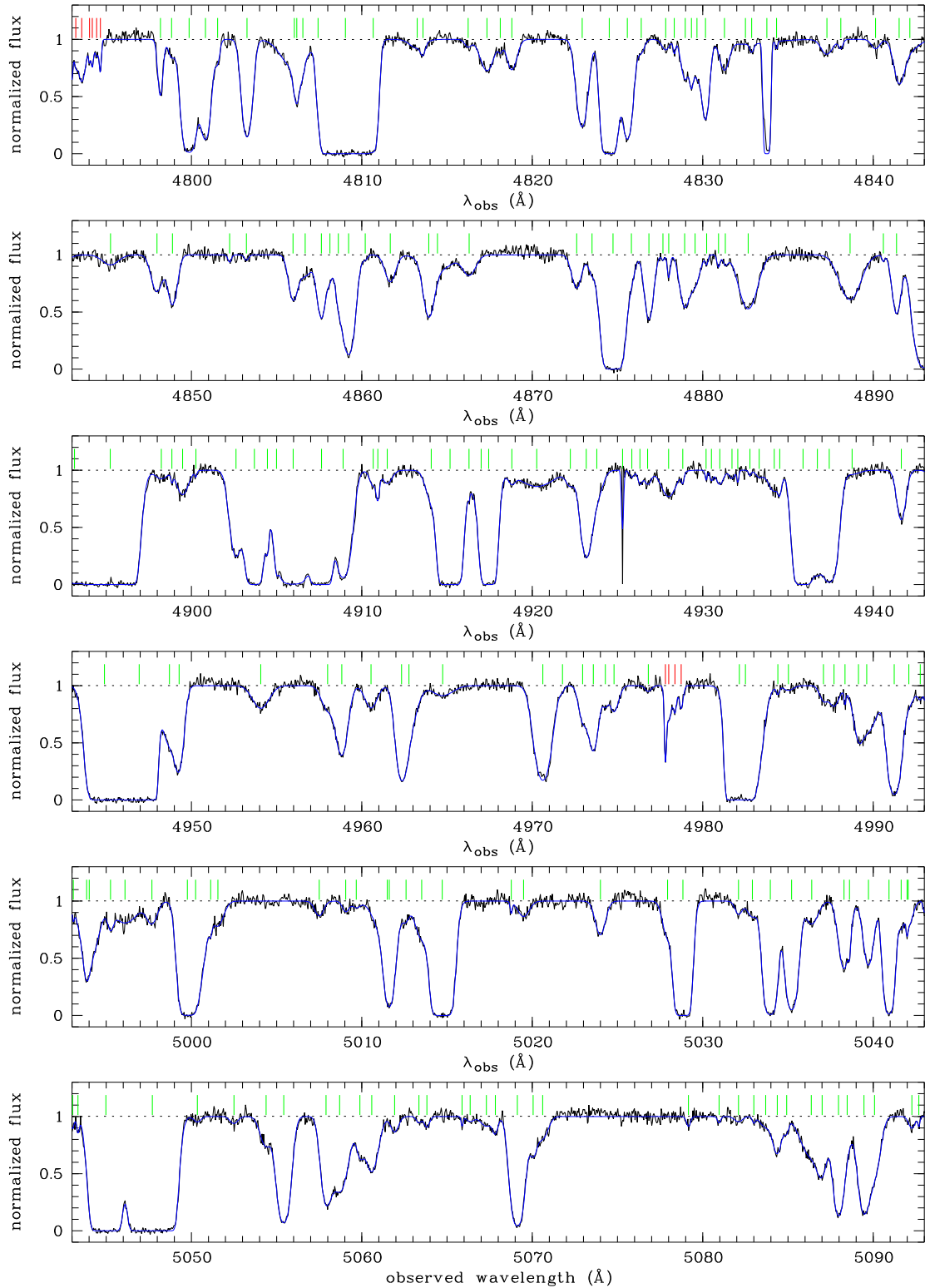


Figure D.5. *Continued*

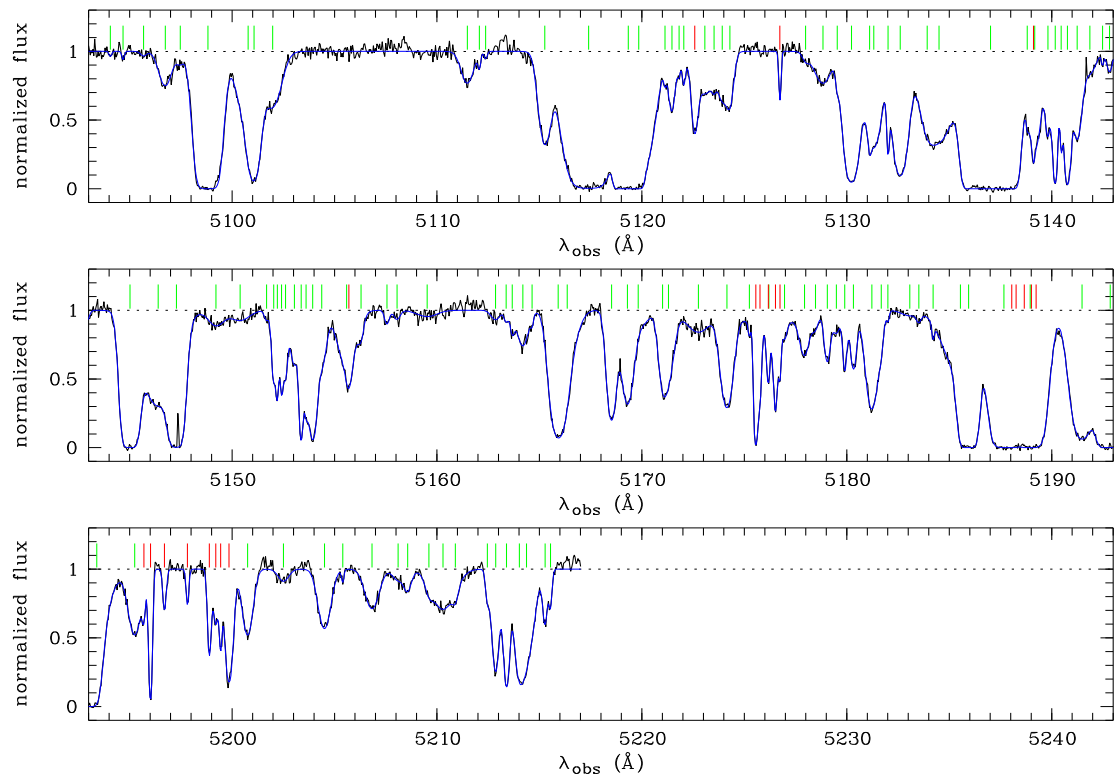


Figure D.5. *Continued*

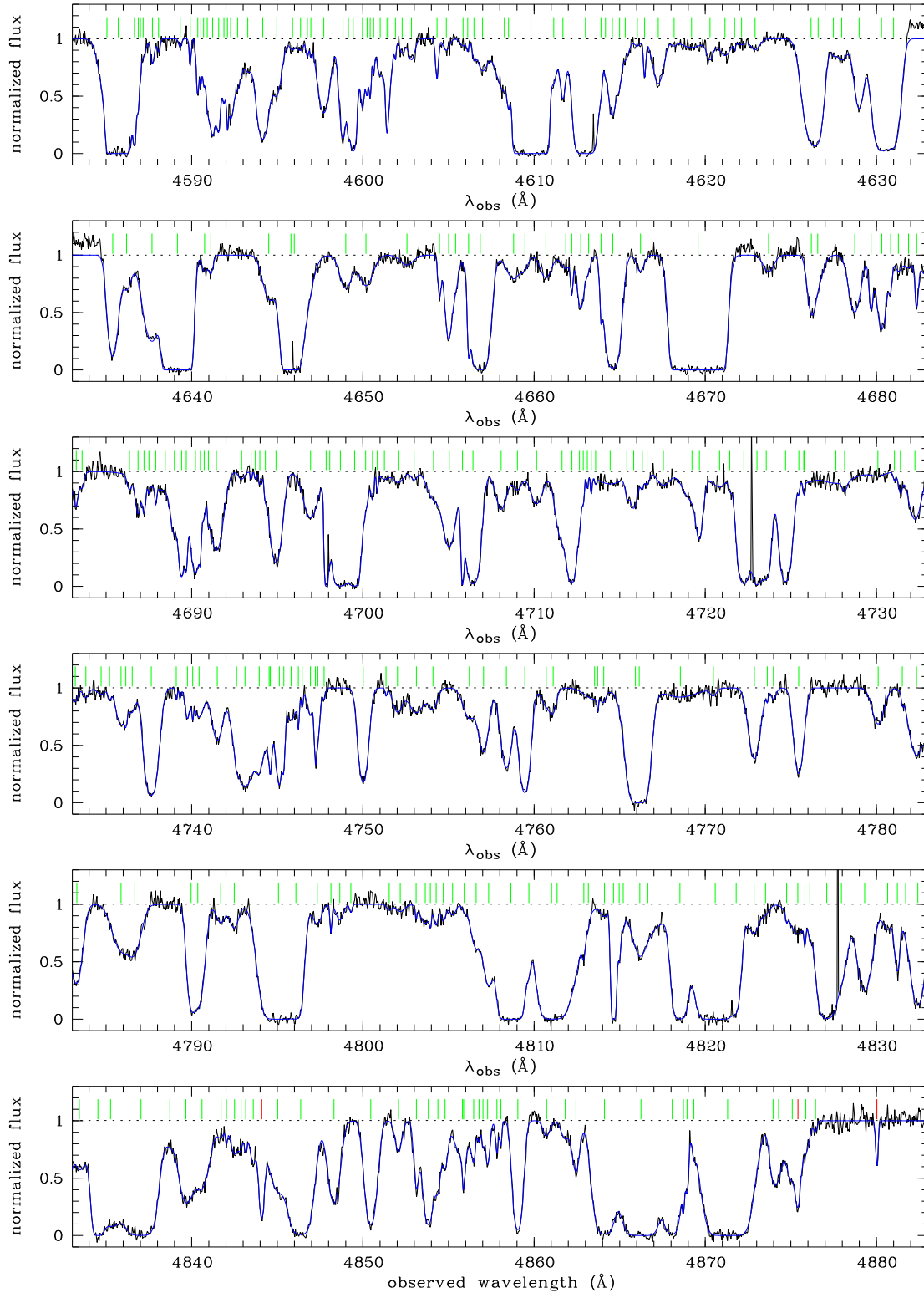


Figure D.6. The normalized absorption spectrum of the quasar J115538+053050 (black solid line) and its fit with CANDALF (blue solid line). Absorption-line components are indicated by vertical lines; assumed H I Ly α transitions (green) and identified metals (red).

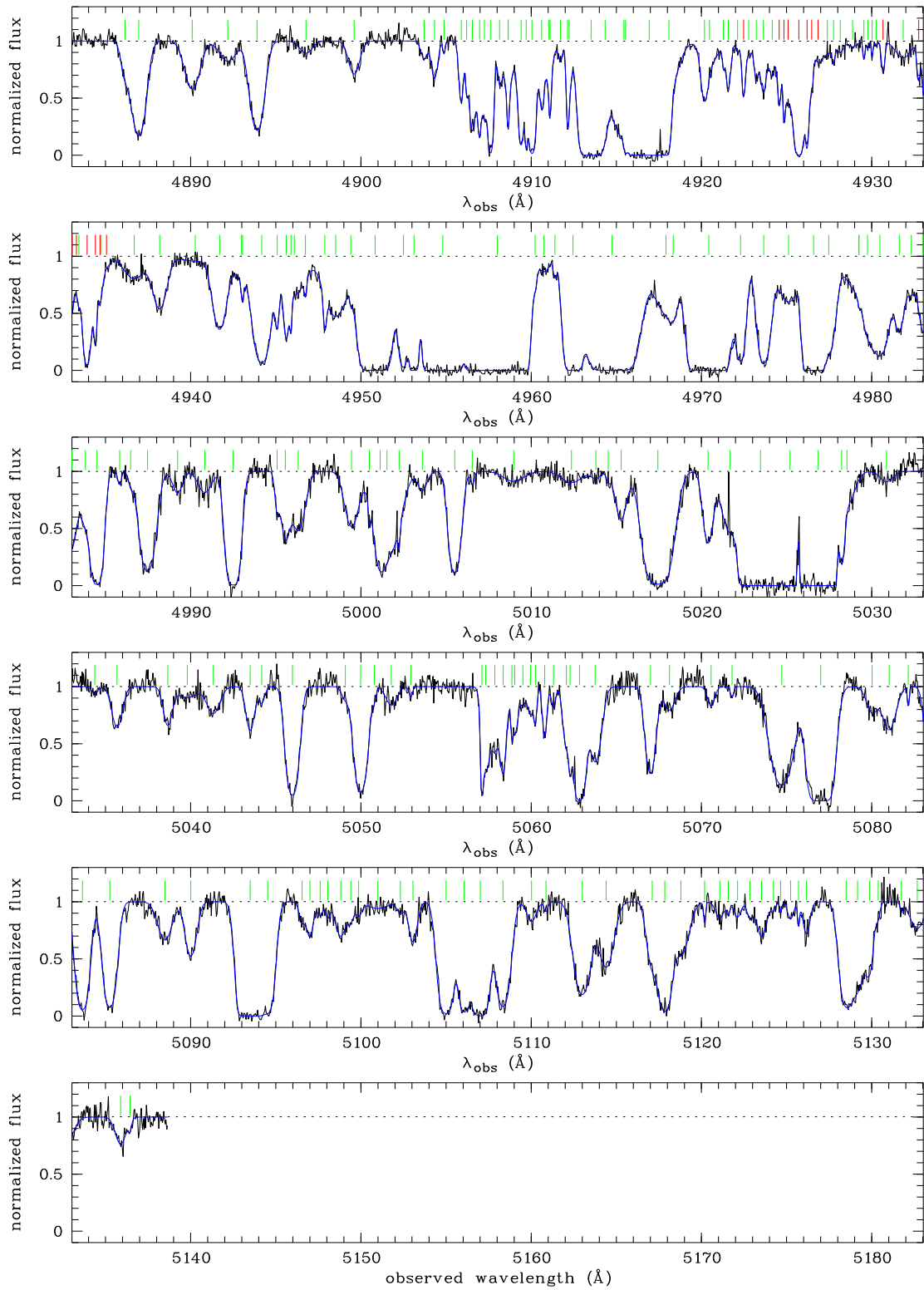


Figure D.6. *Continued*

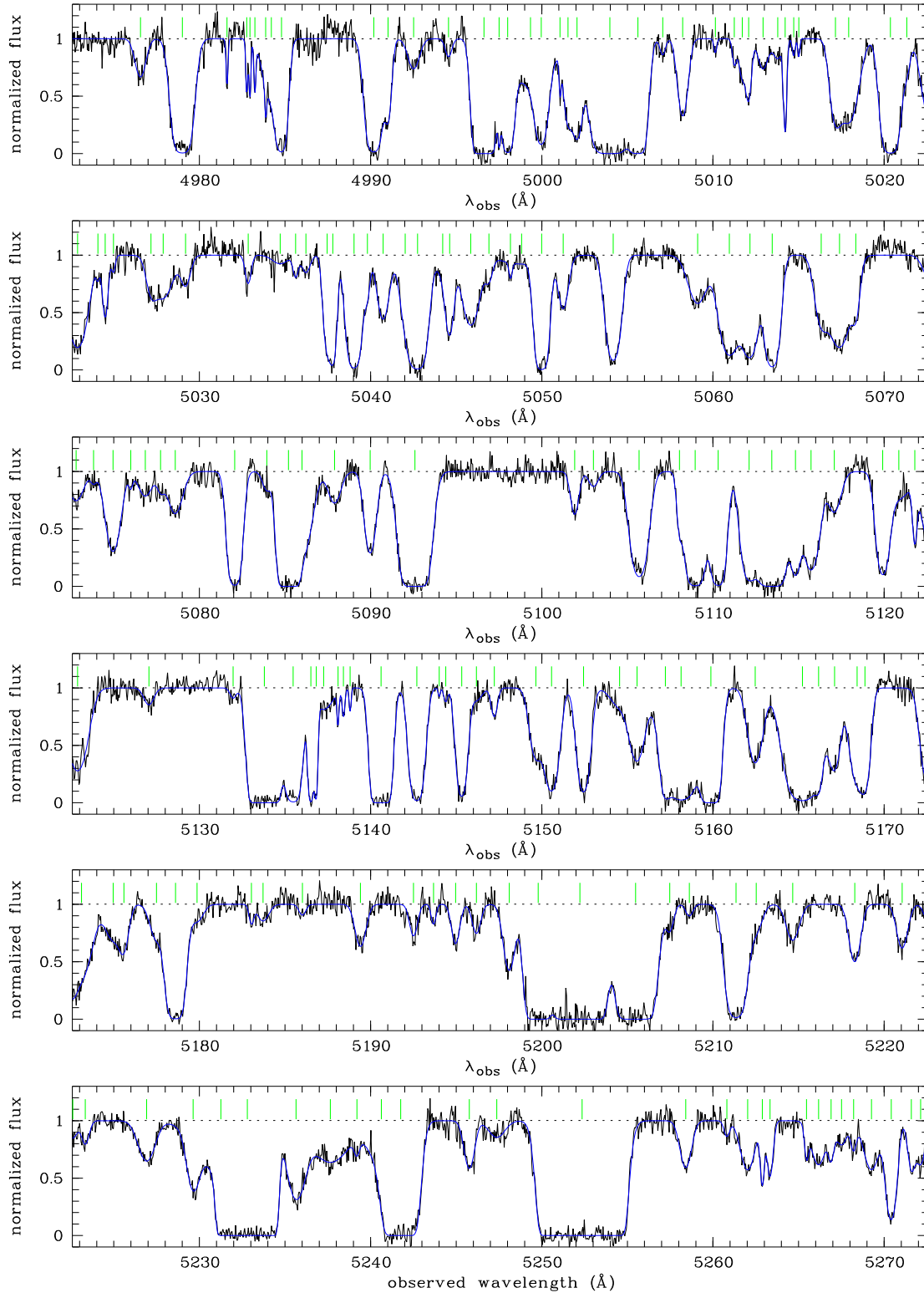


Figure D.7. The normalized absorption spectrum of the quasar J123055-113909 (black solid line) and its fit with CANDALF (blue solid line). Absorption-line components are indicated by vertical lines; assumed H I Ly α transitions (green), no metals could be identified.

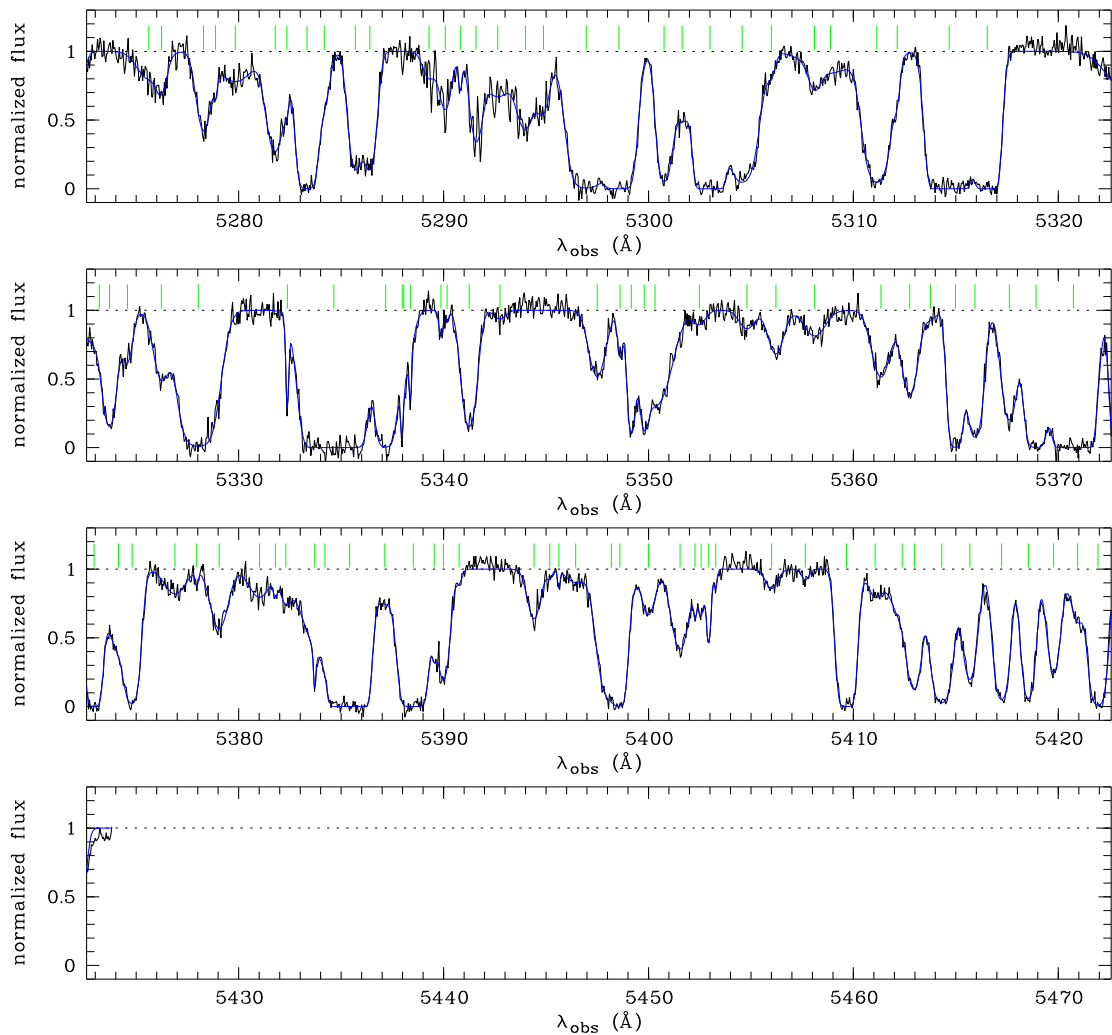


Figure D.7. *Continued*

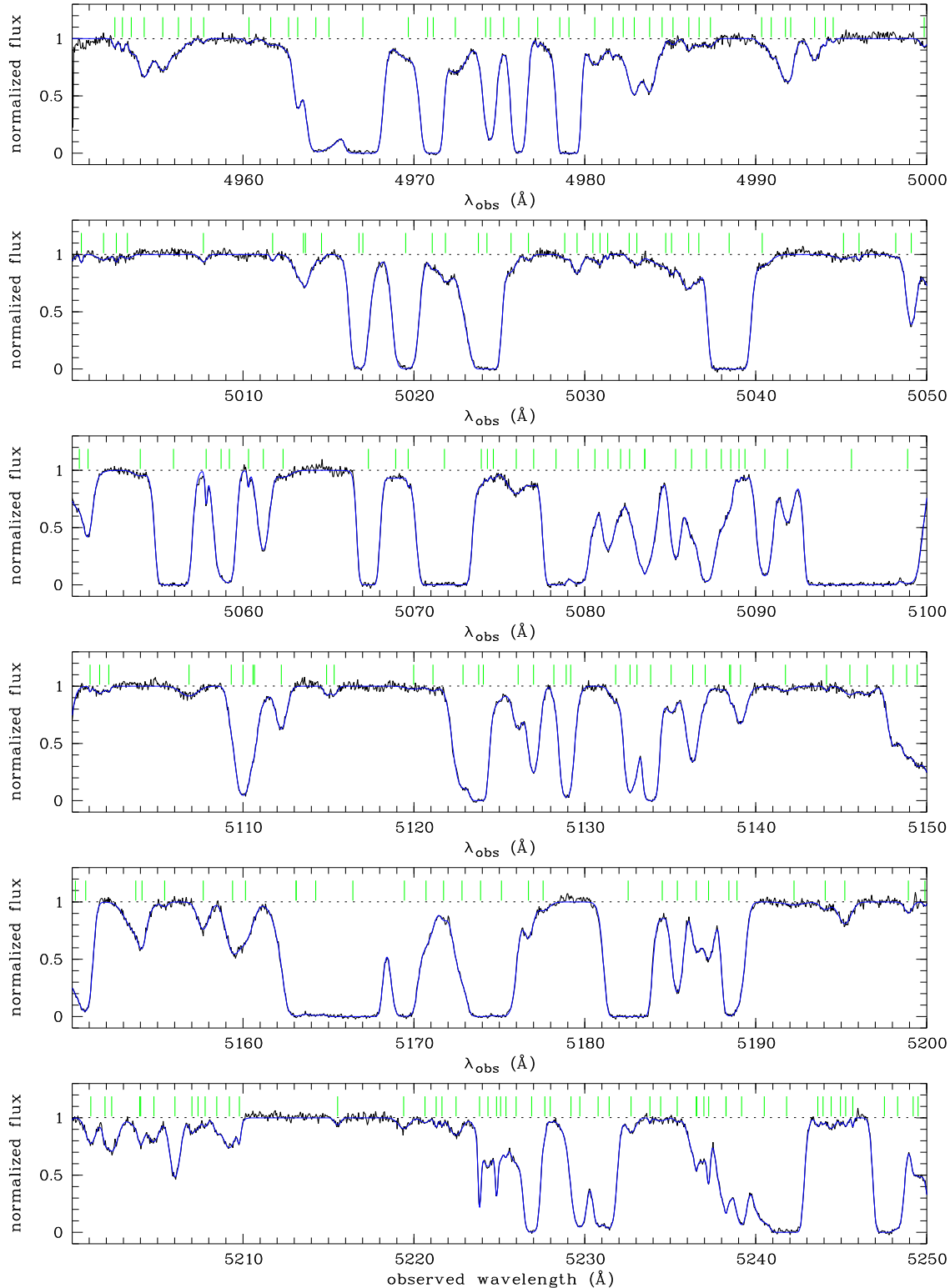


Figure D.8. The normalized absorption spectrum of the quasar J005758-264314 (black solid line) and its fit with CANDALF (blue solid line). Absorption-line components are indicated by vertical lines; assumed H I Ly α transitions (green) and identified metals (red).

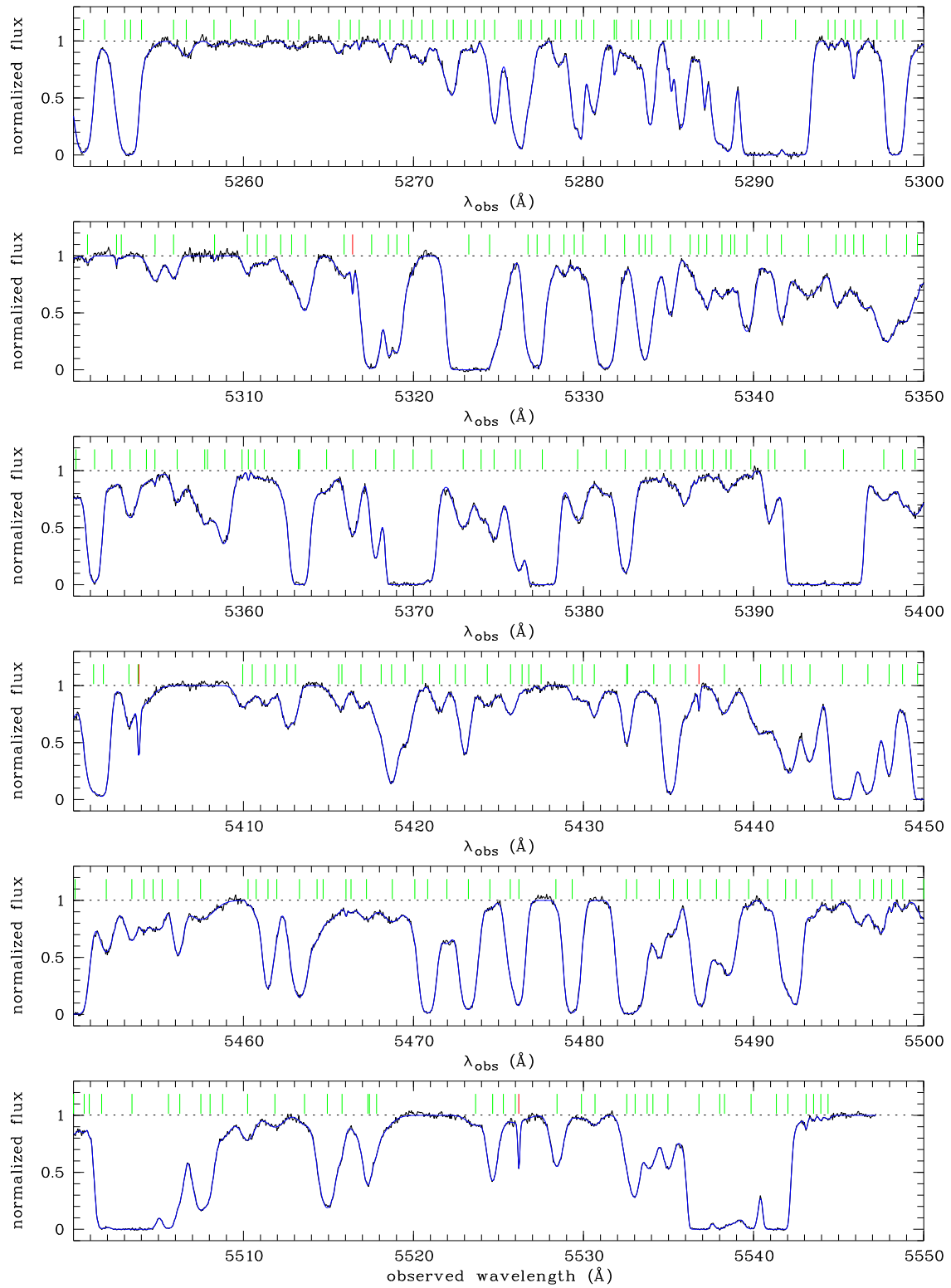


Figure D.8. *Continued*

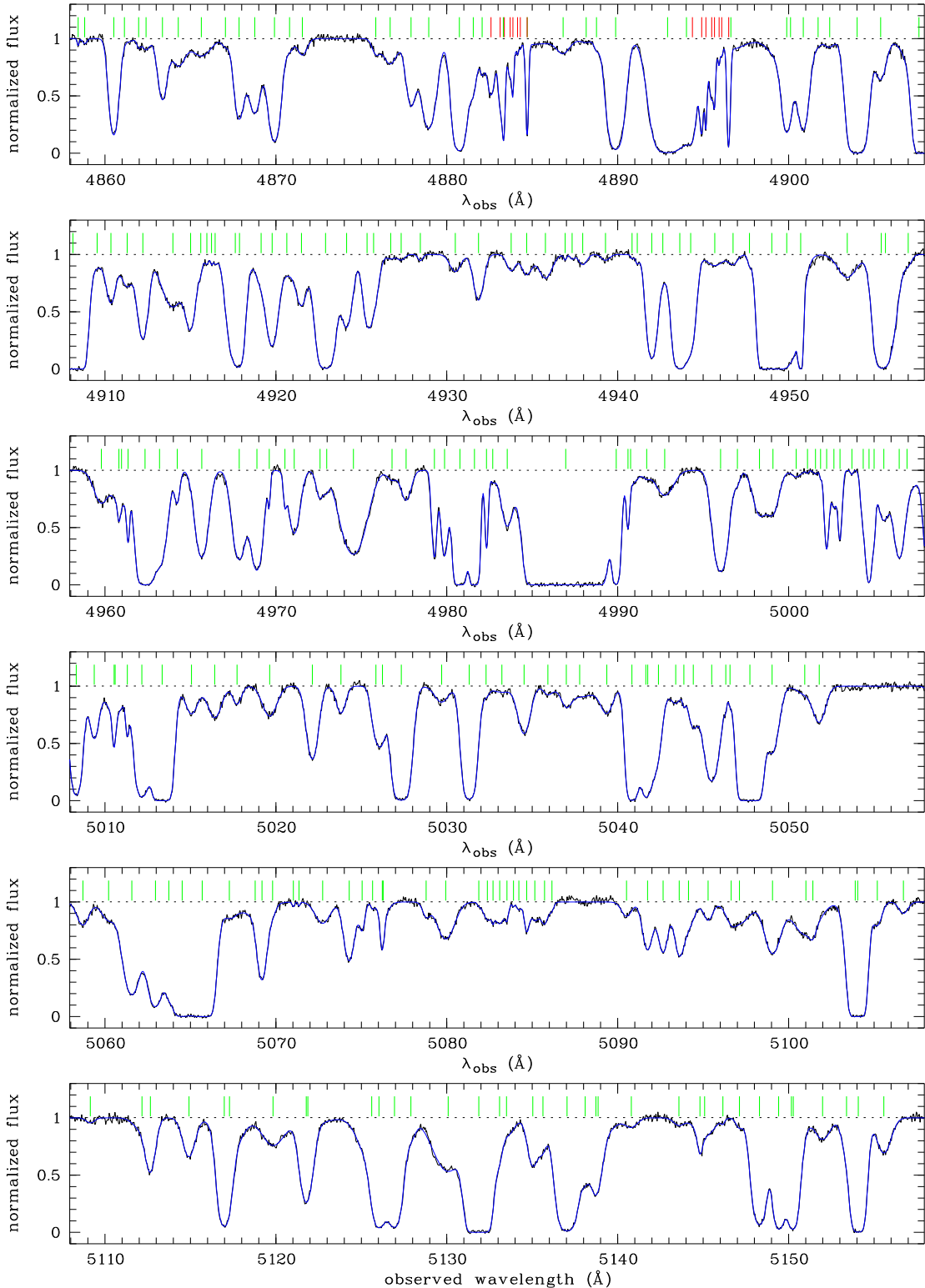


Figure D.9. The normalized absorption spectrum of the quasar J124957-015928 (black solid line) and its fit with CANDALF (blue solid line). Absorption-line components are indicated by vertical lines; assumed H I Ly α transitions (green) and identified metals (red).

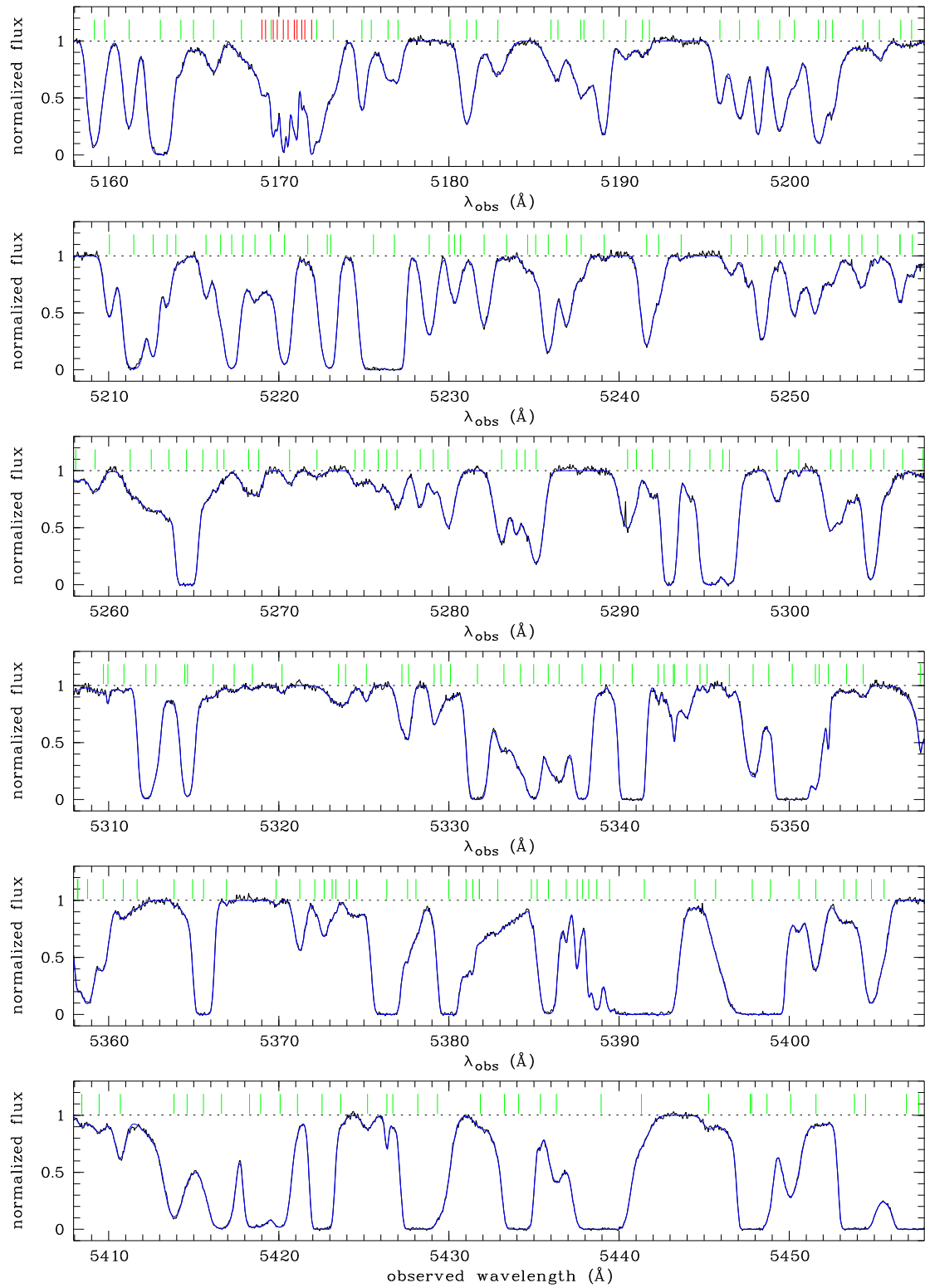


Figure D.9. *Continued*

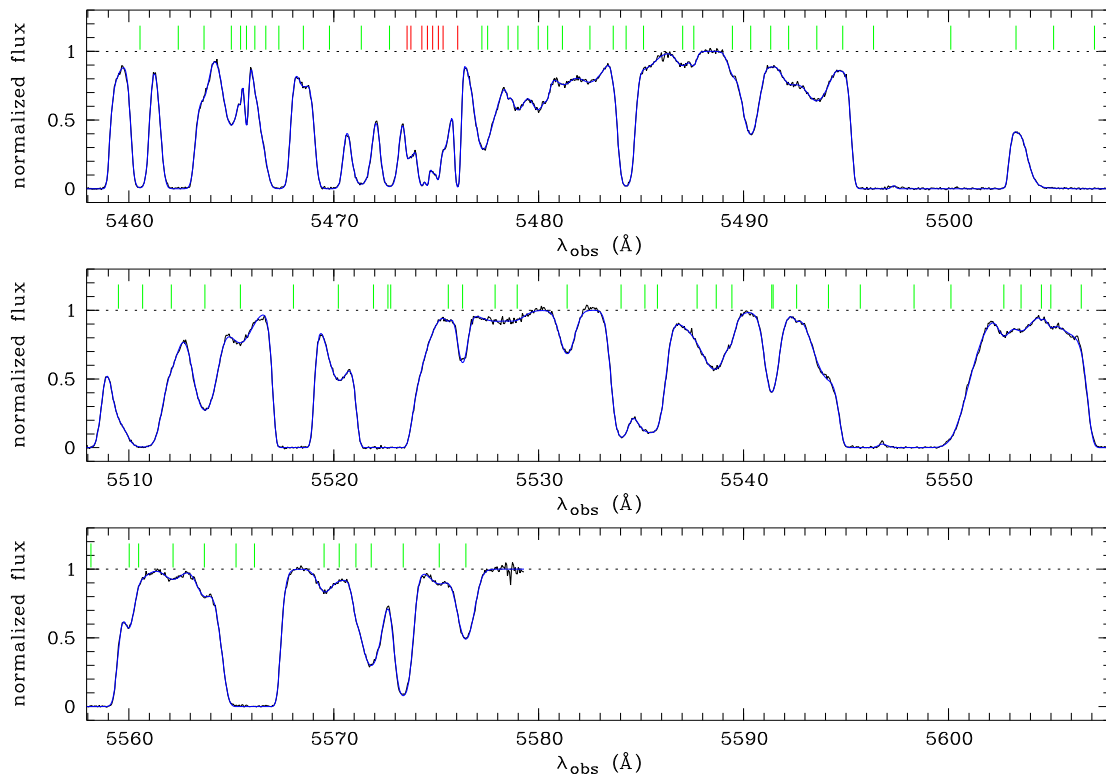


Figure D.9. *Continued*

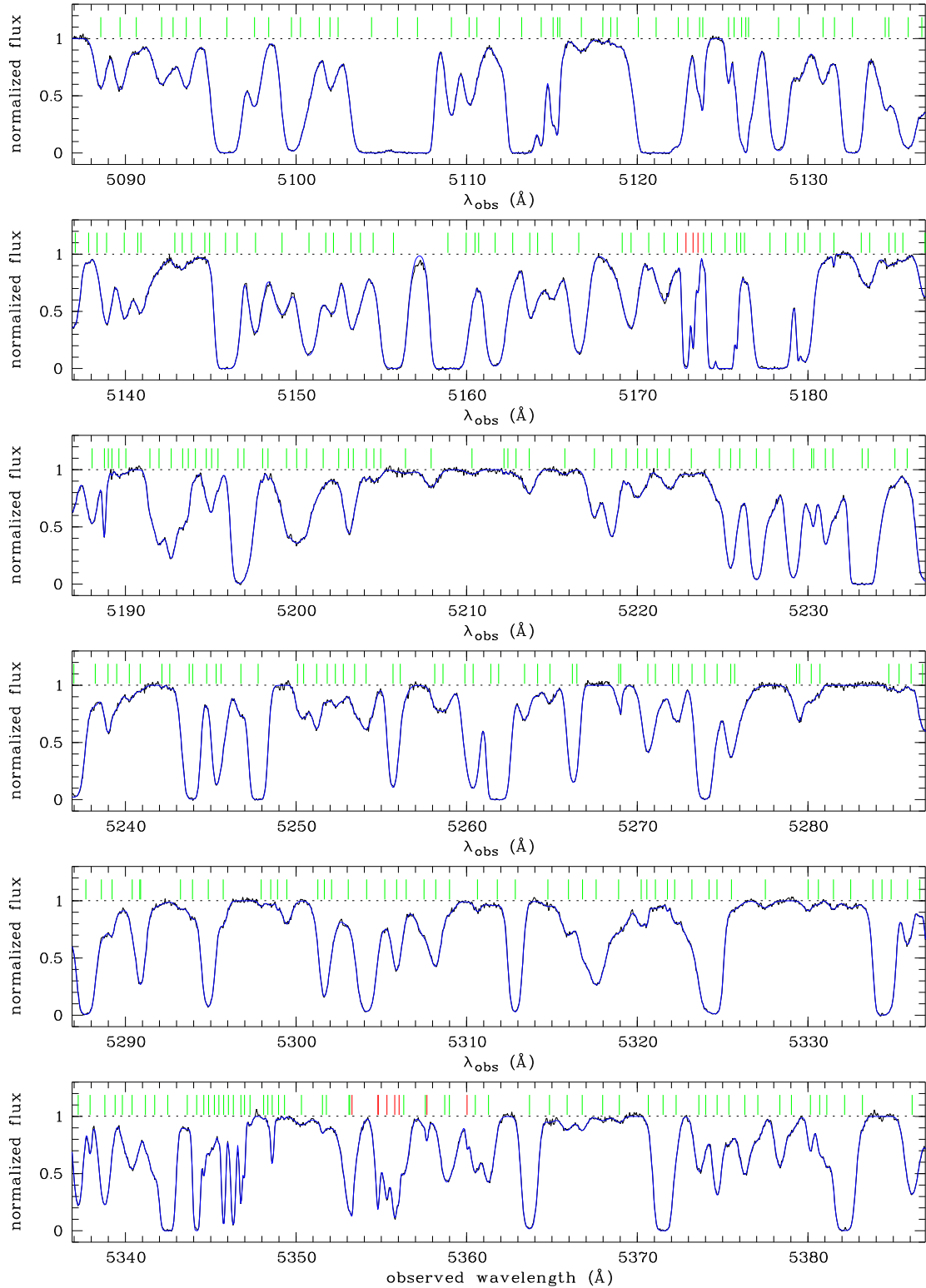


Figure D.10. The normalized absorption spectrum of the quasar J162116-004250 (black solid line) and its fit with CANDALF (blue solid line). Absorption-line components are indicated by vertical lines; assumed H I Ly α transitions (green) and identified metals (red).

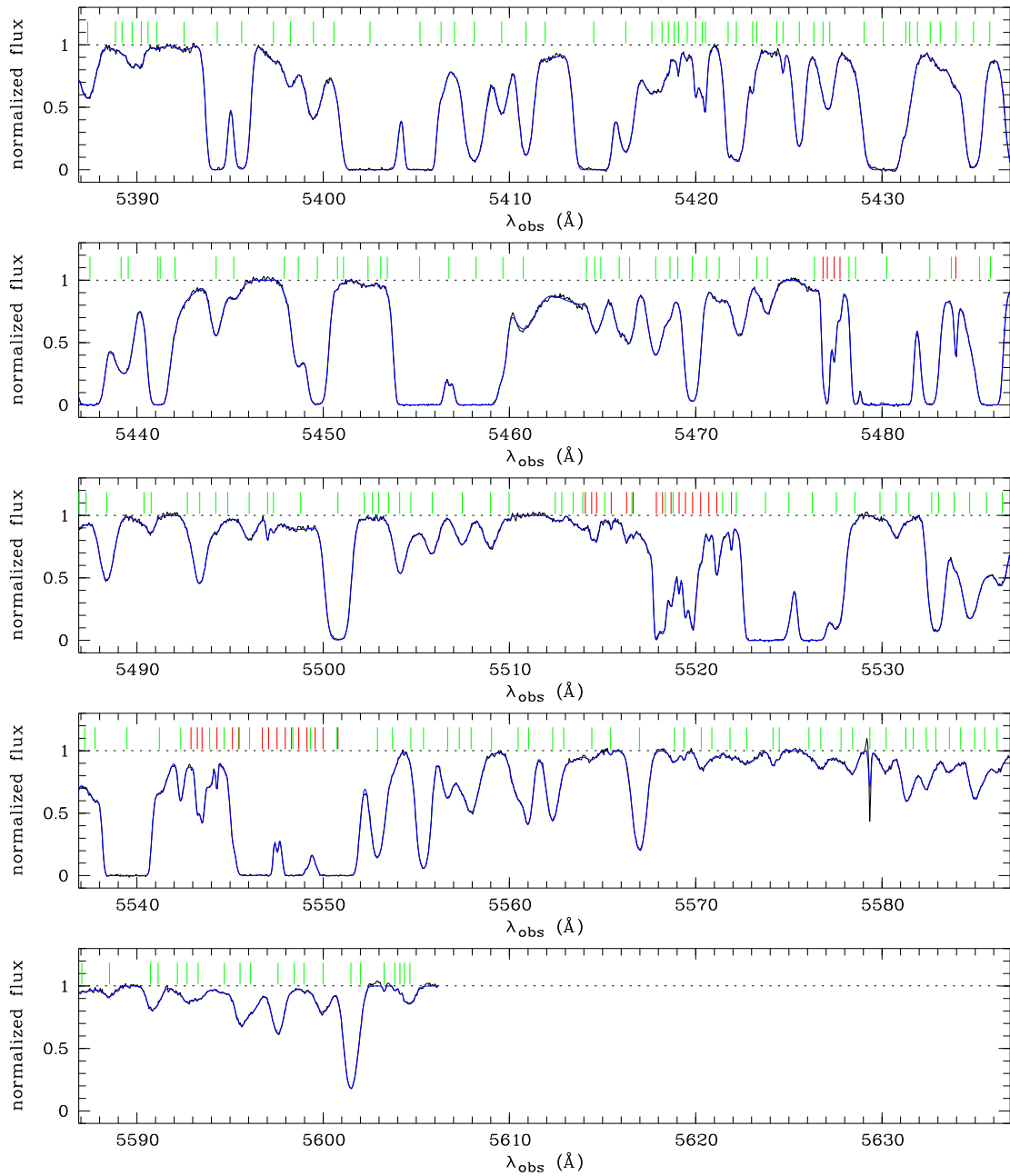


Figure D.10. *Continued*

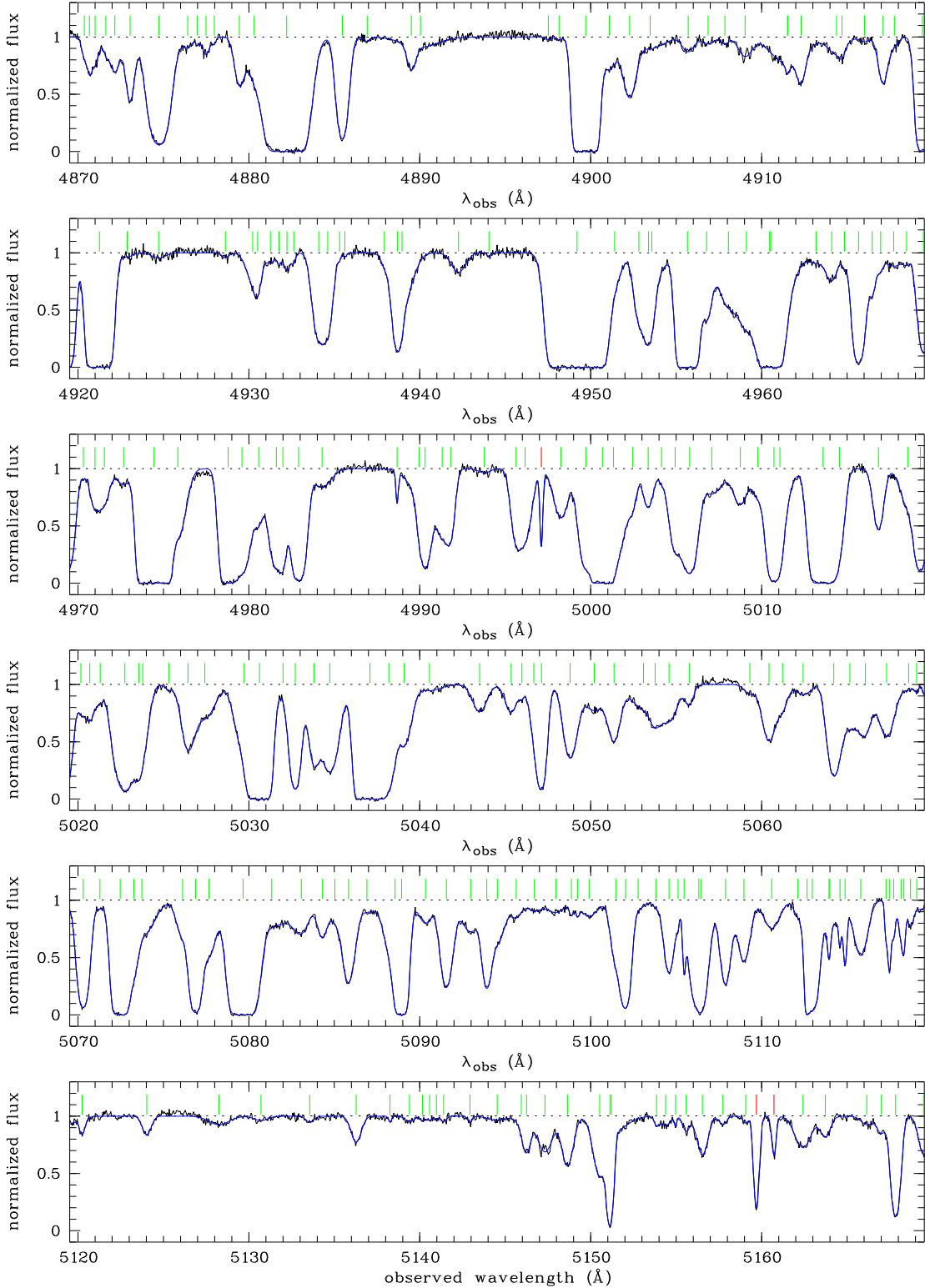
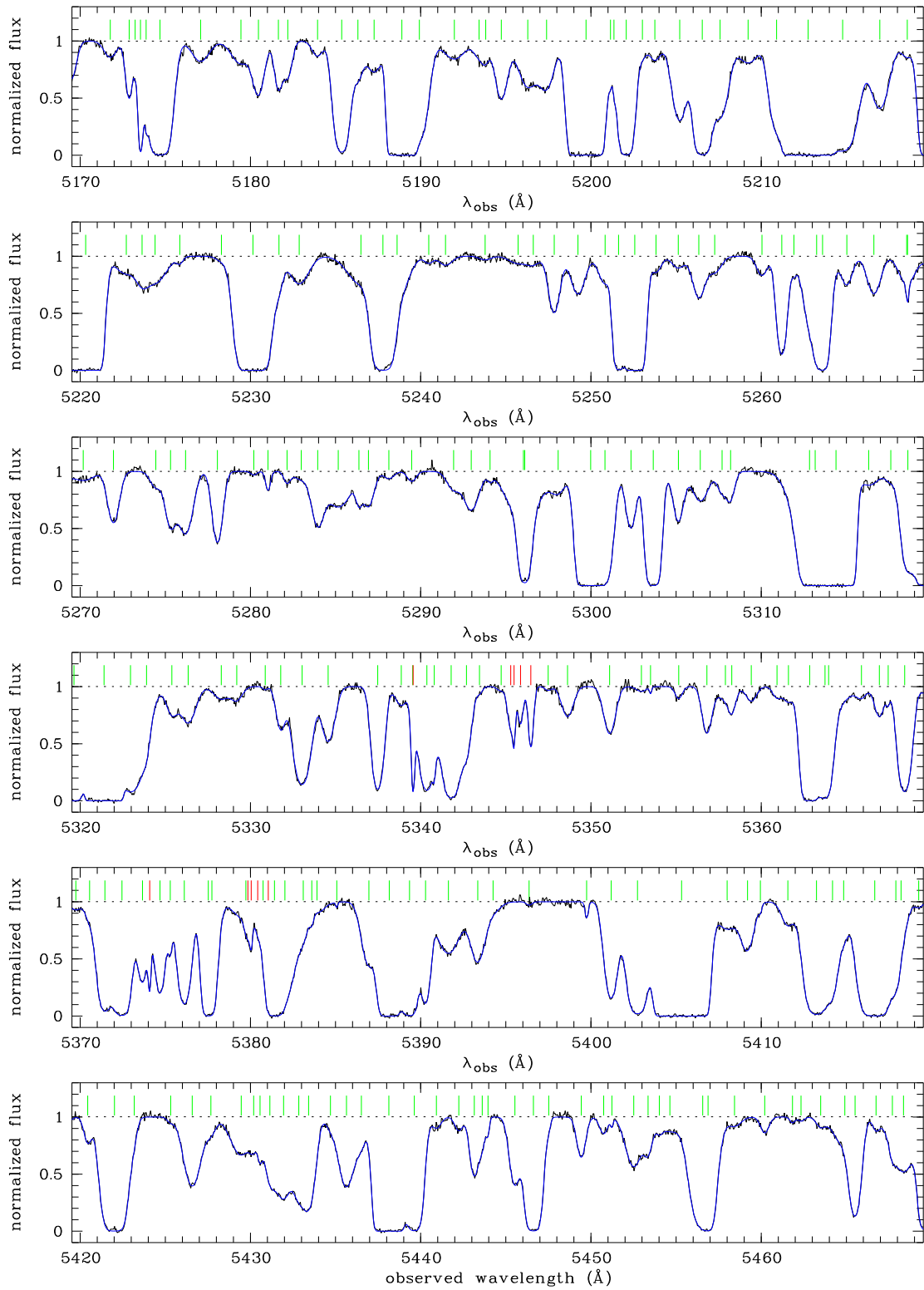


Figure D.11. The normalized absorption spectrum of the quasar J132029-052335 (black solid line) and its fit with CANDALF (blue solid line). Absorption-line components are indicated by vertical lines; assumed H_I Ly_α transitions (green) and identified metals (red).

Figure D.11. *Continued*

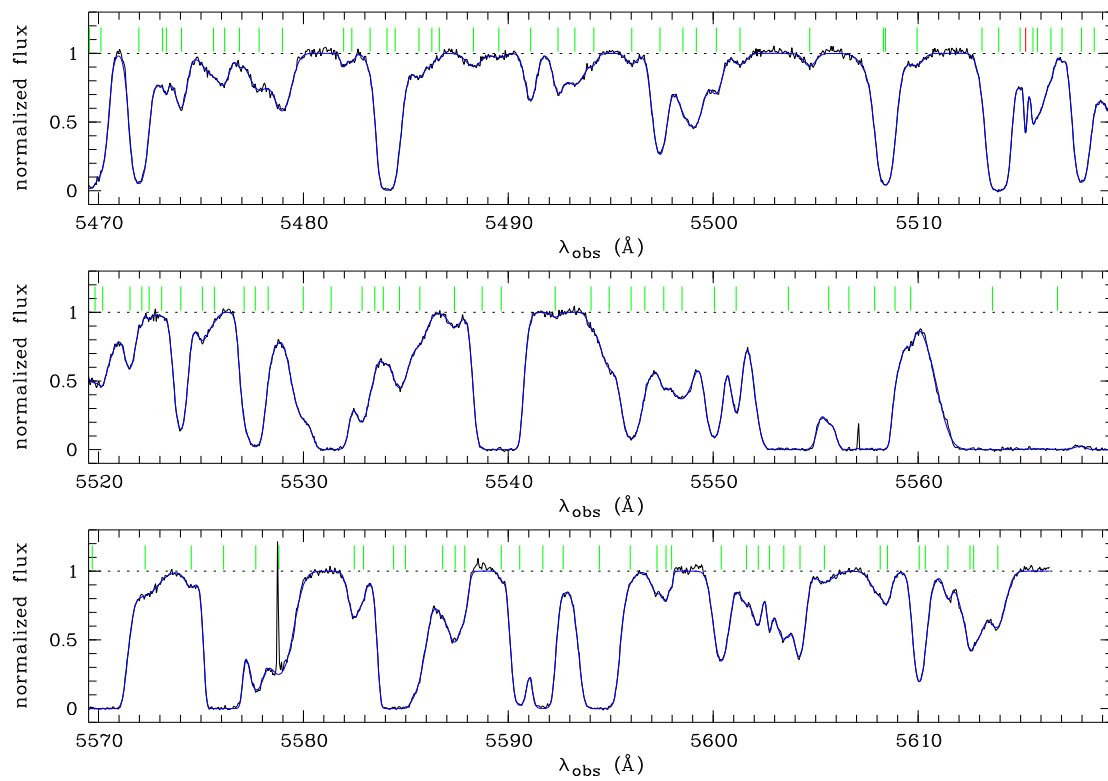


Figure D.11. *Continued*

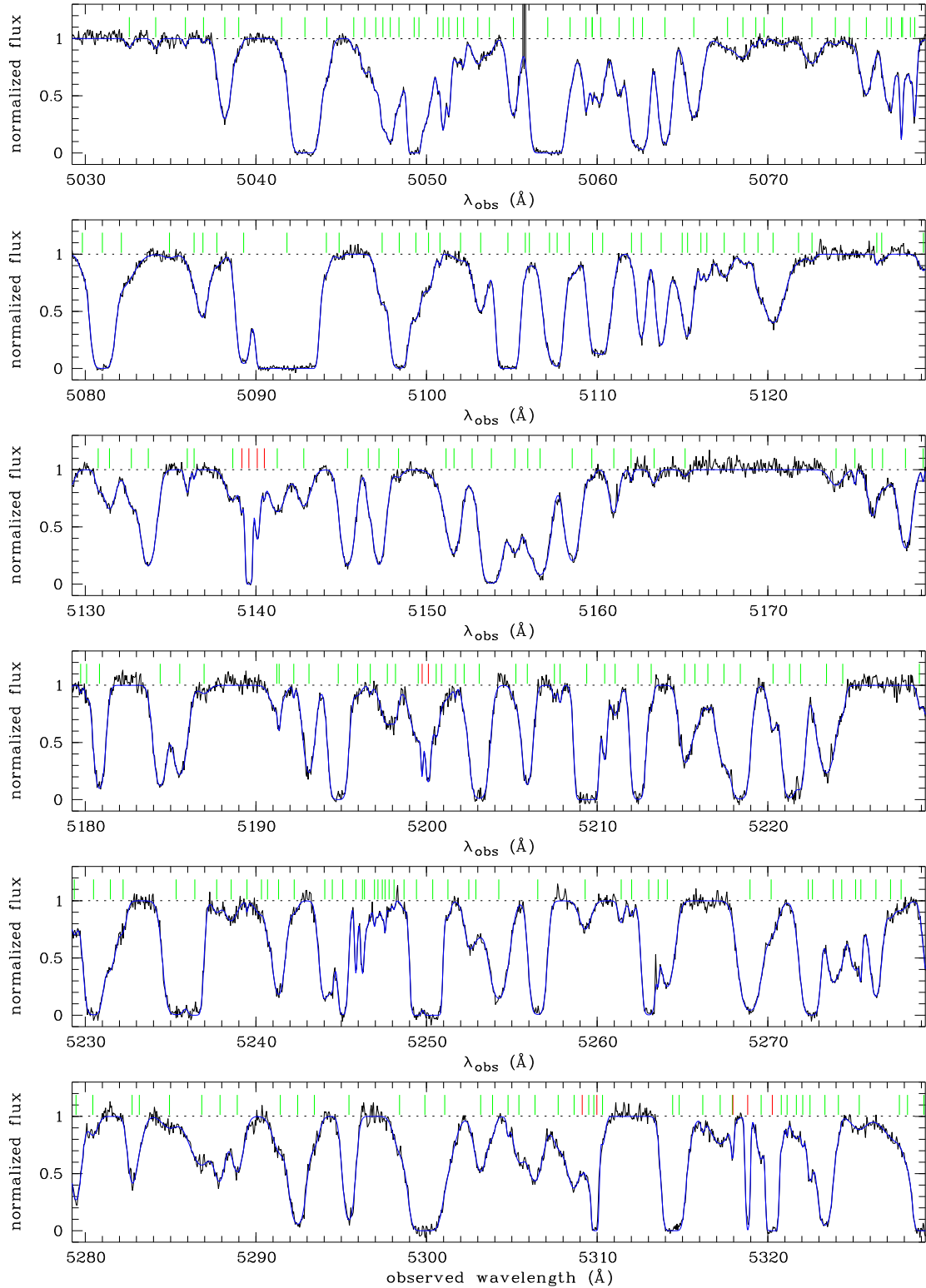


Figure D.12. The normalized absorption spectrum of the quasar J012403+004432 (black solid line) and its fit with CANDALF (blue solid line). Absorption-line components are indicated by vertical lines; assumed H I Ly α transitions (green) and identified metals (red).

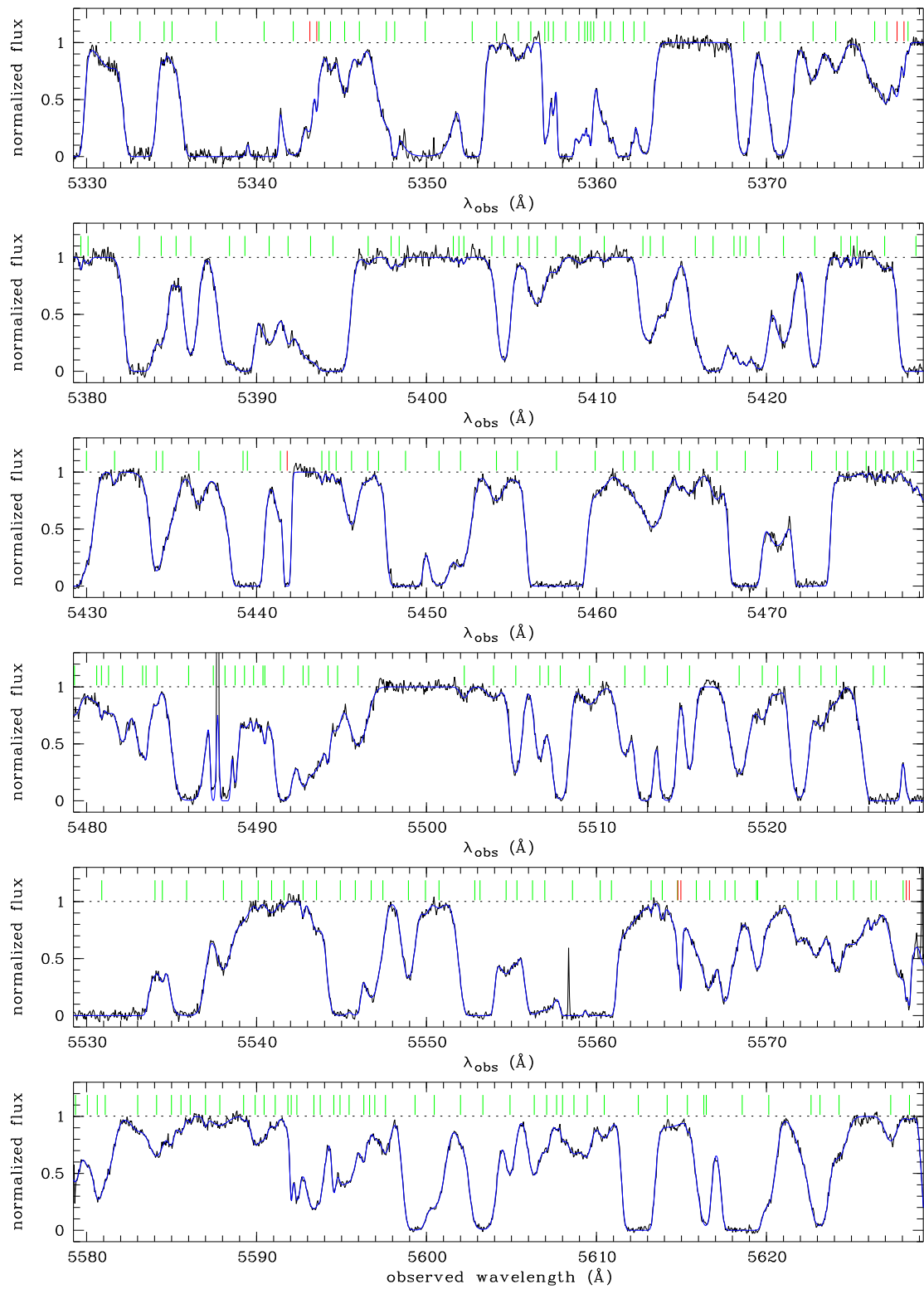


Figure D.12. *Continued*

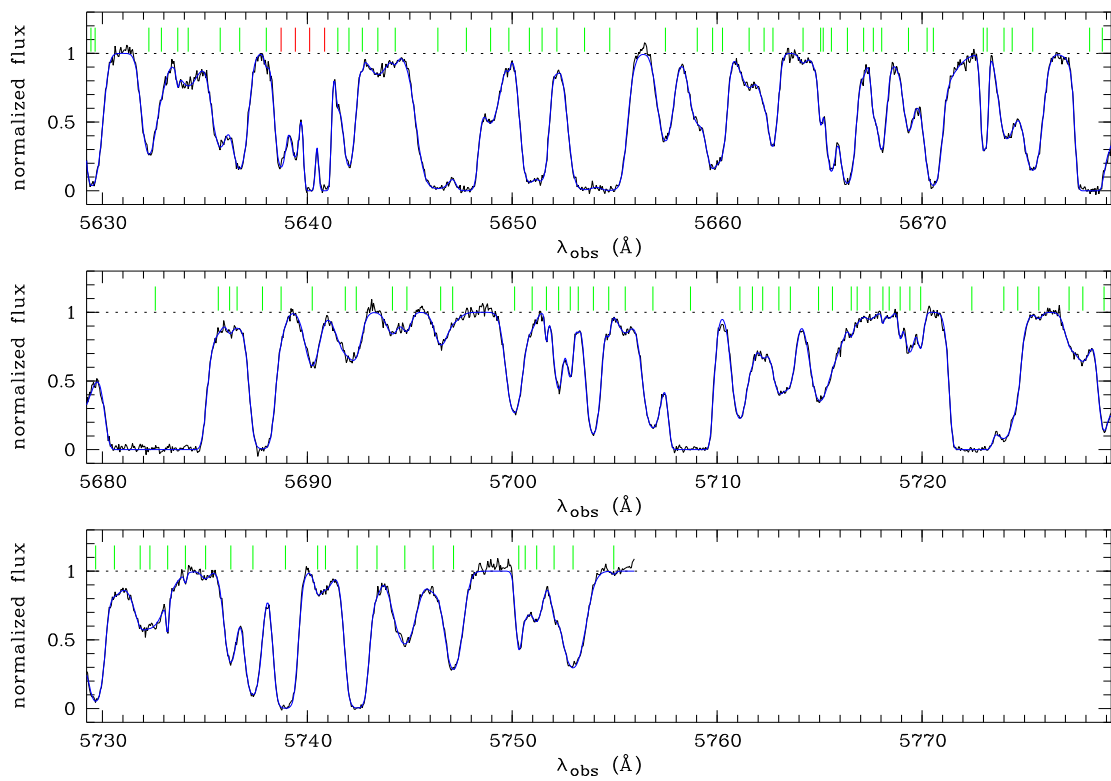


Figure D.12. *Continued*

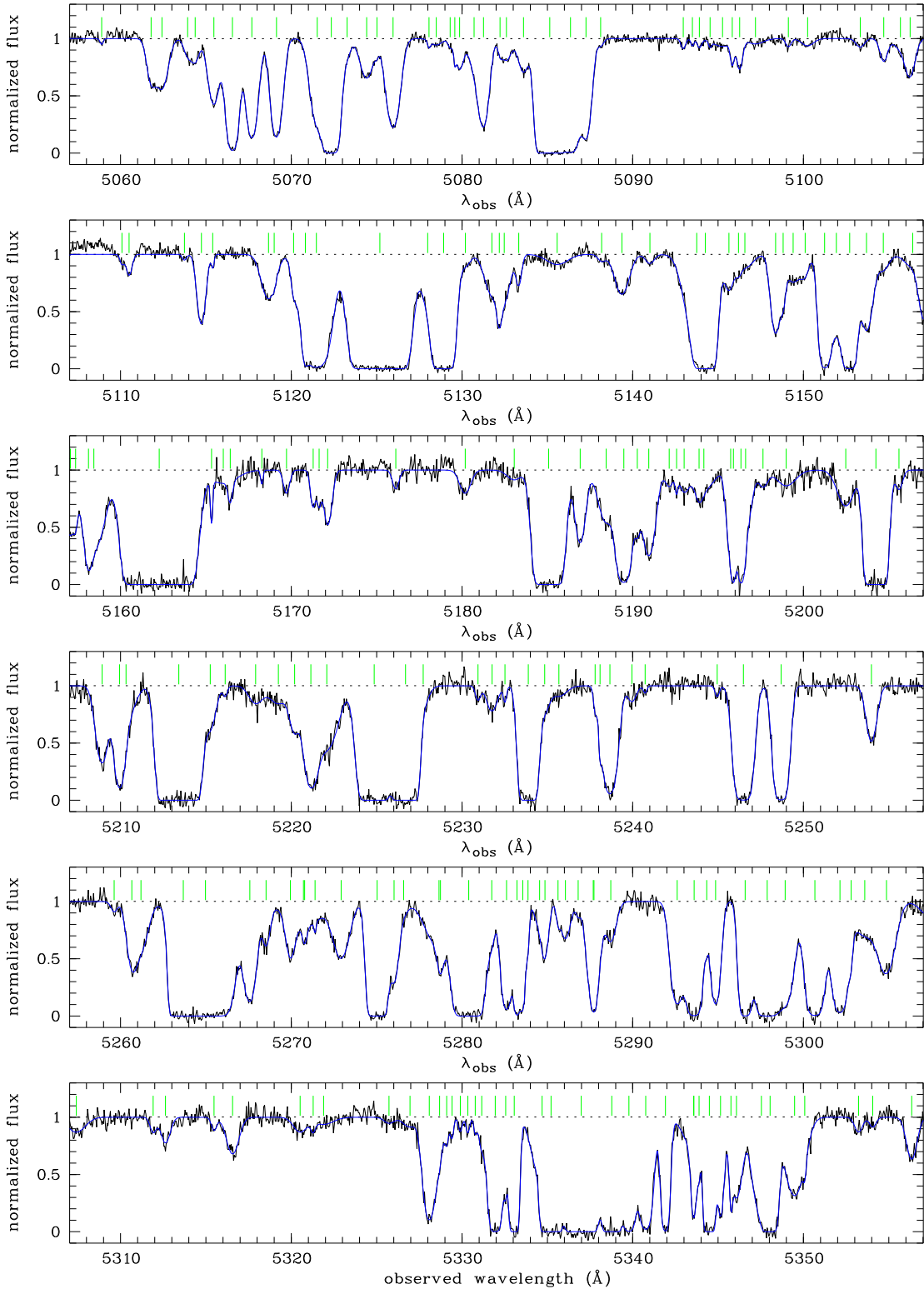


Figure D.13. The normalized absorption spectrum of the quasar J111113-080401 (black solid line) and its fit with CANDALF (blue solid line). Absorption-line components are indicated by vertical lines; assumed H I Ly α transitions (green) and identified metals (red).

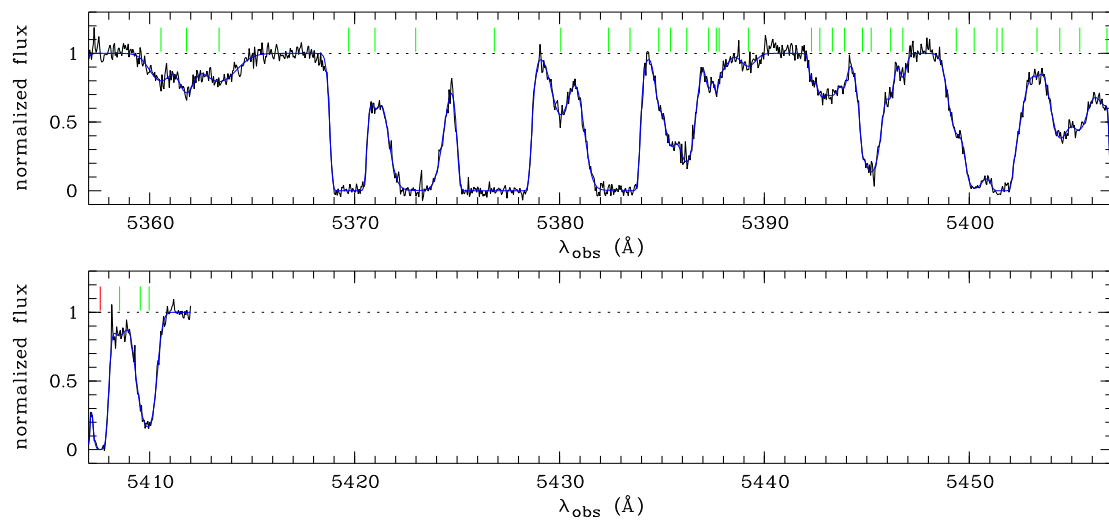


Figure D.13. *Continued*

Appendix E

Absorption line data

Table E.1. Complete sample of absorption lines used in this work with rest-frame wavelength $\lambda_{r,\alpha} = 1215.6701 \text{ \AA}$ and a Doppler parameter $b > 10 \text{ km s}^{-1}$.

No.	QSO	$\lambda (\text{\AA})$	$\log N$	$b (\text{km s}^{-1})$
1	J004131-493611	5065.466 \pm 0.040	12.314 \pm 0.088	17.220 \pm 3.747
2	J004131-493611	5064.248 \pm 0.031	13.059 \pm 0.030	44.170 \pm 4.038
3	J004131-493611	5062.815 \pm 0.012	13.508 \pm 0.020	23.805 \pm 0.832
4	J004131-493611	5061.963 \pm 0.070	12.769 \pm 0.132	28.988 \pm 8.813
5	J004131-493611	5060.881 \pm 0.041	12.795 \pm 0.092	25.944 \pm 5.805
6	J004131-493611	5060.154 \pm 0.124	12.123 \pm 0.273	18.139 \pm 8.027
7	J004131-493611	5057.628 \pm 0.030	12.799 \pm 0.031	31.361 \pm 2.779
8	J004131-493611	5056.587 \pm 0.052	12.280 \pm 0.087	20.055 \pm 4.451
9	J004131-493611	5054.853 \pm 0.068	12.510 \pm 0.330	15.253 \pm 4.935
10	J004131-493611	5054.065 \pm 0.009	13.719 \pm 0.076	19.124 \pm 1.212
11	J004131-493611	5053.789 \pm 0.648	12.914 \pm 0.615	40.351 \pm 18.169
12	J004131-493611	5045.821 \pm 0.022	12.321 \pm 0.051	13.099 \pm 1.952
13	J004131-493611	5044.404 \pm 0.014	12.877 \pm 0.019	22.475 \pm 1.153
14	J004131-493611	5042.050 \pm 0.050	12.824 \pm 0.033	49.034 \pm 4.510
15	J004131-493611	5039.790 \pm 0.017	12.866 \pm 0.056	20.876 \pm 1.833
16	J004131-493611	5039.049 \pm 0.105	13.164 \pm 0.040	68.824 \pm 6.562
17	J004131-493611	5036.450 \pm 0.118	12.990 \pm 0.137	23.738 \pm 4.677
18	J004131-493611	5034.813 \pm 0.031	12.648 \pm 0.115	19.060 \pm 3.827
19	J004131-493611	5033.716 \pm 0.038	13.343 \pm 0.046	46.120 \pm 5.666
20	J004131-493611	5032.487 \pm 0.053	13.121 \pm 0.114	25.887 \pm 5.427
21	J004131-493611	5032.020 \pm 0.030	12.590 \pm 0.255	12.609 \pm 3.199
22	J004131-493611	5031.347 \pm 0.054	12.729 \pm 0.062	29.627 \pm 4.906
23	J004131-493611	5029.120 \pm 0.055	13.633 \pm 0.039	41.271 \pm 2.789
24	J004131-493611	5028.002 \pm 0.041	13.284 \pm 0.110	17.471 \pm 3.429
25	J004131-493611	5027.227 \pm 0.022	13.607 \pm 0.056	30.698 \pm 4.263
26	J004131-493611	5026.466 \pm 0.023	12.944 \pm 0.111	14.571 \pm 1.818
27	J004131-493611	5025.655 \pm 0.012	13.357 \pm 0.013	28.711 \pm 1.286
28	J004131-493611	5023.116 \pm 0.062	12.187 \pm 0.090	21.308 \pm 5.297
29	J004131-493611	5020.671 \pm 0.011	13.194 \pm 0.011	28.952 \pm 0.868

Table E.1. *Continued*

30	J004131-493611	5015.796 ± 0.143	13.566 ± 0.176	31.371 ± 4.326
31	J004131-493611	5015.088 ± 0.017	14.558 ± 0.028	27.278 ± 1.058
32	J004131-493611	5014.003 ± 0.095	12.326 ± 0.358	15.423 ± 11.603
33	J004131-493611	5013.488 ± 0.043	12.799 ± 0.198	14.707 ± 5.087
34	J004131-493611	5012.703 ± 0.006	14.433 ± 0.018	24.599 ± 0.799
35	J004131-493611	5011.150 ± 0.004	14.630 ± 0.017	33.725 ± 0.675
36	J004131-493611	5009.856 ± 0.010	13.202 ± 0.019	17.752 ± 0.764
37	J004131-493611	5008.566 ± 0.010	14.118 ± 0.012	25.388 ± 0.519
38	J004131-493611	5007.871 ± 0.035	13.155 ± 0.136	19.106 ± 4.321
39	J004131-493611	5007.209 ± 0.011	13.707 ± 0.021	21.120 ± 0.980
40	J004131-493611	5005.757 ± 0.061	15.076 ± 0.121	27.493 ± 1.401
41	J004131-493611	5004.935 ± 0.242	13.846 ± 0.447	23.749 ± 10.619
42	J004131-493611	5004.081 ± 0.026	13.865 ± 0.041	27.201 ± 1.773
43	J004131-493611	5003.032 ± 0.171	12.705 ± 0.142	38.249 ± 10.432
44	J004131-493611	4998.146 ± 0.121	12.304 ± 0.095	40.153 ± 10.251
45	J004131-493611	4994.728 ± 0.005	14.181 ± 0.006	27.958 ± 0.362
46	J004131-493611	4993.821 ± 0.042	12.790 ± 0.134	19.945 ± 5.936
47	J004131-493611	4991.869 ± 0.022	17.211 ± 0.296	32.423 ± 1.608
48	J004131-493611	4990.177 ± 0.038	14.088 ± 0.051	26.170 ± 1.532
49	J004131-493611	4988.860 ± 0.013	13.364 ± 0.014	32.062 ± 1.361
50	J004131-493611	4986.673 ± 0.061	13.199 ± 0.044	45.369 ± 4.682
51	J004131-493611	4985.828 ± 0.014	13.012 ± 0.059	19.257 ± 1.510
52	J004131-493611	4984.696 ± 0.024	12.927 ± 0.024	31.847 ± 2.042
53	J004131-493611	4978.589 ± 0.039	12.081 ± 0.107	13.328 ± 3.124
54	J004131-493611	4977.533 ± 0.002	14.563 ± 0.011	28.530 ± 0.325
55	J004131-493611	4975.812 ± 0.102	13.787 ± 0.068	54.993 ± 4.501
56	J004131-493611	4975.335 ± 0.006	13.887 ± 0.039	24.157 ± 0.860
57	J004131-493611	4974.117 ± 0.026	13.346 ± 0.094	28.354 ± 3.729
58	J004131-493611	4973.290 ± 0.085	12.961 ± 0.172	29.982 ± 8.453
59	J004131-493611	4972.287 ± 0.074	12.623 ± 0.132	29.253 ± 7.969
60	J004131-493611	4971.470 ± 0.071	11.953 ± 0.184	16.802 ± 5.319
61	J004131-493611	4969.090 ± 0.044	12.271 ± 0.074	21.961 ± 3.467
62	J004131-493611	4967.964 ± 0.156	12.498 ± 0.187	34.604 ± 13.784
63	J004131-493611	4967.208 ± 0.006	13.546 ± 0.014	21.939 ± 0.346
64	J004131-493611	4965.252 ± 0.009	13.149 ± 0.013	30.974 ± 1.237
65	J004131-493611	4964.322 ± 0.002	13.605 ± 0.006	17.101 ± 0.211
66	J004131-493611	4963.256 ± 0.119	12.731 ± 0.042	47.038 ± 7.910
67	J004131-493611	4962.779 ± 0.035	12.038 ± 0.187	12.624 ± 3.982
68	J004131-493611	4960.994 ± 0.032	12.612 ± 0.035	28.149 ± 2.360
69	J004131-493611	4954.623 ± 0.026	12.825 ± 0.042	18.931 ± 1.621
70	J004131-493611	4953.044 ± 0.003	14.266 ± 0.002	50.387 ± 0.383
71	J004131-493611	4951.530 ± 0.008	13.300 ± 0.011	26.813 ± 0.565
72	J004131-493611	4948.326 ± 0.003	14.812 ± 0.006	52.701 ± 0.316
73	J004131-493611	4946.405 ± 0.005	14.476 ± 0.014	24.708 ± 0.547

Table E.1. *Continued*

74	J004131-493611	4945.264 ± 0.428	13.017 ± 0.623	42.835 ± 51.475
75	J004131-493611	4944.444 ± 0.013	14.091 ± 0.040	28.020 ± 0.692
76	J004131-493611	4943.441 ± 0.054	11.948 ± 1.005	11.756 ± 9.780
77	J004131-493611	4943.039 ± 0.205	12.387 ± 0.602	24.992 ± 29.415
78	J004131-493611	4942.254 ± 0.081	12.670 ± 0.132	25.032 ± 5.254
79	J004131-493611	4941.006 ± 0.061	12.750 ± 0.102	33.488 ± 4.812
80	J004131-493611	4939.817 ± 0.043	13.145 ± 0.056	47.596 ± 5.942
81	J004131-493611	4938.502 ± 0.062	12.581 ± 0.306	16.899 ± 4.651
82	J004131-493611	4937.630 ± 0.022	14.658 ± 0.058	22.274 ± 1.022
83	J004131-493611	4936.700 ± 0.021	14.444 ± 0.063	21.195 ± 2.553
84	J004131-493611	4935.955 ± 0.023	13.907 ± 0.059	21.038 ± 1.118
85	J004131-493611	4936.179 ± 2.916	13.128 ± 1.445	79.818 ± 83.920
86	J004131-493611	4933.439 ± 0.003	13.726 ± 0.005	23.031 ± 0.302
87	J004131-493611	4932.812 ± 0.016	12.558 ± 0.059	12.915 ± 1.527
88	J004131-493611	4932.007 ± 0.006	13.792 ± 0.014	22.846 ± 0.414
89	J004131-493611	4931.306 ± 0.326	12.366 ± 0.405	31.753 ± 22.232
90	J004131-493611	4929.912 ± 0.043	13.007 ± 0.070	33.402 ± 3.346
91	J004131-493611	4928.451 ± 0.345	13.332 ± 0.985	52.480 ± 29.188
92	J004131-493611	4927.741 ± 0.063	12.554 ± 0.501	23.945 ± 8.515
93	J004131-493611	4927.435 ± 2.829	13.155 ± 1.451	77.058 ± 98.626
94	J004131-493611	4925.277 ± 0.714	12.888 ± 1.556	22.534 ± 18.635
95	J004131-493611	4924.966 ± 0.077	13.551 ± 0.333	19.925 ± 1.832
96	J004131-493611	4923.958 ± 0.034	12.630 ± 0.050	30.329 ± 3.696
97	J004131-493611	4922.022 ± 0.013	13.006 ± 0.036	28.993 ± 1.517
98	J004131-493611	4921.316 ± 0.033	13.614 ± 0.011	89.683 ± 2.071
99	J004131-493611	4918.936 ± 0.020	13.824 ± 0.022	33.685 ± 0.823
100	J004131-493611	4918.547 ± 0.015	12.849 ± 0.174	16.146 ± 2.529
101	J004131-493611	4917.061 ± 0.362	13.110 ± 0.333	39.944 ± 16.184
102	J004131-493611	4916.450 ± 0.006	14.346 ± 0.016	22.839 ± 0.766
103	J004131-493611	4915.659 ± 0.014	13.877 ± 0.014	31.434 ± 0.617
104	J004131-493611	4912.716 ± 0.012	13.019 ± 0.011	36.217 ± 1.111
105	J004131-493611	4911.181 ± 0.010	13.245 ± 0.065	18.713 ± 1.083
106	J004131-493611	4910.959 ± 0.015	13.638 ± 0.027	32.484 ± 0.473
107	J004131-493611	4909.471 ± 0.025	12.311 ± 0.039	21.168 ± 2.312
108	J004131-493611	4908.126 ± 0.038	13.421 ± 0.213	22.102 ± 1.937
109	J004131-493611	4907.640 ± 0.856	12.738 ± 1.090	31.281 ± 42.920
110	J004131-493611	4906.660 ± 0.146	11.966 ± 0.700	13.065 ± 19.189
111	J004131-493611	4906.013 ± 0.047	12.658 ± 0.395	15.352 ± 5.917
112	J004131-493611	4905.620 ± 0.204	13.009 ± 0.200	35.768 ± 9.905
113	J004131-493611	4904.319 ± 0.003	13.581 ± 0.010	20.730 ± 0.318
114	J004131-493611	4903.170 ± 0.070	13.041 ± 0.037	58.729 ± 7.734
115	J004131-493611	4902.866 ± 0.028	11.899 ± 0.177	10.152 ± 3.473
116	J004131-493611	4901.899 ± 0.026	11.980 ± 0.117	10.903 ± 2.748
117	J004131-493611	4901.045 ± 0.008	13.252 ± 0.010	30.680 ± 0.847

Table E.1. *Continued*

118	J004131-493611	4899.471 ± 0.201	13.150 ± 0.201	36.359 ± 8.458
119	J004131-493611	4898.977 ± 0.032	12.923 ± 0.325	21.993 ± 4.392
120	J004131-493611	4898.068 ± 0.010	13.383 ± 0.021	27.555 ± 1.467
121	J004131-493611	4897.304 ± 0.024	12.852 ± 0.083	19.147 ± 2.669
122	J004131-493611	4896.560 ± 0.004	13.984 ± 0.005	25.797 ± 0.264
123	J004131-493611	4893.458 ± 0.047	12.901 ± 0.041	46.739 ± 2.448
124	J004131-493611	4893.149 ± 0.018	12.567 ± 0.083	18.728 ± 2.066
125	J004131-493611	4890.424 ± 0.025	12.548 ± 0.027	30.805 ± 2.214
126	J004131-493611	4887.353 ± 0.012	13.118 ± 0.014	28.021 ± 0.927
127	J004131-493611	4886.359 ± 0.017	12.977 ± 0.022	29.530 ± 1.699
128	J004131-493611	4885.097 ± 0.072	12.134 ± 0.102	28.638 ± 7.519
129	J004131-493611	4883.457 ± 0.103	11.964 ± 0.310	19.460 ± 9.755
130	J004131-493611	4882.034 ± 0.262	12.794 ± 0.147	88.577 ± 29.846
131	J004131-493611	4880.032 ± 0.097	12.997 ± 0.070	53.747 ± 6.498
132	J004131-493611	4879.830 ± 0.016	12.435 ± 0.101	14.316 ± 2.089
133	J004131-493611	4878.346 ± 0.056	12.873 ± 0.110	21.656 ± 3.127
134	J004131-493611	4877.743 ± 0.008	13.836 ± 0.012	23.318 ± 0.401
135	J004131-493611	4875.501 ± 0.003	13.709 ± 0.004	30.134 ± 0.311
136	J004131-493611	4874.638 ± 0.012	12.602 ± 0.034	14.337 ± 1.237
137	J004131-493611	4873.494 ± 0.001	15.061 ± 0.024	23.433 ± 0.220
138	J004131-493611	4862.929 ± 0.061	12.288 ± 0.052	37.888 ± 5.340
139	J004131-493611	4860.373 ± 0.102	12.664 ± 0.233	23.122 ± 4.555
140	J004131-493611	4859.819 ± 0.028	13.142 ± 0.200	21.837 ± 2.955
141	J004131-493611	4859.428 ± 0.729	12.733 ± 0.630	42.991 ± 26.457
142	J004131-493611	4856.833 ± 0.003	13.963 ± 0.003	33.200 ± 0.264
143	J004131-493611	4855.467 ± 0.068	13.103 ± 0.078	37.783 ± 5.941
144	J004131-493611	4854.475 ± 0.015	13.257 ± 0.083	20.784 ± 1.621
145	J004131-493611	4853.936 ± 0.141	12.873 ± 0.159	31.130 ± 6.023
146	J004131-493611	4851.650 ± 0.005	13.257 ± 0.006	24.332 ± 0.433
147	J004131-493611	4850.669 ± 0.002	13.532 ± 0.004	20.063 ± 0.199
148	J004131-493611	4848.999 ± 0.009	12.814 ± 0.018	16.207 ± 0.857
149	J004131-493611	4846.269 ± 0.003	13.846 ± 0.006	20.545 ± 0.209
150	J004131-493611	4845.473 ± 0.018	13.375 ± 0.019	34.749 ± 1.537
151	J004131-493611	4844.111 ± 0.002	14.094 ± 0.004	22.530 ± 0.179
152	J004131-493611	4843.124 ± 0.102	12.148 ± 0.117	29.250 ± 8.940
153	J004131-493611	4841.232 ± 0.014	12.887 ± 0.014	34.350 ± 1.255
154	J004131-493611	4839.391 ± 0.007	13.111 ± 0.008	29.020 ± 0.620
155	J004131-493611	4837.660 ± 0.012	13.133 ± 0.019	24.437 ± 0.849
156	J004131-493611	4836.845 ± 0.064	12.533 ± 0.076	29.001 ± 4.760
157	J004131-493611	4835.045 ± 0.565	12.688 ± 0.738	30.599 ± 17.715
158	J004131-493611	4834.666 ± 0.042	12.950 ± 0.399	20.936 ± 4.034
159	J004131-493611	4831.308 ± 0.394	12.931 ± 0.943	21.774 ± 39.107
160	J004131-493611	4830.693 ± 0.082	12.614 ± 0.474	10.496 ± 4.075
161	J004131-493611	4830.170 ± 0.007	12.848 ± 0.122	11.357 ± 1.373

Table E.1. *Continued*

162	J004131-493611	4829.429 ± 0.010	13.675 ± 0.092	20.727 ± 2.165
163	J004131-493611	4829.033 ± 1.006	12.812 ± 0.766	50.790 ± 31.848
164	J004131-493611	4825.521 ± 0.025	13.117 ± 0.030	29.716 ± 2.191
165	J004131-493611	4824.681 ± 0.027	12.567 ± 0.160	12.813 ± 2.419
166	J004131-493611	4824.080 ± 0.102	13.131 ± 0.206	24.013 ± 9.292
167	J004131-493611	4823.313 ± 0.014	14.559 ± 0.137	19.791 ± 1.943
168	J004131-493611	4821.679 ± 0.004	15.320 ± 0.061	32.619 ± 0.859
169	J004131-493611	4820.199 ± 0.024	12.973 ± 0.090	18.192 ± 2.486
170	J004131-493611	4819.496 ± 0.007	13.957 ± 0.010	25.863 ± 0.696
171	J004131-493611	4816.139 ± 0.017	13.473 ± 0.039	28.056 ± 2.548
172	J004131-493611	4811.589 ± 0.123	12.845 ± 0.168	30.803 ± 9.596
173	J004131-493611	4810.720 ± 0.033	12.307 ± 0.136	15.263 ± 4.240
174	J004131-493611	4810.255 ± 0.009	12.749 ± 0.041	11.738 ± 1.001
175	J004131-493611	4809.696 ± 0.033	12.428 ± 0.104	19.258 ± 5.341
176	J004131-493611	4809.085 ± 0.047	12.207 ± 0.136	16.339 ± 5.288
177	J004131-493611	4808.339 ± 0.033	12.900 ± 0.083	14.137 ± 2.030
178	J004131-493611	4807.397 ± 0.016	13.045 ± 0.026	30.878 ± 2.330
179	J004131-493611	4806.632 ± 0.064	11.784 ± 0.295	11.365 ± 6.686
180	J004131-493611	4805.884 ± 0.002	14.226 ± 0.006	22.761 ± 0.228
181	J004131-493611	4804.424 ± 0.041	12.525 ± 0.180	16.548 ± 4.827
182	J004131-493611	4803.405 ± 0.003	13.575 ± 0.010	18.640 ± 0.302
183	J004131-493611	4803.563 ± 0.149	13.051 ± 0.076	71.520 ± 9.933
184	J004131-493611	4800.619 ± 0.044	12.483 ± 0.042	37.610 ± 4.494
185	J004131-493611	4799.252 ± 0.019	12.685 ± 0.023	28.259 ± 1.748
186	J004131-493611	4795.646 ± 0.029	12.192 ± 0.079	13.837 ± 2.439
187	J004131-493611	4794.891 ± 0.010	13.592 ± 0.016	23.994 ± 0.787
188	J004131-493611	4794.189 ± 0.007	13.659 ± 0.021	22.516 ± 0.755
189	J004131-493611	4793.071 ± 0.120	13.317 ± 0.137	41.715 ± 10.761
190	J004131-493611	4792.373 ± 0.025	13.217 ± 0.144	24.627 ± 2.334
191	J004131-493611	4791.451 ± 0.007	13.227 ± 0.009	24.661 ± 0.634
192	J004131-493611	4789.846 ± 0.019	13.680 ± 0.017	39.175 ± 0.803
193	J004131-493611	4789.465 ± 0.012	12.797 ± 0.109	15.985 ± 1.972
194	J004131-493611	4788.512 ± 0.032	12.462 ± 0.066	21.210 ± 3.089
195	J004131-493611	4786.910 ± 0.022	13.114 ± 0.054	46.398 ± 4.390
196	J004131-493611	4786.846 ± 0.003	13.448 ± 0.028	19.810 ± 0.572
197	J004131-493611	4785.097 ± 0.001	14.096 ± 0.003	24.955 ± 0.136
198	J004131-493611	4783.824 ± 0.020	12.593 ± 0.025	26.969 ± 1.893
199	J004131-493611	4782.045 ± 0.002	13.641 ± 0.003	24.441 ± 0.185
200	J004131-493611	4780.718 ± 0.009	13.170 ± 0.012	25.295 ± 0.799
201	J004131-493611	4779.584 ± 0.352	13.586 ± 0.646	24.806 ± 9.252
202	J004131-493611	4779.312 ± 0.024	13.955 ± 0.270	18.226 ± 1.946
203	J004131-493611	4778.543 ± 0.050	13.080 ± 0.058	33.773 ± 3.883
204	J004131-493611	4777.566 ± 0.007	12.894 ± 0.022	14.734 ± 0.811
205	J004131-493611	4776.347 ± 0.058	12.500 ± 0.061	38.782 ± 7.049

Table E.1. *Continued*

206	J004131-493611	4775.036 ± 0.018	13.413 ± 0.041	19.613 ± 0.831
207	J004131-493611	4774.525 ± 0.014	13.702 ± 0.021	22.511 ± 0.636
208	J004131-493611	4773.331 ± 0.020	12.778 ± 0.034	22.501 ± 1.713
209	J004131-493611	4772.538 ± 0.009	13.272 ± 0.011	26.163 ± 0.696
210	J004131-493611	4770.772 ± 0.015	13.384 ± 0.020	24.813 ± 0.836
211	J004131-493611	4769.965 ± 0.003	14.362 ± 0.009	23.581 ± 0.314
212	J004131-493611	4768.937 ± 0.030	12.353 ± 0.051	19.738 ± 2.755
213	J004131-493611	4762.783 ± 0.017	17.203 ± 0.062	40.710 ± 0.446
214	J004131-493611	4761.285 ± 0.444	13.723 ± 0.653	32.863 ± 10.486
215	J004131-493611	4759.609 ± 0.047	12.352 ± 0.051	31.151 ± 4.493
216	J004131-493611	4756.968 ± 0.018	12.865 ± 0.015	40.346 ± 1.640
217	J004131-493611	4755.035 ± 0.002	13.983 ± 0.003	26.152 ± 0.162
218	J004131-493611	4753.823 ± 0.026	13.286 ± 0.035	29.616 ± 1.946
219	J004131-493611	4753.101 ± 0.009	13.616 ± 0.015	24.108 ± 0.514
220	J004131-493611	4752.185 ± 0.029	12.154 ± 0.078	14.458 ± 2.910
221	J004131-493611	4751.366 ± 0.003	13.687 ± 0.003	26.914 ± 0.246
222	J004131-493611	4748.462 ± 0.014	12.688 ± 0.025	17.843 ± 0.893
223	J004131-493611	4746.633 ± 0.007	12.486 ± 0.020	11.340 ± 0.672
224	J004131-493611	4744.986 ± 0.043	12.375 ± 0.060	24.864 ± 3.818
225	J004131-493611	4744.042 ± 0.026	12.988 ± 0.047	24.859 ± 2.439
226	J004131-493611	4743.412 ± 0.040	12.694 ± 0.080	20.707 ± 2.243
227	J004131-493611	4742.016 ± 0.009	13.092 ± 0.011	28.422 ± 0.836
228	J004131-493611	4740.831 ± 0.017	13.200 ± 0.046	32.736 ± 1.661
229	J004131-493611	4739.785 ± 0.087	13.124 ± 0.056	56.102 ± 6.020
230	J004131-493611	4737.665 ± 0.037	12.119 ± 0.062	20.597 ± 3.598
231	J004131-493611	4736.839 ± 0.027	11.856 ± 0.081	10.352 ± 2.568
232	J004131-493611	4733.855 ± 0.029	12.944 ± 0.029	33.070 ± 2.176
233	J004131-493611	4732.999 ± 0.027	12.760 ± 0.043	24.911 ± 1.899
234	J004131-493611	4731.550 ± 0.013	12.906 ± 0.016	26.643 ± 1.247
235	J004131-493611	4729.086 ± 0.010	13.017 ± 0.010	31.586 ± 0.891
236	J004131-493611	4726.175 ± 0.091	12.146 ± 0.113	30.071 ± 8.635
237	J004131-493611	4725.150 ± 0.058	11.961 ± 0.106	19.281 ± 5.636
238	J004131-493611	4722.972 ± 0.001	14.140 ± 0.004	25.287 ± 0.144
239	J004131-493611	4721.596 ± 0.264	12.823 ± 0.700	25.154 ± 9.806
240	J004131-493611	4720.795 ± 0.014	14.030 ± 0.079	21.414 ± 1.394
241	J004131-493611	4720.692 ± 0.162	13.840 ± 0.194	41.541 ± 3.566
242	J004131-493611	4717.978 ± 0.037	12.183 ± 0.231	17.239 ± 4.995
243	J004131-493611	4716.876 ± 0.002	14.396 ± 0.011	26.076 ± 0.420
244	J004131-493611	4715.541 ± 0.052	14.065 ± 0.041	86.178 ± 7.897
245	J004131-493611	4714.689 ± 0.015	13.858 ± 0.029	23.343 ± 0.867
246	J004131-493611	4714.068 ± 0.019	13.784 ± 0.035	25.748 ± 1.008
247	J004131-493611	4712.604 ± 0.159	13.153 ± 0.093	75.948 ± 12.408
248	J004131-493611	4710.548 ± 0.208	12.896 ± 0.251	32.668 ± 10.160
249	J004131-493611	4710.094 ± 0.004	13.739 ± 0.033	18.884 ± 0.517

Table E.1. *Continued*

250	J004131-493611	4709.033 ± 0.151	13.628 ± 0.202	32.755 ± 5.760
251	J004131-493611	4708.277 ± 0.025	14.221 ± 0.082	31.108 ± 4.347
252	J004131-493611	4707.400 ± 0.020	14.567 ± 0.043	24.553 ± 0.498
253	J004131-493611	4705.361 ± 0.030	13.045 ± 0.094	23.335 ± 1.657
254	J004131-493611	4704.524 ± 0.021	13.548 ± 0.066	38.427 ± 5.859
255	J004131-493611	4703.797 ± 0.013	13.291 ± 0.069	20.679 ± 1.077
256	J004131-493611	4701.313 ± 0.194	12.762 ± 0.129	50.658 ± 11.079
257	J004131-493611	4700.605 ± 0.011	12.998 ± 0.066	22.537 ± 1.628
258	J004131-493611	4699.749 ± 0.022	12.647 ± 0.034	24.951 ± 2.042
259	J004131-493611	4693.255 ± 0.011	13.307 ± 0.017	28.960 ± 0.929
260	J004131-493611	4691.614 ± 0.232	12.707 ± 0.201	74.586 ± 37.755
261	J004131-493611	4690.667 ± 0.005	13.629 ± 0.028	18.420 ± 0.473
262	J004131-493611	4689.963 ± 0.086	13.018 ± 0.282	34.900 ± 21.165
263	J004131-493611	4689.237 ± 0.080	12.828 ± 0.285	23.318 ± 5.602
264	J004131-493611	4688.477 ± 0.042	12.366 ± 0.119	19.722 ± 5.428
265	J004131-493611	4687.772 ± 0.030	12.469 ± 0.088	19.166 ± 3.644
266	J004131-493611	4687.014 ± 0.012	13.119 ± 0.018	27.755 ± 1.244
267	J004131-493611	4685.041 ± 0.136	13.038 ± 0.082	59.012 ± 9.144
268	J004131-493611	4683.773 ± 0.004	15.508 ± 0.056	26.681 ± 0.567
269	J004131-493611	4682.861 ± 0.077	13.460 ± 0.086	33.629 ± 2.914
270	J004131-493611	4680.666 ± 0.024	13.000 ± 0.036	25.039 ± 1.552
271	J004131-493611	4679.863 ± 0.009	13.445 ± 0.017	27.684 ± 1.164
272	J004131-493611	4678.905 ± 0.044	12.590 ± 0.221	18.324 ± 6.608
273	J004131-493611	4678.298 ± 0.026	13.320 ± 0.028	30.193 ± 1.483
274	J004131-493611	4675.236 ± 0.235	12.328 ± 0.231	35.132 ± 14.675
275	J004131-493611	4674.531 ± 0.009	13.339 ± 0.022	23.030 ± 0.575
276	J004131-493611	4671.152 ± 1.350	13.132 ± 1.008	57.796 ± 37.885
277	J004131-493611	4671.025 ± 0.021	13.657 ± 0.112	25.380 ± 1.777
278	J004131-493611	4670.353 ± 0.035	13.920 ± 0.118	36.746 ± 2.436
279	J004131-493611	4669.215 ± 0.009	13.505 ± 0.014	26.085 ± 0.518
280	J004131-493611	4665.735 ± 0.105	13.267 ± 0.047	75.486 ± 6.020
281	J004131-493611	4664.321 ± 0.002	15.214 ± 0.023	33.973 ± 0.359
282	J004131-493611	4661.733 ± 0.021	15.185 ± 0.032	41.846 ± 0.640
283	J004131-493611	4660.609 ± 0.090	13.875 ± 0.113	36.149 ± 2.639
284	J004131-493611	4659.004 ± 0.027	12.259 ± 0.060	16.562 ± 2.876
285	J004131-493611	4657.355 ± 0.012	13.058 ± 0.012	35.075 ± 1.170
286	J004131-493611	4656.058 ± 0.017	12.636 ± 0.028	21.249 ± 1.625
287	J004131-493611	4652.347 ± 0.031	12.721 ± 0.046	28.386 ± 3.654
288	J004131-493611	4651.352 ± 0.040	12.208 ± 0.187	17.041 ± 4.981
289	J004131-493611	4650.466 ± 0.029	13.052 ± 0.045	46.152 ± 5.753
290	J004131-493611	4649.297 ± 0.019	12.900 ± 0.035	26.984 ± 1.581
291	J004131-493611	4647.295 ± 0.024	13.575 ± 0.023	35.269 ± 1.209
292	J004131-493611	4646.467 ± 0.006	13.960 ± 0.014	27.481 ± 0.799
293	J004131-493611	4645.712 ± 0.036	12.838 ± 0.137	21.429 ± 4.028

Table E.1. *Continued*

294	J004131-493611	4645.045 ± 0.060	12.892 ± 0.068	30.830 ± 3.581
295	J004131-493611	4643.309 ± 0.002	13.922 ± 0.003	27.858 ± 0.150
296	J004131-493611	4638.428 ± 0.003	14.119 ± 0.004	26.915 ± 0.320
297	J004131-493611	4637.462 ± 0.024	13.057 ± 0.033	26.818 ± 1.892
298	J004131-493611	4636.031 ± 0.013	13.138 ± 0.016	32.878 ± 1.675
299	J004131-493611	4635.147 ± 0.013	12.321 ± 0.044	11.127 ± 1.242
300	J004131-493611	4633.756 ± 0.004	13.700 ± 0.006	24.293 ± 0.353
301	J004131-493611	4626.744 ± 0.047	12.239 ± 0.056	28.992 ± 4.358
302	J004131-493611	4623.997 ± 0.002	14.156 ± 0.003	31.514 ± 0.138
303	J004131-493611	4616.561 ± 0.008	12.949 ± 0.012	24.879 ± 0.778
304	J004131-493611	4614.754 ± 0.070	13.636 ± 0.080	34.219 ± 2.528
305	J004131-493611	4614.268 ± 0.010	13.929 ± 0.041	23.301 ± 0.586
306	J004131-493611	4611.346 ± 0.033	12.373 ± 0.045	25.470 ± 3.303
307	J004131-493611	4609.506 ± 0.031	12.424 ± 0.040	26.695 ± 2.919
308	J004131-493611	4602.386 ± 0.017	12.861 ± 0.018	33.037 ± 1.671
309	J004131-493611	4601.156 ± 0.002	13.802 ± 0.003	24.375 ± 0.218
310	J004131-493611	4600.107 ± 0.072	12.486 ± 0.255	19.922 ± 10.144
311	J004131-493611	4599.563 ± 0.227	12.103 ± 0.471	20.214 ± 15.047
312	J004131-493611	4598.548 ± 0.022	13.715 ± 0.083	23.845 ± 1.106
313	J004131-493611	4597.966 ± 0.047	13.894 ± 0.062	34.621 ± 3.263
314	J004131-493611	4596.882 ± 0.060	13.027 ± 0.072	33.889 ± 3.835
315	J004131-493611	4595.089 ± 0.139	13.013 ± 0.104	50.755 ± 7.066
316	J004131-493611	4594.473 ± 0.045	12.445 ± 0.353	25.888 ± 7.958
317	J004131-493611	4591.425 ± 0.063	12.580 ± 0.075	29.246 ± 4.906
318	J004131-493611	4590.591 ± 0.070	13.065 ± 0.178	23.054 ± 3.863
319	J004131-493611	4590.101 ± 0.352	12.513 ± 0.589	25.440 ± 13.478
320	J004131-493611	4587.629 ± 0.029	12.821 ± 0.026	37.776 ± 2.657
321	J004131-493611	4585.527 ± 0.051	12.340 ± 0.116	18.988 ± 3.715
322	J004131-493611	4584.854 ± 0.025	12.943 ± 0.031	28.036 ± 2.057
323	J004131-493611	4583.642 ± 0.019	12.368 ± 0.037	17.300 ± 1.813
324	J004131-493611	4580.655 ± 0.003	13.719 ± 0.004	25.113 ± 0.270
325	J004131-493611	4579.945 ± 0.005	13.065 ± 0.017	13.897 ± 0.557
326	J004131-493611	4579.232 ± 0.042	12.877 ± 0.080	23.017 ± 3.877
327	J004131-493611	4578.737 ± 0.145	12.061 ± 0.461	16.609 ± 7.948
328	J004131-493611	4576.482 ± 0.054	12.268 ± 0.134	15.452 ± 3.746
329	J004131-493611	4576.013 ± 0.069	12.236 ± 0.151	17.395 ± 5.629
330	J004131-493611	4575.114 ± 0.004	13.440 ± 0.006	19.878 ± 0.387
331	J004131-493611	4573.751 ± 0.009	13.708 ± 0.008	41.892 ± 0.505
332	J004131-493611	4573.308 ± 0.005	13.134 ± 0.025	15.068 ± 0.608
333	J004131-493611	4567.266 ± 0.032	12.011 ± 0.080	13.721 ± 3.171
334	J004131-493611	4566.449 ± 0.027	12.854 ± 0.046	22.323 ± 2.199
335	J004131-493611	4565.890 ± 0.106	12.108 ± 0.241	18.158 ± 6.925
336	J004131-493611	4564.138 ± 0.028	12.344 ± 0.043	22.323 ± 2.651
337	J004131-493611	4561.683 ± 0.031	12.980 ± 0.044	25.612 ± 1.959

Table E.1. *Continued*

338	J004131-493611	4561.007 ± 0.011	13.322 ± 0.024	23.502 ± 1.127
339	J004131-493611	4560.068 ± 0.078	12.771 ± 0.143	24.572 ± 6.399
340	J004131-493611	4559.516 ± 0.069	12.580 ± 0.221	19.457 ± 6.058
341	J004131-493611	4559.003 ± 0.055	11.861 ± 0.234	11.212 ± 5.391
342	J004131-493611	4557.763 ± 0.002	13.918 ± 0.003	27.350 ± 0.216
343	J004131-493611	4555.622 ± 0.005	13.274 ± 0.008	17.009 ± 0.314
344	J004131-493611	4554.636 ± 0.026	12.388 ± 0.049	19.437 ± 2.600
345	J004131-493611	4553.705 ± 0.087	12.588 ± 0.135	23.715 ± 6.217
346	J004131-493611	4552.533 ± 0.013	12.601 ± 0.023	19.823 ± 1.305
347	J004131-493611	4550.058 ± 0.190	12.593 ± 0.646	16.533 ± 6.284
348	J004131-493611	4549.742 ± 0.047	13.341 ± 0.116	18.076 ± 1.709
349	J004131-493611	4548.696 ± 0.029	12.616 ± 0.052	22.203 ± 2.823
350	J004131-493611	4547.483 ± 0.054	12.531 ± 0.046	43.103 ± 5.678
351	J004131-493611	4543.382 ± 0.028	12.776 ± 0.044	22.416 ± 2.157
352	J004131-493611	4542.728 ± 0.156	11.864 ± 0.486	20.192 ± 23.792
353	J004131-493611	4541.802 ± 0.024	12.175 ± 0.060	13.941 ± 2.593
354	J004131-493611	4540.707 ± 0.488	12.017 ± 0.846	23.626 ± 24.693
355	J004131-493611	4540.197 ± 0.065	12.821 ± 0.132	22.104 ± 3.014
356	J004131-493611	4538.366 ± 0.079	12.107 ± 0.192	20.933 ± 6.438
357	J004131-493611	4537.554 ± 0.015	13.296 ± 0.014	36.635 ± 1.277
358	J004131-493611	4536.191 ± 0.069	11.786 ± 0.136	17.509 ± 6.728
359	J004131-493611	4535.459 ± 0.031	11.845 ± 0.106	10.214 ± 3.202
360	J004131-493611	4534.342 ± 0.010	14.172 ± 0.015	33.362 ± 0.495
361	J004131-493611	4533.251 ± 0.006	14.788 ± 0.029	27.803 ± 0.954
362	J004131-493611	4532.751 ± 0.824	13.252 ± 0.505	65.637 ± 27.031
363	J004131-493611	4529.300 ± 0.168	12.522 ± 0.099	65.886 ± 16.948
364	J004131-493611	4528.231 ± 0.121	12.381 ± 0.427	16.306 ± 15.755
365	J004131-493611	4526.291 ± 0.035	12.533 ± 0.181	11.031 ± 2.158
366	J004131-493611	4525.847 ± 0.047	12.706 ± 0.122	23.050 ± 6.999
367	J004131-493611	4524.788 ± 0.012	12.897 ± 0.020	25.512 ± 1.473
368	J004131-493611	4522.819 ± 0.037	12.217 ± 0.070	20.126 ± 4.188
369	J004131-493611	4521.959 ± 0.002	13.840 ± 0.004	21.013 ± 0.171
370	J004131-493611	4520.711 ± 0.004	13.368 ± 0.005	29.243 ± 0.424
371	J004131-493611	4517.659 ± 0.004	13.226 ± 0.006	21.101 ± 0.331
372	J004131-493611	4516.219 ± 0.031	12.917 ± 0.051	20.341 ± 1.748
373	J004131-493611	4515.263 ± 0.003	13.889 ± 0.003	27.107 ± 0.294
374	J004131-493611	4514.167 ± 0.004	13.457 ± 0.006	26.293 ± 0.486
375	J004131-493611	4513.196 ± 0.046	12.242 ± 0.069	24.318 ± 4.638
376	J004131-493611	4510.556 ± 0.018	12.540 ± 0.029	22.016 ± 1.858
377	J004131-493611	4509.433 ± 0.018	12.478 ± 0.050	19.142 ± 1.997
378	J004131-493611	4508.042 ± 0.175	12.814 ± 0.129	56.805 ± 15.661
379	J004131-493611	4507.138 ± 0.017	12.925 ± 0.085	27.159 ± 2.300
380	J004131-493611	4506.371 ± 0.050	11.644 ± 0.172	10.618 ± 5.167
381	J004131-493611	4503.089 ± 0.035	11.831 ± 0.103	11.265 ± 3.645

Table E.1. *Continued*

382	J004131-493611	4502.188 ± 0.041	12.063 ± 0.106	15.593 ± 5.166
383	J004131-493611	4501.546 ± 0.062	11.788 ± 0.184	13.125 ± 7.282
384	J004131-493611	4501.037 ± 0.058	12.159 ± 0.269	13.194 ± 5.412
385	J004131-493611	4500.607 ± 0.015	13.169 ± 0.025	20.316 ± 1.033
386	J004131-493611	4498.875 ± 0.036	12.413 ± 0.045	28.220 ± 3.426
387	J004131-493611	4496.580 ± 0.059	13.428 ± 0.045	62.395 ± 4.101
388	J004131-493611	4496.600 ± 0.003	14.739 ± 0.045	17.359 ± 0.448
389	J004131-493611	4495.974 ± 0.043	12.251 ± 0.269	10.477 ± 4.432
390	J004131-493611	4495.044 ± 0.007	13.488 ± 0.020	26.237 ± 1.119
391	J004131-493611	4493.914 ± 0.013	15.095 ± 0.076	23.728 ± 0.776
392	J004131-493611	4493.000 ± 0.030	14.357 ± 0.022	51.041 ± 1.370
393	J004131-493611	4491.494 ± 0.017	12.762 ± 0.065	15.671 ± 1.586
394	J004131-493611	4490.808 ± 0.004	14.089 ± 0.024	22.554 ± 0.694
395	J004131-493611	4489.870 ± 0.028	13.989 ± 0.075	55.787 ± 9.778
396	J004131-493611	4488.804 ± 0.006	14.489 ± 0.018	27.477 ± 0.912
397	J004131-493611	4487.524 ± 0.004	14.250 ± 0.005	36.152 ± 0.616
398	J004131-493611	4486.140 ± 0.162	12.814 ± 0.244	40.336 ± 21.163
399	J004131-493611	4485.645 ± 0.032	12.276 ± 0.425	14.820 ± 5.878
400	J004131-493611	4484.953 ± 0.008	13.643 ± 0.011	29.092 ± 0.599
401	J004131-493611	4483.468 ± 0.060	12.141 ± 0.106	21.465 ± 5.666
402	J004131-493611	4482.632 ± 0.220	11.991 ± 0.290	26.435 ± 17.080
403	J004131-493611	4480.530 ± 0.042	11.729 ± 0.121	11.630 ± 4.270
404	J004131-493611	4479.116 ± 0.041	11.692 ± 0.131	10.347 ± 4.178
405	J004131-493611	4477.876 ± 0.006	14.148 ± 0.007	31.843 ± 0.359
406	J004131-493611	4477.031 ± 0.027	13.332 ± 0.036	30.366 ± 1.708
407	J004131-493611	4475.976 ± 0.021	12.463 ± 0.050	18.215 ± 2.612
408	J004131-493611	4475.478 ± 0.013	12.477 ± 0.080	10.824 ± 1.525
409	J004131-493611	4475.003 ± 0.006	13.443 ± 0.009	23.193 ± 0.507
410	J004131-493611	4473.104 ± 0.221	12.175 ± 0.328	26.771 ± 12.957
411	J004131-493611	4472.450 ± 0.027	13.088 ± 0.040	26.382 ± 1.570
412	J004131-493611	4470.061 ± 0.044	12.022 ± 0.110	15.673 ± 4.081
413	J004131-493611	4469.314 ± 0.032	12.742 ± 0.095	26.763 ± 3.470
414	J004131-493611	4468.319 ± 0.080	12.843 ± 0.128	48.016 ± 13.737
415	J004131-493611	4467.426 ± 0.031	11.895 ± 0.215	10.735 ± 4.095
416	J004131-493611	4466.829 ± 0.167	12.686 ± 0.136	51.549 ± 14.714
417	J004131-493611	4465.210 ± 0.015	12.900 ± 0.021	28.170 ± 1.603
418	J004131-493611	4463.125 ± 0.019	13.529 ± 0.018	56.780 ± 1.762
419	J004131-493611	4463.013 ± 0.009	13.200 ± 0.037	20.072 ± 1.131
420	J004131-493611	4461.813 ± 0.027	12.675 ± 0.051	26.371 ± 2.446
421	J004131-493611	4459.257 ± 0.092	13.398 ± 0.045	74.650 ± 4.913
422	J004131-493611	4458.732 ± 0.012	13.018 ± 0.058	21.071 ± 1.627
423	J004131-493611	4457.979 ± 0.008	13.252 ± 0.031	19.378 ± 0.916
424	J004131-493611	4456.983 ± 0.046	11.820 ± 0.148	13.312 ± 4.931
425	J004131-493611	4454.599 ± 0.125	12.203 ± 0.165	32.445 ± 10.646

Table E.1. *Continued*

426	J004131-493611	4453.402 ± 0.004	13.406 ± 0.018	18.861 ± 0.481
427	J004131-493611	4453.022 ± 0.065	13.193 ± 0.043	57.118 ± 3.149
428	J004131-493611	4450.715 ± 0.048	12.721 ± 0.073	23.208 ± 3.323
429	J004131-493611	4450.307 ± 0.016	12.575 ± 0.107	12.424 ± 1.674
430	J004131-493611	4449.570 ± 0.004	13.661 ± 0.005	33.287 ± 0.508
431	J004131-493611	4448.356 ± 0.002	13.863 ± 0.005	23.040 ± 0.225
432	J004131-493611	4447.458 ± 0.038	13.013 ± 0.031	43.576 ± 3.148
433	J004131-493611	4444.993 ± 0.029	13.431 ± 0.023	44.865 ± 1.891
434	J004131-493611	4444.327 ± 0.026	12.585 ± 0.153	20.636 ± 3.736
435	J004131-493611	4443.618 ± 0.016	12.795 ± 0.026	23.051 ± 1.529
436	J004131-493611	4442.394 ± 0.005	13.206 ± 0.011	21.711 ± 0.463
437	J004131-493611	4441.375 ± 0.066	12.598 ± 0.053	47.292 ± 6.943
438	J004131-493611	4438.400 ± 0.479	12.657 ± 0.253	69.369 ± 27.482
439	J004131-493611	4437.490 ± 0.003	14.008 ± 0.011	31.530 ± 0.471
440	J004131-493611	4436.189 ± 0.002	14.584 ± 0.013	30.643 ± 0.409
441	J004131-493611	4435.020 ± 0.051	12.544 ± 0.067	28.688 ± 4.447
442	J004131-493611	4433.555 ± 0.090	13.026 ± 0.195	25.717 ± 3.190
443	J004131-493611	4433.063 ± 0.157	12.912 ± 0.255	28.055 ± 6.298
444	J004131-493611	4431.997 ± 0.021	12.304 ± 0.045	17.311 ± 2.250
445	J004131-493611	4431.006 ± 0.006	13.642 ± 0.008	25.286 ± 0.452
446	J004131-493611	4430.368 ± 0.009	13.180 ± 0.022	19.111 ± 0.812
447	J004131-493611	4429.183 ± 0.002	14.600 ± 0.011	29.489 ± 0.226
448	J004131-493611	4427.086 ± 0.059	12.417 ± 0.087	24.875 ± 4.952
449	J004131-493611	4426.469 ± 0.026	12.574 ± 0.060	19.021 ± 2.113
450	J004131-493611	4425.484 ± 0.031	13.338 ± 0.165	21.310 ± 1.736
451	J004131-493611	4425.033 ± 0.055	13.709 ± 0.074	30.927 ± 2.858
452	J004131-493611	4423.784 ± 0.057	12.751 ± 0.074	39.621 ± 7.374
453	J004131-493611	4422.155 ± 0.084	13.108 ± 0.083	41.842 ± 6.224
454	J004131-493611	4421.017 ± 0.005	14.976 ± 0.035	30.151 ± 0.822
455	J004131-493611	4419.935 ± 0.083	13.112 ± 0.214	34.902 ± 15.651
456	J004131-493611	4419.176 ± 0.007	13.761 ± 0.018	22.431 ± 0.376
457	J004131-493611	4416.722 ± 0.008	13.235 ± 0.010	28.539 ± 0.805
458	J004131-493611	4416.124 ± 0.026	12.296 ± 0.145	10.959 ± 2.593
459	J004131-493611	4415.696 ± 0.004	13.627 ± 0.007	18.892 ± 0.309
460	J004131-493611	4414.268 ± 0.014	12.437 ± 0.030	16.729 ± 1.456
461	J004131-493611	4412.735 ± 0.024	12.207 ± 0.069	13.071 ± 2.317
462	J004131-493611	4412.076 ± 0.002	13.817 ± 0.003	21.872 ± 0.206
463	J004131-493611	4410.883 ± 0.032	12.643 ± 0.039	35.871 ± 4.233
464	J004131-493611	4409.845 ± 0.038	12.056 ± 0.099	15.920 ± 4.494
465	J004131-493611	4408.908 ± 0.027	12.572 ± 0.036	30.890 ± 3.356
466	J004131-493611	4407.795 ± 0.013	13.664 ± 0.024	22.908 ± 0.686
467	J004131-493611	4407.147 ± 0.047	13.008 ± 0.223	25.065 ± 11.725
468	J004131-493611	4406.646 ± 0.056	12.508 ± 0.309	14.399 ± 3.786
469	J004131-493611	4406.089 ± 0.051	11.609 ± 0.166	10.684 ± 5.436

Table E.1. *Continued*

470	J004131-493611	4402.852 ± 0.040	12.500 ± 0.062	23.226 ± 3.552
471	J004131-493611	4402.084 ± 0.080	11.694 ± 0.233	12.206 ± 7.822
472	J004131-493611	4399.554 ± 0.079	12.993 ± 0.186	34.132 ± 2.571
473	J004131-493611	4399.371 ± 0.004	13.793 ± 0.029	21.798 ± 0.497
474	J004131-493611	4396.811 ± 0.094	12.065 ± 0.138	25.520 ± 8.602
475	J004131-493611	4395.802 ± 0.122	13.388 ± 0.214	27.615 ± 4.660
476	J004131-493611	4395.295 ± 0.027	13.974 ± 0.061	25.959 ± 1.454
477	J004131-493611	4394.343 ± 0.016	12.483 ± 0.140	12.623 ± 2.285
478	J004131-493611	4394.155 ± 0.085	13.324 ± 0.062	51.588 ± 4.737
479	J004131-493611	4388.994 ± 0.010	13.005 ± 0.020	23.935 ± 1.201
480	J004131-493611	4388.024 ± 0.024	12.775 ± 0.038	34.127 ± 3.664
481	J004131-493611	4386.936 ± 0.045	12.348 ± 0.084	27.456 ± 6.215
482	J004131-493611	4386.060 ± 0.002	13.723 ± 0.003	20.612 ± 0.214
483	J004131-493611	4384.763 ± 0.050	12.101 ± 0.070	26.269 ± 5.164
484	J004131-493611	4383.442 ± 0.038	12.193 ± 0.087	15.790 ± 3.651
485	J004131-493611	4382.014 ± 0.029	12.054 ± 0.065	15.931 ± 3.105
486	J004131-493611	4379.162 ± 0.042	11.767 ± 0.133	11.234 ± 4.746
487	J004131-493611	4376.873 ± 0.117	12.147 ± 0.257	21.797 ± 7.503
488	J004131-493611	4376.243 ± 0.039	12.938 ± 0.041	28.451 ± 2.369
489	J004131-493611	4375.055 ± 0.012	12.193 ± 0.039	10.125 ± 1.220
490	J004131-493611	4374.192 ± 0.011	12.766 ± 0.016	23.866 ± 1.043
491	J004131-493611	4372.791 ± 0.064	12.571 ± 0.213	12.188 ± 3.037
492	J004131-493611	4372.497 ± 0.008	13.452 ± 0.052	11.774 ± 0.977
493	J004131-493611	4371.903 ± 0.008	14.165 ± 0.016	25.599 ± 1.342
494	J004131-493611	4371.255 ± 0.027	13.476 ± 0.069	21.065 ± 2.076
495	J004131-493611	4370.752 ± 0.052	12.009 ± 0.298	11.137 ± 4.634
496	J004131-493611	4369.872 ± 0.074	13.087 ± 0.090	32.465 ± 4.117
497	J004131-493611	4368.336 ± 0.017	13.354 ± 0.024	26.973 ± 1.442
498	J004131-493611	4365.279 ± 0.030	13.520 ± 0.020	52.469 ± 2.855
499	J004131-493611	4363.861 ± 0.005	13.469 ± 0.011	25.038 ± 0.649
500	J004131-493611	4360.985 ± 0.084	11.952 ± 0.235	12.110 ± 6.489
501	J004131-493611	4358.206 ± 0.016	12.796 ± 0.022	27.938 ± 1.712
502	J004131-493611	4357.487 ± 0.027	12.265 ± 0.088	16.233 ± 3.313
503	J004131-493611	4356.822 ± 0.042	12.389 ± 0.075	22.399 ± 3.942
504	J004131-493611	4355.474 ± 0.001	14.781 ± 0.012	28.660 ± 0.193
505	J004131-493611	4353.101 ± 0.021	12.250 ± 0.042	17.745 ± 2.076
506	J212912-153841	5113.398 ± 0.032	11.874 ± 0.107	13.859 ± 4.447
507	J212912-153841	5109.871 ± 0.024	12.323 ± 0.046	22.696 ± 2.895
508	J212912-153841	5109.286 ± 0.074	11.431 ± 0.309	12.609 ± 6.926
509	J212912-153841	5108.619 ± 0.019	12.106 ± 0.044	17.656 ± 2.149
510	J212912-153841	5107.565 ± 0.049	12.227 ± 1.006	20.673 ± 10.207
511	J212912-153841	5107.253 ± 0.532	12.370 ± 0.739	30.481 ± 12.337
512	J212912-153841	5101.851 ± 0.040	12.608 ± 0.144	14.167 ± 1.403
513	J212912-153841	5101.460 ± 0.020	13.137 ± 0.048	17.559 ± 1.428

Table E.1. *Continued*

514	J212912-153841	5100.907 ± 0.036	12.287 ± 0.288	10.421 ± 2.635
515	J212912-153841	5100.556 ± 0.052	12.644 ± 0.176	15.943 ± 6.016
516	J212912-153841	5100.067 ± 0.035	12.255 ± 0.192	10.624 ± 2.733
517	J212912-153841	5099.598 ± 0.008	13.060 ± 0.012	21.366 ± 0.571
518	J212912-153841	5098.411 ± 0.020	12.670 ± 0.030	22.695 ± 1.390
519	J212912-153841	5097.716 ± 0.050	12.246 ± 0.169	18.774 ± 6.559
520	J212912-153841	5096.560 ± 0.065	12.283 ± 0.089	38.637 ± 9.437
521	J212912-153841	5095.240 ± 0.048	12.068 ± 0.153	15.197 ± 5.976
522	J212912-153841	5092.384 ± 0.031	12.444 ± 0.082	11.984 ± 1.430
523	J212912-153841	5091.583 ± 0.017	12.586 ± 0.038	13.349 ± 0.969
524	J212912-153841	5090.304 ± 0.044	11.722 ± 0.063	21.233 ± 3.714
525	J212912-153841	5087.913 ± 0.011	12.714 ± 0.015	21.431 ± 0.828
526	J212912-153841	5086.733 ± 0.051	12.516 ± 0.150	16.341 ± 4.612
527	J212912-153841	5086.291 ± 0.014	12.885 ± 0.130	14.050 ± 1.800
528	J212912-153841	5085.828 ± 0.022	13.286 ± 0.042	22.456 ± 1.804
529	J212912-153841	5084.847 ± 0.010	13.294 ± 0.009	34.872 ± 0.611
530	J212912-153841	5081.830 ± 1.227	12.928 ± 1.449	38.316 ± 26.050
531	J212912-153841	5081.563 ± 0.025	13.528 ± 0.325	24.961 ± 3.471
532	J212912-153841	5080.873 ± 0.013	12.780 ± 0.192	15.018 ± 1.735
533	J212912-153841	5080.469 ± 0.190	12.795 ± 0.224	33.661 ± 11.638
534	J212912-153841	5079.378 ± 0.125	11.922 ± 0.202	24.370 ± 7.267
535	J212912-153841	5078.400 ± 0.010	12.273 ± 0.027	10.561 ± 0.706
536	J212912-153841	5077.348 ± 0.031	11.841 ± 0.061	15.388 ± 2.684
537	J212912-153841	5075.531 ± 0.039	12.859 ± 0.055	22.392 ± 1.712
538	J212912-153841	5074.792 ± 0.106	12.259 ± 0.903	10.320 ± 10.494
539	J212912-153841	5074.492 ± 0.137	12.417 ± 0.332	15.348 ± 6.614
540	J212912-153841	5073.740 ± 0.004	13.279 ± 0.006	23.373 ± 0.389
541	J212912-153841	5072.218 ± 0.011	12.961 ± 0.011	31.399 ± 0.951
542	J212912-153841	5071.122 ± 0.005	13.139 ± 0.012	12.983 ± 0.309
543	J212912-153841	5068.010 ± 0.010	12.318 ± 0.026	14.633 ± 0.992
544	J212912-153841	5067.214 ± 0.007	12.835 ± 0.009	26.402 ± 0.668
545	J212912-153841	5065.691 ± 0.016	13.442 ± 0.081	17.545 ± 0.984
546	J212912-153841	5065.240 ± 0.011	14.236 ± 0.014	29.220 ± 0.310
547	J212912-153841	5063.436 ± 0.024	12.507 ± 0.049	22.986 ± 2.845
548	J212912-153841	5062.653 ± 0.006	13.486 ± 0.015	19.513 ± 0.515
549	J212912-153841	5062.114 ± 0.044	12.575 ± 0.106	18.054 ± 2.758
550	J212912-153841	5061.115 ± 0.036	11.697 ± 0.091	12.098 ± 3.278
551	J212912-153841	5059.635 ± 0.015	12.283 ± 0.021	22.420 ± 1.313
552	J212912-153841	5058.274 ± 0.030	12.389 ± 0.035	30.059 ± 2.689
553	J212912-153841	5057.064 ± 0.076	12.833 ± 0.097	28.181 ± 4.222
554	J212912-153841	5056.611 ± 0.023	12.539 ± 0.206	15.761 ± 2.722
555	J212912-153841	5056.025 ± 0.009	13.145 ± 0.034	21.762 ± 1.533
556	J212912-153841	5055.313 ± 0.004	13.793 ± 0.005	23.076 ± 0.176
557	J212912-153841	5053.611 ± 0.045	12.175 ± 0.117	24.313 ± 6.068

Table E.1. *Continued*

558	J212912-153841	5052.101 ± 0.091	12.740 ± 0.076	55.390 ± 9.671
559	J212912-153841	5051.023 ± 0.003	13.844 ± 0.008	25.452 ± 0.291
560	J212912-153841	5049.865 ± 0.021	13.592 ± 0.022	34.659 ± 0.971
561	J212912-153841	5048.408 ± 0.005	13.482 ± 0.008	25.184 ± 0.422
562	J212912-153841	5047.618 ± 0.014	13.094 ± 0.018	27.139 ± 0.807
563	J212912-153841	5046.270 ± 0.003	12.941 ± 0.005	21.584 ± 0.292
564	J212912-153841	5043.848 ± 0.082	13.479 ± 0.059	50.557 ± 2.607
565	J212912-153841	5043.226 ± 0.003	13.870 ± 0.023	30.113 ± 0.468
566	J212912-153841	5041.690 ± 0.001	14.054 ± 0.001	25.700 ± 0.068
567	J212912-153841	5039.125 ± 0.018	12.440 ± 0.017	33.174 ± 1.529
568	J212912-153841	5036.044 ± 0.153	12.079 ± 0.125	39.740 ± 9.168
569	J212912-153841	5034.796 ± 0.006	13.659 ± 0.009	24.331 ± 0.420
570	J212912-153841	5034.123 ± 0.004	13.677 ± 0.009	19.997 ± 0.359
571	J212912-153841	5033.441 ± 0.015	12.625 ± 0.045	15.138 ± 1.557
572	J212912-153841	5032.695 ± 0.001	13.698 ± 0.002	19.712 ± 0.130
573	J212912-153841	5031.990 ± 0.034	11.666 ± 0.118	11.375 ± 3.775
574	J212912-153841	5031.423 ± 0.052	11.770 ± 0.156	13.720 ± 5.683
575	J212912-153841	5030.902 ± 0.063	12.205 ± 0.209	12.729 ± 5.100
576	J212912-153841	5024.139 ± 0.011	12.519 ± 0.015	23.181 ± 0.987
577	J212912-153841	5023.278 ± 0.025	12.051 ± 0.068	15.784 ± 2.318
578	J212912-153841	5022.519 ± 0.021	12.411 ± 0.039	25.853 ± 2.992
579	J212912-153841	5021.711 ± 0.030	11.999 ± 0.108	14.548 ± 2.986
580	J212912-153841	5020.847 ± 0.012	12.792 ± 0.122	18.069 ± 1.714
581	J212912-153841	5020.752 ± 0.020	13.223 ± 0.047	32.884 ± 1.030
582	J212912-153841	5019.390 ± 0.050	11.822 ± 0.133	13.270 ± 3.758
583	J212912-153841	5018.630 ± 0.010	14.183 ± 0.018	19.506 ± 0.399
584	J212912-153841	5018.026 ± 0.011	14.017 ± 0.033	17.757 ± 1.161
585	J212912-153841	5017.487 ± 0.011	14.057 ± 0.017	23.938 ± 0.353
586	J212912-153841	5015.550 ± 0.020	12.133 ± 0.029	21.073 ± 1.705
587	J212912-153841	5013.734 ± 0.008	12.668 ± 0.024	21.884 ± 0.820
588	J212912-153841	5012.287 ± 0.064	12.921 ± 0.050	60.613 ± 7.281
589	J212912-153841	5011.669 ± 0.029	11.616 ± 0.240	10.499 ± 4.066
590	J212912-153841	5010.754 ± 0.008	13.216 ± 0.015	30.824 ± 0.666
591	J212912-153841	5009.696 ± 0.027	12.307 ± 0.059	19.159 ± 2.735
592	J212912-153841	5009.106 ± 0.010	12.721 ± 0.039	14.223 ± 1.252
593	J212912-153841	5008.398 ± 0.007	12.601 ± 0.023	13.473 ± 0.912
594	J212912-153841	5007.640 ± 0.062	12.014 ± 0.143	13.242 ± 3.734
595	J212912-153841	5006.125 ± 0.005	13.656 ± 0.048	17.567 ± 0.533
596	J212912-153841	5005.971 ± 0.024	13.678 ± 0.037	29.924 ± 1.304
597	J212912-153841	5004.966 ± 0.022	13.247 ± 0.026	30.770 ± 1.247
598	J212912-153841	5003.720 ± 0.003	13.131 ± 0.005	23.422 ± 0.285
599	J212912-153841	5001.820 ± 0.003	13.242 ± 0.003	25.507 ± 0.228
600	J212912-153841	4999.266 ± 0.047	12.128 ± 0.085	17.078 ± 3.290
601	J212912-153841	4997.715 ± 0.041	11.640 ± 0.090	14.821 ± 3.697

Table E.1. *Continued*

602	J212912-153841	4996.356 ± 0.735	12.475 ± 1.528	21.675 ± 23.362
603	J212912-153841	4996.116 ± 0.032	12.678 ± 0.819	14.910 ± 5.044
604	J212912-153841	4995.421 ± 0.048	13.374 ± 0.043	53.456 ± 4.648
605	J212912-153841	4994.352 ± 0.001	13.811 ± 0.004	19.153 ± 0.122
606	J212912-153841	4993.530 ± 0.008	12.871 ± 0.011	22.939 ± 0.633
607	J212912-153841	4991.928 ± 0.042	12.417 ± 0.079	17.960 ± 2.384
608	J212912-153841	4991.534 ± 0.031	12.127 ± 0.300	11.904 ± 3.449
609	J212912-153841	4990.944 ± 0.111	12.495 ± 0.338	33.161 ± 25.950
610	J212912-153841	4990.245 ± 0.035	12.524 ± 0.228	19.080 ± 4.165
611	J212912-153841	4989.540 ± 0.005	13.290 ± 0.013	22.638 ± 0.768
612	J212912-153841	4988.242 ± 0.012	12.253 ± 0.022	17.501 ± 1.085
613	J212912-153841	4986.864 ± 0.038	11.597 ± 0.085	13.469 ± 3.380
614	J212912-153841	4985.481 ± 0.006	12.860 ± 0.007	24.946 ± 0.519
615	J212912-153841	4984.383 ± 0.013	12.570 ± 0.019	21.915 ± 1.169
616	J212912-153841	4982.830 ± 0.007	14.881 ± 0.011	31.958 ± 0.274
617	J212912-153841	4982.055 ± 0.118	13.420 ± 0.144	34.695 ± 3.102
618	J212912-153841	4979.032 ± 0.017	12.086 ± 0.029	18.051 ± 1.473
619	J212912-153841	4973.496 ± 0.007	13.270 ± 0.019	41.357 ± 1.290
620	J212912-153841	4973.519 ± 0.002	13.306 ± 0.019	18.106 ± 0.346
621	J212912-153841	4971.886 ± 0.346	12.265 ± 0.526	24.073 ± 13.933
622	J212912-153841	4971.493 ± 0.036	12.593 ± 0.332	15.855 ± 5.044
623	J212912-153841	4971.109 ± 0.059	12.369 ± 0.221	13.712 ± 3.097
624	J212912-153841	4970.501 ± 0.011	12.891 ± 0.014	25.173 ± 0.823
625	J212912-153841	4967.369 ± 0.208	12.228 ± 0.284	25.362 ± 8.772
626	J212912-153841	4966.840 ± 0.040	12.833 ± 0.169	18.466 ± 3.465
627	J212912-153841	4966.418 ± 0.126	12.382 ± 0.321	17.653 ± 4.677
628	J212912-153841	4965.348 ± 0.032	12.338 ± 0.046	31.105 ± 3.958
629	J212912-153841	4964.030 ± 0.019	12.893 ± 0.019	34.660 ± 1.443
630	J212912-153841	4962.572 ± 0.037	12.317 ± 0.050	22.886 ± 2.602
631	J212912-153841	4958.850 ± 0.001	13.665 ± 0.002	26.626 ± 0.122
632	J212912-153841	4957.957 ± 0.013	12.401 ± 0.023	18.854 ± 1.058
633	J212912-153841	4956.191 ± 0.030	11.664 ± 0.083	12.063 ± 2.690
634	J212912-153841	4955.462 ± 0.019	12.284 ± 0.026	23.922 ± 1.797
635	J212912-153841	4953.593 ± 0.085	11.589 ± 0.312	13.245 ± 5.642
636	J212912-153841	4953.106 ± 0.011	12.915 ± 0.016	21.115 ± 0.708
637	J212912-153841	4951.366 ± 0.050	12.703 ± 0.097	22.540 ± 1.916
638	J212912-153841	4950.507 ± 0.017	13.080 ± 0.847	23.922 ± 7.438
639	J212912-153841	4950.241 ± 0.729	13.000 ± 1.066	33.386 ± 14.917
640	J212912-153841	4947.939 ± 0.006	12.847 ± 0.008	25.947 ± 0.604
641	J212912-153841	4947.152 ± 0.035	11.946 ± 0.152	13.133 ± 2.958
642	J212912-153841	4946.573 ± 0.010	12.841 ± 0.029	23.254 ± 1.857
643	J212912-153841	4945.333 ± 0.036	12.325 ± 0.040	36.018 ± 4.312
644	J212912-153841	4944.199 ± 0.026	12.153 ± 0.096	15.952 ± 2.136
645	J212912-153841	4943.480 ± 0.013	12.889 ± 0.032	29.879 ± 2.442

Table E.1. *Continued*

646	J212912-153841	4942.514 ± 0.005	13.243 ± 0.013	25.473 ± 0.698
647	J212912-153841	4941.549 ± 0.014	13.189 ± 0.030	26.140 ± 1.148
648	J212912-153841	4940.820 ± 0.031	13.032 ± 0.038	29.984 ± 1.532
649	J212912-153841	4938.739 ± 0.095	12.359 ± 0.061	54.013 ± 7.066
650	J212912-153841	4936.035 ± 0.033	11.822 ± 0.156	15.305 ± 4.141
651	J212912-153841	4935.227 ± 0.159	12.030 ± 0.116	44.940 ± 13.101
652	J212912-153841	4932.682 ± 0.015	12.752 ± 0.011	46.251 ± 1.402
653	J212912-153841	4930.862 ± 0.005	13.349 ± 0.010	24.141 ± 0.374
654	J212912-153841	4929.349 ± 0.001	13.674 ± 0.002	25.693 ± 0.124
655	J212912-153841	4928.085 ± 0.017	12.820 ± 0.017	44.120 ± 2.156
656	J212912-153841	4926.290 ± 0.005	13.327 ± 0.005	39.606 ± 0.533
657	J212912-153841	4925.270 ± 0.043	11.845 ± 0.349	15.136 ± 5.553
658	J212912-153841	4924.572 ± 0.018	12.999 ± 0.047	36.979 ± 4.501
659	J212912-153841	4923.839 ± 0.024	11.948 ± 0.203	12.500 ± 3.203
660	J212912-153841	4923.014 ± 0.002	13.796 ± 0.002	23.859 ± 0.158
661	J212912-153841	4921.618 ± 0.025	15.570 ± 0.070	24.364 ± 0.483
662	J212912-153841	4920.762 ± 0.101	13.951 ± 0.294	24.751 ± 7.712
663	J212912-153841	4920.071 ± 0.116	13.898 ± 0.134	35.357 ± 6.341
664	J212912-153841	4919.105 ± 0.139	12.268 ± 0.813	19.753 ± 17.781
665	J212912-153841	4918.557 ± 0.080	12.554 ± 0.291	20.020 ± 10.115
666	J212912-153841	4916.383 ± 0.056	13.406 ± 0.016	36.301 ± 3.104
667	J212912-153841	4915.523 ± 0.006	14.068 ± 0.015	18.616 ± 0.804
668	J212912-153841	4914.604 ± 0.006	14.676 ± 0.027	23.914 ± 1.250
669	J212912-153841	4913.945 ± 0.173	13.012 ± 0.335	23.309 ± 4.405
670	J212912-153841	4911.331 ± 0.024	12.385 ± 0.045	16.860 ± 1.709
671	J212912-153841	4910.087 ± 0.006	12.960 ± 0.009	22.839 ± 0.553
672	J212912-153841	4909.491 ± 0.042	11.993 ± 0.118	11.251 ± 2.896
673	J212912-153841	4903.854 ± 0.008	12.599 ± 0.011	22.996 ± 0.672
674	J212912-153841	4901.954 ± 0.009	12.609 ± 0.011	26.757 ± 0.830
675	J212912-153841	4900.637 ± 0.038	12.280 ± 0.139	21.075 ± 2.806
676	J212912-153841	4899.836 ± 0.092	12.349 ± 0.187	38.083 ± 17.001
677	J212912-153841	4898.775 ± 0.017	12.834 ± 0.027	27.080 ± 1.028
678	J212912-153841	4896.503 ± 0.009	14.089 ± 0.049	26.707 ± 0.492
679	J212912-153841	4896.084 ± 0.463	13.008 ± 0.597	34.837 ± 11.460
680	J212912-153841	4893.819 ± 0.012	12.935 ± 0.012	32.633 ± 0.969
681	J212912-153841	4892.894 ± 0.002	13.615 ± 0.003	22.738 ± 0.126
682	J212912-153841	4891.446 ± 0.008	12.997 ± 0.008	30.077 ± 0.701
683	J212912-153841	4890.731 ± 0.057	11.540 ± 0.195	13.921 ± 5.100
684	J212912-153841	4888.395 ± 0.041	12.209 ± 0.091	19.967 ± 2.496
685	J212912-153841	4887.731 ± 0.022	12.766 ± 0.026	27.604 ± 1.447
686	J212912-153841	4885.414 ± 0.006	12.933 ± 0.008	26.410 ± 0.505
687	J212912-153841	4883.765 ± 0.014	13.346 ± 0.013	51.622 ± 1.189
688	J212912-153841	4883.536 ± 0.007	12.879 ± 0.041	21.855 ± 0.951
689	J212912-153841	4882.281 ± 0.054	11.734 ± 0.250	13.258 ± 4.478

Table E.1. *Continued*

690	J212912-153841	4881.769 ± 0.009	13.052 ± 0.013	24.066 ± 0.674
691	J212912-153841	4880.353 ± 0.025	12.399 ± 0.033	27.449 ± 2.188
692	J212912-153841	4879.056 ± 0.677	12.205 ± 0.776	34.978 ± 30.999
693	J212912-153841	4878.388 ± 0.052	13.046 ± 0.111	28.850 ± 2.249
694	J212912-153841	4877.485 ± 0.006	13.046 ± 0.019	14.232 ± 0.453
695	J212912-153841	4876.826 ± 0.003	13.993 ± 0.008	23.426 ± 0.309
696	J212912-153841	4875.712 ± 0.176	13.271 ± 0.197	43.529 ± 16.016
697	J212912-153841	4875.145 ± 0.012	13.698 ± 0.065	19.383 ± 1.050
698	J212912-153841	4874.242 ± 0.027	14.656 ± 0.044	26.112 ± 1.666
699	J212912-153841	4873.574 ± 0.065	13.609 ± 0.270	17.750 ± 4.362
700	J212912-153841	4872.983 ± 0.020	14.045 ± 0.041	28.558 ± 2.176
701	J212912-153841	4872.255 ± 0.070	12.877 ± 0.161	22.421 ± 2.171
702	J212912-153841	4869.605 ± 0.093	12.653 ± 0.064	46.687 ± 5.345
703	J212912-153841	4868.735 ± 0.007	13.872 ± 0.014	23.354 ± 0.385
704	J212912-153841	4868.199 ± 0.019	13.376 ± 0.035	22.271 ± 0.642
705	J212912-153841	4864.396 ± 0.013	13.015 ± 0.124	25.447 ± 1.749
706	J212912-153841	4864.022 ± 0.151	12.857 ± 0.180	37.881 ± 3.666
707	J212912-153841	4862.516 ± 0.090	12.449 ± 0.165	25.087 ± 4.282
708	J212912-153841	4861.484 ± 0.505	13.393 ± 0.692	33.451 ± 16.949
709	J212912-153841	4860.560 ± 0.020	14.938 ± 0.039	34.376 ± 3.629
710	J212912-153841	4859.471 ± 0.042	13.775 ± 0.087	24.248 ± 2.121
711	J212912-153841	4858.793 ± 0.061	12.281 ± 0.238	16.139 ± 4.726
712	J212912-153841	4858.231 ± 0.058	11.836 ± 0.142	15.798 ± 4.997
713	J212912-153841	4857.201 ± 0.616	12.289 ± 2.472	28.337 ± 30.092
714	J212912-153841	4856.375 ± 0.602	12.872 ± 0.919	44.162 ± 81.853
715	J212912-153841	4855.746 ± 0.257	12.460 ± 1.210	10.652 ± 10.396
716	J212912-153841	4853.930 ± 0.129	12.611 ± 0.385	30.266 ± 21.724
717	J212912-153841	4853.008 ± 0.013	13.664 ± 0.051	30.048 ± 2.799
718	J212912-153841	4852.379 ± 0.066	12.694 ± 0.660	20.656 ± 8.882
719	J212912-153841	4851.744 ± 0.242	13.388 ± 0.207	35.756 ± 12.054
720	J212912-153841	4851.301 ± 0.005	13.910 ± 0.051	19.531 ± 0.595
721	J212912-153841	4850.437 ± 0.065	12.998 ± 0.075	33.544 ± 3.641
722	J212912-153841	4848.697 ± 0.486	12.251 ± 0.642	35.814 ± 38.669
723	J212912-153841	4847.586 ± 0.884	13.326 ± 1.278	31.971 ± 29.587
724	J212912-153841	4847.217 ± 0.024	14.030 ± 0.243	24.227 ± 1.827
725	J212912-153841	4846.208 ± 0.112	13.233 ± 0.259	24.275 ± 3.671
726	J212912-153841	4845.753 ± 0.191	13.072 ± 0.446	25.606 ± 7.924
727	J212912-153841	4844.829 ± 0.333	12.605 ± 0.427	52.168 ± 48.207
728	J212912-153841	4843.756 ± 0.002	13.683 ± 0.012	21.832 ± 0.319
729	J212912-153841	4843.127 ± 0.036	12.333 ± 0.076	18.379 ± 2.491
730	J212912-153841	4842.027 ± 0.002	13.656 ± 0.003	32.587 ± 0.210
731	J212912-153841	4840.685 ± 0.014	13.002 ± 0.010	45.708 ± 1.199
732	J212912-153841	4836.992 ± 0.026	12.720 ± 0.222	23.839 ± 3.103
733	J212912-153841	4836.374 ± 0.336	12.550 ± 0.391	40.052 ± 26.290

Table E.1. *Continued*

734	J212912-153841	4835.311 ± 0.025	12.681 ± 0.055	26.510 ± 1.740
735	J212912-153841	4834.054 ± 0.016	12.766 ± 0.013	41.299 ± 1.504
736	J212912-153841	4829.925 ± 0.009	14.080 ± 0.046	20.284 ± 0.656
737	J212912-153841	4829.777 ± 0.010	14.109 ± 0.040	29.735 ± 0.500
738	J212912-153841	4828.399 ± 0.088	12.158 ± 0.191	36.752 ± 18.043
739	J212912-153841	4827.520 ± 0.032	12.250 ± 0.116	20.773 ± 3.165
740	J212912-153841	4826.452 ± 0.025	12.777 ± 0.038	42.399 ± 4.406
741	J212912-153841	4825.625 ± 0.092	12.244 ± 0.327	14.773 ± 4.653
742	J212912-153841	4825.099 ± 0.011	13.833 ± 0.031	19.219 ± 1.123
743	J212912-153841	4823.235 ± 0.005	18.654 ± 0.352	31.321 ± 1.256
744	J212912-153841	4821.887 ± 0.071	14.199 ± 0.048	59.824 ± 2.066
745	J212912-153841	4819.613 ± 0.025	12.293 ± 0.121	17.365 ± 2.154
746	J212912-153841	4817.991 ± 0.001	15.458 ± 0.020	40.674 ± 0.676
747	J212912-153841	4817.350 ± 1.299	13.319 ± 0.897	67.415 ± 29.532
748	J212912-153841	4812.760 ± 0.022	12.461 ± 0.096	27.972 ± 2.778
749	J212912-153841	4812.462 ± 0.029	13.025 ± 0.026	61.087 ± 1.920
750	J212912-153841	4810.334 ± 0.175	11.863 ± 0.391	24.197 ± 8.971
751	J212912-153841	4808.932 ± 2.330	13.447 ± 2.595	41.563 ± 57.585
752	J212912-153841	4808.500 ± 0.007	15.117 ± 0.016	27.810 ± 1.834
753	J212912-153841	4807.295 ± 0.107	11.820 ± 0.518	13.981 ± 6.433
754	J212912-153841	4804.615 ± 0.041	11.710 ± 0.086	16.066 ± 4.141
755	J212912-153841	4802.756 ± 0.025	12.221 ± 0.027	30.725 ± 2.284
756	J212912-153841	4801.144 ± 0.015	12.397 ± 0.018	28.496 ± 1.382
757	J212912-153841	4799.856 ± 0.006	12.190 ± 0.018	10.374 ± 0.566
758	J212912-153841	4797.900 ± 0.012	13.840 ± 0.019	25.192 ± 0.409
759	J212912-153841	4797.314 ± 0.008	13.859 ± 0.033	23.161 ± 1.050
760	J212912-153841	4796.692 ± 0.027	13.441 ± 0.087	25.008 ± 2.164
761	J212912-153841	4795.793 ± 0.115	12.499 ± 0.885	25.288 ± 12.310
762	J212912-153841	4795.542 ± 1.046	12.739 ± 0.807	52.964 ± 30.234
763	J212912-153841	4791.949 ± 0.008	13.517 ± 0.020	22.582 ± 0.373
764	J212912-153841	4790.956 ± 0.002	14.535 ± 0.008	22.512 ± 0.405
765	J212912-153841	4790.653 ± 0.677	12.840 ± 0.633	45.925 ± 17.758
766	J212912-153841	4785.493 ± 0.005	13.302 ± 0.005	30.896 ± 0.415
767	J212912-153841	4783.700 ± 0.003	13.265 ± 0.004	32.506 ± 0.324
768	J212912-153841	4782.671 ± 0.021	12.287 ± 0.109	18.517 ± 2.196
769	J212912-153841	4781.613 ± 0.143	12.580 ± 0.172	47.275 ± 23.396
770	J212912-153841	4780.319 ± 0.056	13.018 ± 0.051	43.681 ± 2.572
771	J212912-153841	4778.362 ± 0.010	12.613 ± 0.012	29.386 ± 0.941
772	J212912-153841	4774.759 ± 0.005	12.982 ± 0.007	25.426 ± 0.434
773	J212912-153841	4773.491 ± 0.030	12.972 ± 0.032	36.444 ± 2.448
774	J212912-153841	4772.790 ± 0.009	12.923 ± 0.033	21.132 ± 0.702
775	J212912-153841	4770.996 ± 0.016	14.097 ± 0.018	50.470 ± 0.379
776	J212912-153841	4770.591 ± 0.003	14.524 ± 0.007	30.118 ± 0.361
777	J212912-153841	4768.958 ± 0.049	11.999 ± 0.113	16.559 ± 4.194

Table E.1. *Continued*

778	J212912-153841	4768.521 ± 0.046	11.838 ± 0.152	12.751 ± 3.339
779	J212912-153841	4767.280 ± 0.054	12.452 ± 0.059	43.627 ± 4.427
780	J212912-153841	4765.456 ± 0.134	12.308 ± 0.157	67.602 ± 28.377
781	J212912-153841	4764.209 ± 0.078	11.666 ± 0.339	23.552 ± 10.350
782	J212912-153841	4762.543 ± 0.122	13.266 ± 0.138	38.346 ± 3.811
783	J212912-153841	4761.830 ± 0.023	13.894 ± 0.031	33.751 ± 1.087
784	J212912-153841	4761.632 ± 0.020	12.228 ± 0.201	10.088 ± 2.705
785	J212912-153841	4759.871 ± 0.053	13.350 ± 0.044	64.397 ± 8.904
786	J212912-153841	4758.337 ± 0.013	15.044 ± 0.026	29.702 ± 0.481
787	J212912-153841	4757.589 ± 0.654	13.343 ± 0.764	36.717 ± 32.712
788	J212912-153841	4756.453 ± 0.054	13.431 ± 0.238	11.890 ± 2.664
789	J212912-153841	4756.164 ± 0.023	14.419 ± 0.014	32.787 ± 2.046
790	J212912-153841	4755.388 ± 0.013	13.940 ± 0.043	19.212 ± 0.546
791	J212912-153841	4754.460 ± 0.092	12.509 ± 0.226	49.073 ± 27.730
792	J212912-153841	4753.570 ± 0.058	12.168 ± 0.309	18.396 ± 6.952
793	J212912-153841	4752.958 ± 0.028	13.016 ± 0.029	32.317 ± 1.674
794	J212912-153841	4751.347 ± 0.032	13.764 ± 0.064	22.950 ± 0.903
795	J212912-153841	4749.813 ± 0.009	16.560 ± 0.061	39.029 ± 0.557
796	J212912-153841	4747.842 ± 0.075	12.439 ± 0.422	10.698 ± 5.797
797	J212912-153841	4747.291 ± 0.065	12.687 ± 0.278	28.286 ± 20.254
798	J212912-153841	4742.657 ± 0.081	13.738 ± 0.154	21.952 ± 3.326
799	J212912-153841	4741.539 ± 0.036	13.750 ± 0.028	39.288 ± 1.589
800	J212912-153841	4741.261 ± 0.008	13.490 ± 0.063	21.022 ± 0.920
801	J212912-153841	4740.118 ± 0.038	12.811 ± 0.116	24.268 ± 2.614
802	J212912-153841	4739.425 ± 0.201	12.444 ± 0.296	33.563 ± 18.791
803	J212912-153841	4738.040 ± 0.033	12.953 ± 0.047	29.355 ± 2.937
804	J212912-153841	4737.203 ± 0.004	13.925 ± 0.016	11.455 ± 0.757
805	J212912-153841	4736.311 ± 0.016	12.848 ± 0.024	21.386 ± 1.050
806	J212912-153841	4734.961 ± 0.010	12.907 ± 0.013	26.085 ± 0.860
807	J212912-153841	4734.392 ± 0.045	11.831 ± 0.224	12.948 ± 4.605
808	J212912-153841	4733.936 ± 0.066	11.911 ± 0.127	17.572 ± 5.013
809	J212912-153841	4731.947 ± 0.038	12.586 ± 0.024	51.576 ± 3.918
810	J212912-153841	4730.566 ± 0.051	12.744 ± 0.088	23.656 ± 3.755
811	J212912-153841	4729.310 ± 0.085	12.470 ± 0.137	29.740 ± 4.315
812	J212912-153841	4727.345 ± 0.031	12.139 ± 0.037	28.061 ± 2.900
813	J212912-153841	4724.768 ± 1.056	14.288 ± 1.239	48.930 ± 18.531
814	J212912-153841	4724.570 ± 0.022	16.338 ± 0.164	27.228 ± 1.973
815	J212912-153841	4723.231 ± 0.071	13.227 ± 0.481	15.888 ± 5.719
816	J212912-153841	4722.717 ± 0.084	13.533 ± 0.335	25.466 ± 15.994
817	J212912-153841	4722.301 ± 0.014	13.658 ± 0.158	15.916 ± 1.142
818	J212912-153841	4721.437 ± 0.026	12.741 ± 0.041	30.728 ± 2.993
819	J212912-153841	4720.211 ± 0.063	12.231 ± 0.107	30.638 ± 8.231
820	J212912-153841	4719.266 ± 0.448	12.839 ± 1.021	21.323 ± 12.925
821	J212912-153841	4718.908 ± 0.037	13.602 ± 0.434	19.032 ± 4.538

Table E.1. *Continued*

822	J212912-153841	4718.489 ± 0.103	13.832 ± 0.186	25.581 ± 5.971
823	J212912-153841	4717.768 ± 0.008	13.933 ± 0.016	21.140 ± 0.266
824	J212912-153841	4716.239 ± 0.002	12.911 ± 0.005	13.520 ± 0.193
825	J212912-153841	4714.957 ± 0.005	13.998 ± 0.006	30.686 ± 0.401
826	J212912-153841	4713.920 ± 0.005	13.837 ± 0.009	23.035 ± 0.544
827	J212912-153841	4712.643 ± 0.019	12.853 ± 0.031	26.865 ± 1.902
828	J212912-153841	4711.884 ± 0.031	11.981 ± 0.078	16.414 ± 2.557
829	J212912-153841	4710.087 ± 0.012	12.574 ± 0.015	28.051 ± 1.172
830	J212912-153841	4708.897 ± 0.041	12.106 ± 0.046	31.190 ± 4.016
831	J212912-153841	4706.428 ± 0.017	12.816 ± 0.035	18.059 ± 0.898
832	J212912-153841	4705.919 ± 0.007	13.183 ± 0.039	19.063 ± 0.874
833	J212912-153841	4705.338 ± 0.190	12.353 ± 0.226	33.625 ± 12.927
834	J212912-153841	4704.149 ± 0.035	12.072 ± 0.229	22.346 ± 5.301
835	J212912-153841	4702.799 ± 0.016	12.382 ± 0.171	20.145 ± 3.272
836	J212912-153841	4702.381 ± 0.608	12.943 ± 0.225	84.795 ± 57.919
837	J212912-153841	4701.270 ± 0.010	13.233 ± 0.081	28.431 ± 1.792
838	J212912-153841	4700.321 ± 0.008	13.503 ± 0.023	33.507 ± 1.184
839	J212912-153841	4699.334 ± 0.009	13.271 ± 0.026	29.525 ± 1.555
840	J212912-153841	4698.684 ± 0.050	12.041 ± 0.414	16.104 ± 6.146
841	J212912-153841	4698.121 ± 0.053	12.765 ± 0.085	32.686 ± 6.274
842	J212912-153841	4697.331 ± 0.027	12.073 ± 0.137	14.868 ± 3.019
843	J212912-153841	4696.717 ± 0.012	12.703 ± 0.017	23.797 ± 1.081
844	J212912-153841	4692.772 ± 0.028	12.747 ± 0.018	54.612 ± 2.835
845	J212912-153841	4691.548 ± 0.090	11.859 ± 0.394	16.375 ± 8.004
846	J212912-153841	4690.756 ± 0.195	12.239 ± 0.357	34.270 ± 25.229
847	J212912-153841	4689.538 ± 0.317	12.155 ± 0.398	37.222 ± 30.329
848	J212912-153841	4688.362 ± 0.006	13.616 ± 0.010	25.328 ± 0.476
849	J212912-153841	4686.317 ± 0.004	13.571 ± 0.004	33.764 ± 0.466
850	J212912-153841	4685.296 ± 0.053	11.956 ± 0.152	19.416 ± 5.484
851	J212912-153841	4684.460 ± 0.016	12.988 ± 0.027	30.220 ± 2.011
852	J212912-153841	4683.326 ± 0.008	13.084 ± 0.013	24.734 ± 0.865
853	J212912-153841	4682.053 ± 0.002	13.732 ± 0.022	16.005 ± 0.422
854	J212912-153841	4682.078 ± 0.006	13.540 ± 0.035	31.732 ± 1.188
855	J212912-153841	4680.494 ± 0.033	12.989 ± 0.066	20.288 ± 2.213
856	J212912-153841	4678.002 ± 0.007	13.279 ± 0.012	24.029 ± 0.671
857	J212912-153841	4676.940 ± 0.007	12.613 ± 0.028	13.453 ± 0.824
858	J212912-153841	4676.348 ± 0.050	12.478 ± 0.121	20.687 ± 5.031
859	J212912-153841	4673.723 ± 0.035	12.464 ± 0.058	26.371 ± 3.955
860	J212912-153841	4673.191 ± 0.031	11.922 ± 0.175	12.930 ± 3.185
861	J212912-153841	4672.105 ± 0.293	12.311 ± 0.414	31.727 ± 25.098
862	J212912-153841	4671.599 ± 0.032	12.408 ± 0.280	17.540 ± 3.518
863	J212912-153841	4670.962 ± 0.071	12.622 ± 0.058	41.638 ± 4.766
864	J212912-153841	4669.355 ± 0.055	12.438 ± 0.204	15.751 ± 2.663
865	J212912-153841	4668.783 ± 0.251	12.030 ± 0.555	28.091 ± 36.007

Table E.1. *Continued*

866	J212912-153841	4666.379 ± 0.008	13.628 ± 0.058	19.175 ± 2.717
867	J212912-153841	4665.223 ± 0.004	14.250 ± 0.006	28.837 ± 0.544
868	J212912-153841	4664.317 ± 0.029	13.350 ± 0.050	29.063 ± 3.868
869	J212912-153841	4663.639 ± 0.129	12.514 ± 0.524	10.903 ± 7.427
870	J212912-153841	4663.072 ± 0.036	12.637 ± 0.177	10.723 ± 4.288
871	J212912-153841	4662.268 ± 0.015	13.635 ± 0.073	13.968 ± 0.601
872	J212912-153841	4661.485 ± 0.035	14.380 ± 0.057	28.509 ± 4.338
873	J212912-153841	4659.637 ± 0.006	12.927 ± 0.012	20.335 ± 0.667
874	J212912-153841	4658.935 ± 0.020	12.404 ± 0.034	20.304 ± 1.705
875	J212912-153841	4657.460 ± 0.140	12.236 ± 1.030	18.786 ± 8.888
876	J212912-153841	4657.054 ± 0.171	12.864 ± 0.260	27.516 ± 9.304
877	J212912-153841	4655.843 ± 0.005	14.252 ± 0.007	27.269 ± 0.381
878	J212912-153841	4654.812 ± 0.006	13.950 ± 0.017	12.499 ± 0.745
879	J212912-153841	4654.434 ± 0.009	13.606 ± 0.045	11.683 ± 1.073
880	J212912-153841	4652.245 ± 0.026	12.580 ± 0.045	16.566 ± 1.182
881	J212912-153841	4651.061 ± 0.054	13.007 ± 0.146	13.603 ± 2.700
882	J212912-153841	4650.371 ± 0.031	13.723 ± 0.137	12.002 ± 1.012
883	J212912-153841	4649.736 ± 0.018	15.052 ± 0.481	19.357 ± 5.792
884	J212912-153841	4648.375 ± 0.020	15.057 ± 0.033	36.333 ± 0.683
885	J212912-153841	4646.999 ± 0.016	12.793 ± 0.035	20.728 ± 1.244
886	J212912-153841	4645.868 ± 0.015	13.111 ± 0.019	29.911 ± 1.190
887	J212912-153841	4645.046 ± 0.019	13.250 ± 0.044	23.315 ± 1.689
888	J212912-153841	4643.918 ± 0.474	15.162 ± 1.036	25.894 ± 8.924
889	J212912-153841	4643.211 ± 1.616	14.886 ± 2.979	26.155 ± 39.668
890	J212912-153841	4642.299 ± 0.033	13.861 ± 0.121	18.275 ± 1.697
891	J212912-153841	4641.753 ± 0.125	13.347 ± 0.207	38.077 ± 14.907
892	J212912-153841	4640.873 ± 0.096	12.662 ± 0.260	25.652 ± 4.373
893	J212912-153841	4639.707 ± 0.075	12.264 ± 0.126	27.734 ± 6.150
894	J212912-153841	4638.892 ± 0.048	12.603 ± 0.054	31.966 ± 3.114
895	J212912-153841	4637.241 ± 0.138	12.056 ± 0.238	19.581 ± 7.932
896	J212912-153841	4636.608 ± 0.006	13.215 ± 0.015	19.164 ± 0.698
897	J212912-153841	4635.507 ± 0.149	12.693 ± 0.200	36.211 ± 15.309
898	J212912-153841	4634.925 ± 0.185	12.356 ± 0.637	13.512 ± 10.573
899	J212912-153841	4634.651 ± 0.136	12.287 ± 1.059	11.932 ± 9.212
900	J212912-153841	4634.390 ± 0.174	12.535 ± 0.314	21.070 ± 6.720
901	J212912-153841	4633.023 ± 0.013	12.793 ± 0.018	23.941 ± 1.091
902	J212912-153841	4632.061 ± 0.035	12.259 ± 0.046	26.592 ± 3.374
903	J212912-153841	4629.373 ± 0.050	12.355 ± 0.063	28.069 ± 3.684
904	J212912-153841	4628.613 ± 0.056	12.182 ± 0.096	24.503 ± 4.418
905	J212912-153841	4627.260 ± 0.032	12.321 ± 0.031	37.333 ± 3.319
906	J212912-153841	4625.556 ± 0.015	12.629 ± 0.017	30.315 ± 1.514
907	J212912-153841	4624.683 ± 0.065	12.034 ± 0.173	17.128 ± 5.182
908	J212912-153841	4624.179 ± 0.057	12.118 ± 0.166	18.346 ± 5.805
909	J212912-153841	4623.327 ± 0.016	12.753 ± 0.033	30.062 ± 2.645

Table E.1. *Continued*

910	J212912-153841	4622.478 ± 0.008	12.945 ± 0.017	22.577 ± 0.748
911	J212912-153841	4621.270 ± 0.048	12.390 ± 0.053	44.725 ± 7.175
912	J212912-153841	4619.557 ± 0.045	13.367 ± 0.053	32.686 ± 2.454
913	J212912-153841	4618.914 ± 0.004	14.176 ± 0.008	23.062 ± 0.308
914	J212912-153841	4618.169 ± 0.047	11.805 ± 0.165	10.967 ± 4.271
915	J212912-153841	4616.884 ± 0.034	12.522 ± 0.042	28.810 ± 3.340
916	J212912-153841	4615.980 ± 0.065	12.993 ± 0.129	18.653 ± 3.330
917	J212912-153841	4615.116 ± 0.040	14.069 ± 0.067	22.814 ± 1.968
918	J212912-153841	4614.779 ± 0.019	13.626 ± 0.182	12.534 ± 2.376
919	J212912-153841	4611.024 ± 0.045	12.813 ± 0.028	57.407 ± 4.504
920	J212912-153841	4609.771 ± 0.111	12.260 ± 0.279	16.904 ± 6.675
921	J212912-153841	4609.182 ± 0.019	13.838 ± 0.049	19.832 ± 1.335
922	J212912-153841	4608.623 ± 0.321	13.050 ± 1.165	21.224 ± 28.717
923	J212912-153841	4608.209 ± 0.555	12.849 ± 1.502	20.352 ± 20.474
924	J212912-153841	4607.605 ± 0.032	12.582 ± 0.186	14.162 ± 3.824
925	J212912-153841	4607.081 ± 0.005	13.867 ± 0.007	22.325 ± 0.363
926	J212912-153841	4605.949 ± 0.010	12.858 ± 0.014	24.805 ± 1.011
927	J212912-153841	4604.285 ± 0.014	12.782 ± 0.022	23.905 ± 1.283
928	J212912-153841	4603.297 ± 0.025	12.752 ± 0.026	33.465 ± 2.435
929	J212912-153841	4600.494 ± 0.008	12.955 ± 0.014	20.721 ± 0.823
930	J212912-153841	4599.902 ± 0.007	12.799 ± 0.018	13.429 ± 0.585
931	J212912-153841	4594.673 ± 0.387	13.265 ± 0.353	46.051 ± 12.319
932	J212912-153841	4594.226 ± 0.005	13.746 ± 0.110	28.028 ± 1.753
933	J212912-153841	4593.416 ± 0.037	12.450 ± 0.160	19.141 ± 4.306
934	J212912-153841	4592.252 ± 0.004	14.627 ± 0.016	29.321 ± 0.476
935	J212912-153841	4590.016 ± 0.006	15.467 ± 0.058	49.949 ± 1.534
936	J212912-153841	4588.366 ± 0.070	12.843 ± 0.263	22.281 ± 5.840
937	J212912-153841	4587.226 ± 0.204	13.357 ± 0.155	64.359 ± 21.131
938	J212912-153841	4587.020 ± 0.025	12.502 ± 0.198	13.952 ± 2.993
939	J212912-153841	4583.140 ± 0.041	17.814 ± 0.670	66.694 ± 6.847
940	J212912-153841	4578.766 ± 0.018	16.847 ± 1.275	37.254 ± 10.282
941	J212912-153841	4576.773 ± 0.579	13.435 ± 1.042	48.904 ± 48.945
942	J212912-153841	4575.735 ± 1.757	13.216 ± 1.529	55.177 ± 86.007
943	J212912-153841	4574.765 ± 0.011	13.075 ± 0.089	13.085 ± 1.487
944	J212912-153841	4574.048 ± 0.021	12.817 ± 0.170	11.022 ± 3.643
945	J212912-153841	4573.285 ± 0.066	13.272 ± 0.093	41.526 ± 8.836
946	J212912-153841	4571.367 ± 0.036	13.099 ± 0.067	29.515 ± 4.794
947	J212912-153841	4569.124 ± 0.066	13.018 ± 0.088	26.860 ± 3.835
948	J212912-153841	4568.767 ± 0.017	12.536 ± 0.236	12.503 ± 2.822
949	J212912-153841	4568.109 ± 0.002	13.963 ± 0.003	23.586 ± 0.221
950	J212912-153841	4567.258 ± 0.048	12.009 ± 0.294	13.325 ± 5.282
951	J212912-153841	4566.731 ± 0.126	12.230 ± 0.218	27.497 ± 15.077
952	J212912-153841	4565.844 ± 0.064	12.035 ± 0.119	19.890 ± 5.825
953	J212912-153841	4561.327 ± 0.048	12.581 ± 0.077	21.781 ± 3.341

Table E.1. *Continued*

954	J212912-153841	4560.825 ± 0.040	12.385 ± 0.130	16.027 ± 3.146
955	J212912-153841	4559.477 ± 0.749	13.385 ± 0.877	39.408 ± 20.481
956	J212912-153841	4559.519 ± 0.096	12.879 ± 0.851	15.368 ± 7.364
957	J212912-153841	4558.968 ± 0.363	12.401 ± 5.308	17.490 ± 57.987
958	J212912-153841	4558.483 ± 0.101	11.956 ± 1.494	13.937 ± 13.840
959	J212912-153841	4557.660 ± 1.741	12.948 ± 4.032	18.668 ± 79.429
960	J212912-153841	4557.415 ± 0.326	12.893 ± 4.332	13.529 ± 19.368
961	J212912-153841	4556.174 ± 0.029	12.812 ± 0.045	22.865 ± 2.393
962	J212912-153841	4550.872 ± 0.027	12.646 ± 0.037	26.051 ± 2.585
963	J212912-153841	4550.012 ± 0.236	12.713 ± 0.914	10.360 ± 10.040
964	J212912-153841	4547.122 ± 1.732	13.648 ± 0.831	92.555 ± 50.165
965	J212912-153841	4547.885 ± 0.022	13.560 ± 0.039	12.064 ± 1.495
966	J212912-153841	4544.928 ± 0.015	13.460 ± 0.239	14.160 ± 2.559
967	J212912-153841	4544.626 ± 0.100	13.728 ± 0.176	29.662 ± 6.674
968	J212912-153841	4543.710 ± 0.229	12.844 ± 0.392	38.912 ± 20.104
969	J212912-153841	4542.564 ± 0.392	12.740 ± 0.219	64.565 ± 20.626
970	J212912-153841	4538.498 ± 0.074	12.378 ± 0.152	31.896 ± 6.362
971	J212912-153841	4537.224 ± 0.189	12.692 ± 0.132	60.962 ± 18.964
972	J212912-153841	4536.744 ± 0.027	12.013 ± 0.194	11.626 ± 3.655
973	J212912-153841	4535.362 ± 0.061	12.102 ± 0.160	17.672 ± 6.956
974	J212912-153841	4534.883 ± 0.039	12.089 ± 0.186	12.186 ± 5.175
975	J212912-153841	4534.481 ± 0.034	12.149 ± 0.103	12.063 ± 3.080
976	J212912-153841	4533.205 ± 0.019	14.128 ± 0.021	33.001 ± 0.750
977	J212912-153841	4531.951 ± 0.010	16.141 ± 0.133	29.935 ± 0.985
978	J212912-153841	4530.075 ± 0.006	13.648 ± 0.010	32.246 ± 0.933
979	J212912-153841	4528.348 ± 0.006	12.712 ± 0.015	13.729 ± 0.622
980	J212912-153841	4526.870 ± 0.007	14.190 ± 0.011	24.591 ± 0.319
981	J212912-153841	4525.954 ± 0.032	14.347 ± 0.048	25.950 ± 2.116
982	J212912-153841	4525.219 ± 0.027	14.315 ± 0.057	21.989 ± 3.393
983	J212912-153841	4524.565 ± 0.040	13.904 ± 0.082	24.255 ± 2.873
984	J212912-153841	4523.589 ± 0.007	14.186 ± 0.013	33.250 ± 1.383
985	J212912-153841	4521.781 ± 0.116	12.571 ± 0.432	26.790 ± 27.936
986	J212912-153841	4521.085 ± 0.130	13.054 ± 0.714	12.487 ± 16.116
987	J212912-153841	4520.821 ± 0.075	13.136 ± 0.635	10.061 ± 5.564
988	J212912-153841	4520.409 ± 0.413	13.258 ± 0.590	29.595 ± 13.374
989	J212912-153841	4519.146 ± 0.046	12.084 ± 0.078	21.050 ± 4.671
990	J212912-153841	4517.031 ± 0.016	12.640 ± 0.018	31.385 ± 1.496
991	J212912-153841	4511.688 ± 0.016	12.998 ± 0.019	31.005 ± 1.282
992	J212912-153841	4510.814 ± 0.005	13.510 ± 0.006	27.780 ± 0.350
993	J212912-153841	4509.493 ± 0.038	12.205 ± 0.068	21.808 ± 3.381
994	J212912-153841	4508.652 ± 0.015	12.808 ± 0.020	29.947 ± 1.614
995	J212912-153841	4506.834 ± 0.385	12.729 ± 0.325	47.408 ± 15.004
996	J212912-153841	4506.455 ± 0.039	12.523 ± 0.424	22.102 ± 7.376
997	J212912-153841	4505.772 ± 0.034	11.780 ± 0.450	10.426 ± 5.796

Table E.1. *Continued*

998	J212912-153841	4505.219 ± 0.025	12.051 ± 0.277	13.154 ± 4.165
999	J212912-153841	4504.582 ± 0.036	12.514 ± 0.229	21.813 ± 4.101
1000	J212912-153841	4503.897 ± 0.010	13.163 ± 0.058	24.392 ± 1.323
1001	J212912-153841	4503.188 ± 0.701	12.804 ± 0.375	91.688 ± 69.129
1002	J212912-153841	4501.454 ± 0.067	11.966 ± 0.357	23.961 ± 10.916
1003	J212912-153841	4500.244 ± 0.182	13.333 ± 0.661	19.368 ± 3.842
1004	J212912-153841	4499.967 ± 0.489	12.996 ± 1.461	19.885 ± 15.643
1005	J212912-153841	4499.408 ± 0.070	12.192 ± 0.223	14.683 ± 4.022
1006	J212912-153841	4497.437 ± 0.021	13.661 ± 0.012	69.830 ± 1.359
1007	J212912-153841	4495.273 ± 0.023	12.273 ± 0.071	17.177 ± 2.909
1008	J212912-153841	4494.592 ± 0.053	12.193 ± 0.073	25.796 ± 4.985
1009	J212912-153841	4484.285 ± 0.016	12.433 ± 0.025	20.597 ± 1.335
1010	J212912-153841	4482.765 ± 0.002	13.457 ± 0.003	24.141 ± 0.164
1011	J212912-153841	4478.168 ± 0.157	12.304 ± 0.169	32.457 ± 10.125
1012	J212912-153841	4477.765 ± 0.029	12.178 ± 0.232	11.765 ± 3.146
1013	J212912-153841	4477.342 ± 0.016	12.760 ± 0.059	19.167 ± 2.658
1014	J212912-153841	4476.413 ± 0.002	14.283 ± 0.004	27.569 ± 0.326
1015	J212912-153841	4474.470 ± 0.077	14.789 ± 0.169	25.938 ± 1.848
1016	J212912-153841	4473.709 ± 0.012	14.732 ± 0.008	70.370 ± 0.581
1017	J212912-153841	4472.363 ± 0.003	13.890 ± 0.010	16.893 ± 0.295
1018	J212912-153841	4470.825 ± 0.013	13.285 ± 0.009	52.531 ± 1.473
1019	J212912-153841	4469.202 ± 0.003	13.995 ± 0.006	23.965 ± 0.198
1020	J212912-153841	4467.660 ± 0.005	14.708 ± 0.008	57.723 ± 0.621
1021	J212912-153841	4466.056 ± 0.001	13.551 ± 0.005	10.683 ± 0.165
1022	J212912-153841	4464.996 ± 0.003	13.515 ± 0.005	29.663 ± 0.417
1023	J212912-153841	4463.983 ± 0.031	13.068 ± 0.177	20.435 ± 1.665
1024	J212912-153841	4463.610 ± 0.270	12.692 ± 0.429	27.493 ± 10.608
1025	J212912-153841	4461.660 ± 0.041	13.356 ± 0.020	78.418 ± 2.745
1026	J212912-153841	4461.155 ± 0.001	14.066 ± 0.004	21.428 ± 0.154
1027	J212912-153841	4460.027 ± 0.041	12.349 ± 0.140	17.050 ± 3.609
1028	J212912-153841	4459.502 ± 0.054	12.257 ± 0.190	20.344 ± 8.975
1029	J212912-153841	4458.911 ± 0.065	12.006 ± 0.172	17.234 ± 5.740
1030	J212912-153841	4458.261 ± 0.035	11.728 ± 0.165	12.626 ± 4.360
1031	J212912-153841	4455.928 ± 0.062	13.465 ± 0.026	129.989 ± 7.781
1032	J212912-153841	4456.605 ± 0.012	12.563 ± 0.059	15.214 ± 1.342
1033	J212912-153841	4455.769 ± 0.011	13.965 ± 0.015	31.169 ± 0.664
1034	J212912-153841	4454.960 ± 0.011	14.074 ± 0.013	36.524 ± 0.566
1035	J212912-153841	4452.354 ± 0.051	12.484 ± 0.085	35.394 ± 4.193
1036	J212912-153841	4451.062 ± 0.125	12.378 ± 0.146	57.259 ± 22.160
1037	J212912-153841	4450.051 ± 0.032	11.871 ± 0.156	14.811 ± 3.900
1038	J212912-153841	4449.232 ± 0.023	12.500 ± 0.029	32.020 ± 2.604
1039	J212912-153841	4447.775 ± 0.013	12.866 ± 0.012	35.874 ± 1.098
1040	J111350-153333	5123.722 ± 0.053	12.865 ± 0.108	21.350 ± 5.958
1041	J111350-153333	5121.586 ± 0.009	13.405 ± 0.014	18.593 ± 0.659

Table E.1. *Continued*

1042	J111350-153333	5119.764 ± 1.216	13.118 ± 2.235	20.904 ± 39.983
1043	J111350-153333	5119.480 ± 0.069	13.539 ± 0.830	14.855 ± 4.959
1044	J111350-153333	5118.216 ± 0.027	13.558 ± 0.030	29.128 ± 2.045
1045	J111350-153333	5117.413 ± 0.038	13.196 ± 0.107	18.425 ± 3.822
1046	J111350-153333	5116.802 ± 0.120	13.547 ± 0.319	14.716 ± 5.832
1047	J111350-153333	5116.546 ± 0.045	13.453 ± 0.368	10.432 ± 1.774
1048	J111350-153333	5114.682 ± 0.021	13.951 ± 0.031	22.211 ± 0.812
1049	J111350-153333	5112.279 ± 0.016	14.962 ± 0.056	26.318 ± 0.796
1050	J111350-153333	5111.351 ± 0.034	13.358 ± 0.187	12.445 ± 3.935
1051	J111350-153333	5110.740 ± 0.021	14.191 ± 0.025	26.509 ± 0.891
1052	J111350-153333	5109.025 ± 0.013	13.651 ± 0.013	32.248 ± 1.097
1053	J111350-153333	5107.774 ± 0.168	13.711 ± 0.252	26.991 ± 5.891
1054	J111350-153333	5107.067 ± 0.049	14.401 ± 0.068	27.055 ± 2.527
1055	J111350-153333	5105.830 ± 0.037	13.693 ± 0.084	36.138 ± 6.126
1056	J111350-153333	5104.761 ± 0.093	13.421 ± 0.106	34.924 ± 5.286
1057	J111350-153333	5114.016 ± 0.024	13.907 ± 0.033	23.162 ± 1.040
1058	J111350-153333	5103.745 ± 0.067	12.151 ± 0.213	14.517 ± 6.231
1059	J111350-153333	5102.453 ± 0.023	13.522 ± 0.034	23.378 ± 1.396
1060	J111350-153333	5101.529 ± 0.010	14.262 ± 0.012	28.867 ± 0.552
1061	J111350-153333	5098.751 ± 0.186	13.680 ± 0.577	18.781 ± 5.484
1062	J111350-153333	5097.720 ± 0.103	15.150 ± 0.160	35.757 ± 3.331
1063	J111350-153333	5096.450 ± 1.198	13.372 ± 0.548	72.213 ± 56.163
1064	J111350-153333	5089.439 ± 0.083	13.885 ± 0.040	46.617 ± 3.729
1065	J111350-153333	5087.270 ± 0.006	13.825 ± 0.007	28.612 ± 0.531
1066	J111350-153333	5086.083 ± 0.038	12.991 ± 0.043	32.857 ± 3.853
1067	J111350-153333	5085.005 ± 0.053	12.151 ± 0.120	14.573 ± 4.653
1068	J111350-153333	5074.547 ± 0.058	13.107 ± 0.052	33.990 ± 3.714
1069	J111350-153333	5073.434 ± 0.006	14.297 ± 0.013	26.721 ± 0.763
1070	J111350-153333	5072.454 ± 0.088	12.575 ± 0.138	21.279 ± 5.562
1071	J111350-153333	5066.522 ± 0.005	13.576 ± 0.007	22.865 ± 0.376
1072	J111350-153333	5064.819 ± 0.037	12.755 ± 0.046	25.375 ± 3.327
1073	J111350-153333	5064.063 ± 0.079	12.060 ± 0.202	14.577 ± 7.164
1074	J111350-153333	5063.061 ± 0.003	13.907 ± 0.006	22.137 ± 0.267
1075	J111350-153333	5061.246 ± 0.003	13.739 ± 0.006	19.851 ± 0.257
1076	J111350-153333	5057.946 ± 0.052	12.663 ± 0.049	34.227 ± 4.717
1077	J111350-153333	5056.516 ± 0.082	13.951 ± 0.189	19.662 ± 2.041
1078	J111350-153333	5056.070 ± 0.073	14.134 ± 0.145	20.877 ± 1.812
1079	J111350-153333	5053.652 ± 0.076	12.539 ± 0.063	38.032 ± 6.489
1080	J111350-153333	5051.715 ± 0.004	13.796 ± 0.005	28.424 ± 0.375
1081	J111350-153333	5050.348 ± 0.030	12.801 ± 0.034	28.473 ± 2.727
1082	J111350-153333	5048.646 ± 0.028	12.871 ± 0.028	31.593 ± 2.386
1083	J111350-153333	5045.610 ± 0.005	14.521 ± 0.005	61.475 ± 0.415
1084	J111350-153333	5043.173 ± 0.004	14.193 ± 0.011	23.498 ± 0.370
1085	J111350-153333	5042.113 ± 0.042	13.030 ± 0.040	32.758 ± 3.230

Table E.1. *Continued*

1086	J111350-153333	5039.233 ± 0.043	12.146 ± 0.096	13.461 ± 3.779
1087	J111350-153333	5038.264 ± 0.047	12.357 ± 0.086	18.211 ± 4.273
1088	J111350-153333	5036.856 ± 0.822	12.921 ± 0.854	35.543 ± 31.670
1089	J111350-153333	5036.223 ± 0.164	13.085 ± 0.642	26.363 ± 14.246
1090	J111350-153333	5035.377 ± 0.024	13.104 ± 0.046	18.663 ± 1.500
1091	J111350-153333	5032.551 ± 0.039	13.400 ± 0.063	20.867 ± 1.755
1092	J111350-153333	5032.065 ± 0.056	13.065 ± 0.135	17.695 ± 2.420
1093	J111350-153333	5030.386 ± 0.009	13.742 ± 0.013	22.812 ± 0.619
1094	J111350-153333	5027.649 ± 0.005	16.603 ± 0.161	53.235 ± 1.933
1095	J111350-153333	5024.700 ± 0.027	13.497 ± 0.042	38.965 ± 3.821
1096	J111350-153333	5023.372 ± 0.127	12.797 ± 0.119	38.531 ± 9.331
1097	J111350-153333	5021.690 ± 0.090	13.507 ± 0.852	21.363 ± 6.396
1098	J111350-153333	5021.375 ± 0.531	13.510 ± 0.850	28.106 ± 12.267
1099	J111350-153333	5019.475 ± 0.078	12.628 ± 0.059	42.663 ± 7.082
1100	J111350-153333	5016.131 ± 0.063	13.279 ± 0.082	29.392 ± 2.798
1101	J111350-153333	5015.371 ± 0.215	12.787 ± 0.255	30.783 ± 9.748
1102	J111350-153333	5010.973 ± 0.084	12.333 ± 0.108	25.222 ± 7.945
1103	J111350-153333	5008.615 ± 0.031	12.768 ± 0.047	21.889 ± 2.611
1104	J111350-153333	5007.740 ± 0.017	13.122 ± 0.022	24.337 ± 1.446
1105	J111350-153333	5005.832 ± 0.003	14.747 ± 0.022	29.476 ± 0.358
1106	J111350-153333	5002.836 ± 0.027	13.122 ± 0.022	39.396 ± 2.480
1107	J111350-153333	5001.509 ± 0.033	12.750 ± 0.043	25.152 ± 2.783
1108	J111350-153333	4999.156 ± 0.061	13.756 ± 0.200	26.140 ± 2.156
1109	J111350-153333	4998.547 ± 0.245	13.636 ± 0.286	35.298 ± 13.348
1110	J111350-153333	4997.284 ± 0.022	13.666 ± 0.037	30.577 ± 2.377
1111	J111350-153333	4996.252 ± 0.034	13.490 ± 0.415	24.304 ± 5.092
1112	J111350-153333	4995.826 ± 0.496	13.406 ± 0.524	37.134 ± 14.249
1113	J111350-153333	4993.499 ± 0.058	12.806 ± 0.052	28.222 ± 2.964
1114	J111350-153333	4987.809 ± 0.238	13.316 ± 0.483	73.886 ± 87.894
1115	J111350-153333	4986.460 ± 0.048	13.136 ± 0.380	33.217 ± 9.872
1116	J111350-153333	4985.537 ± 0.127	12.160 ± 0.401	18.255 ± 12.287
1117	J111350-153333	4984.487 ± 0.492	12.839 ± 0.568	34.285 ± 28.811
1118	J111350-153333	4983.275 ± 0.011	15.118 ± 0.040	34.734 ± 0.887
1119	J111350-153333	4981.426 ± 0.050	12.900 ± 0.042	35.388 ± 3.707
1120	J111350-153333	4979.626 ± 0.011	13.430 ± 0.019	25.082 ± 0.739
1121	J111350-153333	4978.685 ± 0.055	13.072 ± 0.044	39.047 ± 3.740
1122	J111350-153333	4976.175 ± 0.004	13.551 ± 0.015	21.923 ± 0.491
1123	J111350-153333	4974.811 ± 0.327	12.763 ± 0.304	61.292 ± 44.535
1124	J111350-153333	4973.754 ± 0.014	13.140 ± 0.087	25.931 ± 2.256
1125	J111350-153333	4972.923 ± 0.037	12.337 ± 0.127	11.885 ± 3.022
1126	J111350-153333	4972.458 ± 0.065	12.313 ± 0.127	16.381 ± 4.994
1127	J111350-153333	4967.345 ± 0.028	12.993 ± 0.021	42.423 ± 2.622
1128	J111350-153333	4965.163 ± 0.019	13.173 ± 0.032	21.582 ± 1.254
1129	J111350-153333	4964.413 ± 0.011	13.456 ± 0.021	24.741 ± 1.274

Table E.1. *Continued*

1130	J111350-153333	4963.451 ± 0.005	13.686 ± 0.006	23.517 ± 0.363
1131	J111350-153333	4960.337 ± 0.035	12.990 ± 0.044	28.974 ± 2.868
1132	J111350-153333	4959.477 ± 0.042	12.824 ± 0.063	25.486 ± 3.009
1133	J111350-153333	4957.915 ± 0.038	12.230 ± 0.193	14.996 ± 4.473
1134	J111350-153333	4957.589 ± 0.071	13.035 ± 0.032	52.451 ± 5.654
1135	J111350-153333	4955.954 ± 0.019	13.158 ± 0.029	31.855 ± 2.269
1136	J111350-153333	4954.958 ± 0.030	13.315 ± 0.062	20.698 ± 1.809
1137	J111350-153333	4954.346 ± 0.019	13.621 ± 0.030	22.759 ± 1.251
1138	J111350-153333	4953.002 ± 0.035	13.093 ± 0.031	39.247 ± 3.238
1139	J111350-153333	4951.696 ± 0.052	12.093 ± 0.139	14.338 ± 4.724
1140	J111350-153333	4950.949 ± 0.015	12.987 ± 0.020	25.013 ± 1.468
1141	J111350-153333	4949.443 ± 0.010	13.273 ± 0.012	28.312 ± 0.882
1142	J111350-153333	4948.047 ± 0.025	13.226 ± 0.028	38.343 ± 2.891
1143	J111350-153333	4946.950 ± 0.051	12.729 ± 0.117	25.705 ± 5.828
1144	J111350-153333	4946.069 ± 0.018	13.255 ± 0.025	26.876 ± 1.610
1145	J111350-153333	4944.952 ± 0.016	12.940 ± 0.021	24.712 ± 1.416
1146	J111350-153333	4943.068 ± 0.058	13.164 ± 0.067	27.590 ± 3.009
1147	J111350-153333	4942.655 ± 0.022	12.613 ± 0.216	12.603 ± 2.892
1148	J111350-153333	4941.971 ± 0.006	13.653 ± 0.007	24.730 ± 0.441
1149	J111350-153333	4940.783 ± 0.041	12.081 ± 0.120	12.570 ± 3.726
1150	J111350-153333	4939.883 ± 0.021	13.516 ± 0.026	27.875 ± 1.566
1151	J111350-153333	4939.282 ± 0.032	12.811 ± 0.144	16.345 ± 3.054
1152	J111350-153333	4938.361 ± 0.005	14.103 ± 0.005	32.443 ± 0.459
1153	J111350-153333	4936.574 ± 0.003	14.255 ± 0.005	37.410 ± 0.315
1154	J111350-153333	4934.968 ± 0.006	13.572 ± 0.008	21.097 ± 0.505
1155	J111350-153333	4934.363 ± 0.050	12.218 ± 0.188	13.026 ± 5.147
1156	J111350-153333	4933.761 ± 0.055	12.285 ± 0.097	18.707 ± 5.135
1157	J111350-153333	4932.344 ± 0.074	12.318 ± 0.085	29.230 ± 7.177
1158	J111350-153333	4931.461 ± 0.030	12.229 ± 0.079	13.361 ± 2.817
1159	J111350-153333	4930.547 ± 0.019	12.951 ± 0.030	20.285 ± 1.651
1160	J111350-153333	4930.001 ± 0.051	12.186 ± 0.158	12.720 ± 3.878
1161	J111350-153333	4928.481 ± 0.011	13.271 ± 0.013	25.330 ± 0.924
1162	J111350-153333	4927.781 ± 0.039	12.282 ± 0.105	14.163 ± 3.158
1163	J111350-153333	4926.449 ± 0.003	13.582 ± 0.005	22.025 ± 0.285
1164	J111350-153333	4925.122 ± 0.002	13.932 ± 0.007	18.491 ± 0.192
1165	J111350-153333	4923.617 ± 0.131	12.701 ± 0.136	30.833 ± 7.130
1166	J111350-153333	4921.170 ± 0.108	12.812 ± 0.151	26.290 ± 5.129
1167	J111350-153333	4921.827 ± 0.038	13.237 ± 0.057	25.348 ± 1.806
1168	J111350-153333	4918.193 ± 0.079	12.769 ± 0.080	45.655 ± 10.156
1169	J111350-153333	4917.019 ± 0.016	13.145 ± 0.025	26.828 ± 1.173
1170	J111350-153333	4914.749 ± 0.060	12.237 ± 0.157	11.818 ± 4.509
1171	J111350-153333	4913.876 ± 0.010	13.767 ± 0.016	27.470 ± 0.771
1172	J111350-153333	4912.800 ± 0.022	13.552 ± 0.044	39.755 ± 4.304
1173	J111350-153333	4910.715 ± 0.004	16.051 ± 0.101	39.251 ± 1.101

Table E.1. *Continued*

1174	J111350-153333	4908.747 ± 0.009	13.358 ± 0.023	19.422 ± 1.136
1175	J111350-153333	4908.142 ± 0.053	12.445 ± 0.115	16.143 ± 3.528
1176	J111350-153333	4905.962 ± 0.020	12.496 ± 0.037	17.362 ± 1.794
1177	J111350-153333	4902.770 ± 0.015	12.938 ± 0.017	28.079 ± 1.316
1178	J111350-153333	4901.143 ± 0.013	12.922 ± 0.017	24.019 ± 1.097
1179	J111350-153333	4889.938 ± 0.013	12.914 ± 0.018	23.807 ± 1.219
1180	J111350-153333	4888.854 ± 0.009	13.108 ± 0.015	23.709 ± 0.947
1181	J111350-153333	4887.096 ± 0.120	12.669 ± 0.076	60.958 ± 13.247
1182	J111350-153333	4885.506 ± 0.005	13.221 ± 0.021	12.440 ± 0.841
1183	J111350-153333	4884.443 ± 0.008	13.065 ± 0.027	10.461 ± 0.538
1184	J111350-153333	4883.863 ± 0.009	14.015 ± 0.019	18.702 ± 0.568
1185	J111350-153333	4882.796 ± 0.005	13.505 ± 0.007	22.611 ± 0.479
1186	J111350-153333	4881.687 ± 0.011	13.021 ± 0.016	23.254 ± 1.061
1187	J111350-153333	4880.374 ± 0.039	12.553 ± 0.458	19.739 ± 7.241
1188	J111350-153333	4879.880 ± 0.892	12.320 ± 0.834	37.311 ± 39.011
1189	J111350-153333	4878.126 ± 0.003	14.097 ± 0.006	26.273 ± 0.263
1190	J111350-153333	4877.218 ± 0.016	12.490 ± 0.063	10.741 ± 1.671
1191	J111350-153333	4875.740 ± 0.003	15.092 ± 0.026	39.377 ± 0.498
1192	J111350-153333	4873.308 ± 0.090	13.031 ± 0.080	41.713 ± 4.340
1193	J111350-153333	4872.744 ± 0.012	12.568 ± 0.126	11.170 ± 1.952
1194	J111350-153333	4871.648 ± 0.056	12.372 ± 0.080	25.816 ± 5.869
1195	J111350-153333	4870.572 ± 0.009	13.012 ± 0.016	19.585 ± 0.869
1196	J111350-153333	4869.502 ± 0.014	13.049 ± 0.017	29.183 ± 1.503
1197	J111350-153333	4868.195 ± 0.009	13.431 ± 0.012	26.425 ± 0.790
1198	J111350-153333	4867.260 ± 0.034	12.826 ± 0.042	27.310 ± 2.733
1199	J111350-153333	4862.691 ± 0.044	12.513 ± 0.101	16.853 ± 2.989
1200	J111350-153333	4862.083 ± 0.014	13.246 ± 0.020	22.462 ± 1.024
1201	J111350-153333	4860.737 ± 0.003	13.474 ± 0.006	18.028 ± 0.257
1202	J111350-153333	4859.525 ± 0.014	13.014 ± 0.017	26.338 ± 1.205
1203	J111350-153333	4856.320 ± 0.024	13.269 ± 0.033	23.677 ± 2.064
1204	J111350-153333	4855.452 ± 0.026	13.123 ± 0.034	27.320 ± 2.106
1205	J111350-153333	4854.037 ± 0.015	13.801 ± 0.024	21.648 ± 0.699
1206	J111350-153333	4853.523 ± 0.289	12.396 ± 0.590	20.246 ± 11.535
1207	J111350-153333	4851.098 ± 0.035	12.550 ± 0.040	28.043 ± 3.071
1208	J111350-153333	4849.504 ± 0.003	13.590 ± 0.007	19.240 ± 0.283
1209	J111350-153333	4848.371 ± 0.026	13.153 ± 0.019	45.634 ± 2.509
1210	J111350-153333	4846.331 ± 0.015	12.926 ± 0.018	26.968 ± 1.310
1211	J111350-153333	4844.170 ± 0.005	13.222 ± 0.009	19.934 ± 0.462
1212	J111350-153333	4842.886 ± 0.016	12.726 ± 0.025	20.835 ± 1.468
1213	J111350-153333	4842.037 ± 0.014	12.540 ± 0.042	11.822 ± 1.307
1214	J111350-153333	4841.284 ± 0.005	13.572 ± 0.008	23.972 ± 0.609
1215	J111350-153333	4840.340 ± 0.012	13.197 ± 0.023	24.682 ± 1.624
1216	J111350-153333	4839.479 ± 0.013	12.935 ± 0.035	15.795 ± 1.317
1217	J111350-153333	4838.321 ± 0.003	14.737 ± 0.020	31.413 ± 0.412

Table E.1. *Continued*

1218	J111350-153333	4836.153 ± 0.177	12.241 ± 0.262	22.705 ± 11.764
1219	J111350-153333	4835.541 ± 0.020	12.972 ± 0.061	18.333 ± 2.213
1220	J111350-153333	4834.713 ± 0.006	13.770 ± 0.010	21.692 ± 0.720
1221	J111350-153333	4833.667 ± 0.067	13.414 ± 0.105	25.548 ± 4.879
1222	J111350-153333	4832.796 ± 0.035	13.235 ± 0.052	22.852 ± 1.775
1223	J111350-153333	4831.190 ± 0.005	13.755 ± 0.007	23.062 ± 0.349
1224	J111350-153333	4830.269 ± 0.066	12.687 ± 0.069	31.841 ± 5.491
1225	J111350-153333	4827.516 ± 0.057	12.454 ± 0.123	17.322 ± 3.965
1226	J111350-153333	4826.897 ± 0.014	13.273 ± 0.020	21.917 ± 1.053
1227	J111350-153333	4825.682 ± 0.017	13.665 ± 0.030	18.569 ± 0.818
1228	J111350-153333	4825.198 ± 0.033	13.341 ± 0.181	15.532 ± 3.358
1229	J111350-153333	4824.754 ± 0.062	13.391 ± 0.136	19.817 ± 4.447
1230	J111350-153333	4824.153 ± 0.055	12.500 ± 0.155	14.116 ± 3.260
1231	J111350-153333	4822.868 ± 0.281	12.271 ± 0.590	17.473 ± 17.553
1232	J111350-153333	4822.492 ± 0.104	12.367 ± 0.468	12.804 ± 6.796
1233	J111350-153333	4821.640 ± 0.030	12.046 ± 0.092	10.346 ± 3.095
1234	J111350-153333	4820.627 ± 0.036	12.973 ± 0.059	24.275 ± 2.336
1235	J111350-153333	4819.018 ± 0.050	14.901 ± 0.072	42.774 ± 1.952
1236	J111350-153333	4816.428 ± 0.060	15.031 ± 0.023	116.115 ± 1.634
1237	J111350-153333	4808.426 ± 0.070	12.612 ± 0.141	26.576 ± 4.862
1238	J111350-153333	4807.581 ± 0.016	12.442 ± 0.157	11.038 ± 2.549
1239	J111350-153333	4806.975 ± 0.097	13.504 ± 0.039	57.038 ± 4.853
1240	J111350-153333	4806.250 ± 0.003	14.056 ± 0.010	20.819 ± 0.397
1241	J111350-153333	4804.255 ± 0.075	12.912 ± 0.049	48.698 ± 4.878
1242	J111350-153333	4803.922 ± 0.018	12.626 ± 0.087	16.202 ± 2.137
1243	J111350-153333	4802.435 ± 0.049	13.921 ± 0.245	17.374 ± 1.287
1244	J111350-153333	4802.129 ± 0.339	13.455 ± 0.711	21.043 ± 10.875
1245	J111350-153333	4800.950 ± 0.037	14.135 ± 0.046	28.121 ± 1.995
1246	J111350-153333	4800.494 ± 0.034	13.254 ± 0.315	13.854 ± 4.163
1247	J111350-153333	4799.775 ± 0.317	13.634 ± 2.255	23.562 ± 14.010
1248	J111350-153333	4799.449 ± 2.068	13.436 ± 3.601	28.654 ± 56.585
1249	J111350-153333	4798.243 ± 0.119	13.014 ± 0.388	38.046 ± 31.625
1250	J111350-153333	4797.174 ± 1.354	12.859 ± 2.369	28.723 ± 71.670
1251	J111350-153333	4796.761 ± 0.095	13.422 ± 0.570	21.826 ± 3.973
1252	J111350-153333	4795.724 ± 0.026	12.601 ± 0.066	16.265 ± 2.162
1253	J111350-153333	4795.007 ± 0.022	12.956 ± 0.040	26.085 ± 3.055
1254	J111350-153333	4793.790 ± 0.041	12.608 ± 0.093	25.025 ± 7.015
1255	J111350-153333	4788.611 ± 0.051	12.256 ± 0.171	10.712 ± 3.550
1256	J111350-153333	4788.192 ± 0.061	12.607 ± 0.256	13.450 ± 6.494
1257	J111350-153333	4787.438 ± 0.006	14.634 ± 0.073	20.796 ± 1.274
1258	J111350-153333	4784.896 ± 0.005	15.920 ± 0.122	56.327 ± 2.370
1259	J111350-153333	4781.261 ± 0.012	13.787 ± 0.019	21.028 ± 0.946
1260	J111350-153333	4780.749 ± 0.013	13.443 ± 0.060	12.889 ± 1.533
1261	J111350-153333	4779.823 ± 0.019	13.661 ± 0.153	10.948 ± 3.925

Table E.1. *Continued*

1262	J111350-153333	4777.026 ± 0.053	12.386 ± 0.084	23.496 ± 5.787
1263	J111350-153333	4776.139 ± 0.005	13.597 ± 0.010	20.003 ± 0.494
1264	J111350-153333	4775.232 ± 0.104	12.777 ± 0.129	27.344 ± 7.142
1265	J111350-153333	4774.249 ± 0.052	11.990 ± 0.128	13.790 ± 5.064
1266	J111350-153333	4773.244 ± 0.014	12.915 ± 0.024	21.558 ± 1.519
1267	J111350-153333	4772.045 ± 0.015	13.057 ± 0.016	31.674 ± 1.388
1268	J111350-153333	4768.424 ± 0.003	14.095 ± 0.004	31.746 ± 0.273
1269	J111350-153333	4766.789 ± 0.037	13.033 ± 0.037	42.112 ± 4.039
1270	J111350-153333	4764.724 ± 0.004	14.742 ± 0.011	52.169 ± 0.585
1271	J111350-153333	4760.924 ± 0.014	13.652 ± 0.018	25.170 ± 0.737
1272	J111350-153333	4760.107 ± 0.007	14.067 ± 0.010	26.571 ± 0.681
1273	J111350-153333	4758.860 ± 0.022	13.489 ± 0.022	44.824 ± 3.816
1274	J111350-153333	4757.560 ± 0.221	12.659 ± 0.692	23.511 ± 11.711
1275	J111350-153333	4756.592 ± 0.492	13.658 ± 0.559	38.103 ± 33.127
1276	J111350-153333	4755.924 ± 0.007	15.708 ± 0.434	18.454 ± 2.546
1277	J111350-153333	4755.110 ± 0.196	12.296 ± 0.678	11.507 ± 12.177
1278	J111350-153333	4754.633 ± 0.030	12.376 ± 0.149	10.977 ± 4.614
1279	J111350-153333	4752.291 ± 0.003	16.143 ± 0.064	34.937 ± 0.541
1280	J111350-153333	4750.641 ± 0.038	12.843 ± 0.055	23.208 ± 2.652
1281	J111350-153333	4748.896 ± 0.037	12.676 ± 0.055	24.033 ± 2.989
1282	J111350-153333	4747.909 ± 0.012	13.360 ± 0.020	30.737 ± 1.752
1283	J111350-153333	4746.953 ± 0.005	13.807 ± 0.008	21.567 ± 0.479
1284	J111350-153333	4745.902 ± 0.005	14.189 ± 0.009	29.643 ± 0.574
1285	J111350-153333	4744.814 ± 0.320	12.782 ± 0.228	51.375 ± 22.026
1286	J111350-153333	4743.440 ± 0.010	12.747 ± 0.030	14.927 ± 1.017
1287	J111350-153333	4737.922 ± 0.205	12.991 ± 0.228	32.448 ± 8.566
1288	J111350-153333	4737.473 ± 0.035	12.862 ± 0.313	19.158 ± 4.636
1289	J111350-153333	4735.389 ± 0.005	15.544 ± 0.054	53.273 ± 1.296
1290	J111350-153333	4732.907 ± 0.111	13.329 ± 0.146	51.491 ± 16.712
1291	J111350-153333	4731.640 ± 0.033	12.399 ± 0.262	12.151 ± 3.891
1292	J111350-153333	4731.051 ± 0.017	12.592 ± 0.068	12.392 ± 1.664
1293	J111350-153333	4730.414 ± 0.014	13.199 ± 0.032	24.218 ± 2.220
1294	J111350-153333	4729.793 ± 0.045	12.368 ± 0.167	14.520 ± 4.064
1295	J111350-153333	4728.805 ± 0.014	13.443 ± 0.017	36.509 ± 1.799
1296	J111350-153333	4727.904 ± 0.014	13.103 ± 0.047	20.036 ± 1.526
1297	J111350-153333	4726.896 ± 0.010	13.763 ± 0.012	40.159 ± 1.345
1298	J111350-153333	4724.800 ± 0.004	16.699 ± 0.177	30.819 ± 1.016
1299	J111350-153333	4722.852 ± 0.004	14.046 ± 0.005	28.913 ± 0.380
1300	J111350-153333	4720.154 ± 0.002	16.495 ± 0.061	46.051 ± 0.592
1301	J111350-153333	4716.963 ± 0.004	14.566 ± 0.023	32.542 ± 1.053
1302	J111350-153333	4715.869 ± 0.006	13.685 ± 0.012	17.800 ± 0.425
1303	J111350-153333	4715.109 ± 0.020	12.398 ± 0.051	14.280 ± 2.262
1304	J111350-153333	4713.989 ± 0.023	12.469 ± 0.044	18.210 ± 2.453
1305	J111350-153333	4712.488 ± 0.004	14.359 ± 0.012	27.799 ± 0.474

Table E.1. *Continued*

1306	J111350-153333	4710.873 ± 0.004	15.372 ± 0.045	31.455 ± 0.535
1307	J111350-153333	4709.155 ± 0.029	12.721 ± 0.056	23.349 ± 2.799
1308	J111350-153333	4708.177 ± 0.012	13.439 ± 0.012	36.541 ± 1.186
1309	J111350-153333	4705.515 ± 0.149	13.087 ± 0.059	86.193 ± 8.898
1310	J111350-153333	4705.098 ± 0.050	12.161 ± 0.168	15.338 ± 4.923
1311	J111350-153333	4704.352 ± 0.013	13.108 ± 0.039	26.603 ± 1.646
1312	J111350-153333	4700.203 ± 0.049	13.360 ± 0.043	41.254 ± 2.625
1313	J111350-153333	4697.797 ± 0.010	13.358 ± 0.038	25.548 ± 1.140
1314	J111350-153333	4697.288 ± 0.116	13.166 ± 0.055	59.167 ± 5.415
1315	J111350-153333	4696.246 ± 0.026	12.119 ± 0.162	10.917 ± 3.343
1316	J111350-153333	4695.327 ± 0.017	12.960 ± 0.026	24.408 ± 1.753
1317	J111350-153333	4693.768 ± 0.082	12.373 ± 0.084	35.825 ± 7.740
1318	J111350-153333	4690.551 ± 0.557	13.233 ± 0.213	96.232 ± 25.936
1319	J111350-153333	4687.927 ± 0.006	16.717 ± 0.144	56.273 ± 1.862
1320	J111350-153333	4685.041 ± 0.091	13.943 ± 0.114	34.740 ± 5.725
1321	J111350-153333	4683.496 ± 0.027	15.641 ± 0.075	43.637 ± 1.287
1322	J111350-153333	4681.410 ± 0.003	14.015 ± 0.007	22.639 ± 0.354
1323	J111350-153333	4680.418 ± 0.018	12.846 ± 0.037	19.965 ± 2.068
1324	J111350-153333	4679.381 ± 0.028	13.312 ± 0.040	26.049 ± 2.089
1325	J111350-153333	4678.697 ± 0.008	13.755 ± 0.016	21.097 ± 0.693
1326	J111350-153333	4677.719 ± 0.005	13.957 ± 0.005	29.294 ± 0.402
1327	J111350-153333	4674.209 ± 0.108	13.211 ± 0.051	118.073 ± 10.901
1328	J111350-153333	4674.766 ± 0.003	14.645 ± 0.025	25.378 ± 0.428
1329	J111350-153333	4673.110 ± 0.020	12.553 ± 0.073	16.975 ± 2.384
1330	J111350-153333	4667.602 ± 0.094	13.572 ± 0.058	77.168 ± 4.414
1331	J111350-153333	4667.519 ± 0.024	13.814 ± 0.161	20.531 ± 2.275
1332	J111350-153333	4667.262 ± 0.075	13.924 ± 0.131	30.611 ± 2.074
1333	J111350-153333	4664.309 ± 0.003	16.535 ± 0.109	44.492 ± 1.074
1334	J111350-153333	4662.275 ± 0.035	12.503 ± 0.212	14.420 ± 4.342
1335	J111350-153333	4661.512 ± 0.014	13.627 ± 0.027	39.550 ± 2.905
1336	J111350-153333	4660.112 ± 0.003	15.310 ± 0.047	27.678 ± 0.477
1337	J111350-153333	4656.025 ± 0.015	12.715 ± 0.033	15.352 ± 1.513
1338	J111350-153333	4655.026 ± 0.043	11.980 ± 0.125	11.304 ± 4.551
1339	J111350-153333	4653.641 ± 0.028	12.742 ± 0.030	32.979 ± 2.793
1340	J111350-153333	4651.934 ± 0.022	13.656 ± 0.028	30.546 ± 0.934
1341	J111350-153333	4649.330 ± 0.047	11.964 ± 0.116	13.483 ± 4.621
1342	J111350-153333	4648.388 ± 0.115	12.046 ± 0.178	25.106 ± 11.367
1343	J111350-153333	4646.946 ± 0.071	12.809 ± 0.058	48.087 ± 7.816
1344	J111350-153333	4645.696 ± 0.041	12.347 ± 0.145	10.542 ± 3.154
1345	J111350-153333	4645.320 ± 0.056	12.533 ± 0.283	11.735 ± 6.477
1346	J111350-153333	4644.941 ± 0.039	12.653 ± 0.314	12.869 ± 8.980
1347	J111350-153333	4643.758 ± 0.022	12.570 ± 0.047	18.105 ± 2.707
1348	J111350-153333	4639.603 ± 0.078	12.177 ± 0.097	27.189 ± 7.241
1349	J111350-153333	4635.588 ± 0.021	12.868 ± 0.024	29.913 ± 1.975

Table E.1. *Continued*

1350	J111350-153333	4633.622 ± 0.007	13.371 ± 0.008	30.937 ± 0.682
1351	J111350-153333	4632.267 ± 0.123	12.409 ± 0.189	22.150 ± 8.534
1352	J111350-153333	4631.166 ± 0.009	13.615 ± 0.013	28.596 ± 0.970
1353	J111350-153333	4630.024 ± 0.017	13.703 ± 0.026	33.368 ± 2.161
1354	J111350-153333	4629.300 ± 0.018	13.403 ± 0.047	19.282 ± 0.862
1355	J111350-153333	4626.131 ± 0.044	12.374 ± 0.128	18.205 ± 6.673
1356	J111350-153333	4625.337 ± 0.078	13.210 ± 0.159	20.013 ± 4.072
1357	J111350-153333	4624.911 ± 0.066	13.036 ± 0.266	16.977 ± 5.773
1358	J111350-153333	4624.494 ± 0.032	12.510 ± 0.198	10.395 ± 2.976
1359	J111350-153333	4623.847 ± 0.004	13.851 ± 0.007	24.462 ± 0.574
1360	J111350-153333	4623.004 ± 0.049	12.740 ± 0.072	25.641 ± 4.384
1361	J111350-153333	4621.833 ± 0.033	12.228 ± 0.121	12.015 ± 4.072
1362	J111350-153333	4621.277 ± 0.019	12.712 ± 0.048	17.971 ± 2.664
1363	J111350-153333	4619.952 ± 0.044	12.816 ± 0.082	18.840 ± 3.280
1364	J111350-153333	4619.553 ± 0.044	12.371 ± 0.236	11.763 ± 3.847
1365	J111350-153333	4618.907 ± 0.061	12.412 ± 0.088	24.697 ± 6.326
1366	J111350-153333	4616.554 ± 0.044	13.304 ± 0.038	58.831 ± 6.282
1367	J111350-153333	4616.681 ± 0.054	13.700 ± 0.903	11.441 ± 4.467
1368	J111350-153333	4616.549 ± 0.223	13.730 ± 0.854	14.894 ± 4.636
1369	J111350-153333	4614.707 ± 0.008	13.274 ± 0.015	17.277 ± 0.767
1370	J111350-153333	4613.446 ± 0.088	12.820 ± 0.242	15.932 ± 4.607
1371	J111350-153333	4613.030 ± 0.046	13.140 ± 0.133	17.403 ± 3.973
1372	J111350-153333	4612.441 ± 0.094	12.287 ± 0.243	16.935 ± 9.247
1373	J111350-153333	4611.576 ± 0.107	12.490 ± 0.183	24.779 ± 10.793
1374	J111350-153333	4610.748 ± 0.029	13.265 ± 0.113	22.671 ± 5.679
1375	J111350-153333	4610.123 ± 0.081	12.824 ± 0.283	20.285 ± 9.587
1376	J111350-153333	4608.089 ± 0.005	16.197 ± 0.166	45.569 ± 2.104
1377	J111350-153333	4605.937 ± 0.057	13.186 ± 0.116	34.464 ± 9.337
1378	J111350-153333	4604.908 ± 0.287	12.771 ± 0.948	22.071 ± 39.696
1379	J111350-153333	4604.440 ± 0.039	13.533 ± 0.124	17.660 ± 1.596
1380	J111350-153333	4603.188 ± 0.003	13.561 ± 0.021	13.240 ± 0.472
1381	J111350-153333	4603.257 ± 0.047	13.046 ± 0.053	42.438 ± 7.773
1382	J111350-153333	4600.337 ± 0.039	12.564 ± 0.078	22.543 ± 5.373
1383	J111350-153333	4598.716 ± 0.007	15.085 ± 0.051	34.037 ± 0.959
1384	J111350-153333	4597.569 ± 0.022	13.156 ± 0.078	15.908 ± 2.275
1385	J111350-153333	4596.751 ± 0.020	13.531 ± 0.023	36.955 ± 2.295
1386	J111350-153333	4595.771 ± 0.052	12.172 ± 0.156	14.761 ± 5.049
1387	J111350-153333	4594.860 ± 0.047	12.155 ± 0.102	15.500 ± 4.635
1388	J111350-153333	4594.210 ± 0.022	12.315 ± 0.068	11.141 ± 2.267
1389	J111350-153333	4592.765 ± 0.131	13.612 ± 0.128	42.180 ± 5.833
1390	J111350-153333	4591.965 ± 0.064	13.749 ± 0.092	36.642 ± 2.412
1391	J111350-153333	4590.362 ± 0.032	12.870 ± 0.054	26.530 ± 3.361
1392	J111350-153333	4588.946 ± 0.010	13.691 ± 0.042	23.925 ± 1.245
1393	J111350-153333	4588.830 ± 0.048	13.570 ± 0.061	54.171 ± 3.387

Table E.1. *Continued*

1394	J111350-153333	4581.896 ± 0.017	12.434 ± 0.050	11.106 ± 1.776
1395	J111350-153333	4579.837 ± 0.053	12.678 ± 0.097	18.150 ± 4.002
1396	J111350-153333	4578.562 ± 0.003	14.160 ± 0.011	22.141 ± 0.311
1397	J111350-153333	4577.247 ± 0.009	13.668 ± 0.008	41.007 ± 1.023
1398	J111350-153333	4575.822 ± 0.038	12.767 ± 0.043	32.346 ± 3.652
1399	J111350-153333	4571.964 ± 0.060	13.032 ± 0.132	36.750 ± 12.394
1400	J111350-153333	4569.722 ± 0.249	13.334 ± 0.342	41.341 ± 6.421
1401	J111350-153333	4569.536 ± 0.008	14.183 ± 0.037	21.965 ± 1.230
1402	J111350-153333	4568.436 ± 0.007	14.099 ± 0.010	23.548 ± 0.493
1403	J111350-153333	4567.244 ± 0.005	13.621 ± 0.008	25.716 ± 0.607
1404	J111350-153333	4566.391 ± 0.013	13.029 ± 0.022	20.213 ± 1.182
1405	J111350-153333	4564.281 ± 0.003	14.684 ± 0.019	31.009 ± 0.386
1406	J111350-153333	4560.937 ± 0.055	13.210 ± 0.128	23.764 ± 2.406
1407	J111350-153333	4560.225 ± 0.026	13.683 ± 0.063	32.545 ± 4.746
1408	J111350-153333	4559.591 ± 0.013	13.079 ± 0.099	13.275 ± 1.725
1409	J111350-153333	4558.952 ± 0.005	14.013 ± 0.007	23.421 ± 0.390
1410	J111350-153333	4554.121 ± 0.003	14.047 ± 0.007	23.204 ± 0.253
1411	J111350-153333	4552.394 ± 0.017	12.563 ± 0.050	13.778 ± 2.294
1412	J111350-153333	4551.276 ± 0.075	12.752 ± 0.154	18.818 ± 6.207
1413	J111350-153333	4550.597 ± 0.045	12.157 ± 0.133	13.869 ± 5.411
1414	J111350-153333	4549.792 ± 0.015	12.778 ± 0.038	12.621 ± 1.385
1415	J111350-153333	4548.765 ± 0.035	12.572 ± 0.045	26.548 ± 3.294
1416	J111350-153333	4546.228 ± 0.003	13.740 ± 0.005	24.238 ± 0.292
1417	J111350-153333	4544.626 ± 0.024	13.360 ± 0.028	29.140 ± 1.768
1418	J111350-153333	4543.648 ± 0.012	13.203 ± 0.021	18.349 ± 1.012
1419	J111350-153333	4542.248 ± 0.005	13.917 ± 0.007	26.297 ± 0.375
1420	J111350-153333	4540.799 ± 0.005	14.194 ± 0.013	25.936 ± 0.701
1421	J111350-153333	4540.331 ± 0.048	13.880 ± 0.027	70.686 ± 2.468
1422	J111350-153333	4538.465 ± 0.008	13.481 ± 0.011	30.410 ± 0.787
1423	J111350-153333	4536.646 ± 0.025	13.099 ± 0.035	32.069 ± 2.458
1424	J111350-153333	4535.342 ± 0.162	13.251 ± 0.191	28.478 ± 7.868
1425	J111350-153333	4534.964 ± 0.005	13.670 ± 0.070	14.828 ± 0.861
1426	J111350-153333	4533.998 ± 0.097	12.630 ± 0.170	26.683 ± 10.539
1427	J111350-153333	4533.582 ± 0.035	12.143 ± 0.382	10.669 ± 4.977
1428	J111350-153333	4532.917 ± 0.009	13.464 ± 0.016	24.846 ± 1.024
1429	J111350-153333	4532.076 ± 0.226	13.276 ± 0.588	22.634 ± 7.885
1430	J111350-153333	4531.471 ± 0.043	13.694 ± 1.199	20.456 ± 9.171
1431	J111350-153333	4531.262 ± 1.601	13.457 ± 2.456	31.530 ± 43.272
1432	J111350-153333	4530.103 ± 0.005	13.614 ± 0.009	21.222 ± 0.370
1433	J010604-254651	5150.195 ± 0.252	12.608 ± 0.177	45.582 ± 15.975
1434	J010604-254651	5149.735 ± 0.048	12.107 ± 0.325	10.831 ± 6.081
1435	J010604-254651	5148.922 ± 0.060	12.130 ± 0.204	13.071 ± 5.921
1436	J010604-254651	5147.718 ± 0.007	14.052 ± 0.009	27.568 ± 0.550
1437	J010604-254651	5146.707 ± 0.043	12.915 ± 0.057	23.722 ± 2.956

Table E.1. *Continued*

1438	J010604-254651	5145.020 ± 0.049	12.560 ± 0.073	20.696 ± 4.367
1439	J010604-254651	5144.378 ± 0.059	12.171 ± 0.164	12.689 ± 4.989
1440	J010604-254651	5142.419 ± 0.107	13.070 ± 0.055	63.687 ± 9.402
1441	J010604-254651	5141.144 ± 0.068	12.752 ± 0.161	21.176 ± 5.066
1442	J010604-254651	5140.382 ± 0.023	13.484 ± 0.024	27.490 ± 1.405
1443	J010604-254651	5138.590 ± 0.008	13.200 ± 0.013	18.257 ± 0.624
1444	J010604-254651	5137.060 ± 0.020	12.835 ± 0.031	20.664 ± 1.889
1445	J010604-254651	5135.979 ± 0.062	12.064 ± 0.127	14.412 ± 5.329
1446	J010604-254651	5132.547 ± 0.124	12.733 ± 0.147	25.235 ± 7.425
1447	J010604-254651	5127.697 ± 0.066	13.386 ± 0.164	26.644 ± 2.583
1448	J010604-254651	5126.948 ± 0.782	12.710 ± 0.893	36.977 ± 56.590
1449	J010604-254651	5125.750 ± 0.041	13.547 ± 0.153	23.424 ± 2.681
1450	J010604-254651	5125.065 ± 0.226	13.225 ± 0.445	34.535 ± 24.033
1451	J010604-254651	5123.983 ± 0.163	13.336 ± 0.135	40.515 ± 6.630
1452	J010604-254651	5121.432 ± 0.045	12.133 ± 0.121	10.913 ± 4.470
1453	J010604-254651	5119.548 ± 0.039	12.521 ± 0.057	20.647 ± 3.245
1454	J010604-254651	5117.594 ± 0.046	12.524 ± 0.107	12.686 ± 3.480
1455	J010604-254651	5114.387 ± 0.021	12.680 ± 0.038	16.761 ± 1.781
1456	J010604-254651	5111.671 ± 0.042	12.921 ± 0.033	39.420 ± 3.493
1457	J010604-254651	5105.734 ± 0.031	12.607 ± 0.140	10.312 ± 3.717
1458	J010604-254651	5105.154 ± 0.009	13.470 ± 0.014	19.234 ± 0.848
1459	J010604-254651	5103.706 ± 0.019	13.145 ± 0.028	23.477 ± 1.969
1460	J010604-254651	5102.312 ± 0.005	13.803 ± 0.008	22.626 ± 0.356
1461	J010604-254651	5100.408 ± 0.041	13.042 ± 0.047	28.076 ± 3.462
1462	J010604-254651	5099.070 ± 0.052	12.104 ± 0.183	11.224 ± 5.550
1463	J010604-254651	5097.960 ± 0.093	12.723 ± 0.068	46.814 ± 9.545
1464	J010604-254651	5096.592 ± 0.032	12.176 ± 0.101	10.025 ± 2.996
1465	J010604-254651	5095.511 ± 0.072	12.214 ± 0.121	18.720 ± 6.810
1466	J010604-254651	5092.879 ± 0.025	13.380 ± 0.024	30.561 ± 1.661
1467	J010604-254651	5092.191 ± 0.037	12.404 ± 0.535	10.412 ± 5.896
1468	J010604-254651	5091.764 ± 0.215	12.746 ± 0.389	26.155 ± 22.964
1469	J010604-254651	5091.110 ± 0.068	12.213 ± 0.520	10.172 ± 7.423
1470	J010604-254651	5090.623 ± 0.017	13.521 ± 0.021	22.398 ± 1.163
1471	J010604-254651	5089.183 ± 0.015	13.286 ± 0.014	32.791 ± 1.286
1472	J010604-254651	5086.581 ± 0.005	14.798 ± 0.034	32.510 ± 0.652
1473	J010604-254651	5085.270 ± 0.056	12.424 ± 0.117	16.116 ± 4.454
1474	J010604-254651	5083.786 ± 0.045	12.348 ± 0.231	12.861 ± 4.665
1475	J010604-254651	5083.090 ± 0.024	13.493 ± 0.020	34.238 ± 1.711
1476	J010604-254651	5080.327 ± 0.047	12.898 ± 0.051	28.457 ± 3.931
1477	J010604-254651	5079.644 ± 0.031	12.862 ± 0.124	11.683 ± 2.291
1478	J010604-254651	5079.160 ± 0.013	13.582 ± 0.026	17.383 ± 1.181
1479	J010604-254651	5077.550 ± 0.010	14.563 ± 0.024	42.297 ± 1.429
1480	J010604-254651	5076.304 ± 0.024	13.067 ± 0.129	14.033 ± 2.602
1481	J010604-254651	5075.667 ± 0.031	13.579 ± 0.037	30.789 ± 2.766

Table E.1. *Continued*

1482	J010604-254651	5074.468 ± 0.036	12.954 ± 0.045	26.045 ± 2.944
1483	J010604-254651	5072.183 ± 0.016	13.447 ± 0.102	23.576 ± 2.412
1484	J010604-254651	5072.108 ± 0.023	13.631 ± 0.065	48.761 ± 3.373
1485	J010604-254651	5068.256 ± 0.017	13.062 ± 0.021	24.300 ± 1.402
1486	J010604-254651	5063.206 ± 0.056	12.349 ± 0.089	19.334 ± 4.785
1487	J010604-254651	5060.679 ± 0.221	12.726 ± 0.236	29.720 ± 11.989
1488	J010604-254651	5059.950 ± 0.148	12.804 ± 0.454	20.924 ± 14.069
1489	J010604-254651	5059.382 ± 0.156	12.686 ± 0.592	19.041 ± 15.255
1490	J010604-254651	5058.742 ± 0.499	12.276 ± 0.659	24.848 ± 28.061
1491	J010604-254651	5057.357 ± 0.066	13.905 ± 0.144	20.295 ± 1.858
1492	J010604-254651	5056.913 ± 0.127	13.660 ± 0.239	21.695 ± 3.563
1493	J010604-254651	5055.705 ± 0.014	12.880 ± 0.026	16.667 ± 1.239
1494	J010604-254651	5053.355 ± 0.005	13.834 ± 0.010	19.985 ± 0.404
1495	J010604-254651	5052.397 ± 0.009	13.504 ± 0.011	23.409 ± 0.735
1496	J010604-254651	5050.295 ± 0.024	13.739 ± 0.065	15.871 ± 1.464
1497	J010604-254651	5049.890 ± 0.012	14.139 ± 0.016	39.762 ± 0.531
1498	J010604-254651	5045.350 ± 0.069	12.741 ± 0.051	42.542 ± 5.823
1499	J010604-254651	5040.879 ± 0.029	15.282 ± 0.058	43.265 ± 1.069
1500	J010604-254651	5038.056 ± 0.027	16.796 ± 0.242	36.321 ± 1.639
1501	J010604-254651	5035.885 ± 0.048	12.381 ± 0.154	14.727 ± 5.026
1502	J010604-254651	5034.221 ± 0.552	13.751 ± 0.397	51.242 ± 18.107
1503	J010604-254651	5033.202 ± 0.023	15.377 ± 0.167	33.892 ± 2.703
1504	J010604-254651	5031.386 ± 0.120	13.450 ± 0.071	40.072 ± 5.586
1505	J010604-254651	5029.061 ± 0.018	13.305 ± 0.019	29.774 ± 1.624
1506	J010604-254651	5028.210 ± 0.048	12.416 ± 0.150	13.511 ± 5.456
1507	J010604-254651	5027.274 ± 0.016	13.629 ± 0.051	22.369 ± 1.636
1508	J010604-254651	5026.552 ± 0.220	13.020 ± 0.196	36.235 ± 11.128
1509	J010604-254651	5024.611 ± 0.065	13.494 ± 0.076	26.850 ± 3.032
1510	J010604-254651	5023.984 ± 0.013	14.095 ± 0.043	16.804 ± 1.849
1511	J010604-254651	5023.418 ± 0.015	13.546 ± 0.044	10.754 ± 0.948
1512	J010604-254651	5022.608 ± 0.011	13.375 ± 0.030	16.436 ± 1.413
1513	J010604-254651	5021.993 ± 0.044	12.856 ± 0.075	18.195 ± 3.081
1514	J010604-254651	5020.184 ± 0.059	12.355 ± 0.092	19.686 ± 5.032
1515	J010604-254651	5017.086 ± 0.053	13.126 ± 0.027	61.188 ± 4.365
1516	J010604-254651	5013.396 ± 0.023	13.336 ± 0.017	42.750 ± 2.073
1517	J010604-254651	5011.868 ± 0.012	13.721 ± 0.023	27.058 ± 1.042
1518	J010604-254651	5010.551 ± 0.007	13.911 ± 0.020	20.228 ± 0.797
1519	J010604-254651	5009.999 ± 0.157	13.574 ± 0.073	73.010 ± 8.012
1520	J010604-254651	5007.338 ± 0.005	14.511 ± 0.021	34.342 ± 0.666
1521	J010604-254651	5004.397 ± 0.005	15.953 ± 0.080	47.757 ± 1.031
1522	J010604-254651	5000.847 ± 0.005	14.704 ± 0.020	44.334 ± 0.622
1523	J010604-254651	4991.103 ± 0.013	13.355 ± 0.018	22.280 ± 1.033
1524	J010604-254651	4990.115 ± 0.008	13.776 ± 0.010	25.904 ± 0.664
1525	J010604-254651	4988.879 ± 0.091	12.128 ± 0.184	16.342 ± 8.965

Table E.1. *Continued*

1526	J010604-254651	4988.275 ± 0.044	12.340 ± 0.154	12.169 ± 4.449
1527	J010604-254651	4987.509 ± 0.025	13.101 ± 0.036	27.873 ± 3.043
1528	J010604-254651	4985.403 ± 0.205	12.733 ± 0.136	60.334 ± 23.409
1529	J010604-254651	4983.733 ± 0.082	12.213 ± 0.233	15.748 ± 7.433
1530	J010604-254651	4982.836 ± 0.036	13.141 ± 0.057	30.968 ± 3.942
1531	J010604-254651	4981.137 ± 0.189	13.623 ± 0.135	50.927 ± 11.715
1532	J010604-254651	4980.198 ± 0.024	14.217 ± 0.043	27.079 ± 2.561
1533	J010604-254651	4979.342 ± 0.144	13.243 ± 0.269	26.638 ± 12.849
1534	J010604-254651	4978.542 ± 0.045	13.447 ± 0.153	16.964 ± 3.006
1535	J010604-254651	4978.100 ± 0.155	13.102 ± 0.291	19.677 ± 6.524
1536	J010604-254651	4977.048 ± 0.041	13.236 ± 0.087	21.113 ± 2.447
1537	J010604-254651	4976.294 ± 0.033	13.491 ± 0.080	28.709 ± 4.868
1538	J010604-254651	4975.108 ± 0.032	13.780 ± 0.055	35.638 ± 4.806
1539	J010604-254651	4974.203 ± 0.116	13.625 ± 0.257	20.849 ± 6.452
1540	J010604-254651	4973.717 ± 0.051	13.962 ± 0.113	19.154 ± 1.482
1541	J010604-254651	4969.490 ± 0.050	12.526 ± 0.067	23.953 ± 4.521
1542	J010604-254651	4968.309 ± 0.008	13.409 ± 0.011	22.599 ± 0.662
1543	J010604-254651	4966.342 ± 0.082	12.838 ± 0.083	39.125 ± 6.800
1544	J010604-254651	4966.205 ± 0.006	13.269 ± 0.028	10.634 ± 0.657
1545	J010604-254651	4964.897 ± 0.124	12.572 ± 0.190	24.535 ± 10.414
1546	J010604-254651	4964.034 ± 0.022	13.888 ± 0.037	22.058 ± 1.618
1547	J010604-254651	4963.328 ± 0.025	13.881 ± 0.034	23.087 ± 1.307
1548	J010604-254651	4961.685 ± 0.008	13.533 ± 0.012	21.319 ± 0.663
1549	J010604-254651	4960.229 ± 0.006	14.534 ± 0.025	36.250 ± 0.872
1550	J010604-254651	4958.787 ± 0.025	12.785 ± 0.049	18.272 ± 2.393
1551	J010604-254651	4958.059 ± 0.020	12.469 ± 0.056	10.851 ± 1.851
1552	J010604-254651	4955.863 ± 0.046	13.518 ± 0.038	37.673 ± 2.648
1553	J010604-254651	4954.801 ± 0.068	13.233 ± 0.079	34.548 ± 4.746
1554	J010604-254651	4952.615 ± 0.479	13.034 ± 0.616	31.358 ± 18.062
1555	J010604-254651	4951.963 ± 0.062	13.839 ± 0.097	28.836 ± 2.151
1556	J010604-254651	4950.408 ± 0.073	12.842 ± 0.086	29.716 ± 6.746
1557	J010604-254651	4949.637 ± 0.010	13.433 ± 0.021	17.642 ± 0.722
1558	J010604-254651	4948.527 ± 0.018	13.146 ± 0.031	19.573 ± 1.411
1559	J010604-254651	4947.221 ± 0.006	14.471 ± 0.023	35.463 ± 0.869
1560	J010604-254651	4945.444 ± 0.037	13.012 ± 0.045	32.222 ± 3.895
1561	J010604-254651	4943.935 ± 0.104	12.743 ± 0.111	43.013 ± 14.121
1562	J010604-254651	4941.018 ± 0.016	15.434 ± 0.066	45.603 ± 1.287
1563	J010604-254651	4939.401 ± 0.031	13.407 ± 0.076	17.196 ± 1.597
1564	J010604-254651	4933.981 ± 0.019	12.768 ± 0.039	15.666 ± 1.866
1565	J010604-254651	4930.837 ± 0.023	13.167 ± 0.054	22.027 ± 3.447
1566	J010604-254651	4929.370 ± 0.018	13.005 ± 0.036	16.884 ± 1.742
1567	J010604-254651	4928.444 ± 0.036	12.801 ± 0.077	18.909 ± 2.886
1568	J010604-254651	4927.644 ± 0.016	13.507 ± 0.017	28.777 ± 1.279
1569	J010604-254651	4926.011 ± 0.028	12.843 ± 0.042	22.492 ± 2.768

Table E.1. *Continued*

1570	J010604-254651	4923.735 ± 0.059	12.896 ± 0.053	35.326 ± 4.825
1571	J010604-254651	4920.379 ± 0.004	14.869 ± 0.038	32.530 ± 0.643
1572	J010604-254651	4918.892 ± 0.041	12.976 ± 0.085	16.460 ± 3.306
1573	J010604-254651	4917.417 ± 0.033	13.327 ± 0.291	14.414 ± 3.681
1574	J010604-254651	4917.338 ± 0.017	13.795 ± 0.099	24.029 ± 1.321
1575	J010604-254651	4914.753 ± 0.005	14.391 ± 0.034	21.961 ± 0.588
1576	J010604-254651	4913.672 ± 0.008	13.749 ± 0.011	24.335 ± 0.832
1577	J010604-254651	4912.435 ± 0.008	14.106 ± 0.016	23.578 ± 0.842
1578	J010604-254651	4911.489 ± 0.005	13.527 ± 0.015	10.984 ± 0.491
1579	J010604-254651	4909.731 ± 0.054	12.970 ± 0.081	28.681 ± 6.415
1580	J010604-254651	4908.548 ± 0.011	13.313 ± 0.015	21.943 ± 0.914
1581	J010604-254651	4903.534 ± 0.015	13.957 ± 0.017	26.214 ± 0.850
1582	J010604-254651	4902.748 ± 0.016	13.688 ± 0.053	20.020 ± 1.576
1583	J010604-254651	4902.103 ± 0.199	13.027 ± 0.183	35.426 ± 9.954
1584	J010604-254651	4899.292 ± 0.013	12.917 ± 0.025	16.732 ± 1.203
1585	J010604-254651	4898.580 ± 0.054	12.080 ± 0.187	10.719 ± 5.203
1586	J010604-254651	4897.678 ± 1.058	12.692 ± 1.498	26.441 ± 40.665
1587	J010604-254651	4897.301 ± 0.233	12.573 ± 1.924	17.903 ± 16.891
1588	J010604-254651	4893.651 ± 0.016	13.267 ± 0.015	34.413 ± 1.385
1589	J010604-254651	4883.847 ± 0.042	13.341 ± 0.090	16.322 ± 1.825
1590	J010604-254651	4883.452 ± 0.092	12.876 ± 0.279	14.900 ± 5.424
1591	J010604-254651	4882.545 ± 0.005	14.195 ± 0.020	23.022 ± 0.670
1592	J010604-254651	4881.509 ± 0.069	12.574 ± 0.139	19.288 ± 6.533
1593	J010604-254651	4880.693 ± 0.012	13.403 ± 0.016	23.254 ± 1.042
1594	J010604-254651	4879.013 ± 0.013	13.229 ± 0.016	26.632 ± 1.210
1595	J010604-254651	4877.473 ± 0.134	13.634 ± 0.318	29.833 ± 2.678
1596	J010604-254651	4877.298 ± 0.016	14.122 ± 0.082	19.379 ± 2.200
1597	J010604-254651	4875.921 ± 0.042	13.403 ± 0.055	30.527 ± 4.072
1598	J010604-254651	4874.808 ± 0.092	12.749 ± 0.196	26.082 ± 12.459
1599	J010604-254651	4874.258 ± 0.071	12.217 ± 0.415	12.393 ± 6.817
1600	J010604-254651	4873.258 ± 0.019	13.572 ± 0.031	26.109 ± 1.200
1601	J010604-254651	4872.331 ± 0.095	13.096 ± 0.103	37.511 ± 8.874
1602	J010604-254651	4871.030 ± 0.005	14.022 ± 0.014	21.825 ± 0.452
1603	J010604-254651	4866.073 ± 0.159	13.394 ± 0.208	28.434 ± 5.834
1604	J010604-254651	4865.600 ± 0.093	13.202 ± 0.322	21.521 ± 3.644
1605	J010604-254651	4863.822 ± 0.020	13.391 ± 0.020	30.743 ± 1.643
1606	J010604-254651	4862.539 ± 0.059	12.676 ± 0.075	28.168 ± 7.051
1607	J010604-254651	4861.220 ± 0.048	12.641 ± 0.069	23.033 ± 4.563
1608	J010604-254651	4856.657 ± 0.010	13.391 ± 0.012	26.088 ± 0.910
1609	J010604-254651	4848.381 ± 0.028	12.662 ± 0.045	19.776 ± 2.460
1610	J010604-254651	4847.005 ± 0.038	12.656 ± 0.065	19.505 ± 3.658
1611	J010604-254651	4845.111 ± 0.132	14.060 ± 0.818	22.659 ± 6.441
1612	J010604-254651	4844.768 ± 0.937	13.797 ± 1.485	29.260 ± 22.953
1613	J010604-254651	4843.283 ± 0.066	12.681 ± 0.120	18.899 ± 5.673

Table E.1. *Continued*

1614	J010604-254651	4842.750 ± 0.062	12.330 ± 0.194	12.267 ± 4.670
1615	J010604-254651	4839.953 ± 0.117	12.832 ± 0.290	17.169 ± 4.980
1616	J010604-254651	4839.533 ± 0.241	12.610 ± 0.484	18.711 ± 10.738
1617	J010604-254651	4834.285 ± 0.020	13.007 ± 0.027	24.706 ± 1.763
1618	J010604-254651	4832.573 ± 0.282	13.751 ± 0.432	29.002 ± 7.389
1619	J010604-254651	4832.099 ± 0.087	14.109 ± 0.209	24.921 ± 2.162
1620	J010604-254651	4828.665 ± 0.035	12.493 ± 0.090	14.291 ± 3.144
1621	J010604-254651	4827.704 ± 0.161	12.924 ± 0.198	30.963 ± 11.455
1622	J010604-254651	4826.822 ± 0.018	13.826 ± 0.035	27.463 ± 1.982
1623	J010604-254651	4825.286 ± 0.040	14.277 ± 0.032	50.505 ± 2.143
1624	J010604-254651	4824.834 ± 0.048	13.941 ± 0.114	21.685 ± 3.026
1625	J010604-254651	4823.343 ± 0.040	13.161 ± 0.043	30.450 ± 3.225
1626	J010604-254651	4821.792 ± 0.071	12.844 ± 0.321	19.283 ± 4.985
1627	J010604-254651	4821.176 ± 0.085	13.342 ± 0.136	32.944 ± 8.538
1628	J010604-254651	4819.948 ± 0.164	12.881 ± 0.140	41.918 ± 12.925
1629	J010604-254651	4817.944 ± 0.017	13.509 ± 0.022	27.728 ± 1.463
1630	J010604-254651	4816.645 ± 0.037	13.812 ± 0.040	39.656 ± 3.697
1631	J010604-254651	4815.717 ± 0.019	13.716 ± 0.049	24.992 ± 2.096
1632	J010604-254651	4815.056 ± 0.072	12.457 ± 0.233	14.251 ± 4.889
1633	J010604-254651	4813.327 ± 0.011	14.379 ± 0.020	30.796 ± 0.761
1634	J010604-254651	4812.078 ± 0.036	13.789 ± 0.058	32.630 ± 4.455
1635	J010604-254651	4811.091 ± 0.013	14.664 ± 0.051	24.246 ± 0.780
1636	J010604-254651	4807.461 ± 0.043	12.522 ± 0.065	21.477 ± 3.819
1637	J010604-254651	4801.393 ± 0.071	12.391 ± 0.097	24.163 ± 6.502
1638	J010604-254651	4799.466 ± 0.345	12.979 ± 0.507	25.131 ± 13.107
1639	J010604-254651	4799.086 ± 0.035	13.366 ± 0.206	17.137 ± 2.076
1640	J010604-254651	4797.252 ± 0.110	12.658 ± 0.075	48.608 ± 9.852
1641	J010604-254651	4793.660 ± 0.069	12.278 ± 0.173	16.061 ± 6.145
1642	J010604-254651	4792.796 ± 0.033	13.092 ± 0.035	32.662 ± 3.302
1643	J010604-254651	4791.302 ± 0.024	12.982 ± 0.033	25.073 ± 2.420
1644	J010604-254651	4790.399 ± 0.010	13.244 ± 0.022	16.804 ± 0.987
1645	J010604-254651	4789.005 ± 0.007	14.564 ± 0.035	34.864 ± 1.125
1646	J010604-254651	4787.812 ± 0.114	13.209 ± 0.510	12.468 ± 4.374
1647	J010604-254651	4787.498 ± 0.170	13.261 ± 0.494	15.189 ± 11.854
1648	J010604-254651	4786.246 ± 0.007	14.079 ± 0.015	23.865 ± 0.609
1649	J010604-254651	4782.691 ± 0.046	12.252 ± 0.107	14.018 ± 4.325
1650	J010604-254651	4781.689 ± 0.038	12.744 ± 0.048	26.454 ± 3.485
1651	J010604-254651	4777.981 ± 0.005	13.663 ± 0.009	22.443 ± 0.438
1652	J010604-254651	4773.599 ± 0.061	13.210 ± 0.100	19.812 ± 3.108
1653	J010604-254651	4773.229 ± 0.044	12.786 ± 0.356	12.256 ± 4.526
1654	J010604-254651	4772.686 ± 0.119	13.042 ± 0.342	24.466 ± 14.050
1655	J010604-254651	4772.007 ± 0.131	13.187 ± 0.207	26.691 ± 8.446
1656	J010604-254651	4771.043 ± 0.015	13.343 ± 0.022	22.772 ± 1.202
1657	J010604-254651	4769.127 ± 0.005	13.852 ± 0.008	27.162 ± 0.421

Table E.1. *Continued*

1658	J010604-254651	4766.944 ± 0.013	13.619 ± 0.014	29.081 ± 1.072
1659	J010604-254651	4765.466 ± 0.005	15.542 ± 0.104	28.157 ± 0.871
1660	J010604-254651	4757.773 ± 0.011	14.317 ± 0.025	27.610 ± 0.786
1661	J010604-254651	4756.712 ± 0.020	13.839 ± 0.019	31.999 ± 1.257
1662	J010604-254651	4754.458 ± 0.187	12.652 ± 0.210	30.200 ± 12.974
1663	J010604-254651	4753.761 ± 0.031	13.140 ± 0.066	20.981 ± 1.963
1664	J010604-254651	4750.867 ± 1.277	12.903 ± 1.091	45.827 ± 42.476
1665	J010604-254651	4750.350 ± 0.014	13.802 ± 0.129	27.307 ± 2.463
1666	J010604-254651	4748.685 ± 0.198	12.761 ± 0.113	59.458 ± 17.099
1667	J010604-254651	4742.410 ± 0.048	12.185 ± 0.114	13.455 ± 4.449
1668	J010604-254651	4741.199 ± 0.015	13.146 ± 0.019	26.677 ± 1.336
1669	J010604-254651	4739.008 ± 0.019	12.600 ± 0.045	13.262 ± 1.718
1670	J010604-254651	4737.724 ± 0.026	12.898 ± 0.075	15.363 ± 1.853
1671	J010604-254651	4737.162 ± 0.035	13.108 ± 0.049	23.452 ± 2.601
1672	J010604-254651	4734.297 ± 0.012	13.818 ± 0.010	39.918 ± 0.901
1673	J010604-254651	4732.259 ± 0.180	12.953 ± 1.217	20.746 ± 11.283
1674	J010604-254651	4731.794 ± 0.672	13.049 ± 1.195	30.389 ± 50.593
1675	J010604-254651	4730.777 ± 0.219	13.032 ± 0.306	35.647 ± 21.332
1676	J010604-254651	4729.841 ± 0.113	12.348 ± 0.454	18.369 ± 16.139
1677	J010604-254651	4728.350 ± 0.039	12.441 ± 0.092	15.457 ± 4.177
1678	J010604-254651	4727.559 ± 0.019	13.025 ± 0.027	22.947 ± 1.810
1679	J010604-254651	4725.079 ± 0.031	12.370 ± 0.096	10.570 ± 3.217
1680	J010604-254651	4724.251 ± 0.062	12.116 ± 0.208	11.521 ± 7.936
1681	J010604-254651	4722.797 ± 0.048	13.191 ± 0.058	27.253 ± 3.218
1682	J010604-254651	4721.986 ± 0.009	14.015 ± 0.016	23.316 ± 0.664
1683	J010604-254651	4719.431 ± 0.029	13.542 ± 0.042	22.202 ± 1.638
1684	J010604-254651	4718.916 ± 0.066	12.929 ± 0.167	17.261 ± 3.389
1685	J010604-254651	4717.651 ± 0.043	12.307 ± 0.097	14.221 ± 3.943
1686	J010604-254651	4716.233 ± 0.006	13.714 ± 0.010	24.841 ± 0.516
1687	J010604-254651	4714.566 ± 0.011	13.446 ± 0.013	29.644 ± 0.965
1688	J010604-254651	4713.337 ± 0.098	12.040 ± 0.192	17.008 ± 9.271
1689	J010604-254651	4711.663 ± 0.019	13.568 ± 0.017	36.960 ± 1.487
1690	J010604-254651	4709.484 ± 0.359	14.121 ± 0.256	53.441 ± 14.766
1691	J010604-254651	4708.410 ± 0.033	15.798 ± 0.127	33.203 ± 1.179
1692	J010604-254651	4701.147 ± 0.038	12.558 ± 0.693	13.278 ± 7.546
1693	J010604-254651	4700.819 ± 0.390	12.672 ± 0.571	25.131 ± 18.970
1694	J010604-254651	4699.902 ± 0.133	12.515 ± 0.402	15.165 ± 7.813
1695	J010604-254651	4699.455 ± 0.135	12.628 ± 0.347	18.156 ± 12.943
1696	J010604-254651	4698.292 ± 0.020	12.985 ± 0.026	26.254 ± 1.907
1697	J010604-254651	4693.351 ± 0.015	13.025 ± 0.023	21.700 ± 1.326
1698	J010604-254651	4691.812 ± 0.018	12.837 ± 0.036	16.323 ± 1.723
1699	J010604-254651	4689.876 ± 0.004	14.519 ± 0.029	27.010 ± 0.496
1700	J010604-254651	4686.312 ± 0.006	13.948 ± 0.009	26.816 ± 0.533
1701	J010604-254651	4682.571 ± 0.005	13.947 ± 0.013	21.964 ± 0.467

Table E.1. *Continued*

1702	J010604-254651	4681.464 ± 0.005	14.050 ± 0.015	22.779 ± 0.524
1703	J010604-254651	4680.158 ± 0.056	13.196 ± 0.071	27.606 ± 3.884
1704	J010604-254651	4679.304 ± 0.010	14.014 ± 0.015	24.433 ± 0.689
1705	J010604-254651	4676.956 ± 0.006	14.000 ± 0.014	22.038 ± 0.612
1706	J010604-254651	4676.043 ± 0.014	13.496 ± 0.029	24.414 ± 1.833
1707	J010604-254651	4675.165 ± 0.034	13.210 ± 0.040	28.936 ± 2.658
1708	J010604-254651	4671.242 ± 0.177	12.289 ± 0.232	27.882 ± 14.929
1709	J010604-254651	4670.188 ± 0.071	12.949 ± 0.093	33.100 ± 7.451
1710	J010604-254651	4669.171 ± 0.030	12.616 ± 0.076	15.694 ± 2.904
1711	J010604-254651	4668.093 ± 0.038	13.762 ± 0.062	22.180 ± 1.601
1712	J010604-254651	4667.577 ± 0.061	13.367 ± 0.187	20.170 ± 4.879
1713	J010604-254651	4666.931 ± 0.112	12.942 ± 0.147	26.300 ± 6.457
1714	J010604-254651	4664.569 ± 0.039	12.494 ± 0.126	13.922 ± 4.764
1715	J010604-254651	4663.858 ± 0.030	12.891 ± 0.042	24.949 ± 3.010
1716	J010604-254651	4661.691 ± 0.018	13.657 ± 0.026	22.493 ± 1.373
1717	J010604-254651	4660.428 ± 0.033	12.537 ± 0.243	10.108 ± 3.145
1718	J010604-254651	4660.029 ± 0.051	12.988 ± 0.103	20.576 ± 5.230
1719	J010604-254651	4659.365 ± 0.034	12.426 ± 0.125	12.011 ± 4.270
1720	J010604-254651	4658.179 ± 0.043	12.598 ± 0.078	18.743 ± 4.268
1721	J010604-254651	4657.260 ± 0.099	12.208 ± 0.162	21.179 ± 10.134
1722	J010604-254651	4654.866 ± 0.025	12.939 ± 0.031	27.328 ± 2.262
1723	J010604-254651	4652.347 ± 0.070	12.421 ± 0.151	16.450 ± 5.927
1724	J010604-254651	4651.627 ± 0.079	13.474 ± 0.166	20.304 ± 4.148
1725	J010604-254651	4651.179 ± 0.064	13.537 ± 0.139	19.600 ± 2.350
1726	J010604-254651	4644.726 ± 0.014	13.249 ± 0.019	23.827 ± 1.334
1727	J010604-254651	4639.311 ± 0.044	13.658 ± 0.057	27.557 ± 2.120
1728	J010604-254651	4638.704 ± 0.049	13.444 ± 0.092	23.545 ± 2.203
1729	J010604-254651	4636.557 ± 0.016	12.699 ± 0.045	12.210 ± 1.564
1730	J010604-254651	4635.662 ± 0.011	13.625 ± 0.014	26.546 ± 0.975
1731	J010604-254651	4631.011 ± 0.354	12.929 ± 0.156	77.154 ± 25.789
1732	J010604-254651	4630.071 ± 0.161	12.007 ± 0.794	20.781 ± 22.637
1733	J010604-254651	4628.820 ± 0.020	13.790 ± 0.021	35.761 ± 1.731
1734	J010604-254651	4627.645 ± 0.010	14.329 ± 0.019	31.354 ± 0.904
1735	J010604-254651	4626.255 ± 0.105	12.353 ± 0.136	27.036 ± 10.328
1736	J010604-254651	4618.568 ± 0.340	12.719 ± 0.417	29.471 ± 17.418
1737	J010604-254651	4618.023 ± 0.079	12.961 ± 0.238	21.233 ± 4.325
1738	J010604-254651	4616.317 ± 0.049	13.443 ± 0.037	47.928 ± 3.769
1739	J010604-254651	4614.744 ± 0.022	13.876 ± 0.014	50.608 ± 1.644
1740	J010604-254651	4611.284 ± 0.019	12.767 ± 0.040	15.786 ± 1.765
1741	J010604-254651	4606.915 ± 0.079	12.591 ± 0.080	33.763 ± 7.291
1742	J010604-254651	4605.413 ± 0.036	12.616 ± 0.060	20.530 ± 3.403
1743	J010604-254651	4602.891 ± 0.044	12.731 ± 0.059	26.204 ± 4.332
1744	J010604-254651	4601.836 ± 0.067	12.538 ± 0.090	26.175 ± 6.615
1745	J010604-254651	4596.676 ± 0.054	12.407 ± 0.089	20.764 ± 5.053

Table E.1. *Continued*

1746	J010604-254651	4594.063 ± 0.040	12.209 ± 0.109	11.974 ± 3.866
1747	J010604-254651	4592.525 ± 0.016	13.246 ± 0.025	23.014 ± 1.046
1748	J010604-254651	4591.376 ± 0.041	12.171 ± 0.117	11.279 ± 3.970
1749	J010604-254651	4589.511 ± 0.049	12.545 ± 0.079	21.905 ± 4.816
1750	J010604-254651	4588.508 ± 0.076	12.471 ± 0.114	25.957 ± 8.992
1751	J010604-254651	4587.216 ± 0.029	12.767 ± 0.068	17.254 ± 3.561
1752	J010604-254651	4586.700 ± 0.057	12.322 ± 0.279	11.483 ± 6.319
1753	J010604-254651	4586.201 ± 0.061	12.661 ± 0.125	20.455 ± 7.402
1754	J010604-254651	4584.809 ± 0.008	14.151 ± 0.022	23.681 ± 0.697
1755	J010604-254651	4583.853 ± 0.043	13.570 ± 0.036	41.732 ± 3.559
1756	J010604-254651	4582.510 ± 0.006	13.706 ± 0.013	17.752 ± 0.564
1757	J010604-254651	4581.420 ± 0.033	12.886 ± 0.043	27.859 ± 3.467
1758	J010604-254651	4580.417 ± 0.043	12.345 ± 0.101	14.569 ± 4.208
1759	J010604-254651	4575.199 ± 0.090	12.719 ± 0.210	17.837 ± 9.051
1760	J010604-254651	4574.072 ± 0.092	12.715 ± 0.142	22.639 ± 7.690
1761	J010604-254651	4572.653 ± 0.068	12.749 ± 0.063	38.296 ± 6.707
1762	J010604-254651	4570.634 ± 0.051	14.482 ± 0.129	22.025 ± 1.707
1763	J010604-254651	4569.247 ± 0.066	14.769 ± 0.061	54.800 ± 6.197
1764	J010604-254651	4567.561 ± 0.021	13.825 ± 0.045	26.048 ± 2.278
1765	J010604-254651	4566.409 ± 0.007	15.023 ± 0.088	23.713 ± 0.875
1766	J010604-254651	4560.894 ± 0.168	12.325 ± 0.283	21.591 ± 12.874
1767	J010604-254651	4560.243 ± 0.050	12.803 ± 0.122	21.147 ± 5.985
1768	J010604-254651	4559.389 ± 0.010	13.610 ± 0.012	25.375 ± 0.848
1769	J010604-254651	4556.022 ± 0.035	12.541 ± 0.064	18.832 ± 3.310
1770	J010604-254651	4554.581 ± 0.013	13.339 ± 0.035	19.771 ± 2.202
1771	J010604-254651	4553.517 ± 0.005	13.782 ± 0.010	20.772 ± 0.428
1772	J010604-254651	4551.265 ± 0.019	12.920 ± 0.039	16.307 ± 1.692
1773	J010604-254651	4546.333 ± 0.031	12.833 ± 0.040	26.500 ± 2.825
1774	J010604-254651	4540.843 ± 0.023	12.686 ± 0.044	17.796 ± 2.199
1775	J010604-254651	4536.392 ± 0.008	13.662 ± 0.011	23.240 ± 0.692
1776	J010604-254651	4535.700 ± 0.027	12.760 ± 0.084	15.944 ± 2.787
1777	J010604-254651	4534.813 ± 0.045	12.980 ± 0.050	38.241 ± 5.739
1778	J010604-254651	4532.950 ± 0.034	13.200 ± 0.035	33.359 ± 2.968
1779	J010604-254651	4531.527 ± 0.004	15.708 ± 0.095	28.247 ± 0.731
1780	J010604-254651	4526.718 ± 0.014	15.528 ± 0.045	52.846 ± 1.003
1781	J010604-254651	4524.734 ± 0.074	13.680 ± 0.096	49.351 ± 10.192
1782	J010604-254651	4523.577 ± 0.084	12.920 ± 0.176	28.941 ± 5.580
1783	J010604-254651	4520.875 ± 0.018	13.464 ± 0.082	19.572 ± 1.993
1784	J010604-254651	4520.032 ± 0.025	14.265 ± 0.016	48.691 ± 1.658
1785	J010604-254651	4518.184 ± 0.010	13.829 ± 0.013	26.957 ± 0.611
1786	J010604-254651	4516.760 ± 0.004	14.298 ± 0.015	29.514 ± 0.551
1787	J010604-254651	4515.640 ± 0.065	12.612 ± 0.144	19.939 ± 6.944
1788	J010604-254651	4515.015 ± 0.039	12.716 ± 0.078	18.103 ± 3.156
1789	J010604-254651	4511.647 ± 0.008	13.331 ± 0.012	23.066 ± 0.692

Table E.1. *Continued*

1790	J010604-254651	4509.723 ± 0.033	12.678 ± 0.045	25.859 ± 3.183
1791	J010604-254651	4508.090 ± 0.009	14.030 ± 0.012	25.329 ± 0.620
1792	J010604-254651	4506.674 ± 0.006	16.262 ± 0.206	25.968 ± 1.132
1793	J010604-254651	4504.815 ± 0.008	13.719 ± 0.025	17.732 ± 0.889
1794	J010604-254651	4503.242 ± 0.058	14.601 ± 0.027	81.422 ± 3.503
1795	J010604-254651	4501.190 ± 0.050	14.509 ± 0.032	66.480 ± 4.208
1796	J010604-254651	4499.654 ± 0.039	13.072 ± 0.160	24.458 ± 6.058
1797	J010604-254651	4498.995 ± 0.028	13.025 ± 0.161	18.907 ± 3.601
1798	J010604-254651	4498.288 ± 0.053	13.489 ± 0.072	43.917 ± 7.198
1799	J010604-254651	4495.740 ± 0.007	15.244 ± 0.046	63.744 ± 1.762
1800	J010604-254651	4493.271 ± 0.017	13.261 ± 0.038	16.743 ± 1.514
1801	J010604-254651	4492.318 ± 0.006	13.774 ± 0.007	29.416 ± 0.556
1802	J010604-254651	4490.470 ± 0.003	15.170 ± 0.051	30.969 ± 0.638
1803	J010604-254651	4489.128 ± 0.047	12.617 ± 0.138	18.290 ± 4.839
1804	J010604-254651	4488.445 ± 0.023	13.233 ± 0.039	27.470 ± 2.836
1805	J014214+002324	5214.365 ± 0.271	13.555 ± 0.382	25.649 ± 8.517
1806	J014214+002324	5214.023 ± 0.038	13.426 ± 0.501	16.698 ± 4.319
1807	J014214+002324	5212.862 ± 0.005	13.369 ± 0.013	12.114 ± 0.554
1808	J014214+002324	5210.294 ± 0.054	13.302 ± 0.029	43.622 ± 2.801
1809	J014214+002324	5209.606 ± 0.043	12.173 ± 0.289	12.570 ± 5.815
1810	J014214+002324	5208.569 ± 0.072	12.497 ± 0.259	14.025 ± 4.034
1811	J014214+002324	5208.103 ± 0.229	12.368 ± 0.357	20.275 ± 12.920
1812	J014214+002324	5206.831 ± 0.014	13.073 ± 0.017	26.013 ± 1.218
1813	J014214+002324	5204.509 ± 0.009	13.245 ± 0.011	23.062 ± 0.699
1814	J014214+002324	5202.509 ± 0.043	12.397 ± 0.064	20.079 ± 3.566
1815	J014214+002324	5200.754 ± 0.007	13.228 ± 0.011	19.058 ± 0.599
1816	J014214+002324	5195.250 ± 0.016	13.309 ± 0.038	23.377 ± 2.017
1817	J014214+002324	5193.396 ± 3.174	13.457 ± 2.591	48.085 ± 83.966
1818	J014214+002324	5192.853 ± 0.015	14.659 ± 0.111	29.763 ± 4.724
1819	J014214+002324	5191.479 ± 0.020	14.100 ± 0.020	34.279 ± 0.809
1820	J014214+002324	5188.953 ± 0.115	14.563 ± 0.133	36.573 ± 2.502
1821	J014214+002324	5187.672 ± 0.183	14.510 ± 0.204	34.043 ± 6.257
1822	J014214+002324	5185.942 ± 0.007	14.448 ± 0.035	21.490 ± 1.207
1823	J014214+002324	5185.547 ± 0.296	13.684 ± 0.175	59.642 ± 9.836
1824	J014214+002324	5183.076 ± 0.294	12.221 ± 0.287	31.021 ± 18.111
1825	J014214+002324	5181.224 ± 0.010	13.562 ± 0.013	21.288 ± 0.761
1826	J014214+002324	5180.326 ± 0.007	12.943 ± 0.021	11.045 ± 0.763
1827	J014214+002324	5179.493 ± 0.039	12.525 ± 0.155	13.271 ± 5.752
1828	J014214+002324	5179.046 ± 0.017	12.858 ± 0.056	10.931 ± 1.399
1829	J014214+002324	5178.470 ± 0.046	12.316 ± 0.156	11.566 ± 4.010
1830	J014214+002324	5177.937 ± 0.021	12.956 ± 0.067	18.154 ± 2.349
1831	J014214+002324	5176.200 ± 0.134	13.238 ± 0.066	80.039 ± 21.448
1832	J014214+002324	5174.147 ± 0.006	13.548 ± 0.013	21.696 ± 0.549
1833	J014214+002324	5172.757 ± 0.047	13.036 ± 0.043	47.220 ± 6.112

Table E.1. *Continued*

1834	J014214+002324	5171.296 ± 0.330	13.242 ± 0.633	20.374 ± 9.682
1835	J014214+002324	5171.006 ± 0.109	13.091 ± 0.889	15.276 ± 5.316
1836	J014214+002324	5169.824 ± 0.889	12.798 ± 0.846	36.287 ± 42.323
1837	J014214+002324	5169.292 ± 0.014	13.471 ± 0.164	20.117 ± 2.292
1838	J014214+002324	5168.518 ± 0.005	13.544 ± 0.011	15.887 ± 0.368
1839	J014214+002324	5166.360 ± 0.828	13.250 ± 0.978	34.425 ± 20.829
1840	J014214+002324	5165.911 ± 0.039	13.920 ± 0.208	25.630 ± 2.177
1841	J014214+002324	5164.188 ± 0.023	12.932 ± 0.050	21.214 ± 3.199
1842	J014214+002324	5162.859 ± 0.064	12.225 ± 0.114	17.405 ± 6.001
1843	J014214+002324	5159.522 ± 0.120	12.389 ± 0.094	39.414 ± 10.080
1844	J014214+002324	5158.048 ± 0.051	12.049 ± 0.132	11.580 ± 4.894
1845	J014214+002324	5155.593 ± 0.024	13.362 ± 0.027	33.192 ± 2.243
1846	J014214+002324	5154.375 ± 0.062	13.073 ± 0.123	16.618 ± 3.261
1847	J014214+002324	5153.931 ± 0.012	13.694 ± 0.048	12.423 ± 1.452
1848	J014214+002324	5153.045 ± 0.036	13.060 ± 0.128	16.454 ± 5.544
1849	J014214+002324	5150.389 ± 0.135	12.576 ± 0.121	36.795 ± 11.012
1850	J014214+002324	5149.216 ± 0.078	12.676 ± 0.094	30.135 ± 6.128
1851	J014214+002324	5147.286 ± 0.005	14.181 ± 0.022	20.291 ± 0.637
1852	J014214+002324	5146.397 ± 0.034	13.964 ± 0.018	58.335 ± 2.308
1853	J014214+002324	5145.014 ± 0.004	14.361 ± 0.024	21.198 ± 0.432
1854	J014214+002324	5142.822 ± 0.021	12.374 ± 0.058	10.280 ± 1.924
1855	J014214+002324	5141.866 ± 0.108	12.719 ± 0.159	22.416 ± 7.193
1856	J014214+002324	5141.240 ± 0.014	13.362 ± 0.051	16.691 ± 1.806
1857	J014214+002324	5139.170 ± 0.010	13.580 ± 0.016	22.619 ± 1.316
1858	J014214+002324	5137.012 ± 0.004	16.064 ± 0.115	38.541 ± 1.182
1859	J014214+002324	5134.500 ± 0.120	13.882 ± 0.074	54.790 ± 4.903
1860	J014214+002324	5133.920 ± 0.060	13.011 ± 0.467	25.957 ± 9.976
1861	J014214+002324	5132.607 ± 0.008	13.878 ± 0.013	24.154 ± 0.741
1862	J014214+002324	5131.321 ± 0.013	13.645 ± 0.015	27.358 ± 0.940
1863	J014214+002324	5130.227 ± 0.005	13.976 ± 0.007	23.194 ± 0.524
1864	J014214+002324	5128.835 ± 0.028	13.061 ± 0.038	32.793 ± 3.883
1865	J014214+002324	5127.991 ± 0.068	12.002 ± 0.249	12.337 ± 6.303
1866	J014214+002324	5124.294 ± 0.096	12.950 ± 0.297	13.602 ± 3.305
1867	J014214+002324	5123.921 ± 0.146	12.834 ± 0.448	15.093 ± 11.491
1868	J014214+002324	5123.071 ± 0.112	13.309 ± 0.088	41.386 ± 8.461
1869	J014214+002324	5121.464 ± 0.010	12.981 ± 0.036	12.364 ± 1.412
1870	J014214+002324	5119.842 ± 0.342	14.141 ± 0.297	43.313 ± 9.587
1871	J014214+002324	5119.337 ± 0.011	16.248 ± 1.246	17.811 ± 4.631
1872	J014214+002324	5117.399 ± 0.017	14.653 ± 0.013	58.565 ± 1.241
1873	J014214+002324	5115.258 ± 0.007	13.495 ± 0.011	21.538 ± 0.563
1874	J014214+002324	5111.478 ± 0.020	12.920 ± 0.027	23.502 ± 1.849
1875	J014214+002324	5101.983 ± 0.119	13.338 ± 0.131	32.686 ± 4.593
1876	J014214+002324	5101.070 ± 0.010	13.750 ± 0.113	18.917 ± 1.732
1877	J014214+002324	5100.785 ± 0.240	13.588 ± 0.238	38.201 ± 7.197

Table E.1. *Continued*

1878	J014214+002324	5098.819 ± 0.003	14.537 ± 0.019	30.039 ± 0.451
1879	J014214+002324	5097.470 ± 0.055	12.175 ± 0.158	13.120 ± 5.095
1880	J014214+002324	5096.740 ± 0.022	12.980 ± 0.029	24.671 ± 2.052
1881	J014214+002324	5095.683 ± 0.092	11.731 ± 0.239	11.144 ± 8.156
1882	J014214+002324	5092.271 ± 0.035	12.337 ± 0.073	14.553 ± 3.231
1883	J014214+002324	5090.078 ± 0.092	13.374 ± 0.131	25.332 ± 3.381
1884	J014214+002324	5089.460 ± 0.027	13.750 ± 0.068	22.961 ± 2.359
1885	J014214+002324	5088.476 ± 0.648	12.978 ± 1.048	26.022 ± 35.429
1886	J014214+002324	5087.964 ± 0.057	13.741 ± 0.168	20.887 ± 2.087
1887	J014214+002324	5087.010 ± 0.020	13.217 ± 0.208	23.227 ± 4.048
1888	J014214+002324	5086.366 ± 0.202	13.434 ± 0.141	47.232 ± 9.213
1889	J014214+002324	5084.375 ± 0.045	13.030 ± 0.119	20.579 ± 4.323
1890	J014214+002324	5083.691 ± 0.249	12.510 ± 0.357	25.202 ± 17.127
1891	J014214+002324	5082.096 ± 0.085	12.077 ± 0.139	18.597 ± 7.275
1892	J014214+002324	5070.609 ± 0.123	12.855 ± 0.156	24.822 ± 6.583
1893	J014214+002324	5070.051 ± 0.040	12.941 ± 0.139	17.070 ± 3.193
1894	J014214+002324	5069.124 ± 0.005	14.024 ± 0.008	24.940 ± 0.433
1895	J014214+002324	5067.829 ± 0.042	12.384 ± 0.303	11.925 ± 4.430
1896	J014214+002324	5067.309 ± 0.194	12.493 ± 0.295	26.366 ± 18.834
1897	J014214+002324	5066.355 ± 0.133	12.037 ± 0.269	18.098 ± 12.722
1898	J014214+002324	5063.816 ± 0.051	12.222 ± 0.129	11.969 ± 4.551
1899	J014214+002324	5063.348 ± 0.086	11.953 ± 0.236	11.185 ± 7.675
1900	J014214+002324	5061.921 ± 0.030	12.560 ± 0.050	18.320 ± 2.606
1901	J014214+002324	5060.580 ± 0.026	13.404 ± 0.027	28.740 ± 1.802
1902	J014214+002324	5059.887 ± 0.028	12.901 ± 0.093	16.894 ± 2.451
1903	J014214+002324	5058.697 ± 0.037	13.721 ± 0.035	36.821 ± 2.736
1904	J014214+002324	5057.903 ± 0.017	13.578 ± 0.044	21.948 ± 0.982
1905	J014214+002324	5055.416 ± 0.005	13.949 ± 0.007	24.995 ± 0.404
1906	J014214+002324	5054.380 ± 0.028	13.031 ± 0.033	26.498 ± 2.304
1907	J014214+002324	5052.496 ± 0.065	12.205 ± 0.106	18.607 ± 5.532
1908	J014214+002324	5050.349 ± 0.079	12.031 ± 0.149	16.222 ± 6.874
1909	J014214+002324	5047.712 ± 0.005	15.904 ± 0.068	40.911 ± 0.770
1910	J014214+002324	5044.980 ± 0.005	15.081 ± 0.039	35.538 ± 0.673
1911	J014214+002324	5042.061 ± 0.086	12.828 ± 0.134	19.906 ± 4.630
1912	J014214+002324	5040.928 ± 0.004	14.043 ± 0.013	19.086 ± 0.368
1913	J014214+002324	5039.724 ± 0.007	13.396 ± 0.010	22.347 ± 0.625
1914	J014214+002324	5038.291 ± 0.010	13.455 ± 0.013	23.726 ± 0.651
1915	J014214+002324	5036.393 ± 0.031	12.942 ± 0.034	29.258 ± 2.814
1916	J014214+002324	5035.216 ± 0.004	13.968 ± 0.008	23.032 ± 0.432
1917	J014214+002324	5033.966 ± 0.004	14.172 ± 0.016	22.438 ± 0.520
1918	J014214+002324	5032.917 ± 0.052	12.685 ± 0.095	24.315 ± 6.730
1919	J014214+002324	5032.101 ± 0.050	12.434 ± 0.101	16.498 ± 4.119
1920	J014214+002324	5028.835 ± 0.006	14.591 ± 0.040	22.147 ± 0.604
1921	J014214+002324	5027.937 ± 0.048	13.045 ± 0.068	22.221 ± 2.975

Table E.1. *Continued*

1922	J014214+002324	5023.994 ± 0.015	13.036 ± 0.021	23.126 ± 1.281
1923	J014214+002324	5019.488 ± 0.037	12.716 ± 0.043	26.748 ± 3.245
1924	J014214+002324	5014.720 ± 0.006	14.707 ± 0.029	29.188 ± 0.622
1925	J014214+002324	5013.512 ± 0.046	13.190 ± 0.062	29.656 ± 4.374
1926	J014214+002324	5012.591 ± 0.062	12.379 ± 0.285	14.796 ± 6.632
1927	J014214+002324	5011.613 ± 0.008	13.750 ± 0.033	19.422 ± 0.928
1928	J014214+002324	5011.487 ± 0.075	13.477 ± 0.075	49.061 ± 4.113
1929	J014214+002324	5009.674 ± 0.123	12.162 ± 0.233	18.808 ± 11.505
1930	J014214+002324	5009.055 ± 0.067	12.312 ± 0.145	15.360 ± 5.340
1931	J014214+002324	5007.496 ± 0.033	12.592 ± 0.049	20.812 ± 2.781
1932	J014214+002324	5001.558 ± 0.106	12.931 ± 0.148	27.066 ± 5.264
1933	J014214+002324	5000.246 ± 1.442	13.832 ± 1.678	35.798 ± 42.327
1934	J014214+002324	4999.763 ± 0.112	14.386 ± 0.471	26.858 ± 5.038
1935	J014214+002324	4997.687 ± 0.034	12.844 ± 0.065	25.198 ± 2.970
1936	J014214+002324	4996.104 ± 0.098	13.226 ± 0.078	59.888 ± 12.286
1937	J014214+002324	4995.259 ± 0.026	12.517 ± 0.160	12.894 ± 3.294
1938	J014214+002324	4994.010 ± 0.026	13.574 ± 0.024	37.679 ± 2.326
1939	J014214+002324	4993.857 ± 0.017	12.959 ± 0.111	13.264 ± 2.092
1940	J014214+002324	4992.761 ± 0.059	12.226 ± 0.286	11.813 ± 6.426
1941	J014214+002324	4992.091 ± 0.122	12.792 ± 0.240	25.811 ± 13.602
1942	J014214+002324	4991.237 ± 0.012	14.005 ± 0.014	25.275 ± 0.837
1943	J014214+002324	4989.622 ± 0.063	13.525 ± 0.043	48.102 ± 2.949
1944	J014214+002324	4989.134 ± 0.029	12.916 ± 0.152	19.210 ± 3.690
1945	J014214+002324	4987.699 ± 0.082	12.781 ± 0.131	22.982 ± 6.517
1946	J014214+002324	4987.083 ± 0.100	12.528 ± 0.211	18.366 ± 5.483
1947	J014214+002324	4985.025 ± 0.109	12.128 ± 0.149	23.933 ± 10.497
1948	J014214+002324	4982.509 ± 0.033	14.454 ± 0.049	44.306 ± 0.850
1949	J014214+002324	4982.152 ± 0.019	15.935 ± 0.256	22.803 ± 1.407
1950	J014214+002324	4976.807 ± 0.057	12.014 ± 0.121	14.324 ± 5.012
1951	J014214+002324	4974.799 ± 0.033	12.870 ± 0.048	21.321 ± 2.565
1952	J014214+002324	4974.282 ± 0.034	12.404 ± 0.165	11.668 ± 3.449
1953	J014214+002324	4973.581 ± 0.018	13.407 ± 0.033	22.630 ± 1.766
1954	J014214+002324	4972.953 ± 0.040	12.948 ± 0.081	18.761 ± 2.154
1955	J014214+002324	4970.619 ± 0.004	13.907 ± 0.004	34.455 ± 0.336
1956	J014214+002324	4964.740 ± 0.062	12.776 ± 0.042	48.999 ± 5.747
1957	J014214+002324	4962.765 ± 0.316	13.327 ± 0.352	36.122 ± 9.203
1958	J014214+002324	4962.332 ± 0.017	13.692 ± 0.149	24.118 ± 2.016
1959	J014214+002324	4960.542 ± 0.019	12.917 ± 0.021	28.480 ± 1.659
1960	J014214+002324	4958.823 ± 0.014	13.510 ± 0.019	25.992 ± 0.858
1961	J014214+002324	4957.993 ± 0.058	12.961 ± 0.066	29.212 ± 3.645
1962	J014214+002324	4954.071 ± 0.023	13.063 ± 0.018	39.436 ± 1.916
1963	J014214+002324	4949.280 ± 0.022	13.482 ± 0.160	19.773 ± 2.139
1964	J014214+002324	4948.713 ± 0.141	13.515 ± 0.173	34.134 ± 10.381
1965	J014214+002324	4946.935 ± 0.058	16.746 ± 0.395	25.562 ± 1.839

Table E.1. *Continued*

1966	J014214+002324	4944.899 ± 0.062	15.023 ± 0.080	41.901 ± 1.277
1967	J014214+002324	4941.647 ± 0.007	13.196 ± 0.011	20.344 ± 0.576
1968	J014214+002324	4938.762 ± 0.220	12.237 ± 0.200	35.921 ± 18.333
1969	J014214+002324	4937.424 ± 0.020	14.177 ± 0.022	29.248 ± 1.097
1970	J014214+002324	4936.723 ± 0.032	13.599 ± 0.128	16.988 ± 3.552
1971	J014214+002324	4935.888 ± 0.019	14.567 ± 0.034	27.943 ± 0.770
1972	J014214+002324	4934.193 ± 0.049	12.896 ± 0.057	28.926 ± 3.605
1973	J014214+002324	4933.309 ± 0.065	12.127 ± 0.152	16.283 ± 6.364
1974	J014214+002324	4931.712 ± 0.041	12.134 ± 0.108	12.781 ± 4.404
1975	J014214+002324	4931.001 ± 0.030	12.494 ± 0.063	17.342 ± 3.431
1976	J014214+002324	4927.999 ± 0.019	13.089 ± 0.019	35.283 ± 1.942
1977	J014214+002324	4926.766 ± 0.048	12.482 ± 0.096	17.344 ± 4.431
1978	J014214+002324	4925.841 ± 0.045	12.000 ± 0.128	10.996 ± 4.492
1979	J014214+002324	4923.783 ± 0.158	12.981 ± 0.216	27.114 ± 6.350
1980	J014214+002324	4923.163 ± 0.026	13.662 ± 0.047	24.358 ± 1.413
1981	J014214+002324	4922.233 ± 0.041	12.560 ± 0.083	20.513 ± 3.833
1982	J014214+002324	4920.264 ± 0.061	13.221 ± 0.032	82.100 ± 7.792
1983	J014214+002324	4918.803 ± 0.045	12.242 ± 0.149	15.589 ± 4.628
1984	J014214+002324	4917.441 ± 0.004	14.521 ± 0.032	22.401 ± 0.757
1985	J014214+002324	4917.000 ± 0.220	13.348 ± 0.094	57.529 ± 11.076
1986	J014214+002324	4915.174 ± 0.005	14.966 ± 0.059	27.669 ± 1.001
1987	J014214+002324	4914.073 ± 0.069	13.034 ± 0.088	26.351 ± 3.561
1988	J014214+002324	4911.494 ± 0.039	12.587 ± 0.054	23.310 ± 3.591
1989	J014214+002324	4910.666 ± 0.104	12.527 ± 0.191	17.010 ± 6.143
1990	J014214+002324	4908.902 ± 0.009	14.058 ± 0.008	30.841 ± 0.530
1991	J014214+002324	4907.634 ± 0.009	15.052 ± 0.154	22.258 ± 1.511
1992	J014214+002324	4905.974 ± 0.016	14.608 ± 0.013	54.184 ± 1.245
1993	J014214+002324	4903.696 ± 0.005	14.458 ± 0.032	25.867 ± 1.038
1994	J014214+002324	4902.617 ± 0.012	13.694 ± 0.014	26.552 ± 0.748
1995	J014214+002324	4899.487 ± 0.019	12.945 ± 0.023	27.406 ± 1.886
1996	J014214+002324	4898.234 ± 0.059	12.487 ± 0.069	29.560 ± 5.949
1997	J014214+002324	4895.238 ± 0.055	15.940 ± 0.088	49.599 ± 1.091
1998	J014214+002324	4893.137 ± 0.056	14.395 ± 0.052	41.213 ± 1.739
1999	J014214+002324	4891.374 ± 0.006	13.291 ± 0.010	20.068 ± 0.522
2000	J014214+002324	4888.646 ± 0.011	13.509 ± 0.007	49.051 ± 0.947
2001	J014214+002324	4882.666 ± 0.009	13.551 ± 0.007	41.743 ± 0.794
2002	J014214+002324	4881.327 ± 0.036	12.154 ± 0.100	11.899 ± 3.750
2003	J014214+002324	4879.551 ± 0.067	12.954 ± 0.112	22.575 ± 3.826
2004	J014214+002324	4878.941 ± 0.035	13.262 ± 0.054	22.747 ± 1.784
2005	J014214+002324	4876.843 ± 0.005	13.354 ± 0.009	19.913 ± 0.459
2006	J014214+002324	4875.814 ± 0.052	12.708 ± 0.117	17.966 ± 3.289
2007	J014214+002324	4874.737 ± 0.005	14.597 ± 0.028	32.089 ± 0.979
2008	J014214+002324	4873.509 ± 0.039	12.634 ± 0.086	18.393 ± 3.525
2009	J014214+002324	4872.601 ± 0.013	13.029 ± 0.018	23.187 ± 1.213

Table E.1. *Continued*

2010	J014214+002324	4866.299 ± 0.029	12.912 ± 0.036	31.782 ± 2.477
2011	J014214+002324	4864.440 ± 0.114	13.118 ± 0.048	66.167 ± 6.495
2012	J014214+002324	4863.930 ± 0.009	13.343 ± 0.030	24.511 ± 1.035
2013	J014214+002324	4861.668 ± 0.014	12.965 ± 0.018	25.480 ± 1.252
2014	J014214+002324	4860.199 ± 0.060	11.797 ± 0.180	10.530 ± 5.759
2015	J014214+002324	4859.225 ± 0.013	13.848 ± 0.015	25.559 ± 0.756
2016	J014214+002324	4858.622 ± 0.027	12.982 ± 0.117	15.754 ± 3.146
2017	J014214+002324	4858.132 ± 0.037	12.501 ± 0.215	11.673 ± 4.280
2018	J014214+002324	4857.631 ± 0.013	13.334 ± 0.043	20.005 ± 1.776
2019	J014214+002324	4856.672 ± 0.124	12.966 ± 0.212	33.877 ± 16.282
2020	J014214+002324	4855.963 ± 0.034	13.128 ± 0.109	21.256 ± 1.896
2021	J014214+002324	4853.232 ± 0.049	11.840 ± 0.146	10.129 ± 4.687
2022	J014214+002324	4848.892 ± 0.010	13.231 ± 0.015	22.141 ± 0.848
2023	J014214+002324	4847.977 ± 0.015	13.143 ± 0.019	26.625 ± 1.376
2024	J014214+002324	4845.254 ± 0.051	12.687 ± 0.041	39.887 ± 4.413
2025	J014214+002324	4842.148 ± 0.575	12.752 ± 0.468	43.092 ± 24.386
2026	J014214+002324	4841.527 ± 0.028	13.184 ± 0.168	25.478 ± 2.999
2027	J014214+002324	4840.140 ± 0.040	12.364 ± 0.064	20.111 ± 3.553
2028	J014214+002324	4838.097 ± 0.033	12.068 ± 0.107	10.020 ± 3.176
2029	J014214+002324	4837.282 ± 0.030	12.715 ± 0.037	27.810 ± 2.939
2030	J014214+002324	4832.504 ± 0.797	12.840 ± 0.164	122.626 ± 49.071
2031	J014214+002324	4831.272 ± 0.015	12.925 ± 0.065	21.918 ± 2.189
2032	J014214+002324	4830.163 ± 0.022	13.435 ± 0.051	16.731 ± 1.271
2033	J014214+002324	4829.657 ± 0.048	12.921 ± 0.280	16.370 ± 9.932
2034	J014214+002324	4828.974 ± 0.030	13.060 ± 0.050	19.602 ± 2.211
2035	J014214+002324	4827.825 ± 0.040	12.393 ± 0.069	19.091 ± 3.926
2036	J014214+002324	4826.392 ± 0.037	12.414 ± 0.079	15.614 ± 3.292
2037	J014214+002324	4825.581 ± 0.006	13.785 ± 0.009	22.001 ± 0.574
2038	J014214+002324	4824.517 ± 0.004	14.466 ± 0.023	24.244 ± 0.462
2039	J014214+002324	4822.926 ± 0.004	13.677 ± 0.006	24.457 ± 0.341
2040	J014214+002324	4818.804 ± 0.014	12.999 ± 0.020	24.099 ± 1.407
2041	J014214+002324	4817.344 ± 0.017	13.140 ± 0.019	32.198 ± 1.833
2042	J014214+002324	4816.233 ± 0.048	12.182 ± 0.097	16.632 ± 4.473
2043	J014214+002324	4813.584 ± 0.029	12.170 ± 0.191	10.583 ± 3.654
2044	J014214+002324	4813.245 ± 0.105	12.580 ± 0.095	35.504 ± 5.545
2045	J014214+002324	4810.670 ± 0.060	13.966 ± 0.171	17.081 ± 1.584
2046	J014214+002324	4809.035 ± 0.047	16.986 ± 2.935	34.744 ± 20.451
2047	J014214+002324	4807.433 ± 0.210	12.964 ± 1.331	11.249 ± 9.354
2048	J014214+002324	4806.180 ± 0.017	13.028 ± 0.049	14.240 ± 1.537
2049	J014214+002324	4806.042 ± 0.042	13.379 ± 0.025	61.433 ± 3.241
2050	J014214+002324	4803.261 ± 0.003	13.745 ± 0.006	21.565 ± 0.266
2051	J014214+002324	4800.828 ± 0.008	13.792 ± 0.011	22.326 ± 0.678
2052	J014214+002324	4799.866 ± 0.006	14.185 ± 0.012	26.088 ± 0.646
2053	J014214+002324	4798.836 ± 0.027	12.563 ± 0.061	16.229 ± 2.832

Table E.1. *Continued*

2054	J014214+002324	4798.181 ± 0.005	13.037 ± 0.014	11.387 ± 0.493
2055	J014214+002324	4791.552 ± 0.061	12.493 ± 0.123	21.205 ± 6.405
2056	J014214+002324	4790.817 ± 0.112	12.325 ± 0.164	23.371 ± 8.919
2057	J014214+002324	4788.875 ± 0.007	14.052 ± 0.008	27.375 ± 0.501
2058	J014214+002324	4788.162 ± 0.063	12.675 ± 0.274	13.661 ± 6.141
2059	J014214+002324	4787.751 ± 0.092	12.585 ± 0.329	14.941 ± 8.632
2060	J014214+002324	4786.960 ± 0.008	13.996 ± 0.007	30.943 ± 0.608
2061	J014214+002324	4785.202 ± 0.251	12.716 ± 0.266	31.080 ± 14.714
2062	J014214+002324	4784.484 ± 0.034	12.513 ± 0.178	11.355 ± 3.534
2063	J014214+002324	4783.432 ± 0.037	13.557 ± 0.036	41.086 ± 3.251
2064	J014214+002324	4782.178 ± 0.063	13.263 ± 0.079	39.924 ± 6.685
2065	J014214+002324	4780.177 ± 0.951	13.535 ± 0.829	44.815 ± 32.724
2066	J014214+002324	4779.987 ± 0.056	13.545 ± 0.432	17.855 ± 5.602
2067	J014214+002324	4779.478 ± 0.020	13.626 ± 0.216	13.972 ± 2.530
2068	J014214+002324	4778.873 ± 0.027	14.021 ± 0.051	22.458 ± 1.165
2069	J014214+002324	4777.644 ± 0.028	12.621 ± 0.054	16.921 ± 2.583
2070	J014214+002324	4771.706 ± 0.099	12.562 ± 0.126	24.653 ± 5.777
2071	J014214+002324	4769.586 ± 0.007	13.574 ± 0.009	25.923 ± 0.637
2072	J014214+002324	4767.511 ± 0.118	12.359 ± 0.137	29.595 ± 11.318
2073	J014214+002324	4766.249 ± 0.065	13.375 ± 0.137	30.283 ± 3.484
2074	J014214+002324	4765.451 ± 0.692	12.718 ± 0.640	41.238 ± 39.793
2075	J014214+002324	4763.970 ± 0.077	13.199 ± 0.137	24.258 ± 4.460
2076	J014214+002324	4762.841 ± 0.015	14.771 ± 0.032	37.239 ± 0.996
2077	J014214+002324	4760.768 ± 0.044	13.139 ± 0.050	30.333 ± 3.772
2078	J014214+002324	4760.171 ± 0.028	12.621 ± 0.141	13.293 ± 2.864
2079	J014214+002324	4758.959 ± 0.009	13.485 ± 0.010	29.224 ± 0.791
2080	J014214+002324	4754.166 ± 0.008	13.543 ± 0.009	27.499 ± 0.649
2081	J014214+002324	4745.815 ± 0.048	13.498 ± 0.048	32.362 ± 2.708
2082	J014214+002324	4745.225 ± 0.027	13.125 ± 0.110	18.407 ± 2.066
2083	J014214+002324	4744.459 ± 0.022	12.389 ± 0.070	10.382 ± 2.397
2084	J014214+002324	4742.627 ± 0.039	12.244 ± 0.099	12.658 ± 3.761
2085	J014214+002324	4741.300 ± 0.007	15.478 ± 0.121	24.093 ± 0.886
2086	J014214+002324	4740.172 ± 0.036	13.784 ± 0.029	38.470 ± 1.987
2087	J014214+002324	4729.564 ± 0.034	13.155 ± 0.032	35.882 ± 3.239
2088	J014214+002324	4727.251 ± 0.006	14.214 ± 0.017	24.881 ± 0.603
2089	J014214+002324	4726.220 ± 0.056	13.216 ± 0.109	24.522 ± 5.951
2090	J014214+002324	4725.594 ± 0.058	13.031 ± 0.259	17.867 ± 8.007
2091	J014214+002324	4725.103 ± 0.092	13.043 ± 0.449	14.698 ± 9.033
2092	J014214+002324	4724.663 ± 0.052	13.300 ± 0.358	16.450 ± 11.208
2093	J014214+002324	4723.872 ± 0.020	14.797 ± 0.329	19.887 ± 4.967
2094	J014214+002324	4723.017 ± 0.026	14.190 ± 0.062	17.984 ± 1.321
2095	J014214+002324	4722.067 ± 0.006	13.925 ± 0.010	21.458 ± 0.608
2096	J014214+002324	4721.053 ± 0.063	12.754 ± 0.069	31.774 ± 6.149
2097	J014214+002324	4719.905 ± 0.070	11.918 ± 0.198	11.629 ± 6.920

Table E.1. *Continued*

2098	J014214+002324	4718.985 ± 0.023	13.823 ± 0.044	21.763 ± 1.039
2099	J014214+002324	4718.321 ± 0.038	13.694 ± 0.072	27.375 ± 4.082
2100	J014214+002324	4717.455 ± 0.085	12.950 ± 0.334	21.894 ± 8.836
2101	J014214+002324	4716.860 ± 0.080	13.390 ± 0.097	29.399 ± 3.827
2102	J014214+002324	4715.371 ± 0.130	12.578 ± 0.981	13.956 ± 10.964
2103	J014214+002324	4715.052 ± 0.653	12.463 ± 1.221	20.054 ± 25.727
2104	J014214+002324	4713.592 ± 0.098	12.119 ± 0.158	21.108 ± 9.264
2105	J014214+002324	4712.411 ± 0.027	12.937 ± 0.030	30.390 ± 2.529
2106	J014214+002324	4710.783 ± 0.006	13.521 ± 0.009	24.678 ± 0.551
2107	J014214+002324	4707.237 ± 0.014	12.995 ± 0.022	21.127 ± 1.262
2108	J014214+002324	4701.497 ± 0.223	12.148 ± 0.584	12.496 ± 14.825
2109	J014214+002324	4700.726 ± 0.017	13.079 ± 0.032	21.741 ± 2.107
2110	J014214+002324	4699.985 ± 0.006	13.553 ± 0.011	17.289 ± 0.545
2111	J014214+002324	4699.048 ± 0.035	13.044 ± 0.551	14.334 ± 4.824
2112	J014214+002324	4698.729 ± 0.469	12.908 ± 0.822	23.618 ± 24.845
2113	J014214+002324	4697.915 ± 0.078	12.745 ± 0.118	23.541 ± 5.445
2114	J014214+002324	4696.258 ± 0.046	13.059 ± 0.073	21.952 ± 3.400
2115	J014214+002324	4695.641 ± 0.041	13.098 ± 0.175	17.289 ± 5.444
2116	J014214+002324	4695.087 ± 0.038	13.296 ± 0.100	20.857 ± 4.149
2117	J014214+002324	4694.226 ± 0.045	13.026 ± 0.130	26.696 ± 8.956
2118	J014214+002324	4693.580 ± 0.030	12.879 ± 0.095	15.847 ± 2.071
2119	J014214+002324	4690.485 ± 0.049	14.059 ± 0.057	31.233 ± 1.792
2120	J014214+002324	4689.330 ± 0.032	15.084 ± 0.095	33.201 ± 1.608
2121	J014214+002324	4687.581 ± 0.112	13.676 ± 0.161	26.219 ± 5.157
2122	J014214+002324	4686.391 ± 0.019	16.313 ± 0.205	28.527 ± 1.306
2123	J014214+002324	4684.145 ± 0.096	12.247 ± 0.145	23.683 ± 10.171
2124	J014214+002324	4682.595 ± 0.027	13.040 ± 0.028	33.362 ± 2.490
2125	J014214+002324	4679.831 ± 0.042	13.615 ± 0.084	61.130 ± 12.054
2126	J014214+002324	4679.824 ± 0.005	14.621 ± 0.074	21.144 ± 1.211
2127	J014214+002324	4678.348 ± 0.033	12.856 ± 0.103	22.516 ± 3.779
2128	J014214+002324	4677.328 ± 0.008	13.677 ± 0.011	27.454 ± 0.809
2129	J014214+002324	4675.064 ± 0.031	14.540 ± 0.028	64.604 ± 1.233
2130	J014214+002324	4674.437 ± 0.036	16.586 ± 0.387	24.357 ± 1.684
2131	J014214+002324	4672.557 ± 0.135	11.984 ± 0.368	14.604 ± 12.227
2132	J014214+002324	4671.925 ± 0.160	12.600 ± 0.381	19.718 ± 13.618
2133	J014214+002324	4671.331 ± 0.012	13.886 ± 0.020	20.688 ± 0.912
2134	J014214+002324	4670.383 ± 0.143	12.227 ± 0.209	26.856 ± 16.215
2135	J014214+002324	4669.382 ± 0.025	12.640 ± 0.047	18.404 ± 2.418
2136	J014214+002324	4667.823 ± 0.013	13.416 ± 0.015	32.927 ± 1.315
2137	J014214+002324	4665.794 ± 0.162	13.595 ± 0.110	53.946 ± 7.335
2138	J014214+002324	4665.099 ± 0.007	14.093 ± 0.031	27.108 ± 1.140
2139	J014214+002324	4663.464 ± 0.042	12.577 ± 0.063	23.906 ± 4.334
2140	J014214+002324	4661.320 ± 0.023	12.585 ± 0.047	16.160 ± 2.127
2141	J014214+002324	4659.048 ± 0.068	12.611 ± 0.096	22.584 ± 4.504

Table E.1. *Continued*

2142	J014214+002324	4657.056 ± 0.517	12.804 ± 0.385	47.049 ± 26.653
2143	J014214+002324	4656.050 ± 0.006	14.994 ± 0.057	28.074 ± 0.808
2144	J014214+002324	4652.439 ± 0.157	12.237 ± 0.162	34.145 ± 15.977
2145	J014214+002324	4649.157 ± 0.067	12.978 ± 0.147	20.825 ± 3.421
2146	J014214+002324	4648.523 ± 0.050	13.179 ± 0.142	26.256 ± 7.792
2147	J014214+002324	4647.717 ± 0.026	13.462 ± 0.034	26.034 ± 1.592
2148	J014214+002324	4640.544 ± 0.026	13.020 ± 0.026	33.685 ± 2.323
2149	J014214+002324	4637.895 ± 0.023	12.828 ± 0.035	22.530 ± 2.138
2150	J014214+002324	4636.112 ± 0.027	12.865 ± 0.035	25.953 ± 2.429
2151	J014214+002324	4627.565 ± 0.012	13.523 ± 0.010	40.151 ± 1.044
2152	J014214+002324	4625.495 ± 0.028	12.883 ± 0.037	25.905 ± 2.721
2153	J014214+002324	4624.518 ± 0.040	12.922 ± 0.060	22.025 ± 3.220
2154	J014214+002324	4622.870 ± 0.058	12.749 ± 0.068	28.475 ± 4.997
2155	J014214+002324	4619.820 ± 0.030	12.782 ± 0.053	19.322 ± 2.862
2156	J014214+002324	4619.338 ± 0.077	11.951 ± 0.309	10.307 ± 7.049
2157	J014214+002324	4617.899 ± 0.120	11.998 ± 0.202	20.312 ± 11.474
2158	J014214+002324	4616.790 ± 0.039	12.705 ± 0.048	28.036 ± 3.731
2159	J014214+002324	4612.096 ± 0.007	13.922 ± 0.007	36.121 ± 0.607
2160	J014214+002324	4610.915 ± 0.040	12.772 ± 0.549	16.670 ± 7.091
2161	J014214+002324	4610.448 ± 0.288	13.017 ± 0.373	32.842 ± 21.775
2162	J014214+002324	4609.409 ± 0.052	12.835 ± 0.091	23.905 ± 5.469
2163	J014214+002324	4608.021 ± 0.018	12.531 ± 0.057	11.231 ± 2.204
2164	J014214+002324	4607.295 ± 0.027	12.501 ± 0.058	15.636 ± 2.717
2165	J014214+002324	4606.422 ± 0.018	12.882 ± 0.036	17.637 ± 1.737
2166	J014214+002324	4605.509 ± 0.005	13.967 ± 0.008	25.861 ± 0.480
2167	J014214+002324	4604.429 ± 0.069	12.434 ± 0.195	13.744 ± 5.154
2168	J014214+002324	4603.959 ± 0.034	12.786 ± 0.130	16.479 ± 5.333
2169	J014214+002324	4603.360 ± 0.114	12.501 ± 0.454	16.876 ± 12.007
2170	J014214+002324	4602.682 ± 0.662	12.735 ± 1.327	24.752 ± 54.692
2171	J014214+002324	4602.250 ± 0.205	12.767 ± 1.073	17.445 ± 11.324
2172	J014214+002324	4600.844 ± 0.021	13.668 ± 0.024	27.211 ± 1.508
2173	J014214+002324	4600.221 ± 0.022	13.303 ± 0.115	16.595 ± 2.290
2174	J014214+002324	4599.748 ± 0.191	12.802 ± 0.273	24.999 ± 10.300
2175	J014214+002324	4598.160 ± 0.019	12.678 ± 0.041	15.690 ± 1.847
2176	J014214+002324	4596.620 ± 0.009	14.526 ± 0.019	36.086 ± 0.810
2177	J014214+002324	4595.224 ± 0.201	13.341 ± 0.277	35.227 ± 16.818
2178	J014214+002324	4594.578 ± 0.169	12.892 ± 0.761	24.365 ± 15.771
2179	J014214+002324	4593.768 ± 0.149	12.653 ± 0.484	28.360 ± 28.920
2180	J014214+002324	4592.432 ± 1.275	14.235 ± 3.504	33.995 ± 29.271
2181	J014214+002324	4591.958 ± 0.818	14.724 ± 1.177	39.070 ± 16.532
2182	J014214+002324	4588.679 ± 0.035	14.804 ± 0.037	80.665 ± 1.704
2183	J014214+002324	4587.915 ± 0.119	17.121 ± 0.492	31.819 ± 2.345
2184	J014214+002324	4582.726 ± 0.137	12.735 ± 0.067	71.672 ± 12.767
2185	J014214+002324	4579.237 ± 0.086	12.933 ± 0.050	61.758 ± 10.112

Table E.1. *Continued*

2186	J014214+002324	4577.202 ± 0.137	14.701 ± 0.214	33.247 ± 3.140
2187	J014214+002324	4576.372 ± 0.177	14.154 ± 0.259	30.763 ± 5.496
2188	J014214+002324	4575.402 ± 0.052	12.144 ± 0.239	10.983 ± 5.444
2189	J014214+002324	4574.722 ± 0.086	12.268 ± 0.174	20.568 ± 10.293
2190	J014214+002324	4574.107 ± 0.080	12.128 ± 0.225	15.033 ± 7.620
2191	J014214+002324	4571.832 ± 0.341	12.720 ± 0.151	111.187 ± 49.960
2192	J014214+002324	4569.776 ± 0.042	12.023 ± 0.238	10.107 ± 5.296
2193	J014214+002324	4568.890 ± 0.103	12.915 ± 0.098	57.540 ± 13.923
2194	J014214+002324	4567.710 ± 0.042	12.347 ± 0.152	15.405 ± 4.573
2195	J014214+002324	4566.705 ± 0.070	12.821 ± 0.085	40.568 ± 10.042
2196	J014214+002324	4565.225 ± 0.029	13.074 ± 0.029	36.165 ± 2.873
2197	J014214+002324	4563.404 ± 0.016	13.239 ± 0.017	34.049 ± 1.624
2198	J014214+002324	4562.192 ± 0.090	12.311 ± 0.139	26.884 ± 9.277
2199	J014214+002324	4561.043 ± 0.080	12.146 ± 0.218	20.474 ± 9.184
2200	J014214+002324	4558.686 ± 0.011	12.828 ± 0.040	12.866 ± 1.229
2201	J014214+002324	4558.267 ± 0.109	13.477 ± 0.030	150.942 ± 17.783
2202	J014214+002324	4555.963 ± 0.091	11.676 ± 0.400	10.355 ± 10.470
2203	J014214+002324	4555.060 ± 0.094	12.202 ± 0.200	23.466 ± 10.551
2204	J014214+002324	4554.208 ± 0.035	12.526 ± 0.077	18.777 ± 4.271
2205	J014214+002324	4553.086 ± 0.100	12.688 ± 0.241	26.713 ± 16.829
2206	J014214+002324	4552.595 ± 0.119	12.104 ± 0.873	11.206 ± 15.201
2207	J014214+002324	4552.253 ± 0.013	13.096 ± 0.091	10.488 ± 1.783
2208	J014214+002324	4551.897 ± 0.065	12.728 ± 0.168	15.471 ± 5.430
2209	J014214+002324	4550.835 ± 0.004	14.290 ± 0.013	29.725 ± 0.506
2210	J014214+002324	4549.719 ± 0.027	12.475 ± 0.062	15.190 ± 2.675
2211	J014214+002324	4546.036 ± 0.059	12.499 ± 0.070	29.161 ± 5.530
2212	J014214+002324	4540.501 ± 0.063	12.769 ± 0.084	25.505 ± 3.304
2213	J014214+002324	4538.964 ± 0.092	12.182 ± 0.175	18.013 ± 8.846
2214	J014214+002324	4537.685 ± 0.025	12.423 ± 0.057	14.842 ± 2.411
2215	J014214+002324	4536.008 ± 0.008	14.161 ± 0.014	25.078 ± 0.526
2216	J014214+002324	4534.772 ± 0.957	13.445 ± 0.944	43.319 ± 49.454
2217	J014214+002324	4534.528 ± 0.038	13.025 ± 0.505	14.930 ± 5.989
2218	J014214+002324	4534.160 ± 0.027	12.971 ± 0.206	11.402 ± 2.419
2219	J014214+002324	4533.871 ± 0.562	13.392 ± 0.764	39.759 ± 15.073
2220	J014214+002324	4532.520 ± 0.032	12.172 ± 0.096	11.795 ± 3.220
2221	J014214+002324	4530.495 ± 0.037	12.169 ± 0.092	13.651 ± 3.626
2222	J014214+002324	4529.170 ± 0.012	12.882 ± 0.022	18.127 ± 1.089
2223	J014214+002324	4527.298 ± 0.047	12.521 ± 0.100	17.756 ± 3.846
2224	J014214+002324	4526.651 ± 0.064	12.470 ± 0.147	22.407 ± 9.263
2225	J014214+002324	4524.919 ± 0.150	12.081 ± 0.182	29.471 ± 15.353
2226	J014214+002324	4524.095 ± 0.047	11.962 ± 0.167	10.352 ± 5.122
2227	J014214+002324	4523.383 ± 0.016	13.623 ± 0.029	18.449 ± 0.993
2228	J014214+002324	4522.965 ± 0.041	12.926 ± 0.146	13.999 ± 2.742
2229	J014214+002324	4522.297 ± 0.016	13.277 ± 0.039	17.674 ± 1.475

Table E.1. *Continued*

2230	J014214+002324	4521.732 ± 0.013	13.492 ± 0.023	19.811 ± 1.088
2231	J014214+002324	4518.074 ± 0.004	16.266 ± 0.069	50.211 ± 0.828
2232	J014214+002324	4516.005 ± 0.009	13.056 ± 0.029	13.048 ± 0.834
2233	J014214+002324	4513.690 ± 0.005	13.434 ± 0.009	19.667 ± 0.470
2234	J014214+002324	4512.661 ± 0.016	12.861 ± 0.178	15.296 ± 3.209
2235	J014214+002324	4511.929 ± 0.156	13.269 ± 0.259	39.950 ± 20.978
2236	J014214+002324	4510.825 ± 0.016	14.401 ± 0.017	34.787 ± 2.112
2237	J014214+002324	4509.522 ± 0.013	14.114 ± 0.016	36.825 ± 1.724
2238	J014214+002324	4508.429 ± 0.044	13.021 ± 0.095	27.080 ± 5.101
2239	J014214+002324	4507.268 ± 0.008	14.028 ± 0.009	33.988 ± 1.021
2240	J014214+002324	4506.524 ± 0.005	13.497 ± 0.023	11.231 ± 0.707
2241	J014214+002324	4504.312 ± 0.003	14.476 ± 0.027	23.552 ± 0.452
2242	J014214+002324	4501.764 ± 0.019	13.450 ± 0.020	31.801 ± 1.563
2243	J014214+002324	4500.955 ± 0.042	12.757 ± 0.112	21.652 ± 5.356
2244	J014214+002324	4500.374 ± 0.061	12.132 ± 0.200	12.509 ± 5.642
2245	J014214+002324	4496.703 ± 0.018	13.386 ± 0.025	24.091 ± 1.361
2246	J014214+002324	4496.128 ± 0.080	12.442 ± 0.205	17.243 ± 5.614
2247	J014214+002324	4495.120 ± 0.004	13.662 ± 0.007	19.283 ± 0.315
2248	J115538+053050	5135.891 ± 0.039	12.942 ± 0.050	24.238 ± 3.497
2249	J115538+053050	5132.673 ± 0.035	13.060 ± 0.034	32.336 ± 3.007
2250	J115538+053050	5129.883 ± 0.054	13.219 ± 0.425	15.982 ± 5.315
2251	J115538+053050	5129.169 ± 0.298	13.774 ± 0.517	32.166 ± 29.770
2252	J115538+053050	5128.492 ± 0.129	13.879 ± 0.323	24.941 ± 3.374
2253	J115538+053050	5126.167 ± 0.021	12.842 ± 0.041	15.350 ± 1.826
2254	J115538+053050	5125.238 ± 0.038	12.487 ± 0.082	13.763 ± 3.389
2255	J115538+053050	5123.532 ± 0.030	13.034 ± 0.050	22.246 ± 3.505
2256	J115538+053050	5122.841 ± 0.055	12.413 ± 0.160	12.597 ± 5.010
2257	J115538+053050	5122.116 ± 0.049	12.497 ± 0.100	15.943 ± 4.991
2258	J115538+053050	5121.078 ± 0.061	12.601 ± 0.098	19.223 ± 5.588
2259	J115538+053050	5118.791 ± 0.069	13.461 ± 0.060	34.439 ± 3.933
2260	J115538+053050	5117.850 ± 0.022	13.993 ± 0.036	23.443 ± 2.063
2261	J115538+053050	5117.106 ± 0.067	13.415 ± 0.097	23.040 ± 3.084
2262	J115538+053050	5114.404 ± 0.019	13.562 ± 0.018	32.335 ± 1.537
2263	J115538+053050	5113.000 ± 0.012	13.869 ± 0.011	33.245 ± 0.975
2264	J115538+053050	5110.022 ± 0.043	12.741 ± 0.060	21.800 ± 3.629
2265	J115538+053050	5108.342 ± 0.012	13.948 ± 0.014	26.732 ± 0.861
2266	J115538+053050	5107.011 ± 0.023	14.338 ± 0.043	26.629 ± 2.036
2267	J115538+053050	5106.065 ± 0.025	13.945 ± 0.040	19.966 ± 1.949
2268	J115538+053050	5104.998 ± 0.012	14.141 ± 0.018	27.018 ± 0.878
2269	J115538+053050	5103.053 ± 0.023	13.044 ± 0.037	18.870 ± 2.015
2270	J115538+053050	5102.317 ± 0.088	12.338 ± 0.215	16.141 ± 8.531
2271	J115538+053050	5100.996 ± 0.239	12.581 ± 0.205	47.587 ± 29.363
2272	J115538+053050	5099.867 ± 0.125	12.413 ± 0.335	15.151 ± 10.854
2273	J115538+053050	5099.403 ± 0.085	12.416 ± 0.439	11.845 ± 8.898

Table E.1. *Continued*

2274	J115538+053050	5098.819 ± 0.056	13.077 ± 0.081	24.822 ± 5.373
2275	J115538+053050	5097.609 ± 0.077	12.355 ± 0.269	13.255 ± 10.337
2276	J115538+053050	5097.002 ± 0.059	12.874 ± 0.169	15.179 ± 5.957
2277	J115538+053050	5096.543 ± 0.118	12.543 ± 0.301	13.462 ± 6.663
2278	J115538+053050	5094.521 ± 0.112	14.043 ± 0.181	23.926 ± 3.112
2279	J115538+053050	5093.500 ± 0.103	14.955 ± 0.186	30.318 ± 2.041
2280	J115538+053050	5090.008 ± 0.015	13.331 ± 0.019	24.564 ± 1.211
2281	J115538+053050	5088.491 ± 0.025	13.240 ± 0.024	32.234 ± 2.102
2282	J115538+053050	5085.252 ± 0.007	13.935 ± 0.012	25.024 ± 0.527
2283	J115538+053050	5083.646 ± 0.007	13.982 ± 0.014	24.723 ± 0.529
2284	J115538+053050	5081.026 ± 0.038	13.279 ± 0.039	30.152 ± 2.958
2285	J115538+053050	5080.022 ± 0.065	12.942 ± 0.081	26.189 ± 4.795
2286	J115538+053050	5077.000 ± 0.007	14.651 ± 0.039	35.316 ± 0.910
2287	J115538+053050	5074.718 ± 0.011	14.069 ± 0.009	45.006 ± 0.917
2288	J115538+053050	5070.569 ± 0.038	12.612 ± 0.071	16.347 ± 3.275
2289	J115538+053050	5068.120 ± 0.042	12.897 ± 0.052	25.521 ± 3.791
2290	J115538+053050	5067.007 ± 0.009	13.616 ± 0.014	21.328 ± 0.742
2291	J115538+053050	5063.759 ± 0.023	13.571 ± 0.025	25.815 ± 1.635
2292	J115538+053050	5062.842 ± 0.012	14.114 ± 0.042	18.905 ± 1.471
2293	J115538+053050	5062.068 ± 0.079	13.190 ± 0.159	14.809 ± 3.809
2294	J115538+053050	5059.957 ± 0.077	12.762 ± 0.297	14.826 ± 11.855
2295	J115538+053050	5059.038 ± 0.029	13.037 ± 0.071	14.786 ± 3.016
2296	J115538+053050	5058.353 ± 0.029	13.394 ± 0.091	12.828 ± 1.870
2297	J115538+053050	5057.862 ± 0.045	13.278 ± 0.221	17.114 ± 8.495
2298	J115538+053050	5057.330 ± 0.047	13.464 ± 0.077	15.725 ± 2.027
2299	J115538+053050	5051.785 ± 0.047	12.785 ± 0.056	25.916 ± 3.982
2300	J115538+053050	5049.986 ± 0.008	13.929 ± 0.013	24.352 ± 0.821
2301	J115538+053050	5049.086 ± 0.090	12.435 ± 0.169	17.451 ± 7.526
2302	J115538+053050	5045.973 ± 0.006	13.966 ± 0.014	23.217 ± 0.495
2303	J115538+053050	5044.176 ± 0.052	12.455 ± 0.123	13.502 ± 4.571
2304	J115538+053050	5043.496 ± 0.021	13.096 ± 0.033	18.954 ± 1.840
2305	J115538+053050	5041.334 ± 0.052	13.027 ± 0.063	30.026 ± 4.092
2306	J115538+053050	5039.806 ± 0.179	12.820 ± 0.182	49.133 ± 25.797
2307	J115538+053050	5038.655 ± 0.027	13.038 ± 0.069	20.117 ± 2.421
2308	J115538+053050	5035.675 ± 0.021	13.147 ± 0.027	23.702 ± 1.737
2309	J115538+053050	5034.370 ± 0.105	12.102 ± 0.215	14.783 ± 9.115
2310	J115538+053050	5030.868 ± 0.097	12.580 ± 0.102	29.794 ± 8.201
2311	J115538+053050	5028.230 ± 0.025	13.373 ± 0.173	11.706 ± 2.823
2312	J115538+053050	5028.543 ± 0.369	13.198 ± 0.349	34.482 ± 15.214
2313	J115538+053050	5026.861 ± 0.012	21.049 ± 8.030	15.980 ± 8.758
2314	J115538+053050	5023.473 ± 0.061	16.152 ± 0.650	34.562 ± 6.283
2315	J115538+053050	5021.686 ± 0.137	13.575 ± 0.127	37.407 ± 8.584
2316	J115538+053050	5020.385 ± 0.016	13.457 ± 0.023	21.774 ± 1.185
2317	J115538+053050	5017.445 ± 0.008	14.431 ± 0.015	46.592 ± 0.785

Table E.1. *Continued*

2318	J115538+053050	5015.281 ± 0.019	13.264 ± 0.025	25.294 ± 1.839
2319	J115538+053050	5013.796 ± 0.133	12.261 ± 0.222	21.615 ± 12.780
2320	J115538+053050	5012.367 ± 0.118	12.805 ± 0.082	46.725 ± 10.915
2321	J115538+053050	5008.971 ± 0.122	12.767 ± 0.079	48.219 ± 10.090
2322	J115538+053050	5005.509 ± 0.007	13.850 ± 0.012	23.291 ± 0.537
2323	J115538+053050	5003.608 ± 0.045	12.723 ± 0.064	21.874 ± 3.816
2324	J115538+053050	5001.129 ± 0.028	13.411 ± 0.095	19.634 ± 2.864
2325	J115538+053050	5001.528 ± 0.039	13.970 ± 0.030	50.425 ± 1.607
2326	J115538+053050	4999.452 ± 0.020	13.435 ± 0.020	30.960 ± 1.712
2327	J115538+053050	4996.311 ± 0.049	13.478 ± 0.047	30.811 ± 3.109
2328	J115538+053050	4995.556 ± 0.027	13.323 ± 0.088	18.681 ± 3.379
2329	J115538+053050	4992.493 ± 0.006	14.219 ± 0.028	23.858 ± 0.632
2330	J115538+053050	4990.832 ± 0.049	12.933 ± 0.049	31.339 ± 4.222
2331	J115538+053050	4989.230 ± 0.042	12.802 ± 0.057	22.715 ± 3.575
2332	J115538+053050	4987.467 ± 0.009	13.936 ± 0.012	30.898 ± 0.773
2333	J115538+053050	4986.472 ± 0.045	12.222 ± 0.144	10.382 ± 4.133
2334	J115538+053050	4984.500 ± 0.026	14.097 ± 0.060	20.888 ± 1.006
2335	J115538+053050	4983.818 ± 0.178	13.385 ± 0.360	29.940 ± 22.016
2336	J115538+053050	4983.024 ± 0.032	13.403 ± 0.156	18.414 ± 3.539
2337	J115538+053050	4982.326 ± 0.074	13.137 ± 0.290	25.533 ± 16.314
2338	J115538+053050	4981.624 ± 0.036	13.428 ± 0.110	19.948 ± 3.079
2339	J115538+053050	4980.483 ± 0.079	13.999 ± 0.125	38.117 ± 5.431
2340	J115538+053050	4979.752 ± 0.099	13.126 ± 0.583	21.264 ± 9.531
2341	J115538+053050	4979.251 ± 0.918	13.479 ± 0.575	58.536 ± 49.480
2342	J115538+053050	4977.480 ± 0.066	13.813 ± 0.100	25.943 ± 3.724
2343	J115538+053050	4976.584 ± 0.021	15.170 ± 0.156	22.344 ± 1.447
2344	J115538+053050	4975.120 ± 0.037	13.532 ± 0.038	50.492 ± 5.378
2345	J115538+053050	4973.657 ± 0.006	13.963 ± 0.010	25.279 ± 0.504
2346	J115538+053050	4972.299 ± 0.009	13.830 ± 0.014	20.254 ± 0.607
2347	J115538+053050	4970.427 ± 0.008	15.426 ± 0.117	42.775 ± 2.253
2348	J115538+053050	4968.343 ± 0.040	12.908 ± 0.315	18.602 ± 5.959
2349	J115538+053050	4967.915 ± 0.123	13.668 ± 0.087	50.911 ± 6.142
2350	J115538+053050	4964.753 ± 0.012	14.967 ± 0.026	67.832 ± 1.725
2351	J115538+053050	4962.457 ± 0.009	14.571 ± 0.043	25.384 ± 0.780
2352	J115538+053050	4960.748 ± 0.083	12.725 ± 0.138	27.084 ± 10.470
2353	J115538+053050	4958.018 ± 0.017	17.640 ± 0.685	40.226 ± 4.134
2354	J115538+053050	4954.803 ± 0.016	16.102 ± 0.574	32.522 ± 5.023
2355	J115538+053050	4953.120 ± 0.010	14.575 ± 0.431	10.645 ± 2.461
2356	J115538+053050	4952.495 ± 0.016	13.934 ± 0.026	17.848 ± 1.207
2357	J115538+053050	4950.833 ± 0.007	14.854 ± 0.043	42.354 ± 1.347
2358	J115538+053050	4948.517 ± 0.024	13.706 ± 0.018	50.929 ± 2.501
2359	J115538+053050	4946.082 ± 0.166	13.439 ± 0.109	50.074 ± 9.818
2360	J115538+053050	4945.611 ± 0.010	13.209 ± 0.096	11.684 ± 1.715
2361	J115538+053050	4944.174 ± 0.010	14.067 ± 0.011	32.310 ± 1.064

Table E.1. *Continued*

2362	J115538+053050	4942.984 ± 0.069	12.949 ± 0.094	29.850 ± 7.867
2363	J115538+053050	4941.703 ± 0.013	13.621 ± 0.023	30.899 ± 1.374
2364	J115538+053050	4940.270 ± 0.436	12.572 ± 0.274	64.036 ± 45.906
2365	J115538+053050	4938.181 ± 0.018	13.416 ± 0.022	32.059 ± 1.590
2366	J115538+053050	4936.684 ± 0.054	13.157 ± 0.039	49.496 ± 5.428
2367	J115538+053050	4934.744 ± 0.026	12.597 ± 0.079	11.622 ± 2.722
2368	J115538+053050	4931.849 ± 0.048	12.891 ± 0.043	36.760 ± 4.447
2369	J115538+053050	4928.879 ± 0.130	12.175 ± 0.210	21.437 ± 13.320
2370	J115538+053050	4928.159 ± 0.096	12.304 ± 0.331	14.444 ± 8.069
2371	J115538+053050	4927.388 ± 0.220	12.622 ± 0.332	27.343 ± 24.564
2372	J115538+053050	4924.154 ± 0.025	12.848 ± 0.077	13.933 ± 3.042
2373	J115538+053050	4923.641 ± 0.017	13.039 ± 0.067	13.014 ± 2.386
2374	J115538+053050	4922.774 ± 0.071	12.400 ± 0.220	14.031 ± 8.581
2375	J115538+053050	4921.575 ± 0.013	12.927 ± 0.037	11.123 ± 1.300
2376	J115538+053050	4920.476 ± 0.108	13.061 ± 0.100	37.230 ± 5.002
2377	J115538+053050	4920.173 ± 0.015	13.085 ± 0.091	15.615 ± 1.830
2378	J115538+053050	4918.083 ± 0.763	13.470 ± 0.660	44.055 ± 23.744
2379	J115538+053050	4916.933 ± 0.037	16.970 ± 0.871	28.063 ± 4.437
2380	J115538+053050	4915.446 ± 0.469	14.126 ± 0.351	53.870 ± 32.746
2381	J115538+053050	4914.342 ± 0.231	13.139 ± 1.003	14.411 ± 13.048
2382	J115538+053050	4913.517 ± 0.056	14.844 ± 0.102	30.073 ± 1.654
2383	J115538+053050	4911.716 ± 0.034	12.455 ± 0.142	10.980 ± 4.581
2384	J115538+053050	4911.041 ± 0.090	13.005 ± 0.086	17.531 ± 9.146
2385	J115538+053050	4910.048 ± 0.009	13.893 ± 0.024	13.310 ± 0.913
2386	J115538+053050	4909.409 ± 0.007	13.588 ± 0.023	11.392 ± 0.795
2387	J115538+053050	4908.654 ± 0.039	13.246 ± 0.069	26.830 ± 7.579
2388	J115538+053050	4907.609 ± 0.008	13.783 ± 0.029	10.436 ± 0.692
2389	J115538+053050	4906.549 ± 0.010	13.491 ± 0.033	14.483 ± 1.669
2390	J115538+053050	4904.322 ± 0.015	12.897 ± 0.033	14.349 ± 1.393
2391	J115538+053050	4903.711 ± 0.033	12.555 ± 0.070	15.111 ± 3.136
2392	J115538+053050	4899.600 ± 0.019	13.074 ± 0.023	25.816 ± 1.587
2393	J115538+053050	4896.773 ± 0.056	12.653 ± 0.061	29.647 ± 4.860
2394	J115538+053050	4893.898 ± 0.007	13.787 ± 0.008	30.080 ± 0.547
2395	J115538+053050	4892.183 ± 0.038	13.014 ± 0.032	39.823 ± 3.537
2396	J115538+053050	4890.095 ± 0.014	13.409 ± 0.013	35.168 ± 1.172
2397	J115538+053050	4886.948 ± 0.013	13.844 ± 0.012	29.813 ± 0.875
2398	J115538+053050	4886.146 ± 0.039	12.930 ± 0.080	19.145 ± 2.580
2399	J115538+053050	4875.876 ± 0.062	12.810 ± 0.197	17.792 ± 4.558
2400	J115538+053050	4875.079 ± 0.036	13.499 ± 0.073	32.216 ± 6.129
2401	J115538+053050	4874.283 ± 0.207	13.014 ± 0.726	15.492 ± 9.093
2402	J115538+053050	4873.959 ± 0.181	13.162 ± 0.474	16.410 ± 5.712
2403	J115538+053050	4871.305 ± 0.006	14.916 ± 0.021	62.645 ± 0.909
2404	J115538+053050	4868.072 ± 0.014	14.215 ± 0.020	28.901 ± 1.393
2405	J115538+053050	4866.240 ± 0.015	14.800 ± 0.039	52.931 ± 2.766

Table E.1. *Continued*

2406	J115538+053050	4864.112 ± 0.012	14.331 ± 0.013	36.606 ± 0.785
2407	J115538+053050	4862.445 ± 0.016	13.128 ± 0.032	16.797 ± 1.249
2408	J115538+053050	4861.819 ± 0.055	12.653 ± 0.092	19.803 ± 4.553
2409	J115538+053050	4860.731 ± 0.031	12.504 ± 0.060	16.574 ± 2.808
2410	J115538+053050	4859.052 ± 0.004	13.873 ± 0.011	18.437 ± 0.302
2411	J115538+053050	4857.289 ± 0.013	12.854 ± 0.037	10.239 ± 1.210
2412	J115538+053050	4855.814 ± 0.031	13.263 ± 0.035	35.428 ± 4.192
2413	J115538+053050	4854.800 ± 0.026	12.972 ± 0.076	13.081 ± 2.108
2414	J115538+053050	4854.384 ± 0.017	13.138 ± 0.087	11.884 ± 2.031
2415	J115538+053050	4853.825 ± 0.010	13.825 ± 0.016	20.937 ± 1.040
2416	J115538+053050	4853.126 ± 0.008	13.133 ± 0.023	11.181 ± 0.651
2417	J115538+053050	4852.077 ± 0.015	12.843 ± 0.029	16.350 ± 1.292
2418	J115538+053050	4850.461 ± 0.004	13.866 ± 0.008	23.191 ± 0.346
2419	J115538+053050	4848.307 ± 0.007	13.644 ± 0.009	26.110 ± 0.547
2420	J115538+053050	4846.363 ± 0.015	14.388 ± 0.015	39.025 ± 0.902
2421	J115538+053050	4845.024 ± 0.043	13.712 ± 0.043	42.361 ± 4.060
2422	J115538+053050	4843.594 ± 0.019	13.023 ± 0.052	17.260 ± 2.722
2423	J115538+053050	4842.884 ± 0.046	12.473 ± 0.492	10.175 ± 7.240
2424	J115538+053050	4842.503 ± 0.081	12.965 ± 0.158	19.954 ± 6.741
2425	J115538+053050	4841.710 ± 0.053	12.532 ± 0.144	17.570 ± 6.215
2426	J115538+053050	4840.600 ± 0.067	13.593 ± 0.075	34.648 ± 4.079
2427	J115538+053050	4839.660 ± 0.040	13.719 ± 0.064	32.841 ± 3.852
2428	J115538+053050	4838.728 ± 0.075	12.700 ± 0.197	21.114 ± 6.987
2429	J115538+053050	4837.035 ± 0.029	14.615 ± 0.030	46.025 ± 1.715
2430	J115538+053050	4835.264 ± 0.080	14.292 ± 0.062	59.076 ± 7.968
2431	J115538+053050	4834.520 ± 0.017	14.175 ± 0.083	17.551 ± 2.260
2432	J115538+053050	4833.434 ± 0.060	13.232 ± 0.176	26.646 ± 7.418
2433	J115538+053050	4832.417 ± 0.014	13.894 ± 0.024	27.589 ± 1.951
2434	J115538+053050	4831.708 ± 0.076	12.654 ± 0.349	16.282 ± 9.862
2435	J115538+053050	4831.223 ± 0.014	13.146 ± 0.062	12.021 ± 1.355
2436	J115538+053050	4830.651 ± 0.053	12.930 ± 0.080	25.770 ± 5.379
2437	J115538+053050	4829.312 ± 0.009	13.774 ± 0.010	31.968 ± 0.936
2438	J115538+053050	4827.952 ± 0.089	13.560 ± 0.124	28.495 ± 4.268
2439	J115538+053050	4827.095 ± 0.028	14.319 ± 0.031	31.365 ± 1.532
2440	J115538+053050	4825.408 ± 0.056	13.184 ± 0.050	38.331 ± 4.776
2441	J115538+053050	4823.521 ± 0.175	12.338 ± 0.351	19.771 ± 10.764
2442	J115538+053050	4822.846 ± 0.052	12.975 ± 0.121	24.790 ± 6.652
2443	J115538+053050	4821.807 ± 0.052	13.557 ± 0.215	16.431 ± 3.655
2444	J115538+053050	4820.580 ± 0.047	14.881 ± 0.051	53.456 ± 2.561
2445	J115538+053050	4818.523 ± 0.007	14.300 ± 0.021	25.617 ± 0.787
2446	J115538+053050	4816.175 ± 0.033	13.173 ± 0.132	29.910 ± 4.508
2447	J115538+053050	4816.643 ± 0.222	13.463 ± 0.076	85.550 ± 14.692
2448	J115538+053050	4814.112 ± 0.064	12.444 ± 0.127	20.315 ± 6.483
2449	J115538+053050	4811.346 ± 0.076	14.397 ± 0.076	66.172 ± 2.377

Table E.1. *Continued*

2450	J115538+053050	4811.025 ± 0.038	14.362 ± 0.073	36.026 ± 5.163
2451	J115538+053050	4808.648 ± 0.007	14.921 ± 0.098	31.988 ± 2.192
2452	J115538+053050	4807.346 ± 0.019	13.560 ± 0.056	22.703 ± 2.615
2453	J115538+053050	4806.615 ± 0.051	13.191 ± 0.080	24.589 ± 3.856
2454	J115538+053050	4805.243 ± 0.050	12.318 ± 0.108	15.586 ± 5.063
2455	J115538+053050	4804.697 ± 0.030	12.400 ± 0.103	11.419 ± 3.589
2456	J115538+053050	4803.645 ± 0.067	12.772 ± 0.099	24.295 ± 6.077
2457	J115538+053050	4802.183 ± 0.085	12.297 ± 0.128	22.679 ± 8.478
2458	J115538+053050	4801.533 ± 0.077	11.891 ± 0.251	10.979 ± 7.307
2459	J115538+053050	4798.647 ± 0.030	12.539 ± 0.057	17.255 ± 2.858
2460	J115538+053050	4797.338 ± 0.036	12.699 ± 0.066	19.553 ± 3.165
2461	J115538+053050	4796.089 ± 0.168	14.114 ± 0.372	21.692 ± 6.150
2462	J115538+053050	4795.066 ± 0.094	14.772 ± 0.093	51.005 ± 2.101
2463	J115538+053050	4792.486 ± 0.030	12.815 ± 0.049	21.044 ± 2.723
2464	J115538+053050	4791.694 ± 0.039	12.708 ± 0.065	21.793 ± 3.913
2465	J115538+053050	4790.353 ± 0.086	13.862 ± 0.130	24.907 ± 2.903
2466	J115538+053050	4789.966 ± 0.049	13.616 ± 0.230	17.506 ± 2.136
2467	J115538+053050	4786.681 ± 0.073	13.293 ± 0.129	31.521 ± 3.316
2468	J115538+053050	4785.869 ± 0.110	13.438 ± 0.093	41.464 ± 5.149
2469	J115538+053050	4783.286 ± 0.014	13.577 ± 0.020	25.015 ± 0.938
2470	J115538+053050	4782.343 ± 0.020	13.595 ± 0.020	33.720 ± 1.763
2471	J115538+053050	4780.098 ± 0.016	13.151 ± 0.019	28.066 ± 1.425
2472	J115538+053050	4775.459 ± 0.005	13.587 ± 0.009	21.087 ± 0.435
2473	J115538+053050	4773.983 ± 0.040	12.265 ± 0.098	13.035 ± 3.961
2474	J115538+053050	4772.869 ± 0.007	13.527 ± 0.009	26.338 ± 0.627
2475	J115538+053050	4770.474 ± 0.065	12.115 ± 0.175	15.216 ± 6.518
2476	J115538+053050	4768.542 ± 0.149	12.967 ± 0.072	84.099 ± 17.822
2477	J115538+053050	4766.139 ± 0.027	14.391 ± 0.106	30.361 ± 3.031
2478	J115538+053050	4765.924 ± 0.154	13.923 ± 0.362	42.666 ± 3.665
2479	J115538+053050	4763.533 ± 0.144	12.820 ± 0.098	47.952 ± 9.015
2480	J115538+053050	4761.113 ± 0.120	12.659 ± 0.536	16.584 ± 5.901
2481	J115538+053050	4760.706 ± 0.312	12.711 ± 0.485	23.303 ± 14.627
2482	J115538+053050	4759.456 ± 0.004	13.857 ± 0.008	22.099 ± 0.417
2483	J115538+053050	4758.380 ± 0.007	13.606 ± 0.009	25.389 ± 0.641
2484	J115538+053050	4757.050 ± 0.016	13.412 ± 0.024	23.881 ± 1.168
2485	J115538+053050	4756.212 ± 0.045	13.079 ± 0.050	29.608 ± 3.403
2486	J115538+053050	4754.095 ± 0.043	12.737 ± 0.090	21.439 ± 3.448
2487	J115538+053050	4753.127 ± 0.044	13.084 ± 0.060	37.795 ± 6.508
2488	J115538+053050	4752.025 ± 0.032	12.836 ± 0.056	22.193 ± 2.787
2489	J115538+053050	4750.019 ± 0.005	13.691 ± 0.008	21.157 ± 0.383
2490	J115538+053050	4746.932 ± 0.039	12.746 ± 0.091	15.270 ± 3.602
2491	J115538+053050	4745.804 ± 0.036	13.095 ± 0.082	28.163 ± 6.431
2492	J115538+053050	4745.114 ± 0.017	13.503 ± 0.114	13.227 ± 2.338
2493	J115538+053050	4744.525 ± 0.130	13.385 ± 0.325	24.928 ± 22.577

Table E.1. *Continued*

2494	J115538+053050	4743.949 ± 0.083	13.337 ± 0.316	17.553 ± 4.964
2495	J115538+053050	4743.113 ± 0.024	14.029 ± 0.014	40.811 ± 1.458
2496	J115538+053050	4741.496 ± 0.012	13.313 ± 0.017	25.191 ± 1.215
2497	J115538+053050	4740.428 ± 0.027	12.985 ± 0.045	24.630 ± 3.266
2498	J115538+053050	4739.751 ± 0.017	12.674 ± 0.057	11.406 ± 1.644
2499	J115538+053050	4737.635 ± 0.004	13.993 ± 0.008	26.892 ± 0.367
2500	J115538+053050	4736.522 ± 0.053	12.690 ± 0.138	16.469 ± 3.657
2501	J115538+053050	4735.872 ± 0.064	13.097 ± 0.095	23.786 ± 4.785
2502	J115538+053050	4734.712 ± 0.101	12.223 ± 0.170	21.716 ± 11.194
2503	J115538+053050	4733.816 ± 0.049	12.258 ± 0.111	15.090 ± 5.073
2504	J115538+053050	4733.196 ± 0.036	12.312 ± 0.101	12.579 ± 3.723
2505	J115538+053050	4732.252 ± 0.013	13.333 ± 0.015	30.061 ± 1.390
2506	J115538+053050	4730.085 ± 0.208	12.264 ± 0.230	38.099 ± 20.356
2507	J115538+053050	4728.142 ± 0.040	12.209 ± 0.182	11.632 ± 4.586
2508	J115538+053050	4727.631 ± 0.288	13.081 ± 0.111	84.670 ± 27.530
2509	J115538+053050	4725.756 ± 0.228	12.690 ± 0.371	43.681 ± 28.788
2510	J115538+053050	4724.689 ± 0.007	14.005 ± 0.011	24.135 ± 0.606
2511	J115538+053050	4723.561 ± 0.035	13.867 ± 0.062	20.041 ± 1.591
2512	J115538+053050	4723.021 ± 0.025	13.985 ± 0.056	17.848 ± 2.313
2513	J115538+053050	4722.252 ± 0.014	14.081 ± 0.018	24.160 ± 0.927
2514	J115538+053050	4720.834 ± 0.085	12.838 ± 0.151	36.165 ± 13.932
2515	J115538+053050	4719.658 ± 0.010	13.176 ± 0.093	16.095 ± 1.729
2516	J115538+053050	4719.225 ± 0.150	13.234 ± 0.121	44.517 ± 8.036
2517	J115538+053050	4717.555 ± 0.049	12.725 ± 0.058	31.231 ± 5.068
2518	J115538+053050	4716.596 ± 0.077	12.246 ± 0.243	10.743 ± 6.622
2519	J115538+053050	4715.818 ± 0.034	12.991 ± 0.095	20.167 ± 4.879
2520	J115538+053050	4714.445 ± 0.122	13.037 ± 0.098	71.789 ± 19.849
2521	J115538+053050	4712.209 ± 0.011	13.922 ± 0.035	18.152 ± 1.442
2522	J115538+053050	4711.633 ± 0.061	13.555 ± 0.072	29.213 ± 3.113
2523	J115538+053050	4710.146 ± 0.020	13.134 ± 0.024	30.923 ± 2.224
2524	J115538+053050	4709.026 ± 0.038	12.718 ± 0.067	23.110 ± 4.169
2525	J115538+053050	4708.073 ± 0.018	13.164 ± 0.023	27.446 ± 1.758
2526	J115538+053050	4706.429 ± 0.006	14.131 ± 0.010	26.693 ± 0.498
2527	J115538+053050	4705.046 ± 0.018	13.631 ± 0.023	30.322 ± 1.503
2528	J115538+053050	4704.124 ± 0.072	13.047 ± 0.083	31.658 ± 5.045
2529	J115538+053050	4702.990 ± 0.056	12.173 ± 0.136	14.567 ± 5.625
2530	J115538+053050	4702.066 ± 0.086	12.549 ± 0.126	26.158 ± 8.846
2531	J115538+053050	4701.259 ± 0.109	12.295 ± 0.231	21.233 ± 12.298
2532	J115538+053050	4700.165 ± 0.084	12.859 ± 0.256	15.288 ± 6.685
2533	J115538+053050	4699.512 ± 0.031	14.202 ± 0.064	20.085 ± 2.823
2534	J115538+053050	4698.684 ± 0.037	14.345 ± 0.047	28.121 ± 2.925
2535	J115538+053050	4696.947 ± 0.014	13.383 ± 0.014	35.175 ± 1.325
2536	J115538+053050	4694.919 ± 0.006	13.746 ± 0.008	26.321 ± 0.573
2537	J115538+053050	4692.917 ± 0.058	12.150 ± 0.126	15.014 ± 5.482

Table E.1. *Continued*

2538	J115538+053050	4691.443 ± 0.011	13.665 ± 0.018	30.024 ± 0.988
2539	J115538+053050	4690.217 ± 0.011	13.766 ± 0.035	20.594 ± 1.390
2540	J115538+053050	4689.410 ± 0.014	13.566 ± 0.056	11.352 ± 1.660
2541	J115538+053050	4688.985 ± 0.042	13.169 ± 0.119	17.380 ± 3.220
2542	J115538+053050	4688.450 ± 0.596	13.403 ± 0.169	107.829 ± 30.725
2543	J115538+053050	4686.867 ± 0.018	12.838 ± 0.061	12.801 ± 2.254
2544	J115538+053050	4686.364 ± 0.034	12.300 ± 0.144	10.543 ± 3.761
2545	J115538+053050	4682.878 ± 0.166	12.901 ± 0.331	32.967 ± 26.550
2546	J115538+053050	4681.873 ± 0.140	12.483 ± 0.386	19.923 ± 16.424
2547	J115538+053050	4681.280 ± 0.098	12.565 ± 0.267	18.381 ± 10.634
2548	J115538+053050	4680.310 ± 0.009	13.487 ± 0.016	21.763 ± 1.157
2549	J115538+053050	4678.733 ± 0.010	13.407 ± 0.012	27.806 ± 0.905
2550	J115538+053050	4676.565 ± 0.529	12.988 ± 0.759	27.702 ± 18.569
2551	J115538+053050	4676.199 ± 0.062	13.193 ± 0.469	19.051 ± 4.476
2552	J115538+053050	4673.696 ± 0.034	12.749 ± 0.043	26.535 ± 3.063
2553	J115538+053050	4669.578 ± 0.003	16.784 ± 0.093	42.780 ± 0.710
2554	J115538+053050	4666.214 ± 0.026	12.577 ± 0.049	17.799 ± 2.421
2555	J115538+053050	4664.600 ± 0.004	14.181 ± 0.010	27.436 ± 0.441
2556	J115538+053050	4663.189 ± 0.045	12.304 ± 0.165	10.755 ± 3.712
2557	J115538+053050	4662.729 ± 0.013	13.160 ± 0.030	17.101 ± 1.459
2558	J115538+053050	4661.854 ± 0.079	12.599 ± 0.124	23.681 ± 7.673
2559	J115538+053050	4660.690 ± 0.025	12.916 ± 0.031	27.955 ± 2.456
2560	J115538+053050	4659.467 ± 0.064	12.302 ± 0.315	16.087 ± 6.835
2561	J115538+053050	4658.804 ± 0.069	13.047 ± 0.064	36.281 ± 5.455
2562	J115538+053050	4656.851 ± 0.005	14.388 ± 0.015	30.632 ± 0.467
2563	J115538+053050	4655.419 ± 0.057	12.798 ± 0.155	14.147 ± 3.222
2564	J115538+053050	4655.006 ± 0.016	13.447 ± 0.037	15.580 ± 1.170
2565	J115538+053050	4652.569 ± 0.057	12.597 ± 0.059	33.128 ± 5.236
2566	J115538+053050	4650.182 ± 0.023	13.148 ± 0.023	34.166 ± 2.187
2567	J115538+053050	4649.002 ± 0.019	13.124 ± 0.023	29.272 ± 1.782
2568	J115538+053050	4645.995 ± 0.070	14.103 ± 0.081	50.512 ± 1.810
2569	J115538+053050	4645.799 ± 0.010	14.858 ± 0.148	23.153 ± 2.067
2570	J115538+053050	4644.500 ± 0.057	13.251 ± 0.077	30.439 ± 3.105
2571	J115538+053050	4641.119 ± 0.038	12.415 ± 0.131	10.648 ± 2.920
2572	J115538+053050	4640.756 ± 0.047	12.449 ± 0.125	12.816 ± 3.877
2573	J115538+053050	4639.165 ± 0.004	15.964 ± 0.105	27.110 ± 0.679
2574	J115538+053050	4637.679 ± 0.014	13.865 ± 0.012	39.853 ± 1.218
2575	J115538+053050	4636.190 ± 0.023	13.072 ± 0.036	25.016 ± 2.364
2576	J115538+053050	4635.387 ± 0.005	13.788 ± 0.008	21.549 ± 0.412
2577	J115538+053050	4630.999 ± 0.033	13.947 ± 0.059	26.437 ± 1.153
2578	J115538+053050	4630.295 ± 0.034	14.193 ± 0.037	33.212 ± 1.509
2579	J115538+053050	4628.987 ± 0.008	13.454 ± 0.014	22.650 ± 0.829
2580	J115538+053050	4627.967 ± 0.072	12.926 ± 0.111	31.104 ± 8.413
2581	J115538+053050	4627.483 ± 0.046	12.076 ± 0.548	11.282 ± 7.649

Table E.1. *Continued*

2582	J115538+053050	4626.592 ± 0.049	13.618 ± 0.365	24.314 ± 4.423
2583	J115538+053050	4626.182 ± 0.132	13.979 ± 0.160	35.499 ± 3.838
2584	J115538+053050	4622.905 ± 0.046	12.500 ± 0.069	23.475 ± 4.507
2585	J115538+053050	4622.120 ± 0.089	12.116 ± 0.210	19.600 ± 10.906
2586	J115538+053050	4621.150 ± 0.032	12.806 ± 0.047	30.284 ± 4.290
2587	J115538+053050	4620.274 ± 0.023	12.611 ± 0.094	16.577 ± 2.719
2588	J115538+053050	4619.200 ± 0.119	12.782 ± 0.123	57.565 ± 20.689
2589	J115538+053050	4618.177 ± 0.074	11.866 ± 0.388	12.333 ± 9.226
2590	J115538+053050	4617.251 ± 0.010	13.245 ± 0.014	26.446 ± 0.984
2591	J115538+053050	4616.031 ± 0.071	12.164 ± 0.188	16.247 ± 8.991
2592	J115538+053050	4615.328 ± 0.109	12.697 ± 0.235	18.349 ± 8.811
2593	J115538+053050	4614.570 ± 0.013	13.484 ± 0.032	20.324 ± 1.810
2594	J115538+053050	4612.996 ± 0.005	14.679 ± 0.026	33.056 ± 0.750
2595	J115538+053050	4611.682 ± 0.010	13.142 ± 0.028	13.712 ± 1.004
2596	J115538+053050	4611.152 ± 0.029	13.001 ± 0.094	15.130 ± 3.377
2597	J115538+053050	4609.818 ± 0.005	17.973 ± 0.740	22.435 ± 2.060
2598	J115538+053050	4608.261 ± 0.090	13.526 ± 0.092	41.526 ± 7.705
2599	J115538+053050	4606.986 ± 0.029	13.051 ± 0.072	26.632 ± 4.447
2600	J115538+053050	4605.849 ± 0.098	12.102 ± 0.231	14.291 ± 9.327
2601	J115538+053050	4604.876 ± 0.033	12.364 ± 0.071	16.028 ± 3.319
2602	J115538+053050	4602.840 ± 0.022	12.656 ± 0.047	16.352 ± 2.300
2603	J115538+053050	4602.292 ± 0.029	12.375 ± 0.085	12.502 ± 3.102
2604	J115538+053050	4601.479 ± 0.046	13.189 ± 0.131	14.836 ± 1.882
2605	J115538+053050	4601.008 ± 0.058	12.929 ± 0.154	16.485 ± 5.384
2606	J115538+053050	4599.978 ± 0.010	13.126 ± 0.047	10.020 ± 1.407
2607	J115538+053050	4599.433 ± 0.008	13.877 ± 0.018	14.094 ± 0.853
2608	J115538+053050	4598.838 ± 0.006	13.628 ± 0.012	15.279 ± 0.509
2609	J115538+053050	4597.720 ± 0.006	13.597 ± 0.008	28.600 ± 0.626
2610	J115538+053050	4596.356 ± 0.082	12.324 ± 0.269	14.725 ± 9.283
2611	J115538+053050	4595.889 ± 0.100	12.329 ± 0.246	15.832 ± 8.597
2612	J115538+053050	4594.972 ± 0.023	13.320 ± 0.037	23.855 ± 1.833
2613	J115538+053050	4594.146 ± 0.008	13.863 ± 0.016	26.318 ± 1.241
2614	J115538+053050	4593.277 ± 0.098	12.944 ± 0.247	21.146 ± 9.558
2615	J115538+053050	4592.679 ± 0.105	13.152 ± 0.374	19.205 ± 12.583
2616	J115538+053050	4592.274 ± 0.031	13.318 ± 0.247	13.563 ± 4.906
2617	J115538+053050	4591.218 ± 0.018	13.600 ± 0.119	15.434 ± 4.918
2618	J115538+053050	4587.158 ± 0.085	12.530 ± 0.214	13.441 ± 6.619
2619	J115538+053050	4585.710 ± 0.008	16.406 ± 0.860	19.223 ± 3.439
2620	J115538+053050	4585.045 ± 0.353	13.547 ± 0.431	33.635 ± 11.257
2621	J123055-113909	5421.937 ± 0.008	14.133 ± 0.018	22.472 ± 0.581
2622	J123055-113909	5420.944 ± 0.030	13.175 ± 0.042	23.240 ± 2.521
2623	J123055-113909	5419.774 ± 0.007	13.601 ± 0.011	21.092 ± 0.599
2624	J123055-113909	5418.543 ± 0.005	13.868 ± 0.013	19.061 ± 0.406
2625	J123055-113909	5417.233 ± 0.005	13.942 ± 0.012	21.865 ± 0.410

Table E.1. *Continued*

2626	J123055-113909	5415.686 ± 0.008	13.693 ± 0.010	22.643 ± 0.590
2627	J123055-113909	5414.309 ± 0.009	14.125 ± 0.013	28.219 ± 0.769
2628	J123055-113909	5412.981 ± 0.019	13.731 ± 0.216	21.494 ± 3.196
2629	J123055-113909	5412.379 ± 0.634	13.363 ± 0.578	39.050 ± 33.307
2630	J123055-113909	5411.060 ± 0.109	12.878 ± 0.173	25.839 ± 6.372
2631	J123055-113909	5409.666 ± 0.004	14.356 ± 0.034	20.733 ± 0.510
2632	J123055-113909	5407.652 ± 0.058	12.188 ± 0.121	13.407 ± 4.735
2633	J123055-113909	5406.003 ± 0.041	12.655 ± 0.053	22.020 ± 3.221
2634	J123055-113909	5402.564 ± 0.024	12.767 ± 0.121	10.263 ± 4.038
2635	J123055-113909	5401.543 ± 0.012	13.535 ± 0.013	29.295 ± 1.085
2636	J123055-113909	5399.999 ± 0.020	13.103 ± 0.026	23.411 ± 1.784
2637	J123055-113909	5398.605 ± 0.042	13.921 ± 0.125	15.195 ± 2.148
2638	J123055-113909	5398.182 ± 0.026	14.153 ± 0.031	35.559 ± 0.994
2639	J123055-113909	5396.444 ± 0.102	12.670 ± 0.104	34.324 ± 10.404
2640	J123055-113909	5394.413 ± 0.018	13.140 ± 0.022	22.903 ± 1.449
2641	J123055-113909	5390.756 ± 0.058	12.171 ± 0.171	10.016 ± 4.860
2642	J123055-113909	5389.991 ± 0.022	13.637 ± 0.031	19.294 ± 1.547
2643	J123055-113909	5388.525 ± 0.014	14.623 ± 0.081	28.715 ± 2.428
2644	J123055-113909	5387.135 ± 0.158	13.175 ± 0.339	40.179 ± 32.633
2645	J123055-113909	5385.412 ± 0.016	15.537 ± 0.290	29.009 ± 3.002
2646	J123055-113909	5384.208 ± 0.346	13.961 ± 0.169	65.179 ± 15.786
2647	J123055-113909	5382.296 ± 0.045	12.756 ± 0.151	18.594 ± 5.208
2648	J123055-113909	5381.015 ± 0.055	13.055 ± 0.046	37.279 ± 4.915
2649	J123055-113909	5379.046 ± 0.017	13.356 ± 0.017	29.885 ± 1.347
2650	J123055-113909	5376.892 ± 0.049	13.001 ± 0.039	37.841 ± 4.211
2651	J123055-113909	5374.801 ± 0.016	13.972 ± 0.071	20.378 ± 1.761
2652	J123055-113909	5374.133 ± 0.192	13.657 ± 0.175	39.132 ± 11.406
2653	J123055-113909	5372.942 ± 0.008	14.239 ± 0.045	18.214 ± 0.763
2654	J123055-113909	5370.742 ± 0.014	15.212 ± 0.085	35.273 ± 1.308
2655	J123055-113909	5368.909 ± 0.014	14.345 ± 0.043	24.985 ± 1.432
2656	J123055-113909	5367.610 ± 0.011	13.719 ± 0.013	24.272 ± 0.833
2657	J123055-113909	5365.934 ± 0.011	13.904 ± 0.014	23.166 ± 0.746
2658	J123055-113909	5364.980 ± 0.008	14.157 ± 0.039	17.464 ± 0.734
2659	J123055-113909	5363.762 ± 0.179	12.302 ± 0.263	23.151 ± 15.406
2660	J123055-113909	5362.750 ± 0.015	13.526 ± 0.019	26.413 ± 1.444
2661	J123055-113909	5361.349 ± 0.017	13.454 ± 0.016	32.048 ± 1.403
2662	J123055-113909	5358.111 ± 0.046	13.027 ± 0.035	38.757 ± 3.700
2663	J123055-113909	5356.215 ± 0.024	13.150 ± 0.025	27.649 ± 1.968
2664	J123055-113909	5354.806 ± 0.058	12.739 ± 0.061	28.406 ± 4.917
2665	J123055-113909	5352.479 ± 0.072	12.523 ± 0.094	23.237 ± 5.918
2666	J123055-113909	5350.317 ± 0.094	13.910 ± 0.054	51.180 ± 4.249
2667	J123055-113909	5349.791 ± 0.015	13.354 ± 0.109	13.001 ± 2.092
2668	J123055-113909	5349.164 ± 0.008	13.526 ± 0.048	11.451 ± 0.863
2669	J123055-113909	5347.495 ± 0.015	13.404 ± 0.016	28.830 ± 1.192

Table E.1. *Continued*

2670	J123055-113909	5342.754 ± 0.108	12.273 ± 0.149	21.240 ± 8.754
2671	J123055-113909	5341.247 ± 0.007	13.766 ± 0.012	23.023 ± 0.539
2672	J123055-113909	5338.055 ± 0.167	13.375 ± 0.187	26.205 ± 6.104
2673	J123055-113909	5337.170 ± 0.029	14.243 ± 0.046	23.933 ± 2.248
2674	J123055-113909	5334.647 ± 0.013	15.379 ± 0.079	52.830 ± 1.779
2675	J123055-113909	5328.025 ± 0.011	14.447 ± 0.017	46.577 ± 1.002
2676	J123055-113909	5326.224 ± 0.023	13.386 ± 0.027	26.914 ± 1.814
2677	J123055-113909	5324.572 ± 0.027	12.974 ± 0.140	16.949 ± 3.209
2678	J123055-113909	5323.697 ± 0.012	13.658 ± 0.044	20.813 ± 1.279
2679	J123055-113909	5323.193 ± 0.271	13.420 ± 0.128	66.203 ± 10.527
2680	J123055-113909	5316.532 ± 0.021	14.724 ± 0.078	24.270 ± 1.084
2681	J123055-113909	5314.678 ± 0.021	15.278 ± 0.091	35.401 ± 1.344
2682	J123055-113909	5311.143 ± 0.012	14.162 ± 0.013	36.157 ± 1.148
2683	J123055-113909	5308.882 ± 0.234	13.274 ± 0.056	83.677 ± 14.065
2684	J123055-113909	5308.104 ± 0.048	12.787 ± 0.129	22.131 ± 4.810
2685	J123055-113909	5306.001 ± 0.049	12.491 ± 0.127	13.774 ± 4.119
2686	J123055-113909	5304.572 ± 0.029	14.220 ± 0.019	41.037 ± 1.980
2687	J123055-113909	5302.996 ± 0.021	15.103 ± 0.300	25.162 ± 3.713
2688	J123055-113909	5301.640 ± 0.123	13.583 ± 0.361	40.798 ± 34.329
2689	J123055-113909	5300.760 ± 0.025	13.892 ± 0.096	20.841 ± 1.971
2690	J123055-113909	5298.561 ± 0.052	14.635 ± 0.080	33.204 ± 1.641
2691	J123055-113909	5296.967 ± 0.060	14.477 ± 0.049	43.420 ± 2.305
2692	J123055-113909	5294.871 ± 0.071	13.232 ± 0.122	23.351 ± 3.868
2693	J123055-113909	5293.996 ± 0.055	13.514 ± 0.150	30.863 ± 7.243
2694	J123055-113909	5292.644 ± 0.116	13.430 ± 0.231	50.660 ± 28.747
2695	J123055-113909	5291.584 ± 0.020	13.444 ± 0.105	21.151 ± 2.404
2696	J123055-113909	5290.085 ± 0.037	13.203 ± 0.056	21.603 ± 2.813
2697	J123055-113909	5289.290 ± 0.096	12.825 ± 0.127	23.115 ± 6.545
2698	J123055-113909	5286.399 ± 0.030	13.724 ± 0.042	20.465 ± 1.427
2699	J123055-113909	5285.697 ± 0.030	13.747 ± 0.040	21.463 ± 1.477
2700	J123055-113909	5284.178 ± 0.100	13.071 ± 0.168	19.500 ± 4.669
2701	J123055-113909	5283.337 ± 0.019	14.332 ± 0.050	24.007 ± 1.588
2702	J123055-113909	5281.781 ± 0.027	13.701 ± 0.031	28.972 ± 2.248
2703	J123055-113909	5279.834 ± 0.099	13.334 ± 0.072	65.341 ± 13.671
2704	J123055-113909	5278.283 ± 0.019	13.428 ± 0.036	24.312 ± 1.682
2705	J123055-113909	5276.234 ± 0.041	12.832 ± 0.275	19.032 ± 5.998
2706	J123055-113909	5275.619 ± 0.230	13.110 ± 0.161	43.434 ± 9.972
2707	J123055-113909	5272.128 ± 0.065	13.109 ± 0.096	20.132 ± 3.685
2708	J123055-113909	5271.587 ± 0.045	13.043 ± 0.110	15.253 ± 2.384
2709	J123055-113909	5270.414 ± 0.009	13.729 ± 0.014	20.177 ± 0.659
2710	J123055-113909	5269.264 ± 0.026	13.392 ± 0.027	33.298 ± 2.715
2711	J123055-113909	5268.214 ± 0.036	12.654 ± 0.134	11.978 ± 3.160
2712	J123055-113909	5267.510 ± 0.071	12.889 ± 0.155	24.429 ± 10.629
2713	J123055-113909	5266.902 ± 0.036	12.735 ± 0.202	11.764 ± 3.512

Table E.1. *Continued*

2714	J123055-113909	5266.169 ± 0.037	13.305 ± 0.057	31.280 ± 5.260
2715	J123055-113909	5263.331 ± 0.014	13.066 ± 0.031	12.408 ± 1.215
2716	J123055-113909	5262.030 ± 0.021	13.357 ± 0.021	30.483 ± 1.910
2717	J123055-113909	5260.810 ± 0.042	12.391 ± 0.101	12.061 ± 3.597
2718	J123055-113909	5258.409 ± 0.019	13.239 ± 0.023	24.621 ± 1.479
2719	J123055-113909	5252.357 ± 0.007	17.095 ± 0.153	57.091 ± 1.431
2720	J123055-113909	5247.374 ± 0.070	12.880 ± 0.058	36.474 ± 5.822
2721	J123055-113909	5245.765 ± 0.019	13.208 ± 0.025	22.304 ± 1.493
2722	J123055-113909	5241.761 ± 0.050	15.004 ± 0.087	38.586 ± 2.035
2723	J123055-113909	5240.633 ± 1.850	13.517 ± 1.180	56.325 ± 77.173
2724	J123055-113909	5239.199 ± 0.050	12.419 ± 0.295	11.430 ± 5.847
2725	J123055-113909	5237.651 ± 0.090	13.708 ± 0.068	85.634 ± 15.785
2726	J123055-113909	5235.649 ± 0.024	13.726 ± 0.039	36.900 ± 2.292
2727	J123055-113909	5232.797 ± 0.012	17.857 ± 0.701	34.392 ± 3.298
2728	J123055-113909	5229.635 ± 0.035	13.390 ± 0.119	25.914 ± 3.585
2729	J123055-113909	5231.253 ± 2.099	13.885 ± 0.624	96.036 ± 57.812
2730	J123055-113909	5226.916 ± 0.027	13.325 ± 0.023	36.696 ± 2.165
2731	J123055-113909	5223.337 ± 0.044	12.716 ± 0.082	16.715 ± 3.585
2732	J123055-113909	5222.600 ± 0.065	12.651 ± 0.100	20.044 ± 5.596
2733	J123055-113909	5221.052 ± 0.020	13.186 ± 0.025	23.805 ± 1.553
2734	J123055-113909	5218.282 ± 0.015	13.352 ± 0.019	24.163 ± 1.176
2735	J123055-113909	5214.661 ± 0.027	13.158 ± 0.029	28.597 ± 2.164
2736	J123055-113909	5212.524 ± 0.101	12.976 ± 0.119	27.025 ± 6.246
2737	J123055-113909	5211.349 ± 0.015	14.266 ± 0.021	32.603 ± 1.081
2738	J123055-113909	5208.620 ± 0.066	12.372 ± 0.123	15.959 ± 5.571
2739	J123055-113909	5207.477 ± 0.040	12.765 ± 0.076	17.062 ± 3.321
2740	J123055-113909	5205.482 ± 0.018	14.980 ± 0.079	45.122 ± 2.249
2741	J123055-113909	5202.227 ± 0.058	15.580 ± 0.259	49.265 ± 5.445
2742	J123055-113909	5199.793 ± 0.058	14.792 ± 0.145	31.536 ± 2.913
2743	J123055-113909	5198.100 ± 0.018	13.447 ± 0.022	24.428 ± 1.503
2744	J123055-113909	5196.184 ± 0.029	12.870 ± 0.047	18.680 ± 2.407
2745	J123055-113909	5194.966 ± 0.021	13.007 ± 0.036	17.735 ± 1.706
2746	J123055-113909	5192.507 ± 0.026	12.888 ± 0.044	17.625 ± 2.101
2747	J123055-113909	5189.410 ± 0.022	13.162 ± 0.028	23.690 ± 1.774
2748	J123055-113909	5186.015 ± 0.071	12.316 ± 0.136	15.384 ± 5.979
2749	J123055-113909	5183.718 ± 0.074	12.735 ± 0.089	25.783 ± 6.671
2750	J123055-113909	5179.864 ± 0.111	12.781 ± 0.123	27.879 ± 8.362
2751	J123055-113909	5178.603 ± 0.013	14.334 ± 0.037	28.057 ± 1.597
2752	J123055-113909	5177.492 ± 0.089	13.136 ± 0.097	28.305 ± 5.270
2753	J123055-113909	5175.593 ± 0.071	13.074 ± 0.400	20.710 ± 6.128
2754	J123055-113909	5174.966 ± 0.296	13.250 ± 0.295	36.033 ± 17.404
2755	J123055-113909	5173.110 ± 0.223	13.755 ± 0.184	42.726 ± 9.297
2756	J123055-113909	5172.486 ± 0.040	13.606 ± 0.246	25.097 ± 4.541
2757	J123055-113909	5168.878 ± 0.099	13.655 ± 0.540	19.592 ± 5.598

Table E.1. *Continued*

2758	J123055-113909	5168.423 ± 0.306	13.822 ± 0.374	29.150 ± 10.982
2759	J123055-113909	5167.100 ± 0.030	13.588 ± 0.057	24.789 ± 2.681
2760	J123055-113909	5166.168 ± 0.054	13.253 ± 0.274	12.852 ± 5.332
2761	J123055-113909	5165.224 ± 0.059	14.478 ± 0.034	56.872 ± 2.412
2762	J123055-113909	5162.471 ± 0.014	13.635 ± 0.015	30.629 ± 1.107
2763	J123055-113909	5159.875 ± 0.022	14.555 ± 0.078	25.647 ± 1.303
2764	J123055-113909	5158.141 ± 0.058	14.455 ± 0.029	58.119 ± 3.148
2765	J123055-113909	5157.222 ± 0.061	13.596 ± 0.148	16.511 ± 3.766
2766	J123055-113909	5155.564 ± 0.053	13.632 ± 0.073	32.501 ± 3.375
2767	J123055-113909	5154.550 ± 0.394	12.981 ± 0.310	41.138 ± 19.665
2768	J123055-113909	5152.437 ± 0.008	13.888 ± 0.016	24.395 ± 0.663
2769	J123055-113909	5150.570 ± 0.024	13.918 ± 0.025	27.354 ± 1.376
2770	J123055-113909	5149.656 ± 0.045	13.519 ± 0.052	26.530 ± 2.508
2771	J123055-113909	5147.225 ± 0.026	12.736 ± 0.056	13.561 ± 2.213
2772	J123055-113909	5146.183 ± 0.149	12.585 ± 0.195	24.774 ± 12.446
2773	J123055-113909	5145.322 ± 0.010	13.886 ± 0.021	19.712 ± 0.780
2774	J123055-113909	5142.702 ± 0.007	14.113 ± 0.023	24.369 ± 0.615
2775	J123055-113909	5140.610 ± 0.006	14.781 ± 0.072	24.779 ± 0.809
2776	J123055-113909	5137.258 ± 0.188	13.053 ± 0.163	40.790 ± 15.613
2777	J123055-113909	5135.479 ± 0.016	14.244 ± 0.032	27.029 ± 1.622
2778	J123055-113909	5133.792 ± 0.014	15.281 ± 0.114	32.183 ± 1.433
2779	J123055-113909	5131.972 ± 0.068	12.257 ± 0.145	14.028 ± 5.965
2780	J123055-113909	5127.049 ± 0.051	12.690 ± 0.068	22.927 ± 4.239
2781	J123055-113909	5122.881 ± 0.021	13.846 ± 0.015	41.234 ± 1.473
2782	J123055-113909	5120.854 ± 0.335	13.260 ± 0.303	50.455 ± 32.986
2783	J123055-113909	5119.918 ± 0.016	13.862 ± 0.059	24.681 ± 1.656
2784	J123055-113909	5117.085 ± 0.036	13.233 ± 0.038	29.400 ± 2.947
2785	J123055-113909	5115.732 ± 0.028	13.915 ± 0.027	31.661 ± 2.326
2786	J123055-113909	5114.821 ± 0.031	13.738 ± 0.080	19.297 ± 2.827
2787	J123055-113909	5113.440 ± 0.053	14.635 ± 0.100	39.927 ± 7.372
2788	J123055-113909	5112.113 ± 0.071	14.049 ± 0.086	29.738 ± 2.528
2789	J123055-113909	5110.305 ± 0.016	14.201 ± 0.034	24.826 ± 1.159
2790	J123055-113909	5108.965 ± 0.017	14.340 ± 0.039	31.559 ± 2.853
2791	J123055-113909	5108.045 ± 0.032	12.959 ± 0.152	11.217 ± 2.447
2792	J123055-113909	5105.687 ± 0.009	14.026 ± 0.013	32.355 ± 0.694
2793	J123055-113909	5103.017 ± 0.058	12.618 ± 0.082	22.026 ± 4.997
2794	J123055-113909	5101.923 ± 0.018	13.062 ± 0.030	18.122 ± 1.492
2795	J123055-113909	5092.593 ± 0.007	14.720 ± 0.034	39.936 ± 0.833
2796	J123055-113909	5089.978 ± 0.009	13.592 ± 0.013	23.517 ± 0.734
2797	J123055-113909	5087.892 ± 0.032	13.090 ± 0.035	28.681 ± 2.786
2798	J123055-113909	5085.994 ± 0.276	13.818 ± 0.246	39.572 ± 9.282
2799	J123055-113909	5085.205 ± 0.034	14.798 ± 0.131	26.405 ± 2.237
2800	J123055-113909	5083.937 ± 0.073	12.668 ± 0.120	19.271 ± 5.925
2801	J123055-113909	5082.060 ± 0.006	14.154 ± 0.027	23.020 ± 0.606

Table E.1. *Continued*

2802	J123055-113909	5078.586 ± 0.041	13.305 ± 0.037	33.243 ± 3.387
2803	J123055-113909	5077.732 ± 0.077	12.533 ± 0.250	16.154 ± 7.382
2804	J123055-113909	5076.841 ± 0.062	13.014 ± 0.075	32.178 ± 7.364
2805	J123055-113909	5074.955 ± 0.013	13.687 ± 0.014	30.683 ± 1.113
2806	J123055-113909	5073.820 ± 0.081	12.243 ± 0.211	13.423 ± 7.493
2807	J123055-113909	5072.795 ± 0.042	13.131 ± 0.039	34.488 ± 3.828
2808	J123055-113909	5068.346 ± 0.034	13.128 ± 0.181	16.873 ± 3.602
2809	J123055-113909	5067.393 ± 0.048	13.972 ± 0.066	43.572 ± 7.427
2810	J123055-113909	5066.320 ± 0.074	13.503 ± 0.129	28.675 ± 3.337
2811	J123055-113909	5063.460 ± 0.013	14.091 ± 0.022	25.729 ± 0.955
2812	J123055-113909	5062.164 ± 0.033	13.966 ± 0.039	32.286 ± 2.835
2813	J123055-113909	5060.960 ± 0.041	14.033 ± 0.032	39.693 ± 2.737
2814	J123055-113909	5059.107 ± 0.033	13.482 ± 0.024	41.924 ± 2.750
2815	J123055-113909	5054.173 ± 0.008	13.970 ± 0.013	28.182 ± 0.601
2816	J123055-113909	5051.250 ± 0.019	13.273 ± 0.068	22.518 ± 2.247
2817	J123055-113909	5049.993 ± 0.007	14.204 ± 0.033	22.090 ± 1.002
2818	J123055-113909	5048.820 ± 0.974	13.031 ± 0.372	100.747 ± 86.928
2819	J123055-113909	5046.911 ± 0.047	12.661 ± 0.143	16.269 ± 4.386
2820	J123055-113909	5045.854 ± 0.019	13.666 ± 0.020	37.087 ± 2.108
2821	J123055-113909	5044.619 ± 0.078	13.424 ± 0.502	17.665 ± 4.488
2822	J123055-113909	5044.213 ± 1.500	12.802 ± 2.202	25.659 ± 66.327
2823	J123055-113909	5042.740 ± 0.096	14.290 ± 0.104	31.320 ± 4.167
2824	J123055-113909	5042.020 ± 0.455	13.325 ± 0.804	26.642 ± 14.298
2825	J123055-113909	5040.731 ± 0.017	13.448 ± 0.021	25.612 ± 1.625
2826	J123055-113909	5039.812 ± 0.035	12.777 ± 0.124	11.329 ± 2.850
2827	J123055-113909	5039.029 ± 0.012	14.137 ± 0.025	25.462 ± 1.102
2828	J123055-113909	5037.793 ± 0.070	13.725 ± 0.214	13.580 ± 2.219
2829	J123055-113909	5037.461 ± 0.124	13.547 ± 0.299	15.395 ± 3.907
2830	J123055-113909	5036.225 ± 0.064	12.627 ± 0.107	18.835 ± 5.872
2831	J123055-113909	5035.622 ± 0.043	12.523 ± 0.149	11.664 ± 4.066
2832	J123055-113909	5034.716 ± 0.165	12.580 ± 0.148	36.510 ± 15.714
2833	J123055-113909	5032.848 ± 0.025	12.718 ± 0.058	13.147 ± 2.189
2834	J123055-113909	5029.192 ± 0.050	12.954 ± 0.091	22.271 ± 3.796
2835	J123055-113909	5027.883 ± 0.254	13.427 ± 0.217	42.959 ± 16.727
2836	J123055-113909	5027.175 ± 0.086	12.946 ± 0.580	22.507 ± 10.596
2837	J123055-113909	5024.498 ± 0.014	13.115 ± 0.038	11.920 ± 1.582
2838	J123055-113909	5022.885 ± 0.013	13.943 ± 0.011	40.312 ± 1.093
2839	J123055-113909	5021.320 ± 0.061	12.807 ± 0.148	15.381 ± 4.388
2840	J123055-113909	5020.361 ± 0.014	14.329 ± 0.033	29.598 ± 1.186
2841	J123055-113909	5017.924 ± 0.077	13.835 ± 0.059	39.414 ± 3.688
2842	J123055-113909	5017.153 ± 0.043	13.540 ± 0.114	23.366 ± 2.496
2843	J123055-113909	5013.784 ± 0.076	12.714 ± 0.190	20.289 ± 10.434
2844	J123055-113909	5012.928 ± 0.047	12.986 ± 0.074	23.702 ± 5.028
2845	J123055-113909	5012.084 ± 0.062	13.081 ± 0.237	11.667 ± 2.997

Table E.1. *Continued*

2846	J123055-113909	5011.713 ± 0.133	12.948 ± 0.363	15.228 ± 11.135
2847	J123055-113909	5008.233 ± 0.010	13.509 ± 0.016	21.422 ± 0.827
2848	J123055-113909	5007.064 ± 0.042	12.417 ± 0.102	12.306 ± 3.737
2849	J123055-113909	5005.613 ± 0.050	14.410 ± 0.094	26.643 ± 1.662
2850	J123055-113909	5003.979 ± 0.063	14.747 ± 0.062	53.254 ± 4.857
2851	J123055-113909	5002.061 ± 0.061	13.723 ± 0.113	20.129 ± 3.934
2852	J123055-113909	5001.533 ± 0.083	13.460 ± 0.191	17.602 ± 4.198
2853	J123055-113909	4999.973 ± 0.016	13.827 ± 0.045	23.898 ± 1.845
2854	J123055-113909	4999.341 ± 0.352	13.801 ± 0.069	89.654 ± 25.953
2855	J123055-113909	4998.007 ± 0.016	14.080 ± 0.049	19.880 ± 2.088
2856	J123055-113909	4996.623 ± 0.013	14.871 ± 0.111	26.994 ± 1.524
2857	J123055-113909	4994.555 ± 0.047	12.549 ± 0.095	15.155 ± 4.062
2858	J123055-113909	4992.517 ± 0.037	13.035 ± 0.044	26.543 ± 3.095
2859	J123055-113909	4991.023 ± 0.027	13.364 ± 0.064	14.527 ± 1.650
2860	J123055-113909	4990.188 ± 0.020	14.199 ± 0.032	27.917 ± 1.403
2861	J123055-113909	4984.796 ± 0.025	14.031 ± 0.090	20.126 ± 2.105
2862	J123055-113909	4984.201 ± 0.299	13.557 ± 0.265	36.167 ± 13.068
2863	J123055-113909	4979.003 ± 0.008	14.360 ± 0.031	32.908 ± 0.872
2864	J123055-113909	4976.555 ± 0.026	13.125 ± 0.033	24.561 ± 2.152
2865	J005758-264314	5544.378 ± 0.052	11.753 ± 0.128	11.499 ± 4.739
2866	J005758-264314	5542.017 ± 2.173	12.898 ± 1.627	44.010 ± 75.846
2867	J005758-264314	5541.341 ± 0.003	15.260 ± 0.084	21.953 ± 0.984
2868	J005758-264314	5539.859 ± 0.005	14.011 ± 0.020	18.142 ± 0.705
2869	J005758-264314	5538.295 ± 0.043	14.583 ± 0.005	87.924 ± 2.017
2870	J005758-264314	5538.009 ± 0.016	13.646 ± 0.072	12.245 ± 1.620
2871	J005758-264314	5536.788 ± 0.007	15.042 ± 0.073	18.584 ± 0.542
2872	J005758-264314	5534.965 ± 0.014	13.260 ± 0.022	23.376 ± 1.105
2873	J005758-264314	5534.085 ± 0.172	13.090 ± 0.323	19.259 ± 7.053
2874	J005758-264314	5533.738 ± 0.078	12.816 ± 0.619	13.877 ± 4.874
2875	J005758-264314	5533.039 ± 0.090	13.545 ± 0.187	22.486 ± 4.040
2876	J005758-264314	5532.546 ± 0.282	13.043 ± 0.553	22.580 ± 6.261
2877	J005758-264314	5530.679 ± 0.041	12.376 ± 0.335	21.788 ± 6.533
2878	J005758-264314	5529.876 ± 0.751	12.209 ± 0.605	45.912 ± 54.513
2879	J005758-264314	5528.441 ± 0.007	13.287 ± 0.011	24.261 ± 0.473
2880	J005758-264314	5525.986 ± 0.135	12.599 ± 0.078	44.087 ± 9.322
2881	J005758-264314	5525.286 ± 0.060	11.807 ± 0.334	10.573 ± 5.786
2882	J005758-264314	5524.655 ± 0.006	13.356 ± 0.013	20.068 ± 0.544
2883	J005758-264314	5523.657 ± 0.065	12.643 ± 0.052	35.881 ± 4.620
2884	J005758-264314	5517.411 ± 0.019	13.392 ± 0.016	59.655 ± 2.559
2885	J005758-264314	5517.316 ± 0.008	13.180 ± 0.026	17.448 ± 0.758
2886	J005758-264314	5515.798 ± 0.016	12.562 ± 0.061	12.716 ± 1.319
2887	J005758-264314	5514.936 ± 0.005	13.856 ± 0.004	32.404 ± 0.463
2888	J005758-264314	5513.590 ± 0.045	12.412 ± 0.057	24.666 ± 3.594
2889	J005758-264314	5511.854 ± 0.030	12.712 ± 0.026	35.380 ± 2.650

Table E.1. *Continued*

2890	J005758-264314	5510.249 ± 0.018	12.983 ± 0.022	29.469 ± 1.581
2891	J005758-264314	5508.774 ± 0.088	13.014 ± 0.087	36.583 ± 5.836
2892	J005758-264314	5508.040 ± 0.027	12.950 ± 0.229	15.852 ± 2.758
2893	J005758-264314	5507.498 ± 0.036	13.881 ± 0.037	32.409 ± 2.051
2894	J005758-264314	5506.255 ± 0.038	13.480 ± 0.076	19.124 ± 1.737
2895	J005758-264314	5505.596 ± 0.012	14.110 ± 0.025	20.799 ± 1.308
2896	J005758-264314	5503.444 ± 0.024	15.152 ± 0.058	55.918 ± 3.544
2897	J005758-264314	5501.662 ± 0.019	13.985 ± 0.055	17.898 ± 1.007
2898	J005758-264314	5500.634 ± 0.041	12.443 ± 0.159	15.374 ± 4.097
2899	J005758-264314	5500.010 ± 0.049	12.738 ± 0.062	23.036 ± 2.965
2900	J005758-264314	5498.774 ± 0.026	12.306 ± 0.042	17.432 ± 2.169
2901	J005758-264314	5497.529 ± 0.028	12.897 ± 0.050	17.412 ± 1.838
2902	J005758-264314	5497.059 ± 0.036	12.476 ± 0.138	12.257 ± 2.332
2903	J005758-264314	5496.248 ± 0.017	12.958 ± 0.018	28.421 ± 1.480
2904	J005758-264314	5494.602 ± 0.031	12.465 ± 0.040	23.501 ± 2.688
2905	J005758-264314	5493.458 ± 0.026	12.711 ± 0.039	23.008 ± 2.435
2906	J005758-264314	5492.493 ± 0.014	13.766 ± 0.030	19.515 ± 0.663
2907	J005758-264314	5491.883 ± 0.030	13.647 ± 0.039	24.456 ± 1.305
2908	J005758-264314	5490.833 ± 0.033	12.271 ± 0.063	15.987 ± 2.633
2909	J005758-264314	5489.712 ± 0.038	11.959 ± 0.089	12.270 ± 3.175
2910	J005758-264314	5488.571 ± 0.026	13.569 ± 0.030	26.644 ± 1.108
2911	J005758-264314	5487.819 ± 0.028	13.298 ± 0.076	23.342 ± 2.831
2912	J005758-264314	5486.865 ± 0.006	13.950 ± 0.008	25.594 ± 0.574
2913	J005758-264314	5485.286 ± 0.025	12.970 ± 0.040	21.067 ± 1.532
2914	J005758-264314	5484.453 ± 0.012	13.355 ± 0.029	24.368 ± 1.610
2915	J005758-264314	5483.127 ± 0.122	14.046 ± 0.146	30.286 ± 3.784
2916	J005758-264314	5482.511 ± 0.061	14.146 ± 0.123	25.807 ± 1.247
2917	J005758-264314	5479.334 ± 0.002	14.110 ± 0.006	23.053 ± 0.170
2918	J005758-264314	5476.202 ± 0.015	13.801 ± 0.025	19.080 ± 0.531
2919	J005758-264314	5475.690 ± 0.039	13.317 ± 0.074	18.539 ± 1.342
2920	J005758-264314	5474.494 ± 0.039	12.312 ± 0.060	19.979 ± 3.440
2921	J005758-264314	5473.226 ± 0.004	14.057 ± 0.004	27.002 ± 0.305
2922	J005758-264314	5471.964 ± 0.020	13.270 ± 0.033	30.064 ± 2.491
2923	J005758-264314	5470.834 ± 0.012	14.138 ± 0.019	24.126 ± 0.743
2924	J005758-264314	5470.082 ± 0.231	12.951 ± 0.321	29.336 ± 12.725
2925	J005758-264314	5468.757 ± 0.050	13.044 ± 0.068	40.251 ± 6.512
2926	J005758-264314	5467.233 ± 0.038	12.913 ± 0.054	34.484 ± 4.290
2927	J005758-264314	5466.325 ± 0.046	12.050 ± 0.211	12.261 ± 5.067
2928	J005758-264314	5464.686 ± 0.455	13.267 ± 0.233	63.140 ± 21.644
2929	J005758-264314	5464.331 ± 0.028	12.573 ± 0.307	16.595 ± 4.610
2930	J005758-264314	5463.294 ± 0.015	13.879 ± 0.039	31.052 ± 0.946
2931	J005758-264314	5461.960 ± 0.075	12.645 ± 0.235	14.523 ± 3.007
2932	J005758-264314	5461.442 ± 0.014	13.591 ± 0.036	19.685 ± 1.596
2933	J005758-264314	5460.750 ± 0.082	12.418 ± 0.210	16.348 ± 6.437

Table E.1. *Continued*

2934	J005758-264314	5457.481 ± 0.036	13.130 ± 0.019	55.968 ± 2.906
2935	J005758-264314	5456.153 ± 0.006	13.242 ± 0.013	20.881 ± 0.562
2936	J005758-264314	5455.217 ± 0.180	12.622 ± 1.063	16.354 ± 8.344
2937	J005758-264314	5454.683 ± 0.190	12.979 ± 0.728	25.154 ± 37.671
2938	J005758-264314	5454.152 ± 0.053	12.524 ± 0.697	12.423 ± 5.763
2939	J005758-264314	5453.441 ± 0.019	13.206 ± 0.022	27.711 ± 1.392
2940	J005758-264314	5451.935 ± 0.007	13.396 ± 0.008	31.179 ± 0.713
2941	J005758-264314	5450.100 ± 0.009	14.452 ± 0.014	33.749 ± 0.411
2942	J005758-264314	5448.764 ± 0.039	12.750 ± 0.119	21.550 ± 5.648
2943	J005758-264314	5447.970 ± 0.006	13.593 ± 0.010	19.161 ± 0.473
2944	J005758-264314	5446.721 ± 0.004	14.064 ± 0.004	29.943 ± 0.396
2945	J005758-264314	5445.241 ± 0.003	14.541 ± 0.013	28.300 ± 0.327
2946	J005758-264314	5443.319 ± 0.014	13.625 ± 0.015	28.960 ± 0.680
2947	J005758-264314	5442.216 ± 0.055	13.497 ± 0.647	24.318 ± 6.213
2948	J005758-264314	5441.736 ± 0.568	13.548 ± 0.631	35.537 ± 20.973
2949	J005758-264314	5440.414 ± 0.074	13.492 ± 0.053	43.462 ± 3.015
2950	J005758-264314	5438.284 ± 0.012	13.035 ± 0.013	28.926 ± 0.980
2951	J005758-264314	5435.996 ± 0.035	13.066 ± 0.042	28.286 ± 2.307
2952	J005758-264314	5435.094 ± 0.005	13.941 ± 0.006	22.278 ± 0.325
2953	J005758-264314	5434.131 ± 0.037	12.136 ± 0.131	13.654 ± 3.597
2954	J005758-264314	5432.587 ± 0.239	13.066 ± 0.076	130.586 ± 28.654
2955	J005758-264314	5432.546 ± 0.005	13.188 ± 0.012	17.587 ± 0.442
2956	J005758-264314	5430.631 ± 0.019	12.878 ± 0.038	19.856 ± 1.588
2957	J005758-264314	5429.909 ± 0.046	12.449 ± 0.138	16.342 ± 5.457
2958	J005758-264314	5429.408 ± 0.049	12.272 ± 0.159	12.014 ± 3.126
2959	J005758-264314	5427.511 ± 0.051	11.738 ± 0.139	10.178 ± 4.368
2960	J005758-264314	5426.777 ± 0.050	11.984 ± 0.105	14.144 ± 4.578
2961	J005758-264314	5425.706 ± 0.013	13.000 ± 0.017	25.572 ± 1.192
2962	J005758-264314	5424.341 ± 0.022	12.947 ± 0.023	34.080 ± 2.396
2963	J005758-264314	5423.036 ± 0.013	13.399 ± 0.019	20.365 ± 0.839
2964	J005758-264314	5422.469 ± 0.084	12.284 ± 0.234	14.933 ± 5.043
2965	J005758-264314	5421.528 ± 0.013	12.928 ± 0.016	24.334 ± 1.127
2966	J005758-264314	5419.500 ± 0.026	13.431 ± 0.026	28.345 ± 1.300
2967	J005758-264314	5418.714 ± 0.016	13.682 ± 0.084	21.142 ± 1.364
2968	J005758-264314	5418.102 ± 0.179	13.334 ± 0.188	33.231 ± 9.027
2969	J005758-264314	5416.908 ± 0.032	12.789 ± 0.067	21.801 ± 2.753
2970	J005758-264314	5415.789 ± 0.045	12.206 ± 0.321	13.459 ± 5.182
2971	J005758-264314	5415.601 ± 0.064	12.859 ± 0.082	31.977 ± 2.725
2972	J005758-264314	5413.060 ± 0.042	12.767 ± 0.123	15.484 ± 1.813
2973	J005758-264314	5412.556 ± 0.039	13.094 ± 0.062	20.915 ± 2.275
2974	J005758-264314	5411.311 ± 0.026	12.863 ± 0.046	28.726 ± 3.909
2975	J005758-264314	5410.517 ± 0.075	11.988 ± 0.438	13.036 ± 7.375
2976	J005758-264314	5409.958 ± 0.049	12.879 ± 0.052	26.855 ± 2.929
2977	J005758-264314	5403.799 ± 0.045	13.176 ± 0.029	51.651 ± 2.128

Table E.1. *Continued*

2978	J005758-264314	5403.270 ± 0.011	12.786 ± 0.051	15.729 ± 1.235
2979	J005758-264314	5401.762 ± 0.019	13.844 ± 0.056	19.103 ± 0.699
2980	J005758-264314	5401.185 ± 0.035	13.984 ± 0.041	28.152 ± 1.427
2981	J005758-264314	5399.505 ± 0.024	13.447 ± 0.026	43.456 ± 2.905
2982	J005758-264314	5398.761 ± 0.025	12.233 ± 0.168	11.056 ± 2.975
2983	J005758-264314	5397.661 ± 0.027	13.249 ± 0.022	45.288 ± 2.549
2984	J005758-264314	5395.292 ± 0.016	15.864 ± 0.074	29.235 ± 0.598
2985	J005758-264314	5393.026 ± 0.016	15.872 ± 0.161	29.223 ± 1.438
2986	J005758-264314	5391.259 ± 0.291	12.952 ± 0.518	21.274 ± 15.413
2987	J005758-264314	5390.868 ± 0.072	12.992 ± 0.431	15.194 ± 2.847
2988	J005758-264314	5388.674 ± 0.211	12.845 ± 0.171	42.338 ± 7.476
2989	J005758-264314	5388.389 ± 0.073	12.255 ± 0.495	16.458 ± 8.821
2990	J005758-264314	5386.979 ± 0.128	12.308 ± 0.248	23.864 ± 14.930
2991	J005758-264314	5385.950 ± 0.019	13.059 ± 0.041	24.428 ± 2.561
2992	J005758-264314	5385.150 ± 0.054	12.450 ± 0.168	18.191 ± 4.583
2993	J005758-264314	5383.681 ± 0.139	12.836 ± 0.181	55.123 ± 25.692
2994	J005758-264314	5382.454 ± 0.005	13.857 ± 0.012	24.367 ± 0.468
2995	J005758-264314	5381.329 ± 0.035	13.055 ± 0.036	36.250 ± 3.465
2996	J005758-264314	5379.660 ± 0.009	13.429 ± 0.009	34.986 ± 0.890
2997	J005758-264314	5377.574 ± 0.008	15.000 ± 0.032	30.574 ± 0.522
2998	J005758-264314	5376.280 ± 0.026	13.389 ± 1.039	15.954 ± 7.739
2999	J005758-264314	5376.000 ± 0.433	13.605 ± 0.670	24.401 ± 12.160
3000	J005758-264314	5374.738 ± 0.012	13.549 ± 0.026	28.412 ± 1.911
3001	J005758-264314	5373.975 ± 0.021	12.950 ± 0.071	16.799 ± 1.580
3002	J005758-264314	5372.925 ± 0.010	13.546 ± 0.008	38.630 ± 0.939
3003	J005758-264314	5371.066 ± 0.018	13.445 ± 0.060	12.225 ± 1.025
3004	J005758-264314	5369.979 ± 0.086	14.657 ± 0.056	50.557 ± 2.131
3005	J005758-264314	5368.856 ± 0.067	14.558 ± 0.170	17.123 ± 2.060
3006	J005758-264314	5367.777 ± 0.008	13.571 ± 0.014	19.307 ± 0.441
3007	J005758-264314	5366.437 ± 0.005	13.462 ± 0.006	26.054 ± 0.423
3008	J005758-264314	5364.890 ± 0.059	12.881 ± 0.073	32.947 ± 3.838
3009	J005758-264314	5363.303 ± 0.004	14.392 ± 0.024	21.442 ± 0.756
3010	J005758-264314	5363.223 ± 0.034	13.676 ± 0.060	51.971 ± 5.903
3011	J005758-264314	5361.225 ± 0.108	12.505 ± 0.188	32.826 ± 13.595
3012	J005758-264314	5358.909 ± 0.008	13.399 ± 0.040	23.503 ± 1.026
3013	J005758-264314	5357.886 ± 0.050	13.638 ± 0.027	57.192 ± 3.858
3014	J005758-264314	5356.101 ± 0.014	12.932 ± 0.028	21.300 ± 1.191
3015	J005758-264314	5354.292 ± 0.292	12.807 ± 0.179	49.078 ± 16.145
3016	J005758-264314	5353.332 ± 0.018	13.258 ± 0.062	27.057 ± 1.726
3017	J005758-264314	5352.262 ± 0.083	12.604 ± 0.352	20.359 ± 6.611
3018	J005758-264314	5351.247 ± 0.004	14.014 ± 0.030	20.683 ± 0.820
3019	J005758-264314	5350.151 ± 0.216	13.386 ± 0.459	68.084 ± 72.027
3020	J005758-264314	5349.004 ± 0.031	13.363 ± 0.208	28.201 ± 3.990
3021	J005758-264314	5347.817 ± 0.026	13.895 ± 0.034	42.759 ± 2.825

Table E.1. *Continued*

3022	J005758-264314	5346.455 ± 0.063	13.342 ± 0.118	30.406 ± 5.803
3023	J005758-264314	5345.384 ± 0.247	13.160 ± 0.533	28.459 ± 27.437
3024	J005758-264314	5344.845 ± 0.085	12.988 ± 0.573	18.092 ± 5.134
3025	J005758-264314	5343.233 ± 0.018	13.553 ± 0.012	62.584 ± 2.277
3026	J005758-264314	5341.637 ± 0.007	13.355 ± 0.013	20.895 ± 0.634
3027	J005758-264314	5340.795 ± 0.029	12.548 ± 0.055	18.314 ± 2.735
3028	J005758-264314	5339.612 ± 0.010	13.605 ± 0.011	27.820 ± 0.721
3029	J005758-264314	5338.144 ± 0.031	13.349 ± 0.066	37.605 ± 6.302
3030	J005758-264314	5337.251 ± 0.045	13.074 ± 0.138	16.740 ± 3.146
3031	J005758-264314	5336.761 ± 0.054	12.837 ± 0.308	15.565 ± 6.311
3032	J005758-264314	5336.269 ± 0.214	12.542 ± 0.349	19.917 ± 9.531
3033	J005758-264314	5335.107 ± 0.011	13.298 ± 0.017	20.018 ± 0.782
3034	J005758-264314	5334.012 ± 0.706	13.232 ± 1.037	25.507 ± 20.909
3035	J005758-264314	5333.619 ± 0.096	13.664 ± 1.013	18.571 ± 7.816
3036	J005758-264314	5333.270 ± 0.937	13.324 ± 1.582	23.601 ± 24.505
3037	J005758-264314	5332.413 ± 0.055	12.195 ± 0.244	11.446 ± 4.886
3038	J005758-264314	5331.268 ± 0.004	14.254 ± 0.007	32.364 ± 0.461
3039	J005758-264314	5329.964 ± 0.033	12.676 ± 0.074	21.352 ± 4.174
3040	J005758-264314	5328.853 ± 0.025	12.737 ± 0.049	20.991 ± 2.989
3041	J005758-264314	5327.996 ± 0.092	12.782 ± 0.197	18.254 ± 5.497
3042	J005758-264314	5327.273 ± 0.025	14.032 ± 0.046	20.467 ± 1.928
3043	J005758-264314	5326.736 ± 0.048	13.541 ± 0.116	17.367 ± 1.384
3044	J005758-264314	5324.480 ± 0.125	14.049 ± 0.095	46.996 ± 3.463
3045	J005758-264314	5323.252 ± 0.020	15.450 ± 0.046	36.949 ± 0.591
3046	J005758-264314	5319.721 ± 0.139	12.798 ± 0.179	24.790 ± 5.905
3047	J005758-264314	5319.024 ± 0.016	13.714 ± 0.047	20.743 ± 1.844
3048	J005758-264314	5318.523 ± 0.013	13.486 ± 0.052	13.028 ± 0.778
3049	J005758-264314	5317.537 ± 0.003	14.209 ± 0.007	27.693 ± 0.339
3050	J005758-264314	5315.915 ± 0.027	12.927 ± 0.025	31.789 ± 2.131
3051	J005758-264314	5313.639 ± 0.028	13.323 ± 0.053	25.906 ± 1.207
3052	J005758-264314	5312.834 ± 0.101	13.061 ± 0.108	34.737 ± 6.670
3053	J005758-264314	5311.335 ± 0.143	12.217 ± 0.303	16.435 ± 8.854
3054	J005758-264314	5310.812 ± 0.117	12.172 ± 0.467	15.641 ± 13.894
3055	J005758-264314	5310.230 ± 0.046	12.620 ± 0.080	17.296 ± 2.801
3056	J005758-264314	5305.892 ± 0.015	12.785 ± 0.022	20.023 ± 1.220
3057	J005758-264314	5304.801 ± 0.015	12.945 ± 0.017	26.769 ± 1.308
3058	J005758-264314	5300.831 ± 0.038	12.043 ± 0.085	12.995 ± 3.182
3059	J005758-264314	5298.779 ± 0.728	13.108 ± 0.523	49.375 ± 20.701
3060	J005758-264314	5298.319 ± 0.005	14.354 ± 0.019	22.835 ± 1.038
3061	J005758-264314	5297.256 ± 0.080	12.303 ± 0.385	15.455 ± 6.087
3062	J005758-264314	5296.312 ± 0.046	12.035 ± 0.131	10.292 ± 3.912
3063	J005758-264314	5292.471 ± 0.010	14.910 ± 0.032	27.964 ± 0.462
3064	J005758-264314	5290.466 ± 0.010	15.693 ± 0.087	32.485 ± 0.923
3065	J005758-264314	5288.533 ± 0.017	13.908 ± 0.032	18.322 ± 0.754

Table E.1. *Continued*

3066	J005758-264314	5287.908 ± 0.022	13.825 ± 0.046	22.191 ± 1.814
3067	J005758-264314	5286.770 ± 0.161	12.950 ± 0.218	34.654 ± 16.522
3068	J005758-264314	5285.745 ± 0.006	13.573 ± 0.015	19.440 ± 0.531
3069	J005758-264314	5283.928 ± 0.004	13.475 ± 0.018	16.934 ± 0.463
3070	J005758-264314	5283.243 ± 0.023	12.345 ± 0.148	12.144 ± 2.659
3071	J005758-264314	5282.824 ± 0.157	13.082 ± 0.078	59.016 ± 7.877
3072	J005758-264314	5280.606 ± 0.007	13.492 ± 0.009	23.105 ± 0.530
3073	J005758-264314	5279.564 ± 0.025	13.594 ± 0.038	20.131 ± 1.250
3074	J005758-264314	5278.652 ± 0.100	12.642 ± 0.239	14.279 ± 5.461
3075	J005758-264314	5278.341 ± 0.094	12.296 ± 0.497	10.258 ± 4.057
3076	J005758-264314	5277.540 ± 0.064	11.919 ± 0.148	12.698 ± 5.758
3077	J005758-264314	5276.914 ± 0.108	12.731 ± 0.516	14.314 ± 6.184
3078	J005758-264314	5276.340 ± 0.021	13.174 ± 0.231	10.841 ± 2.845
3079	J005758-264314	5276.182 ± 0.063	13.933 ± 0.073	30.571 ± 1.906
3080	J005758-264314	5274.771 ± 0.004	13.506 ± 0.006	18.565 ± 0.341
3081	J005758-264314	5273.167 ± 0.100	12.296 ± 0.311	17.247 ± 9.985
3082	J005758-264314	5272.335 ± 0.036	12.999 ± 1.048	18.597 ± 9.543
3083	J005758-264314	5271.976 ± 0.633	13.154 ± 0.776	29.494 ± 19.953
3084	J005758-264314	5270.492 ± 0.027	12.834 ± 0.045	23.142 ± 2.865
3085	J005758-264314	5269.896 ± 0.040	12.296 ± 0.238	11.477 ± 3.794
3086	J005758-264314	5269.404 ± 0.200	12.044 ± 0.388	20.019 ± 19.102
3087	J005758-264314	5268.622 ± 0.019	12.554 ± 0.040	14.763 ± 1.610
3088	J005758-264314	5266.286 ± 0.040	11.931 ± 0.111	10.693 ± 3.540
3089	J005758-264314	5265.620 ± 0.024	12.466 ± 0.040	18.210 ± 2.158
3090	J005758-264314	5263.256 ± 0.062	12.290 ± 0.087	21.756 ± 5.323
3091	J005758-264314	5262.623 ± 0.049	12.008 ± 0.145	12.045 ± 3.950
3092	J005758-264314	5260.683 ± 0.080	12.214 ± 0.079	30.017 ± 6.460
3093	J005758-264314	5259.230 ± 0.081	11.809 ± 0.152	15.804 ± 6.986
3094	J005758-264314	5258.272 ± 0.053	12.129 ± 0.081	19.766 ± 4.579
3095	J005758-264314	5256.636 ± 0.023	12.694 ± 0.028	25.327 ± 2.070
3096	J005758-264314	5254.002 ± 1.228	12.894 ± 1.168	39.608 ± 32.767
3097	J005758-264314	5253.358 ± 0.025	14.068 ± 0.282	20.443 ± 3.575
3098	J005758-264314	5253.031 ± 0.334	14.008 ± 0.424	32.033 ± 8.569
3099	J005758-264314	5251.839 ± 0.128	12.201 ± 0.278	20.048 ± 9.416
3100	J005758-264314	5250.597 ± 0.006	14.122 ± 0.007	26.650 ± 0.428
3101	J005758-264314	5249.504 ± 0.028	13.475 ± 0.031	31.897 ± 2.363
3102	J005758-264314	5248.306 ± 0.040	13.910 ± 0.071	19.720 ± 1.655
3103	J005758-264314	5247.530 ± 0.029	14.572 ± 0.059	23.233 ± 0.647
3104	J005758-264314	5244.415 ± 0.035	12.405 ± 0.066	19.605 ± 4.081
3105	J005758-264314	5241.806 ± 0.018	15.073 ± 0.041	31.083 ± 0.527
3106	J005758-264314	5240.502 ± 0.060	14.153 ± 0.046	45.566 ± 3.943
3107	J005758-264314	5239.172 ± 0.007	13.807 ± 0.018	19.599 ± 0.627
3108	J005758-264314	5238.265 ± 0.012	13.809 ± 0.011	33.223 ± 1.143
3109	J005758-264314	5236.970 ± 0.052	12.467 ± 0.568	10.479 ± 7.990

Table E.1. *Continued*

3110	J005758-264314	5236.554 ± 0.089	13.278 ± 0.104	29.183 ± 3.193
3111	J005758-264314	5235.402 ± 0.060	11.717 ± 0.170	10.614 ± 5.412
3112	J005758-264314	5234.438 ± 0.113	11.926 ± 0.150	23.758 ± 10.522
3113	J005758-264314	5232.706 ± 0.021	12.580 ± 0.030	20.810 ± 1.786
3114	J005758-264314	5231.423 ± 0.015	13.978 ± 0.021	22.088 ± 0.595
3115	J005758-264314	5230.777 ± 0.016	13.849 ± 0.029	19.859 ± 0.910
3116	J005758-264314	5229.709 ± 0.010	14.013 ± 0.122	25.925 ± 1.851
3117	J005758-264314	5229.191 ± 1.511	12.995 ± 1.339	41.126 ± 47.530
3118	J005758-264314	5226.893 ± 0.005	14.247 ± 0.013	21.157 ± 0.461
3119	J005758-264314	5225.977 ± 0.039	13.347 ± 0.073	33.625 ± 5.911
3120	J005758-264314	5225.072 ± 0.051	12.718 ± 0.339	12.849 ± 9.824
3121	J005758-264314	5224.332 ± 0.026	13.398 ± 0.020	34.002 ± 1.492
3122	J005758-264314	5222.462 ± 0.020	12.782 ± 0.022	27.856 ± 1.803
3123	J005758-264314	5220.647 ± 0.060	12.037 ± 0.099	18.592 ± 5.487
3124	J005758-264314	5219.401 ± 0.029	12.524 ± 0.035	25.292 ± 2.485
3125	J005758-264314	5215.541 ± 0.034	12.082 ± 0.073	13.530 ± 2.878
3126	J005758-264314	5209.200 ± 0.021	13.068 ± 0.036	28.939 ± 2.898
3127	J005758-264314	5208.463 ± 0.037	12.326 ± 0.134	14.529 ± 3.375
3128	J005758-264314	5207.785 ± 0.058	12.129 ± 0.163	11.959 ± 5.140
3129	J005758-264314	5207.016 ± 0.077	12.434 ± 0.172	13.851 ± 4.522
3130	J005758-264314	5206.021 ± 0.005	13.328 ± 0.007	21.784 ± 0.455
3131	J005758-264314	5204.788 ± 0.110	12.854 ± 0.231	24.742 ± 5.056
3132	J005758-264314	5204.015 ± 0.026	12.436 ± 0.249	11.656 ± 3.192
3133	J005758-264314	5203.954 ± 0.471	12.684 ± 0.460	36.915 ± 18.322
3134	J005758-264314	5202.319 ± 0.036	13.097 ± 0.045	27.110 ± 2.483
3135	J005758-264314	5201.093 ± 0.016	12.882 ± 0.022	22.500 ± 1.319
3136	J005758-264314	5198.933 ± 0.026	12.367 ± 0.046	16.907 ± 2.251
3137	J005758-264314	5195.210 ± 0.018	12.901 ± 0.020	28.376 ± 1.597
3138	J005758-264314	5194.068 ± 0.048	12.316 ± 0.068	22.779 ± 4.263
3139	J005758-264314	5192.244 ± 0.146	12.155 ± 0.108	41.475 ± 12.231
3140	J005758-264314	5188.907 ± 0.058	13.865 ± 0.083	25.474 ± 1.692
3141	J005758-264314	5188.425 ± 0.024	14.056 ± 0.065	19.161 ± 0.783
3142	J005758-264314	5187.243 ± 0.015	13.370 ± 0.022	25.357 ± 1.321
3143	J005758-264314	5186.517 ± 0.017	13.132 ± 0.034	19.097 ± 1.077
3144	J005758-264314	5185.413 ± 0.004	13.662 ± 0.005	22.091 ± 0.336
3145	J005758-264314	5184.528 ± 0.031	12.532 ± 0.064	19.588 ± 3.311
3146	J005758-264314	5182.538 ± 0.002	15.407 ± 0.026	41.324 ± 0.401
3147	J005758-264314	5177.564 ± 0.075	12.462 ± 0.085	27.527 ± 5.802
3148	J005758-264314	5176.703 ± 0.014	13.002 ± 0.029	20.350 ± 1.330
3149	J005758-264314	5175.126 ± 0.050	14.434 ± 0.050	36.817 ± 1.490
3150	J005758-264314	5173.904 ± 0.045	14.584 ± 0.059	33.027 ± 3.929
3151	J005758-264314	5172.814 ± 0.128	13.641 ± 0.139	34.042 ± 5.216
3152	J005758-264314	5171.734 ± 0.034	12.404 ± 0.124	14.988 ± 3.241
3153	J005758-264314	5170.708 ± 0.038	13.281 ± 0.043	32.717 ± 2.841

Table E.1. *Continued*

3154	J005758-264314	5169.443 ± 0.006	14.458 ± 0.010	34.007 ± 0.604
3155	J005758-264314	5166.426 ± 0.052	15.766 ± 0.081	48.749 ± 1.267
3156	J005758-264314	5164.256 ± 0.335	14.318 ± 0.611	36.879 ± 17.962
3157	J005758-264314	5163.105 ± 0.171	14.150 ± 0.741	29.265 ± 10.285
3158	J005758-264314	5163.106 ± 2.434	14.027 ± 2.100	55.032 ± 45.340
3159	J005758-264314	5160.141 ± 0.099	13.226 ± 0.110	32.960 ± 4.393
3160	J005758-264314	5159.386 ± 0.060	13.313 ± 0.088	29.433 ± 2.219
3161	J005758-264314	5157.673 ± 0.012	12.965 ± 0.015	25.418 ± 1.016
3162	J005758-264314	5155.415 ± 0.060	11.906 ± 0.127	14.447 ± 5.219
3163	J005758-264314	5154.090 ± 0.015	12.810 ± 0.064	16.736 ± 1.587
3164	J005758-264314	5153.723 ± 0.033	13.252 ± 0.026	44.923 ± 1.526
3165	J005758-264314	5150.798 ± 0.062	13.876 ± 0.291	21.364 ± 2.594
3166	J005758-264314	5150.190 ± 0.202	13.784 ± 0.523	31.551 ± 30.696
3167	J005758-264314	5149.452 ± 0.087	13.349 ± 0.623	20.333 ± 8.692
3168	J005758-264314	5148.833 ± 0.089	13.511 ± 0.187	26.623 ± 8.453
3169	J005758-264314	5148.039 ± 0.046	13.335 ± 0.074	23.552 ± 1.781
3170	J005758-264314	5146.518 ± 0.076	12.449 ± 0.094	27.443 ± 6.007
3171	J005758-264314	5145.507 ± 0.081	12.473 ± 0.088	29.210 ± 6.132
3172	J005758-264314	5141.740 ± 0.080	12.259 ± 0.081	31.447 ± 6.684
3173	J005758-264314	5139.106 ± 0.012	13.090 ± 0.032	24.980 ± 1.314
3174	J005758-264314	5138.475 ± 0.478	12.607 ± 0.097	89.441 ± 34.421
3175	J005758-264314	5137.048 ± 0.030	12.143 ± 0.134	10.628 ± 2.915
3176	J005758-264314	5136.310 ± 0.005	13.562 ± 0.008	25.334 ± 0.530
3177	J005758-264314	5135.046 ± 0.019	13.016 ± 0.026	29.592 ± 2.200
3178	J005758-264314	5133.850 ± 0.003	14.317 ± 0.016	21.712 ± 0.443
3179	J005758-264314	5133.053 ± 0.026	13.072 ± 0.163	11.441 ± 1.950
3180	J005758-264314	5132.643 ± 0.018	13.838 ± 0.031	19.533 ± 1.072
3181	J005758-264314	5131.809 ± 0.058	12.675 ± 0.073	24.398 ± 3.891
3182	J005758-264314	5129.174 ± 2.725	13.071 ± 4.786	27.798 ± 51.677
3183	J005758-264314	5128.913 ± 0.029	13.972 ± 0.593	21.135 ± 4.527
3184	J005758-264314	5126.998 ± 0.005	13.621 ± 0.006	22.145 ± 0.353
3185	J005758-264314	5126.096 ± 0.012	13.135 ± 0.026	22.856 ± 1.228
3186	J005758-264314	5124.066 ± 0.771	13.382 ± 0.405	67.709 ± 28.230
3187	J005758-264314	5123.792 ± 0.010	14.472 ± 0.035	22.011 ± 0.725
3188	J005758-264314	5122.877 ± 0.032	13.982 ± 0.080	34.542 ± 2.254
3189	J005758-264314	5121.119 ± 0.091	12.063 ± 0.184	20.591 ± 8.453
3190	J005758-264314	5119.986 ± 0.179	12.093 ± 0.158	36.577 ± 16.531
3191	J005758-264314	5115.329 ± 0.079	12.212 ± 0.166	14.752 ± 5.580
3192	J005758-264314	5114.889 ± 0.070	12.120 ± 0.200	11.995 ± 4.612
3193	J005758-264314	5112.239 ± 0.011	13.171 ± 0.018	23.769 ± 0.846
3194	J005758-264314	5110.590 ± 0.814	13.258 ± 0.635	47.679 ± 26.082
3195	J005758-264314	5110.668 ± 0.033	12.854 ± 0.242	13.288 ± 2.986
3196	J005758-264314	5109.997 ± 0.013	13.988 ± 0.089	25.059 ± 1.635
3197	J005758-264314	5109.309 ± 0.068	12.812 ± 0.291	17.023 ± 4.219

Table E.1. *Continued*

3198	J005758-264314	5106.840 ± 0.044	12.679 ± 0.034	39.959 ± 3.643
3199	J005758-264314	5101.610 ± 0.062	12.281 ± 0.108	21.957 ± 7.251
3200	J005758-264314	5098.889 ± 0.019	14.365 ± 0.016	39.489 ± 0.687
3201	J005758-264314	5095.601 ± 0.014	18.267 ± 0.129	51.213 ± 0.824
3202	J005758-264314	5091.858 ± 0.007	13.339 ± 0.008	26.858 ± 0.654
3203	J005758-264314	5090.534 ± 0.003	13.956 ± 0.004	26.462 ± 0.232
3204	J005758-264314	5089.374 ± 0.043	12.140 ± 0.108	13.125 ± 4.326
3205	J005758-264314	5087.984 ± 0.061	13.497 ± 0.064	35.461 ± 4.124
3206	J005758-264314	5087.111 ± 0.010	14.078 ± 0.020	25.832 ± 1.100
3207	J005758-264314	5086.246 ± 0.027	13.432 ± 0.047	24.851 ± 2.177
3208	J005758-264314	5085.314 ± 0.006	13.628 ± 0.008	21.492 ± 0.408
3209	J005758-264314	5083.505 ± 0.008	14.006 ± 0.006	37.267 ± 0.568
3210	J005758-264314	5082.622 ± 0.080	12.627 ± 0.315	15.592 ± 5.548
3211	J005758-264314	5082.094 ± 0.050	13.005 ± 0.229	21.127 ± 7.937
3212	J005758-264314	5081.353 ± 0.026	13.645 ± 0.036	27.962 ± 2.040
3213	J005758-264314	5080.590 ± 0.016	12.658 ± 0.104	10.447 ± 1.740
3214	J005758-264314	5079.608 ± 0.016	14.320 ± 0.014	34.099 ± 1.267
3215	J005758-264314	5078.313 ± 0.012	14.757 ± 0.042	26.883 ± 0.806
3216	J005758-264314	5077.007 ± 0.056	12.555 ± 0.149	23.488 ± 6.576
3217	J005758-264314	5075.992 ± 0.044	13.086 ± 0.037	40.392 ± 3.708
3218	J005758-264314	5074.650 ± 0.058	12.182 ± 0.141	14.028 ± 5.378
3219	J005758-264314	5073.941 ± 0.038	12.396 ± 0.103	14.900 ± 4.244
3220	J005758-264314	5071.790 ± 0.003	15.789 ± 0.047	44.183 ± 0.632
3221	J005758-264314	5068.933 ± 0.229	12.944 ± 0.122	92.734 ± 28.172
3222	J005758-264314	5067.340 ± 0.002	14.678 ± 0.026	23.286 ± 0.357
3223	J005758-264314	5062.348 ± 0.071	12.461 ± 0.068	33.853 ± 6.479
3224	J005758-264314	5061.188 ± 0.004	13.566 ± 0.006	23.194 ± 0.347
3225	J005758-264314	5059.203 ± 0.027	13.933 ± 0.067	19.591 ± 0.783
3226	J005758-264314	5058.717 ± 0.047	13.876 ± 0.071	24.039 ± 1.517
3227	J005758-264314	5055.936 ± 0.002	15.199 ± 0.026	34.063 ± 0.342
3228	J005758-264314	5053.986 ± 0.070	12.302 ± 0.075	29.992 ± 6.381
3229	J005758-264314	5050.933 ± 0.008	13.164 ± 0.033	18.065 ± 0.852
3230	J005758-264314	5050.421 ± 0.034	13.408 ± 0.020	47.045 ± 1.637
3231	J005758-264314	5049.101 ± 0.005	13.406 ± 0.010	20.581 ± 0.488
3232	J005758-264314	5048.197 ± 0.150	11.854 ± 0.215	22.509 ± 13.583
3233	J005758-264314	5045.135 ± 0.104	12.327 ± 0.083	40.876 ± 9.674
3234	J005758-264314	5040.379 ± 0.069	12.733 ± 0.058	38.360 ± 5.409
3235	J005758-264314	5038.449 ± 0.003	15.378 ± 0.038	37.933 ± 0.559
3236	J005758-264314	5036.669 ± 0.033	12.446 ± 0.268	14.435 ± 4.071
3237	J005758-264314	5036.073 ± 0.047	13.159 ± 0.162	32.122 ± 7.168
3238	J005758-264314	5035.071 ± 0.031	12.129 ± 0.306	11.426 ± 4.818
3239	J005758-264314	5034.736 ± 0.442	12.970 ± 0.247	62.432 ± 26.314
3240	J005758-264314	5033.045 ± 0.064	12.346 ± 0.158	17.896 ± 6.149
3241	J005758-264314	5032.598 ± 0.091	11.782 ± 0.388	10.178 ± 6.896

Table E.1. *Continued*

3242	J005758-264314	5030.885 ± 0.067	12.130 ± 0.345	11.274 ± 4.570
3243	J005758-264314	5030.472 ± 0.230	12.076 ± 0.435	18.912 ± 17.773
3244	J005758-264314	5029.546 ± 0.023	12.698 ± 0.045	20.535 ± 2.668
3245	J005758-264314	5028.824 ± 0.105	11.944 ± 0.202	17.279 ± 8.699
3246	J005758-264314	5026.701 ± 0.050	12.059 ± 0.097	16.034 ± 4.487
3247	J005758-264314	5025.685 ± 0.135	12.672 ± 0.262	23.385 ± 6.626
3248	J005758-264314	5024.275 ± 0.012	14.862 ± 0.073	28.614 ± 3.362
3249	J005758-264314	5023.775 ± 0.352	14.154 ± 0.289	50.625 ± 9.262
3250	J005758-264314	5021.849 ± 0.028	13.041 ± 0.047	31.472 ± 3.472
3251	J005758-264314	5021.071 ± 0.037	12.354 ± 0.121	15.655 ± 3.171
3252	J005758-264314	5019.516 ± 0.002	14.420 ± 0.008	33.587 ± 0.259
3253	J005758-264314	5017.014 ± 0.038	13.502 ± 0.067	44.094 ± 1.866
3254	J005758-264314	5016.783 ± 0.004	14.209 ± 0.014	23.509 ± 0.560
3255	J005758-264314	5013.530 ± 0.016	13.137 ± 0.017	36.608 ± 1.602
3256	J005758-264314	5007.682 ± 0.034	12.177 ± 0.063	16.510 ± 2.935
3257	J005758-264314	5003.234 ± 0.076	11.986 ± 0.121	20.034 ± 7.193
3258	J005758-264314	5001.841 ± 0.064	12.258 ± 0.078	27.090 ± 6.119
3259	J005758-264314	4999.859 ± 0.032	12.212 ± 0.060	16.680 ± 2.846
3260	J005758-264314	4993.446 ± 0.015	12.824 ± 0.020	23.674 ± 1.379
3261	J005758-264314	4992.050 ± 0.032	12.246 ± 0.232	11.237 ± 3.733
3262	J005758-264314	4991.742 ± 0.032	13.270 ± 0.021	31.005 ± 1.558
3263	J005758-264314	4990.907 ± 0.038	12.489 ± 0.137	16.321 ± 4.413
3264	J005758-264314	4990.350 ± 0.092	12.133 ± 0.186	16.389 ± 6.626
3265	J005758-264314	4987.348 ± 0.088	12.249 ± 0.161	18.453 ± 6.053
3266	J005758-264314	4986.689 ± 0.082	12.255 ± 0.266	19.832 ± 12.956
3267	J005758-264314	4986.088 ± 0.054	12.352 ± 0.126	15.494 ± 3.633
3268	J005758-264314	4985.156 ± 0.044	12.063 ± 0.091	15.474 ± 4.156
3269	J005758-264314	4983.794 ± 0.034	13.353 ± 0.116	27.987 ± 2.096
3270	J005758-264314	4982.892 ± 0.019	13.256 ± 0.274	24.866 ± 4.263
3271	J005758-264314	4982.247 ± 0.944	13.140 ± 0.617	61.172 ± 65.076
3272	J005758-264314	4980.586 ± 0.047	13.036 ± 0.132	33.120 ± 5.686
3273	J005758-264314	4979.068 ± 0.002	15.073 ± 0.063	22.208 ± 0.780
3274	J005758-264314	4978.540 ± 0.527	13.196 ± 0.395	49.963 ± 16.841
3275	J005758-264314	4976.137 ± 0.002	14.197 ± 0.009	21.609 ± 0.244
3276	J005758-264314	4975.251 ± 0.058	12.483 ± 0.157	18.332 ± 5.164
3277	J005758-264314	4974.474 ± 0.053	13.737 ± 0.745	21.162 ± 4.837
3278	J005758-264314	4974.194 ± 1.759	13.131 ± 3.042	27.426 ± 39.967
3279	J005758-264314	4972.427 ± 0.029	13.385 ± 0.028	51.629 ± 3.784
3280	J005758-264314	4971.134 ± 0.074	14.573 ± 0.391	22.382 ± 2.934
3281	J005758-264314	4970.805 ± 1.091	13.869 ± 1.898	28.260 ± 23.902
3282	J005758-264314	4969.672 ± 0.217	13.178 ± 0.133	57.983 ± 13.055
3283	J005758-264314	4967.017 ± 0.010	15.047 ± 0.025	39.900 ± 0.606
3284	J005758-264314	4965.031 ± 0.208	14.320 ± 0.146	56.623 ± 12.374
3285	J005758-264314	4964.266 ± 0.020	14.045 ± 0.231	29.521 ± 5.112

Table E.1. *Continued*

3286	J005758-264314	4963.204 ± 0.016	13.281 ± 0.145	17.563 ± 1.895
3287	J005758-264314	4962.668 ± 0.371	12.715 ± 0.508	34.591 ± 33.193
3288	J005758-264314	4961.625 ± 0.188	12.287 ± 0.289	26.270 ± 9.935
3289	J005758-264314	4960.345 ± 0.044	11.955 ± 0.090	15.088 ± 3.923
3290	J005758-264314	4957.699 ± 0.049	11.755 ± 0.129	11.507 ± 4.506
3291	J005758-264314	4956.219 ± 0.122	12.663 ± 0.181	29.236 ± 8.489
3292	J005758-264314	4955.308 ± 0.040	13.140 ± 0.076	32.102 ± 5.028
3293	J005758-264314	4954.219 ± 0.018	13.179 ± 0.033	28.351 ± 2.204
3294	J005758-264314	4953.460 ± 0.028	12.300 ± 0.105	13.239 ± 3.040
3295	J124957-015928	5576.447 ± 0.004	13.412 ± 0.004	27.165 ± 0.312
3296	J124957-015928	5575.150 ± 0.026	12.700 ± 0.023	33.408 ± 2.141
3297	J124957-015928	5573.394 ± 0.001	13.890 ± 0.002	22.785 ± 0.111
3298	J124957-015928	5571.827 ± 0.006	13.729 ± 0.005	33.299 ± 0.425
3299	J124957-015928	5571.080 ± 0.016	12.396 ± 0.130	11.692 ± 1.891
3300	J124957-015928	5570.270 ± 0.472	12.567 ± 0.579	35.317 ± 37.094
3301	J124957-015928	5569.526 ± 0.107	12.709 ± 0.347	24.278 ± 4.246
3302	J124957-015928	5566.128 ± 0.057	15.418 ± 0.092	33.358 ± 0.786
3303	J124957-015928	5565.229 ± 0.548	14.068 ± 0.612	35.910 ± 12.146
3304	J124957-015928	5563.684 ± 0.042	12.867 ± 0.054	26.395 ± 2.174
3305	J124957-015928	5562.160 ± 0.029	12.477 ± 0.031	29.098 ± 2.677
3306	J124957-015928	5560.472 ± 0.455	12.484 ± 0.457	30.965 ± 17.162
3307	J124957-015928	5560.017 ± 0.008	13.039 ± 0.117	16.885 ± 1.402
3308	J124957-015928	5558.146 ± 0.003	15.112 ± 0.015	39.670 ± 0.411
3309	J124957-015928	5556.476 ± 0.262	13.362 ± 0.119	81.828 ± 17.911
3310	J124957-015928	5554.994 ± 0.029	11.924 ± 0.203	12.156 ± 3.809
3311	J124957-015928	5553.543 ± 0.040	12.834 ± 0.067	32.865 ± 4.305
3312	J124957-015928	5552.698 ± 0.025	12.660 ± 0.067	20.082 ± 1.667
3313	J124957-015928	5550.118 ± 0.751	13.873 ± 0.553	69.849 ± 13.573
3314	J124957-015928	5548.322 ± 0.101	14.984 ± 0.032	75.687 ± 7.697
3315	J124957-015928	5545.696 ± 0.014	14.847 ± 0.027	33.400 ± 0.755
3316	J124957-015928	5544.141 ± 0.030	13.633 ± 0.019	47.627 ± 1.543
3317	J124957-015928	5541.440 ± 0.081	12.782 ± 0.266	41.128 ± 16.531
3318	J124957-015928	5541.373 ± 0.005	13.350 ± 0.081	20.912 ± 1.155
3319	J124957-015928	5539.429 ± 0.021	12.064 ± 0.162	10.302 ± 2.545
3320	J124957-015928	5538.662 ± 0.105	13.409 ± 0.539	40.939 ± 9.926
3321	J124957-015928	5537.736 ± 1.795	13.131 ± 1.072	60.081 ± 71.128
3322	J124957-015928	5535.798 ± 0.017	13.419 ± 0.150	22.463 ± 2.052
3323	J124957-015928	5535.187 ± 0.053	14.033 ± 0.047	40.641 ± 2.867
3324	J124957-015928	5534.025 ± 0.006	13.883 ± 0.010	23.991 ± 0.252
3325	J124957-015928	5531.390 ± 0.006	13.111 ± 0.006	25.326 ± 0.423
3326	J124957-015928	5528.952 ± 0.091	12.236 ± 0.476	29.780 ± 12.017
3327	J124957-015928	5527.877 ± 0.256	12.812 ± 0.148	59.741 ± 16.891
3328	J124957-015928	5526.288 ± 0.005	13.030 ± 0.013	16.771 ± 0.460
3329	J124957-015928	5525.587 ± 0.027	11.969 ± 0.075	11.312 ± 2.373

Table E.1. *Continued*

3330	J124957-015928	5522.778 ± 0.113	14.302 ± 0.070	70.234 ± 2.490
3331	J124957-015928	5522.639 ± 0.957	15.175 ± 1.602	30.212 ± 14.024
3332	J124957-015928	5521.941 ± 0.662	14.762 ± 1.388	25.653 ± 11.233
3333	J124957-015928	5520.224 ± 0.036	13.506 ± 0.039	36.206 ± 1.539
3334	J124957-015928	5518.033 ± 0.001	15.220 ± 0.019	27.553 ± 0.191
3335	J124957-015928	5515.444 ± 0.013	13.138 ± 0.010	38.621 ± 1.055
3336	J124957-015928	5513.715 ± 0.004	13.805 ± 0.003	36.967 ± 0.350
3337	J124957-015928	5512.072 ± 0.040	13.230 ± 0.051	30.271 ± 2.036
3338	J124957-015928	5510.675 ± 0.009	14.450 ± 0.007	40.312 ± 1.098
3339	J124957-015928	5509.491 ± 0.022	13.584 ± 0.041	25.852 ± 1.173
3340	J124957-015928	5507.128 ± 0.073	15.214 ± 0.074	46.948 ± 1.393
3341	J124957-015928	5505.126 ± 0.089	14.632 ± 0.047	60.235 ± 3.398
3342	J124957-015928	5503.295 ± 0.039	12.999 ± 0.130	18.361 ± 3.028
3343	J124957-015928	5500.114 ± 0.009	17.996 ± 0.332	50.684 ± 2.449
3344	J124957-015928	5496.344 ± 0.010	15.230 ± 0.042	30.091 ± 0.601
3345	J124957-015928	5494.836 ± 0.043	12.253 ± 0.130	15.617 ± 3.827
3346	J124957-015928	5493.577 ± 0.026	13.435 ± 0.023	46.268 ± 2.450
3347	J124957-015928	5492.197 ± 0.035	13.042 ± 0.059	35.023 ± 3.691
3348	J124957-015928	5491.321 ± 0.044	12.074 ± 0.183	14.646 ± 4.237
3349	J124957-015928	5490.347 ± 0.005	13.532 ± 0.006	27.577 ± 0.510
3350	J124957-015928	5489.456 ± 0.021	12.532 ± 0.043	16.995 ± 1.450
3351	J124957-015928	5487.571 ± 0.024	12.109 ± 0.126	10.312 ± 2.099
3352	J124957-015928	5487.025 ± 0.043	12.535 ± 0.056	23.339 ± 3.292
3353	J124957-015928	5485.119 ± 0.087	12.862 ± 0.063	40.970 ± 5.132
3354	J124957-015928	5484.271 ± 0.002	13.991 ± 0.006	18.511 ± 0.228
3355	J124957-015928	5482.500 ± 0.055	13.216 ± 0.041	49.348 ± 4.372
3356	J124957-015928	5481.162 ± 0.051	13.027 ± 0.100	33.057 ± 5.219
3357	J124957-015928	5479.979 ± 0.024	13.332 ± 0.070	29.942 ± 4.280
3358	J124957-015928	5478.983 ± 0.023	13.262 ± 0.059	26.460 ± 2.728
3359	J124957-015928	5477.505 ± 0.035	13.615 ± 0.026	41.341 ± 1.891
3360	J124957-015928	5477.227 ± 0.013	13.190 ± 0.086	20.201 ± 1.474
3361	J124957-015928	5472.718 ± 0.002	14.089 ± 0.005	21.843 ± 0.236
3362	J124957-015928	5471.343 ± 0.002	14.092 ± 0.003	27.115 ± 0.227
3363	J124957-015928	5469.792 ± 0.002	14.483 ± 0.011	26.598 ± 0.296
3364	J124957-015928	5468.516 ± 0.012	12.910 ± 0.022	20.973 ± 1.285
3365	J124957-015928	5467.321 ± 0.011	14.287 ± 0.021	21.388 ± 0.422
3366	J124957-015928	5466.685 ± 0.062	13.550 ± 0.080	25.555 ± 2.190
3367	J124957-015928	5465.004 ± 0.006	13.427 ± 0.006	25.948 ± 0.456
3368	J124957-015928	5463.667 ± 0.011	12.957 ± 0.018	18.417 ± 0.786
3369	J124957-015928	5462.412 ± 0.002	14.627 ± 0.011	29.535 ± 0.240
3370	J124957-015928	5460.544 ± 0.001	14.081 ± 0.006	18.149 ± 0.135
3371	J124957-015928	5457.607 ± 0.006	16.757 ± 0.162	28.759 ± 0.931
3372	J124957-015928	5456.889 ± 0.149	14.448 ± 0.032	88.876 ± 7.529
3373	J124957-015928	5454.489 ± 0.564	14.114 ± 0.601	36.678 ± 17.046

Table E.1. *Continued*

3374	J124957-015928	5453.827 ± 0.045	15.222 ± 0.104	26.011 ± 0.990
3375	J124957-015928	5451.574 ± 0.216	13.005 ± 0.139	81.047 ± 26.877
3376	J124957-015928	5450.086 ± 0.013	13.706 ± 0.031	32.279 ± 1.074
3377	J124957-015928	5448.696 ± 0.050	13.682 ± 0.107	20.239 ± 2.311
3378	J124957-015928	5447.782 ± 0.015	15.155 ± 0.058	23.627 ± 0.625
3379	J124957-015928	5447.712 ± 0.212	13.629 ± 0.091	83.589 ± 9.400
3380	J124957-015928	5445.265 ± 0.031	12.506 ± 0.079	24.669 ± 3.003
3381	J124957-015928	5441.317 ± 0.037	13.061 ± 0.034	35.358 ± 1.983
3382	J124957-015928	5438.942 ± 0.003	15.111 ± 0.017	56.926 ± 0.683
3383	J124957-015928	5436.317 ± 0.007	13.578 ± 0.008	32.920 ± 0.628
3384	J124957-015928	5434.096 ± 0.014	14.910 ± 0.031	29.083 ± 0.790
3385	J124957-015928	5433.269 ± 0.813	13.463 ± 0.635	45.063 ± 34.124
3386	J124957-015928	5431.844 ± 0.153	12.539 ± 0.293	27.011 ± 6.497
3387	J124957-015928	5429.329 ± 0.034	14.023 ± 0.029	36.611 ± 1.074
3388	J124957-015928	5428.175 ± 0.012	15.105 ± 0.035	29.979 ± 0.467
3389	J124957-015928	5425.215 ± 0.018	12.588 ± 0.023	22.165 ± 1.418
3390	J124957-015928	5423.648 ± 0.058	12.334 ± 0.092	18.844 ± 3.921
3391	J124957-015928	5422.542 ± 0.002	14.851 ± 0.029	22.800 ± 0.352
3392	J124957-015928	5421.095 ± 0.150	12.470 ± 0.251	22.957 ± 8.351
3393	J124957-015928	5420.078 ± 0.020	14.177 ± 0.025	29.178 ± 1.423
3394	J124957-015928	5418.936 ± 0.047	14.172 ± 0.074	31.086 ± 4.726
3395	J124957-015928	5418.281 ± 0.027	13.847 ± 0.118	17.733 ± 1.372
3396	J124957-015928	5416.634 ± 0.004	14.329 ± 0.008	36.063 ± 0.515
3397	J124957-015928	5415.569 ± 0.034	12.399 ± 0.136	12.377 ± 2.957
3398	J124957-015928	5414.611 ± 0.090	14.026 ± 0.013	112.854 ± 5.102
3399	J124957-015928	5413.836 ± 0.004	13.792 ± 0.012	29.411 ± 0.521
3400	J124957-015928	5410.685 ± 0.007	13.137 ± 0.012	22.563 ± 0.616
3401	J124957-015928	5409.444 ± 0.025	12.846 ± 0.031	33.299 ± 3.038
3402	J124957-015928	5408.419 ± 0.033	12.359 ± 0.064	18.613 ± 2.499
3403	J124957-015928	5405.571 ± 0.026	13.143 ± 0.054	19.226 ± 1.073
3404	J124957-015928	5404.837 ± 0.008	13.909 ± 0.012	26.135 ± 0.843
3405	J124957-015928	5403.933 ± 0.040	12.619 ± 0.161	18.348 ± 4.004
3406	J124957-015928	5403.212 ± 0.055	12.966 ± 0.053	31.392 ± 3.305
3407	J124957-015928	5401.561 ± 0.004	13.513 ± 0.005	26.192 ± 0.360
3408	J124957-015928	5400.567 ± 0.011	12.743 ± 0.029	15.795 ± 1.072
3409	J124957-015928	5398.894 ± 0.255	15.799 ± 0.821	19.596 ± 3.157
3410	J124957-015928	5397.827 ± 0.022	14.792 ± 0.021	70.139 ± 1.417
3411	J124957-015928	5395.674 ± 0.046	13.023 ± 0.106	29.169 ± 3.495
3412	J124957-015928	5394.464 ± 0.058	12.313 ± 0.085	25.070 ± 5.716
3413	J124957-015928	5391.484 ± 0.014	15.630 ± 0.029	54.788 ± 0.634
3414	J124957-015928	5389.440 ± 0.014	13.717 ± 0.043	15.432 ± 1.152
3415	J124957-015928	5388.695 ± 0.005	13.882 ± 0.010	17.059 ± 0.670
3416	J124957-015928	5386.891 ± 0.007	12.881 ± 0.016	13.011 ± 0.629
3417	J124957-015928	5385.847 ± 0.009	14.220 ± 0.012	23.375 ± 0.484

Table E.1. *Continued*

3418	J124957-015928	5385.188 ± 0.053	12.733 ± 0.206	13.367 ± 4.024
3419	J124957-015928	5381.791 ± 0.081	12.342 ± 0.205	16.624 ± 6.651
3420	J124957-015928	5381.791 ± 0.055	13.834 ± 0.014	137.412 ± 3.454
3421	J124957-015928	5381.009 ± 0.016	13.273 ± 0.054	18.757 ± 2.541
3422	J124957-015928	5379.986 ± 0.005	14.576 ± 0.022	23.105 ± 0.424
3423	J124957-015928	5378.060 ± 0.054	12.935 ± 0.097	18.599 ± 2.632
3424	J124957-015928	5377.571 ± 0.022	13.105 ± 0.074	15.324 ± 1.659
3425	J124957-015928	5376.342 ± 0.003	14.789 ± 0.022	30.159 ± 0.463
3426	J124957-015928	5374.583 ± 0.051	12.848 ± 0.042	35.279 ± 3.392
3427	J124957-015928	5372.669 ± 0.011	13.043 ± 0.023	21.442 ± 1.518
3428	J124957-015928	5371.238 ± 0.005	13.211 ± 0.007	20.946 ± 0.375
3429	J124957-015928	5369.840 ± 0.040	11.868 ± 0.096	11.733 ± 3.401
3430	J124957-015928	5365.583 ± 0.003	14.609 ± 0.021	20.460 ± 0.435
3431	J124957-015928	5364.933 ± 0.316	13.062 ± 0.267	38.453 ± 12.245
3432	J124957-015928	5361.676 ± 0.179	12.351 ± 0.223	26.510 ± 8.933
3433	J124957-015928	5360.855 ± 0.062	12.781 ± 0.096	26.575 ± 4.644
3434	J124957-015928	5359.680 ± 0.022	13.404 ± 0.103	21.868 ± 1.476
3435	J124957-015928	5358.758 ± 0.007	13.817 ± 0.136	24.549 ± 2.156
3436	J124957-015928	5358.192 ± 0.524	13.578 ± 0.344	56.983 ± 12.852
3437	J124957-015928	5354.349 ± 0.039	12.391 ± 0.163	18.671 ± 3.648
3438	J124957-015928	5353.368 ± 0.143	12.519 ± 0.252	42.206 ± 27.098
3439	J124957-015928	5351.759 ± 0.821	13.454 ± 0.941	31.222 ± 23.246
3440	J124957-015928	5351.538 ± 0.045	13.559 ± 0.530	15.423 ± 4.894
3441	J124957-015928	5350.176 ± 0.019	15.648 ± 0.146	28.370 ± 1.512
3442	J124957-015928	5348.800 ± 0.025	12.754 ± 0.085	12.061 ± 1.721
3443	J124957-015928	5347.879 ± 0.004	13.814 ± 0.004	30.468 ± 0.318
3444	J124957-015928	5346.477 ± 0.021	12.314 ± 0.041	14.659 ± 1.729
3445	J124957-015928	5343.982 ± 0.021	12.942 ± 0.033	20.667 ± 1.376
3446	J124957-015928	5343.192 ± 0.020	13.046 ± 0.030	23.203 ± 2.069
3447	J124957-015928	5342.294 ± 0.014	12.346 ± 0.041	10.270 ± 1.265
3448	J124957-015928	5340.771 ± 0.002	15.342 ± 0.049	22.097 ± 0.354
3449	J124957-015928	5339.652 ± 0.046	12.301 ± 0.107	14.693 ± 3.969
3450	J124957-015928	5338.922 ± 0.033	12.159 ± 0.077	13.808 ± 3.254
3451	J124957-015928	5337.827 ± 0.003	14.244 ± 0.011	22.546 ± 0.313
3452	J124957-015928	5336.473 ± 0.024	13.939 ± 0.024	35.406 ± 1.798
3453	J124957-015928	5335.840 ± 0.019	13.045 ± 0.154	15.141 ± 2.510
3454	J124957-015928	5334.977 ± 0.014	14.120 ± 0.019	23.253 ± 0.990
3455	J124957-015928	5334.210 ± 0.039	13.583 ± 0.093	25.507 ± 3.258
3456	J124957-015928	5333.234 ± 0.043	13.660 ± 0.039	40.503 ± 3.123
3457	J124957-015928	5331.677 ± 0.003	14.393 ± 0.012	25.227 ± 0.327
3458	J124957-015928	5330.088 ± 0.109	12.678 ± 0.123	28.803 ± 7.448
3459	J124957-015928	5329.527 ± 0.079	12.454 ± 0.361	13.138 ± 5.464
3460	J124957-015928	5329.133 ± 0.041	12.921 ± 0.084	14.983 ± 1.765
3461	J124957-015928	5327.626 ± 0.033	12.985 ± 0.131	14.452 ± 1.278

Table E.1. *Continued*

3462	J124957-015928	5327.239 ± 0.069	13.042 ± 0.115	19.286 ± 2.607
3463	J124957-015928	5325.146 ± 0.016	12.487 ± 0.031	15.725 ± 1.368
3464	J124957-015928	5323.927 ± 0.059	12.031 ± 0.308	15.593 ± 6.911
3465	J124957-015928	5323.506 ± 0.054	12.991 ± 0.040	42.633 ± 2.258
3466	J124957-015928	5320.193 ± 0.031	12.158 ± 0.059	15.368 ± 2.593
3467	J124957-015928	5318.449 ± 0.059	11.887 ± 0.110	15.579 ± 4.906
3468	J124957-015928	5317.380 ± 0.055	12.141 ± 0.122	20.187 ± 4.849
3469	J124957-015928	5316.143 ± 0.069	12.133 ± 0.314	22.060 ± 9.067
3470	J124957-015928	5314.640 ± 0.002	13.942 ± 0.007	19.104 ± 0.248
3471	J124957-015928	5314.476 ± 0.066	13.367 ± 0.037	86.596 ± 14.118
3472	J124957-015928	5312.774 ± 0.026	13.438 ± 0.057	17.316 ± 1.132
3473	J124957-015928	5312.191 ± 0.010	14.134 ± 0.017	19.918 ± 0.380
3474	J124957-015928	5310.899 ± 0.062	12.050 ± 0.144	18.071 ± 5.463
3475	J124957-015928	5309.693 ± 0.078	12.601 ± 0.060	44.515 ± 7.406
3476	J124957-015928	5307.865 ± 0.060	12.390 ± 0.059	32.484 ± 5.254
3477	J124957-015928	5305.557 ± 0.095	13.065 ± 0.088	34.406 ± 5.071
3478	J124957-015928	5304.800 ± 0.005	13.929 ± 0.012	21.277 ± 0.433
3479	J124957-015928	5303.741 ± 0.040	13.037 ± 0.069	25.447 ± 3.952
3480	J124957-015928	5303.047 ± 0.022	13.077 ± 0.092	18.112 ± 2.214
3481	J124957-015928	5302.426 ± 0.023	13.371 ± 0.028	23.931 ± 1.108
3482	J124957-015928	5299.277 ± 0.009	13.003 ± 0.011	23.282 ± 0.705
3483	J124957-015928	5296.108 ± 0.360	13.814 ± 0.306	42.430 ± 11.359
3484	J124957-015928	5296.486 ± 0.027	14.037 ± 0.092	20.112 ± 1.554
3485	J124957-015928	5295.340 ± 0.034	14.411 ± 0.074	25.704 ± 1.327
3486	J124957-015928	5294.156 ± 0.020	12.880 ± 0.033	20.693 ± 1.649
3487	J124957-015928	5292.962 ± 0.002	14.216 ± 0.012	19.282 ± 0.247
3488	J124957-015928	5291.953 ± 0.016	12.917 ± 0.023	23.147 ± 1.520
3489	J124957-015928	5290.497 ± 0.012	13.457 ± 0.010	30.811 ± 0.778
3490	J124957-015928	5285.126 ± 0.008	13.767 ± 0.008	26.293 ± 0.466
3491	J124957-015928	5284.471 ± 0.020	12.961 ± 0.086	13.548 ± 1.803
3492	J124957-015928	5283.981 ± 0.016	13.248 ± 0.037	16.815 ± 1.253
3493	J124957-015928	5283.096 ± 0.007	13.567 ± 0.007	28.381 ± 0.530
3494	J124957-015928	5279.948 ± 0.007	13.384 ± 0.007	26.852 ± 0.548
3495	J124957-015928	5279.083 ± 0.016	12.589 ± 0.041	14.797 ± 1.538
3496	J124957-015928	5278.313 ± 0.008	13.016 ± 0.013	19.578 ± 0.750
3497	J124957-015928	5276.947 ± 0.016	13.165 ± 0.017	27.902 ± 1.285
3498	J124957-015928	5275.844 ± 0.058	12.727 ± 0.188	19.991 ± 6.519
3499	J124957-015928	5275.021 ± 0.197	12.600 ± 0.549	26.377 ± 30.857
3500	J124957-015928	5274.484 ± 0.103	12.323 ± 0.693	15.272 ± 7.168
3501	J124957-015928	5272.247 ± 0.045	12.301 ± 0.053	25.664 ± 3.679
3502	J124957-015928	5270.634 ± 0.019	12.538 ± 0.027	20.313 ± 1.524
3503	J124957-015928	5268.822 ± 0.032	12.580 ± 0.173	17.164 ± 2.767
3504	J124957-015928	5268.229 ± 0.078	12.965 ± 0.076	31.772 ± 4.228
3505	J124957-015928	5266.779 ± 0.075	12.120 ± 0.292	16.741 ± 6.606

Table E.1. *Continued*

3506	J124957-015928	5265.538 ± 0.163	13.307 ± 0.146	45.730 ± 13.247
3507	J124957-015928	5264.573 ± 0.004	14.724 ± 0.037	22.510 ± 0.727
3508	J124957-015928	5263.543 ± 0.032	13.110 ± 0.162	25.310 ± 4.282
3509	J124957-015928	5262.506 ± 0.067	13.531 ± 0.090	57.758 ± 12.035
3510	J124957-015928	5261.264 ± 0.041	12.680 ± 0.232	25.511 ± 5.314
3511	J124957-015928	5259.203 ± 0.038	12.868 ± 0.055	27.335 ± 2.219
3512	J124957-015928	5258.062 ± 0.110	12.683 ± 0.166	39.048 ± 15.168
3513	J124957-015928	5257.238 ± 0.063	12.367 ± 0.454	13.824 ± 5.941
3514	J124957-015928	5256.516 ± 0.032	12.929 ± 0.192	16.719 ± 2.870
3515	J124957-015928	5256.505 ± 0.312	12.929 ± 0.339	40.942 ± 9.246
3516	J124957-015928	5254.268 ± 0.014	13.049 ± 0.017	25.645 ± 1.199
3517	J124957-015928	5253.507 ± 0.066	12.029 ± 0.171	15.623 ± 5.686
3518	J124957-015928	5252.446 ± 0.027	13.026 ± 0.034	27.252 ± 2.088
3519	J124957-015928	5251.511 ± 0.010	13.355 ± 0.022	24.564 ± 1.333
3520	J124957-015928	5250.861 ± 0.024	12.481 ± 0.130	11.827 ± 2.351
3521	J124957-015928	5250.285 ± 0.010	13.357 ± 0.014	22.678 ± 0.844
3522	J124957-015928	5249.216 ± 0.034	12.357 ± 0.076	16.331 ± 3.177
3523	J124957-015928	5248.409 ± 0.004	13.606 ± 0.006	22.198 ± 0.416
3524	J124957-015928	5247.558 ± 0.010	12.787 ± 0.022	15.221 ± 0.915
3525	J124957-015928	5246.588 ± 0.016	12.751 ± 0.020	23.649 ± 1.371
3526	J124957-015928	5242.324 ± 0.020	13.101 ± 0.032	20.523 ± 1.103
3527	J124957-015928	5241.618 ± 0.007	13.663 ± 0.009	22.689 ± 0.430
3528	J124957-015928	5239.122 ± 0.048	11.785 ± 0.119	11.611 ± 4.199
3529	J124957-015928	5237.771 ± 0.024	12.811 ± 0.036	21.148 ± 1.635
3530	J124957-015928	5236.910 ± 0.006	13.490 ± 0.011	24.747 ± 0.739
3531	J124957-015928	5235.839 ± 0.003	13.754 ± 0.005	22.854 ± 0.363
3532	J124957-015928	5235.101 ± 0.024	12.407 ± 0.130	11.155 ± 2.270
3533	J124957-015928	5234.621 ± 0.051	12.623 ± 0.073	21.095 ± 3.406
3534	J124957-015928	5233.392 ± 0.070	11.952 ± 0.107	19.934 ± 6.069
3535	J124957-015928	5232.066 ± 0.004	13.510 ± 0.005	25.790 ± 0.335
3536	J124957-015928	5230.668 ± 0.901	12.650 ± 1.516	22.633 ± 24.974
3537	J124957-015928	5230.330 ± 0.063	13.008 ± 0.750	16.317 ± 8.912
3538	J124957-015928	5228.841 ± 0.003	13.605 ± 0.004	25.249 ± 0.234
3539	J124957-015928	5226.799 ± 0.024	14.777 ± 0.060	21.890 ± 0.507
3540	J124957-015928	5225.562 ± 0.025	14.636 ± 0.035	31.958 ± 0.591
3541	J124957-015928	5223.058 ± 0.015	13.657 ± 0.063	15.505 ± 1.000
3542	J124957-015928	5222.846 ± 0.013	13.965 ± 0.027	27.392 ± 0.515
3543	J124957-015928	5221.701 ± 0.074	12.319 ± 0.107	23.837 ± 6.282
3544	J124957-015928	5220.336 ± 0.006	13.973 ± 0.007	23.450 ± 0.340
3545	J124957-015928	5219.499 ± 0.045	13.042 ± 0.151	24.419 ± 5.315
3546	J124957-015928	5218.601 ± 0.037	13.352 ± 0.080	33.255 ± 6.014
3547	J124957-015928	5217.898 ± 0.044	12.560 ± 0.260	12.532 ± 3.814
3548	J124957-015928	5217.238 ± 0.010	14.095 ± 0.016	21.232 ± 1.042
3549	J124957-015928	5216.585 ± 0.054	13.300 ± 0.098	20.939 ± 2.652

Table E.1. *Continued*

3550	J124957-015928	5215.726 ± 0.010	13.074 ± 0.017	19.110 ± 0.782
3551	J124957-015928	5213.951 ± 0.250	12.529 ± 0.247	31.256 ± 12.025
3552	J124957-015928	5213.429 ± 0.009	13.081 ± 0.068	16.073 ± 1.139
3553	J124957-015928	5212.617 ± 0.004	13.756 ± 0.007	20.200 ± 0.378
3554	J124957-015928	5211.482 ± 0.004	14.274 ± 0.006	30.478 ± 0.321
3555	J124957-015928	5210.045 ± 0.004	13.328 ± 0.006	20.413 ± 0.347
3556	J124957-015928	5207.194 ± 0.250	12.236 ± 0.231	32.841 ± 15.944
3557	J124957-015928	5206.553 ± 0.092	11.883 ± 0.473	15.543 ± 8.924
3558	J124957-015928	5205.302 ± 0.031	12.774 ± 0.040	25.473 ± 2.251
3559	J124957-015928	5204.333 ± 0.086	12.364 ± 0.187	27.688 ± 10.076
3560	J124957-015928	5202.551 ± 0.011	13.172 ± 0.091	17.283 ± 1.501
3561	J124957-015928	5202.149 ± 0.082	13.558 ± 0.091	65.414 ± 9.274
3562	J124957-015928	5201.708 ± 0.009	13.800 ± 0.037	24.505 ± 0.877
3563	J124957-015928	5200.310 ± 0.019	13.138 ± 0.053	23.415 ± 2.073
3564	J124957-015928	5199.440 ± 0.008	13.733 ± 0.009	27.057 ± 0.542
3565	J124957-015928	5198.178 ± 0.003	13.619 ± 0.005	18.111 ± 0.226
3566	J124957-015928	5197.080 ± 0.004	13.632 ± 0.005	28.244 ± 0.420
3567	J124957-015928	5195.923 ± 0.005	13.367 ± 0.006	21.701 ± 0.381
3568	J124957-015928	5191.375 ± 0.040	12.591 ± 0.086	20.863 ± 4.410
3569	J124957-015928	5190.400 ± 0.026	12.799 ± 0.031	27.942 ± 2.405
3570	J124957-015928	5189.090 ± 0.004	13.659 ± 0.011	20.693 ± 0.347
3571	J124957-015928	5187.938 ± 0.022	13.603 ± 0.014	50.252 ± 2.803
3572	J124957-015928	5186.405 ± 0.028	12.821 ± 0.380	18.690 ± 4.428
3573	J124957-015928	5185.998 ± 0.255	12.983 ± 0.281	31.500 ± 8.361
3574	J124957-015928	5182.877 ± 0.013	13.231 ± 0.011	36.582 ± 1.153
3575	J124957-015928	5181.604 ± 0.242	12.755 ± 0.436	23.397 ± 8.863
3576	J124957-015928	5181.047 ± 0.036	13.599 ± 0.065	23.643 ± 1.672
3577	J124957-015928	5180.066 ± 0.260	11.969 ± 0.293	27.824 ± 18.202
3578	J124957-015928	5177.004 ± 0.042	12.962 ± 0.116	18.398 ± 1.672
3579	J124957-015928	5176.426 ± 0.047	13.126 ± 0.105	24.715 ± 5.069
3580	J124957-015928	5175.436 ± 0.160	12.670 ± 0.336	24.968 ± 15.874
3581	J124957-015928	5174.883 ± 0.017	13.345 ± 0.055	17.783 ± 0.724
3582	J124957-015928	5173.204 ± 0.035	13.332 ± 0.046	26.732 ± 1.480
3583	J124957-015928	5172.230 ± 0.035	13.939 ± 0.051	29.781 ± 2.866
3584	J124957-015928	5169.549 ± 0.577	13.750 ± 0.310	72.052 ± 43.888
3585	J124957-015928	5167.805 ± 0.149	12.493 ± 0.808	30.154 ± 18.387
3586	J124957-015928	5166.168 ± 0.029	13.057 ± 0.054	27.875 ± 1.966
3587	J124957-015928	5164.981 ± 0.115	12.727 ± 0.224	43.720 ± 24.374
3588	J124957-015928	5164.245 ± 0.012	12.680 ± 0.114	14.034 ± 1.904
3589	J124957-015928	5163.036 ± 0.003	14.419 ± 0.008	31.874 ± 0.279
3590	J124957-015928	5161.206 ± 0.003	13.628 ± 0.004	22.401 ± 0.216
3591	J124957-015928	5159.768 ± 0.040	12.807 ± 0.090	16.929 ± 1.919
3592	J124957-015928	5159.160 ± 0.007	13.880 ± 0.009	22.268 ± 0.384
3593	J124957-015928	5155.574 ± 0.010	13.192 ± 0.010	31.874 ± 0.868

Table E.1. *Continued*

3594	J124957-015928	5154.076 ± 0.008	14.277 ± 0.014	22.940 ± 0.422
3595	J124957-015928	5153.389 ± 0.093	12.988 ± 0.149	22.478 ± 3.995
3596	J124957-015928	5151.986 ± 0.022	12.990 ± 0.023	35.283 ± 2.439
3597	J124957-015928	5150.160 ± 0.099	13.797 ± 0.184	34.182 ± 4.923
3598	J124957-015928	5150.270 ± 0.027	13.744 ± 0.162	18.066 ± 2.194
3599	J124957-015928	5149.412 ± 0.022	13.953 ± 0.052	20.485 ± 1.005
3600	J124957-015928	5148.292 ± 0.004	14.003 ± 0.004	27.708 ± 0.312
3601	J124957-015928	5147.122 ± 0.027	12.288 ± 0.052	15.818 ± 2.361
3602	J124957-015928	5145.082 ± 0.038	13.007 ± 0.027	43.179 ± 2.831
3603	J124957-015928	5144.814 ± 0.011	12.545 ± 0.057	11.030 ± 1.182
3604	J124957-015928	5143.581 ± 0.048	12.345 ± 0.064	24.748 ± 4.078
3605	J124957-015928	5140.798 ± 0.069	12.496 ± 0.127	28.499 ± 4.872
3606	J124957-015928	5138.855 ± 1.989	13.187 ± 1.210	60.700 ± 66.231
3607	J124957-015928	5138.727 ± 0.039	13.475 ± 0.224	24.196 ± 2.801
3608	J124957-015928	5138.093 ± 0.033	13.112 ± 0.517	18.995 ± 5.618
3609	J124957-015928	5137.033 ± 0.025	14.306 ± 0.029	35.134 ± 0.989
3610	J124957-015928	5135.625 ± 0.036	12.868 ± 0.094	18.449 ± 2.315
3611	J124957-015928	5135.035 ± 0.027	13.231 ± 0.040	23.429 ± 1.647
3612	J124957-015928	5133.498 ± 0.195	12.888 ± 0.186	34.108 ± 9.702
3613	J124957-015928	5133.086 ± 0.018	12.704 ± 0.217	13.669 ± 2.870
3614	J124957-015928	5131.870 ± 0.004	14.770 ± 0.022	33.745 ± 0.590
3615	J124957-015928	5130.085 ± 0.023	13.736 ± 0.011	65.260 ± 1.764
3616	J124957-015928	5127.896 ± 0.050	12.729 ± 0.084	21.880 ± 3.045
3617	J124957-015928	5126.944 ± 0.011	14.052 ± 0.023	27.928 ± 0.980
3618	J124957-015928	5126.034 ± 0.014	13.968 ± 0.067	25.362 ± 1.447
3619	J124957-015928	5125.611 ± 0.352	13.548 ± 0.235	54.185 ± 10.985
3620	J124957-015928	5121.870 ± 0.277	12.838 ± 0.146	75.556 ± 20.355
3621	J124957-015928	5121.778 ± 0.005	13.650 ± 0.015	26.249 ± 0.533
3622	J124957-015928	5119.830 ± 0.040	13.251 ± 0.037	49.710 ± 3.085
3623	J124957-015928	5117.285 ± 0.040	13.393 ± 0.039	52.026 ± 2.264
3624	J124957-015928	5116.976 ± 0.004	13.930 ± 0.012	24.110 ± 0.417
3625	J124957-015928	5114.913 ± 0.008	13.188 ± 0.009	27.743 ± 0.654
3626	J124957-015928	5112.660 ± 0.011	13.236 ± 0.107	21.919 ± 1.716
3627	J124957-015928	5112.165 ± 0.368	12.747 ± 0.340	37.727 ± 12.493
3628	J124957-015928	5109.146 ± 0.054	12.082 ± 0.083	19.929 ± 4.558
3629	J124957-015928	5106.719 ± 0.024	12.475 ± 0.035	21.216 ± 2.032
3630	J124957-015928	5105.192 ± 0.043	12.792 ± 0.072	20.621 ± 2.444
3631	J124957-015928	5104.041 ± 0.010	14.536 ± 0.039	22.242 ± 1.962
3632	J124957-015928	5103.902 ± 0.128	13.839 ± 0.346	32.665 ± 1.832
3633	J124957-015928	5101.416 ± 0.024	12.343 ± 0.099	14.315 ± 2.594
3634	J124957-015928	5101.008 ± 0.024	13.414 ± 0.010	57.908 ± 1.730
3635	J124957-015928	5099.061 ± 0.008	13.441 ± 0.009	34.989 ± 0.765
3636	J124957-015928	5097.122 ± 0.071	13.136 ± 0.046	50.413 ± 3.107
3637	J124957-015928	5096.637 ± 0.047	12.363 ± 0.238	20.478 ± 5.860

Table E.1. *Continued*

3638	J124957-015928	5095.292 ± 0.019	12.685 ± 0.036	20.953 ± 1.946
3639	J124957-015928	5094.141 ± 0.171	12.936 ± 0.225	27.316 ± 7.647
3640	J124957-015928	5093.597 ± 0.040	13.215 ± 0.118	21.133 ± 1.911
3641	J124957-015928	5092.656 ± 0.007	13.230 ± 0.013	21.860 ± 0.834
3642	J124957-015928	5091.750 ± 0.007	13.210 ± 0.011	22.350 ± 0.660
3643	J124957-015928	5090.520 ± 0.020	12.632 ± 0.026	23.896 ± 1.725
3644	J124957-015928	5085.718 ± 0.063	12.692 ± 0.229	17.452 ± 7.756
3645	J124957-015928	5085.148 ± 0.070	12.628 ± 0.290	18.210 ± 10.909
3646	J124957-015928	5084.676 ± 0.021	12.645 ± 0.112	10.936 ± 1.749
3647	J124957-015928	5084.216 ± 0.034	12.008 ± 0.121	10.044 ± 3.790
3648	J124957-015928	5083.095 ± 0.049	12.856 ± 0.095	25.748 ± 5.548
3649	J124957-015928	5082.374 ± 0.059	12.629 ± 0.138	20.166 ± 5.238
3650	J124957-015928	5079.937 ± 0.011	13.315 ± 0.009	39.862 ± 0.983
3651	J124957-015928	5078.794 ± 0.021	12.453 ± 0.044	16.656 ± 1.771
3652	J124957-015928	5076.277 ± 0.037	12.642 ± 0.075	24.621 ± 3.705
3653	J124957-015928	5075.045 ± 0.009	12.668 ± 0.024	12.308 ± 0.801
3654	J124957-015928	5074.289 ± 0.005	13.357 ± 0.007	23.551 ± 0.480
3655	J124957-015928	5072.736 ± 0.016	12.973 ± 0.015	34.234 ± 1.378
3656	J124957-015928	5069.804 ± 0.062	12.254 ± 0.237	15.256 ± 5.203
3657	J124957-015928	5069.187 ± 0.007	13.451 ± 0.036	20.281 ± 0.915
3658	J124957-015928	5068.790 ± 0.297	12.981 ± 0.088	55.554 ± 14.594
3659	J124957-015928	5067.274 ± 0.071	12.841 ± 0.148	36.119 ± 9.009
3660	J124957-015928	5065.687 ± 0.069	14.688 ± 0.096	32.279 ± 1.715
3661	J124957-015928	5064.516 ± 0.062	14.429 ± 0.082	28.777 ± 7.690
3662	J124957-015928	5063.737 ± 0.077	13.436 ± 0.304	17.252 ± 3.922
3663	J124957-015928	5062.951 ± 0.011	14.013 ± 0.013	31.664 ± 0.988
3664	J124957-015928	5061.575 ± 0.006	13.898 ± 0.007	35.878 ± 0.709
3665	J124957-015928	5060.215 ± 0.034	12.887 ± 0.036	33.715 ± 2.946
3666	J124957-015928	5058.711 ± 0.013	12.922 ± 0.015	27.817 ± 1.177
3667	J124957-015928	5051.796 ± 0.031	13.149 ± 0.047	28.546 ± 1.536
3668	J124957-015928	5050.944 ± 0.215	12.528 ± 0.201	35.857 ± 11.670
3669	J124957-015928	5049.032 ± 0.011	13.518 ± 0.011	28.381 ± 0.709
3670	J124957-015928	5047.735 ± 0.003	14.959 ± 0.031	28.328 ± 0.471
3671	J124957-015928	5045.500 ± 0.004	13.861 ± 0.004	30.908 ± 0.393
3672	J124957-015928	5044.421 ± 0.012	13.121 ± 0.024	22.842 ± 1.326
3673	J124957-015928	5043.392 ± 0.045	12.765 ± 0.116	27.242 ± 7.692
3674	J124957-015928	5042.386 ± 0.071	12.804 ± 0.621	16.393 ± 7.709
3675	J124957-015928	5041.642 ± 0.025	13.423 ± 0.191	13.862 ± 3.054
3676	J124957-015928	5041.759 ± 0.075	14.024 ± 0.097	36.757 ± 4.707
3677	J124957-015928	5040.831 ± 0.013	14.158 ± 0.033	18.939 ± 0.517
3678	J124957-015928	5039.363 ± 0.015	12.977 ± 0.054	28.606 ± 1.893
3679	J124957-015928	5037.775 ± 0.305	13.016 ± 0.179	79.285 ± 29.786
3680	J124957-015928	5036.997 ± 0.038	12.609 ± 0.201	22.239 ± 4.961
3681	J124957-015928	5035.912 ± 0.063	12.240 ± 0.334	20.012 ± 8.302

Table E.1. *Continued*

3682	J124957-015928	5034.522 ± 0.011	13.287 ± 0.024	27.474 ± 0.910
3683	J124957-015928	5033.227 ± 0.145	12.586 ± 0.207	53.531 ± 29.728
3684	J124957-015928	5032.295 ± 0.034	12.150 ± 0.217	13.632 ± 4.450
3685	J124957-015928	5031.317 ± 0.002	14.151 ± 0.006	24.641 ± 0.215
3686	J124957-015928	5029.698 ± 0.021	12.817 ± 0.021	32.763 ± 1.856
3687	J124957-015928	5027.341 ± 0.003	14.330 ± 0.008	29.796 ± 0.289
3688	J124957-015928	5026.238 ± 0.065	13.061 ± 0.226	16.792 ± 2.764
3689	J124957-015928	5025.857 ± 0.086	13.187 ± 0.164	19.952 ± 2.884
3690	J124957-015928	5023.807 ± 0.010	12.892 ± 0.014	21.574 ± 0.829
3691	J124957-015928	5022.132 ± 0.004	13.533 ± 0.005	25.126 ± 0.282
3692	J124957-015928	5019.634 ± 0.011	13.127 ± 0.010	33.112 ± 0.885
3693	J124957-015928	5017.728 ± 0.015	12.670 ± 0.023	20.186 ± 1.293
3694	J124957-015928	5016.417 ± 0.011	13.132 ± 0.012	31.696 ± 1.075
3695	J124957-015928	5015.062 ± 0.012	13.031 ± 0.014	29.189 ± 1.206
3696	J124957-015928	5013.349 ± 0.004	14.633 ± 0.017	27.424 ± 0.361
3697	J124957-015928	5012.160 ± 0.005	14.069 ± 0.006	25.718 ± 0.404
3698	J124957-015928	5010.592 ± 0.021	13.179 ± 0.020	38.361 ± 4.188
3699	J124957-015928	5009.371 ± 0.007	13.231 ± 0.013	20.918 ± 0.646
3700	J124957-015928	5008.320 ± 0.003	13.949 ± 0.007	21.906 ± 0.282
3701	J124957-015928	5006.934 ± 0.826	13.087 ± 0.653	46.502 ± 41.436
3702	J124957-015928	5006.471 ± 0.007	13.570 ± 0.143	21.182 ± 1.882
3703	J124957-015928	5005.568 ± 0.059	13.325 ± 0.112	27.984 ± 3.274
3704	J124957-015928	5004.702 ± 0.005	13.771 ± 0.019	10.348 ± 0.834
3705	J124957-015928	5004.365 ± 0.028	12.971 ± 0.092	10.256 ± 1.209
3706	J124957-015928	5002.647 ± 0.012	12.816 ± 0.056	11.872 ± 1.873
3707	J124957-015928	5001.576 ± 0.056	11.678 ± 0.170	10.172 ± 5.899
3708	J124957-015928	5000.443 ± 0.043	12.255 ± 0.062	22.615 ± 4.085
3709	J124957-015928	4999.080 ± 0.033	13.228 ± 0.045	27.990 ± 1.647
3710	J124957-015928	4998.297 ± 0.034	13.285 ± 0.039	30.272 ± 1.739
3711	J124957-015928	4997.006 ± 0.020	12.305 ± 0.052	12.994 ± 1.855
3712	J124957-015928	4996.019 ± 0.003	13.927 ± 0.003	29.364 ± 0.223
3713	J124957-015928	4992.752 ± 0.018	13.125 ± 0.014	40.669 ± 1.656
3714	J124957-015928	4991.698 ± 0.059	12.076 ± 0.184	16.107 ± 5.620
3715	J124957-015928	4990.757 ± 0.104	12.766 ± 0.115	32.933 ± 7.551
3716	J124957-015928	4989.914 ± 0.003	13.982 ± 0.014	14.112 ± 0.394
3717	J124957-015928	4986.956 ± 0.003	16.501 ± 0.058	63.802 ± 0.874
3718	J124957-015928	4983.535 ± 0.007	13.371 ± 0.009	26.681 ± 0.702
3719	J124957-015928	4982.686 ± 0.031	12.219 ± 0.099	12.151 ± 3.422
3720	J124957-015928	4981.621 ± 0.003	14.415 ± 0.041	13.452 ± 0.350
3721	J124957-015928	4980.765 ± 0.004	14.398 ± 0.026	19.318 ± 0.516
3722	J124957-015928	4979.865 ± 0.003	13.445 ± 0.007	14.691 ± 0.348
3723	J124957-015928	4979.272 ± 0.002	13.325 ± 0.006	10.271 ± 0.193
3724	J124957-015928	4977.619 ± 0.014	12.979 ± 0.019	23.397 ± 1.157
3725	J124957-015928	4976.797 ± 0.044	12.407 ± 0.068	21.601 ± 3.673

Table E.1. *Continued*

3726	J124957-015928	4974.533 ± 0.004	13.972 ± 0.003	53.673 ± 0.362
3727	J124957-015928	4972.978 ± 0.038	12.269 ± 0.178	10.740 ± 2.676
3728	J124957-015928	4972.583 ± 0.029	12.809 ± 0.052	17.259 ± 1.880
3729	J124957-015928	4971.076 ± 0.005	13.430 ± 0.006	25.140 ± 0.461
3730	J124957-015928	4968.888 ± 0.003	13.820 ± 0.004	24.071 ± 0.287
3731	J124957-015928	4967.857 ± 0.004	13.760 ± 0.005	28.587 ± 0.338
3732	J124957-015928	4965.661 ± 0.003	13.717 ± 0.003	27.479 ± 0.215
3733	J124957-015928	4964.227 ± 0.007	12.733 ± 0.019	11.742 ± 0.606
3734	J124957-015928	4963.196 ± 0.023	13.832 ± 0.027	29.001 ± 1.047
3735	J124957-015928	4962.341 ± 0.009	14.400 ± 0.017	25.931 ± 0.836
3736	J124957-015928	4960.969 ± 0.042	13.246 ± 0.055	35.473 ± 5.280
3737	J124957-015928	4959.786 ± 0.029	13.180 ± 0.029	34.412 ± 1.780
3738	J124957-015928	4956.997 ± 0.038	12.302 ± 0.082	17.527 ± 3.125
3739	J124957-015928	4955.663 ± 0.021	14.059 ± 0.042	38.596 ± 0.818
3740	J124957-015928	4955.421 ± 0.015	13.961 ± 0.054	23.633 ± 1.248
3741	J124957-015928	4953.432 ± 0.017	13.112 ± 0.012	43.837 ± 1.534
3742	J124957-015928	4949.894 ± 0.130	14.256 ± 0.102	44.070 ± 3.443
3743	J124957-015928	4949.012 ± 0.035	15.220 ± 0.082	28.470 ± 0.799
3744	J124957-015928	4946.750 ± 0.038	12.397 ± 0.073	21.154 ± 3.161
3745	J124957-015928	4945.678 ± 0.044	12.728 ± 0.046	39.243 ± 5.355
3746	J124957-015928	4944.273 ± 0.030	13.675 ± 0.057	20.924 ± 1.103
3747	J124957-015928	4943.631 ± 0.014	14.227 ± 0.027	23.390 ± 1.251
3748	J124957-015928	4942.640 ± 0.331	13.102 ± 0.644	38.555 ± 50.447
3749	J124957-015928	4941.990 ± 0.008	13.805 ± 0.085	20.730 ± 1.277
3750	J124957-015928	4939.289 ± 0.042	12.140 ± 0.068	19.501 ± 3.711
3751	J124957-015928	4937.954 ± 0.027	12.395 ± 0.044	19.767 ± 2.610
3752	J124957-015928	4935.771 ± 0.017	12.982 ± 0.018	31.075 ± 1.603
3753	J124957-015928	4934.677 ± 0.019	12.804 ± 0.032	24.626 ± 2.151
3754	J124957-015928	4933.769 ± 0.020	12.630 ± 0.033	20.636 ± 1.804
3755	J124957-015928	4931.857 ± 0.005	13.196 ± 0.008	22.903 ± 0.465
3756	J124957-015928	4930.496 ± 0.016	12.754 ± 0.020	26.153 ± 1.429
3757	J124957-015928	4928.455 ± 0.031	11.941 ± 0.084	11.366 ± 2.900
3758	J124957-015928	4927.334 ± 0.099	12.053 ± 0.204	17.071 ± 6.965
3759	J124957-015928	4926.720 ± 0.117	12.026 ± 0.275	19.938 ± 13.756
3760	J124957-015928	4925.717 ± 0.175	13.232 ± 0.341	22.413 ± 5.593
3761	J124957-015928	4925.332 ± 0.092	13.328 ± 0.272	20.287 ± 2.455
3762	J124957-015928	4924.137 ± 0.006	13.536 ± 0.008	25.760 ± 0.526
3763	J124957-015928	4922.905 ± 0.003	14.315 ± 0.006	30.892 ± 0.349
3764	J124957-015928	4921.501 ± 0.036	13.298 ± 0.070	25.872 ± 1.938
3765	J124957-015928	4920.636 ± 0.096	12.930 ± 0.327	33.867 ± 23.105
3766	J124957-015928	4919.140 ± 0.169	13.031 ± 0.234	28.462 ± 8.726
3767	J124957-015928	4919.784 ± 0.019	13.697 ± 0.072	24.054 ± 1.915
3768	J124957-015928	4917.872 ± 0.014	13.644 ± 0.065	16.669 ± 1.314
3769	J124957-015928	4917.627 ± 0.017	14.019 ± 0.028	30.628 ± 0.474

Table E.1. *Continued*

3770	J124957-015928	4916.448 ± 0.040	12.070 ± 0.127	10.222 ± 3.891
3771	J124957-015928	4915.958 ± 0.033	12.122 ± 0.142	10.666 ± 4.868
3772	J124957-015928	4915.014 ± 0.006	13.460 ± 0.018	22.813 ± 0.703
3773	J124957-015928	4913.976 ± 0.020	13.622 ± 0.013	51.489 ± 1.702
3774	J124957-015928	4912.213 ± 0.005	13.603 ± 0.008	22.505 ± 0.423
3775	J124957-015928	4911.302 ± 0.018	13.100 ± 0.035	28.736 ± 2.736
3776	J124957-015928	4910.349 ± 0.019	13.195 ± 0.053	21.635 ± 1.608
3777	J124957-015928	4909.538 ± 0.370	12.665 ± 0.711	30.982 ± 27.507
3778	J124957-015928	4908.126 ± 0.005	15.073 ± 0.057	30.824 ± 2.401
3779	J124957-015928	4907.624 ± 2.055	13.482 ± 1.543	56.335 ± 53.041
3780	J124957-015928	4905.385 ± 0.011	13.177 ± 0.018	25.573 ± 1.173
3781	J124957-015928	4904.008 ± 0.003	14.452 ± 0.011	31.303 ± 0.334
3782	J124957-015928	4902.401 ± 0.066	12.327 ± 0.157	22.577 ± 5.569
3783	J124957-015928	4901.721 ± 0.191	11.515 ± 1.961	12.218 ± 27.041
3784	J124957-015928	4900.858 ± 0.006	13.619 ± 0.072	22.624 ± 1.695
3785	J124957-015928	4899.894 ± 0.007	13.576 ± 0.036	20.445 ± 0.781
3786	J124957-015928	4900.115 ± 0.251	13.529 ± 0.150	71.788 ± 7.972
3787	J124957-015928	4896.620 ± 0.151	12.939 ± 0.081	67.704 ± 11.675
3788	J124957-015928	4894.024 ± 0.040	13.662 ± 0.085	27.476 ± 2.583
3789	J124957-015928	4892.919 ± 0.023	14.567 ± 0.017	52.180 ± 0.764
3790	J124957-015928	4889.878 ± 0.002	14.144 ± 0.004	30.866 ± 0.195
3791	J124957-015928	4888.762 ± 0.030	12.155 ± 0.130	11.850 ± 2.988
3792	J124957-015928	4888.156 ± 0.154	12.019 ± 0.300	26.352 ± 16.224
3793	J124957-015928	4886.806 ± 0.028	12.696 ± 0.103	31.418 ± 4.226
3794	J124957-015928	4884.711 ± 0.404	12.973 ± 0.183	133.128 ± 61.856
3795	J124957-015928	4882.066 ± 0.014	12.681 ± 0.072	11.080 ± 1.461
3796	J124957-015928	4881.548 ± 0.011	13.157 ± 0.036	17.528 ± 1.417
3797	J124957-015928	4880.732 ± 0.004	14.124 ± 0.006	26.034 ± 0.308
3798	J124957-015928	4878.940 ± 0.004	13.810 ± 0.004	31.572 ± 0.371
3799	J124957-015928	4877.907 ± 0.006	13.414 ± 0.010	22.397 ± 0.550
3800	J124957-015928	4876.687 ± 0.023	13.057 ± 0.028	34.372 ± 2.719
3801	J124957-015928	4875.847 ± 0.030	12.493 ± 0.078	18.129 ± 2.377
3802	J124957-015928	4871.547 ± 0.024	12.669 ± 0.036	22.348 ± 2.214
3803	J124957-015928	4870.798 ± 0.034	12.418 ± 0.087	17.618 ± 3.790
3804	J124957-015928	4869.914 ± 0.003	13.878 ± 0.005	24.861 ± 0.360
3805	J124957-015928	4868.759 ± 0.007	13.617 ± 0.010	29.463 ± 0.869
3806	J124957-015928	4867.844 ± 0.006	13.547 ± 0.010	22.019 ± 0.551
3807	J124957-015928	4867.046 ± 0.041	12.174 ± 0.096	15.633 ± 3.894
3808	J124957-015928	4865.640 ± 0.039	12.997 ± 0.032	45.328 ± 3.852
3809	J124957-015928	4864.289 ± 0.021	13.066 ± 0.035	32.448 ± 2.709
3810	J124957-015928	4863.363 ± 0.006	13.330 ± 0.012	21.077 ± 0.567
3811	J124957-015928	4862.404 ± 0.041	12.414 ± 0.080	18.700 ± 4.196
3812	J124957-015928	4861.141 ± 0.768	12.193 ± 0.839	35.142 ± 54.994
3813	J124957-015928	4860.515 ± 0.006	13.688 ± 0.024	19.702 ± 0.450

Table E.1. *Continued*

3814	J162116-004250	5604.657 ± 0.029	12.625 ± 0.039	20.075 ± 1.799
3815	J162116-004250	5602.010 ± 0.041	12.281 ± 0.163	12.474 ± 2.226
3816	J162116-004250	5601.491 ± 0.006	13.686 ± 0.007	21.103 ± 0.302
3817	J162116-004250	5599.998 ± 0.009	12.962 ± 0.009	28.810 ± 0.785
3818	J162116-004250	5598.969 ± 0.045	11.824 ± 0.127	11.071 ± 3.745
3819	J162116-004250	5598.450 ± 0.067	11.729 ± 0.183	12.842 ± 6.525
3820	J162116-004250	5597.574 ± 0.006	13.165 ± 0.008	22.756 ± 0.529
3821	J162116-004250	5596.111 ± 0.127	13.018 ± 0.118	33.735 ± 5.833
3822	J162116-004250	5595.538 ± 0.024	12.819 ± 0.180	18.882 ± 2.480
3823	J162116-004250	5594.701 ± 0.123	12.415 ± 0.162	34.090 ± 13.348
3824	J162116-004250	5593.289 ± 0.105	12.606 ± 0.150	26.476 ± 7.488
3825	J162116-004250	5592.690 ± 0.076	12.352 ± 0.477	15.889 ± 6.410
3826	J162116-004250	5592.177 ± 0.355	12.181 ± 0.507	22.632 ± 18.071
3827	J162116-004250	5591.141 ± 0.153	12.429 ± 0.370	16.063 ± 5.956
3828	J162116-004250	5590.732 ± 0.104	12.616 ± 0.233	16.276 ± 3.291
3829	J162116-004250	5588.529 ± 0.031	12.371 ± 0.119	21.739 ± 3.209
3830	J162116-004250	5587.043 ± 0.486	12.556 ± 0.358	57.583 ± 44.669
3831	J162116-004250	5586.176 ± 0.050	12.647 ± 0.208	20.315 ± 4.602
3832	J162116-004250	5585.512 ± 0.072	12.633 ± 0.249	17.597 ± 5.665
3833	J162116-004250	5584.966 ± 0.043	13.116 ± 0.071	20.483 ± 1.976
3834	J162116-004250	5583.618 ± 0.020	12.831 ± 0.036	26.605 ± 2.772
3835	J162116-004250	5582.379 ± 0.029	13.002 ± 0.089	20.236 ± 3.966
3836	J162116-004250	5581.678 ± 0.257	12.715 ± 0.756	17.486 ± 13.300
3837	J162116-004250	5581.281 ± 0.128	13.023 ± 0.324	17.105 ± 3.197
3838	J162116-004250	5580.224 ± 0.012	12.755 ± 0.015	23.035 ± 1.049
3839	J162116-004250	5578.423 ± 0.038	12.618 ± 0.293	17.771 ± 3.574
3840	J162116-004250	5577.802 ± 0.293	12.571 ± 0.420	31.862 ± 26.448
3841	J162116-004250	5576.717 ± 0.038	12.651 ± 0.121	22.169 ± 4.988
3842	J162116-004250	5576.084 ± 0.116	11.848 ± 0.333	14.436 ± 6.407
3843	J162116-004250	5574.155 ± 0.020	12.281 ± 0.052	10.720 ± 1.628
3844	J162116-004250	5572.731 ± 0.032	12.700 ± 0.027	35.213 ± 2.732
3845	J162116-004250	5571.842 ± 0.051	11.845 ± 0.213	13.009 ± 4.700
3846	J162116-004250	5570.866 ± 0.279	12.452 ± 0.282	33.374 ± 16.671
3847	J162116-004250	5570.305 ± 0.020	12.470 ± 0.232	16.215 ± 3.318
3848	J162116-004250	5568.856 ± 0.019	12.329 ± 0.034	16.131 ± 1.666
3849	J162116-004250	5566.978 ± 0.002	13.675 ± 0.002	22.400 ± 0.127
3850	J162116-004250	5564.424 ± 0.033	12.183 ± 0.087	18.579 ± 2.975
3851	J162116-004250	5562.908 ± 0.117	12.916 ± 0.055	59.480 ± 5.739
3852	J162116-004250	5562.321 ± 0.005	13.312 ± 0.017	20.631 ± 0.491
3853	J162116-004250	5561.028 ± 0.009	13.218 ± 0.031	15.770 ± 0.536
3854	J162116-004250	5560.466 ± 0.027	13.175 ± 0.033	24.013 ± 1.393
3855	J162116-004250	5559.041 ± 0.191	11.967 ± 0.250	25.950 ± 13.624
3856	J162116-004250	5557.942 ± 0.014	13.411 ± 0.023	28.414 ± 1.525
3857	J162116-004250	5557.308 ± 0.027	12.466 ± 0.166	13.883 ± 2.695

Table E.1. *Continued*

3858	J162116-004250	5556.683 ± 0.011	13.138 ± 0.014	21.431 ± 0.748
3859	J162116-004250	5555.388 ± 0.002	13.876 ± 0.003	19.651 ± 0.148
3860	J162116-004250	5554.706 ± 0.048	11.918 ± 0.136	11.440 ± 3.444
3861	J162116-004250	5553.727 ± 0.025	12.600 ± 0.043	18.210 ± 1.553
3862	J162116-004250	5552.916 ± 0.003	13.770 ± 0.004	23.039 ± 0.238
3863	J162116-004250	5550.743 ± 0.019	15.143 ± 0.029	35.981 ± 0.423
3864	J162116-004250	5549.315 ± 0.028	13.085 ± 0.119	12.166 ± 2.516
3865	J162116-004250	5548.374 ± 0.014	14.469 ± 0.091	24.998 ± 1.938
3866	J162116-004250	5546.047 ± 0.236	14.699 ± 0.197	23.558 ± 18.905
3867	J162116-004250	5545.449 ± 1.816	13.460 ± 4.535	20.422 ± 40.568
3868	J162116-004250	5544.681 ± 0.172	12.510 ± 0.428	16.006 ± 7.702
3869	J162116-004250	5543.905 ± 0.017	12.831 ± 0.058	14.820 ± 1.521
3870	J162116-004250	5542.355 ± 0.005	12.800 ± 0.051	10.169 ± 0.662
3871	J162116-004250	5541.210 ± 0.028	13.251 ± 0.041	32.178 ± 2.970
3872	J162116-004250	5539.466 ± 0.003	16.497 ± 0.121	27.492 ± 0.720
3873	J162116-004250	5537.753 ± 0.048	13.178 ± 0.118	22.550 ± 5.337
3874	J162116-004250	5537.196 ± 0.067	12.682 ± 0.328	16.055 ± 4.843
3875	J162116-004250	5536.458 ± 0.066	13.326 ± 0.316	23.861 ± 4.625
3876	J162116-004250	5535.611 ± 0.099	13.485 ± 0.457	37.879 ± 33.422
3877	J162116-004250	5534.705 ± 0.049	13.765 ± 0.141	26.661 ± 2.712
3878	J162116-004250	5533.877 ± 0.022	13.044 ± 0.085	18.484 ± 2.402
3879	J162116-004250	5533.033 ± 0.059	13.765 ± 0.111	19.184 ± 2.198
3880	J162116-004250	5532.671 ± 0.053	13.425 ± 0.232	15.661 ± 1.223
3881	J162116-004250	5531.447 ± 0.108	12.015 ± 0.187	18.106 ± 6.529
3882	J162116-004250	5530.762 ± 0.023	12.708 ± 0.045	19.719 ± 2.139
3883	J162116-004250	5529.892 ± 0.072	11.936 ± 0.114	18.739 ± 5.754
3884	J162116-004250	5527.547 ± 0.006	13.882 ± 0.007	23.650 ± 0.300
3885	J162116-004250	5526.258 ± 0.003	14.800 ± 0.031	27.810 ± 0.663
3886	J162116-004250	5525.001 ± 0.033	13.377 ± 0.101	13.303 ± 1.627
3887	J162116-004250	5523.742 ± 0.011	15.809 ± 0.052	29.054 ± 0.454
3888	J162116-004250	5521.441 ± 0.214	12.836 ± 0.323	24.807 ± 14.787
3889	J162116-004250	5518.371 ± 0.098	13.704 ± 0.091	50.821 ± 9.879
3890	J162116-004250	5516.577 ± 0.365	12.822 ± 0.225	48.920 ± 20.152
3891	J162116-004250	5515.117 ± 0.043	11.890 ± 0.189	11.853 ± 4.453
3892	J162116-004250	5513.936 ± 0.062	12.332 ± 0.096	19.214 ± 4.332
3893	J162116-004250	5513.417 ± 0.079	11.830 ± 0.315	11.829 ± 5.521
3894	J162116-004250	5512.456 ± 0.109	12.000 ± 0.184	16.563 ± 7.249
3895	J162116-004250	5508.991 ± 0.008	13.035 ± 0.008	27.272 ± 0.641
3896	J162116-004250	5507.467 ± 0.008	12.956 ± 0.009	25.771 ± 0.675
3897	J162116-004250	5505.858 ± 0.030	13.035 ± 0.099	23.558 ± 1.683
3898	J162116-004250	5504.710 ± 0.556	13.014 ± 0.557	43.249 ± 43.797
3899	J162116-004250	5504.109 ± 0.017	13.154 ± 0.263	20.386 ± 3.155
3900	J162116-004250	5503.519 ± 0.230	11.897 ± 1.323	16.678 ± 15.326
3901	J162116-004250	5500.798 ± 0.001	14.326 ± 0.005	27.455 ± 0.162

Table E.1. *Continued*

3902	J162116-004250	5498.788 ± 0.057	13.137 ± 0.033	87.020 ± 8.148
3903	J162116-004250	5497.327 ± 0.022	12.146 ± 0.082	10.116 ± 2.110
3904	J162116-004250	5496.034 ± 0.016	12.844 ± 0.026	24.808 ± 1.448
3905	J162116-004250	5494.878 ± 0.353	12.098 ± 0.491	25.828 ± 23.945
3906	J162116-004250	5494.238 ± 0.054	12.509 ± 0.205	18.052 ± 4.557
3907	J162116-004250	5493.373 ± 0.008	13.404 ± 0.018	23.930 ± 1.116
3908	J162116-004250	5492.713 ± 0.076	12.106 ± 0.230	14.762 ± 4.220
3909	J162116-004250	5490.764 ± 0.020	12.329 ± 0.128	14.175 ± 2.361
3910	J162116-004250	5490.381 ± 0.115	12.473 ± 0.103	34.320 ± 4.226
3911	J162116-004250	5488.383 ± 0.006	13.406 ± 0.006	26.071 ± 0.435
3912	J162116-004250	5487.267 ± 0.393	12.317 ± 0.582	22.405 ± 19.963
3913	J162116-004250	5486.895 ± 0.090	11.984 ± 1.216	12.072 ± 11.437
3914	J162116-004250	5485.816 ± 0.008	14.670 ± 0.029	22.027 ± 1.483
3915	J162116-004250	5485.229 ± 0.410	13.795 ± 0.367	38.819 ± 15.825
3916	J162116-004250	5483.722 ± 0.117	12.895 ± 0.161	29.837 ± 7.497
3917	J162116-004250	5482.570 ± 0.002	14.192 ± 0.007	21.189 ± 0.219
3918	J162116-004250	5480.260 ± 0.003	16.436 ± 0.072	31.450 ± 0.489
3919	J162116-004250	5478.577 ± 0.003	13.885 ± 0.055	10.015 ± 0.835
3920	J162116-004250	5478.228 ± 0.795	12.639 ± 1.448	21.452 ± 56.167
3921	J162116-004250	5476.378 ± 0.066	12.606 ± 0.057	33.116 ± 4.566
3922	J162116-004250	5473.836 ± 0.010	12.988 ± 0.012	23.568 ± 0.832
3923	J162116-004250	5472.351 ± 0.009	13.305 ± 0.011	25.623 ± 0.591
3924	J162116-004250	5471.253 ± 0.026	12.903 ± 0.035	32.435 ± 3.109
3925	J162116-004250	5469.810 ± 0.002	14.011 ± 0.004	21.156 ± 0.148
3926	J162116-004250	5468.615 ± 0.018	12.862 ± 0.056	17.870 ± 2.036
3927	J162116-004250	5467.854 ± 0.009	13.493 ± 0.017	25.708 ± 0.836
3928	J162116-004250	5466.451 ± 0.018	13.200 ± 0.036	19.367 ± 1.059
3929	J162116-004250	5465.890 ± 0.025	12.935 ± 0.060	16.978 ± 1.421
3930	J162116-004250	5464.904 ± 0.218	12.507 ± 0.694	14.468 ± 6.869
3931	J162116-004250	5464.576 ± 0.146	12.772 ± 0.366	15.353 ± 4.239
3932	J162116-004250	5464.133 ± 0.140	13.561 ± 0.040	125.256 ± 10.290
3933	J162116-004250	5460.744 ± 0.012	13.475 ± 0.014	47.674 ± 1.268
3934	J162116-004250	5459.650 ± 0.019	13.269 ± 0.076	14.607 ± 0.975
3935	J162116-004250	5458.202 ± 0.005	15.262 ± 0.094	37.716 ± 2.164
3936	J162116-004250	5456.754 ± 0.010	13.227 ± 0.074	10.677 ± 1.075
3937	J162116-004250	5455.175 ± 0.003	15.960 ± 0.077	33.165 ± 0.734
3938	J162116-004250	5453.443 ± 0.058	11.888 ± 0.265	10.989 ± 6.999
3939	J162116-004250	5452.404 ± 0.062	12.338 ± 0.058	32.662 ± 5.513
3940	J162116-004250	5449.694 ± 0.003	14.251 ± 0.006	24.216 ± 0.209
3941	J162116-004250	5448.658 ± 0.005	13.559 ± 0.008	23.075 ± 0.535
3942	J162116-004250	5447.904 ± 0.034	12.000 ± 0.106	10.975 ± 2.627
3943	J162116-004250	5445.199 ± 0.026	12.788 ± 0.027	27.990 ± 1.954
3944	J162116-004250	5444.259 ± 0.007	13.219 ± 0.019	21.572 ± 0.671
3945	J162116-004250	5442.050 ± 1.621	13.279 ± 0.825	68.092 ± 50.169

Table E.1. *Continued*

3946	J162116-004250	5441.250 ± 0.034	13.781 ± 0.194	37.767 ± 8.416
3947	J162116-004250	5441.132 ± 0.007	14.258 ± 0.028	20.527 ± 0.870
3948	J162116-004250	5439.531 ± 0.024	12.883 ± 0.236	18.124 ± 3.386
3949	J162116-004250	5439.152 ± 0.050	13.796 ± 0.044	38.120 ± 1.967
3950	J162116-004250	5437.478 ± 0.003	14.577 ± 0.012	31.048 ± 0.479
3951	J162116-004250	5435.787 ± 0.227	12.884 ± 0.249	42.841 ± 22.247
3952	J162116-004250	5434.909 ± 0.004	14.073 ± 0.013	22.290 ± 0.465
3953	J162116-004250	5433.978 ± 0.026	13.109 ± 0.072	23.771 ± 3.235
3954	J162116-004250	5433.129 ± 0.052	12.875 ± 0.126	26.324 ± 6.556
3955	J162116-004250	5431.903 ± 0.593	12.680 ± 0.729	29.200 ± 32.992
3956	J162116-004250	5431.488 ± 0.111	12.892 ± 0.556	13.480 ± 7.837
3957	J162116-004250	5430.071 ± 0.009	14.797 ± 0.019	37.927 ± 1.611
3958	J162116-004250	5429.045 ± 1.914	13.236 ± 0.996	65.493 ± 72.093
3959	J162116-004250	5427.194 ± 0.329	13.151 ± 0.851	18.052 ± 7.784
3960	J162116-004250	5426.838 ± 0.411	12.925 ± 1.655	17.342 ± 22.974
3961	J162116-004250	5426.344 ± 0.601	12.258 ± 1.430	16.981 ± 23.333
3962	J162116-004250	5425.565 ± 0.003	13.593 ± 0.011	17.263 ± 0.342
3963	J162116-004250	5424.346 ± 0.152	12.828 ± 0.121	68.632 ± 21.304
3964	J162116-004250	5422.185 ± 0.004	13.992 ± 0.005	27.418 ± 0.205
3965	J162116-004250	5420.357 ± 0.022	13.058 ± 0.017	16.069 ± 1.118
3966	J162116-004250	5419.545 ± 0.021	12.413 ± 0.055	15.490 ± 2.699
3967	J162116-004250	5418.192 ± 0.036	12.437 ± 0.259	11.748 ± 4.050
3968	J162116-004250	5417.648 ± 0.043	13.409 ± 0.044	39.333 ± 3.777
3969	J162116-004250	5416.244 ± 0.004	13.823 ± 0.005	25.545 ± 0.351
3970	J162116-004250	5414.521 ± 0.002	14.994 ± 0.018	32.898 ± 0.334
3971	J162116-004250	5411.913 ± 0.203	13.140 ± 0.100	87.465 ± 19.464
3972	J162116-004250	5410.891 ± 0.002	13.775 ± 0.010	21.303 ± 0.306
3973	J162116-004250	5409.585 ± 0.007	13.430 ± 0.018	25.915 ± 0.644
3974	J162116-004250	5408.109 ± 0.002	14.035 ± 0.002	31.432 ± 0.212
3975	J162116-004250	5407.050 ± 0.025	12.448 ± 0.116	12.672 ± 2.072
3976	J162116-004250	5406.332 ± 0.046	13.229 ± 0.078	25.325 ± 4.061
3977	J162116-004250	5405.200 ± 0.004	15.441 ± 0.069	23.134 ± 0.599
3978	J162116-004250	5402.515 ± 0.006	15.481 ± 0.038	44.112 ± 0.814
3979	J162116-004250	5400.581 ± 0.085	13.024 ± 0.180	33.588 ± 11.139
3980	J162116-004250	5399.479 ± 0.019	13.563 ± 0.025	31.021 ± 1.310
3981	J162116-004250	5398.237 ± 0.015	13.126 ± 0.028	24.964 ± 1.463
3982	J162116-004250	5397.326 ± 0.054	12.686 ± 0.059	27.995 ± 3.295
3983	J162116-004250	5395.623 ± 0.001	14.138 ± 0.006	19.514 ± 0.146
3984	J162116-004250	5394.313 ± 0.001	14.456 ± 0.011	21.932 ± 0.181
3985	J162116-004250	5392.536 ± 0.055	12.195 ± 0.061	26.978 ± 4.661
3986	J162116-004250	5391.083 ± 0.105	12.051 ± 0.124	27.726 ± 10.085
3987	J162116-004250	5390.240 ± 0.022	12.357 ± 0.170	10.653 ± 2.249
3988	J162116-004250	5389.746 ± 0.042	12.772 ± 0.084	22.470 ± 4.761
3989	J162116-004250	5388.855 ± 0.091	12.030 ± 0.166	16.086 ± 6.695

Table E.1. *Continued*

3990	J162116-004250	5387.359 ± 0.006	13.350 ± 0.006	29.965 ± 0.537
3991	J162116-004250	5386.108 ± 0.003	13.592 ± 0.004	25.696 ± 0.265
3992	J162116-004250	5383.192 ± 0.037	12.133 ± 0.090	13.067 ± 2.772
3993	J162116-004250	5382.147 ± 0.002	14.340 ± 0.009	26.075 ± 0.348
3994	J162116-004250	5381.110 ± 0.022	13.036 ± 0.061	15.041 ± 1.819
3995	J162116-004250	5380.693 ± 0.027	12.760 ± 0.100	11.858 ± 1.654
3996	J162116-004250	5380.149 ± 0.007	12.774 ± 0.017	11.673 ± 0.600
3997	J162116-004250	5379.033 ± 0.048	12.584 ± 0.071	20.984 ± 2.899
3998	J162116-004250	5378.355 ± 0.011	13.181 ± 0.018	19.575 ± 0.680
3999	J162116-004250	5377.061 ± 0.033	12.774 ± 0.051	20.849 ± 1.907
4000	J162116-004250	5376.301 ± 0.009	13.328 ± 0.020	22.490 ± 1.064
4001	J162116-004250	5375.370 ± 0.024	12.888 ± 0.056	21.023 ± 2.765
4002	J162116-004250	5374.682 ± 0.006	13.416 ± 0.022	16.614 ± 0.751
4003	J162116-004250	5374.007 ± 0.217	12.709 ± 0.627	17.437 ± 10.198
4004	J162116-004250	5373.608 ± 0.090	13.180 ± 0.196	18.383 ± 2.412
4005	J162116-004250	5372.273 ± 0.035	12.721 ± 0.092	14.245 ± 1.589
4006	J162116-004250	5371.511 ± 0.004	14.354 ± 0.014	22.434 ± 0.544
4007	J162116-004250	5370.648 ± 0.094	11.898 ± 0.270	12.203 ± 5.795
4008	J162116-004250	5368.946 ± 0.039	12.114 ± 0.067	17.351 ± 3.260
4009	J162116-004250	5367.970 ± 0.065	12.083 ± 0.086	23.975 ± 6.099
4010	J162116-004250	5366.773 ± 0.023	12.532 ± 0.039	19.525 ± 1.961
4011	J162116-004250	5365.887 ± 0.025	12.605 ± 0.044	23.085 ± 2.805
4012	J162116-004250	5364.857 ± 0.055	12.235 ± 0.085	23.988 ± 5.868
4013	J162116-004250	5363.683 ± 0.002	14.071 ± 0.004	21.525 ± 0.131
4014	J162116-004250	5361.282 ± 0.007	13.399 ± 0.010	21.990 ± 0.476
4015	J162116-004250	5360.504 ± 0.008	13.245 ± 0.017	20.084 ± 0.865
4016	J162116-004250	5358.991 ± 0.030	13.458 ± 0.038	32.502 ± 0.810
4017	J162116-004250	5358.714 ± 0.020	12.802 ± 0.161	17.202 ± 2.536
4018	J162116-004250	5357.581 ± 0.040	12.414 ± 0.068	20.233 ± 2.933
4019	J162116-004250	5356.313 ± 0.012	13.294 ± 0.016	20.478 ± 0.725
4020	J162116-004250	5353.143 ± 0.010	13.205 ± 0.069	13.017 ± 0.924
4021	J162116-004250	5353.099 ± 0.013	13.525 ± 0.025	30.361 ± 1.410
4022	J162116-004250	5351.781 ± 0.067	12.690 ± 0.050	32.739 ± 4.902
4023	J162116-004250	5350.321 ± 0.035	12.465 ± 0.038	28.058 ± 3.005
4024	J162116-004250	5345.218 ± 0.155	12.570 ± 0.824	10.313 ± 11.357
4025	J162116-004250	5344.877 ± 0.104	12.809 ± 0.575	12.273 ± 13.826
4026	J162116-004250	5343.631 ± 0.217	12.886 ± 0.311	49.427 ± 36.377
4027	J162116-004250	5342.477 ± 0.004	14.412 ± 0.022	16.969 ± 0.419
4028	J162116-004250	5341.719 ± 0.027	13.442 ± 0.045	28.214 ± 2.925
4029	J162116-004250	5340.391 ± 0.016	13.360 ± 0.027	27.828 ± 1.852
4030	J162116-004250	5339.825 ± 0.040	12.117 ± 0.348	11.814 ± 5.535
4031	J162116-004250	5338.795 ± 0.003	13.610 ± 0.004	20.361 ± 0.240
4032	J162116-004250	5337.236 ± 0.002	13.534 ± 0.004	16.743 ± 0.192
4033	J162116-004250	5336.558 ± 0.016	12.258 ± 0.054	10.134 ± 1.532

Table E.1. *Continued*

4034	J162116-004250	5335.840 ± 0.006	13.137 ± 0.010	21.128 ± 0.683
4035	J162116-004250	5334.880 ± 0.042	13.630 ± 0.114	15.706 ± 1.188
4036	J162116-004250	5334.345 ± 0.021	14.284 ± 0.056	19.835 ± 1.675
4037	J162116-004250	5333.808 ± 1.172	12.730 ± 1.375	30.210 ± 41.428
4038	J162116-004250	5332.504 ± 0.088	12.368 ± 0.123	27.274 ± 7.900
4039	J162116-004250	5331.496 ± 0.030	12.235 ± 0.058	16.582 ± 2.501
4040	J162116-004250	5330.013 ± 0.030	12.398 ± 0.043	20.638 ± 2.639
4041	J162116-004250	5327.507 ± 0.036	12.326 ± 0.042	25.156 ± 2.906
4042	J162116-004250	5325.522 ± 0.219	12.592 ± 0.209	32.760 ± 9.454
4043	J162116-004250	5324.669 ± 0.023	13.784 ± 0.158	17.199 ± 1.850
4044	J162116-004250	5324.201 ± 0.061	14.123 ± 0.103	30.446 ± 3.674
4045	J162116-004250	5323.201 ± 0.230	13.403 ± 0.195	43.847 ± 13.051
4046	J162116-004250	5322.188 ± 0.019	12.367 ± 0.166	12.900 ± 2.627
4047	J162116-004250	5321.063 ± 0.127	12.508 ± 0.153	35.629 ± 13.329
4048	J162116-004250	5320.229 ± 0.032	12.752 ± 0.090	18.401 ± 2.630
4049	J162116-004250	5318.907 ± 0.051	13.239 ± 0.046	41.962 ± 3.811
4050	J162116-004250	5317.587 ± 0.010	13.799 ± 0.020	36.102 ± 1.529
4051	J162116-004250	5316.794 ± 0.016	12.957 ± 0.081	17.679 ± 1.566
4052	J162116-004250	5315.967 ± 0.017	13.163 ± 0.020	30.708 ± 1.638
4053	J162116-004250	5314.761 ± 0.056	12.132 ± 0.087	21.573 ± 4.801
4054	J162116-004250	5312.848 ± 0.001	13.971 ± 0.004	19.955 ± 0.146
4055	J162116-004250	5311.800 ± 0.224	12.664 ± 0.070	81.732 ± 12.350
4056	J162116-004250	5310.632 ± 0.022	12.144 ± 0.084	13.320 ± 2.350
4057	J162116-004250	5308.992 ± 0.072	12.525 ± 0.104	22.964 ± 4.292
4058	J162116-004250	5308.192 ± 0.034	13.358 ± 0.134	22.545 ± 2.220
4059	J162116-004250	5307.499 ± 0.155	13.187 ± 0.232	33.049 ± 14.062
4060	J162116-004250	5306.461 ± 0.389	12.421 ± 1.015	21.926 ± 28.794
4061	J162116-004250	5305.899 ± 0.031	13.383 ± 0.110	19.750 ± 2.623
4062	J162116-004250	5305.203 ± 0.064	12.841 ± 0.160	22.630 ± 6.736
4063	J162116-004250	5304.143 ± 0.009	14.104 ± 0.022	28.386 ± 0.777
4064	J162116-004250	5303.059 ± 0.147	13.161 ± 0.294	46.835 ± 30.580
4065	J162116-004250	5302.081 ± 0.230	12.950 ± 0.589	19.084 ± 10.263
4066	J162116-004250	5301.658 ± 0.028	13.572 ± 0.206	16.729 ± 2.598
4067	J162116-004250	5301.275 ± 0.439	12.734 ± 0.783	21.353 ± 11.827
4068	J162116-004250	5299.458 ± 0.010	12.803 ± 0.015	21.014 ± 0.927
4069	J162116-004250	5298.516 ± 0.061	11.929 ± 0.149	15.552 ± 7.151
4070	J162116-004250	5297.960 ± 0.044	11.890 ± 0.124	10.911 ± 3.626
4071	J162116-004250	5295.731 ± 0.013	12.716 ± 0.024	16.814 ± 1.050
4072	J162116-004250	5294.862 ± 0.002	13.874 ± 0.004	21.568 ± 0.258
4073	J162116-004250	5293.935 ± 0.029	12.642 ± 0.072	20.174 ± 3.417
4074	J162116-004250	5293.227 ± 0.076	12.278 ± 0.128	19.932 ± 5.171
4075	J162116-004250	5290.845 ± 0.152	12.988 ± 0.080	62.613 ± 9.408
4076	J162116-004250	5290.889 ± 0.007	13.469 ± 0.018	18.146 ± 0.583
4077	J162116-004250	5290.401 ± 0.037	12.385 ± 0.166	11.811 ± 2.729

Table E.1. *Continued*

4078	J162116-004250	5289.224 ± 0.016	12.310 ± 0.108	10.066 ± 1.839
4079	J162116-004250	5288.595 ± 0.110	13.369 ± 0.087	47.317 ± 7.714
4080	J162116-004250	5287.680 ± 0.004	14.204 ± 0.010	24.707 ± 0.475
4081	J162116-004250	5286.717 ± 0.011	13.010 ± 0.020	17.863 ± 0.843
4082	J162116-004250	5285.340 ± 0.043	12.224 ± 0.070	20.641 ± 4.446
4083	J162116-004250	5280.202 ± 0.288	12.672 ± 0.555	22.753 ± 16.373
4084	J162116-004250	5279.514 ± 0.052	12.720 ± 1.282	16.077 ± 9.425
4085	J162116-004250	5279.330 ± 1.136	12.730 ± 1.684	27.264 ± 25.963
4086	J162116-004250	5275.708 ± 0.265	13.350 ± 0.224	44.543 ± 6.819
4087	J162116-004250	5275.473 ± 0.030	13.237 ± 0.200	20.198 ± 2.998
4088	J162116-004250	5274.680 ± 0.029	12.856 ± 0.240	14.932 ± 3.633
4089	J162116-004250	5273.946 ± 0.004	14.231 ± 0.008	22.321 ± 0.523
4090	J162116-004250	5272.419 ± 0.064	12.954 ± 0.108	18.805 ± 2.822
4091	J162116-004250	5272.060 ± 0.060	12.412 ± 0.392	12.450 ± 3.727
4092	J162116-004250	5271.065 ± 0.102	13.090 ± 0.063	43.938 ± 3.390
4093	J162116-004250	5270.617 ± 0.008	13.336 ± 0.040	22.153 ± 0.861
4094	J162116-004250	5268.917 ± 0.014	12.539 ± 0.028	14.075 ± 0.944
4095	J162116-004250	5266.462 ± 0.058	12.991 ± 0.552	13.360 ± 3.187
4096	J162116-004250	5266.199 ± 0.064	13.625 ± 0.129	18.593 ± 1.719
4097	J162116-004250	5264.877 ± 0.017	12.700 ± 0.023	22.739 ± 1.577
4098	J162116-004250	5264.157 ± 0.030	12.090 ± 0.102	11.807 ± 2.764
4099	J162116-004250	5263.396 ± 0.009	13.081 ± 0.012	24.979 ± 0.946
4100	J162116-004250	5261.876 ± 0.008	14.480 ± 0.019	27.198 ± 0.293
4101	J162116-004250	5260.384 ± 0.020	13.835 ± 0.029	22.333 ± 1.006
4102	J162116-004250	5259.899 ± 0.059	12.996 ± 0.191	16.950 ± 2.045
4103	J162116-004250	5258.611 ± 0.032	13.072 ± 0.029	34.149 ± 1.777
4104	J162116-004250	5258.129 ± 0.026	12.142 ± 0.198	12.251 ± 3.466
4105	J162116-004250	5256.109 ± 0.202	12.823 ± 0.303	23.366 ± 6.638
4106	J162116-004250	5245.604 ± 0.307	13.403 ± 0.466	24.632 ± 9.027
4107	J162116-004250	5255.681 ± 0.011	13.721 ± 0.038	17.921 ± 0.417
4108	J162116-004250	5254.109 ± 0.032	13.276 ± 0.033	29.311 ± 1.603
4109	J162116-004250	5253.431 ± 0.039	12.695 ± 0.150	19.671 ± 4.351
4110	J162116-004250	5252.773 ± 0.144	12.373 ± 0.524	14.550 ± 8.555
4111	J162116-004250	5252.302 ± 0.084	12.685 ± 0.316	17.726 ± 11.341
4112	J162116-004250	5251.831 ± 0.056	12.216 ± 0.353	10.604 ± 4.469
4113	J162116-004250	5251.212 ± 0.020	13.127 ± 0.045	20.879 ± 2.000
4114	J162116-004250	5250.447 ± 0.093	12.963 ± 0.211	20.795 ± 7.723
4115	J162116-004250	5250.086 ± 0.057	12.291 ± 0.776	11.660 ± 6.352
4116	J162116-004250	5247.779 ± 0.002	14.384 ± 0.011	21.725 ± 0.218
4117	J162116-004250	5246.772 ± 0.014	12.940 ± 0.032	21.303 ± 1.826
4118	J162116-004250	5245.314 ± 0.011	13.509 ± 0.348	15.766 ± 2.776
4119	J162116-004250	5243.940 ± 0.013	14.083 ± 0.286	19.679 ± 3.018
4120	J162116-004250	5243.739 ± 0.316	13.739 ± 0.673	26.208 ± 4.598
4121	J162116-004250	5240.870 ± 0.148	12.073 ± 0.276	18.048 ± 8.201

Table E.1. *Continued*

4122	J162116-004250	5240.234 ± 0.043	12.564 ± 0.156	19.731 ± 6.769
4123	J162116-004250	5239.492 ± 0.067	12.728 ± 0.189	18.978 ± 6.723
4124	J162116-004250	5238.983 ± 0.026	13.033 ± 0.084	15.770 ± 1.659
4125	J162116-004250	5238.237 ± 0.028	12.783 ± 0.058	24.920 ± 3.698
4126	J162116-004250	5236.982 ± 0.003	14.191 ± 0.004	30.534 ± 0.264
4127	J162116-004250	5235.820 ± 0.029	12.236 ± 0.086	13.646 ± 2.731
4128	J162116-004250	5235.101 ± 0.033	12.549 ± 0.078	22.274 ± 3.877
4129	J162116-004250	5233.523 ± 0.117	14.011 ± 0.114	44.594 ± 2.641
4130	J162116-004250	5233.178 ± 0.005	15.309 ± 0.122	21.222 ± 1.131
4131	J162116-004250	5231.461 ± 0.137	13.423 ± 0.170	36.173 ± 11.314
4132	J162116-004250	5231.022 ± 0.007	13.140 ± 0.179	14.369 ± 1.862
4133	J162116-004250	5230.212 ± 0.061	13.202 ± 0.096	24.342 ± 2.700
4134	J162116-004250	5229.151 ± 0.002	13.937 ± 0.004	22.247 ± 0.240
4135	J162116-004250	5227.741 ± 0.053	13.399 ± 0.049	37.650 ± 3.366
4136	J162116-004250	5226.981 ± 0.004	13.954 ± 0.014	21.130 ± 0.453
4137	J162116-004250	5226.009 ± 0.105	13.072 ± 0.176	23.995 ± 6.845
4138	J162116-004250	5225.468 ± 0.014	13.646 ± 0.053	18.200 ± 0.865
4139	J162116-004250	5224.818 ± 0.061	13.137 ± 0.063	31.984 ± 3.455
4140	J162116-004250	5223.171 ± 0.081	12.349 ± 0.093	35.494 ± 9.320
4141	J162116-004250	5221.874 ± 0.020	12.854 ± 0.028	29.175 ± 2.239
4142	J162116-004250	5220.020 ± 0.013	13.074 ± 0.015	31.544 ± 1.363
4143	J162116-004250	5218.503 ± 0.005	13.467 ± 0.006	25.069 ± 0.392
4144	J162116-004250	5217.483 ± 0.007	13.238 ± 0.009	24.462 ± 0.559
4145	J162116-004250	5215.752 ± 0.050	12.108 ± 0.068	22.304 ± 4.143
4146	J162116-004250	5213.667 ± 0.021	12.875 ± 0.026	24.675 ± 1.569
4147	J162116-004250	5212.892 ± 0.084	12.026 ± 0.201	18.632 ± 8.759
4148	J162116-004250	5210.312 ± 0.058	12.121 ± 0.069	25.203 ± 4.752
4149	J162116-004250	5207.918 ± 0.017	12.794 ± 0.019	28.500 ± 1.464
4150	J162116-004250	5206.417 ± 0.100	12.193 ± 0.084	38.127 ± 9.218
4151	J162116-004250	5204.962 ± 0.185	11.803 ± 1.013	11.187 ± 9.759
4152	J162116-004250	5204.561 ± 0.113	12.431 ± 0.310	17.787 ± 12.230
4153	J162116-004250	5203.361 ± 2.487	12.973 ± 3.567	27.664 ± 69.480
4154	J162116-004250	5203.071 ± 0.055	13.199 ± 1.929	18.951 ± 12.516
4155	J162116-004250	5202.502 ± 0.505	12.403 ± 1.270	22.102 ± 20.733
4156	J162116-004250	5201.592 ± 0.191	12.734 ± 0.343	41.614 ± 25.167
4157	J162116-004250	5200.039 ± 0.039	13.869 ± 0.016	54.463 ± 1.763
4158	J162116-004250	5196.944 ± 0.025	13.982 ± 0.033	31.095 ± 0.623
4159	J162116-004250	5196.596 ± 0.009	13.913 ± 0.038	18.173 ± 0.827
4160	J162116-004250	5195.425 ± 0.118	12.504 ± 0.314	13.315 ± 5.013
4161	J162116-004250	5195.053 ± 0.086	12.833 ± 0.573	12.446 ± 6.827
4162	J162116-004250	5194.743 ± 0.261	12.671 ± 0.679	14.562 ± 9.905
4163	J162116-004250	5194.107 ± 0.153	11.973 ± 0.707	11.911 ± 11.610
4164	J162116-004250	5193.359 ± 0.028	13.343 ± 0.122	23.746 ± 6.312
4165	J162116-004250	5192.688 ± 0.015	13.540 ± 0.069	18.742 ± 1.706

Table E.1. *Continued*

4166	J162116-004250	5191.973 ± 0.014	13.534 ± 0.056	24.211 ± 3.154
4167	J162116-004250	5191.433 ± 0.026	12.683 ± 0.183	12.455 ± 1.932
4168	J162116-004250	5189.620 ± 0.051	12.033 ± 0.135	12.251 ± 4.588
4169	J162116-004250	5188.048 ± 0.005	13.317 ± 0.006	24.472 ± 0.441
4170	J162116-004250	5186.860 ± 0.006	13.164 ± 0.008	23.235 ± 0.494
4171	J162116-004250	5185.560 ± 0.070	12.224 ± 0.116	19.880 ± 5.074
4172	J162116-004250	5184.747 ± 0.069	12.522 ± 0.120	22.860 ± 6.569
4173	J162116-004250	5183.624 ± 0.144	12.958 ± 0.250	23.515 ± 5.617
4174	J162116-004250	5183.131 ± 0.204	12.710 ± 0.431	22.067 ± 5.911
4175	J162116-004250	5180.719 ± 0.121	12.537 ± 0.131	30.310 ± 7.416
4176	J162116-004250	5179.807 ± 0.005	13.977 ± 0.008	24.980 ± 0.469
4177	J162116-004250	5178.704 ± 0.057	13.827 ± 0.220	15.340 ± 2.548
4178	J162116-004250	5177.782 ± 0.064	14.809 ± 0.076	37.214 ± 1.391
4179	J162116-004250	5176.287 ± 0.029	12.511 ± 0.097	10.618 ± 2.432
4180	J162116-004250	5171.574 ± 0.007	13.344 ± 0.007	32.320 ± 0.751
4181	J162116-004250	5169.637 ± 0.010	13.518 ± 0.132	28.353 ± 2.201
4182	J162116-004250	5169.117 ± 0.342	13.194 ± 0.286	45.247 ± 9.442
4183	J162116-004250	5166.568 ± 0.003	13.900 ± 0.003	29.516 ± 0.206
4184	J162116-004250	5165.017 ± 0.027	13.375 ± 0.026	35.712 ± 2.010
4185	J162116-004250	5164.159 ± 0.143	12.966 ± 0.329	20.663 ± 6.815
4186	J162116-004250	5163.703 ± 0.060	13.281 ± 0.144	19.386 ± 2.231
4187	J162116-004250	5162.694 ± 0.037	13.006 ± 0.063	26.768 ± 3.328
4188	J162116-004250	5161.672 ± 0.005	14.186 ± 0.005	30.479 ± 0.418
4189	J162116-004250	5159.971 ± 0.192	13.529 ± 0.266	28.207 ± 8.723
4190	J162116-004250	5158.905 ± 0.023	15.087 ± 0.038	33.481 ± 0.511
4191	J162116-004250	5155.706 ± 0.003	14.481 ± 0.007	34.062 ± 0.257
4192	J162116-004250	5154.518 ± 0.053	12.565 ± 0.236	15.895 ± 3.968
4193	J162116-004250	5153.778 ± 0.285	13.222 ± 0.453	27.258 ± 15.774
4194	J162116-004250	5153.224 ± 0.094	13.460 ± 0.244	22.968 ± 3.333
4195	J162116-004250	5152.191 ± 0.079	13.329 ± 0.133	23.010 ± 4.213
4196	J162116-004250	5151.744 ± 0.096	12.826 ± 0.409	17.327 ± 4.463
4197	J162116-004250	5150.759 ± 0.004	13.986 ± 0.004	34.066 ± 0.435
4198	J162116-004250	5149.181 ± 0.007	13.584 ± 0.006	38.654 ± 0.701
4199	J162116-004250	5147.627 ± 0.004	13.634 ± 0.004	27.780 ± 0.339
4200	J162116-004250	5146.552 ± 0.037	13.449 ± 0.103	15.517 ± 1.265
4201	J162116-004250	5145.873 ± 0.014	14.617 ± 0.032	23.387 ± 0.741
4202	J162116-004250	5144.655 ± 0.207	12.264 ± 0.370	32.357 ± 29.847
4203	J162116-004250	5143.876 ± 0.081	12.023 ± 0.397	12.779 ± 7.123
4204	J162116-004250	5143.334 ± 0.037	12.543 ± 0.160	18.412 ± 7.660
4205	J162116-004250	5140.725 ± 0.205	13.601 ± 0.108	72.715 ± 6.367
4206	J162116-004250	5140.912 ± 0.025	12.913 ± 0.118	19.092 ± 2.308
4207	J162116-004250	5139.937 ± 0.008	13.192 ± 0.150	21.194 ± 2.948
4208	J162116-004250	5138.898 ± 0.009	13.413 ± 0.044	21.621 ± 1.247
4209	J162116-004250	5138.337 ± 0.062	12.011 ± 0.278	12.028 ± 6.173

Table E.1. *Continued*

4210	J162116-004250	5137.842 ± 0.034	12.082 ± 0.130	11.672 ± 3.896
4211	J162116-004250	5137.065 ± 0.043	13.380 ± 0.073	19.924 ± 1.931
4212	J162116-004250	5136.673 ± 0.034	13.008 ± 0.196	14.207 ± 2.382
4213	J162116-004250	5135.881 ± 0.007	14.094 ± 0.013	31.295 ± 0.754
4214	J162116-004250	5134.743 ± 0.044	13.715 ± 0.024	48.555 ± 2.807
4215	J162116-004250	5134.530 ± 0.015	12.543 ± 0.106	11.846 ± 1.858
4216	J162116-004250	5132.608 ± 0.002	14.433 ± 0.008	27.936 ± 0.265
4217	J162116-004250	5131.558 ± 0.027	12.353 ± 0.119	13.663 ± 2.771
4218	J162116-004250	5130.889 ± 0.012	13.269 ± 0.015	28.205 ± 1.142
4219	J162116-004250	5129.481 ± 0.011	13.263 ± 0.014	31.972 ± 1.212
4220	J162116-004250	5128.283 ± 0.002	14.156 ± 0.004	27.543 ± 0.199
4221	J162116-004250	5126.525 ± 0.058	13.651 ± 0.080	25.972 ± 1.847
4222	J162116-004250	5126.111 ± 0.024	13.639 ± 0.096	16.503 ± 1.349
4223	J162116-004250	5125.352 ± 0.004	12.865 ± 0.011	10.212 ± 0.360
4224	J162116-004250	5123.654 ± 0.007	13.232 ± 0.011	18.054 ± 0.393
4225	J162116-004250	5122.965 ± 0.055	12.455 ± 0.374	11.450 ± 3.614
4226	J162116-004250	5122.402 ± 0.049	13.884 ± 0.105	22.260 ± 3.239
4227	J162116-004250	5121.101 ± 0.031	15.226 ± 0.204	34.009 ± 6.538
4228	J162116-004250	5120.062 ± 0.777	13.519 ± 0.936	34.705 ± 21.403
4229	J162116-004250	5118.823 ± 0.082	12.221 ± 0.223	19.552 ± 7.644
4230	J162116-004250	5117.976 ± 0.049	11.955 ± 0.099	15.733 ± 4.508
4231	J162116-004250	5116.721 ± 0.021	12.664 ± 0.024	29.077 ± 1.998
4232	J162116-004250	5115.455 ± 0.246	12.778 ± 0.473	18.230 ± 8.273
4233	J162116-004250	5115.069 ± 0.024	13.435 ± 0.084	14.621 ± 1.043
4234	J162116-004250	5114.369 ± 0.004	13.674 ± 0.011	13.212 ± 0.316
4235	J162116-004250	5113.227 ± 0.003	14.902 ± 0.037	29.887 ± 0.784
4236	J162116-004250	5111.907 ± 0.032	12.851 ± 0.097	23.151 ± 4.188
4237	J162116-004250	5110.604 ± 1.338	13.041 ± 1.457	35.740 ± 45.391
4238	J162116-004250	5110.143 ± 0.063	13.391 ± 0.629	25.086 ± 6.048
4239	J162116-004250	5109.108 ± 0.005	13.525 ± 0.008	22.382 ± 0.316
4240	J162116-004250	5107.119 ± 0.070	15.066 ± 0.118	31.491 ± 1.171
4241	J162116-004250	5105.950 ± 0.105	14.259 ± 0.148	30.897 ± 7.946
4242	J162116-004250	5104.427 ± 0.030	14.778 ± 0.026	48.280 ± 0.893
4243	J162116-004250	5102.463 ± 0.110	12.741 ± 0.272	18.721 ± 4.535
4244	J162116-004250	5101.987 ± 0.053	13.188 ± 0.098	20.768 ± 2.566
4245	J162116-004250	5100.259 ± 0.073	13.878 ± 0.061	46.395 ± 2.085
4246	J162116-004250	5099.733 ± 0.007	14.072 ± 0.036	27.907 ± 0.905
4247	J162116-004250	5098.398 ± 0.119	11.677 ± 0.379	15.089 ± 11.683
4248	J162116-004250	5097.567 ± 0.005	13.514 ± 0.007	27.515 ± 0.569
4249	J162116-004250	5095.947 ± 0.002	14.551 ± 0.006	37.646 ± 0.233
4250	J162116-004250	5094.379 ± 0.041	11.793 ± 0.157	10.223 ± 3.895
4251	J162116-004250	5093.566 ± 0.012	13.318 ± 0.017	27.722 ± 1.185
4252	J162116-004250	5092.797 ± 0.042	12.605 ± 0.203	19.224 ± 4.296
4253	J162116-004250	5092.120 ± 0.030	13.348 ± 0.034	32.883 ± 2.227

Table E.1. *Continued*

4254	J162116-004250	5090.635 ± 0.052	12.766 ± 0.071	33.284 ± 5.599
4255	J162116-004250	5089.689 ± 0.011	13.296 ± 0.018	25.348 ± 0.818
4256	J162116-004250	5088.557 ± 0.005	13.261 ± 0.006	23.932 ± 0.430
4257	J132029-052335	5613.888 ± 0.016	13.233 ± 0.020	26.518 ± 0.831
4258	J132029-052335	5612.711 ± 0.015	13.557 ± 0.008	36.322 ± 1.293
4259	J132029-052335	5611.450 ± 0.012	12.593 ± 0.030	14.182 ± 1.002
4260	J132029-052335	5610.352 ± 0.204	12.822 ± 0.295	27.659 ± 4.127
4261	J132029-052335	5610.055 ± 0.006	13.560 ± 0.054	17.815 ± 0.656
4262	J132029-052335	5608.508 ± 0.017	12.390 ± 0.141	12.504 ± 2.156
4263	J132029-052335	5608.150 ± 0.049	12.874 ± 0.051	29.006 ± 1.710
4264	J132029-052335	5605.424 ± 0.033	12.537 ± 0.031	30.643 ± 2.726
4265	J132029-052335	5604.238 ± 0.008	13.310 ± 0.023	17.269 ± 0.474
4266	J132029-052335	5603.448 ± 0.014	13.440 ± 0.023	30.406 ± 1.852
4267	J132029-052335	5602.195 ± 0.014	12.950 ± 0.068	15.132 ± 1.141
4268	J132029-052335	5601.618 ± 0.055	12.965 ± 0.070	25.952 ± 3.529
4269	J132029-052335	5600.394 ± 0.004	13.529 ± 0.004	23.644 ± 0.279
4270	J132029-052335	5595.946 ± 0.079	12.119 ± 0.135	19.135 ± 5.413
4271	J132029-052335	5592.682 ± 0.177	12.881 ± 0.226	38.943 ± 18.507
4272	J132029-052335	5597.702 ± 0.018	12.483 ± 0.118	10.598 ± 1.905
4273	J132029-052335	5597.253 ± 0.051	12.678 ± 0.073	19.748 ± 2.837
4274	J132029-052335	5594.444 ± 0.004	14.640 ± 0.012	34.834 ± 0.492
4275	J132029-052335	5591.686 ± 0.004	14.346 ± 0.011	22.828 ± 0.499
4276	J132029-052335	5590.561 ± 0.003	13.995 ± 0.006	19.509 ± 0.223
4277	J132029-052335	5587.872 ± 0.030	12.602 ± 0.291	11.227 ± 2.499
4278	J132029-052335	5587.404 ± 0.042	13.293 ± 0.171	21.191 ± 5.985
4279	J132029-052335	5586.796 ± 0.150	12.952 ± 0.264	21.385 ± 5.358
4280	J132029-052335	5584.983 ± 0.029	14.259 ± 0.023	46.183 ± 0.861
4281	J132029-052335	5584.403 ± 0.011	14.918 ± 0.070	21.607 ± 0.802
4282	J132029-052335	5582.936 ± 0.043	12.342 ± 0.211	11.963 ± 3.019
4283	J132029-052335	5582.485 ± 0.029	13.030 ± 0.042	19.411 ± 1.455
4284	J132029-052335	5578.810 ± 0.013	13.866 ± 0.009	39.996 ± 0.660
4285	J132029-052335	5577.678 ± 0.006	13.804 ± 0.011	25.862 ± 0.576
4286	J132029-052335	5576.105 ± 0.002	15.388 ± 0.046	24.782 ± 0.389
4287	J132029-052335	5574.523 ± 0.024	12.544 ± 0.033	21.025 ± 2.003
4288	J132029-052335	5572.273 ± 0.049	13.055 ± 0.032	44.899 ± 3.113
4289	J132029-052335	5569.696 ± 0.024	15.441 ± 0.042	47.275 ± 0.886
4290	J132029-052335	5566.803 ± 0.093	14.740 ± 0.049	69.663 ± 8.396
4291	J132029-052335	5563.624 ± 0.099	15.093 ± 0.045	90.706 ± 1.917
4292	J132029-052335	5559.641 ± 0.077	12.589 ± 0.376	15.335 ± 3.908
4293	J132029-052335	5558.874 ± 0.464	13.288 ± 0.652	27.592 ± 26.139
4294	J132029-052335	5557.879 ± 0.036	14.935 ± 0.170	25.040 ± 4.230
4295	J132029-052335	5556.620 ± 0.042	14.445 ± 0.048	27.869 ± 2.989
4296	J132029-052335	5555.638 ± 0.035	13.491 ± 0.078	19.410 ± 1.804
4297	J132029-052335	5553.669 ± 0.005	15.008 ± 0.012	52.687 ± 0.454

Table E.1. *Continued*

4298	J132029-052335	5551.121 ± 0.003	13.492 ± 0.005	18.020 ± 0.264
4299	J132029-052335	5550.055 ± 0.004	13.889 ± 0.006	24.500 ± 0.314
4300	J132029-052335	5548.479 ± 0.170	13.780 ± 0.145	46.911 ± 6.327
4301	J132029-052335	5546.663 ± 1.123	13.631 ± 0.998	55.545 ± 94.365
4302	J132029-052335	5547.592 ± 0.022	12.607 ± 0.241	13.908 ± 3.181
4303	J132029-052335	5545.990 ± 0.022	13.879 ± 0.308	26.448 ± 3.896
4304	J132029-052335	5544.921 ± 0.293	13.300 ± 0.532	31.518 ± 10.984
4305	J132029-052335	5544.042 ± 0.051	12.146 ± 0.239	13.773 ± 3.994
4306	J132029-052335	5542.290 ± 0.051	11.837 ± 0.103	13.745 ± 4.102
4307	J132029-052335	5539.657 ± 0.102	15.083 ± 0.163	31.165 ± 1.527
4308	J132029-052335	5538.724 ± 0.159	13.875 ± 0.403	20.550 ± 3.238
4309	J132029-052335	5537.377 ± 0.023	12.545 ± 0.030	22.833 ± 1.966
4310	J132029-052335	5535.688 ± 0.056	12.868 ± 0.081	25.130 ± 2.515
4311	J132029-052335	5534.689 ± 0.014	13.531 ± 0.034	32.035 ± 2.654
4312	J132029-052335	5533.900 ± 0.124	12.758 ± 0.386	14.964 ± 6.313
4313	J132029-052335	5533.482 ± 0.100	12.766 ± 0.506	14.801 ± 8.403
4314	J132029-052335	5532.861 ± 0.018	13.719 ± 0.043	25.227 ± 2.308
4315	J132029-052335	5531.352 ± 0.010	14.651 ± 0.024	34.707 ± 1.514
4316	J132029-052335	5529.996 ± 0.040	13.835 ± 0.044	36.721 ± 2.733
4317	J132029-052335	5528.276 ± 0.443	13.214 ± 0.433	35.959 ± 19.743
4318	J132029-052335	5527.650 ± 0.015	14.042 ± 0.071	22.178 ± 1.717
4319	J132029-052335	5527.106 ± 0.033	13.240 ± 0.120	14.395 ± 1.081
4320	J132029-052335	5525.658 ± 0.162	11.900 ± 0.529	14.891 ± 8.814
4321	J132029-052335	5525.068 ± 0.045	12.858 ± 0.068	23.417 ± 3.609
4322	J132029-052335	5524.014 ± 0.003	13.684 ± 0.006	18.683 ± 0.293
4323	J132029-052335	5523.082 ± 0.146	12.001 ± 0.317	24.660 ± 22.075
4324	J132029-052335	5521.536 ± 0.007	13.095 ± 0.015	19.070 ± 0.615
4325	J132029-052335	5519.835 ± 0.030	13.717 ± 0.013	54.504 ± 2.409
4326	J132029-052335	5518.598 ± 0.154	12.763 ± 0.321	22.110 ± 8.689
4327	J132029-052335	5517.974 ± 0.013	13.896 ± 0.019	21.219 ± 0.461
4328	J132029-052335	5516.484 ± 0.053	12.354 ± 0.236	13.894 ± 3.748
4329	J132029-052335	5515.825 ± 0.035	13.328 ± 0.046	26.232 ± 2.824
4330	J132029-052335	5514.979 ± 0.026	12.544 ± 0.101	11.347 ± 2.710
4331	J132029-052335	5513.936 ± 0.006	14.314 ± 0.010	25.035 ± 0.540
4332	J132029-052335	5513.118 ± 0.119	12.568 ± 0.221	19.170 ± 4.719
4333	J132029-052335	5509.954 ± 0.041	12.367 ± 0.061	21.880 ± 3.193
4334	J132029-052335	5508.407 ± 0.004	13.915 ± 0.015	22.268 ± 0.418
4335	J132029-052335	5508.309 ± 0.023	13.416 ± 0.046	47.087 ± 2.433
4336	J132029-052335	5504.710 ± 0.026	12.450 ± 0.033	21.635 ± 1.995
4337	J132029-052335	5501.303 ± 0.032	12.412 ± 0.042	22.118 ± 2.678
4338	J132029-052335	5500.153 ± 0.031	12.975 ± 0.054	21.559 ± 1.712
4339	J132029-052335	5499.180 ± 0.258	13.364 ± 0.506	28.604 ± 8.347
4340	J132029-052335	5498.523 ± 0.513	13.274 ± 0.628	32.295 ± 18.560
4341	J132029-052335	5497.399 ± 0.009	13.600 ± 0.015	22.445 ± 0.465

Table E.1. *Continued*

4342	J132029-052335	5496.026 ± 0.030	12.331 ± 0.044	19.162 ± 2.393
4343	J132029-052335	5494.178 ± 0.045	11.933 ± 0.238	11.727 ± 4.697
4344	J132029-052335	5493.247 ± 0.045	13.101 ± 0.056	36.647 ± 5.160
4345	J132029-052335	5492.425 ± 0.018	12.838 ± 0.076	17.851 ± 1.480
4346	J132029-052335	5491.092 ± 0.006	13.038 ± 0.009	19.225 ± 0.497
4347	J132029-052335	5489.539 ± 0.085	11.968 ± 0.116	21.529 ± 7.019
4348	J132029-052335	5488.300 ± 0.032	12.561 ± 0.034	27.369 ± 2.634
4349	J132029-052335	5486.271 ± 0.049	11.963 ± 0.383	10.046 ± 6.096
4350	J132029-052335	5485.640 ± 0.094	12.820 ± 0.190	25.532 ± 9.798
4351	J132029-052335	5484.478 ± 1.538	13.465 ± 2.302	27.156 ± 39.269
4352	J132029-052335	5484.077 ± 0.099	14.184 ± 0.439	21.996 ± 3.207
4353	J132029-052335	5483.255 ± 0.153	12.271 ± 0.315	16.272 ± 6.946
4354	J132029-052335	5481.964 ± 0.043	12.200 ± 0.111	10.882 ± 3.028
4355	J132029-052335	5478.978 ± 0.019	13.322 ± 0.021	29.773 ± 1.060
4356	J132029-052335	5477.834 ± 0.032	13.159 ± 0.037	35.571 ± 3.178
4357	J132029-052335	5476.880 ± 0.045	11.986 ± 0.224	11.022 ± 4.178
4358	J132029-052335	5476.153 ± 0.030	12.619 ± 0.483	18.557 ± 6.486
4359	J132029-052335	5475.617 ± 0.305	12.921 ± 0.275	36.210 ± 14.274
4360	J132029-052335	5474.053 ± 0.016	13.023 ± 0.114	18.626 ± 2.041
4361	J132029-052335	5473.127 ± 0.098	13.226 ± 0.135	47.167 ± 15.278
4362	J132029-052335	5471.970 ± 0.005	13.944 ± 0.011	22.330 ± 0.343
4363	J132029-052335	5470.118 ± 0.026	13.688 ± 0.042	19.815 ± 0.870
4364	J132029-052335	5469.558 ± 0.015	13.976 ± 0.027	18.408 ± 0.638
4365	J132029-052335	5468.355 ± 0.022	13.626 ± 0.014	48.477 ± 1.671
4366	J132029-052335	5467.707 ± 0.023	12.333 ± 0.128	11.609 ± 2.641
4367	J132029-052335	5466.745 ± 0.028	12.319 ± 0.084	14.250 ± 2.686
4368	J132029-052335	5465.515 ± 0.004	13.716 ± 0.021	20.725 ± 0.538
4369	J132029-052335	5464.910 ± 0.101	13.253 ± 0.070	45.687 ± 4.382
4370	J132029-052335	5463.492 ± 0.040	12.339 ± 0.075	19.646 ± 3.182
4371	J132029-052335	5462.340 ± 0.089	11.841 ± 0.189	13.602 ± 7.505
4372	J132029-052335	5461.834 ± 0.056	11.895 ± 0.156	10.522 ± 4.446
4373	J132029-052335	5460.210 ± 0.017	12.568 ± 0.026	18.188 ± 1.334
4374	J132029-052335	5458.435 ± 0.046	12.504 ± 0.049	28.601 ± 3.836
4375	J132029-052335	5456.879 ± 0.022	13.864 ± 0.059	18.363 ± 1.215
4376	J132029-052335	5456.567 ± 0.018	14.223 ± 0.013	38.800 ± 0.910
4377	J132029-052335	5454.634 ± 0.287	13.112 ± 0.376	71.396 ± 62.407
4378	J132029-052335	5454.020 ± 0.049	11.975 ± 0.608	11.050 ± 7.579
4379	J132029-052335	5453.357 ± 0.027	12.818 ± 0.181	17.068 ± 2.694
4380	J132029-052335	5452.511 ± 0.030	13.404 ± 0.053	33.930 ± 1.473
4381	J132029-052335	5450.749 ± 0.019	12.584 ± 0.030	17.940 ± 1.653
4382	J132029-052335	5449.427 ± 0.006	13.033 ± 0.010	18.260 ± 0.500
4383	J132029-052335	5446.622 ± 0.003	14.278 ± 0.011	24.041 ± 0.351
4384	J132029-052335	5445.535 ± 0.007	13.423 ± 0.009	21.855 ± 0.507
4385	J132029-052335	5443.617 ± 0.046	12.700 ± 0.219	13.563 ± 4.632

Table E.1. *Continued*

4386	J132029-052335	5443.145 ± 0.031	13.250 ± 0.053	18.236 ± 1.607
4387	J132029-052335	5442.239 ± 0.024	12.476 ± 0.041	17.165 ± 2.037
4388	J132029-052335	5440.925 ± 0.029	12.437 ± 0.044	19.563 ± 2.465
4389	J132029-052335	5439.627 ± 0.008	14.248 ± 0.013	24.400 ± 0.438
4390	J132029-052335	5438.128 ± 0.007	15.361 ± 0.074	27.660 ± 0.805
4391	J132029-052335	5436.519 ± 0.052	12.892 ± 0.130	21.976 ± 4.050
4392	J132029-052335	5435.641 ± 0.017	13.598 ± 0.033	31.402 ± 2.505
4393	J132029-052335	5434.701 ± 0.097	12.384 ± 0.222	20.073 ± 6.357
4394	J132029-052335	5433.421 ± 0.077	13.703 ± 0.121	24.368 ± 2.175
4395	J132029-052335	5432.838 ± 0.075	13.487 ± 0.337	23.113 ± 7.638
4396	J132029-052335	5431.945 ± 0.052	13.737 ± 0.201	33.178 ± 13.411
4397	J132029-052335	5431.141 ± 0.100	13.343 ± 0.303	23.302 ± 5.644
4398	J132029-052335	5430.189 ± 0.077	12.622 ± 0.252	15.626 ± 6.038
4399	J132029-052335	5429.460 ± 0.052	13.380 ± 0.035	44.563 ± 3.140
4400	J132029-052335	5427.674 ± 0.034	12.655 ± 0.059	22.075 ± 2.670
4401	J132029-052335	5426.582 ± 0.008	13.624 ± 0.007	34.134 ± 0.716
4402	J132029-052335	5425.315 ± 0.059	11.958 ± 0.120	15.031 ± 4.890
4403	J132029-052335	5423.175 ± 0.031	12.307 ± 0.108	11.702 ± 2.435
4404	J132029-052335	5422.011 ± 0.003	14.484 ± 0.010	34.814 ± 0.413
4405	J132029-052335	5420.445 ± 0.012	12.738 ± 0.022	16.104 ± 0.970
4406	J132029-052335	5419.248 ± 0.096	12.064 ± 0.194	16.294 ± 6.487
4407	J132029-052335	5418.209 ± 0.929	13.077 ± 1.357	24.958 ± 26.482
4408	J132029-052335	5417.910 ± 0.030	13.226 ± 0.900	16.133 ± 7.040
4409	J132029-052335	5416.669 ± 0.011	14.600 ± 0.012	43.912 ± 0.780
4410	J132029-052335	5414.842 ± 0.073	12.967 ± 0.152	19.263 ± 3.550
4411	J132029-052335	5414.186 ± 0.023	13.596 ± 0.084	21.821 ± 2.845
4412	J132029-052335	5413.243 ± 0.019	14.315 ± 0.015	36.795 ± 0.822
4413	J132029-052335	5411.563 ± 0.020	12.917 ± 0.022	26.921 ± 1.544
4414	J132029-052335	5409.192 ± 0.018	13.280 ± 0.040	27.632 ± 1.311
4415	J132029-052335	5407.997 ± 0.051	13.250 ± 0.062	49.124 ± 7.584
4416	J132029-052335	5405.324 ± 0.003	16.553 ± 0.099	37.945 ± 0.792
4417	J132029-052335	5402.734 ± 0.004	14.239 ± 0.005	33.186 ± 0.388
4418	J132029-052335	5401.185 ± 0.003	13.783 ± 0.004	24.581 ± 0.254
4419	J132029-052335	5396.369 ± 0.068	11.690 ± 0.163	11.661 ± 5.767
4420	J132029-052335	5394.253 ± 0.221	12.583 ± 0.227	32.051 ± 9.914
4421	J132029-052335	5393.348 ± 0.024	13.462 ± 0.034	29.922 ± 1.538
4422	J132029-052335	5391.628 ± 0.013	13.606 ± 0.011	50.836 ± 1.695
4423	J132029-052335	5390.284 ± 0.009	13.690 ± 0.017	17.417 ± 0.526
4424	J132029-052335	5389.346 ± 0.015	14.263 ± 0.019	24.532 ± 1.388
4425	J132029-052335	5388.155 ± 0.014	14.691 ± 0.048	26.196 ± 1.201
4426	J132029-052335	5386.960 ± 0.026	13.504 ± 0.025	29.609 ± 1.247
4427	J132029-052335	5383.906 ± 0.264	12.653 ± 0.230	34.369 ± 12.799
4428	J132029-052335	5383.099 ± 0.142	12.944 ± 0.594	22.036 ± 9.467
4429	J132029-052335	5382.028 ± 0.765	13.941 ± 0.736	38.736 ± 35.508

Table E.1. *Continued*

4430	J132029-052335	5381.415 ± 0.047	14.306 ± 0.272	24.555 ± 6.090
4431	J132029-052335	5380.739 ± 0.215	12.385 ± 1.273	11.718 ± 10.935
4432	J132029-052335	5379.735 ± 0.103	13.069 ± 0.065	51.855 ± 8.116
4433	J132029-052335	5377.739 ± 1.699	13.496 ± 4.015	23.541 ± 24.603
4434	J132029-052335	5377.523 ± 0.064	14.204 ± 0.768	19.505 ± 4.485
4435	J132029-052335	5376.117 ± 0.003	13.872 ± 0.004	24.860 ± 0.330
4436	J132029-052335	5374.688 ± 0.004	13.655 ± 0.007	20.965 ± 0.485
4437	J132029-052335	5373.660 ± 0.007	13.534 ± 0.016	20.974 ± 0.948
4438	J132029-052335	5372.452 ± 0.012	14.267 ± 0.015	26.921 ± 0.828
4439	J132029-052335	5371.450 ± 0.014	14.023 ± 0.020	25.700 ± 1.212
4440	J132029-052335	5370.553 ± 0.060	12.613 ± 0.167	18.694 ± 5.406
4441	J132029-052335	5369.750 ± 0.093	12.372 ± 0.129	24.117 ± 7.753
4442	J132029-052335	5368.421 ± 0.003	13.913 ± 0.004	24.305 ± 0.217
4443	J132029-052335	5366.943 ± 0.017	12.944 ± 0.028	21.525 ± 1.729
4444	J132029-052335	5365.884 ± 0.053	12.453 ± 0.234	22.811 ± 6.203
4445	J132029-052335	5363.956 ± 2.173	13.368 ± 1.133	66.005 ± 76.302
4446	J132029-052335	5363.747 ± 0.023	14.036 ± 0.083	23.639 ± 1.496
4447	J132029-052335	5362.846 ± 0.017	14.397 ± 0.050	24.397 ± 1.990
4448	J132029-052335	5361.602 ± 0.141	12.632 ± 0.556	22.807 ± 16.010
4449	J132029-052335	5360.924 ± 0.121	12.399 ± 0.229	18.681 ± 5.530
4450	J132029-052335	5359.416 ± 0.031	12.617 ± 0.043	22.838 ± 2.517
4451	J132029-052335	5358.274 ± 0.027	12.603 ± 0.189	15.782 ± 3.195
4452	J132029-052335	5357.898 ± 0.185	12.781 ± 0.137	37.012 ± 7.687
4453	J132029-052335	5356.813 ± 0.011	13.150 ± 0.020	20.331 ± 0.738
4454	J132029-052335	5355.151 ± 0.022	12.378 ± 0.040	15.825 ± 1.821
4455	J132029-052335	5352.959 ± 0.077	12.104 ± 0.105	22.195 ± 6.862
4456	J132029-052335	5351.095 ± 0.007	13.246 ± 0.008	24.798 ± 0.518
4457	J132029-052335	5348.624 ± 0.011	13.013 ± 0.013	25.277 ± 0.880
4458	J132029-052335	5347.489 ± 0.069	11.800 ± 0.144	13.680 ± 5.776
4459	J132029-052335	5344.724 ± 0.149	11.960 ± 0.255	17.214 ± 10.050
4460	J132029-052335	5343.454 ± 0.055	12.017 ± 0.137	12.737 ± 4.392
4461	J132029-052335	5342.687 ± 0.020	13.381 ± 0.040	20.600 ± 1.248
4462	J132029-052335	5341.791 ± 0.008	14.153 ± 0.008	29.104 ± 0.803
4463	J132029-052335	5340.365 ± 0.006	13.976 ± 0.007	29.873 ± 0.666
4464	J132029-052335	5339.530 ± 0.017	12.774 ± 0.126	10.151 ± 1.774
4465	J132029-052335	5338.864 ± 0.032	12.812 ± 0.038	27.002 ± 2.887
4466	J132029-052335	5337.476 ± 0.003	13.823 ± 0.005	21.692 ± 0.199
4467	J132029-052335	5334.562 ± 0.007	13.384 ± 0.007	27.763 ± 0.564
4468	J132029-052335	5333.033 ± 0.004	13.927 ± 0.004	32.541 ± 0.352
4469	J132029-052335	5331.781 ± 0.009	13.085 ± 0.013	19.576 ± 0.701
4470	J132029-052335	5329.198 ± 0.070	12.616 ± 0.109	25.018 ± 3.893
4471	J132029-052335	5328.291 ± 0.098	12.710 ± 0.092	33.392 ± 6.375
4472	J132029-052335	5326.344 ± 0.026	13.220 ± 0.025	32.632 ± 1.807
4473	J132029-052335	5325.387 ± 0.029	12.955 ± 0.044	24.958 ± 1.910

Table E.1. *Continued*

4474	J132029-052335	5323.898 ± 0.021	12.609 ± 0.093	11.735 ± 2.004
4475	J132029-052335	5322.953 ± 0.026	14.235 ± 0.013	50.752 ± 1.070
4476	J132029-052335	5321.400 ± 0.010	19.088 ± 2.333	17.902 ± 3.894
4477	J132029-052335	5319.639 ± 0.013	14.444 ± 0.022	29.134 ± 2.644
4478	J132029-052335	5318.613 ± 0.033	13.836 ± 0.047	25.621 ± 1.649
4479	J132029-052335	5317.607 ± 0.072	12.419 ± 0.177	21.268 ± 6.910
4480	J132029-052335	5316.310 ± 0.108	12.881 ± 0.115	44.301 ± 12.536
4481	J132029-052335	5314.388 ± 1.971	16.406 ± 4.802	27.341 ± 22.086
4482	J132029-052335	5313.171 ± 0.950	14.769 ± 1.240	36.184 ± 23.831
4483	J132029-052335	5312.834 ± 2.423	13.933 ± 1.778	63.187 ± 43.350
4484	J132029-052335	5308.199 ± 0.069	12.819 ± 0.159	17.812 ± 2.623
4485	J132029-052335	5307.703 ± 0.115	12.739 ± 0.201	20.408 ± 5.606
4486	J132029-052335	5306.423 ± 0.016	13.148 ± 0.017	35.215 ± 1.786
4487	J132029-052335	5305.133 ± 0.007	13.234 ± 0.010	22.372 ± 0.575
4488	J132029-052335	5303.657 ± 0.002	14.299 ± 0.012	21.983 ± 0.221
4489	J132029-052335	5302.349 ± 0.006	13.310 ± 0.008	22.245 ± 0.514
4490	J132029-052335	5300.826 ± 0.223	13.979 ± 0.372	27.105 ± 4.647
4491	J132029-052335	5299.979 ± 0.087	15.040 ± 0.144	30.515 ± 1.526
4492	J132029-052335	5298.073 ± 0.029	12.950 ± 0.039	34.451 ± 2.951
4493	J132029-052335	5296.110 ± 0.003	13.941 ± 0.010	20.536 ± 0.377
4494	J132029-052335	5296.038 ± 0.018	13.692 ± 0.012	67.021 ± 2.582
4495	J132029-052335	5294.072 ± 0.040	11.954 ± 0.136	10.981 ± 3.719
4496	J132029-052335	5292.973 ± 0.024	13.250 ± 0.025	32.540 ± 1.794
4497	J132029-052335	5291.934 ± 0.055	12.834 ± 0.061	29.721 ± 3.304
4498	J132029-052335	5289.472 ± 0.031	12.385 ± 0.045	19.742 ± 2.491
4499	J132029-052335	5288.130 ± 0.050	12.308 ± 0.067	23.222 ± 4.442
4500	J132029-052335	5286.930 ± 0.032	13.062 ± 0.042	24.373 ± 2.279
4501	J132029-052335	5286.368 ± 0.026	12.630 ± 0.122	13.794 ± 2.151
4502	J132029-052335	5285.158 ± 0.045	13.449 ± 0.040	56.866 ± 5.709
4503	J132029-052335	5283.948 ± 0.024	13.297 ± 0.069	25.890 ± 1.995
4504	J132029-052335	5282.982 ± 0.208	12.540 ± 0.344	36.131 ± 29.141
4505	J132029-052335	5282.149 ± 0.034	12.277 ± 0.208	13.987 ± 3.767
4506	J132029-052335	5281.033 ± 0.012	12.435 ± 0.030	10.573 ± 0.987
4507	J132029-052335	5280.201 ± 0.069	11.771 ± 0.149	13.278 ± 5.814
4508	J132029-052335	5278.063 ± 0.004	13.447 ± 0.005	21.457 ± 0.293
4509	J132029-052335	5276.188 ± 0.018	13.506 ± 0.018	30.645 ± 1.051
4510	J132029-052335	5275.312 ± 0.016	13.303 ± 0.038	23.557 ± 1.624
4511	J132029-052335	5274.446 ± 0.056	12.710 ± 0.069	25.358 ± 3.583
4512	J132029-052335	5271.955 ± 0.006	13.295 ± 0.008	24.720 ± 0.499
4513	J132029-052335	5270.180 ± 0.071	12.728 ± 0.051	48.753 ± 7.134
4514	J132029-052335	5268.548 ± 0.020	13.107 ± 0.019	34.716 ± 1.770
4515	J132029-052335	5266.618 ± 0.009	13.195 ± 0.009	29.531 ± 0.737
4516	J132029-052335	5265.026 ± 0.015	12.979 ± 0.019	24.838 ± 1.294
4517	J132029-052335	5263.600 ± 0.007	14.100 ± 0.020	20.264 ± 0.717

Table E.1. *Continued*

4518	J132029-052335	5263.252 ± 0.024	13.933 ± 0.026	41.053 ± 0.734
4519	J132029-052335	5261.924 ± 0.022	12.269 ± 0.075	10.368 ± 2.043
4520	J132029-052335	5261.207 ± 0.003	13.713 ± 0.005	19.553 ± 0.246
4521	J132029-052335	5260.047 ± 0.018	12.776 ± 0.022	24.141 ± 1.515
4522	J132029-052335	5257.270 ± 0.066	12.776 ± 0.070	29.516 ± 4.034
4523	J132029-052335	5256.337 ± 0.019	13.207 ± 0.030	26.852 ± 1.659
4524	J132029-052335	5255.128 ± 0.041	12.622 ± 0.050	29.047 ± 4.131
4525	J132029-052335	5253.822 ± 0.035	12.666 ± 0.052	22.828 ± 3.174
4526	J132029-052335	5252.572 ± 0.014	14.762 ± 0.044	23.763 ± 0.706
4527	J132029-052335	5251.623 ± 0.015	14.065 ± 0.030	16.753 ± 0.751
4528	J132029-052335	5250.831 ± 0.044	13.021 ± 0.048	28.620 ± 2.979
4529	J132029-052335	5249.239 ± 0.010	13.218 ± 0.010	30.749 ± 0.929
4530	J132029-052335	5247.840 ± 0.006	13.343 ± 0.009	24.160 ± 0.583
4531	J132029-052335	5246.610 ± 0.182	12.449 ± 0.355	28.737 ± 10.919
4532	J132029-052335	5245.717 ± 0.355	12.541 ± 0.284	39.942 ± 17.816
4533	J132029-052335	5243.781 ± 0.097	12.055 ± 0.113	26.118 ± 8.123
4534	J132029-052335	5241.462 ± 0.052	12.514 ± 0.055	29.672 ± 4.625
4535	J132029-052335	5240.469 ± 0.060	12.191 ± 0.116	19.162 ± 5.398
4536	J132029-052335	5238.614 ± 0.278	13.428 ± 0.208	46.563 ± 9.260
4537	J132029-052335	5237.779 ± 0.013	14.404 ± 0.023	32.240 ± 0.929
4538	J132029-052335	5236.494 ± 0.104	13.341 ± 0.053	59.207 ± 5.170
4539	J132029-052335	5232.861 ± 0.020	13.191 ± 0.015	42.351 ± 1.758
4540	J132029-052335	5231.679 ± 0.026	12.819 ± 0.065	18.633 ± 2.040
4541	J132029-052335	5230.151 ± 0.004	14.858 ± 0.021	41.629 ± 0.685
4542	J132029-052335	5228.294 ± 0.125	12.117 ± 0.162	25.113 ± 9.590
4543	J132029-052335	5225.849 ± 0.044	12.039 ± 0.150	13.852 ± 4.296
4544	J132029-052335	5224.398 ± 0.198	13.241 ± 0.133	49.688 ± 10.225
4545	J132029-052335	5223.635 ± 0.068	12.730 ± 0.414	26.081 ± 7.994
4546	J132029-052335	5222.706 ± 0.169	13.044 ± 0.120	50.751 ± 11.884
4547	J132029-052335	5220.325 ± 0.002	15.481 ± 0.044	32.031 ± 0.484
4548	J132029-052335	5218.577 ± 0.035	12.739 ± 0.046	27.494 ± 3.362
4549	J132029-052335	5216.965 ± 0.008	13.660 ± 0.007	38.692 ± 0.728
4550	J132029-052335	5214.781 ± 0.039	14.330 ± 0.025	49.111 ± 1.600
4551	J132029-052335	5212.749 ± 0.020	16.269 ± 0.451	38.636 ± 4.562
4552	J132029-052335	5210.901 ± 0.060	13.766 ± 0.075	29.197 ± 2.231
4553	J132029-052335	5209.232 ± 0.030	13.110 ± 0.032	45.410 ± 4.161
4554	J132029-052335	5207.585 ± 0.019	13.688 ± 0.021	33.164 ± 1.411
4555	J132029-052335	5206.540 ± 0.006	14.288 ± 0.011	26.635 ± 0.571
4556	J132029-052335	5205.213 ± 0.007	13.692 ± 0.007	30.978 ± 0.661
4557	J132029-052335	5203.752 ± 0.043	12.854 ± 0.056	28.995 ± 4.157
4558	J132029-052335	5203.020 ± 0.047	12.430 ± 0.177	15.663 ± 4.820
4559	J132029-052335	5202.069 ± 0.004	14.278 ± 0.015	24.525 ± 0.607
4560	J132029-052335	5199.709 ± 0.003	15.467 ± 0.046	34.329 ± 0.544
4561	J132029-052335	5197.397 ± 0.034	13.357 ± 0.041	33.464 ± 1.859

Table E.1. *Continued*

4562	J132029-052335	5196.288 ± 0.041	13.446 ± 0.036	41.464 ± 2.961
4563	J132029-052335	5194.736 ± 0.008	13.398 ± 0.012	26.458 ± 0.867
4564	J132029-052335	5193.819 ± 0.174	12.569 ± 1.026	17.554 ± 8.910
4565	J132029-052335	5193.430 ± 0.549	12.661 ± 0.847	24.095 ± 20.230
4566	J132029-052335	5191.977 ± 0.037	13.039 ± 0.030	47.882 ± 4.224
4567	J132029-052335	5189.925 ± 0.041	13.929 ± 0.041	32.288 ± 1.572
4568	J132029-052335	5188.890 ± 0.009	15.976 ± 0.144	22.552 ± 0.784
4569	J132029-052335	5187.260 ± 0.031	13.213 ± 0.051	38.843 ± 5.310
4570	J132029-052335	5186.312 ± 0.021	12.985 ± 0.071	20.284 ± 2.215
4571	J132029-052335	5185.358 ± 0.004	14.108 ± 0.005	26.572 ± 0.298
4572	J132029-052335	5183.940 ± 0.022	12.671 ± 0.028	24.681 ± 1.944
4573	J132029-052335	5182.195 ± 0.031	12.989 ± 0.053	19.086 ± 1.673
4574	J132029-052335	5181.643 ± 0.021	13.115 ± 0.040	17.818 ± 1.169
4575	J132029-052335	5180.472 ± 0.011	13.318 ± 0.022	25.473 ± 0.841
4576	J132029-052335	5179.444 ± 0.053	13.108 ± 0.037	43.555 ± 3.605
4577	J132029-052335	5177.076 ± 0.020	13.009 ± 0.016	39.185 ± 1.683
4578	J132029-052335	5174.692 ± 0.005	14.434 ± 0.008	34.195 ± 0.374
4579	J132029-052335	5172.882 ± 0.007	13.184 ± 0.013	15.980 ± 0.623
4580	J132029-052335	5171.771 ± 0.022	12.770 ± 0.024	28.583 ± 1.983
4581	J132029-052335	5169.478 ± 0.008	13.078 ± 0.010	21.951 ± 0.608
4582	J132029-052335	5167.843 ± 0.003	13.710 ± 0.005	17.940 ± 0.219
4583	J132029-052335	5167.008 ± 0.029	12.639 ± 0.066	20.181 ± 3.136
4584	J132029-052335	5166.152 ± 0.078	12.447 ± 0.088	27.621 ± 6.152
4585	J132029-052335	5163.726 ± 0.017	12.785 ± 0.024	22.728 ± 1.424
4586	J132029-052335	5162.419 ± 0.014	13.192 ± 0.012	36.496 ± 1.212
4587	J132029-052335	5159.068 ± 0.035	12.015 ± 0.087	11.729 ± 3.149
4588	J132029-052335	5157.735 ± 0.031	12.233 ± 0.058	16.071 ± 2.681
4589	J132029-052335	5156.535 ± 0.009	13.126 ± 0.011	24.280 ± 0.756
4590	J132029-052335	5155.589 ± 0.019	12.470 ± 0.038	15.339 ± 1.670
4591	J132029-052335	5154.377 ± 0.072	12.441 ± 0.116	23.643 ± 7.488
4592	J132029-052335	5151.214 ± 0.123	13.123 ± 0.065	65.455 ± 4.975
4593	J132029-052335	5151.130 ± 0.003	13.690 ± 0.011	12.148 ± 0.262
4594	J132029-052335	5150.530 ± 0.017	13.370 ± 0.041	27.213 ± 1.703
4595	J132029-052335	5148.640 ± 0.007	13.276 ± 0.010	24.799 ± 0.649
4596	J132029-052335	5147.326 ± 0.014	13.230 ± 0.016	33.999 ± 1.551
4597	J132029-052335	5146.248 ± 0.131	12.923 ± 1.434	18.395 ± 9.202
4598	J132029-052335	5145.943 ± 3.309	12.347 ± 5.507	24.740 ± 89.877
4599	J132029-052335	5144.529 ± 0.149	12.327 ± 0.112	42.571 ± 13.023
4600	J132029-052335	5141.393 ± 0.048	11.931 ± 0.119	12.471 ± 4.714
4601	J132029-052335	5140.572 ± 0.111	11.799 ± 0.407	12.158 ± 13.633
4602	J132029-052335	5140.156 ± 0.116	11.764 ± 0.370	10.756 ± 8.957
4603	J132029-052335	5139.395 ± 0.049	12.149 ± 0.076	20.036 ± 4.468
4604	J132029-052335	5136.278 ± 0.010	12.899 ± 0.014	22.877 ± 0.857
4605	J132029-052335	5133.563 ± 0.043	12.142 ± 0.068	19.257 ± 3.634

Table E.1. *Continued*

4606	J132029-052335	5130.706 ± 0.076	12.239 ± 0.070	33.415 ± 6.337
4607	J132029-052335	5128.244 ± 0.046	12.689 ± 0.030	47.946 ± 3.843
4608	J132029-052335	5124.025 ± 0.013	12.685 ± 0.020	20.130 ± 1.099
4609	J132029-052335	5120.251 ± 0.013	12.400 ± 0.059	11.877 ± 1.430
4610	J132029-052335	5119.075 ± 0.314	12.843 ± 0.169	61.222 ± 17.536
4611	J132029-052335	5118.711 ± 0.027	12.494 ± 0.139	12.028 ± 2.544
4612	J132029-052335	5118.162 ± 0.248	12.744 ± 0.787	10.875 ± 11.349
4613	J132029-052335	5115.801 ± 0.010	13.411 ± 0.012	29.459 ± 0.726
4614	J132029-052335	5113.994 ± 0.072	13.231 ± 0.078	48.781 ± 10.000
4615	J132029-052335	5112.969 ± 0.010	13.985 ± 0.017	22.317 ± 0.614
4616	J132029-052335	5112.121 ± 0.064	12.556 ± 0.107	19.325 ± 3.902
4617	J132029-052335	5110.588 ± 0.012	13.133 ± 0.011	36.427 ± 1.119
4618	J132029-052335	5108.967 ± 0.005	13.430 ± 0.006	26.322 ± 0.476
4619	J132029-052335	5107.885 ± 0.003	13.591 ± 0.005	22.033 ± 0.290
4620	J132029-052335	5106.444 ± 0.017	13.326 ± 0.081	12.111 ± 1.639
4621	J132029-052335	5106.324 ± 0.005	14.089 ± 0.011	31.711 ± 0.540
4622	J132029-052335	5104.588 ± 0.005	13.475 ± 0.010	21.992 ± 0.691
4623	J132029-052335	5103.808 ± 0.072	12.113 ± 0.195	17.282 ± 7.439
4624	J132029-052335	5102.776 ± 0.224	12.496 ± 0.276	30.317 ± 16.704
4625	J132029-052335	5102.036 ± 0.009	13.869 ± 0.025	19.562 ± 0.757
4626	J132029-052335	5101.466 ± 0.040	13.348 ± 0.063	22.051 ± 1.710
4627	J132029-052335	5099.904 ± 0.040	12.917 ± 0.036	41.772 ± 4.255
4628	J132029-052335	5097.959 ± 0.084	12.786 ± 0.096	40.837 ± 9.343
4629	J132029-052335	5096.703 ± 0.082	12.629 ± 0.157	33.797 ± 10.915
4630	J132029-052335	5095.640 ± 0.046	12.722 ± 0.111	25.102 ± 5.051
4631	J132029-052335	5094.543 ± 0.070	13.291 ± 0.096	32.338 ± 6.018
4632	J132029-052335	5093.916 ± 0.010	13.521 ± 0.050	19.240 ± 0.828
4633	J132029-052335	5092.976 ± 0.029	13.263 ± 0.030	43.136 ± 3.373
4634	J132029-052335	5091.558 ± 0.004	13.676 ± 0.006	24.907 ± 0.355
4635	J132029-052335	5090.337 ± 0.020	12.953 ± 0.028	30.146 ± 2.390
4636	J132029-052335	5088.933 ± 0.004	14.311 ± 0.020	19.018 ± 0.641
4637	J132029-052335	5088.557 ± 0.063	13.678 ± 0.060	37.909 ± 1.965
4638	J132029-052335	5086.906 ± 0.133	12.844 ± 0.196	49.624 ± 23.089
4639	J132029-052335	5085.824 ± 0.008	13.634 ± 0.026	25.744 ± 0.968
4640	J132029-052335	5085.030 ± 0.040	12.673 ± 0.126	19.812 ± 4.700
4641	J132029-052335	5084.310 ± 0.019	13.069 ± 0.046	22.583 ± 1.690
4642	J132029-052335	5083.066 ± 0.019	13.108 ± 0.201	35.868 ± 5.762
4643	J132029-052335	5081.335 ± 0.269	13.503 ± 0.263	93.979 ± 56.136
4644	J132029-052335	5079.660 ± 0.003	14.766 ± 0.015	38.470 ± 0.869
4645	J132029-052335	5077.662 ± 0.030	13.439 ± 0.036	31.211 ± 2.083
4646	J132029-052335	5076.880 ± 0.005	14.037 ± 0.011	20.937 ± 0.541
4647	J132029-052335	5076.123 ± 0.040	13.152 ± 0.048	27.329 ± 2.257
4648	J132029-052335	5073.267 ± 0.032	13.230 ± 0.110	17.998 ± 2.240
4649	J132029-052335	5073.734 ± 0.140	13.431 ± 0.084	54.387 ± 5.992

Table E.1. *Continued*

4650	J132029-052335	5072.476 ± 0.007	14.502 ± 0.019	24.476 ± 0.451
4651	J132029-052335	5071.284 ± 0.035	12.169 ± 0.080	14.892 ± 3.518
4652	J132029-052335	5070.306 ± 0.002	13.927 ± 0.004	22.699 ± 0.203
4653	J132029-052335	5068.606 ± 0.122	12.177 ± 0.220	23.995 ± 13.468
4654	J132029-052335	5067.317 ± 0.011	13.451 ± 0.013	34.789 ± 1.246
4655	J132029-052335	5066.070 ± 0.083	13.283 ± 0.234	29.038 ± 4.170
4656	J132029-052335	5065.162 ± 0.093	13.415 ± 0.285	42.521 ± 24.531
4657	J132029-052335	5064.223 ± 0.021	13.739 ± 0.058	26.975 ± 0.943
4658	J132029-052335	5062.434 ± 0.040	12.635 ± 0.039	33.994 ± 3.854
4659	J132029-052335	5061.229 ± 0.046	12.845 ± 0.088	23.226 ± 2.892
4660	J132029-052335	5060.433 ± 0.018	13.428 ± 0.026	29.734 ± 1.735
4661	J132029-052335	5059.312 ± 0.061	12.476 ± 0.074	27.181 ± 4.706
4662	J132029-052335	5055.769 ± 0.018	12.676 ± 0.039	18.683 ± 1.479
4663	J132029-052335	5054.581 ± 0.069	13.275 ± 0.091	38.630 ± 4.584
4664	J132029-052335	5053.767 ± 0.048	12.929 ± 0.312	25.336 ± 5.597
4665	J132029-052335	5053.093 ± 0.350	13.265 ± 0.217	59.215 ± 20.811
4666	J132029-052335	5051.368 ± 0.012	13.370 ± 0.033	27.394 ± 1.139
4667	J132029-052335	5050.209 ± 0.039	13.224 ± 0.049	48.995 ± 6.071
4668	J132029-052335	5048.798 ± 0.007	13.601 ± 0.009	29.502 ± 0.470
4669	J132029-052335	5047.117 ± 0.027	13.807 ± 0.067	19.747 ± 0.762
4670	J132029-052335	5046.675 ± 0.187	13.106 ± 0.342	21.959 ± 7.329
4671	J132029-052335	5045.978 ± 0.034	12.112 ± 0.183	10.307 ± 3.408
4672	J132029-052335	5045.348 ± 0.017	13.012 ± 0.019	27.785 ± 1.485
4673	J132029-052335	5043.504 ± 0.012	13.077 ± 0.011	33.323 ± 0.992
4674	J132029-052335	5040.570 ± 0.138	12.589 ± 0.082	53.504 ± 10.972
4675	J132029-052335	5039.085 ± 0.032	13.497 ± 0.040	31.428 ± 2.059
4676	J132029-052335	5038.186 ± 0.087	13.804 ± 0.154	24.447 ± 4.119
4677	J132029-052335	5037.087 ± 0.028	15.319 ± 0.059	31.958 ± 0.649
4678	J132029-052335	5034.735 ± 0.010	13.849 ± 0.008	36.840 ± 0.693
4679	J132029-052335	5033.807 ± 0.008	13.533 ± 0.017	23.025 ± 0.674
4680	J132029-052335	5032.712 ± 0.006	13.867 ± 0.009	22.244 ± 0.473
4681	J132029-052335	5031.996 ± 0.111	12.433 ± 0.271	21.294 ± 11.594
4682	J132029-052335	5030.625 ± 0.008	14.931 ± 0.042	28.211 ± 0.792
4683	J132029-052335	5029.727 ± 0.095	13.647 ± 0.088	38.031 ± 3.483
4684	J132029-052335	5027.421 ± 0.057	13.328 ± 0.042	45.949 ± 3.619
4685	J132029-052335	5026.438 ± 0.014	13.485 ± 0.028	29.217 ± 0.959
4686	J132029-052335	5025.329 ± 0.058	12.092 ± 0.099	19.014 ± 5.155
4687	J132029-052335	5023.789 ± 0.224	13.409 ± 0.358	26.497 ± 5.676
4688	J132029-052335	5023.562 ± 0.019	13.137 ± 0.537	15.815 ± 5.016
4689	J132029-052335	5022.742 ± 0.020	14.152 ± 0.015	41.037 ± 0.924
4690	J132029-052335	5021.298 ± 0.048	12.241 ± 0.378	11.935 ± 4.676
4691	J132029-052335	5020.685 ± 0.094	13.128 ± 0.196	26.444 ± 10.864
4692	J132029-052335	5020.170 ± 0.081	12.589 ± 0.532	15.931 ± 6.157
4693	J132029-052335	5019.295 ± 0.008	13.862 ± 0.017	24.734 ± 0.616

Table E.1. *Continued*

4694	J132029-052335	5018.552 ± 0.071	13.249 ± 0.069	34.381 ± 3.274
4695	J132029-052335	5016.835 ± 0.004	13.369 ± 0.006	22.789 ± 0.354
4696	J132029-052335	5014.553 ± 0.059	13.437 ± 0.121	22.252 ± 1.945
4697	J132029-052335	5013.597 ± 0.017	14.776 ± 0.025	34.888 ± 0.617
4698	J132029-052335	5011.072 ± 1.090	13.409 ± 1.123	41.180 ± 26.853
4699	J132029-052335	5010.724 ± 0.010	14.133 ± 0.191	25.622 ± 2.754
4700	J132029-052335	5009.779 ± 0.127	12.932 ± 0.305	24.046 ± 5.758
4701	J132029-052335	5008.751 ± 0.018	13.212 ± 0.027	32.520 ± 2.062
4702	J132029-052335	5007.083 ± 0.048	13.216 ± 0.045	49.923 ± 5.585
4703	J132029-052335	5005.790 ± 0.012	13.979 ± 0.017	29.400 ± 0.911
4704	J132029-052335	5004.945 ± 0.021	13.637 ± 0.033	26.789 ± 1.463
4705	J132029-052335	5004.139 ± 0.041	12.262 ± 0.143	14.042 ± 3.922
4706	J132029-052335	5003.366 ± 0.013	13.117 ± 0.023	23.437 ± 1.250
4707	J132029-052335	5002.458 ± 0.042	12.887 ± 0.378	18.142 ± 4.888
4708	J132029-052335	5001.334 ± 0.754	14.012 ± 0.631	44.520 ± 34.051
4709	J132029-052335	5000.690 ± 0.019	15.096 ± 0.240	23.215 ± 4.088
4710	J132029-052335	4999.724 ± 0.029	13.893 ± 0.038	28.443 ± 1.262
4711	J132029-052335	4998.260 ± 0.008	13.395 ± 0.008	33.405 ± 0.760
4712	J132029-052335	4996.164 ± 0.059	13.542 ± 0.077	28.018 ± 2.231
4713	J132029-052335	4995.635 ± 0.039	13.431 ± 0.099	22.732 ± 1.317
4714	J132029-052335	4993.777 ± 0.081	12.138 ± 0.092	27.735 ± 6.937
4715	J132029-052335	4991.809 ± 0.035	13.272 ± 0.188	18.195 ± 1.847
4716	J132029-052335	4991.313 ± 0.085	13.514 ± 0.158	27.728 ± 6.206
4717	J132029-052335	4990.313 ± 0.012	13.793 ± 0.081	24.751 ± 1.480
4718	J132029-052335	4989.956 ± 0.810	13.181 ± 0.526	56.759 ± 26.676
4719	J132029-052335	4984.285 ± 0.033	13.000 ± 0.025	42.120 ± 2.921
4720	J132029-052335	4982.905 ± 0.007	14.137 ± 0.009	26.142 ± 0.484
4721	J132029-052335	4981.993 ± 0.012	13.333 ± 0.223	13.896 ± 2.632
4722	J132029-052335	4981.611 ± 0.060	13.907 ± 0.074	29.786 ± 3.259
4723	J132029-052335	4980.576 ± 0.030	13.235 ± 0.093	21.738 ± 2.866
4724	J132029-052335	4979.596 ± 0.065	14.015 ± 0.082	32.475 ± 4.632
4725	J132029-052335	4978.789 ± 0.026	14.451 ± 0.052	24.785 ± 0.653
4726	J132029-052335	4975.840 ± 0.031	13.622 ± 0.028	35.095 ± 1.476
4727	J132029-052335	4974.450 ± 0.004	15.766 ± 0.085	30.308 ± 0.783
4728	J132029-052335	4972.666 ± 0.044	12.838 ± 0.076	35.186 ± 7.359
4729	J132029-052335	4971.550 ± 0.113	13.012 ± 0.231	22.869 ± 5.454
4730	J132029-052335	4970.997 ± 0.101	13.118 ± 0.176	23.676 ± 4.797
4731	J132029-052335	4969.471 ± 0.004	13.802 ± 0.006	23.268 ± 0.316
4732	J132029-052335	4968.488 ± 0.048	11.995 ± 0.489	13.275 ± 8.435
4733	J132029-052335	4967.731 ± 0.100	12.947 ± 0.150	53.753 ± 20.447
4734	J132029-052335	4966.968 ± 0.036	12.182 ± 0.226	10.178 ± 3.602
4735	J132029-052335	4966.472 ± 0.014	13.005 ± 0.050	17.617 ± 1.921
4736	J132029-052335	4965.674 ± 0.004	14.002 ± 0.006	22.454 ± 0.345
4737	J132029-052335	4964.852 ± 0.022	12.241 ± 0.095	10.230 ± 2.301

Table E.1. *Continued*

4738	J132029-052335	4964.101 ± 0.047	13.002 ± 0.091	27.887 ± 3.396
4739	J132029-052335	4963.186 ± 0.192	12.644 ± 0.242	37.921 ± 17.949
4740	J132029-052335	4960.467 ± 0.451	14.166 ± 0.337	67.720 ± 10.398
4741	J132029-052335	4960.537 ± 0.026	14.769 ± 0.061	30.455 ± 2.443
4742	J132029-052335	4959.107 ± 0.246	13.540 ± 0.944	38.836 ± 28.638
4743	J132029-052335	4958.060 ± 0.325	13.580 ± 0.275	47.691 ± 17.437
4744	J132029-052335	4956.782 ± 0.014	13.401 ± 0.048	22.579 ± 1.680
4745	J132029-052335	4955.659 ± 0.004	14.956 ± 0.044	25.889 ± 0.619
4746	J132029-052335	4953.573 ± 0.373	13.244 ± 0.227	60.388 ± 18.406
4747	J132029-052335	4953.388 ± 0.035	13.617 ± 0.071	22.710 ± 1.929
4748	J132029-052335	4952.817 ± 0.059	13.351 ± 0.185	22.519 ± 4.098
4749	J132029-052335	4951.402 ± 0.094	13.053 ± 0.168	32.172 ± 9.527
4750	J132029-052335	4949.202 ± 0.008	16.013 ± 0.044	51.938 ± 0.685
4751	J132029-052335	4942.266 ± 0.021	12.922 ± 0.020	33.805 ± 1.786
4752	J132029-052335	4938.964 ± 0.137	13.536 ± 0.116	45.886 ± 4.098
4753	J132029-052335	4938.695 ± 0.011	13.609 ± 0.070	19.832 ± 1.275
4754	J132029-052335	4937.926 ± 0.107	12.118 ± 0.831	14.870 ± 12.220
4755	J132029-052335	4934.616 ± 0.037	13.486 ± 0.086	21.480 ± 1.407
4756	J132029-052335	4934.089 ± 0.039	13.690 ± 0.054	26.135 ± 1.476
4757	J132029-052335	4932.226 ± 0.034	12.565 ± 0.110	16.070 ± 5.079
4758	J132029-052335	4931.260 ± 0.191	12.420 ± 0.414	22.281 ± 15.760
4759	J132029-052335	4930.512 ± 0.024	12.794 ± 0.784	16.552 ± 7.654
4760	J132029-052335	4930.225 ± 0.403	13.066 ± 0.499	30.420 ± 12.748
4761	J132029-052335	4928.627 ± 0.064	11.993 ± 0.115	17.366 ± 5.666
4762	J132029-052335	4924.723 ± 0.074	12.312 ± 0.074	31.988 ± 6.407
4763	J132029-052335	4922.879 ± 0.092	12.102 ± 0.122	24.872 ± 8.658
4764	J132029-052335	4921.254 ± 0.002	15.082 ± 0.030	29.806 ± 0.366
4765	J132029-052335	4919.410 ± 0.002	14.228 ± 0.011	21.717 ± 0.229
4766	J132029-052335	4917.768 ± 0.097	12.323 ± 0.172	19.850 ± 6.457
4767	J132029-052335	4917.108 ± 0.016	13.184 ± 0.026	21.785 ± 1.285
4768	J132029-052335	4916.026 ± 0.083	12.136 ± 0.119	24.318 ± 8.405
4769	J132029-052335	4914.702 ± 0.041	12.190 ± 0.224	13.922 ± 4.820
4770	J132029-052335	4914.380 ± 0.060	12.946 ± 0.046	41.429 ± 3.320
4771	J132029-052335	4912.308 ± 0.012	12.951 ± 0.043	19.520 ± 1.372
4772	J132029-052335	4911.543 ± 0.049	13.452 ± 0.021	79.257 ± 3.275
4773	J132029-052335	4907.856 ± 0.050	12.169 ± 0.105	17.204 ± 4.738
4774	J132029-052335	4906.870 ± 0.075	12.389 ± 0.100	29.793 ± 8.707
4775	J132029-052335	4909.034 ± 0.023	12.897 ± 0.026	32.772 ± 2.184
4776	J132029-052335	4905.702 ± 0.036	12.717 ± 0.047	28.271 ± 3.490
4777	J132029-052335	4903.483 ± 0.155	12.964 ± 0.084	64.871 ± 12.537
4778	J132029-052335	4902.272 ± 0.011	13.444 ± 0.028	28.788 ± 1.200
4779	J132029-052335	4901.090 ± 0.026	13.184 ± 0.042	34.712 ± 3.865
4780	J132029-052335	4899.713 ± 0.003	15.261 ± 0.041	27.099 ± 0.412
4781	J132029-052335	4898.147 ± 0.075	11.684 ± 0.195	11.999 ± 7.235

Table E.1. *Continued*

4782	J132029-052335	4897.521 ± 0.090	11.674 ± 0.208	13.649 ± 8.583
4783	J132029-052335	4890.038 ± 0.078	13.026 ± 0.029	88.106 ± 5.606
4784	J132029-052335	4889.508 ± 0.012	12.856 ± 0.031	20.356 ± 1.227
4785	J132029-052335	4886.925 ± 0.056	11.878 ± 0.125	14.054 ± 5.093
4786	J132029-052335	4885.468 ± 0.002	13.845 ± 0.004	23.812 ± 0.192
4787	J132029-052335	4882.207 ± 0.007	15.011 ± 0.013	55.645 ± 0.541
4788	J132029-052335	4880.312 ± 0.036	13.221 ± 0.079	32.892 ± 5.502
4789	J132029-052335	4879.446 ± 0.019	13.211 ± 0.036	22.678 ± 1.094
4790	J132029-052335	4877.487 ± 0.021	12.623 ± 0.045	18.881 ± 2.739
4791	J132029-052335	4876.418 ± 0.034	12.466 ± 0.055	22.010 ± 3.604
4792	J132029-052335	4874.737 ± 0.003	14.188 ± 0.004	41.063 ± 0.287
4793	J132029-052335	4873.050 ± 0.007	13.343 ± 0.011	19.820 ± 0.573
4794	J132029-052335	4872.160 ± 0.033	13.075 ± 0.059	24.404 ± 3.456
4795	J132029-052335	4871.634 ± 0.050	12.358 ± 0.313	13.173 ± 5.968
4796	J132029-052335	4871.004 ± 0.182	12.820 ± 0.390	18.042 ± 11.368
4797	J132029-052335	4870.676 ± 0.061	12.671 ± 0.722	11.311 ± 7.845
4798	J132029-052335	4870.378 ± 0.136	12.528 ± 0.404	12.302 ± 5.609
4799	J012403+004432	5752.966 ± 0.007	13.752 ± 0.005	34.864 ± 0.519
4800	J012403+004432	5752.045 ± 0.018	12.539 ± 0.067	11.202 ± 1.612
4801	J012403+004432	5751.192 ± 0.060	13.092 ± 0.088	20.337 ± 3.129
4802	J012403+004432	5750.633 ± 0.128	12.766 ± 0.486	13.834 ± 9.862
4803	J012403+004432	5747.132 ± 0.007	13.641 ± 0.007	26.000 ± 0.452
4804	J012403+004432	5746.145 ± 0.043	12.571 ± 0.073	20.501 ± 3.462
4805	J012403+004432	5744.759 ± 0.008	13.550 ± 0.006	35.372 ± 0.691
4806	J012403+004432	5743.396 ± 0.034	12.421 ± 0.079	13.462 ± 2.493
4807	J012403+004432	5742.434 ± 0.003	14.224 ± 0.011	23.306 ± 0.338
4808	J012403+004432	5740.887 ± 0.167	12.634 ± 0.211	22.695 ± 7.307
4809	J012403+004432	5740.502 ± 0.034	12.258 ± 0.464	10.887 ± 5.037
4810	J012403+004432	5738.931 ± 0.002	14.257 ± 0.012	22.754 ± 0.243
4811	J012403+004432	5737.345 ± 0.004	13.829 ± 0.005	21.827 ± 0.269
4812	J012403+004432	5736.267 ± 0.005	13.454 ± 0.007	19.355 ± 0.373
4813	J012403+004432	5735.034 ± 0.047	12.036 ± 0.090	13.925 ± 3.646
4814	J012403+004432	5732.320 ± 0.038	13.554 ± 0.021	50.705 ± 1.568
4815	J012403+004432	5731.846 ± 0.042	12.326 ± 0.226	14.393 ± 4.841
4816	J012403+004432	5730.587 ± 0.064	12.691 ± 0.129	22.444 ± 5.962
4817	J012403+004432	5729.672 ± 0.007	13.918 ± 0.010	21.060 ± 0.726
4818	J012403+004432	5728.881 ± 0.008	13.596 ± 0.019	15.443 ± 0.605
4819	J012403+004432	5727.850 ± 0.063	13.277 ± 0.081	32.257 ± 5.883
4820	J012403+004432	5727.173 ± 0.055	12.500 ± 0.376	16.072 ± 5.298
4821	J012403+004432	5725.695 ± 0.055	11.865 ± 0.127	11.433 ± 4.437
4822	J012403+004432	5723.992 ± 0.017	14.027 ± 0.013	31.957 ± 0.877
4823	J012403+004432	5722.432 ± 0.008	15.300 ± 0.049	28.491 ± 0.515
4824	J012403+004432	5719.404 ± 0.014	12.864 ± 0.036	15.546 ± 1.760
4825	J012403+004432	5717.450 ± 0.115	12.094 ± 0.186	17.939 ± 8.968

Table E.1. *Continued*

4826	J012403+004432	5716.833 ± 0.180	11.989 ± 0.597	11.230 ± 14.478
4827	J012403+004432	5715.626 ± 0.516	13.273 ± 0.469	36.912 ± 19.803
4828	J012403+004432	5714.952 ± 0.080	13.496 ± 0.270	26.933 ± 3.037
4829	J012403+004432	5713.576 ± 0.079	13.171 ± 0.196	17.767 ± 2.346
4830	J012403+004432	5713.014 ± 0.059	13.389 ± 0.162	21.601 ± 6.309
4831	J012403+004432	5712.223 ± 0.049	12.973 ± 0.232	18.556 ± 8.215
4832	J012403+004432	5711.726 ± 0.058	12.615 ± 0.323	12.121 ± 4.283
4833	J012403+004432	5711.108 ± 0.010	13.647 ± 0.011	22.220 ± 0.560
4834	J012403+004432	5708.697 ± 0.003	15.304 ± 0.041	29.218 ± 0.427
4835	J012403+004432	5706.865 ± 0.005	13.819 ± 0.005	26.772 ± 0.423
4836	J012403+004432	5705.513 ± 0.025	12.694 ± 0.033	22.791 ± 2.253
4837	J012403+004432	5703.958 ± 0.003	13.740 ± 0.006	18.717 ± 0.243
4838	J012403+004432	5702.832 ± 0.008	12.968 ± 0.025	10.423 ± 0.780
4839	J012403+004432	5702.264 ± 0.007	13.217 ± 0.013	14.624 ± 0.584
4840	J012403+004432	5700.970 ± 0.045	12.296 ± 0.094	14.451 ± 3.331
4841	J012403+004432	5700.111 ± 0.006	13.621 ± 0.006	23.670 ± 0.427
4842	J012403+004432	5697.091 ± 0.548	12.367 ± 0.674	25.424 ± 20.127
4843	J012403+004432	5696.509 ± 0.098	12.849 ± 0.221	20.572 ± 3.366
4844	J012403+004432	5694.857 ± 0.038	12.450 ± 0.082	14.562 ± 2.551
4845	J012403+004432	5694.157 ± 0.039	12.686 ± 0.051	21.006 ± 2.812
4846	J012403+004432	5692.392 ± 0.068	12.824 ± 0.353	18.746 ± 4.122
4847	J012403+004432	5691.857 ± 0.178	13.119 ± 0.183	29.325 ± 6.640
4848	J012403+004432	5690.239 ± 0.010	13.185 ± 0.011	23.161 ± 0.725
4849	J012403+004432	5688.722 ± 0.101	12.449 ± 0.218	15.854 ± 4.774
4850	J012403+004432	5686.574 ± 0.762	12.702 ± 1.192	33.295 ± 82.331
4851	J012403+004432	5685.651 ± 0.310	12.359 ± 1.221	16.840 ± 16.277
4852	J012403+004432	5678.798 ± 0.040	13.950 ± 0.023	50.047 ± 1.411
4853	J012403+004432	5687.810 ± 0.010	14.232 ± 0.014	24.747 ± 1.147
4854	J012403+004432	5682.580 ± 0.005	16.304 ± 0.097	55.674 ± 1.350
4855	J012403+004432	5678.179 ± 0.007	14.875 ± 0.090	19.574 ± 0.802
4856	J012403+004432	5675.405 ± 0.025	13.804 ± 0.029	25.033 ± 0.923
4857	J012403+004432	5674.399 ± 1.091	13.338 ± 1.581	25.699 ± 38.206
4858	J012403+004432	5674.001 ± 0.282	13.164 ± 2.243	19.085 ± 14.136
4859	J012403+004432	5670.249 ± 0.037	13.633 ± 0.026	64.463 ± 2.373
4860	J012403+004432	5670.555 ± 0.005	13.843 ± 0.014	18.497 ± 0.516
4861	J012403+004432	5669.337 ± 0.012	13.032 ± 0.042	14.522 ± 1.096
4862	J012403+004432	5668.028 ± 0.012	13.375 ± 0.023	14.466 ± 0.774
4863	J012403+004432	5667.145 ± 0.035	12.388 ± 0.118	11.657 ± 3.761
4864	J012403+004432	5666.356 ± 0.006	13.885 ± 0.009	19.543 ± 0.601
4865	J012403+004432	5665.580 ± 0.021	13.522 ± 0.170	13.421 ± 1.926
4866	J012403+004432	5665.175 ± 0.501	12.962 ± 0.676	24.002 ± 17.676
4867	J012403+004432	5664.192 ± 0.072	12.105 ± 0.175	13.132 ± 5.122
4868	J012403+004432	5662.728 ± 0.033	13.332 ± 0.081	14.434 ± 1.094
4869	J012403+004432	5662.294 ± 0.104	12.879 ± 0.283	16.022 ± 6.159

Table E.1. *Continued*

4870	J012403+004432	5661.562 ± 0.062	13.022 ± 0.064	27.610 ± 3.690
4871	J012403+004432	5660.259 ± 0.040	13.311 ± 0.135	14.436 ± 1.330
4872	J012403+004432	5659.776 ± 0.034	13.655 ± 0.084	19.568 ± 2.819
4873	J012403+004432	5659.029 ± 0.051	13.359 ± 0.059	24.909 ± 2.189
4874	J012403+004432	5657.476 ± 0.005	13.506 ± 0.007	23.555 ± 0.399
4875	J012403+004432	5654.761 ± 0.031	14.379 ± 0.035	32.089 ± 0.842
4876	J012403+004432	5653.531 ± 0.033	14.300 ± 0.033	32.056 ± 1.073
4877	J012403+004432	5651.456 ± 0.023	13.743 ± 0.043	17.569 ± 1.049
4878	J012403+004432	5650.833 ± 0.024	13.886 ± 0.032	21.097 ± 0.849
4879	J012403+004432	5648.943 ± 0.021	13.432 ± 0.021	28.726 ± 1.547
4880	J012403+004432	5647.761 ± 0.012	14.352 ± 0.037	22.142 ± 0.948
4881	J012403+004432	5646.371 ± 0.016	14.373 ± 0.011	42.635 ± 0.732
4882	J012403+004432	5643.443 ± 0.036	12.839 ± 0.039	31.158 ± 3.743
4883	J012403+004432	5642.029 ± 0.006	13.614 ± 0.009	17.649 ± 0.499
4884	J012403+004432	5636.701 ± 0.009	13.727 ± 0.011	21.928 ± 0.519
4885	J012403+004432	5635.752 ± 0.013	13.584 ± 0.015	25.252 ± 0.972
4886	J012403+004432	5634.189 ± 0.042	13.108 ± 0.041	35.666 ± 3.939
4887	J012403+004432	5632.875 ± 0.116	12.837 ± 0.231	19.470 ± 5.734
4888	J012403+004432	5632.268 ± 0.029	13.573 ± 0.040	21.242 ± 1.159
4889	J012403+004432	5629.639 ± 0.042	13.683 ± 0.096	21.464 ± 0.789
4890	J012403+004432	5629.436 ± 0.019	13.558 ± 0.126	13.590 ± 1.651
4891	J012403+004432	5628.411 ± 0.115	11.695 ± 0.261	12.076 ± 9.637
4892	J012403+004432	5627.315 ± 0.020	12.897 ± 0.023	24.326 ± 1.538
4893	J012403+004432	5624.273 ± 0.072	13.214 ± 0.098	29.453 ± 2.636
4894	J012403+004432	5623.148 ± 0.010	13.968 ± 0.117	25.347 ± 2.195
4895	J012403+004432	5622.627 ± 0.430	13.608 ± 0.311	46.242 ± 11.627
4896	J012403+004432	5620.135 ± 0.030	13.625 ± 0.037	24.294 ± 1.276
4897	J012403+004432	5618.576 ± 0.012	15.206 ± 0.062	35.958 ± 1.106
4898	J012403+004432	5616.457 ± 0.016	13.444 ± 0.081	12.494 ± 1.455
4899	J012403+004432	5616.314 ± 0.017	13.783 ± 0.035	26.641 ± 0.995
4900	J012403+004432	5614.160 ± 0.285	12.957 ± 0.177	68.604 ± 29.795
4901	J012403+004432	5612.460 ± 0.004	14.982 ± 0.043	28.441 ± 0.583
4902	J012403+004432	5610.460 ± 0.031	12.860 ± 0.037	25.637 ± 2.734
4903	J012403+004432	5609.451 ± 0.055	12.960 ± 0.210	19.483 ± 3.598
4904	J012403+004432	5608.677 ± 0.090	13.236 ± 0.147	32.882 ± 11.199
4905	J012403+004432	5607.069 ± 0.033	12.880 ± 0.073	17.647 ± 2.620
4906	J012403+004432	5606.336 ± 0.020	13.345 ± 0.023	22.831 ± 1.196
4907	J012403+004432	5604.915 ± 0.008	13.268 ± 0.011	19.446 ± 0.619
4908	J012403+004432	5603.314 ± 0.005	14.328 ± 0.011	33.939 ± 0.566
4909	J012403+004432	5602.003 ± 0.037	12.720 ± 0.071	19.211 ± 2.994
4910	J012403+004432	5600.451 ± 0.032	13.874 ± 0.025	36.193 ± 1.607
4911	J012403+004432	5599.323 ± 0.013	14.345 ± 0.021	27.843 ± 0.607
4912	J012403+004432	5597.583 ± 0.059	13.010 ± 0.089	19.789 ± 2.859
4913	J012403+004432	5596.957 ± 0.079	12.663 ± 0.264	17.737 ± 9.394

Table E.1. *Continued*

4914	J012403+004432	5596.307 ± 0.022	12.878 ± 0.123	12.451 ± 2.243
4915	J012403+004432	5595.446 ± 0.180	13.509 ± 0.215	29.010 ± 10.352
4916	J012403+004432	5594.908 ± 0.054	13.062 ± 0.603	16.284 ± 9.324
4917	J012403+004432	5593.377 ± 0.009	13.873 ± 0.007	33.789 ± 0.766
4918	J012403+004432	5592.375 ± 0.012	13.327 ± 0.032	12.813 ± 0.954
4919	J012403+004432	5591.846 ± 0.222	12.356 ± 0.489	13.027 ± 11.336
4920	J012403+004432	5591.100 ± 0.086	12.213 ± 0.260	12.654 ± 6.359
4921	J012403+004432	5590.444 ± 0.179	12.726 ± 0.397	18.967 ± 12.579
4922	J012403+004432	5589.914 ± 0.143	12.787 ± 0.302	17.399 ± 5.403
4923	J012403+004432	5587.833 ± 0.076	12.574 ± 0.065	34.022 ± 6.362
4924	J012403+004432	5585.551 ± 0.042	12.430 ± 0.104	12.899 ± 3.643
4925	J012403+004432	5584.991 ± 0.029	12.657 ± 0.117	13.809 ± 3.104
4926	J012403+004432	5584.118 ± 0.035	13.256 ± 0.058	31.830 ± 4.465
4927	J012403+004432	5583.007 ± 0.142	12.694 ± 0.157	29.830 ± 8.421
4928	J012403+004432	5581.096 ± 0.169	13.485 ± 0.171	30.951 ± 5.569
4929	J012403+004432	5580.627 ± 0.038	13.316 ± 0.282	17.426 ± 4.539
4930	J012403+004432	5580.044 ± 0.059	13.037 ± 0.215	17.117 ± 6.540
4931	J012403+004432	5579.343 ± 0.036	13.343 ± 0.054	20.497 ± 2.777
4932	J012403+004432	5578.041 ± 0.016	13.783 ± 0.011	39.519 ± 1.022
4933	J012403+004432	5576.451 ± 0.047	12.573 ± 0.115	16.804 ± 3.739
4934	J012403+004432	5575.130 ± 0.070	13.432 ± 0.058	43.817 ± 5.897
4935	J012403+004432	5574.133 ± 0.019	13.401 ± 0.060	23.130 ± 1.719
4936	J012403+004432	5572.919 ± 0.023	13.471 ± 0.034	34.995 ± 3.230
4937	J012403+004432	5571.856 ± 0.035	13.069 ± 0.060	23.161 ± 2.140
4938	J012403+004432	5569.416 ± 0.070	13.415 ± 0.029	65.160 ± 7.715
4939	J012403+004432	5569.482 ± 0.012	13.168 ± 0.049	17.879 ± 1.308
4940	J012403+004432	5568.146 ± 0.062	12.967 ± 0.160	15.207 ± 3.069
4941	J012403+004432	5567.565 ± 0.016	13.706 ± 0.040	18.647 ± 1.724
4942	J012403+004432	5566.660 ± 0.066	13.642 ± 0.153	24.693 ± 4.236
4943	J012403+004432	5565.876 ± 0.244	13.320 ± 0.339	30.980 ± 17.108
4944	J012403+004432	5564.773 ± 0.113	12.994 ± 0.150	25.676 ± 5.251
4945	J012403+004432	5560.880 ± 0.595	13.655 ± 0.246	77.119 ± 18.435
4946	J012403+004432	5560.222 ± 0.020	15.376 ± 0.177	24.099 ± 1.743
4947	J012403+004432	5558.593 ± 0.020	15.293 ± 0.438	19.994 ± 3.335
4948	J012403+004432	5556.957 ± 0.091	14.322 ± 0.060	52.473 ± 6.154
4949	J012403+004432	5556.235 ± 0.029	13.819 ± 0.122	19.004 ± 3.099
4950	J012403+004432	5554.681 ± 0.084	13.705 ± 0.189	38.736 ± 15.603
4951	J012403+004432	5553.144 ± 0.040	15.121 ± 0.413	23.256 ± 7.759
4952	J012403+004432	5552.842 ± 0.540	14.422 ± 0.692	36.902 ± 8.534
4953	J012403+004432	5550.736 ± 0.093	12.187 ± 0.144	19.716 ± 8.314
4954	J012403+004432	5549.934 ± 0.046	12.370 ± 0.100	15.491 ± 4.282
4955	J012403+004432	5548.934 ± 0.007	13.549 ± 0.008	23.898 ± 0.530
4956	J012403+004432	5547.428 ± 0.055	12.231 ± 0.462	10.079 ± 6.463
4957	J012403+004432	5546.747 ± 0.015	13.869 ± 0.021	30.068 ± 1.836

Table E.1. *Continued*

4958	J012403+004432	5545.814 ± 0.031	13.970 ± 0.079	14.741 ± 1.549
4959	J012403+004432	5544.924 ± 0.036	14.416 ± 0.042	30.386 ± 1.563
4960	J012403+004432	5543.529 ± 0.033	12.911 ± 0.046	21.254 ± 2.363
4961	J012403+004432	5540.889 ± 0.049	12.476 ± 0.069	21.927 ± 4.598
4962	J012403+004432	5539.125 ± 0.108	12.860 ± 0.124	29.551 ± 6.688
4963	J012403+004432	5538.048 ± 0.024	13.575 ± 0.028	31.623 ± 2.001
4964	J012403+004432	5535.886 ± 0.010	14.571 ± 0.020	43.484 ± 1.135
4965	J012403+004432	5534.454 ± 0.033	12.989 ± 0.578	11.268 ± 5.059
4966	J012403+004432	5534.025 ± 0.132	13.416 ± 0.377	23.334 ± 16.987
4967	J012403+004432	5530.892 ± 0.023	17.156 ± 0.510	55.403 ± 5.382
4968	J012403+004432	5526.936 ± 0.024	16.382 ± 0.752	20.759 ± 3.200
4969	J012403+004432	5526.281 ± 0.411	14.049 ± 0.457	34.703 ± 8.702
4970	J012403+004432	5524.114 ± 0.077	12.405 ± 0.184	17.209 ± 5.193
4971	J012403+004432	5523.209 ± 0.028	13.240 ± 0.044	31.053 ± 3.912
4972	J012403+004432	5521.943 ± 0.007	14.057 ± 0.012	24.568 ± 0.510
4973	J012403+004432	5520.660 ± 0.090	12.131 ± 0.181	15.890 ± 7.590
4974	J012403+004432	5519.757 ± 0.023	13.031 ± 0.034	24.201 ± 2.387
4975	J012403+004432	5518.400 ± 0.008	13.797 ± 0.007	32.574 ± 0.625
4976	J012403+004432	5515.479 ± 0.005	13.466 ± 0.010	16.685 ± 0.402
4977	J012403+004432	5514.167 ± 0.005	14.196 ± 0.020	21.391 ± 0.476
4978	J012403+004432	5512.837 ± 0.005	14.294 ± 0.030	21.658 ± 0.682
4979	J012403+004432	5511.673 ± 0.013	13.495 ± 0.013	25.536 ± 0.908
4980	J012403+004432	5509.590 ± 0.037	12.863 ± 0.032	32.894 ± 2.953
4981	J012403+004432	5507.869 ± 0.007	14.105 ± 0.013	22.719 ± 0.526
4982	J012403+004432	5506.670 ± 0.013	13.419 ± 0.018	19.141 ± 0.889
4983	J012403+004432	5505.256 ± 0.005	13.587 ± 0.008	20.498 ± 0.392
4984	J012403+004432	5503.942 ± 0.051	12.566 ± 0.055	26.664 ± 4.131
4985	J012403+004432	5502.218 ± 0.041	12.357 ± 0.069	16.586 ± 3.219
4986	J012403+004432	5495.975 ± 0.014	13.523 ± 0.011	34.990 ± 0.998
4987	J012403+004432	5494.764 ± 0.028	12.703 ± 0.130	15.382 ± 2.831
4988	J012403+004432	5493.055 ± 0.067	14.124 ± 0.036	66.423 ± 4.914
4989	J012403+004432	5492.739 ± 0.026	13.063 ± 0.121	12.629 ± 2.715
4990	J012403+004432	5491.589 ± 0.012	14.161 ± 0.029	21.560 ± 1.275
4991	J012403+004432	5490.380 ± 0.073	13.315 ± 0.108	34.204 ± 10.499
4992	J012403+004432	5489.289 ± 0.060	13.164 ± 0.169	26.173 ± 8.544
4993	J012403+004432	5486.005 ± 0.005	14.442 ± 0.014	39.393 ± 0.516
4994	J012403+004432	5483.292 ± 0.014	13.510 ± 0.014	26.194 ± 1.094
4995	J012403+004432	5482.112 ± 0.022	13.332 ± 0.035	24.783 ± 2.261
4996	J012403+004432	5481.288 ± 0.084	12.689 ± 0.532	18.308 ± 8.873
4997	J012403+004432	5480.592 ± 0.466	12.830 ± 0.494	35.501 ± 33.954
4998	J012403+004432	5479.290 ± 0.041	12.978 ± 0.078	25.004 ± 4.297
4999	J012403+004432	5478.282 ± 0.089	12.227 ± 0.194	13.497 ± 7.069
5000	J012403+004432	5477.458 ± 0.059	12.136 ± 0.121	14.374 ± 5.387
5001	J012403+004432	5476.430 ± 0.053	12.058 ± 0.126	11.833 ± 4.644

Table E.1. *Continued*

5002	J012403+004432	5474.775 ± 0.209	12.368 ± 0.178	38.902 ± 19.807
5003	J012403+004432	5472.660 ± 0.005	15.791 ± 0.131	25.989 ± 0.864
5004	J012403+004432	5470.653 ± 0.019	13.842 ± 0.018	50.872 ± 2.689
5005	J012403+004432	5468.752 ± 0.006	15.117 ± 0.078	28.112 ± 0.914
5006	J012403+004432	5467.086 ± 0.027	12.955 ± 0.035	24.808 ± 2.528
5007	J012403+004432	5465.473 ± 0.046	12.924 ± 0.050	30.524 ± 4.179
5008	J012403+004432	5463.321 ± 0.039	13.563 ± 0.026	41.598 ± 2.375
5009	J012403+004432	5462.259 ± 0.109	12.741 ± 0.281	23.985 ± 11.265
5010	J012403+004432	5461.567 ± 0.158	12.466 ± 0.326	19.421 ± 8.492
5011	J012403+004432	5459.923 ± 0.157	13.097 ± 0.111	44.551 ± 9.634
5012	J012403+004432	5457.650 ± 0.006	16.317 ± 0.162	39.714 ± 1.547
5013	J012403+004432	5455.342 ± 0.174	12.407 ± 0.275	26.877 ± 16.734
5014	J012403+004432	5454.111 ± 0.029	13.078 ± 0.029	31.012 ± 2.389
5015	J012403+004432	5452.000 ± 0.020	13.893 ± 0.016	33.502 ± 1.018
5016	J012403+004432	5450.736 ± 0.011	14.272 ± 0.015	30.585 ± 1.139
5017	J012403+004432	5448.767 ± 0.006	15.177 ± 0.058	32.537 ± 0.803
5018	J012403+004432	5446.542 ± 0.073	12.282 ± 0.133	18.427 ± 6.675
5019	J012403+004432	5445.585 ± 0.012	13.314 ± 0.015	25.085 ± 1.094
5020	J012403+004432	5441.403 ± 0.051	13.139 ± 0.087	19.230 ± 3.367
5021	J012403+004432	5439.463 ± 0.008	15.279 ± 0.160	25.706 ± 1.596
5022	J012403+004432	5439.204 ± 0.052	13.997 ± 0.070	57.258 ± 2.306
5023	J012403+004432	5436.602 ± 0.018	13.063 ± 0.021	26.122 ± 1.461
5024	J012403+004432	5434.474 ± 0.024	13.717 ± 0.022	42.191 ± 0.945
5025	J012403+004432	5434.090 ± 0.012	13.494 ± 0.036	17.970 ± 1.040
5026	J012403+004432	5431.647 ± 0.027	12.212 ± 0.074	10.013 ± 2.310
5027	J012403+004432	5429.994 ± 0.062	13.676 ± 0.080	25.509 ± 2.090
5028	J012403+004432	5428.795 ± 0.023	14.985 ± 0.060	32.233 ± 1.054
5029	J012403+004432	5426.956 ± 0.047	12.515 ± 0.065	21.686 ± 3.981
5030	J012403+004432	5422.848 ± 0.004	13.967 ± 0.010	22.604 ± 0.314
5031	J012403+004432	5421.002 ± 0.011	13.789 ± 0.009	33.098 ± 0.776
5032	J012403+004432	5419.561 ± 0.023	14.131 ± 0.024	26.667 ± 1.327
5033	J012403+004432	5418.790 ± 0.039	13.709 ± 0.111	14.152 ± 3.496
5034	J012403+004432	5418.087 ± 0.046	13.707 ± 0.126	19.588 ± 5.004
5035	J012403+004432	5416.863 ± 0.021	14.487 ± 0.039	32.560 ± 3.954
5036	J012403+004432	5415.812 ± 0.076	13.502 ± 0.130	23.530 ± 2.503
5037	J012403+004432	5413.909 ± 0.072	13.536 ± 0.057	36.617 ± 3.369
5038	J012403+004432	5413.168 ± 0.106	13.405 ± 0.255	19.228 ± 5.424
5039	J012403+004432	5412.730 ± 0.106	13.286 ± 0.268	17.443 ± 2.838
5040	J012403+004432	5410.455 ± 0.077	11.775 ± 0.204	10.288 ± 6.475
5041	J012403+004432	5409.033 ± 0.078	12.116 ± 0.121	18.711 ± 6.298
5042	J012403+004432	5407.614 ± 0.048	12.507 ± 0.086	18.785 ± 3.592
5043	J012403+004432	5406.516 ± 0.026	13.346 ± 0.031	32.003 ± 2.788
5044	J012403+004432	5405.373 ± 0.213	12.122 ± 0.500	18.797 ± 19.079
5045	J012403+004432	5404.551 ± 0.010	13.823 ± 0.018	21.368 ± 1.118

Table E.1. *Continued*

5046	J012403+004432	5403.846 ± 0.243	12.283 ± 0.436	18.488 ± 11.842
5047	J012403+004432	5398.391 ± 0.081	12.200 ± 0.172	13.598 ± 6.339
5048	J012403+004432	5397.919 ± 0.059	12.194 ± 0.167	10.700 ± 4.413
5049	J012403+004432	5396.567 ± 0.066	12.098 ± 0.122	15.463 ± 5.400
5050	J012403+004432	5394.498 ± 0.048	14.691 ± 0.071	34.353 ± 1.705
5051	J012403+004432	5393.177 ± 0.209	14.259 ± 0.132	60.302 ± 15.041
5052	J012403+004432	5391.856 ± 0.020	13.237 ± 0.131	16.318 ± 2.428
5053	J012403+004432	5390.737 ± 0.026	13.857 ± 0.029	39.766 ± 2.501
5054	J012403+004432	5389.311 ± 0.031	14.345 ± 0.061	23.978 ± 1.556
5055	J012403+004432	5388.405 ± 0.049	14.067 ± 0.046	32.706 ± 1.647
5056	J012403+004432	5386.126 ± 0.006	13.771 ± 0.008	23.169 ± 0.465
5057	J012403+004432	5385.267 ± 0.026	12.621 ± 0.081	12.658 ± 2.421
5058	J012403+004432	5384.390 ± 0.022	13.666 ± 0.029	25.249 ± 1.615
5059	J012403+004432	5383.103 ± 0.012	14.598 ± 0.028	32.642 ± 0.788
5060	J012403+004432	5380.081 ± 0.065	11.933 ± 0.173	10.561 ± 5.993
5061	J012403+004432	5377.078 ± 0.027	13.215 ± 0.105	20.041 ± 2.631
5062	J012403+004432	5376.367 ± 0.086	13.357 ± 0.071	35.223 ± 4.046
5063	J012403+004432	5374.078 ± 0.023	13.018 ± 0.024	27.374 ± 1.873
5064	J012403+004432	5372.741 ± 0.016	13.165 ± 0.018	27.148 ± 1.370
5065	J012403+004432	5370.823 ± 0.013	14.228 ± 0.015	29.101 ± 0.714
5066	J012403+004432	5369.908 ± 0.095	12.774 ± 0.179	19.553 ± 5.189
5067	J012403+004432	5368.670 ± 0.004	14.031 ± 0.014	21.372 ± 0.358
5068	J012403+004432	5362.821 ± 0.010	14.071 ± 0.014	23.934 ± 0.593
5069	J012403+004432	5361.578 ± 0.013	14.493 ± 0.106	21.803 ± 2.569
5070	J012403+004432	5360.466 ± 0.076	13.649 ± 0.100	27.655 ± 5.777
5071	J012403+004432	5358.964 ± 0.023	13.796 ± 0.072	22.431 ± 4.648
5072	J012403+004432	5355.408 ± 0.035	12.726 ± 0.042	24.794 ± 2.962
5073	J012403+004432	5354.122 ± 0.050	12.048 ± 0.129	10.715 ± 4.268
5074	J012403+004432	5352.689 ± 0.005	14.604 ± 0.045	23.418 ± 0.578
5075	J012403+004432	5347.638 ± 0.058	13.678 ± 0.049	36.426 ± 2.780
5076	J012403+004432	5346.046 ± 0.033	12.679 ± 0.061	17.091 ± 2.825
5077	J012403+004432	5345.180 ± 0.015	13.235 ± 0.025	21.621 ± 1.644
5078	J012403+004432	5344.353 ± 0.026	12.786 ± 0.056	16.306 ± 2.532
5079	J012403+004432	5342.160 ± 0.011	14.274 ± 0.015	33.052 ± 1.207
5080	J012403+004432	5337.626 ± 0.015	15.828 ± 0.211	53.220 ± 3.980
5081	J012403+004432	5335.026 ± 0.134	12.681 ± 0.327	24.947 ± 16.807
5082	J012403+004432	5333.144 ± 0.007	14.784 ± 0.048	32.826 ± 0.984
5083	J012403+004432	5331.426 ± 0.089	13.232 ± 0.055	50.962 ± 6.781
5084	J012403+004432	5329.142 ± 0.011	14.594 ± 0.044	24.982 ± 0.845
5085	J012403+004432	5328.188 ± 0.100	12.826 ± 0.447	18.088 ± 8.687
5086	J012403+004432	5327.711 ± 0.508	13.319 ± 0.269	60.054 ± 23.073
5087	J012403+004432	5325.362 ± 0.073	12.728 ± 0.072	33.562 ± 5.921
5088	J012403+004432	5323.349 ± 0.007	14.000 ± 0.012	24.498 ± 0.848
5089	J012403+004432	5322.471 ± 0.012	13.140 ± 0.036	12.928 ± 1.233

Table E.1. *Continued*

5090	J012403+004432	5321.672 ± 0.064	12.797 ± 0.106	21.274 ± 6.067
5091	J012403+004432	5320.791 ± 0.090	12.674 ± 0.265	10.554 ± 6.029
5092	J012403+004432	5319.606 ± 0.033	13.043 ± 0.052	17.284 ± 2.213
5093	J012403+004432	5317.208 ± 0.035	13.150 ± 0.029	38.976 ± 3.256
5094	J012403+004432	5314.808 ± 1.318	13.592 ± 1.778	33.497 ± 25.324
5095	J012403+004432	5314.423 ± 0.040	14.515 ± 0.177	24.595 ± 3.482
5096	J012403+004432	5310.316 ± 0.040	12.650 ± 0.100	11.057 ± 2.773
5097	J012403+004432	5309.509 ± 0.232	13.249 ± 0.555	17.099 ± 15.235
5098	J012403+004432	5308.649 ± 0.035	13.602 ± 0.096	30.598 ± 6.770
5099	J012403+004432	5307.717 ± 0.145	12.993 ± 0.232	26.106 ± 8.324
5100	J012403+004432	5306.354 ± 0.028	13.549 ± 0.033	32.032 ± 2.656
5101	J012403+004432	5305.409 ± 0.040	13.154 ± 0.072	23.247 ± 3.018
5102	J012403+004432	5303.865 ± 0.056	12.369 ± 0.180	13.211 ± 4.178
5103	J012403+004432	5303.173 ± 0.020	13.362 ± 0.022	26.256 ± 1.582
5104	J012403+004432	5301.062 ± 0.311	13.471 ± 0.308	38.124 ± 9.219
5105	J012403+004432	5299.906 ± 0.038	14.662 ± 0.048	38.770 ± 3.355
5106	J012403+004432	5298.418 ± 0.093	13.044 ± 0.126	25.817 ± 4.394
5107	J012403+004432	5295.452 ± 0.005	13.811 ± 0.010	20.414 ± 0.363
5108	J012403+004432	5293.424 ± 0.051	12.900 ± 0.079	20.624 ± 3.146
5109	J012403+004432	5292.451 ± 0.012	14.010 ± 0.015	26.928 ± 1.244
5110	J012403+004432	5291.430 ± 0.073	13.193 ± 0.070	31.125 ± 4.009
5111	J012403+004432	5288.909 ± 0.017	13.355 ± 0.019	25.665 ± 1.295
5112	J012403+004432	5287.895 ± 0.019	13.335 ± 0.056	22.865 ± 1.945
5113	J012403+004432	5286.823 ± 0.053	13.564 ± 0.037	49.915 ± 4.468
5114	J012403+004432	5284.930 ± 0.082	12.651 ± 0.082	32.499 ± 6.677
5115	J012403+004432	5283.169 ± 0.361	12.853 ± 0.610	21.379 ± 11.864
5116	J012403+004432	5282.741 ± 0.079	13.296 ± 0.220	18.172 ± 2.445
5117	J012403+004432	5280.443 ± 0.036	12.716 ± 0.050	21.478 ± 3.096
5118	J012403+004432	5279.458 ± 0.007	13.563 ± 0.010	20.635 ± 0.550
5119	J012403+004432	5277.811 ± 0.257	12.456 ± 0.313	24.790 ± 14.802
5120	J012403+004432	5277.189 ± 0.093	12.527 ± 0.296	17.264 ± 7.891
5121	J012403+004432	5276.332 ± 0.007	13.703 ± 0.011	20.760 ± 0.732
5122	J012403+004432	5275.146 ± 0.019	13.537 ± 0.021	27.581 ± 1.587
5123	J012403+004432	5274.328 ± 0.084	12.930 ± 0.607	14.592 ± 6.159
5124	J012403+004432	5273.832 ± 0.080	13.619 ± 0.163	25.230 ± 8.345
5125	J012403+004432	5272.612 ± 0.032	14.104 ± 0.558	20.660 ± 8.105
5126	J012403+004432	5272.371 ± 0.537	13.948 ± 0.906	29.366 ± 9.060
5127	J012403+004432	5270.198 ± 0.046	13.125 ± 0.050	28.955 ± 2.840
5128	J012403+004432	5268.955 ± 0.010	14.170 ± 0.009	35.275 ± 0.648
5129	J012403+004432	5264.104 ± 0.010	13.711 ± 0.010	27.695 ± 0.750
5130	J012403+004432	5263.024 ± 0.006	14.157 ± 0.026	18.335 ± 0.549
5131	J012403+004432	5262.019 ± 0.029	12.343 ± 0.075	11.263 ± 2.706
5132	J012403+004432	5261.404 ± 0.020	12.545 ± 0.048	11.701 ± 1.757
5133	J012403+004432	5259.295 ± 0.021	12.986 ± 0.024	25.238 ± 1.648

Table E.1. *Continued*

5134	J012403+004432	5256.514 ± 0.004	14.191 ± 0.017	23.318 ± 0.382
5135	J012403+004432	5254.234 ± 0.013	13.940 ± 0.010	34.159 ± 0.819
5136	J012403+004432	5252.888 ± 0.143	13.239 ± 0.108	35.051 ± 4.777
5137	J012403+004432	5252.478 ± 0.045	12.840 ± 0.286	17.848 ± 4.841
5138	J012403+004432	5251.250 ± 0.047	12.395 ± 0.126	10.945 ± 3.867
5139	J012403+004432	5250.358 ± 0.020	15.455 ± 0.381	15.196 ± 1.722
5140	J012403+004432	5249.414 ± 0.021	14.360 ± 0.109	14.453 ± 1.293
5141	J012403+004432	5248.681 ± 0.078	12.082 ± 0.216	10.720 ± 6.734
5142	J012403+004432	5246.365 ± 0.088	12.961 ± 0.126	23.040 ± 4.702
5143	J012403+004432	5245.087 ± 0.007	14.020 ± 0.034	14.420 ± 0.605
5144	J012403+004432	5244.474 ± 0.024	13.236 ± 0.129	11.039 ± 2.136
5145	J012403+004432	5244.039 ± 0.030	13.721 ± 0.041	20.111 ± 1.308
5146	J012403+004432	5242.244 ± 0.069	12.360 ± 0.134	16.238 ± 5.573
5147	J012403+004432	5241.330 ± 0.013	13.735 ± 0.018	23.736 ± 1.121
5148	J012403+004432	5240.324 ± 0.271	12.689 ± 0.295	27.899 ± 15.800
5149	J012403+004432	5238.553 ± 0.051	12.826 ± 0.060	26.093 ± 4.494
5150	J012403+004432	5237.698 ± 0.076	12.363 ± 0.151	16.700 ± 6.289
5151	J012403+004432	5236.416 ± 0.031	14.371 ± 0.089	19.491 ± 1.096
5152	J012403+004432	5235.322 ± 0.035	14.367 ± 0.043	32.577 ± 1.323
5153	J012403+004432	5232.213 ± 0.077	12.757 ± 0.203	16.137 ± 4.304
5154	J012403+004432	5231.468 ± 0.058	13.485 ± 0.117	25.810 ± 6.717
5155	J012403+004432	5230.485 ± 0.022	14.286 ± 0.042	25.700 ± 1.891
5156	J012403+004432	5229.354 ± 0.043	12.896 ± 0.122	17.170 ± 5.618
5157	J012403+004432	5224.392 ± 0.039	12.431 ± 0.143	10.778 ± 3.547
5158	J012403+004432	5223.439 ± 0.013	13.829 ± 0.012	34.875 ± 1.151
5159	J012403+004432	5221.922 ± 0.048	13.680 ± 0.100	16.775 ± 1.831
5160	J012403+004432	5221.274 ± 0.039	14.079 ± 0.053	22.150 ± 2.180
5161	J012403+004432	5220.306 ± 0.029	13.089 ± 0.046	18.535 ± 2.091
5162	J012403+004432	5218.385 ± 0.022	14.249 ± 0.034	26.171 ± 1.102
5163	J012403+004432	5217.432 ± 0.058	13.664 ± 0.065	29.599 ± 3.676
5164	J012403+004432	5215.734 ± 0.648	13.280 ± 0.766	32.878 ± 39.244
5165	J012403+004432	5215.131 ± 0.110	13.466 ± 0.449	22.469 ± 4.916
5166	J012403+004432	5212.393 ± 0.006	14.197 ± 0.041	19.306 ± 0.726
5167	J012403+004432	5211.049 ± 0.029	12.884 ± 0.047	18.499 ± 2.634
5168	J012403+004432	5209.386 ± 0.005	15.206 ± 0.150	21.371 ± 1.053
5169	J012403+004432	5205.904 ± 0.013	13.726 ± 0.019	19.513 ± 0.851
5170	J012403+004432	5205.235 ± 0.109	12.558 ± 0.205	16.996 ± 7.022
5171	J012403+004432	5203.091 ± 0.011	14.217 ± 0.024	27.491 ± 0.880
5172	J012403+004432	5202.203 ± 0.080	12.394 ± 0.277	12.279 ± 6.800
5173	J012403+004432	5200.881 ± 1.034	12.902 ± 0.943	36.298 ± 47.887
5174	J012403+004432	5200.561 ± 0.042	12.898 ± 0.548	12.674 ± 6.297
5175	J012403+004432	5199.515 ± 0.092	13.468 ± 0.085	33.447 ± 4.770
5176	J012403+004432	5198.182 ± 0.058	12.611 ± 0.473	13.494 ± 6.342
5177	J012403+004432	5197.706 ± 0.123	13.188 ± 0.135	27.536 ± 6.415

Table E.1. *Continued*

5178	J012403+004432	5195.961 ± 0.085	12.321 ± 0.154	17.128 ± 7.575
5179	J012403+004432	5194.824 ± 0.006	14.360 ± 0.038	24.453 ± 0.718
5180	J012403+004432	5193.109 ± 0.008	13.634 ± 0.012	22.292 ± 0.580
5181	J012403+004432	5191.229 ± 0.038	12.974 ± 0.048	28.136 ± 3.019
5182	J012403+004432	5186.962 ± 0.094	12.377 ± 0.121	23.854 ± 8.063
5183	J012403+004432	5185.537 ± 0.010	13.762 ± 0.010	28.613 ± 0.856
5184	J012403+004432	5184.392 ± 0.009	13.829 ± 0.012	23.976 ± 0.652
5185	J012403+004432	5180.832 ± 0.006	13.794 ± 0.014	19.904 ± 0.498
5186	J012403+004432	5178.068 ± 0.013	13.600 ± 0.016	25.914 ± 0.970
5187	J012403+004432	5176.729 ± 0.354	12.961 ± 0.342	37.793 ± 23.437
5188	J012403+004432	5176.113 ± 0.028	13.039 ± 0.246	18.605 ± 4.179
5189	J012403+004432	5174.004 ± 0.044	12.763 ± 0.045	29.446 ± 3.595
5190	J012403+004432	5165.151 ± 0.084	12.097 ± 0.164	15.258 ± 7.158
5191	J012403+004432	5163.337 ± 0.038	12.447 ± 0.069	16.442 ± 3.214
5192	J012403+004432	5160.971 ± 0.012	13.109 ± 0.017	20.577 ± 0.944
5193	J012403+004432	5159.680 ± 0.052	12.101 ± 0.124	12.493 ± 4.515
5194	J012403+004432	5158.538 ± 0.005	13.803 ± 0.006	30.146 ± 0.458
5195	J012403+004432	5156.656 ± 0.014	14.070 ± 0.011	35.138 ± 0.842
5196	J012403+004432	5155.928 ± 0.026	12.847 ± 0.153	12.013 ± 2.775
5197	J012403+004432	5155.173 ± 0.014	13.751 ± 0.024	32.964 ± 2.199
5198	J012403+004432	5153.799 ± 0.008	14.307 ± 0.013	32.235 ± 0.946
5199	J012403+004432	5152.673 ± 0.072	12.388 ± 0.303	15.852 ± 6.897
5200	J012403+004432	5151.610 ± 0.020	13.653 ± 0.404	28.844 ± 5.935
5201	J012403+004432	5151.142 ± 1.603	13.110 ± 1.458	43.985 ± 40.317
5202	J012403+004432	5148.359 ± 0.060	12.220 ± 0.102	18.177 ± 5.328
5203	J012403+004432	5147.211 ± 0.007	13.769 ± 0.009	24.902 ± 0.626
5204	J012403+004432	5145.367 ± 0.005	13.818 ± 0.006	26.976 ± 0.340
5205	J012403+004432	5142.807 ± 0.016	13.179 ± 0.017	29.872 ± 1.344
5206	J012403+004432	5141.252 ± 0.016	13.347 ± 0.015	36.468 ± 1.707
5207	J012403+004432	5138.643 ± 0.035	13.102 ± 0.034	30.563 ± 2.688
5208	J012403+004432	5133.695 ± 0.008	13.853 ± 0.008	29.253 ± 0.566
5209	J012403+004432	5132.701 ± 0.026	13.057 ± 0.039	23.559 ± 2.137
5210	J012403+004432	5131.418 ± 0.022	13.190 ± 0.027	27.809 ± 2.147
5211	J012403+004432	5130.752 ± 0.034	12.377 ± 0.139	12.357 ± 2.988
5212	J012403+004432	5129.119 ± 0.026	12.612 ± 0.040	19.638 ± 2.150
5213	J012403+004432	5126.675 ± 0.148	12.093 ± 0.284	15.529 ± 10.795
5214	J012403+004432	5122.587 ± 0.074	11.966 ± 0.473	13.019 ± 9.140
5215	J012403+004432	5121.803 ± 0.300	12.411 ± 0.480	38.004 ± 38.385
5216	J012403+004432	5120.309 ± 0.020	13.746 ± 0.027	46.037 ± 3.265
5217	J012403+004432	5119.427 ± 0.027	12.460 ± 0.199	12.338 ± 3.655
5218	J012403+004432	5118.624 ± 0.053	12.293 ± 0.112	16.903 ± 4.597
5219	J012403+004432	5117.447 ± 0.026	12.939 ± 0.030	28.879 ± 2.581
5220	J012403+004432	5116.428 ± 0.036	12.751 ± 0.082	17.197 ± 3.361
5221	J012403+004432	5115.301 ± 0.015	13.419 ± 0.093	20.246 ± 1.961

Table E.1. *Continued*

5222	J012403+004432	5114.984 ± 0.153	13.345 ± 0.106	45.702 ± 6.773
5223	J012403+004432	5113.754 ± 0.007	13.628 ± 0.016	20.227 ± 0.566
5224	J012403+004432	5112.587 ± 0.005	13.516 ± 0.009	18.201 ± 0.487
5225	J012403+004432	5110.323 ± 0.033	13.891 ± 0.035	28.695 ± 1.336
5226	J012403+004432	5109.730 ± 0.026	13.534 ± 0.079	18.691 ± 1.415
5227	J012403+004432	5108.361 ± 0.268	13.088 ± 0.224	41.601 ± 16.497
5228	J012403+004432	5107.651 ± 0.061	13.925 ± 0.211	19.144 ± 2.373
5229	J012403+004432	5107.202 ± 0.189	13.739 ± 0.321	24.613 ± 7.728
5230	J012403+004432	5106.023 ± 0.308	12.827 ± 0.668	46.811 ± 74.198
5231	J012403+004432	5104.770 ± 0.008	14.719 ± 0.042	25.706 ± 0.786
5232	J012403+004432	5103.171 ± 0.011	13.430 ± 0.013	29.089 ± 1.149
5233	J012403+004432	5101.995 ± 0.113	12.304 ± 0.134	27.180 ± 9.723
5234	J012403+004432	5100.113 ± 0.046	13.002 ± 0.079	20.518 ± 2.807
5235	J012403+004432	5099.378 ± 0.023	13.395 ± 0.064	22.900 ± 3.274
5236	J012403+004432	5098.402 ± 0.008	14.302 ± 0.020	25.253 ± 1.110
5237	J012403+004432	5097.397 ± 0.028	13.229 ± 0.037	23.206 ± 1.714
5238	J012403+004432	5094.877 ± 0.105	11.857 ± 0.219	14.810 ± 9.573
5239	J012403+004432	5094.126 ± 0.045	12.534 ± 0.109	15.840 ± 3.810
5240	J012403+004432	5091.818 ± 0.004	16.715 ± 0.181	42.999 ± 1.538
5241	J012403+004432	5089.280 ± 0.006	13.991 ± 0.009	23.457 ± 0.430
5242	J012403+004432	5087.707 ± 0.188	12.583 ± 0.231	26.628 ± 10.742
5243	J012403+004432	5086.898 ± 0.105	13.360 ± 0.292	23.188 ± 5.357
5244	J012403+004432	5086.377 ± 0.542	12.893 ± 0.788	26.963 ± 17.691
5245	J012403+004432	5084.937 ± 0.161	12.102 ± 0.178	29.112 ± 14.665
5246	J012403+004432	5082.117 ± 0.155	13.385 ± 0.090	54.355 ± 7.291
5247	J012403+004432	5081.003 ± 0.008	14.438 ± 0.021	31.089 ± 0.982
5248	J012403+004432	5079.827 ± 0.063	12.523 ± 0.116	18.711 ± 4.566
5249	J012403+004432	5077.899 ± 0.043	13.376 ± 0.041	37.953 ± 3.795
5250	J012403+004432	5076.976 ± 0.071	13.249 ± 0.131	18.550 ± 3.193
5251	J012403+004432	5075.776 ± 0.010	13.386 ± 0.011	27.133 ± 0.925
5252	J012403+004432	5074.781 ± 0.084	11.974 ± 0.193	14.332 ± 7.939
5253	J012403+004432	5073.954 ± 0.081	12.152 ± 0.135	19.516 ± 7.615
5254	J012403+004432	5072.579 ± 0.025	13.067 ± 0.023	36.028 ± 2.282
5255	J012403+004432	5070.855 ± 0.093	12.300 ± 0.104	28.194 ± 8.141
5256	J012403+004432	5068.544 ± 0.127	12.863 ± 0.189	30.340 ± 7.869
5257	J012403+004432	5067.636 ± 0.342	12.629 ± 0.313	36.559 ± 17.698
5258	J012403+004432	5065.665 ± 0.006	13.667 ± 0.007	29.655 ± 0.515
5259	J012403+004432	5063.974 ± 0.004	13.909 ± 0.008	23.751 ± 0.361
5260	J012403+004432	5062.660 ± 0.043	13.995 ± 0.070	21.650 ± 1.501
5261	J012403+004432	5062.119 ± 0.057	13.730 ± 0.122	19.418 ± 2.718
5262	J012403+004432	5061.281 ± 0.019	13.309 ± 0.051	22.384 ± 2.569
5263	J012403+004432	5060.200 ± 0.028	12.963 ± 0.200	16.846 ± 3.826
5264	J012403+004432	5059.705 ± 0.091	13.580 ± 0.070	47.546 ± 4.741
5265	J012403+004432	5058.407 ± 0.044	12.948 ± 0.119	16.873 ± 3.258

Table E.1. *Continued*

5266	J012403+004432	5057.107 ± 0.009	15.121 ± 0.049	35.041 ± 0.857
5267	J012403+004432	5055.087 ± 0.006	13.506 ± 0.009	21.241 ± 0.466
5268	J012403+004432	5053.681 ± 0.096	12.573 ± 0.172	20.234 ± 5.645
5269	J012403+004432	5053.001 ± 0.055	12.892 ± 0.093	23.462 ± 4.924
5270	J012403+004432	5051.814 ± 0.060	12.858 ± 0.141	22.447 ± 7.962
5271	J012403+004432	5049.556 ± 0.037	14.034 ± 0.030	45.321 ± 1.600
5272	J012403+004432	5048.383 ± 0.057	13.029 ± 0.257	13.106 ± 4.411
5273	J012403+004432	5047.869 ± 0.022	13.757 ± 0.087	17.671 ± 3.886
5274	J012403+004432	5047.438 ± 0.034	13.236 ± 0.279	11.125 ± 3.084
5275	J012403+004432	5047.028 ± 0.068	13.201 ± 0.209	19.813 ± 8.478
5276	J012403+004432	5046.379 ± 0.067	12.943 ± 0.134	18.632 ± 4.206
5277	J012403+004432	5044.158 ± 0.031	12.940 ± 0.064	18.342 ± 2.004
5278	J012403+004432	5042.872 ± 0.006	14.687 ± 0.033	35.817 ± 1.080
5279	J012403+004432	5041.502 ± 0.054	12.416 ± 0.126	15.881 ± 4.200
5280	J012403+004432	5038.991 ± 0.046	12.246 ± 0.118	13.284 ± 3.997
5281	J012403+004432	5038.176 ± 0.007	13.614 ± 0.008	25.567 ± 0.580
5282	J012403+004432	5034.128 ± 0.039	12.241 ± 0.084	13.976 ± 3.369
5283	J012403+004432	5032.580 ± 0.044	12.183 ± 0.095	14.150 ± 3.868
5284	J111113-080401	5409.974 ± 0.170	13.666 ± 0.320	21.746 ± 4.131
5285	J111113-080401	5409.536 ± 0.346	13.276 ± 0.799	20.593 ± 10.544
5286	J111113-080401	5408.529 ± 0.116	12.793 ± 0.226	25.094 ± 11.774
5287	J111113-080401	5406.717 ± 0.354	13.447 ± 0.445	43.476 ± 40.267
5288	J111113-080401	5405.387 ± 0.066	13.461 ± 0.199	29.512 ± 8.135
5289	J111113-080401	5404.418 ± 0.069	13.586 ± 0.077	31.162 ± 4.035
5290	J111113-080401	5403.304 ± 0.084	12.428 ± 0.242	17.158 ± 7.935
5291	J111113-080401	5401.347 ± 0.100	14.297 ± 0.047	53.765 ± 5.993
5292	J111113-080401	5401.602 ± 0.036	14.558 ± 0.472	15.555 ± 3.942
5293	J111113-080401	5400.235 ± 0.031	13.962 ± 0.083	21.720 ± 2.696
5294	J111113-080401	5399.365 ± 0.051	13.451 ± 0.059	26.324 ± 2.496
5295	J111113-080401	5396.757 ± 0.032	12.516 ± 0.074	12.298 ± 2.821
5296	J111113-080401	5396.162 ± 0.024	12.735 ± 0.074	12.353 ± 2.392
5297	J111113-080401	5395.212 ± 0.015	13.885 ± 0.015	28.775 ± 0.994
5298	J111113-080401	5393.315 ± 0.189	13.189 ± 0.255	31.990 ± 17.030
5299	J111113-080401	5392.706 ± 0.079	12.728 ± 0.615	16.611 ± 11.503
5300	J111113-080401	5389.211 ± 0.083	12.541 ± 0.094	26.349 ± 7.039
5301	J111113-080401	5387.792 ± 0.716	12.728 ± 0.833	26.892 ± 28.656
5302	J111113-080401	5387.278 ± 0.064	12.555 ± 0.784	10.574 ± 7.444
5303	J111113-080401	5386.206 ± 0.043	13.718 ± 0.051	25.354 ± 2.406
5304	J111113-080401	5385.422 ± 0.040	13.468 ± 0.134	21.346 ± 5.736
5305	J111113-080401	5384.843 ± 0.080	12.863 ± 0.249	14.509 ± 3.776
5306	J111113-080401	5383.444 ± 0.090	14.434 ± 0.260	16.291 ± 2.561
5307	J111113-080401	5382.397 ± 0.057	14.551 ± 0.055	47.347 ± 1.650
5308	J111113-080401	5380.060 ± 0.019	13.385 ± 0.018	31.004 ± 1.496
5309	J111113-080401	5376.814 ± 0.005	16.820 ± 0.175	37.599 ± 1.123

Table E.1. *Continued*

5310	J111113-080401	5372.982 ± 0.009	14.646 ± 0.021	53.807 ± 1.132
5311	J111113-080401	5370.992 ± 0.033	13.008 ± 0.070	18.291 ± 3.147
5312	J111113-080401	5369.709 ± 0.006	15.443 ± 0.139	23.602 ± 0.996
5313	J111113-080401	5363.382 ± 0.075	13.281 ± 0.036	62.775 ± 6.164
5314	J111113-080401	5361.796 ± 0.042	13.021 ± 0.077	26.728 ± 3.654
5315	J111113-080401	5360.547 ± 0.070	13.091 ± 0.050	41.760 ± 5.497
5316	J111113-080401	5356.340 ± 0.016	13.135 ± 0.021	22.248 ± 1.212
5317	J111113-080401	5354.059 ± 0.060	12.260 ± 0.119	14.585 ± 5.118
5318	J111113-080401	5353.228 ± 0.042	12.514 ± 0.072	17.359 ± 3.678
5319	J111113-080401	5349.481 ± 0.018	13.770 ± 0.013	38.412 ± 1.221
5320	J111113-080401	5348.044 ± 0.037	14.541 ± 0.133	18.838 ± 2.730
5321	J111113-080401	5347.532 ± 0.361	13.900 ± 0.383	32.475 ± 11.573
5322	J111113-080401	5346.072 ± 0.029	13.583 ± 0.043	23.345 ± 2.128
5323	J111113-080401	5345.139 ± 0.015	13.548 ± 0.036	12.497 ± 1.345
5324	J111113-080401	5344.484 ± 0.014	15.185 ± 1.093	10.261 ± 3.647
5325	J111113-080401	5343.576 ± 1.035	13.268 ± 0.825	42.207 ± 32.701
5326	J111113-080401	5341.915 ± 0.005	13.965 ± 0.037	13.123 ± 0.495
5327	J111113-080401	5340.759 ± 0.018	14.062 ± 0.026	22.211 ± 1.033
5328	J111113-080401	5339.777 ± 0.044	14.171 ± 0.072	19.738 ± 3.412
5329	J111113-080401	5338.773 ± 0.032	15.131 ± 1.170	17.504 ± 9.181
5330	J111113-080401	5336.982 ± 0.034	15.146 ± 0.600	36.614 ± 14.999
5331	J111113-080401	5335.213 ± 0.032	16.510 ± 1.799	14.232 ± 4.601
5332	J111113-080401	5334.687 ± 0.540	13.620 ± 0.480	38.519 ± 16.223
5333	J111113-080401	5333.056 ± 0.009	14.656 ± 0.238	10.585 ± 1.086
5334	J111113-080401	5331.945 ± 0.011	14.249 ± 0.076	19.456 ± 2.263
5335	J111113-080401	5331.160 ± 0.056	12.747 ± 0.198	12.444 ± 5.791
5336	J111113-080401	5328.689 ± 0.059	12.866 ± 0.274	13.657 ± 6.521
5337	J111113-080401	5328.084 ± 0.022	13.835 ± 0.030	22.455 ± 1.568
5338	J111113-080401	5326.954 ± 0.144	12.574 ± 0.175	31.630 ± 15.335
5339	J111113-080401	5325.723 ± 0.135	12.206 ± 0.192	22.147 ± 11.147
5340	J111113-080401	5321.889 ± 0.377	12.587 ± 0.248	45.180 ± 24.950
5341	J111113-080401	5320.517 ± 0.094	12.735 ± 0.114	29.946 ± 6.368
5342	J111113-080401	5316.564 ± 0.018	13.142 ± 0.020	26.839 ± 1.447
5343	J111113-080401	5315.478 ± 0.035	12.288 ± 0.088	11.427 ± 3.026
5344	J111113-080401	5312.633 ± 0.028	12.844 ± 0.041	20.384 ± 2.460
5345	J111113-080401	5311.910 ± 0.041	12.414 ± 0.093	13.260 ± 3.324
5346	J111113-080401	5307.408 ± 0.054	12.877 ± 0.040	40.585 ± 4.298
5347	J111113-080401	5304.861 ± 0.045	13.648 ± 0.064	35.488 ± 1.979
5348	J111113-080401	5303.586 ± 0.138	13.384 ± 0.164	51.908 ± 19.338
5349	J111113-080401	5302.135 ± 0.011	14.090 ± 0.015	26.552 ± 1.101
5350	J111113-080401	5300.670 ± 0.007	14.300 ± 0.021	28.192 ± 0.838
5351	J111113-080401	5298.928 ± 0.111	13.967 ± 0.126	31.516 ± 3.807
5352	J111113-080401	5297.878 ± 0.057	14.547 ± 0.075	33.171 ± 4.811
5353	J111113-080401	5296.585 ± 0.014	14.251 ± 0.047	17.451 ± 0.714

Table E.1. *Continued*

5354	J111113-080401	5294.853 ± 0.006	13.742 ± 0.011	17.989 ± 0.482
5355	J111113-080401	5293.596 ± 0.012	14.270 ± 0.033	24.179 ± 1.399
5356	J111113-080401	5292.603 ± 0.019	13.852 ± 0.022	23.841 ± 0.938
5357	J111113-080401	5288.711 ± 0.027	13.124 ± 0.034	23.150 ± 1.960
5358	J111113-080401	5287.728 ± 0.021	13.373 ± 0.185	10.495 ± 2.721
5359	J111113-080401	5287.687 ± 0.012	13.768 ± 0.070	23.352 ± 2.173
5360	J111113-080401	5286.056 ± 0.040	13.061 ± 0.065	21.694 ± 3.763
5361	J111113-080401	5284.862 ± 0.071	13.064 ± 0.982	14.803 ± 7.538
5362	J111113-080401	5284.545 ± 1.086	12.835 ± 1.710	22.581 ± 36.649
5363	J111113-080401	5282.611 ± 0.016	13.882 ± 0.021	19.629 ± 1.200
5364	J111113-080401	5281.745 ± 0.050	12.890 ± 0.176	14.847 ± 4.065
5365	J111113-080401	5280.389 ± 0.014	14.902 ± 0.108	35.514 ± 3.172
5366	J111113-080401	5278.740 ± 0.023	12.942 ± 0.154	13.107 ± 2.698
5367	J111113-080401	5278.649 ± 0.237	13.582 ± 0.140	56.654 ± 9.127
5368	J111113-080401	5276.580 ± 0.500	12.473 ± 0.839	20.733 ± 21.505
5369	J111113-080401	5276.019 ± 0.033	13.473 ± 0.115	18.484 ± 3.760
5370	J111113-080401	5275.027 ± 0.011	14.818 ± 0.066	22.449 ± 0.796
5371	J111113-080401	5272.917 ± 0.017	13.489 ± 0.019	34.652 ± 1.294
5372	J111113-080401	5270.717 ± 0.120	13.415 ± 0.044	75.638 ± 8.762
5373	J111113-080401	5269.945 ± 0.017	13.100 ± 0.062	18.698 ± 1.818
5374	J111113-080401	5268.525 ± 0.017	13.040 ± 0.036	17.436 ± 1.518
5375	J111113-080401	5267.575 ± 0.008	13.807 ± 0.012	23.697 ± 0.777
5376	J111113-080401	5264.971 ± 0.074	15.121 ± 0.091	62.005 ± 2.137
5377	J111113-080401	5263.671 ± 3.437	15.872 ± 9.847	22.114 ± 41.793
5378	J111113-080401	5261.197 ± 0.240	13.342 ± 0.260	31.293 ± 8.755
5379	J111113-080401	5260.661 ± 0.067	13.330 ± 0.264	21.971 ± 3.183
5380	J111113-080401	5259.628 ± 0.048	12.266 ± 0.099	14.278 ± 4.144
5381	J111113-080401	5253.980 ± 0.010	13.303 ± 0.013	22.498 ± 0.780
5382	J111113-080401	5248.690 ± 0.004	14.239 ± 0.022	22.708 ± 0.430
5383	J111113-080401	5246.482 ± 0.004	14.373 ± 0.023	27.103 ± 0.482
5384	J111113-080401	5239.955 ± 0.046	12.587 ± 0.072	19.177 ± 3.909
5385	J111113-080401	5238.661 ± 0.011	13.999 ± 0.013	26.050 ± 0.829
5386	J111113-080401	5235.678 ± 0.306	12.651 ± 0.264	34.988 ± 18.468
5387	J111113-080401	5234.838 ± 0.102	12.837 ± 0.288	20.955 ± 10.284
5388	J111113-080401	5233.880 ± 0.010	14.734 ± 0.070	22.332 ± 0.925
5389	J111113-080401	5231.757 ± 0.034	12.904 ± 0.045	23.970 ± 3.249
5390	J111113-080401	5230.937 ± 0.044	12.302 ± 0.120	10.915 ± 3.757
5391	J111113-080401	5227.726 ± 0.719	12.778 ± 0.988	24.878 ± 24.679
5392	J111113-080401	5226.693 ± 0.031	15.363 ± 0.470	24.451 ± 4.875
5393	J111113-080401	5224.854 ± 0.037	14.961 ± 0.073	37.473 ± 1.560
5394	J111113-080401	5222.080 ± 0.108	13.700 ± 0.071	46.602 ± 5.510
5395	J111113-080401	5221.148 ± 0.020	13.850 ± 0.053	26.299 ± 2.095
5396	J111113-080401	5220.192 ± 0.042	13.158 ± 0.141	22.008 ± 4.586
5397	J111113-080401	5219.240 ± 0.175	12.960 ± 0.248	40.452 ± 24.394

Table E.1. *Continued*

5398	J111113-080401	5217.914 ± 0.119	12.834 ± 0.136	30.950 ± 7.536
5399	J111113-080401	5215.253 ± 0.047	13.175 ± 0.064	24.244 ± 3.406
5400	J111113-080401	5213.414 ± 0.009	15.744 ± 0.118	37.784 ± 1.337
5401	J111113-080401	5210.319 ± 0.826	13.239 ± 0.808	36.708 ± 24.368
5402	J111113-080401	5209.935 ± 0.014	13.726 ± 0.234	20.010 ± 3.390
5403	J111113-080401	5208.919 ± 0.034	13.590 ± 0.042	26.009 ± 1.740
5404	J111113-080401	5205.595 ± 0.039	12.600 ± 0.075	15.738 ± 3.408
5405	J111113-080401	5204.243 ± 0.005	15.090 ± 0.107	24.116 ± 0.962
5406	J111113-080401	5202.477 ± 0.031	13.268 ± 0.027	37.052 ± 2.873
5407	J111113-080401	5198.992 ± 0.088	12.927 ± 0.060	43.225 ± 7.554
5408	J111113-080401	5197.632 ± 0.101	12.651 ± 0.181	21.406 ± 8.696
5409	J111113-080401	5196.611 ± 0.612	13.379 ± 0.916	23.595 ± 22.156
5410	J111113-080401	5196.343 ± 0.025	13.811 ± 0.295	11.991 ± 3.802
5411	J111113-080401	5195.737 ± 0.336	13.458 ± 0.747	16.379 ± 9.628
5412	J111113-080401	5194.162 ± 1.266	13.038 ± 1.004	43.955 ± 45.621
5413	J111113-080401	5193.884 ± 0.169	12.594 ± 1.604	17.466 ± 20.814
5414	J111113-080401	5193.010 ± 0.265	12.763 ± 0.872	21.975 ± 23.715
5415	J111113-080401	5192.135 ± 0.070	12.578 ± 0.133	18.218 ± 6.548
5416	J111113-080401	5190.938 ± 0.017	13.689 ± 0.019	26.422 ± 1.392
5417	J111113-080401	5190.269 ± 0.027	12.974 ± 0.126	11.745 ± 2.635
5418	J111113-080401	5189.479 ± 0.013	14.127 ± 0.019	25.422 ± 1.484
5419	J111113-080401	5188.440 ± 0.061	13.434 ± 0.055	33.779 ± 3.813
5420	J111113-080401	5186.919 ± 0.010	13.473 ± 0.014	21.969 ± 0.862
5421	J111113-080401	5185.068 ± 0.005	14.996 ± 0.054	33.690 ± 0.852
5422	J111113-080401	5183.056 ± 0.098	12.590 ± 0.094	32.846 ± 8.778
5423	J111113-080401	5180.185 ± 0.032	12.878 ± 0.039	24.822 ± 2.642
5424	J111113-080401	5176.120 ± 0.031	12.557 ± 0.063	14.527 ± 2.648
5425	J111113-080401	5172.134 ± 0.018	13.199 ± 0.029	17.876 ± 1.502
5426	J111113-080401	5171.278 ± 0.038	12.791 ± 0.098	11.162 ± 2.663
5427	J111113-080401	5169.718 ± 0.025	12.638 ± 0.053	13.810 ± 2.101
5428	J111113-080401	5166.017 ± 0.191	13.012 ± 0.075	63.225 ± 13.725
5429	J111113-080401	5162.262 ± 0.007	16.154 ± 0.091	59.487 ± 1.405
5430	J111113-080401	5158.437 ± 0.060	13.838 ± 0.046	44.001 ± 2.441
5431	J111113-080401	5158.117 ± 0.016	13.349 ± 0.094	14.766 ± 1.922
5432	J111113-080401	5157.059 ± 0.048	13.351 ± 0.214	21.911 ± 5.553
5433	J111113-080401	5156.403 ± 0.667	12.760 ± 0.581	37.793 ± 29.550
5434	J111113-080401	5154.674 ± 0.082	12.706 ± 0.113	25.606 ± 6.655
5435	J111113-080401	5153.695 ± 0.019	13.572 ± 0.033	25.570 ± 2.169
5436	J111113-080401	5152.704 ± 0.044	14.320 ± 0.108	20.593 ± 2.204
5437	J111113-080401	5151.922 ± 0.134	13.697 ± 0.769	32.014 ± 52.749
5438	J111113-080401	5151.237 ± 0.043	14.058 ± 0.179	18.866 ± 2.200
5439	J111113-080401	5150.101 ± 0.125	12.586 ± 0.955	18.522 ± 12.676
5440	J111113-080401	5149.397 ± 0.160	13.119 ± 0.464	35.677 ± 38.739
5441	J111113-080401	5148.813 ± 0.029	12.723 ± 0.287	10.198 ± 3.385

Table E.1. *Continued*

5442	J111113-080401	5148.365 ± 0.021	13.495 ± 0.045	19.966 ± 1.166
5443	J111113-080401	5146.567 ± 0.412	12.782 ± 0.360	35.855 ± 19.134
5444	J111113-080401	5146.193 ± 0.080	12.259 ± 0.744	12.417 ± 9.650
5445	J111113-080401	5145.631 ± 0.053	13.008 ± 0.148	20.999 ± 5.011
5446	J111113-080401	5144.248 ± 0.011	14.756 ± 0.073	26.994 ± 3.392
5447	J111113-080401	5143.751 ± 0.581	13.896 ± 0.507	46.560 ± 13.752
5448	J111113-080401	5141.003 ± 0.052	12.350 ± 0.078	20.084 ± 4.335
5449	J111113-080401	5139.364 ± 0.014	13.264 ± 0.014	32.135 ± 1.264
5450	J111113-080401	5138.182 ± 0.068	12.155 ± 0.122	17.324 ± 5.894
5451	J111113-080401	5135.576 ± 0.067	12.785 ± 0.042	49.351 ± 5.523
5452	J111113-080401	5133.322 ± 0.019	12.726 ± 0.061	12.533 ± 1.442
5453	J111113-080401	5132.475 ± 0.250	13.232 ± 0.403	26.625 ± 10.770
5454	J111113-080401	5132.181 ± 0.015	12.840 ± 0.249	10.062 ± 2.626
5455	J111113-080401	5131.755 ± 0.252	13.274 ± 0.277	32.922 ± 8.625
5456	J111113-080401	5130.195 ± 0.091	12.518 ± 0.141	22.606 ± 7.286
5457	J111113-080401	5128.921 ± 0.015	14.759 ± 0.050	27.740 ± 1.270
5458	J111113-080401	5127.992 ± 0.143	13.278 ± 0.196	26.733 ± 6.344
5459	J111113-080401	5125.184 ± 0.004	15.596 ± 0.041	57.719 ± 0.879
5460	J111113-080401	5121.469 ± 0.014	14.408 ± 0.013	45.529 ± 0.668
5461	J111113-080401	5120.136 ± 0.024	12.628 ± 0.106	11.607 ± 2.156
5462	J111113-080401	5118.665 ± 0.015	13.318 ± 0.014	31.685 ± 0.908
5463	J111113-080401	5114.733 ± 0.005	13.360 ± 0.009	17.965 ± 0.408
5464	J111113-080401	5110.502 ± 0.024	12.565 ± 0.055	13.020 ± 2.109
5465	J111113-080401	5106.244 ± 0.094	13.062 ± 0.332	22.508 ± 3.754
5466	J111113-080401	5105.675 ± 0.926	12.560 ± 1.130	31.058 ± 49.746
5467	J111113-080401	5104.701 ± 0.030	12.710 ± 0.072	17.232 ± 2.105
5468	J111113-080401	5103.323 ± 0.043	12.300 ± 0.069	19.164 ± 3.672
5469	J111113-080401	5100.243 ± 0.060	12.382 ± 0.067	27.729 ± 5.133
5470	J111113-080401	5099.118 ± 0.036	12.094 ± 0.089	12.011 ± 3.208
5471	J111113-080401	5097.187 ± 0.137	12.372 ± 0.118	37.345 ± 11.841
5472	J111113-080401	5096.262 ± 0.015	12.724 ± 0.069	12.999 ± 1.570
5473	J111113-080401	5095.261 ± 0.205	12.640 ± 0.202	46.401 ± 23.565
5474	J111113-080401	5093.906 ± 0.036	12.060 ± 0.149	10.016 ± 3.901
5475	J111113-080401	5088.120 ± 0.052	12.083 ± 0.122	13.345 ± 4.570
5476	J111113-080401	5087.258 ± 0.023	13.751 ± 0.040	20.985 ± 1.056
5477	J111113-080401	5086.351 ± 0.073	14.267 ± 0.095	27.010 ± 4.477
5478	J111113-080401	5085.138 ± 0.060	15.315 ± 0.142	27.915 ± 1.341
5479	J111113-080401	5083.603 ± 0.019	13.047 ± 0.036	24.060 ± 2.451
5480	J111113-080401	5082.597 ± 0.101	12.803 ± 0.170	22.447 ± 7.593
5481	J111113-080401	5081.259 ± 0.045	13.631 ± 0.089	22.179 ± 1.539
5482	J111113-080401	5080.707 ± 0.260	12.946 ± 0.465	24.187 ± 14.743
5483	J111113-080401	5079.858 ± 0.030	12.883 ± 0.110	18.171 ± 4.560
5484	J111113-080401	5078.487 ± 0.109	12.316 ± 0.139	26.711 ± 9.624
5485	J111113-080401	5075.962 ± 0.004	13.744 ± 0.005	27.789 ± 0.336

Table E.1. *Continued*

5486	J111113-080401	5074.416 ± 0.017	13.234 ± 0.020	30.299 ± 1.759
5487	J111113-080401	5073.266 ± 0.071	12.556 ± 0.161	16.484 ± 4.523
5488	J111113-080401	5072.340 ± 0.012	14.436 ± 0.034	24.593 ± 1.276
5489	J111113-080401	5071.523 ± 0.044	13.728 ± 0.050	29.233 ± 1.675
5490	J111113-080401	5069.132 ± 0.003	13.789 ± 0.005	23.247 ± 0.257
5491	J111113-080401	5067.691 ± 0.004	13.801 ± 0.006	23.223 ± 0.321
5492	J111113-080401	5066.553 ± 0.003	14.040 ± 0.008	21.809 ± 0.343
5493	J111113-080401	5065.463 ± 0.007	13.457 ± 0.010	25.061 ± 0.760
5494	J111113-080401	5064.373 ± 0.134	12.748 ± 0.268	18.824 ± 6.360
5495	J111113-080401	5063.925 ± 0.174	12.560 ± 0.403	17.528 ± 6.891
5496	J111113-080401	5062.424 ± 0.038	13.312 ± 0.044	26.917 ± 2.034
5497	J111113-080401	5061.793 ± 0.033	13.079 ± 0.074	19.968 ± 1.664

Bibliography

- Abel T., Haehnelt M.G., 1999, ApJ, 520, L13
- Agafonova I.I., Centurión M., Levshakov S.A., Molaro P., 2005, A&A, 441, 9
- Agafonova I.I., Levshakov S.A., Reimers D., Fechner C., Tytler D., Simcoe R.A., Songaila A., 2007, A&A, 461, 893
- Aguirre A., Schaye J., Kim T.S., Theuns T., Rauch M., Sargent W.L.W., 2004, ApJ, 602, 38
- Anderson S.F., Hogan C.J., Williams B.F., Carswell R.F., 1999, AJ, 117, 56
- Arons J., Wingert D.W., 1972, ApJ, 177, 1
- Bahcall J.N., Peebles P.J.E., 1969, ApJ, 156, L7
- Bajtlik S., Duncan R.C., Ostriker J.P., 1988, ApJ, 327, 570
- Barthel P.D., 1989, ApJ, 336, 606
- Beaver E.A., Burbidge E.M., Cohen R.D., Junkkarinen V.T., Lyons R.W., Rosenblatt E.I., Hartig G.F., Margon B., Davidsen A.F., 1991, ApJ, 377, L1
- Bechtold J., 1994, ApJS, 91, 1
- Bechtold J., Green R.F., Weymann R.J., Schmidt M., Estabrook F.B., Sherman R.D., Wahlquist H.D., Heckman T.M., 1984, ApJ, 281, 76
- Becker G.D., Bolton J.S., Haehnelt M.G., Sargent W.L.W., 2011, MNRAS, 410, 1096
- Becker G.D., Hewett P.C., Worseck G., Prochaska J.X., 2013, MNRAS, 430, 2067
- Becker R.H., Fan X., White R.L., Strauss M.A., Narayanan V.K., Lupton R.H., Gunn J.E., Annis J., Bahcall N.A., Brinkmann J., Connolly A.J., Csabai I., Czarapata P.C., Doi M., Heckman T.M., Hennessy G.S., Ivezić Ž., Knapp G.R., Lamb D.Q., McKay T.A., Munn J.A., Nash T., Nichol R., Pier J.R., Richards G.T., Schneider D.P., Stoughton C., Szalay A.S., Thakar A.R., York D.G., 2001, AJ, 122, 2850
- Benson A.J., Lacey C.G., Baugh C.M., Cole S., Frenk C.S., 2002, MNRAS, 333, 156
- Bernardi M., Sheth R.K., SubbaRao M., Richards G.T., Burles S., Connolly A.J., Frieman J., Nichol R., Schaye J., Schneider D.P., Vanden Berk D.E., York D.G., Brinkmann J., Lamb D.Q., 2003, AJ, 125, 32

- Bi H., Davidsen A.F., 1997, ApJ, 479, 523
- Boera E., Murphy M.T., Becker G.D., Bolton J.S., 2014, MNRAS, 441, 1916
- Boksenberg A., Sargent W.L.W., Rauch M., 1998, submitted, astro-ph/9810502
- Boksenberg A., Sargent W.L.W., Rauch M., 2003, ApJS, submitted, astro-ph/0307557
- Bolton J.S., Becker G.D., Raskutti S., Wyithe J.S.B., Haehnelt M.G., Sargent W.L.W., 2012, MNRAS, 419, 2880
- Bolton J.S., Haehnelt M.G., Viel M., Carswell R.F., 2006, MNRAS, 366, 1378
- Bolton J.S., Oh S.P., Furlanetto S.R., 2009a, MNRAS, 395, 736
- Bolton J.S., Oh S.P., Furlanetto S.R., 2009b, MNRAS, 396, 2405
- Bond J.R., Kofman L., Pogosyan D., 1996, Nature, 380, 603
- Brotherton M.S., Tran H.D., Becker R.H., Gregg M.D., Laurent-Muehleisen S.A., White R.L., 2001, ApJ, 546, 775
- Brusa M., Comastri A., Gilli R., Hasinger G., Iwasawa K., Mainieri V., Mignoli M., Salvato M., Zamorani G., Bongiorno A., Cappelluti N., Civano F., Fiore F., Merloni A., Silverman J., Trump J., Vignali C., Capak P., Elvis M., Ilbert O., Impey C., Lilly S., 2009, ApJ, 693, 8
- Burbidge E.M., 1967, ARA&A, 5, 399
- Calura F., Tescari E., D'Odorico V., Viel M., Cristiani S., Kim T.S., Bolton J.S., 2012, MNRAS, 422, 3019
- Carswell R.F., Webb J.K., Baldwin J.A., Atwood B., 1987, ApJ, 319, 709
- Carswell R.F., Whelan J.A.J., Smith M.G., Boksenberg A., Tytler D., 1982, MNRAS, 198, 91
- Cen R., 1997, ApJ, 479, L85
- Cen R., Bryan G.L., 2001, ApJ, 546, L81
- Chang P., Broderick A.E., Pfrommer C., 2012, ApJ, 752, 23
- Compostella M., Cantalupo S., Porciani C., 2013, MNRAS, 435, 3169
- Cooke A.J., Espey B., Carswell R.F., 1997, MNRAS, 284, 552
- Dall'Aglio A., Wisotzki L., Worseck G., 2008, A&A, 491, 465
- Dall'Aglio A., Wisotzki L., Worseck G., 2009, ApJ, submitted, arXiv:0906.1484
- Davé R., Hernquist L., Katz N., Weinberg D.H., 1999, ApJ, 511, 521
- Davé R., Hernquist L., Weinberg D.H., Katz N., 1997, ApJ, 477, 21

- Davidsen A.F., Kriss G.A., Zheng W., 1996, Nature, 380, 47
- Davies F.B., Furlanetto S.R., 2014, MNRAS, 437, 1141
- Davis T.M., Lineweaver C.H., 2004, PASA, 21, 97
- Dekker H., D'Odorico S., Kaufer A., Delabre B., Kotzlowski H., in M. Iye, A.F. Moorwood (eds.), *Society of Photo-Optical Instrumentation Engineers (SPIE) Conference Series, Society of Photo-Optical Instrumentation Engineers (SPIE) Conference Series*, vol. 4008, 534–545 (2000)
- Dixon K.L., Furlanetto S.R., 2009, ApJ, 706, 970
- Ellis R.S., 1978, MNRAS, 185, 613
- Fan X., Narayanan V.K., Lupton R.H., Strauss M.A., Knapp G.R., Becker R.H., White R.L., Pentericci L., Leggett S.K., Haiman Z., Gunn J.E., Ivezić Ž., Schneider D.P., Anderson S.F., Brinkmann J., Bahcall N.A., Connolly A.J., Csabai I., Doi M., Fukugita M., Geballe T., Grebel E.K., Harbeck D., Hennessy G., Lamb D.Q., Miknaitis G., Munn J.A., Nichol R., Okamura S., Pier J.R., Prada F., Richards G.T., Szalay A., York D.G., 2001, AJ, 122, 2833
- Fan X., Strauss M.A., Becker R.H., White R.L., Gunn J.E., Knapp G.R., Richards G.T., Schneider D.P., Brinkmann J., Fukugita M., 2006, AJ, 132, 117
- Faucher-Giguère C.A., Lidz A., Hernquist L., Zaldarriaga M., 2008a, ApJ, 688, 85
- Faucher-Giguère C.A., Lidz A., Zaldarriaga M., Hernquist L., 2009, ApJ, 703, 1416
- Faucher-Giguère C.A., Prochaska J.X., Lidz A., Hernquist L., Zaldarriaga M., 2008b, ApJ, 681, 831
- Fechner C., Reimers D., Kriss G.A., Baade R., Blair W.P., Giroux M.L., Green R.F., Moos H.W., Morton D.C., Scott J.E., Shull J.M., Simcoe R., Songaila A., Zheng W., 2006, A&A, 455, 91
- Franceschini A., Hasinger G., Miyaji T., Malquori D., 1999, MNRAS, 310, L5
- Furlanetto S.R., 2009, ApJ, 700, 1666
- Furlanetto S.R., Oh S.P., 2008a, ApJ, 682, 14
- Furlanetto S.R., Oh S.P., 2008b, ApJ, 681, 1
- Giallongo E., Cristiani S., 1990, MNRAS, 247, 696
- Gleser L., Nusser A., Benson A.J., Ohno H., Sugiyama N., 2005, MNRAS, 361, 1399
- Gnedin N.Y., 2000, ApJ, 535, 530
- Gunn J.E., Peterson B.A., 1965, ApJ, 142, 1633
- Haardt F., Madau P., 1996, ApJ, 461, 20

- Haehnelt M.G., Steinmetz M., 1998, MNRAS, 298, L21
- Haiman Z., Knox L., in A. de Oliveira-Costa, M. Tegmark (eds.), *Microwave Foregrounds, Astronomical Society of the Pacific Conference Series*, vol. 181, 227 (1999)
- Heap S.R., Williger G.M., Smette A., Hubeny I., Sahu M.S., Jenkins E.B., Tripp T.M., Winkler J.N., 2000, ApJ, 534, 69
- Hernquist L., Springel V., 2003, MNRAS, 341, 1253
- Hinshaw G., Larson D., Komatsu E., Spergel D.N., Bennett C.L., Dunkley J., Nolta M.R., Halpern M., Hill R.S., Odegard N., Page L., Smith K.M., Weiland J.L., Gold B., Jarosik N., Kogut A., Limon M., Meyer S.S., Tucker G.S., Wollack E., Wright E.L., 2013, ApJS, 208, 19
- Hogan C.J., Anderson S.F., Rutgers M.H., 1997, AJ, 113, 1495
- Hopkins P.F., Hernquist L., Cox T.J., Di Matteo T., Robertson B., Springel V., 2006, ApJS, 163, 1
- Hopkins P.F., Richards G.T., Hernquist L., 2007, ApJ, 654, 731
- Hu E.M., Kim T.S., Cowie L.L., Songaila A., Rauch M., 1995, AJ, 110, 1526
- Hui L., Gnedin N.Y., 1997, MNRAS, 292, 27
- Hui L., Haiman Z., 2003, ApJ, 596, 9
- Hui L., Rutledge R.E., 1999, ApJ, 517, 541
- Jakobsen P., Boksenberg A., Deharveng J.M., Greenfield P., Jedrzejewski R., Paresce F., 1994, Nature, 370, 35
- Jakobsen P., Jansen R.A., Wagner S., Reimers D., 2003, A&A, 397, 891
- Janknecht E., Reimers D., Lopez S., Tytler D., 2006, A&A, 458, 427
- Jenkins E.B., Ostriker J.P., 1991, ApJ, 376, 33
- Kazanas D., Fukumura K., Behar E., Contopoulos I., Shrader C., 2012, The Astronomical Review, 7, 3, 030000
- Kennefick J.D., Djorgovski S.G., de Carvalho R.R., 1995, AJ, 110, 2553
- Kim T.S., Bolton J.S., Viel M., Haehnelt M.G., Carswell R.F., 2007, MNRAS, 382, 1657
- Kim T.S., Carswell R.F., Cristiani S., D'Odorico S., Giallongo E., 2002a, MNRAS, 335, 555
- Kim T.S., Cristiani S., D'Odorico S., 2001, A&A, 373, 757
- Kim T.S., Cristiani S., D'Odorico S., 2002b, A&A, 383, 747
- Kim T.S., Hu E.M., Cowie L.L., Songaila A., 1997, AJ, 114, 1

- Kirkman D., Tytler D., 1997, ApJ, 484, 672
- Kriss G.A., Shull J.M., Oegerle W., Zheng W., Davidsen A.F., Songaila A., Tumlinson J., Cowie L.L., Deharveng J.M., Friedman S.D., Giroux M.L., Green R.F., Hutchings J.B., Jenkins E.B., Kruk J.W., Moos H.W., Morton D.C., Sembach K.R., Tripp T.M., 2001, Science, 293, 1112
- Lidz A., Faucher-Giguère C.A., Dall'Aglio A., McQuinn M., Fechner C., Zaldarriaga M., Hernquist L., Dutta S., 2010, ApJ, 718, 199
- Liske J., Webb J.K., Carswell R.F., 1998, MNRAS, 301, 787
- Liu X.D., Jones B.J.T., 1988, MNRAS, 230, 481
- Lu L., Sargent W.L.W., Womble D.S., Takada-Hidai M., 1996, ApJ, 472, 509
- Lu L., Wolfe A.M., Turnshek D.A., 1991, ApJ, 367, 19
- Lynds R., 1971, ApJ, 164, L73
- Machacek M.E., Bryan G.L., Meiksin A., Anninos P., Thayer D., Norman M., Zhang Y., 2000, ApJ, 532, 118
- Madau P., Haardt F., Rees M.J., 1999, ApJ, 514, 648
- Madau P., Rees M.J., Volonteri M., Haardt F., Oh S.P., 2004, ApJ, 604, 484
- Maselli A., Ferrara A., 2005, MNRAS, 364, 1429
- McDonald P., Miralda-Escudé J., 2001, ApJ, 549, L11
- McDonald P., Miralda-Escudé J., Rauch M., Sargent W.L.W., Barlow T.A., Cen R., 2001, ApJ, 562, 52
- McDonald P., Miralda-Escudé J., Rauch M., Sargent W.L.W., Barlow T.A., Cen R., Ostriker J.P., 2000, ApJ, 543, 1
- McQuinn M., Lidz A., Zaldarriaga M., Hernquist L., Hopkins P.F., Dutta S., Faucher-Giguère C.A., 2009, ApJ, 694, 842
- Meiksin A., 2005, MNRAS, 356, 596
- Meiksin A., Tittley E.R., Brown C.K., 2010, MNRAS, 401, 77
- Meiksin A.A., 2009, Reviews of Modern Physics, 81, 1405
- Miralda-Escudé J., 1998, ApJ, 501, 15
- Miralda-Escudé J., 2005, ApJ, 620, L91
- Miralda-Escudé J., Cen R., Ostriker J.P., Rauch M., 1996, ApJ, 471, 582
- Miralda-Escudé J., Haehnelt M., Rees M.J., 2000, ApJ, 530, 1

- Miralda-Escudé J., Rees M.J., 1994, MNRAS, 266, 343
- Momjian E., Carilli C.L., Walter F., Venemans B., 2014, AJ, 147, 6
- Murdoch H.S., Hunstead R.W., Pettini M., Blades J.C., 1986, ApJ, 309, 19
- O'Brien P.T., Wilson R., Gondhalekar P.M., 1988, MNRAS, 233, 801
- Oemler Jr. A., Lynds C.R., 1975, ApJ, 199, 558
- Oke J.B., Korycansky D.G., 1982, ApJ, 255, 11
- Pâris I., Petitjean P., Rollinde E., Aubourg E., Busca N., Charlassier R., Delubac T., Hamilton J.C., Le Goff J.M., Palanque-Delabrouille N., Peirani S., Pichon C., Rich J., Vargas-Magaña M., Yèche C., 2011, A&A, 530, A50
- Paschos P., Norman M.L., Bordner J.O., Harkness R., 2007, submitted, arXiv:0711.1904
- Peebles P.J.E., 1968, ApJ, 153, 1
- Peimbert M., Luridiana V., Peimbert A., 2007, ApJ, 666, 636
- Peterson B.A., in M.S. Longair, J. Einasto (eds.), *Large Scale Structures in the Universe, IAU Symposium*, vol. 79, 389–392 (1978)
- Petitjean P., Webb J.K., Rauch M., Carswell R.F., Lanzetta K., 1993, MNRAS, 262, 499
- Pettini M., Hunstead R.W., Smith L.J., Mar D.P., 1990, MNRAS, 246, 545
- Planck Collaboration, Ade P.A.R., Aghanim N., Armitage-Caplan C., Arnaud M., Ashdown M., Atrio-Barandela F., Aumont J., Baccigalupi C., Banday A.J., et al., 2013, A&A, submitted, arXiv:1303.5076
- Press W.H., Rybicki G.B., Schneider D.P., 1993, ApJ, 414, 64
- Puchwein E., Pfrommer C., Springel V., Broderick A.E., Chang P., 2012, MNRAS, 423, 149
- Rauch M., Carswell R.F., Chaffee F.H., Foltz C.B., Webb J.K., Weymann R.J., Bechtold J., Green R.F., 1992, ApJ, 390, 387
- Rauch M., Carswell R.F., Webb J.K., Weymann R.J., 1993, MNRAS, 260, 589
- Rauch M., Miralda-Escude J., Sargent W.L.W., Barlow T.A., Weinberg D.H., Hernquist L., Katz N., Cen R., Ostriker J.P., 1997, ApJ, 489, 7
- Rees M.J., Sciama D.W., 1967, ApJ, 147, 353
- Reimers D., Fechner C., Hagen H.J., Jakobsen P., Tytler D., Kirkman D., 2005, A&A, 442, 63
- Reimers D., Kohler S., Wisotzki L., Groote D., Rodriguez-Pascual P., Wamsteker W., 1997, A&A, 327, 890

- Reimers D., Vogel S., 1993, A&A, 276, L13
- Reimers D., Vogel S., Hagen H.J., Engels D., Groote D., Wamsteker W., Clavel J., Rosa M.R., 1992, Nature, 360, 561
- Richards G.T., Strauss M.A., Fan X., Hall P.B., Jester S., Schneider D.P., Vanden Berk D.E., Stoughton C., Anderson S.F., Brunner R.J., Gray J., Gunn J.E., Ivezić Ž., Kirkland M.K., Knapp G.R., Loveday J., Meiksin A., Pope A., Szalay A.S., Thakar A.R., Yanny B., York D.G., Barentine J.C., Brewington H.J., Brinkmann J., Fukugita M., Harvanek M., Kent S.M., Kleinman S.J., Krzesiński J., Long D.C., Lupton R.H., Nash T., Neilson Jr. E.H., Nitta A., Schlegel D.J., Snedden S.A., 2006, AJ, 131, 2766
- Richter P., Fox A.J., Wakker B.P., Lehner N., Howk J.C., Bland-Hawthorn J., Ben Bekhti N., Fechner C., 2013, ApJ, 772, 111
- Richter P., Krause F., Fechner C., Charlton J.C., Murphy M.T., 2011, A&A, 528, A12
- Ricotti M., Gnedin N.Y., Shull J.M., 2000, ApJ, 534, 41
- Ricotti M., Gnedin N.Y., Shull J.M., 2002, ApJ, 575, 49
- Salpeter E.E., 1964, ApJ, 140, 796
- Sandage A., 1961, ApJ, 133, 355
- Sargent W.L.W., Young P.J., Boksenberg A., Tytler D., 1980, ApJS, 42, 41
- Schaye J., 2006, ApJ, 643, 59
- Schaye J., Aguirre A., Kim T.S., Theuns T., Rauch M., Sargent W.L.W., 2003, ApJ, 596, 768
- Schaye J., Theuns T., Leonard A., Efstathiou G., 1999, MNRAS, 310, 57
- Schaye J., Theuns T., Rauch M., Efstathiou G., Sargent W.L.W., 2000, MNRAS, 318, 817
- Schmidt M., 1963, Nature, 197, 1040
- Schmidt M., 1969, ARA&A, 7, 527
- Schneider D.P., Schmidt M., Gunn J.E., 1989a, AJ, 98, 1507
- Schneider D.P., Schmidt M., Gunn J.E., 1989b, AJ, 98, 1951
- Schneider D.P., Schmidt M., Gunn J.E., 1991, AJ, 101, 2004
- Shaver P.A., Hook I.M., Jackson C.A., Wall J.V., Kellermann K.I., in C.L. Carilli, S.J.E. Radford, K.M. Menten, G.I. Langston (eds.), *Highly Redshifted Radio Lines, Astronomical Society of the Pacific Conference Series*, vol. 156, 163 (1999a)
- Shaver P.A., Windhorst R.A., Madau P., de Bruyn A.G., 1999b, A&A, 345, 380

- Shull J.M., France K., Danforth C.W., Smith B., Tumlinson J., 2010, ApJ, 722, 1312
- Shull J.M., Tumlinson J., Giroux M.L., Kriss G.A., Reimers D., 2004, ApJ, 600, 570
- Smette A., Heap S.R., Williger G.M., Tripp T.M., Jenkins E.B., Songaila A., 2002, ApJ, 564, 542
- Sokasian A., Abel T., Hernquist L., 2002, MNRAS, 332, 601
- Songaila A., 1998, AJ, 115, 2184
- Songaila A., 2004, AJ, 127, 2598
- Songaila A., Cowie L.L., 1996, AJ, 112, 335
- Songaila A., Cowie L.L., 2002, AJ, 123, 2183
- Spergel D.N., Verde L., Peiris H.V., Komatsu E., Nolta M.R., Bennett C.L., Halpern M., Hinshaw G., Jarosik N., Kogut A., Limon M., Meyer S.S., Page L., Tucker G.S., Weiland J.L., Wollack E., Wright E.L., 2003, ApJS, 148, 175
- Springel V., White S.D.M., Jenkins A., Frenk C.S., Yoshida N., Gao L., Navarro J., Thacker R., Croton D., Helly J., Peacock J.A., Cole S., Thomas P., Couchman H., Evrard A., Colberg J., Pearce F., 2005, Nature, 435, 629
- Steer I., 2012, Nature, 490, 176
- Steidel C.C., Sargent W.L.W., 1987, ApJ, 313, 171
- Stoer J., *Numerische Mathematik 1*, 5 edn. (Springer-Verlag, 1989). ISBN: 3-540-51481-3
- Strömgren B., 1939, ApJ, 89, 526
- Syphers D., Anderson S.F., Zheng W., Haggard D., Meiksin A., Chiu K., Hogan C., Schneider D.P., York D.G., 2009a, ApJ, 690, 1181
- Syphers D., Anderson S.F., Zheng W., Haggard D., Meiksin A., Schneider D.P., York D.G., 2009b, ApJS, 185, 20
- Syphers D., Anderson S.F., Zheng W., Meiksin A., Haggard D., Schneider D.P., York D.G., 2011a, ApJ, 726, 111
- Syphers D., Anderson S.F., Zheng W., Meiksin A., Schneider D.P., York D.G., 2012, AJ, 143, 100
- Syphers D., Anderson S.F., Zheng W., Smith B., Pieri M., Kriss G.A., Meiksin A., Schneider D.P., Shull J.M., York D.G., 2011b, ApJ, 742, 99
- Syphers D., Shull J.M., 2014, ApJ, 784, 42
- Syunyaev R.A., 1968, Soviet Physics Doklady, 13, 183
- Tepper-García T., Fritze U., 2008, MNRAS, 383, 1671

- Theuns T., Bernardi M., Frieman J., Hewett P., Schaye J., Sheth R.K., Subbarao M., 2002a, ApJ, 574, L111
- Theuns T., Schaye J., Zaroubi S., Kim T.S., Tzanavaris P., Carswell B., 2002b, ApJ, 567, L103
- Theuns T., Zaroubi S., Kim T.S., Tzanavaris P., Carswell R.F., 2002c, MNRAS, 332, 367
- Tittley E.R., Meiksin A., 2007, MNRAS, 380, 1369
- Tytler D., 1987, ApJ, 321, 49
- Tytler D., Kirkman D., O'Meara J.M., Suzuki N., Orin A., Lubin D., Paschos P., Jena T., Lin W.C., Norman M.L., Meiksin A., 2004, ApJ, 617, 1
- Vanden Berk D.E., Richards G.T., Bauer A., Strauss M.A., Schneider D.P., Heckman T.M., York D.G., Hall P.B., Fan X., Knapp G.R., Anderson S.F., Annis J., Bahcall N.A., Bernardi M., Briggs J.W., Brinkmann J., Brunner R., Burles S., Carey L., Castander F.J., Connolly A.J., Crocker J.H., Csabai I., Doi M., Finkbeiner D., Friedman S., Frieman J.A., Fukugita M., Gunn J.E., Hennessy G.S., Ivezić Ž., Kent S., Kunszt P.Z., Lamb D.Q., Leger R.F., Long D.C., Loveday J., Lupton R.H., Meiksin A., Merelli A., Munn J.A., Newberg H.J., Newcomb M., Nichol R.C., Owen R., Pier J.R., Pope A., Rockosi C.M., Schlegel D.J., Siegmund W.A., Smee S., Snir Y., Stoughton C., Stubbs C., SubbaRao M., Szalay A.S., Szokoly G.P., Tremonti C., Uomoto A., Waddell P., Yanny B., Zheng W., 2001, AJ, 122, 549
- Venkatesan A., Tumlinson J., Shull J.M., 2003, ApJ, 584, 621
- Viel M., Haehnelt M.G., Springel V., 2004, MNRAS, 354, 684
- Vladilo G., Centurión M., D'Odorico V., Péroux C., 2003, A&A, 402, 487
- Weinberg D.H., Miralda-Escude J., Hernquist L., Katz N., 1997, ApJ, 490, 564
- Weymann R.J., Carswell R.F., Smith M.G., 1981, ARA&A, 19, 41
- Woosley S.E., Bloom J.S., 2006, ARA&A, 44, 507
- Worseck G., Fechner C., Wisotzki L., Dall'Aglio A., 2007, A&A, 473, 805
- Worseck G., Prochaska J.X., McQuinn M., Dall'Aglio A., Fechner C., Hennawi J.F., Reimers D., Richter P., Wisotzki L., 2011, ApJ, 733, L24
- Worseck G., Wisotzki L., 2006, A&A, 450, 495
- Young P.J., Sargent W.L.W., Boksenberg A., Carswell R.F., Whelan J.A.J., 1979, ApJ, 229, 891
- Zaldarriaga M., Hui L., Tegmark M., 2001, ApJ, 557, 519
- Zhang Y., Anninos P., Norman M.L., 1995, ApJ, 453, L57

Zheng W., Chiu K., Anderson S.F., Schneider D.P., Hogan C.J., York D.G., Burles S., Brinkmann J., 2004a, AJ, 127, 656

Zheng W., Kriss G.A., Deharveng J.M., Dixon W.V., Kruk J.W., Shull J.M., Giroux M.L., Morton D.C., Williger G.M., Friedman S.D., Moos H.W., 2004b, ApJ, 605, 631

Zheng W., Meiksin A., Pifko K., Anderson S.F., Hogan C.J., Tittley E., Kriss G.A., Chiu K., Schneider D.P., York D.G., Weinberg D.H., 2008, ApJ, 686, 195

Zuo L., 1993, A&A, 278, 343

Zuo L., Phinney E.S., 1993, ApJ, 418, 28

Selbstständigkeitserklärung

Hiermit erkläre ich, dass diese Arbeit an keiner anderen Hochschule eingereicht sowie selbstständig von mir und nur mit den angegebenen Mitteln angefertigt wurde.

Dominik Hildebrandt
Potsdam, den 30. Januar 2015

Danksagung

Ich möchte mich herzlich bei meinem Doktorvater Prof. Philipp Richter für die Möglichkeit bedanken, in seiner Arbeitsgruppe ein tolles Forschungsprojekt bearbeiten zu können, für seine Unterstützung in schwierigen Phasen und nicht zuletzt für das Erleichtern des Verständnisses (astro)physikalischer Zusammenhänge.

Im Rahmen dieser Arbeit habe ich viele tolle Menschen kennengelernt, deren Unterstützung ich mir stets sicher sein konnte. Deshalb möchte ich mich ebenfalls bedanken

bei Dr. Cora Fechner, die mir all die Jahre mit Rat und Tat unermüdlich zur Seite stand und immer wieder neue Denkanstöße gab,

bei Dr. Thorsten Tepper-García, von dem ich viel lernte und der mir mit unzähligen Anregungen zur Stelle war,

bei Andrea Brockhaus, die mich mit ihrer Fürsorge und Unterstützung stets auf dem richtigen Weg hielt,

und außerdem bei Dr. Martin Wendt, Dr. Nadya Draganova, Dr. Peter Herenz, Anne Fox, Philipp Ehrlich, Carlo Steiner, Patrick Neubert und Christoph Guber.

Ein großer Danke gilt meiner Familie und meinen Freunden. Mit euch ist alles möglich!